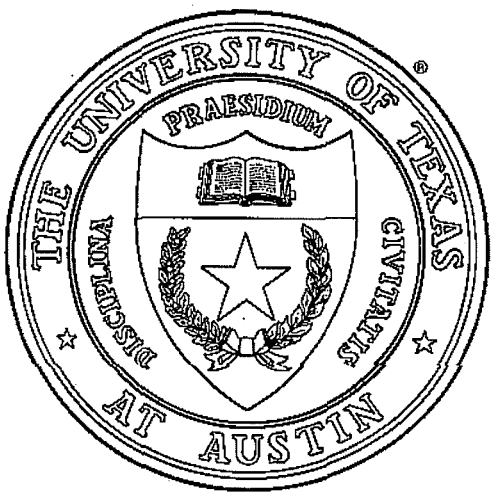

PMFSEL REPORT NO. 96-4
March, 1997

BEHAVIOR OF MULTIPLE-ANCHOR CONNECTIONS TO CONCRETE FROM THE PERSPECTIVE OF PLASTIC THEORY

Dieter Lotze

Richard E. Klingner

PHIL M. FERGUSON STRUCTURAL ENGINEERING LABORATORY

Department of Civil Engineering / Bureau of Engineering Research

The University of Texas at Austin

DISCLAIMER

This report presents partial results of a research program supported by U.S. Nuclear Regulatory Commission (NRC) under Contract No. NRC-03-92-05 (*"Anchor Bolt Behavior and Strength During Earthquakes"*). The technical contact is Herman L. Graves, III. His support is gratefully acknowledged. Any conclusions expressed in this thesis are those of the author. They are not to be considered NRC policy or recommendations.

ACKNOWLEDGEMENTS

The work described here was conducted while Dieter Lotze was a Visiting Scholar at The University of Texas at Austin. His stay was made possible by the German government (DFG); their support is gratefully acknowledged. The work was conducted as part of a research study sponsored by the U.S. Nuclear Regulatory Commission (Contract No. NRC-03-92-025, *"Anchor Bolt Behavior and Strength During Earthquakes"*). The technical contact for that study was Herman L. Graves, III. The work was performed at the Phil M. Ferguson Structural Engineering Laboratory of The University of Texas at Austin. The support of laboratory staff is gratefully acknowledged.

CHAPTER 1

INTRODUCTION

A multiple-anchor connection consists of a steel member (for example, an I-section) with a baseplate, attached to the concrete surface with two or more rows of anchor bolts or headed studs. Any single anchor of a group could fail by concrete breakout or by fracture of the steel. Other possible failure modes in tension are pullout due to insufficient holding force (undercut or friction), or for torque-controlled expansion anchors, pull-through of the cone through the anchor sleeve (CEB 1991; Eligehausen, Fuchs, Lotze and Reuter 1989; Rehm, Eligehausen and Mallée, 1992).

The capacity of an anchor group is a function of the type of load (tension, shear, moment or combined load), the capacities of the individual anchors, and the distribution of the load among the anchors (Lotze, 1986, 1992; Rehm, Eligehausen and Mallée 1992).

Current design methods for multiple-anchor connections with anchor bolts or headed studs to concrete are based primarily on elastic behavior and the equivalent stiffness of individual anchors. Recently, more work has been conducted on methods in which the plastic behavior of the steel anchor shank is considered (Cook, Doerr and Klingner 1989; Cook 1989; Cook and Klingner 1989, 1992-1, 1992-2; Klingner, Eligehausen and Balogh 1992).

In elastic design, the distribution of tension and shear among multiple anchors is based on the assumption that all anchors have the same stiffness. The tension on each anchor is then a function of that anchor's distance from the neutral axis. The failure mode has no influence on the load distribution (Rehm, Eligehausen and Mallée, 1992). Failure occurs when the maximum load on an individual anchor reaches that anchor's capacity. Anchors close to the neutral axis are not fully utilized.

In anchor groups located far from edges and designed for steel failure, shear forces are assumed to be uniformly distributed among the anchors. For near-edge anchors, to evaluate concrete capacity, all shear is assigned to the near-edge anchors. The smaller value of concrete and steel capacity governs. The combined tension and shear loading is evaluated separately for each anchor using an interaction diagram (Rehm, Eligehausen, Mallée, 1992).

The elastic design approach gives a generally conservative understanding of results. For anchors in thin, narrow members, it describes the actual behavior, and therefore leads to an economical design. The ultimate capacity of a multiple-anchor connections that fails by steel fracture is underestimated, however, because the redistribution of loads due to nonlinear material behavior is not considered in elastic design.

The plastic design of multiple-anchor connections was initially developed in the USA (Cook, Doerr and Klingner 1989; Cook 1989; Cook and Klingner 1989, 1992-1, 1992-2; Klingner, Eligehausen and Balogh 1992). The advantage of this design model lies in the utilization of the plastic deformation of the steel anchor shank. It is clear that an anchor shank yields before fracture. Under moment, all anchors of a multiple-anchor connection loaded in tension can therefore be fully utilized. This is analogous to the evaluation of the plastic section modulus of a steel cross-section. Plastic design leads to a simply, very economical design.

The prerequisites for the plastic design method are that the fastening fail by anchor fracture, and that the anchors have a large elongation at fracture. The required plastic deformation depends on the

configuration of the baseplate, on the number of the anchors, and also on the direction and line of application of the load; the influence of these factors has not been clarified so far. Furthermore, few data exist regarding the inelastic load-displacement behavior of currently used anchors under combined tension and shear, that might give clues about their plastic strain capacity. Questions also exist regarding the maximum deformation capacity, and especially regarding the rotation of the baseplate with respect to the serviceability of the connection.

So far, only a few experiments with particular multiple-anchor connections have been carried out to check the basic applicability of the plastic design method (Cook 1989; Cook and Klingner 1989, 1992-1, 1992-2). In those experiments, the calculated ultimate capacity was reached. However, the ultimate capacity in experiments with multiple-anchor connections depends on numerous factors, and the calculated capacities were based on relatively conservative assumptions. Systematic theoretical and experimental investigations of single anchors in tension, oblique tension and shear required to clarify the available plastic deformation have not been carried out, nor have experiments been conducted with multiple-anchor connections in which the distribution of load was measured, and the necessary plastic strain reserve was considered, depending on the proper parameters.

Anchors under earthquake loading are subjected to large deformations at a loading frequency of about 1 Hz to 10 Hz. Investigations of single anchors (Eibl and Keintzel 1989; Rodriguez 1995) had found that at high loading rates (about 0.05 to 0.5 seconds to reach the failure load), concrete breakout capacity is about 10% to 40% higher than under quasi-static load (about 2-4 minutes to reach the failure load). This increase in capacity is expected to be based on more than the pure material properties. It can also be based on changes of the fracture cone surface or on the higher local strain rate near the crack tip of the fracture cone, due to high strain gradients. The modified crack contour will influence the interaction between adjacent anchors, as well as between anchors and structural member edges. Experimental results concerning this have been sparse.

In this report, the status of the plastic design approach is summarized. Experiments conducted at the Phil M. Ferguson Structural Engineering Laboratory of The University of Texas at Austin are then reported. The interpretation of those experiments and calculations based on those test results, provide a significant contribution to the understanding of the capacity of multiple-anchor connections.

Finally, a program developed at the University of Stuttgart was checked against the test data. The purpose of this check was to permit the use of that program to design and carry out analytical parametric studies of multiple-anchor connections. Such studies are necessary to safely extend plastic design methods to situations that have not yet been tested.

CHAPTER 2

BACKGROUND

2.1 BEHAVIOR OF SINGLE ANCHORS

In CEB (1991), research on fastening technology is extensively described. Further summaries are included in Eligehausen, Fuchs, Lotze, and Reuter (1989) and Rehm, Eligehausen, and Mallée (1992). Of those results, only those essential for the present research are again summarized briefly below. Emphasis is placed on the influence of loading direction and loading rate on the ultimate capacity and the load-deformation behavior of single anchors failing by concrete breakout or by fracture of the anchor shank.

2.1.1 FAILURE MODE AND DISPLACEMENT UNDER TENSION AND SHEAR

Anchor bolts or headed studs can fail in the anchor itself, or by failure of the concrete. Most steel failures are failure of the anchor shank, failure of the anchor sleeve, or both. Possible modes of concrete failure are concrete breakout, lateral blowout failure for near edge anchors, splitting of the base concrete, or pullout of the anchors due to local failure of the concrete. The latter depends on the available bearing area, and also on the concrete strength around undercut anchors and headed studs. Pullout can also occur with torque-controlled expansion anchors, depending on the geometry and the coefficient of friction in the expansion zone. In pull-through failure, the cone is pulled through the sleeve of the anchor. Finally, a shallow anchor can fail in shear by formation of a shallow concrete breakout cone on the side of the anchor opposite to the direction of the applied load.

The displacement of anchors consists of the deformation of the attachment, the anchors, and the concrete in which the anchors are embedded. In shear, the additional possibility exists for shell-shaped local concrete spalling in front of the anchor.

Analytical investigation of the deformation of anchors exists up to now only for form-locking anchors (Furche 1994) and expansion anchors (Lehmann 1994) in concentric tension. The work of Fuchs (1990) gives some clues regarding shear behavior.

2.1.2 ULTIMATE CAPACITY UNDER TENSION OR SHEAR

The ultimate tension capacity of single anchors failing by concrete breakout in uncracked concrete is well predicted by Equation (2.1):

$$F_{Z,u,0} = A \cdot \sqrt{f_c} \cdot h_{ef}^{1.5} \tag{2.1}$$

where: $F_{Z,u,0}$ = ultimate capacity [N], A = 15.0 for expansion anchors, A = 17.0 for headed anchors, f_c = cylinder compressive strength of the concrete [N/mm^2], and h_{ef} = effective embedment depth [mm].

Equation (2.1) is valid for single anchors with an edge distance of at least 1.5 h_{ef}. A member thickness of $d = 2 \cdot h_{ef}$ is presupposed. In cracked concrete, a decrease of about 30% in ultimate capacity is expected.

Concrete capacity in shear is calculated as proposed by Rehm, Eligehausen, Mallée (1992) as

$$F_{S,u,0} = 1.0 \cdot \sqrt{\phi_1 f_c} \cdot \left(\frac{h_{ef}}{\phi_1}\right)^{0.2} \cdot c_1^{1.5} \qquad (2.2)$$

where: ϕ_1 = diameter of the anchor [mm], h_{ef} = embedment length [mm], and c_1 = edge distance in the loading direction [mm]. In Equation (2.2), a member thickness of at least $d = 1.4\ c_1$ is presupposed. The influence of the interaction of several anchors in a group as well as the reduction of the capacity by the structural member edge can be considered by the Concrete Capacity Method (CC-Method) described in CEB (1991).

For steel failure, the product of the ultimate tensile strength and the cross-sectional area of the anchor shank give:

$$F_{Z,u,0} = A_s \cdot f_{u,t} \qquad (2.3a)$$

The ratio of the ultimate shear and tensile capacities (with a uniform cross-section) is determined by tests as:

$$F_{S,u,0} / F_{Z,u,0} \approx 0.6 \qquad (2.3b)$$

This value agrees with the observed relationship of bolted joints. If the anchor sleeve goes through the baseplate, higher steel capacity could be achieved in shear. Estimates of capacity must consider in this case the degree of the interaction between anchor shank and anchor sleeve, as well as different materials. Current technical literature does not address this.

2.1.3 Tension - Shear Interaction at Ultimate Capacity

Figure 2.1 shows different models for the description of the interaction between ultimate capacity in shear and tension.

For the interaction at failure by steel fracture, an elliptical interaction relation is used:

$$\left(F_{S,u} / F_{S,u,0}\right)^p + \left(F_{Z,u} / F_{Z,u,0}\right)^p = 1 \qquad (2.4)$$

The exponent p varies between p = 5/3 (McMackin, Slutter and Fisher 1973) and p = 2.0 (Turner 1985; Shaikh and Whayong 1985).

For interaction at failure by concrete breakout, Johnson and Lew (1990) proposed a linear interaction as a lower bond (Figure 2.1). Bode and Roik (1987) proposed trilinear interactions described by Equations 2.5a to 2.5c:

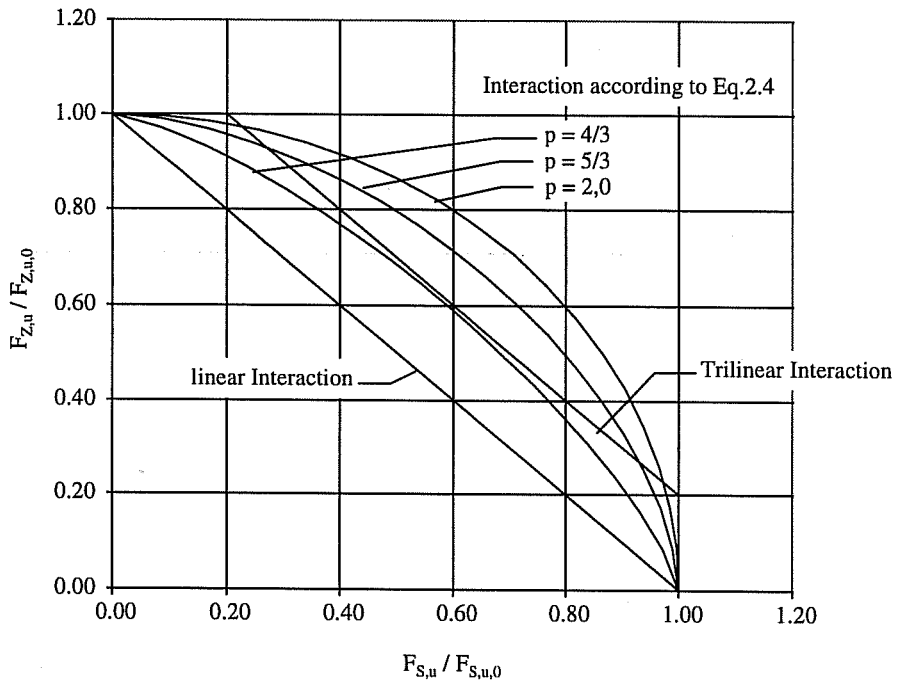

Figure 2. 1 *Tension and shear interaction for anchors at ultimate capacity*

$$F_s/F_{S,u,0} \leq 1.0 \tag{2.5a}$$

$$F_Z/F_{Z,u,0} \leq 1.0 \tag{2.5b}$$

$$F_S/F_{S,u,0} + F_Z/F_{Z,u,0} \leq 1.2 \tag{2.5c}$$

The elliptical interaction of Equation 2.4 has also been proposed for concrete failure. In that application, the exponent p varies from p = 4/3 (PCI 1985), to p = 5/3 (Cook and Klingner 1989), to p = 2.0 (Shaikh and Whayong 1985)

Where failure modes in tension and shear differ, the above interaction relations are probably conservative. A better description of the real behavior should probably use separate interaction relations for each individual failure mode, and should determine the critical oblique capacity separately for each failure mode. The smaller of the values for each failure load determines the capacity and the failure mode. An example for the results achieved with both procedures is compared in Figure 2.2 (torque-controlled expansion anchor) and Figure 2.3 (undercut anchor) with test results of Dieterle et al. (1989).

2.1.4 TENSION-SHEAR DISPLACEMENT INTERACTION

Displacement interaction has not been widely investigated. The elastic design procedure does not require knowledge of the displacement behavior of individual anchors of a group. In principle, the assumption of elastic load distribution to the individual anchors is conservative. Critical cases (such as a row of

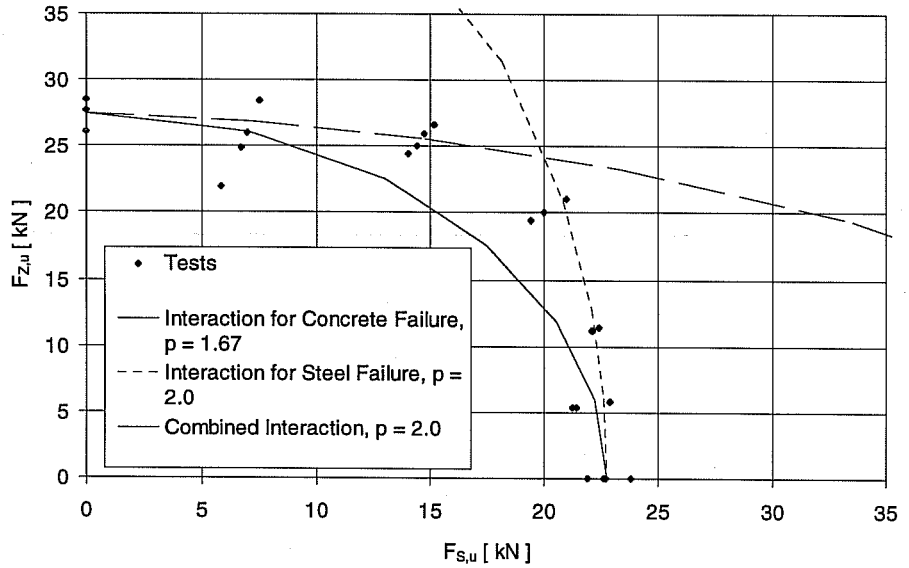

Figure 2. 2 *Tension-shear interaction of an undercut anchor (flush-sleeve installation, concrete breakout in tension, steel fracture in shear)*

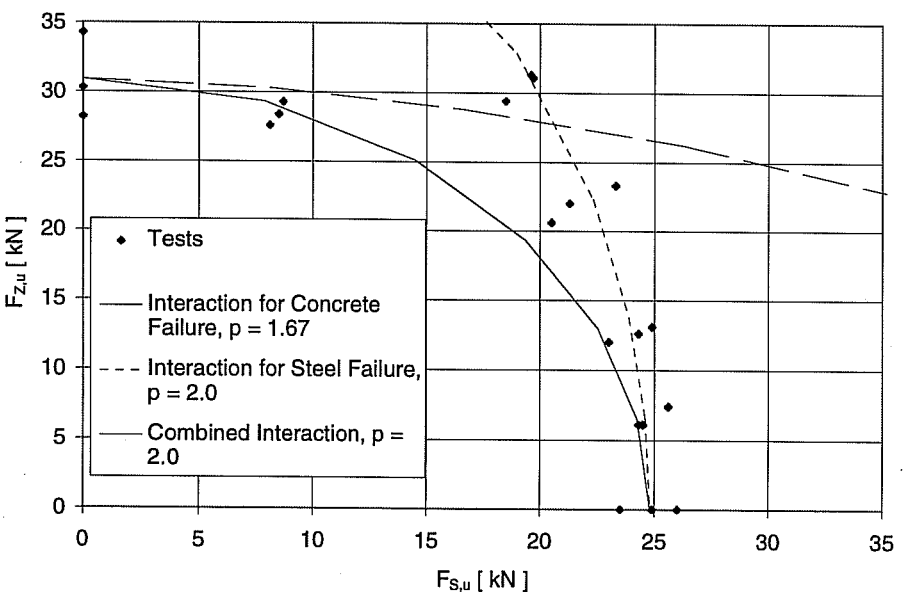

Figure 2. 3 *Tension-shear displacement interaction for a torque-controlled expansion anchor (flush-sleeve installation, concrete breakout in tension, steel fracture in shear)*

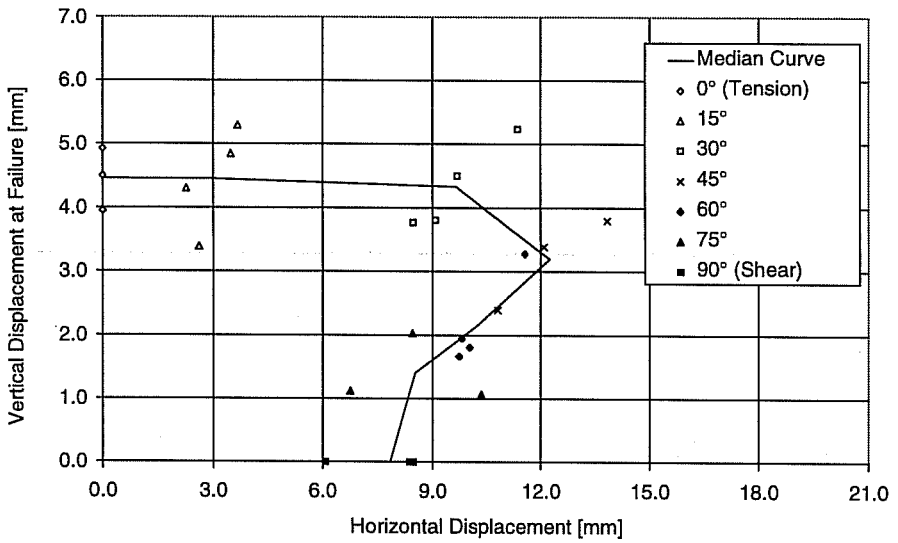

Figure 2. 4 *Tension-shear displacement interaction of a torque-controlled expansion anchor (flush-sleeve installation, concrete breakout under tension, steel fracture under shear)*

anchors placed perpendicular to the edge of a structural member and loaded in shear) are covered by special provisions. Dieterle et al. (1989) report test results for different types of anchors in hairline cracks of width w ≈ 0.4 mm, subjected to loads in different directions, Shear and tension deformations were recorded separately. However, the embedment length and edge distance in all tests were chosen so that, for loading angles exceeding 30° from the anchor axis, the failure mode shifted from concrete breakout (under pure tension) to steel failure (in pure shear). Thus, a complete set of load-displacement curves did not exist with the same failure mode over the entire range of loading angles. In those tests, concrete compressive strengths varied between $f_c = 27$ N/mm^2 and $f_c = 33$ N/mm^2. Figures 2.4 (torque-controlled expansion anchor) and 2.5 (undercut anchor) show the interaction of displacements as reported by Dieterle et al. (1989).

Figures 2.4 and 2.5 show a distinct maximum of the combined displacement at failure, at a loading angle of about 30° to 45°, for both types of anchors. Anchors loaded at that angle exhibit steel fracture, but withstand more displacement than anchors loaded in pure shear. Generally, the failure displacement is greater in shear than in tension. This is because before reaching the ultimate load, a conchoidal ("shell-shaped") concrete spalling occurs in front of the anchor in the loading direction. The anchor deforms significantly due to the elimination of confinement on the concrete. The magnitude of the spalling load was not reported.

2.1.5 Influence of Loading Rate on Ultimate Loads and Displacements

Only a few systematic investigations exist regarding the influence of the loading rate on the ultimate capacity and the load-displacement behavior of anchors.

Tests under both static and dynamic load of torque-controlled expansion anchors of the sleeve and the clip types, and also with undercut anchors, are described in Rodriguez (1995). The anchors were

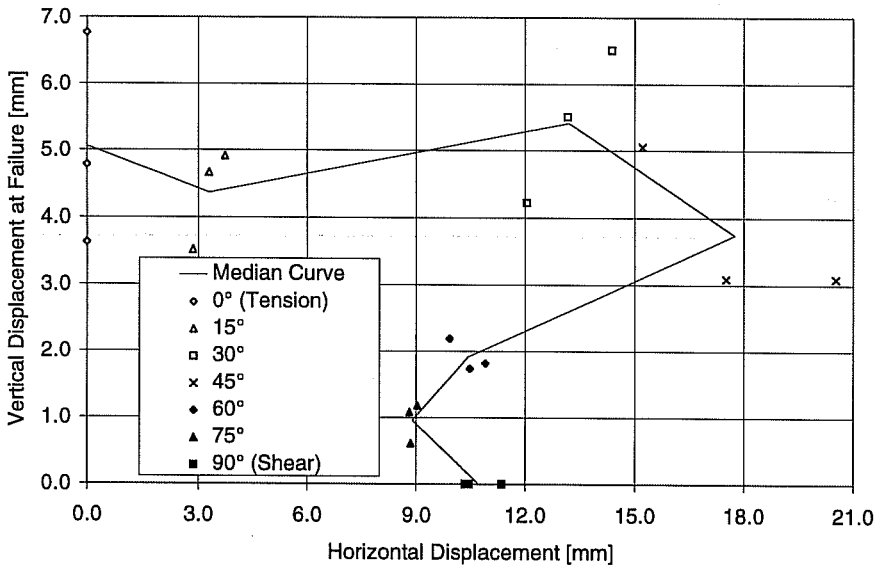

Figure 2. 5 *Tension-shear displacement interaction of an undercut anchor (flush-sleeve installation, concrete breakout under tension, steel fracture under shear)*

installed in uncracked concrete. The loading rate was equivalent to about 2-4 minutes to failure in static tests, and to about 0.1 seconds to failure in dynamic tests. Efforts were made to hold the loading rate constant during a test. These were largely successful in static tests. In dynamic tests, however, the loading rate decreased near the maximum load due to large deformations. In most of the tests, failure occurred by concrete breakout. Only a few of the torque-controlled expansion anchors failed by pull-through of the cone through the anchor sleeve. With concrete breakout failure, the ultimate capacity in dynamic tests increased by 15% to 25% over those in static tests. In tests with pull-through failure, no increase in capacity was reached under dynamic load than under static load. In some test series involving torque-controlled expansion anchors of the clip type, a shift in failure mode was observed depending on the loading rate. Under static load, those anchors failed by concrete breakout; under dynamic load, they failed by pull-through. Significant deviations of the displacements at failure under dynamic compared to static load could not be established.

The test results of Rodriguez (1995) imply that the concrete break-out capacity increases with increased loading rate. However, an increase in the pull-through or pull-out capacity of torque-controlled expansion anchors was not observed under dynamic load. This is because these failure modes are governed by the stiffness of the pressure-displacement behavior when the sleeves are pushed into the concrete surrounding the hole, and on the friction coefficients between steel and steel, and between steel and concrete. No increase can be expected for the effects listed above. Therefore, with certain types of anchors, a shift in failure mode was observed from concrete breakout in static tests, to pull-out or pull-through in the dynamic tests.

Eibl and Keintzel (1989) conducted comparable tests in cracked concrete with crack widths of $w \approx 0.7$ mm and $w \approx 1.1$ mm with 12-mm undercut anchors. The concrete compressive strength was between $f_c = 23.2$ N/mm^2 and $f_c = 26.9$ N/mm^2. Load was applied by a servo-hydraulic test machine, and reached its

maximum value in about 40 ms. For comparison, static tests were conducted, in which the ultimate load was reached in 3 to 5 minutes. In Table 2.1, the ultimate loads and displacements of those dynamic and static tests are compared.

Capacity increases by 25% as loading rate increases by a factor of 6×10^3. The associated increase of 12% to 50% in the ultimate displacement is basically ascribed to the higher load. The increase in concrete breakout capacity is bigger than expected based on the material properties alone. Possible causes are a change of the contour of the fracture cone, or local strengthening near the crack tip.

The possibility of changes in the contour of the fracture cone under dynamic load is significant because it would imply that expressions for critical spacing and edge distance, previously developed based on static loading, might not be valid for dynamic loading. This point is examined later in this study.

Table 2. 1 *Comparison of Dynamic and Static Results (Eibl and Keintzel, 1989)*

	Crack Width	**Static**		**Dynamic**	
	w [mm]	**F_u** [kN]	**d_u** [mm]	**F_u** [kN]	**d_u** [mm]
	0.7	44.20	7.00	47.50	11.00
	0.7	39.20	8.30	47.10	9.20
	0.7	41.60	7.50	48.50	11.00
	0.7	35.40	7.50	49.00	11.40
	0.7	32.40	5.40	46.50	16.30
	0.7	40.00	12.50	50.50	13.80
Average:	0.7	**38.80**	**8.03**	**48.18**	**12.12**
COV:	0.7	**11.00**	**29.77**	**3.02**	**20.83**
	F_u: Dynamic / Static = 1.24 d_u: Dynamic / Static = 1.51				
	1.1	24.80	6.40	33.30	8.50
	1.1	32.60	9.20	39.00	9.00
Average:	1.1	**28.70**	**7.80**	**36.15**	**8.75**
COV:	1.1	**19.22**	**25.38**	**11.15**	**4.04**
	F_u: Dynamic / Static = 1.26 d_u: Dynamic / Static = 1.12				

2.2 DESIGN OF ANCHOR GROUPS LOADED IN SHEAR AND MOMENT

2.2.1 DESIGN BY ELASTIC THEORY

The elastic design of a connection normally proceeds as follows:

- The baseplate is assumed to be stiff, and to rotate about its compression edge. All anchors are assumed to have sufficient area to remain elastic. Anchor layout and embedment depth are presumed.
- For a given load, the forces acting on each anchor are predicted according to elastic theory. Therefore, if all anchors are identical, shear is distributed uniformly to all anchors, and the tension in each anchor varies linearly with that anchor's distance from the axis of rotation of the attachment. Friction between the baseplate and the concrete could be considered by reducing the design loads on anchors.
- The capacity of the attachment is calculated by comparing the anchor forces with the anchor capacities corresponding to steel fracture, pullout or pull-through, and concrete breakout. The concrete breakout capacity is based on the embedment depth as well as the spacing and edge distance of the anchors for tension and shear, and is predicted by a method such as the Concrete Capacity Method (CC-Method).
- For anchors loaded simultaneously in tension and shear, capacity is calculated using the above-mentioned interaction relations.

The elastic design method leads in principle to a conservative design because it represents a classical lower-bound solution satisfying equilibrium in which the stress nowhere exceeds the elastic limit. For failures with relatively small deformation, such as concrete breakout, it gives a good description of the actual failure load. However, it does not address conditions such as gaps between the anchors and the baseplate, which can lead to under-prediction of anchor forces, and hence to unsafe designs.

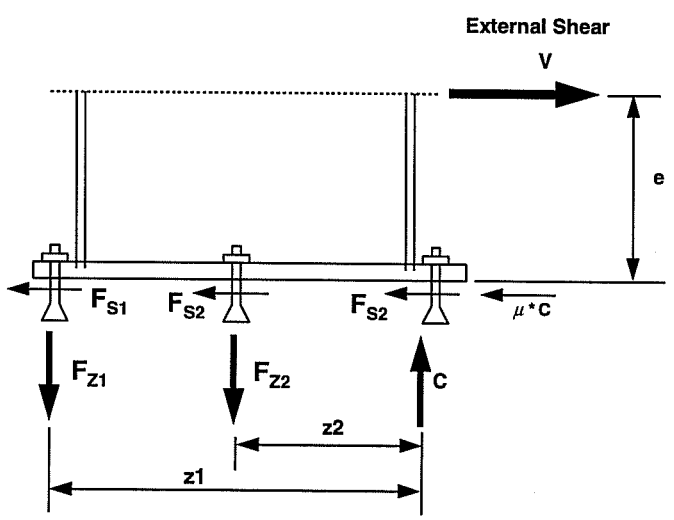

Figure 2. 6 *Anchor group with three anchor rows under eccentric shear loading*

2.2.2 DESIGN BY PLASTIC THEORY

The plastic design procedure for connections has been developed essentially in the USA (Cook 1989; Cook and Klingner 1989; Cook, Doerr and Klingner 1989; Cook and Klingner 1992-1; Cook and Klingner 1992-2). For the plastic design method, in general, a valid interaction diagram is assumed for each anchor at any state. The

distribution of the forces within the group could thus be chosen so that the maximum failure load of the group could be reached.

The particular design method based on plastic theory as proposed by Cook and Klingner (1989) is explained below, using as an example a connection with three rows of anchors (Figure 2.6). The connection is loaded in shear, V, with an eccentricity, e, from the concrete surface. The anchors are loaded in shear $F_{S,1}$ to $F_{S,3}$ and in tension $F_{Z,1}$ and $F_{Z,2}$. Anchor Row 3 is in the zone of compression. The line of action of the resultant compression, C, is assumed at the compression edge of a very thick (stiff) baseplate. For a flexible baseplate, the line of action of the resultant compression might generally be assumed at the extreme compression fiber of the connected beam. This line of action is used in design of the baseplate. Once the baseplate thickness has been determined, the yield capacity of that baseplate limits the internal lever arm (distance between tensile and compressive resultants). Conservatively, the compression resultant can also be assumed to act at the edge of the associated member on a ductile baseplate.

First of all, a simplifying assumption is that the anchors in the tension zone are loaded exclusively in tension. These anchors are then dimensioned in accordance with Equation (2.6), using the applied shear at an eccentricity, e.

$$F_{Z,1} \cdot z_1 + F_{Z,2} \cdot z_2 = V \cdot e \tag{2.6a}$$

$$F_{Z,u,1} = F_{Z,u,2} = F_{Z,u,0} = (V \cdot e)/(z_1 + z_2) \tag{2.6b}$$

or for an n^{th} - row anchor in tension:

$$F_{Z,u,0} = \frac{(V \cdot e)}{\sum_{i=1}^{n} (z_i)} \tag{2.6c}$$

The magnitude of the compression is then:

$$C = F_{Z,u,1} + F_{Z,u,2} \tag{2.7a}$$

or:

$$C = \sum_{i=1}^{n} (F_{Z,u,i}) \tag{2.7b}$$

Considering the friction between the baseplate and concrete, the shear on Anchor Row 3 is:

$$F_{S,3} = V - \mu \ C \tag{2.8}$$

The number and size of the anchors in the compression zone are then chosen based on that $F_{S,3}$.

2.3 ULTIMATE CAPACITY OF AN ANCHOR GROUP UNDER SHEAR AND MOMENT LOADING

For a scientific evaluation of the plastic design approach, the maximum capacity of a set of anchors calculated using plastic theory has to be compared with the maximum capacity calculated using elastic theory, with the maximum capacity calculated using measured load-displacement behavior of anchors, and with the results of group testing. Furthermore, deformation issues with respect to serviceability must be discussed.

2.3.1 ULTIMATE CAPACITY USING PLASTIC THEORY

Calculation of the capacity of an attachment loaded in eccentric shear can be categorized into three ranges, according to the eccentricity of the applied shear:

- $e < e_1$: Anchors in the compression zone reach their maximum shear capacity. Anchors in the tension zone are loaded in tension and shear.
- $e_1 < e < e_2$: Anchors in the compression zone resist that portion of the shear that exceeds the frictional resistance. Anchors in the tension zone are loaded in tension only, and reach their full tension capacity. The connection reaches its maximum flexural capacity.
- $e > e_2$: The shear resistance is provided entirely by friction with the concrete. The anchors in the tension zone are loaded in tension only, and reach their full tension capacity. The connection reaches its maximum flexural capacity.

Calculation of the critical eccentricity, e_2, starts from the condition that:

$$V = \mu \ C \tag{2.9}$$

Invoking vertical and rotational equilibrium leads to:

$$e_2 = \frac{\sum_{i=1}^{n}(z_i)}{(n \ \mu)} \tag{2.10}$$

To calculate the critical eccentricity, e_1, the shear capacity $F_{S,u,3}$ of Anchor Row 3 is included. Instead of Equation (2.9), Equation (2.11) is used:

$$V = \mu \ C + F_{S,u,3} \tag{2.11}$$

The critical eccentricity e_1 is:

$$e_1 = \frac{\sum_{i=1}^{n}(z_i)}{(n \ \ \mu + F_{S,u,0} / F_{Z,u,0})} \tag{2.12}$$

The ultimate capacity of the anchor group for $e > e_1$ is:

$$V = F_{Z,u,0} \cdot \left[\frac{\sum_{i=1}^{n}(z_i)}{e} \right] \tag{2.13}$$

An attachment loaded predominantly in shear ($e < e_1$) with two anchor rows in the tension zone is considered by Cook and Klingner (1992-2) with an elliptical interaction (exponent p = 2.0):

$$\frac{e}{z_1} = \frac{\delta(1+\alpha\beta)}{\left(\frac{V}{F_{Z,u,0}}\right)} \tag{2.14}$$

and

$$\frac{V}{F_{Z,u,0}} = \mu \cdot \delta \cdot (1+\alpha) + \gamma \cdot \sqrt{1-\delta^2} + \gamma \cdot \sqrt{1-\delta^2 \cdot \alpha^2} + \gamma \tag{2.15}$$

where: $F_{Z,u,0}$ = ultimate anchor capacity in pure tension: $\delta = \left(F_{Z,1} / F_{Z,u,0}\right)$, $\alpha = \left(F_{Z,2} / F_{Z,1}\right)$, $\beta = z_2/z_1$, μ = friction coefficient between the baseplate and the concrete, and $\gamma = \left(F_{S,u,0} / F_{Z,u,0}\right)$ = ratio between shear and tensile capacity of the anchor.

Equations (2.14) and (2.15) can be evaluated iteratively. The full plastic capacity is the maximum attainable value $V/F_{Z,u,0}$. For given boundary conditions (geometry, friction coefficient, and ratio of shear to torsion capacities), $V/F_{Z,u,0}$ depends on the distribution of the shear on the anchors in the tension zone of the connection, and on the associated tensile capacity. This influence is expressed in Equations (2.14) and (2.15) by the value α. Cook and Klingner (1992-2) calculated the maximum capacity of a connection with uniform distribution of shear on the tension anchors ($\alpha = 1$), provided that the distance of the first tension anchor row from the compression resultant is at least a quarter of the distance of the outermost row tension anchor from the compression resultant ($\beta > 0.25$).

With $\alpha = 1$, a closed-form solution to the equation is possible:

$$V/F_{Z,u,0} = D \cdot F_{Z,u,0} \cdot (z_1 + z_2)/e \tag{2.16}$$

where: $D = \dfrac{\left[\eta^2 + 3 \cdot (4 \cdot e^2 \cdot \gamma^2 + \eta^2)\right]^{0.5}}{\left(4 \cdot e^2 \cdot \gamma^2 + \eta^2\right)}$ and $\eta = z_1 + z_2 - 2 \cdot \mu \cdot e$

This calculation is now extended to the case of a connection loaded predominantly in shear ($e < e_1$), with n anchor rows in the tension zone and k anchor rows in the compression zone. A uniform distribution of shear ($\alpha = 1$)

$$F_{S,1} = F_{S,2} = \ldots = F_{S,n} \tag{2.17}$$

is still assumed for the tension anchors. The condition on β is also retained:

$$\beta = z_n/z_1 > 0.25 \tag{2.18}$$

From equilibrium, it follows that:

$$F_{Z,i} = \frac{V \cdot e}{\sum_{i=1}^{n} (z_i)} \tag{2.19}$$

and

$$F_{S,i} = \left[\frac{1}{n} - \frac{\mu \cdot e}{\sum_{i=1}^{n} (z_i)}\right] \cdot V - \left(\frac{k}{n}\right) \cdot F_{S,u,0} \tag{2.20}$$

For the interaction relationship of the loads, an arbitrary exponent p is permitted:

$$\left(\frac{F_{Z,i}}{F_{Z,u,0}}\right)^p + \left(\frac{F_{S,i}}{F_{S,u,0}}\right)^p = 1 \tag{2.21}$$

Substitution gives Equation (2.22):

$$\left[\frac{e}{\sum_{i=1}^{n}(z_i)}\cdot\frac{V}{F_{Z,u,0}}\right]^{P} + \left[\left(\frac{1}{n}-\frac{\mu\cdot e}{\sum_{i=1}^{n}(z_i)}\right)\cdot\frac{V}{F_{S,u,0}}-\frac{k}{n}\right]^{p} = 1 \qquad (2.22)$$

Equation (2.22) can be solved iteratively.

2.3.2 Ultimate Capacity by Elastic Theory

For calculations according to elastic theory, the eccentricity is divided into only two ranges. The eccentricity, e_2, from Equation (2.10) forms the dividing line between a connection loaded predominantly in moment (in which all shear is transferred by friction) and a connection in which the anchors are loaded in shear. For $e \geq e_2$, the ultimate capacity of the group is calculated from equilibrium of moments:

$$V/F_{Z,u,0} = \left(z_1^2 + z_2^2 + \cdots + z_n^2\right)\Big/ z_1 \cdot e \qquad (2.23)$$

For $e < e_2$, the portion of the shear that is not transferred by friction can be distributed uniformly among all anchors of the connection. The tension in each anchor is a function of that anchor's distance from the rotational axis of the baseplate. Tension-shear interaction is assumed in accordance with Equation (2.21). From equilibrium, it follows that:

$$\frac{V}{F_{Z,u,0}} = \frac{\sum_{i=1}^{n}\left(z_i^2\right)}{z_1 \cdot e \cdot \left(1+\frac{\vartheta^p}{\gamma^p}\right)^{(1/p)}} \qquad (2.24)$$

where:

$$\vartheta = \frac{\sum_{i=1}^{n}\left(z_i^2\right) - \mu \cdot e \cdot \sum_{i=1}^{n} z_i}{n \cdot z_1 \cdot e}$$

$$\text{and} \quad \gamma = F_{S,u,0}/F_{Z,u,0}$$

2.3.3 Ultimate Capacity Based on the Real Deformation Behavior of Individual Anchors

For a realistic calculation of the ultimate capacity of a multiple-anchor connection, the actual nonlinear load-displacement behavior of individual anchors should be used. From equilibrium and compatibility, a nonlinear system of equations results, which cannot have a closed-form solution. Li and Eligehausen

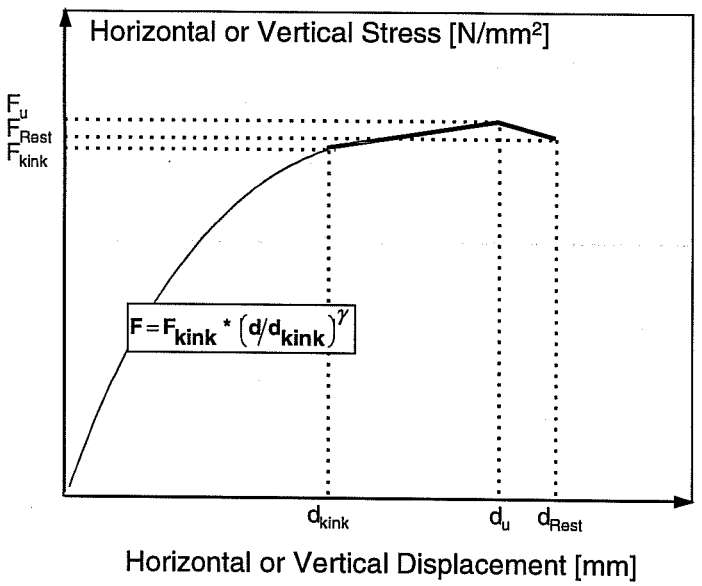

Figure 2. 7 *Idealization and mathematical description of the load-displacement curve*

(1993) proposed a program for calculating the load-displacement behavior of a multiple-anchor connection using modified Newton-Raphson iteration to get the numerical solution to this system of equations.

The typical load-displacement curve of a single anchor for a discrete loading angle is shown in Figure 2.7. For angles between the given load-displacement curves, a suitable interaction diagram of the displacements is developed by interpolation. The gap between the anchor and the baseplate could significantly influence the distribution of shear force among individual anchors. In the program, this could be considered separately for each row. When the program is used, the external load or each of the three deformations of the baseplate could be maximized in specified steps. For each load or deformation step as well as the entire deformation history, all anchor forces and the external load are predicted.

The results are written in data files from which graphs could be plotted using other programs, such as spreadsheets.

Li and Eligehausen (1993) conducted example calculations with this program using the results of Dieterle et al. (1989) and Cook (1989). The results of Dieterle et al. (1989) include no tests with multiple-anchor connections, so a comparison between calculated and actual behavior was not possible. Cook conducted tests with multiple-anchor connections in combined shear and moment. The load-displacement behavior at different loading angles of the anchors used in those tests was not available. A reliable calibration using those tests was therefore not possible, either.

CHAPTER 3

TEST REPORT

3.1 Test Program

The test program is divided into three subject sections:

- interaction between adjacent anchors at high loading rate;
- load-displacement behavior of anchors at various loading angles; and
- behavior of two-anchor connections under shear with moderate eccentricity

Each section includes two test series, which are then divided into subsections.

The first section of the test program (Series 2.1 and 2.2) investigates the influence of high loading rate on the interaction of anchors in a two-anchor connection under pure tension, with a concrete breakout failure mode.

In tests on single anchors (Eibl, Keintzel, 1989; Rodriguez, 1995), concrete breakout capacity increased by as much as 40% when the loading rate was increased by a factor of about 10^3. From existing results on concrete of different tensile and compressive strengths, the increased loading rate itself is known to cause an increase in capacity of only about 10% to 15%. Therefore, it is assumed that the additional increase in capacity is due to changes in the basic fracture mechanism, such as a local increase in the strain rate near the crack tip, or to a change in the form of the concrete breakout cone. The latter would cause a change on the interaction between adjacent anchors. This interaction is investigated using pure tension tests on two-achor attachments with moderately spaced anchors. The spacing ($s = 1.5 \cdot h_{ef}$ or $s = 2.5 \cdot h_{ef}$) is varied, as well as the type of anchor (undercut anchor and torque-controlled expansion sleeve anchor). The loading rate corresponded to about 100 to 200 seconds to ultimate load in the quasi-static tests, and to about 0.1 second to fracture in the dynamic tests. This gives a ratio of about $2 \cdot 10^3$ between loading rates. Table 3.1 gives an overview of these tests.

Table 3. 1 Series 2.1 and 2.2: Influence of Loading Rate on the Interaction of the Double Anchors Loaded in Pure Tension

Test Series	Anchor	Embedment h_{ef}, (in) mm	Time to Ultimate Load, sec	Sub-Series	Relative Axial Spacing / h_{ef}	Replicates
2.1	UC1 5/8" (16 mm)	4 (101.6)	≈ 150	21SM25	2.5	5
				21SM15	1.5	5
	Sleeve M16	4 (101.6)	≈ 150	21SH25	2.5	5
				21SH15	1.5	5
2.2	UC1 5/8" (16 mm)	4 (101.6)	≈ 0.1	22DM25	2.5	4
				22DM15	1.5	4
	Sleeve M16	4 (101.6)	≈ 0.1	22DH25	2.5	4
				22DH15	1.5	5

The second section of the test program accommodated investigation of the effects of loading direction, failure mode (concrete fracture or steel fracture), type of anchor, size of anchor, concrete strength and assembly method (anchor sleeve flush with concrete or extended through baseplate) on the load-displacement behavior of single anchors.

Originally, it had been planned to conduct 5 replicate tests instead of the actual 3 to 5 replicates for each of the following loading directions: 0° (pure tension); 30°; 45°; 60°; and 90° (pure shear). Based on the original test results, additional tests at 15° were conducted in some series. Furthermore, two key series (2 tests each at 30°, 45°, 60° and 90°) were added, in which the anchor sleeve extended through the baseplate ("through-sleeve installation"). This is referred to as a "through-sleeve" installation. In the other series, the anchor sleeve ended at the concrete surface or closely beneath it ("flush-sleeve installation"). This is referred to as a "flush-sleeve" installation. Flush-sleeve anchor installations, loaded at angles ≥ 30°, showed little or no shell-shaped concrete spalling in front of the anchor in the loading direction. This resulted in very small deformation (relatively brittle behavior of the connection), although failure was by steel fracture and the anchor shank was made of comparatively ductile material (ASTM 193 B7 or 8.8). The complementary tests with through-sleeve installation were expected to show a higher shear capacity, shell-shaped concrete spalling, and a more ductile behavior. Additional tests were necessary in the test series with concrete fracture, because in the previous tests with an edge distance of 5.5 inches (140 mm), equivalent to $1.57 \cdot h_{ef}$, full tensile strength was not reached, and the results of these tests could therefore not be applied to the tension anchors of a two-anchor connection far from an edge. The tests of Section 2 are compiled in Table 3.2 (Series 2.3) and Table 3.3 (Series 2.4).

In the third section of the test program (Series 2.5 and 2.6), two-anchor connections (anchor spacing 10 inches or 254 mm) were loaded in shear at moderate eccentricities (12 inches, or 305 mm, and 18 inches, or 457 mm), and the distribution of shear between anchors was investigated. The tests were used to check the predictions of the computer program (Li and Eligehausen 1993) developed at the Institute for Construction Materials (IWB) of the University of Stuttgart. The test program (Table 3.4) was coordinated with Series 2.3 and 2.4, in that the load-displacement curves from those earlier tests were used to calculate the load-displacement behavior of the two-anchor connection in Series 2.5 and 2.6. All tests in this series were conducted in concrete of medium strength ($f_c \approx 32.4$ N/mm²). The anchors were always installed with flush sleeves.

3.2 Test Description

3.2.1 Concrete Specimen

Concrete blocks of 224 x 101 x 61 cm were used for all tests. Three or four such blocks were usually cast simultaneously in the lab. The mixture design of concrete specimens is given in Table 3.5. Together with the specimens, 18 cylinders (diameter 6 inches, or 152.4 mm, height 12 inches, or 304.8 mm) were usually cast. Both the specimens and the cylinders were consolidated with vibrators. Surplus bleed water was partially skimmed off.

After casting and finishing, the specimens and the cylinders were stored inside the laboratory for 7 days, covered with plastic sheets. The forms were then stripped, and the specimens were stored outside until being tested.

Table 3. 2 *Series 2.3: Load-Displacement Behavior of Single Anchors, Failing by Steel Fracture, for Various Loading Orientations*

Test Series	Sub-series	Anchor	Embedment h_{ef} inch/mm	edge distance c1; mm	Concrete Strength f_c N/mm²	Installation	Loading Angle Devices	Replicates
2.3	23H64	Sleeve M16	7" (178 mm)	≥ 279	32.4	Flush-sleeve	0 (tension)	4
							15	3
							30	3
							45	3
							60	4
							90	4
2.3	23H74	Sleeve M16	7" (178 mm)	≥ 279	32.4	Through-sleeve	30	2
							45	2
							60	2
							90	2
2.3	23M54	UC1 5/8"	7" (178 mm)	≥ 279	32.4	Flush-sleeve	0 (tension)	4
							15	3
							30	3
							45	4
							60	4
							90	5
2.3	23M74	UC1 5/8"	7" (178 mm)	≥ 279	32.4	Through-sleeve	30	2
							45	2
							60	2
							90	2
2.3	23M53	UC1 5/8"	7" (178 mm)	≥ 279	20.7	Flush-sleeve	0 (tension)	3
							15	3
							30	3
							45	3
							60	3
							90	3
2.3	23M34	UC1 3/8"	3.5" (89 mm)	≥ 140	32.4	Flush-sleeve	0 (tension)	4
							15	3
							30	3
							45	5
							60	4
							90	4

Table 3. 4 Series 2.4: Load-Displacement Behavior of Single Anchors, Failing by Concrete Breakout, at Various Loading Orientations

Test Series	Sub-series	Anchor Bolt	Embedment h_{ef} inch/mm	Edge Distance c1 mm	Concrete Strength f_c N/mm²		Loading Angle, degrees	Replicates
2.4	24M54	UC1 5/8"	3.5" (89)	140	32.4	Flush-sleeve installation	0 (tension)	2
							30	4
							45	3
							60	3
							90	3
2.4	24A54	UC1 5/8"	3.5" (89)	≥ 279	32.4	Through-sleeve installation	0 (tension)	3
							15	1
							30	1
							45	2

Table 3. 3 Test Series 2.5 and 2.6: Two Anchor Connections Under Shear and Bending Moment

Test Series	Sub-series	Anchor Bolt	Embedment h_{ef}, mm	Edge Distance c_1 [1)], mm	Eccentricity inch/mm	Replicates
2.5	25H642	Sleeve M16	178	≥ 279	12 / 305	3
	25H648	Sleeve M16	178	≥ 279	18 / 457	3
2.5	25M542	UC1 5/8"	178	≥ 279	12 / 305	3
	25M548	UC1 5/8"	178	≥ 279	18 / 457	3
2.5	25M342	UC1 3/8"	89	≥ 279	12 / 305	3
	25M348	UC1 3/8"	89	≥ 279	18 / 457	3
2.6	26M542	UC1 5/8"	89	140	12 / 305	3
	26M548	UC1 5/8"	89	140	18 / 457	3

1) edge distance of the near edge anchor

Table 3. 5 Concrete Mixture Proportions

Ingredient		Quantities in lbs/yd^3	Quantities in kg/m^3
Cement		400	390
Aggregate	coarse:[1]	1876	1923
	fine:	1432	1468
Water		250	256
Superplasticizer		48	49.2
Gradation (% passing)		Coarse Aggregate:	Fine Aggregate:
1 in. =	25.4 mm	100%	
3/4 in. =	19.1 mm	90 - 95%	
1/2 in. =	12.7 mm	41 - 50%	
3/8 in. =	9.50 mm	16 - 25%	100%
No. 4 =	4.75 mm	1 - 3%	95 - 100%
No. 8 =	2.36 mm	0 - 2%	80 - 100%
No. 16 =	1.18 mm	0%	50 - 85%
No. 30 =	0.60 mm		25 - 60%
No. 50 =	0.30 mm		10 - 30%
No. 100 =	0.15 mm		2 - 10%
Water / Cement Ratio		0.64	

[1] Soft limestone, 28% loss by ASTM C131

Concrete compressive strength was generally estimated at 7 days by testing three cylinders. More compressive strength tests were conducted during the respective test period. At least three cylinders were normally tested at the start and end of the test period. Furthermore, cores (ϕ of 2.75 inches, or 70 mm, height of 5.5 inches, or 140 mm) were drilled in specimens to get a rough indication about the surface strength of the test specimen after some tests. The results of the cylinder compression tests are presented in Table 3.6

3.2.2 ANCHORS TESTED

In Series 2.1 and 2.2, an undercut anchor with a diameter of 3/4-inch and a torque-controlled expansion sleeve anchor with a diameter M20 were tested. The embedment depth was 4 inches (101.6 mm) for both types of anchor, different from the respective manufacturer's recommendations. Anchor diameters and embedment depths were chosen in agreement with earlier tests conducted at Texas (Rodriguez, 1995) (see Chapter 2). The anchors and their basic dimensions are shown in Figures 3.1 and 3.2. In Series 2.3, an embedment depth of 3.5 inches (89 mm) was chosen for the anchor of diameter 3/8-inch (9 mm), and a depth of 7 inches (178 mm) for the anchor of diameter 5/8-inch (16 mm) and M16. In Series 2.4, 5/8-inch (16 mm) anchors were installed at 3.5 inches (189 mm). The lengths of sleeve were correspondingly reduced by cutting (see Figures 3.1 and 3.2, and Tables 3.7 and 3.8). Table 3.7 gives the basic dimensions for the undercut anchor. The basic dimensions of the torque-controlled expansion anchor are presented in Table 3.8.

Table 3. 6 Cylinder Compression Test Results

Casting Date (D-M-Y)	Block No.	Test date	Concrete Age, days	Individual Strength Results N/mm²			Average N/mm²	Remarks
22-2-93	53	1-3-93	7	13.73	12.76	12.69	13.1	
		8-3-93	14	15.46	14.65	14.83	15.0	
		15-3-93	21	14.91	16.07	15.71	15.6	
		22-3-93	28	17.02	17.33	16.91	17.1	
		19-10-93	239	19.13	19.94	20.71	19.9	
		14-9-94	569	20.53	21.07	21.60	21.1	
23-9-93	L1/2/3/4	30-9-93	7	18.76	18.44	19.46	18.9	
		7-10-93	14	21.74	21.54	21.42	21.6	
		4-2-94	134	26.86	27.88	28.63	27.8	
		21-4-94	210	28.52	28.27	27.79	28.2	
		2-8-94	313	28.36	30.32	28.74	29.1	
		10-8-94	321	30.02	28.61	30.20	29.6	
		15-8-94	326	33.92	37.27	35.60	35.6	core L4-B (2)
		24-8-94	335	31.00	33.43	33.75	32.7	core L2-B (2)
4-4-94	L28/29/30	11-4-94	7	20.15	18.66	20.69	19.8	
		12-5-94	38	24.70	25.22	25.14	25.0	
		7-7-94	94	25.66	26.34	25.82	25.9	
		29-7-94	116	27.20	27.70	27.35	27.4	
		2-8-94	120	27.68	28.24	28.15	28.0	
		5-8-94	128	27.12	28.48		27.8	core L28-B (2)
		10-8-94	123	28.91	29.94	29.90	29.6	
12-4-94	L31/32/33	19-4-94	7	12.38	10.94	12.61	12.0	(1)
		19-4-94	7	19.46			19.5	
		21-5-94	39	27.35	26.67	29.23	27.7	
		14-9-94	155	31.46	30.68	28.72	30.3	
		23-9-94	164	37.86	32.89	30.86	33.9	core L33-T (2)
		23-9-94	164	31.65	32.44	30.41	31.5	core L33-B (2)
		5-10-94	176	30.45	32.83	32.29	31.9	
		17-10-94	188	41.56	41.39	42.49	41.8	core L32-T (2)
		17-10-94	188	33.33	35.60	33.78	34.2	core L32-B (2)
		24-10-94	195	30.68	30.90	30.42	30.8	
				31.33				
		26-10-94	197	35.56	35.97	33.03	34.9	core L31-T (2)
		26-10-94	197	32.65	34.53	34.33	33.8	core L31-B (2)
1-6-94	L34/35/36	8-6-94	7	26.51	25.73	25.32	25.9	
		19-7-94	48	31.17	31.01	31.59	31.3	
		19-8-94	79	31.76	30.93	31.45	31.4	
		21-9-94	112	34.66	34.24	34.06	34.3	
		17-10-94	138	27.43	29.15	32.06	29.5	core L34-T (2)
		23-11-94	175	32.83	34.36	34.25	33.8	

[1] tested without Neoprene pad; [2] T = Top = top side of concrete block, B = Bottom = bottom side of concrete block

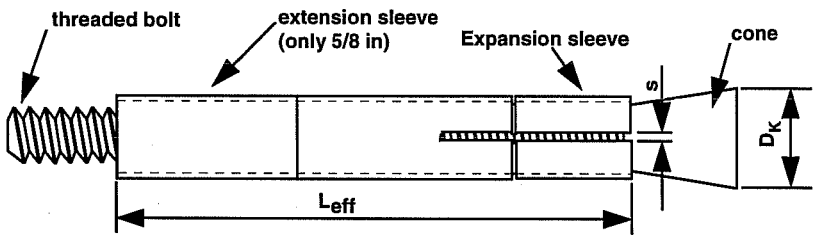

a) unexpanded

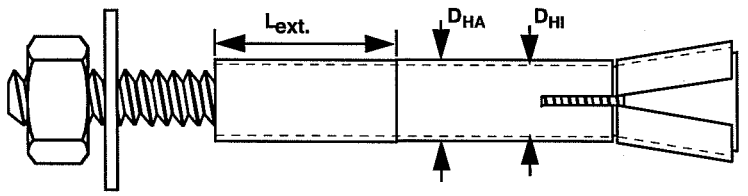

b) expanded

Figure 3. 1 Undercut Anchor

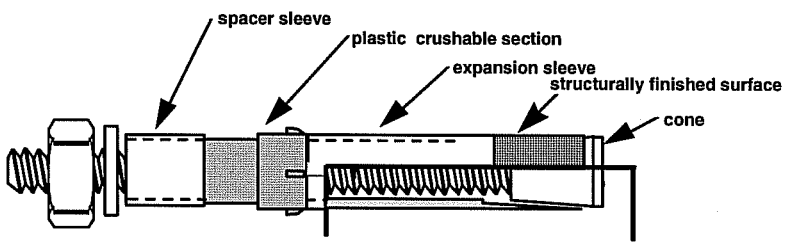

a) M20

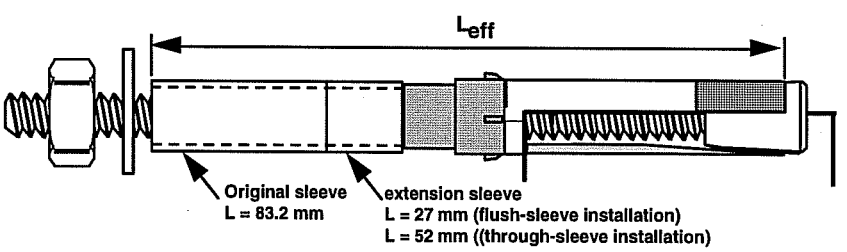

b) M16: In the form which has never been marketed (anchor length extension, expansion sleeve and cone from old inventory of an earlier version of this anchor

Figure 3. 2 Torque-Controlled Expansion Sleeve Anchor

Table 3. 7 Basic Dimensions of the Undercut Anchor

Key Anchor Dimensions	L_{ef} mm	L_{ext} mm	D_{HA} mm	D_{HI} mm	D_K mm	s mm	α_K [1] degrees
UC1 3/8 inch (9.5 mm)	89	-	16.0	9.6	16.2	1.3	8.6
UC1 5/8 inch (16 mm)	89 [2]	-	23.3	16.3	24.0	1.5	10.0
	178 [3]	89 [3]					
	203 [4]	114 [4]					
UC1 3/4 inch (19 mm)	178	-	28.1	19.3	29.2	1.5	10.8

[1] α_K = cone angle
[2] Series 24M5
[3] Series 23M5
[4] Series 23M7

Table 3. 8 Basic Dimensions of Torque-Controlled Expansion Sleeve Anchor

Basic Anchor and Drill Bit Dimensions [1]	L_{ef} mm	D_{HA} mm	D_{HI} mm	D_K mm	s mm	α_K [2] deg	Drill Bit Diameter, mm
Sleeve M16	178 [3]	23.4	16.3	23.7	2.0	≈7.6	24.4
	203 [4]						
Sleeve M20	101.6	27.3	20.5	27.8	2.0	≈8.2	28.45

[1] Dimensions are explained in Figure 3.1.
[2] α_K = cone angle
[3] Series 23H6 and 25H6
[4] Series 23H7

Additional tension tests were conducted on a test machine with the anchor shank used in Series 2.3 to determine basic material characteristics. The stress-strain curves for anchor diameters of M16 and 5/8 inch are plotted in Figure 3.3. Other characteristic data were also obtained. For 3/8-inch anchors, two tension tests were conducted. The fracture strain of the anchor shank was determined, using a gage length of 5 diameters. The fracture load reached 49.1 kN with an associated fracture strain of 12.0% and 55.0 kN with an associated fracture strain of 10.0%. Stress-strain curves could not be measured, due to the small length of the anchor shank.

3.2.3 Anchor Bolt Installation

The torque-controlled expansion sleeve anchor was inserted directly into a cylindrical hole made with a rotary hammer drill, using a drill bit diameter of 24.40 mm (M16) or 28.45 mm (M20), and with the nut and washer already hand-tightened against the anchor sleeve. The correct penetration depth is reached when the washer touches the concrete surface (flush-sleeve installation) or the baseplate (through-sleeve installation). In the former case, the nut and washer must be removed from the insert assembly. The inserts were finally held against the concrete by the application of the tightening torque. The plastic crushable section on the anchor prevents rotation of the anchor, and ensures (by reducing the compressive stiffness of the sleeve) that the prestressing force acts between the baseplate and the concrete, and is not transferred by the anchor sleeve.

For the undercut anchor, after the cylindrical hole was drilled with a rotary hammer using a drill bit diameter of 16.45 mm for 3/8-inch anchors, 24.90 mm for 5/8-inch anchors, and 29.70 mm for ¾-inch anchors, a special tool was used to form the undercut with a hammer drill operating in drill mode only. The basic dimensions of the fully expanded undercutting tool are shown in Figure 3.4. Figure 3.5 illustrates the installation sequence.

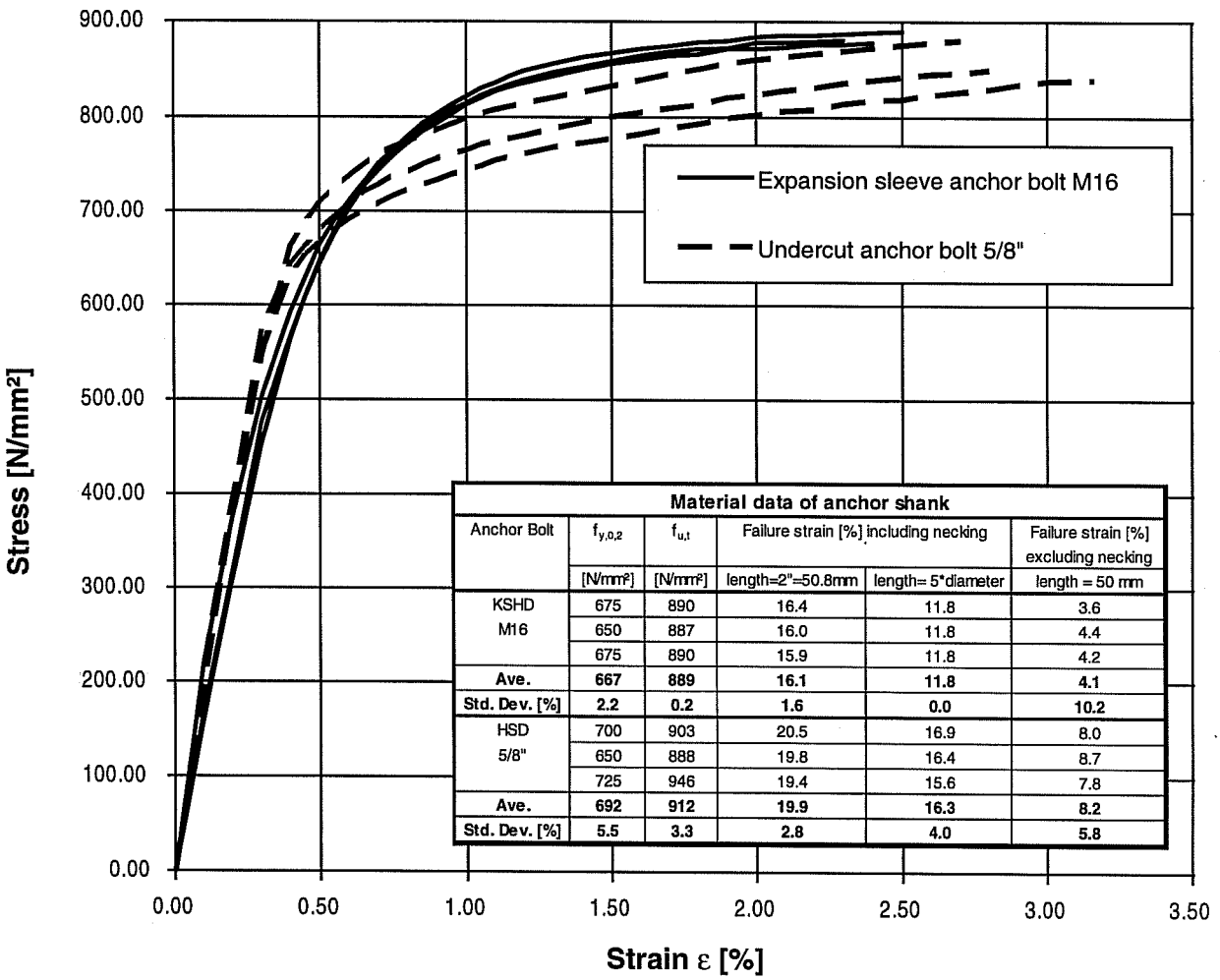

Material data of anchor shank

Anchor Bolt	$f_{y,0,2}$	$f_{u,t}$	Failure strain [%] including necking		Failure strain [%] excluding necking
	[N/mm²]	[N/mm²]	length=2"=50.8mm	length= 5*diameter	length = 50 mm
KSHD M16	675	890	16.4	11.8	3.6
	650	887	16.0	11.8	4.4
	675	890	15.9	11.8	4.2
Ave.	**667**	**889**	**16.1**	**11.8**	**4.1**
Std. Dev. [%]	**2.2**	**0.2**	**1.6**	**0.0**	**10.2**
HSD 5/8"	700	903	20.5	16.9	8.0
	650	888	19.8	16.4	8.7
	725	946	19.4	15.6	7.8
Ave.	**692**	**912**	**19.9**	**16.3**	**8.2**
Std. Dev. [%]	**5.5**	**3.3**	**2.8**	**4.0**	**5.8**

Figure 3. 3 Material Characteristics of Anchor Shank

Anchor diameter	Embedment, h_{eff}	L_{HS}	$\varnothing_S$	max $\varnothing_{HS}$
3/8 in. = 9.52 mm	88.9 mm	87.0 mm	15.7 mm	21.5 mm
5/8 in. = 15.9 mm	177.8 mm	177.5 mm	23.0 mm	28.8 mm
3/4 in. = 19.1 mm	101.6 mm	101.6 mm	27.1 mm	37.9 mm

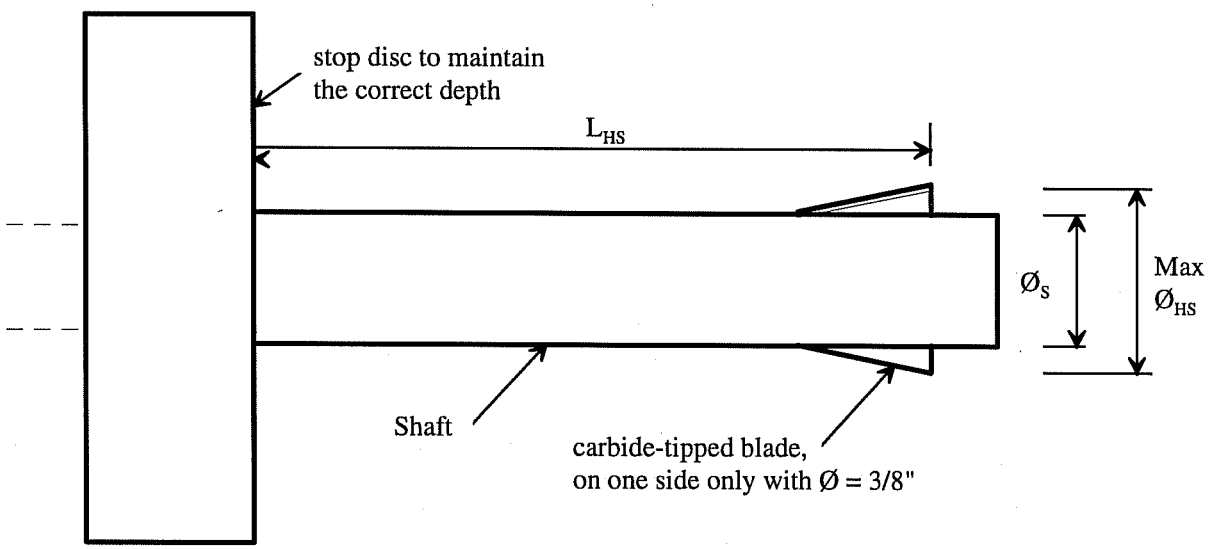

Figure 3. 4 Dimensions of Undercutting Tool

The undercut anchor was expanded by a special setting tool to ensure correct expansion. The setting tool has a collar extending about 1.5 mm beyond the bearing surface of the setting tool, which holds the top edge of the sleeve. This ensures that the anchor sleeve does not protrude past the mouth of a hole even on an uneven concrete surface, and that the insert is supported against the concrete when the tightening torque is applied.

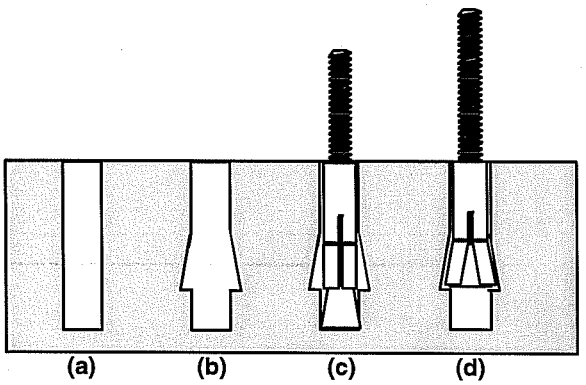

Figure 3. 5 *Installation Sequence for Undercut Anchors: (a) drill cylindrical hole; b) undercut; c) place anchor in hole; and d) expand anchor*

All anchors were torqued using the following sequence:

- Apply the torque specified by the manufacturer. In tests in which concrete fracture was the anticipated failure mode (due to the embedment depth), the torque was chosen at the low end of the recommended range. In tests with deeper embedments, the selected torque was at the high end.
- Wait for about 10 minutes to permit a decrease of prestressing force due to relaxation.
- Loosen the nut, and then apply a torque equal to half the original value, to simulate the decrease in prestressing force over a long period.

The installation torques used are given in the tables of test results.

3.2.4 Loading and Instrumentation

3.2.4.1 Series 2.1 and 2.2: Pure tension on two-anchor connection

Anchors were loaded through a baseplate welded to a tension strap connected to a tension rod (Appendix 1). The load was applied by a hydraulic actuator. The actuator was set on a beam made of two C-channels, which in turn was supported by two stiffened I-section stands, each with a nearly square footprint. Those stands were spaced at least 2.5 times the embedment depth from the anchors (Appendix 2 above).

In tests in which the ultimate load was reached in 2 to 4 minutes, a one-way actuator supplied by an electric pump was used (Appendix 1 above). In tests at seismic loading rates, a two-way ram (Appendix 2 below) was used in combination with the laboratory's central hydraulic system and a programmable servo-controller. The control unit was programmed for a linear load increase up to 267 kN (60 kips) in 0.1 seconds with a small initial load (< 1 kN). The expected failure loads were between 70% and 90% of the programmed maximum value, so that (allowing for some deviation of the actual load from the command signal near failure), the maximum load was reached in about 0.1 second. This loading rate is higher by a factor of about $2 \cdot 10^3$ than that of the quasi-static tests.

The force was measured with an electronic load cell with a capacity of 445 kN (100 kips). The displacement of the baseplate was measured with linear potentiometers (LP) attached to stands set outside the expected breakout cone. The LP's were set against cantilever glass plates placed

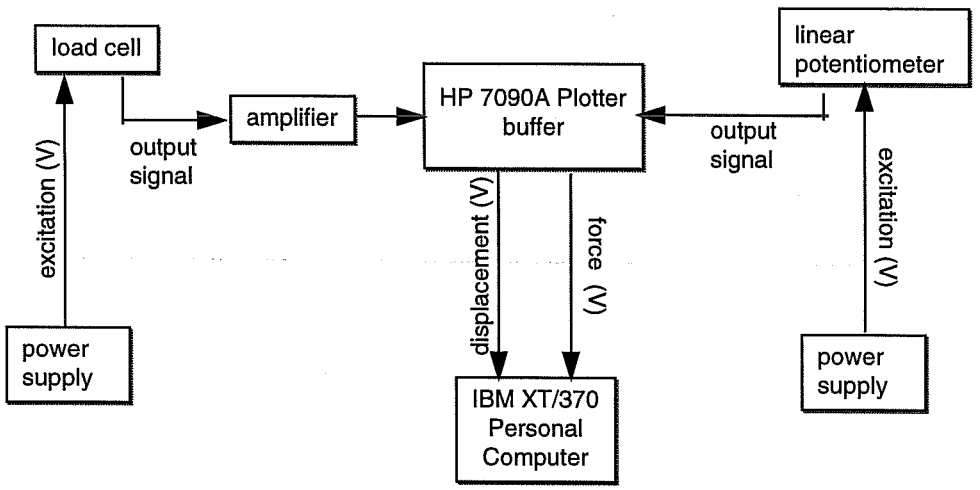

Figure 3. 6 Data Acquisition System

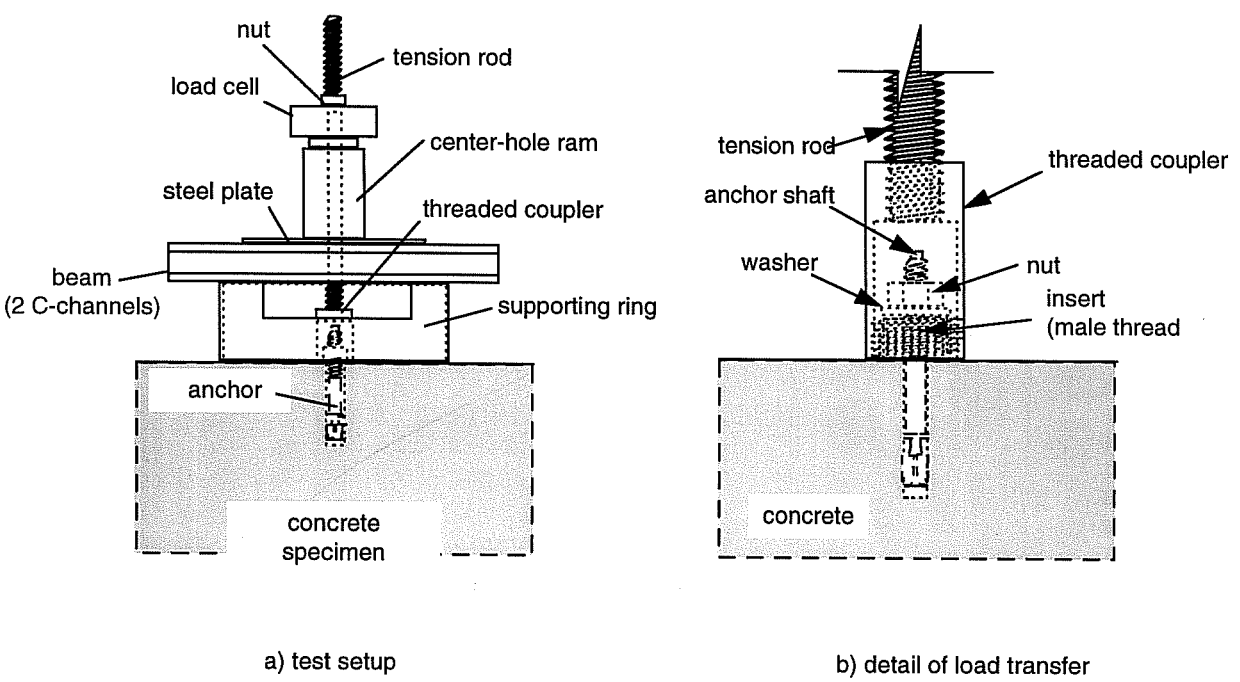

Figure 3. 7 Setup for pure tension tests with single anchors

symmetrically about the center of the attachment over the edge of the baseplate (Appendix 1). The data acquisition system is shown in Figure 3.6.

3.2.4.2 Series 2.3 and 2.4: Load-displacement behavior of single anchors loaded at various orientations

In these tests, a loading rate of 25% to 50% of the maximum load per minute was consistently used. The force could be applied with an one-way actuator and an electric pump.

The overall setup for the pure tension tests is portrayed in Figure 3.7. The interior diameter of the supporting ring is 640 mm (25 in). This is equivalent to a support spacing of about $7 \cdot h_{ef}$ in the tests with expected concrete breakout, and $3.5 \cdot h_{ef}$ in the tests showing steel failure. The measuring equipment was essentially the same as that used in Series 2.1 and 2.2. However, the displacements were measured with two potentiometers placed symmetrically about the anchor axis, and reacting upwards against a Plexiglas plate screwed onto the tension rod.

For the oblique tension tests at 15° a beam with double C-channels was used, inclined at 15° with one end on the edge of the concrete specimen and the other end on a steel support. At the support end, a welded 15° wedge element was clamped to the beam, thereby giving a purely vertical force on the support. The horizontal component of force was resisted by the steel plate bolted to the beam, and by an angle on the concrete. Appendices 3 and 4 show photos of this setup. In Series 2.4, anchors were installed at a small edge distance (concrete failure expected). In this case, the lower end of the beam was supported on a structural steel member oriented perpendicular to the floor of the lab instead of on the concrete, and the horizontal surface of the specimen was braced on both sides of the anchor (Appendix 4). The spacing of the supports from the anchor axis was at least twice the anchor edge distance. The specimens in these tests were also braced against the floor.

In all oblique tension tests, the load was directly applied to the anchor through an insert made of high-strength steel with a male thread similar to those in the pure tension tests (Figure 3.7). The thickness of the insert was the same as the diameter of the anchor shank (flush-sleeve installation) or the outside diameter of the sleeve (through-sleeve installation). The diameter of the hole in the insert was 11.5 mm for the 3/8-inch anchor. For anchors of 5/8 inch and M16, the hole diameter was 17.5 mm for flush-sleeve installation and 25.4 mm for through-sleeve installation.

The insert was embedded into a loading shoe, connected to the tension rod by a machine bolt. The loading shoe for the tests with a loading angle of 15° is shown in a photo in Appendix 4. Linear potentiometers were used for measuring the vertical displacement on both sides of the loading shoe against a glued Plexiglas plate. The horizontal displacement was measured with another potentiometer against a Plexiglas plate bonded to the back end of the loading shoe.

For the tests at 30°, 45°, and 60°, the loading setup shown in Appendix 5 was used. In tests with near-edge anchors and concrete breakout, an additional structural steel section was required, like that used in the tests at 15° (Appendix 5 below). The specimen was anchored to the lab floor to prevent it from being lifted up during the test. The loading setup was first inclined at an angle of 45°. In the tests at 30° and 60°, a welded 15° wedge element was therefore used under the actuator, and was clamped to the main beam (double C-channel) of the loading setup (Appendix 6). The loading shoe for the tests at 30° and 60° is portrayed in Figure 3.8. In Appendix 6, the arrangement of the potentiometers can be seen beside the loading shoe, which is essentially identical to that used in the tests at 15°. The same data acquisition system was used.

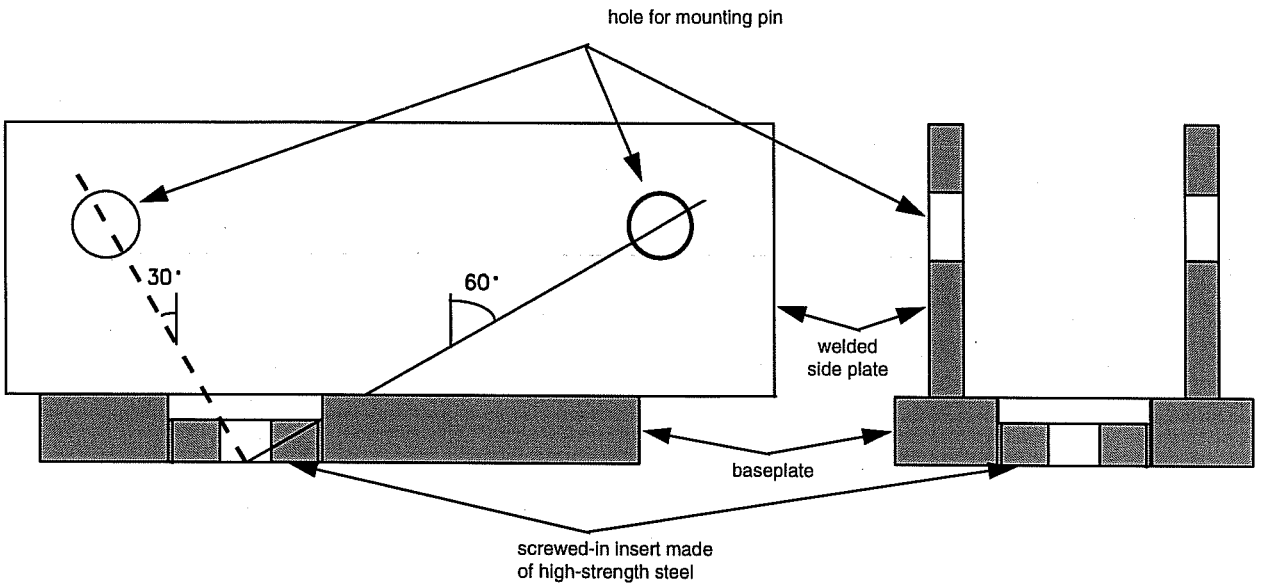

Figure 3. 8 Loading Shoe for Tests at 30° and 60°

The setup for the shear tests is portrayed in Figure 3.9. The horizontal reactions on the specimen had a spacing to the anchor axis of at least twice the edge distance of the anchor (clearance $\geq 4 \cdot c_1$). A high-strength insert with the same thickness and hole diameter as in the pure and the oblique tension tests was used to apply the load to the anchor. The inserts embedded in the loading plate are shown in Figure 3.10. The loading plate extends out over the concrete edge and increases in thickness there, so that the axis of the tension rod is at the height of the concrete top surface, to minimize the eccentricity of the load.

In the shear tests, the horizontal displacement at the end of the loading plate away from the actuator, and the vertical displacement, were measured at the top surface of the loading plate at the end opposite the load. The data acquisition system was the same as that shown in Figure 3.6.

3.2.4.3 Series 2.5 and 2.6: Load-displacement behavior of two-anchor connection loaded in eccentric shear

The test setup for Series 2.5 and 2.6 is portrayed schematically in Figure 3.11. Photos are given in Appendices 7 through 10. As shown in Figure 3.11, the force was applied by a diagonal rod connecting the upper end of a loading beam and a floor-mounted hydraulic ram. The load on two-anchor connections was applied along a horizontal tension rod by the rotation of a vertical loading beam about its lower support pin. The loading rate was chosen so that the capacity of the connection was reached in 2 to 4 minutes. The rotation of the beam reached a maximum of about 3° in tests with ductile connections. In this case, an initial opposite rotation of about 1.5° was applied before the test was begun.

The test setup required that vertical forces be resisted through the diagonal rod of the ram and through clamping rods tying the specimen to the lab floor. Horizontal forces were self-equilibrated.

The anchors of the two-anchor connection were spaced at 10 in, or 254 mm. A 0.8-mm Teflon sheet was inserted between the baseplate and the concrete. The baseplate extended out at both ends by a length of 2 inches (50.8 mm). The projecting length on the compression side was beveled at 5° over a length of 42

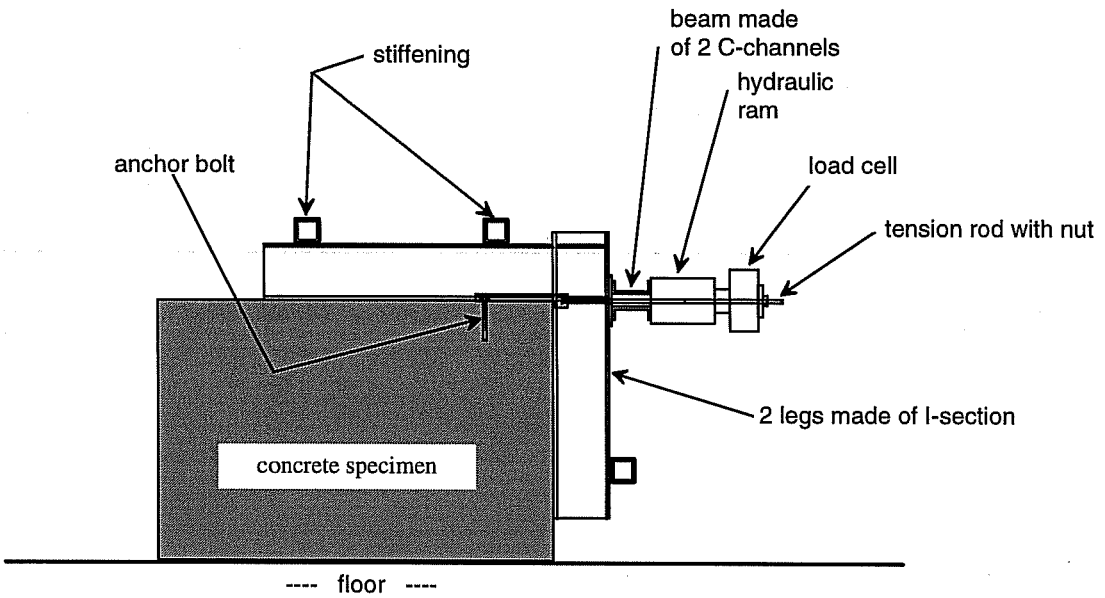

Figure 3. 9 Setup for Shear Test

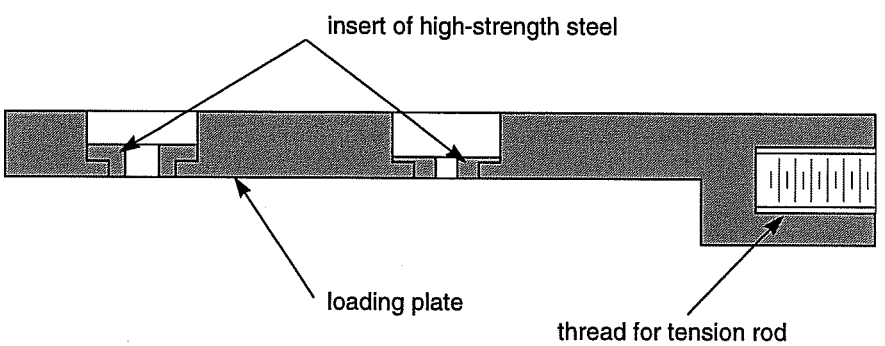

Figure 3. 10 Loading Plate for the Shear Test

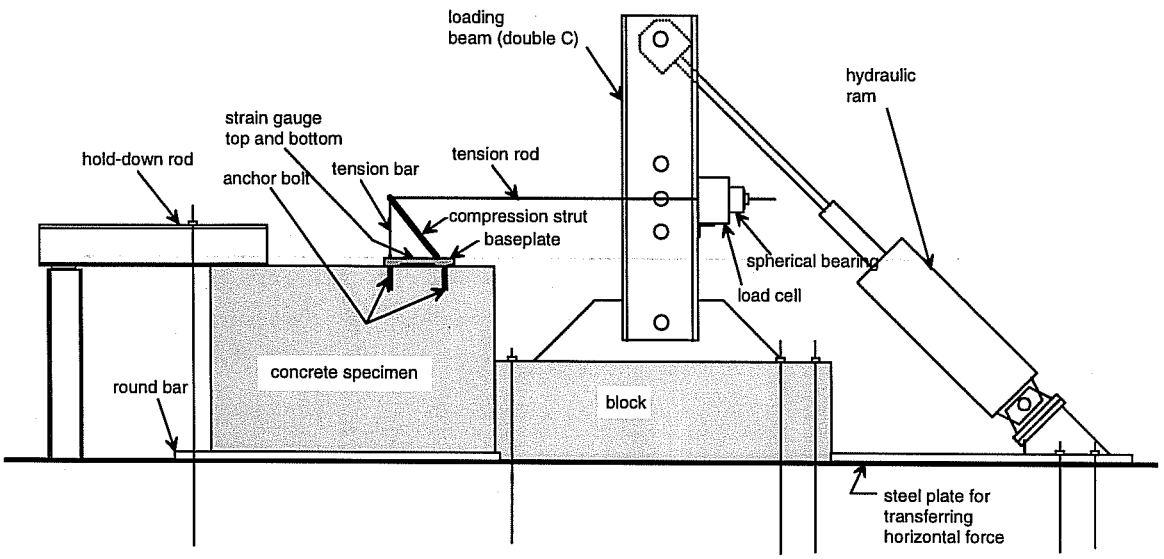

Figure 3. 11 Test Setup for Series 2.5 and 2.6

mm (Figure 3.11, Appendix 10). This was intended to reduce tensile prying on the anchor on the compression side, which would have increased the compression force between the baseplate, Teflon sheet, and concrete, and would therefore have increased the comparatively uncertain amount of friction.

A conventional multi-anchor attachment (consisting of a baseplate and a cantilever beam), installed against a concrete surface, is internally statically indeterminate. In this test setup, the cantilever beam was reduced to its functional components: a compression strut and a tension bar. This created a free sector on the baseplate, in which the strain distribution could be measured with resistance strain gauges (Appendix 9). Using the strain gauge data, the moment and normal force in the baseplate could subsequently be determined, thereby giving the load distribution on individual anchors. The tension bar, the compression strut and the tension rod (for applying the external force) were connected by a pin (Appendix 10). The lower end of the compression strut rested on a pin, which aligned its axis with the anchor axis and with the concrete surface. For smaller applied eccentricities, the exact alignment of the compression strut was maintained with a spacer (Appendix 10).

The strain distribution was measured directly between the anchors with maintained three gages on top and bottom. The width of the baseplate was reduced to 4 inches (101.6 mm) in this region to achieve a more uniform stress distribution. The gages were distributed evenly across the width of the baseplate (edge distance 1 inch, or 25.4 mm; spacing 1 inch).

The vertical displacement of the baseplate was measured with a linear potentiometer at the distance of 7 inches (177.8 mm) and 12 inches (304.8 mm) from the axis of the anchor on the compression side, and reacting against a glued glass plate. The horizontal displacement of the anchor plate was measured with a potentiometer at the side opposite the load. The horizontal force applied to the connection was measured with a load cell where the tension rod was attached to the vertical beam. To eliminate angular deviation during the tests, a spherical bearing was used between the load cell and the nut on the tension rod. The data acquisition system was similar to that portrayed in Figure 3.6. However, the HP Plotter was replaced by a multi-channel data scanner and analog-to-digital converter.

3.3 Test Results and Interpretations

3.3.1 Series 2.1 and 2.2 Pure Tension Tests of Two-Component Groups

Appendix 11 and 12 include result tables for Series 2.1 and 2.2. The corresponding load-displacement curves are plotted in Appendices 13 through 20. Appendices 21 through 24 also include load versus time curves for dynamic tests. Fracture cones were measured in two to four tests of each sub-series. Fracture cones were measured in the plane defined by both anchor axes. Fracture cone profiles are plotted in Appendices 25 and 26. Appendices 27 through 33 include photos of typical failures. Appendices 34 and 35 show photos of anchor after tests.

Some load-displacement curves have portions in which the measured baseplate displacement decreases despite increasing external load. These portions show where the load lifted the baseplate from the concrete surface. Small deviations in the loading direction lead to a "hunting" of the baseplate. This can cause a decrease in the measurements through lateral deflection of the displacement pickup pins. This slight imprecision in measurement has no influence on the load results.

The following failure modes were observed in tests:

- concrete breakout at both anchors simultaneously (Appendices 28, 30, 32, 33, and 34)

  This failure mode usually occurred with attachments installed near the middle of the test blocks. With a attachment installed at the end of a test block (2 of 3 tests, because only 3 tests were done on each surface), the short edge of the test block was frequently split off (see below).

- concrete breakout only at one of two anchors (Appendices 27, 29, and 31)

  This failure mode occurred mostly in connections with a spacing of $2.5 \cdot h_{ef}$ (Appendices 27, 29). However, it was also observed in one static test with $s = 1.5 \cdot h_{ef}$ (Test 21sh1502, Appendix 31).

- concrete breakout combined with splitting (Appendices 27, 28,30, 31, 32, and 33)

  This failure mode occurred only at attachments installed at the ends of test blocks. It was the most frequent failure mode of those attachments, although the edge distance of the anchor to all edges was at least $3.5h_{ef}$. The above-mentioned appendices show typical failure modes. In general, a normal fracture cone formed in the test blocks. However, part of the fracture cone about $1.0\ h_{ef}$ from the anchor axis at the ends of the test blocks was inclined toward the side faces, and in some tests the entire ends of specimens were broken off.

No influence of the different failure mode on failure loads and the displacement behavior of anchors could be determined.

Table 3.9 shows mean failure loads and displacements at failure, for individual sub-series. Typical load-displacement curves are plotted in Figure 3.12 (undercut anchor) and Figure 3.13 (sleeve anchor).

The observed load-displacement behavior of the undercut anchor agrees well overall with the other test results. Table 3.9 shows that for the undercut anchor, the increase in the failure load in dynamic tests relative to static tests is 13% (spacing $s = 2.5\ h_{ef}$) or 16% (spacing $s = 1.5\ h_{ef}$). In tests on

Table 3. 9 *Average Maximum Loads and Displacements of Two-Anchor Connections Under Pure Tension*

Series	Sub-series	Anchor Bolt 5)	Spacing s/h_{ef}	F_u (f_c = 32.4) kN	$F_{u,dyn}$ / $F_{u,stat}$	COV. F_u %	Failure Displ. d_u mm	COV d_u %	Note
2.1 Static	21SM25	HSD 3/4"	2.5	205.4	-	5.3	0.68	36.13	1)
	21SM15	HSD 3/4"	1.5	177.8	-	6.0	0.61	74.86	2)
	21SH25	KSHD M20	2.5	173.3	-	11.8	2.34	22.27	3)
	21SH15	KSHD M20	1.5	146.9	-	6.3	1.83	46.48	4)
2.2 Dynamic	22SM25	HSD 3/4"	2.5	232.3	1.13	7.4	3.64	27.35	
	22SM15	HSD 3/4"	1.5	206.6	1.16	3.7	1.30	12.71	
	22SH25	KSHD M20	2.5	246.3	1.42	4.9	2.61	9.74	
	22SH15	KSHD M20	1.5	213.1	1.45	6.5	3.62	32.33	

1) d_u of Test 1 of this sub-series was not included
2) mean d_u = 0.88 mm, COV. = 42.7% without Tests 2 and 3 of this sub-series
3) d_u of Test 4 of this sub-series not included
4) d_u of Test 3 of this sub-series not included
5) HSD = UC1, KSHD = Sleeve anchor

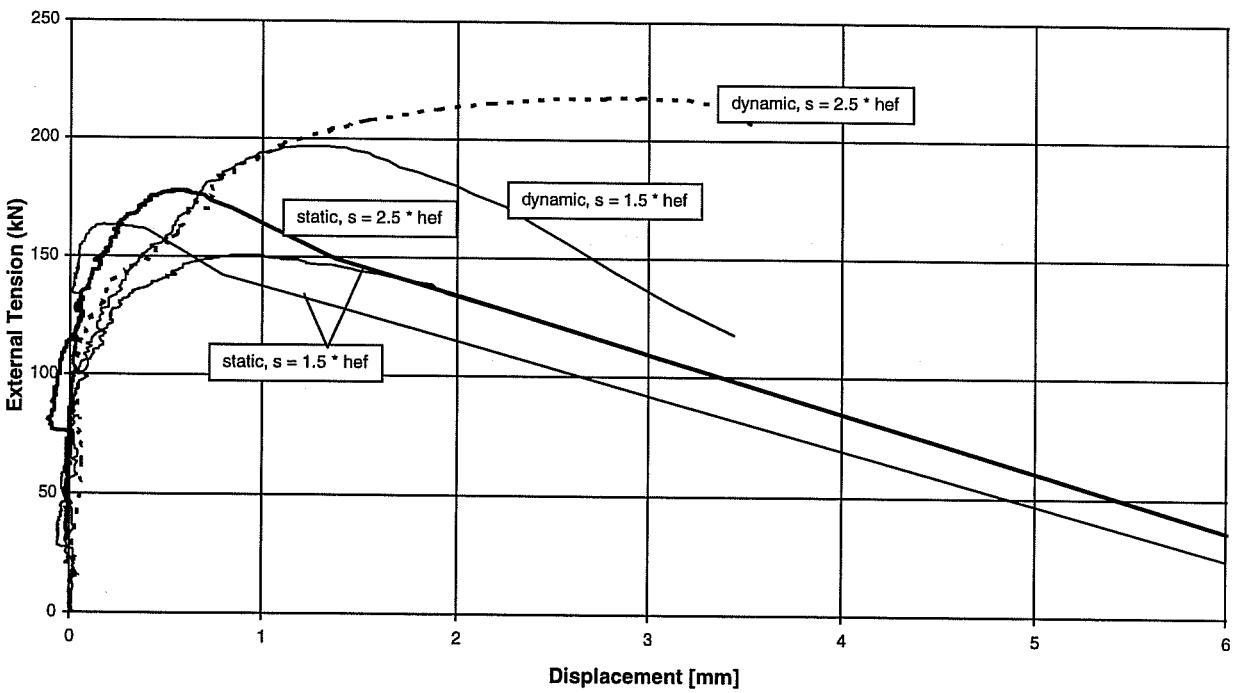

Figure 3. 12 *Typical Load-Displacement Curves for Undercut Anchors*

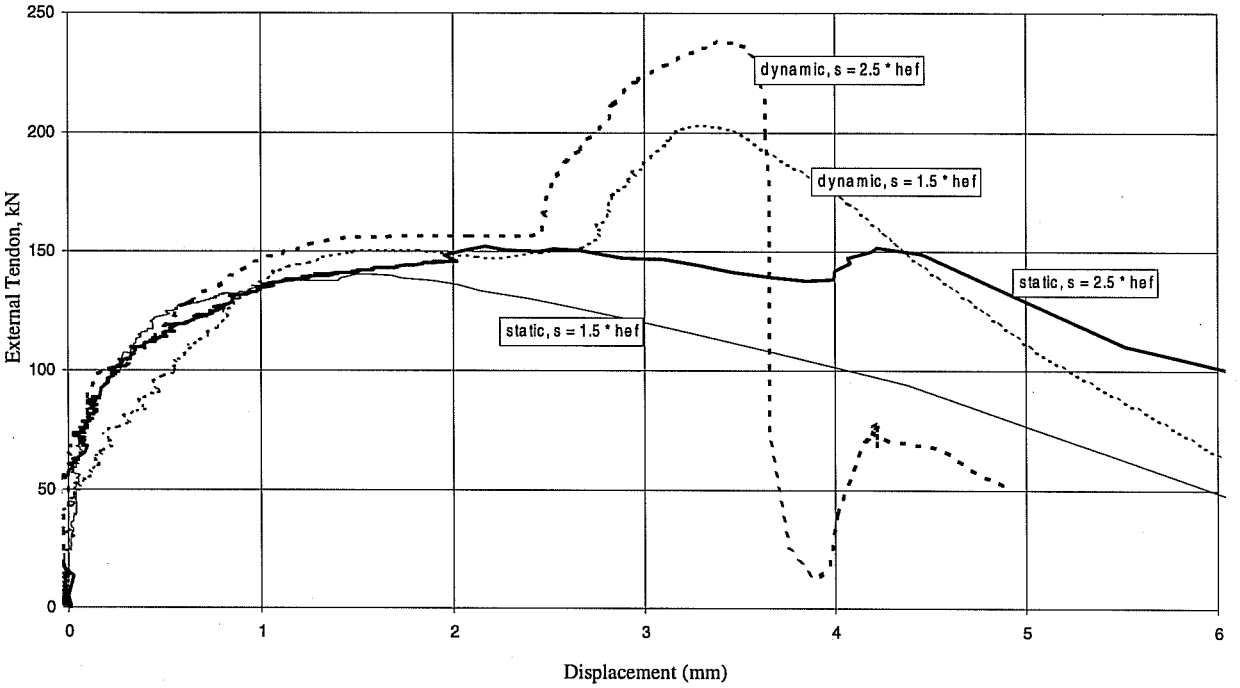

Figure 3. 13 Typical Load-Displacement Curves of Torque-Controlled Expansion Sleeve Anchors

single anchors (Rodriguez, 1995) with comparable loading time to fracture, a mean load increase of 14% was observed. Tests on another type of undercut anchor (h_{ef} = 80 mm) were reported by Eibl and Keintzel (1989), who tested anchors installed in line cracks 0.7 and 1.1 mm wide. In those tests, the increase in failure load was about 25% with a loading time of 0.04 second before fracture (dynamic), compared to static tests with loading time of about 300 seconds (factor between loading times: $7.5 \cdot 10^3$).

For loads up to about 130 kN the load-displacement curves of all tests with undercut anchor are close together, independent of spacing and loading rate. However, the increase in the maximum load (with increased spacing and loading rate) leads to an increase in displacement at failure. Particularly in dynamic tests with an anchor spacing of s = 2.5 h_{ef}, the load-displacement curves have comparatively long and nearly horizontal portions near the maximum load. Photos of the undercut anchor after dynamic tests (Appendix 34) show that the cone was drawn far into the expansion sleeve. This suggests that the local bearing strength where load was induced into the concrete increased less than the concrete breakout load.

The behavior of the torque-controlled expansion sleeve anchor is affected by a peculiarity in its design. As noted in Figure 3.2(a), there is a step inside the sleeve of the M20 sleeve anchor. The cone reaches this step at approximately maximum expansion of the anchor, immediately before reaching the maximum load for pull-through failure. Further pull-through of this cone is prevented by the step, so a larger friction force can develop between the outside surface of sleeve and the concrete.

This results in a unique load-displacement behavior for this anchor. At first, the load-displacement curve of the sleeve anchor is shallower than that of UC1. The gradual transition in the horizontal or falling branch follows a steep secondary increase at comparatively large displacement. This secondary increase in load was observed in all tests on M20 Sleeve Anchors except three static tests with a spacing of 1.5h_{ef}

(Series 21sh15). Without a doubt, failure by concrete breakout or concrete breakout combined with splitting of the concrete occurred in these tests, before the cone reached the edge. In dynamic tests, the secondary load increase is even more distinct than in static tests, and the maximum load is always reached in this phase of response. The load-time curves in Appendices 23 and 24 show that with the steep increase in the load-displacement curve, there is a distinct increase in loading rate.

Appendix 35 shows photos of the Sleeve Anchor after dynamic tests. In only one dynamic test (with a spacing of $s = 2.5h_{ef}$,) was the anchor expanded past the step by the load.

As shown in Table 3, for Sleeve Anchors, the increase in the failure load in dynamic tests compared to static tests is about 42% ($s/h_{ef} = 2.5$) or 45% ($s/h_{ef} = 1.5$). This increase is clearly much higher than observed for undercut anchors. Other torque-controlled expansion anchors showed less load increase than undercut and grouted anchors (Rodriguez, 1995). The extremely high increase for the Sleeve Anchors tested here is therefore due to the unique form of the expansion mechanism. If the cone reaches the step inside the expansion sleeve, it is prevented from sliding further into the shell. This leads to a sudden stiffening of the load-displacement behavior of the anchor, which has a massive influence on the instantaneous loading rate in dynamic tests. This becomes clear from the load-time diagram in Appendices 21-24. The undercut anchor shows an approximately linear load increase up to the maximum load. However, the Sleeve Achor shows first of all a flattened sector (which indicates a pull-through failure), followed by a steep increase when the cone is stopped by the edge of the expansion sleeve. The instantaneous loading rate is then about twice the nominal value.

From the assessment of the measured failure load increase in dynamic versus static tests, additional observations are as follows:

A zone of very high strain gradients exists at the tip of the critical concrete breakout crack. The effects of high loading rate are accentuated by the mechanics of fracture propagation. Through the particular geometry of this torque-controlled expansion sleeve anchor, this effect is especially evident.

In single-anchor tests with the sleeve anchor, the load increase of 24% for dynamic versus static loading was already bigger than for UC1 (Rodriguez, 1995). However, the effect there was less distinct because the small hydraulic ram, combined with a small valve used in the single-anchor tests, could not maintain as high a loading rate for large displacements close to the maximum load.

Furthermore, Figure 3.14 shows that there is little difference between the absolute failure loads of UC1 and the Sleeve Anchor in dynamic tests. The undercut anchor has high failure loads in static tests. This, combined with the peculiar form of the Sleeve Anchor, explains the difference in the quotient ($F_{u,dyn}/F_{u,stat}$) for these two anchor types.

Loading rate appears to have little effect on the interaction of anchor within a group for either anchor type. In Figure 3.14, the capacities of the two-anchor connection and the tests described by Rodriguez (1995) on single anchors are plotted as a function of the relative spacing of anchors (s/h_{ef}). For comparison, the maximum loads calculated from Equation 3.1 (static) or 3.2 (dynamic) are also shown.

$$F_{u,Gr.stat} = (1 + s/s_k)15.5\sqrt{1.18 * f_c} * h_{ef}^{1.5} \qquad (3.1)$$

where: $s_k = 3\ h_{ef}$

$$F_{u,Gr,dyn} = 1.25\ F_{u,Gr,stat} \qquad (3.2)$$

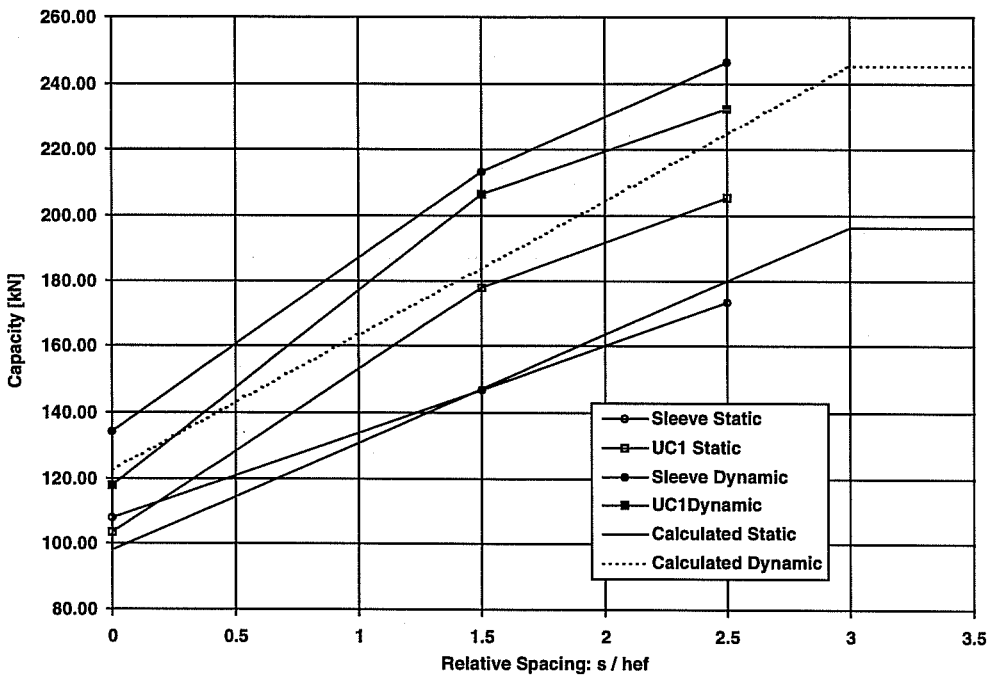

Figure 3. 14 Maximum loads of static and dynamic tests depending on the relative spacing of anchors

Figure 3.14 shows that in dynamic tests, the increase in the maximum load with the relative spacing of anchor, is nearly parallel to the calculated values. Therefore, despite the higher failure loads under dynamic load, the same rule holds for interaction between two anchors as under static load.

Measurements of fracture cones (Appendices 25 and 26) do not suggest a bigger fracture cone in dynamic tests than in static ones. Rather, they suggest a steeper crack development, and so a smaller fracture cone in tests with dynamic load. This agrees with the observations reported for single anchors by Rodriguez (1995). Based on the large scatter of the fracture cone contours, more experimental and theoretical investigations are required to confirm these observations. However, it seems safe to say that the critical anchor spacing is not larger under dynamic load than under static load.

The following conclusions are derived from the test results of Series 2.1 and 2.2:

- An increase in the loading rate by a factor of 10^3 to 10^4 leads to an increase of 15% to 25% in the concrete breakout load of two-anchor groups of UC1 anchors. This value agrees well with the results of single-anchor tests (Eibl and Keintzel, 1989; Rodriguez, 1995).
- The interaction of group anchors follows the well-known rule for single anchors (Figure 3.14).
- Measured fracture cone contours (Appendices 25 and 26) do not suggest any enlargement of fracture cones under dynamic load. Rather, a steeper fracture cone was observed. Due to large scatter, this result requires additional confirmation.
- In the tests with the Sleeve Anchor, the geometry of the expansion sleeve significantly influences the test results, as seen from the load-displacement (Appendices 13 - 20) and load-time curves

(Appendices 21 - 24). In particular, the sudden stop of the cone at the step in the anchor sleeve caused the instantaneous loading rate to jump to about double the nominal value. Failure loads were 42% to 45% higher in dynamic compared to static tests. The nearly doubled loading rate is not enough to substantiate an inherently greater increase in maximum capacity of expansion anchors as compared to undercut anchors. Rather the results reflect the effect of high strain gradient near the crack tip, which in combination with crack propagation amplifies the effect of changes in loading rate.

- The load-displacement behavior of anchor was independent of loading rate. The higher displacements at failure in dynamic tests result from higher failure loads. However, the flattening of the load-displacement curves of UC1 near the high failure loads in dynamic tests, as well as the cone being drawn far into the sleeve after the tests, shows that the local strength of the concrete around the expansion mechanism does not increase as much as the concrete breakout load.

3.3.2 Series 2.3 and 2.4: Load-Displacement Behavior of Single Anchor at Various Loading Directions

3.3.2.1 Summary of Results

The average maximum loads and displacements at failure for each test are compared in Table 3.11 for Series 2.3, and in Table 3.12 for Series 2.4. More detailed results, load-displacement curves and their mathematical description, photos of failure modes, and interaction diagrams for loads and displacements are given in Appendices 36 to 144. The appendices corresponding to each sub-series are given in Table 3.10.

3.3.2.2 Interpretation and Discussion of the Results

Anchors in Series 2.3 were intended to fail by fracture of the anchor shank. Therefore, large embedment depths were used: 7 inches (178 mm) for anchor with diameter of 5/8 inch and M16, and 3.5 inches (89 mm) for anchors with a diameter of 3/8 inch (9mm). Large edge distances of 11 inches (280 mm) or 5.5 inches (140 mm) were chosen. The intended failure mode of steel fracture was achieved with only a few exceptions, all under pure tension.

Table 3. 10 Appendices Corresponding to Each Sub-Series in Series 2.3 and 2.4

Type of Result	Sub-series							
	23H64	**23H74**	**23M54**	**23M74**	**23M53**	**23M34**	**24M54**	**24A54**
Result charts	36	53	64	81	92	108	122	122
Interaction diagram for forces	37	54	65	82	93	109	123	134
Interaction diagram for displacements	38	55	66	83	94	110	124	135
Mathematical description of load-displacement curves[1)]	39-41	56-57	67-69	84-85	95-96	111-112	125-126	136-137
Load-displacement curves	42-46	58-61	70-74	86-89	97-101	113-117	127-130	138-141
Photos of failure modes	47-52	62-63	75-80	90-91	102-107	118-121	131-133	142-144

[1)] curve parameters and curve groups

Table 3. 11 Average Maximum Loads and Displacements at Failure, Series 2.3

Series	Anchor Bolt	h_{ef} mm	Installation (1)	Loading Angle, degrees	Torque Nm	Concrete Strength N/mm²	Failure Load F_u kN	Horizontal Displacement $d_{H,u}$ mm	Vertical Displacement $d_{V,u}$ mm	Shell, t mm	Note
23H64	KSHD M 16	178	Flush-sleeve installation	Tension	203/102	32.4	126.2	0.00	21.20	-	(1)
				15	203/102	32.4	127.5	7.34	9.67	28	
				30	203/102	32.4	106.6	4.02	2.08	11	
				45	203/102	32.4	89.7	4.14	1.26	6	
				60	203/102	32.4	83.2	3.66	0.85	2	
				90	203/102	32.4	78.0	3.14	0.09	0	
23H74	KSHD M16	178	Through-sleeve installation	30	203/102	32.4	136.8	19.65	10.96	38	
				45	203/102	32.4	137.0	27.77	11.56	43	
				60	203/102	32.4	138.1	15.96	5.22	35	
				90	203/102	32.4	149.7	15.02	2.35	13	
23M54	HSD 5/8	178	Flush-sleeve installation	Tension	244/122	32.4	135.3	0.00	21.34	-	
				15	244/122	32.4	126.6	9.07	10.33	21	
				30	244/122	32.4	112.2	6.65	3.46	13	
				45	244/122	32.4	93.5	6.91	2.00	9	
				60	244/122	32.4	86.2	6.40	1.11	6	
				90	244/122	32.4	82.2	5.69	0.00	2	
23M74	HSD 5/8	178	Through-sleeve installation	30	244/122	32.4	145.0	21.11	11.34	51	
				45	244/122	32.4	133.2	20.09	6.07	35	
				60	244/122	32.4	131.9	25.85	6.97	38	
				90	244/122	32.4	155.9	13.65	0.00	8	
23M53	HSD 5/8	178	UC1	Tension	244/122	20.7	134.8	0.00	41.13	-	(2)
				15	244/122	20.7	130.2	18.61	19.82	35	
				30	244/122	20.7	106.8	14.86	6.63	25	
				45	244/122	20.7	95.2	9.61	2.70	18	
				60	244/122	20.7	84.4	9.42	1.79	14	
				90	244/122	20.7	80.4	6.18	0.21	5	
23M34	HSD 3/8	89	Flush-sleeve installation	Tension	54/27	32.4	50.6	0.00	1.96	-	
				15	54/27	32.4	44.6	2.26	1.85	0	
				30	54/27	32.4	38.7	2.86	1.11	0	
				45	54/27	32.4	35.2	2.51	0.49	0	
				60	54/27	32.4	30.8	2.66	0.36	0	
				90	54/27	32.4	30.0	2.58	0.15	0	

1) pull-through failure for 3 of 4 anchors ; 1 test with steel fracture at F_u = 140.1 kN ($d_{V,u}$ = 20.98 mm)
2) median value for tests with steel failure only (2 out of 3)

Table 3. 12 Average Maximum Loads and Displacements at Failure, Series 2.4

Series	Edge Distance c1 mm	Installation 1)	Loading Angle degrees	Torque 2) Nm	Concrete Strength N/mm²	F_u (f_c = 32.4) kN	Horizontal Displacement $d_{H,u}$ mm	Vertical Displacement $d_{V,u}$ mm	Height BA h mm	Note
24M54	140	Flush-sleeve installation	Tension	244/122	32.4	75.86	0.00	1.19	-	
			30	244/122	32.4	69.17	1.94	0.41	186	
			45	244/122	32.4	70.25	2.64	0.52	210	
			60	244/122	32.4	57.20	2.24	0.25	174	
			90	244/122	32.4	65.08	3.74	0.00	254	
24A54	279	Flush-sleeve installation	Tension	244/122	32.4	91.28	0.00	1.72	-	
			15	244/122	32.4	92.69	Md	Md	-	2)
			30	244/122	32.4	99.68	5.10	2.02	-	3)
			45	244/122	32.4	90.57	6.56	1.91	-	4)

1) In some tests a torque of only 203 Nm instead of 244 Nm was applied to avoid splitting of the concrete edge.
2) Md = measurement failure
3) only 1 test
4) 2 tests, 1 with concrete failure and 1 with steel failure

In Sub-Series 24M54, concrete failure was expected. In Sub-Series 24A54, the failure mode changed from concrete breakout under tension to steel fracture under shear. This agrees with the behavior of the far-edge anchor of a group of anchor with relatively small embedment depth, as tested in Series 2.6 (see Section 3.3.3).

In the following sections, the results of each individual test series are described and discussed.

Series 23H64: Torque-controlled expansion sleeve anchor M16, h_{ef} = 7 inches (178 mm), $c_1 \geq 11$ inches (279 mm), f_c = 32.4 N/mm², flush-sleeve installation:

The expected failure mode in these tests was fracture of the anchor shank. This was achieved in all oblique and shear tests. There was only one case with steel fracture, in pure tension. In three tests, the cone was pulled through the sleeve (photos in Appendix 47).

The interaction diagram of failure loads is plotted in Appendix 37. For the values on the load axis, only the tests with steel failure were included. The interaction is well described by Equation (2.4), using an exponent, p, of 1.8. The ratio of the calculated to observed failure loads is then (cal F_u / $F_{u,Vers.}$) = 1.01, with a coefficient of variation of 2.0%.

Under pure tension, virtually no displacement was measured before the prestressing force was overcome, at 60 to 80 kN. Starting from that point, displacement increased almost linearly with load, to a maximum value of about 20 mm at failure. No significant differences were observed between the load-displacement curves corresponding to steel fracture and pull-through failure (Appendix 42).

In pure tension tests by Collins et al. (1989), using a sleeve anchor of similar type and equal size in concrete with a compressive strength of f_c = 4520 to 5760 psi (31.2 N/mm² to 39.7 N/mm²), considerably

smaller displacements at maximum load were measured, with a mean value of 0.41 inches (10.4 mm). This is because the lower failure load, the lower ductility of the anchor shank, and the smaller embedment depth (6 inches, or 152.4 mm), resulted in a smaller elongation. The average failure load in Collins' tests was 110 kN instead of 139 kN (steel fracture) in that test series. Considering that the displacement at failure in Collins' tests was measured over a gage length of (h_{ef} + 0.5in), the elongation was 6.3%. With the material data of the anchor shank in the tests described here (see Figure 3.3), a value of 7.8% results from pure steel deformation ([2 in · 16.1% + 4.5 in · 4.1%] / 6.5 in).

In oblique tests at 15°, before reaching the maximum load, a shell-shaped spalling of the concrete occurred in front of anchors (Appendix 48). The depth of the spalling was about 25 to 29 mm. At maximum load, a comparatively large horizontal displacement of 7 to 8 mm was reached. In contrast, the vertical displacement of about 7 to 12 mm was only half that observed in the pure tension tests. Nevertheless, these tests showed ductile failure overall.

In oblique tension tests at 30° to 60°, shell-shaped spalling of the concrete was also observed. However this spalling was restrained by the baseplate. Therefore, the concrete surface was almost flat after the test (Appendix 49). Loose concrete about the size and depth of the observed spalling was removed with a screwdriver, and is shown by photos in Appendices 50 and 51. The depth of the spalling decreased to 6 to 13 mm at 30°, and to 0 to 6 mm at 60° (see Table in Appendix 36). Both the vertical and the horizontal displacements at maximum load decreased with the increasing transverse component of the load, which resulted in a decrease in the overall displacement to about 4.5 mm at 30°, and to about 3.8 mm at 60°.

Under pure shear, little or no concrete spalled in front of anchors. Failure occurred at a displacement of about 3 mm by a small-deformation shear failure of anchor shank.

An overview of the interaction diagram of displacements at maximum load of the anchor at different loading directions is given in Appendix 38. The diagram shows a significant decrease in the displacement at failure as the load deviated only slightly from pure tension.

Anchors under oblique and shear load therefore failed in a relatively brittle manner, even though failure was by steel fracture, and the material of the anchor shank has a comparatively high fracture elongation.

Series 23H74: Torque-controlled expansion sleeve anchor M16, h_{ef} = 7 inches (178 mm) $c_1 \geq 11$ in (279 mm), f_c = 32.4 N/mm², through-sleeve installation:

In these tests the anchor sleeve passed through the baseplate, and therefore transferred shear directly. This inherently gives a higher shear strength of the connection for the failure mode of steel fracture. This failure mode was always achieved in the shear tests (90°) and the oblique tests (30°, 45°, and 60°). In evaluating test results for pure tension, the results of Series 23H64 were used, because under pure tension load the location of the critical shear plane has no influence on results.

The interaction diagram of the failure loads is plotted in Appendix 54. Equation (2.4), with an exponent of p = 1.8, again proved applicable for describing the results. The ratio of the calculated and the test values is (cal $F_u/F_{u,Vers.}$) = 1.01. The coefficient of variation was 5.1%, slightly higher than in the tests with anchors with flush-sleeve installation.

In the oblique tension tests at an angle of 30° from the anchor axis, the transverse displacements at maximum load were 15.5 and 23.7 mm. The vertical displacements were 7.7 mm and 14.2 mm, clearly greater than those of the anchors installed with flush sleeves. The load-displacement curves of the

anchors are approximately the same as in Series 23H6. The larger displacements are due to the inherently higher failure loads of the anchors installed with through sleeves, under oblique and shear load. The plateau of the load-displacement curves was achieved at a load higher than the failure load in Series 23H6. In essence, the displacement increased because of shell-shaped concrete spalling in front of the anchor in the loading direction. In the tests of Series 23H7, the depth of the concrete spalling was measured at 25 mm and 51 mm at an oblique tension angle of 30°, about 42 mm at 45°, about 35 mm at 60°, and at 9 mm to 16 mm under pure shear. The depth of the concrete spalling is therefore several times of the values measured in Series 23H6.

The interaction diagram of the displacements at maximum load is plotted in Appendix 55. For all loading directions, displacements at maximum load were at least 15 mm. Therefore, regardless of loading direction, failure of the anchor was ductile.

Series 23M54: UC1 5/8 inch (9.5 mm), h_{ef} = 7 inches (178 mm), $c_1 \geq 11$ inches (279 mm), f_c = 32.4 N/mm², flush-sleeve installation:

The intended failure mode of steel fracture was achieved in all tests of this series.

The interaction diagram of the failure loads is plotted in Appendix 65. The interaction is well described by Equation (2.4). To investigate the plotted interaction curves, the tests of Series 23M54 (f_c = 32.2 N/mm²) and Series 23M53 (f_c = 21.1 N/mm²) were evaluated together. The best match to the test results was achieved using an exponent p = 1.8. For each sub-series, and for both sub-series together, the ratio of the calculated failure load to the failure load in tests is (cal F_u / $F_{u,Vers.}$) = 1.00

Coefficients of variation are 3.0% for Sub-series 23M54, 4.1% for Sub-series 23M53, and 3.5% for both Sub-series together.

In the pure tension tests, before overcoming the prestressing force at about 60 to 80 kN, virtually no displacement was measured. Further loading caused a progressive displacement increase to 16 to 28 mm at maximum load (Appendix 70). In all tests, the anchor shank fractured beneath the nut inside the insert (Appendix 75).

In the pure tension tests (Collins et al. 1989) of anchors of the same type and diameter were tested in concrete of f_c = 4520 psi (31.2 N/mm²). The average failure load was 129 kN, similar to that of this series (135 kN). The load-displacement curves measured by Collins agreed very well with those of this series, except for a somewhat smaller failure load.

The behavior of UC1 under oblique loading at 15° agreed largely with that of the Sleeve Anchor. However, about 20% to 25% higher transverse displacement (6 to 13 mm) was reached than with the Sleeve Anchor, which led to about 15% larger total displacement. The vertical displacement was 7 to 15 mm, similar in magnitude to that of the Sleeve Anchor. The depth of shell-shaped spalling in the loading direction in front of the anchor is the same (16 mm to 32), as shown in Appendix 64 and in the photos in Appendix 76.

Under oblique tension tests at 30°, only 6- mm to 7.5-mm horizontal displacement and about 3.5-mm vertical displacement were measured. The depth of the shell-shaped concrete spalling was only about 13 mm. At larger oblique tension angles, up to pure shear, the displacement and the depth of the shell-shaped concrete spalling was much smaller. Under pure shear, the horizontal displacement only reached 5 to 6 mm, and the depth of spalling was 0 to 3 mm.

Appendix 66 shows the development of the interaction diagram for displacements. Clearly, the displacement decreases with an increasing angle of oblique tension, or with an increasing transverse component of the applied load. At oblique tension angles greater than 15°, a small-deformation shear fracture of the anchor shank occurred. Photos in Appendix 76 to 80 show fractures and the broken anchor shanks.

Series 23M74: UC1 5/8 inch (9.5 mm), h_{ef} = 7 inches (178 mm), $c_1 \geq 11$ in (279 mm), f_c = 32.4 N/mm², through-sleeve installation.

In these specimens, the anchor sleeve passed directly through the baseplate, and therefore transferred shear. This increased the shear strength of the anchor for the failure mode of steel fracture. In the oblique tension tests (30°, 45°, and 60°), anchors failed by fracture of threaded shank, and the anchor sleeve was bent but not broken (photos in Appendices 90 and 91). In pure shear tests (90°), however, the anchor sleeve and anchor shank were both stripped. In evaluating results for pure tension, the results of Series 23M54 were used because tension behavior was not affected by the additional shear area provided by the anchor sleeve.

The interaction diagram of failure loads is plotted in Appendix 82. To describe the results, Equation (2.4) again proved applicable, with an exponent of p = 1.8. The ratio of the calculated to the measured failure load is (cal F_u / $F_{u,Vers.}$) = 1.01, with a coefficient of variation of 5.7%.

In the oblique tension tests at 30° from the anchor axis, transverse displacement at maximum load reached 20 to 23 mm. The vertical displacement was 10.0 to 12.6 mm, distinctly greater than that of the anchor with flush sleeves. The load-displacement curves of the anchor are approximately the same as those of Series 23M5. The larger displacement here are also due to the inherently higher failure loads of the through-sleeve anchor under oblique and shear load (See Series 23H7). In the tests of Series 23M7, the depth of concrete spalling was measured at 51 mm at an oblique tension angle of 30°, at about 36 mm at 45° and 60°, and at 6 to 9 mm under pure shear. The depth of the concrete spalling is therefore a multiple of that measured in Series 23M5.

The interaction diagram of displacements at maximum load is plotted in Appendix 83. In all loading directions the displacements at maximum load are at least 13 mm. Therefore, regardless of the loading direction, failure of the anchor was ductile.

Series 23M53: UC1 5/8 inch (9.5 mm), h_{ef} = 7 inches (178 mm), $c_1 \geq 11$ in (279 mm), f_c = 21.1 N/mm², flush-sleeve installation:

The expected failure mode of steel fracture was achieved (despite the low concrete strength of f_c = 21.2 N/mm²) in all oblique and shear tests, as well as in 2 of 3 pure tension tests. In one pure tension test, pullout failure occurred via a comparatively smaller fracture cone with a large displacement (photos in Appendix 102). The displacement at maximum load reached 43.7 mm in this test.

The interaction of failure loads is already described and discussed for Series 23M54, by which the tests of Series 23M53 were evaluated. The interaction diagram for Series 23M53 is plotted in Appendix 93. Displacements at maximum load in pure tension tests failing by steel fracture were also very large, about 41 mm.

In oblique tension tests at 15°, both transverse and vertical displacements still reached 15 to 25 mm. However, shell-shaped spalling occurred with a maximum depth of 32 to 38 mm in front of the anchors, in the loading direction.

The mean depth of spalling decreased with increasing angles between the external load and the anchor axis. At 30° it was 25 mm; at 45°, 18 mm; at 60°, 14 mm; and at 90° (pure shear), 5 mm. The associated displacement also decreased. Under pure shear, the average displacement at maximum load was 6.2 mm, not much greater than in Series 23M54 with $f_c = 32.2$ N/mm².

The interaction diagram in Appendix 94 clearly shows a large displacement under tension, as well as huge decrease in displacement at loading angles greater than 15°. However, with overall displacements of about 15 mm at 30° and 9 mm to 10 mm at 45° and 60°, the behavior can still be deemed ductile.

Series 23M34: UC1 3/8 inch (9.5 mm), h_{ef} = 3.5 in (89 mm), $c_1 \geq 5.5$ inches (140 mm), f_c = 32.2 N/mm², flush-sleeve installation:

These tests were a means of investigating the influence of anchor diameter on displacement behavior. The expected failure mode of steel fracture was achieved in all oblique and shear tests, as well as in 3 of 4 pure tension tests. In one test with UC1 of 3/8 in, concrete breakout occurred, likely due to damaged concrete from a preceding test.

Equation (2.4) proved applicable to the interaction of failure loads. However, the best match to the test results in this series was achieved with an exponent of p = 1.67. The interaction diagram is plotted in Appendix 109. The average ratio of calculated to experimentally determined failure loads is: (cal F_u / $F_{u,Vers.}$) = 1.01. The coefficient of variation was 5.6%. Using an exponent of p = 1.8 yields (cal F_u / $F_{u,Vers.}$) = 1.02 and a COV of 5.8 %, also in good agreement with the test results.

With 7 to 13 mm for steel failure and 14.1 mm for concrete breakout, comparatively large displacements were reached in pure tension tests. In the oblique and shear tests, total displacements reached at most only about 3 mm. The interaction diagram of displacements (Appendix 110) resembles that of an anchor of 5/8 inch or M16 (flush-sleeve installation). However, the total displacements are about 50% to 60% smaller, and the displacements at a oblique tension angle of 15° are so much smaller that ductile behavior could no longer be achieved. In all oblique and shear tests with anchors of 3/8 inch (9 mm), little or no spalling was noticed in front of the anchors.

Series 24M54: UC1 5/8 inch (9.5 mm), h_{ef} = 3.5 inches (89 mm), $c_1 \geq 5.5$ inches (140 mm), f_c = 32.4 N/mm², flush-sleeve installation.

In the tests of Series 2.4, the expected failure by concrete breakout enabled comparison of the behavior of steel fracture and concrete fracture, and especially consideration of the interaction relations for loads and displacements. For this purpose, anchors were installed with smaller embedment depth and edge distance. The desired failure mode was achieved in all tests.

Again, Equation (2.4) proved meaningful for the interaction of failure loads. The best match to the test results in this series is achieved with an exponent of p = 1.6. The interaction diagram was plotted in Appendix 123. For comparison, the curves corresponding to p = 1.4 and p = 1.8 are also plotted. The average ratios between calculated and observed failure loads, and the associated coefficients of variation, are:

$$(\text{cal } F_u / F_{u,Vers.}) = 0.96, \ \text{COV} = 9.4\ \% \quad (p = 1.4)$$

$$(\text{cal } F_u / F_{u,Vers.}) = 1.00, \ \text{COV} = 8.7\ \% \quad (p = 1.6)$$

$$(\text{cal } F_u / F_{u,Vers.}) = 1.03, \ \text{COV} = 8.7\ \% \quad (p = 1.8)$$

Therefore, the use of an exponent of p = 1.8 also provides good agreement with test results, and consistent exponents can be used for steel and concrete failure.

The displacements at maximum load under pure tension are 0.7 to 1.7 mm, naturally much smaller than those in the tests with steel failure. This is because the load-displacement curves are almost identical and the failure loads are smaller.

In the oblique and shear tests, with increasingly oblique loading angle, the vertical displacement decreases, but the transverse displacement increases. As the diagram in Appendix 124 shows, the interaction of displacements can be approximated by a straight line. This result is based on only one test series. Furthermore, the small number of tests does not allow the derivation of a relation between the loading angle and the necessary second geometrical point for the determination of the corresponding point on the interaction lines.

The average displacement at maximum load under shear was 3.7 mm. The ratio between the displacements at failure in this series and in tests with flush-sleeve installation at steel failure, agrees well with the ratio of failure loads. The reason for this is the comparatively poor curvature of the load-displacement curves under shear as well as the virtually identical shape of the curves for steel or concrete fracture up to the concrete failure load.

Series 24A54: UC1 (HSD) 5/8 inch (9.5 mm), h_{ef} = 3.5 in (89 mm), $c_1 \geq 11$ inches (279 mm), f_c = 32.4 N/mm², flush-sleeve installation:

This test series permits exploration of the load-displacement behavior of an anchor with a smaller embedment depth, failing by concrete breakout in tension and with large edge distance, and failing by steel fracture under shear. The embedment and edge distance were chosen to correspond to the far-edge anchor tested in Series 2.6 (two-anchor connections), and to prepare data for the calculation of this connection with the program BDA5. In the tests, concrete breakout occurred under pure tension as well as under oblique tension at 30°, and in 1of 2 tests at 45°. The test results in the force interaction diagram (Appendix 134) were compared with the following description of interaction:

For angles up to and including 30°, the interaction for concrete fracture was estimated from Equation (2.4) with an exponent of p = 1.6, using the average maximum test capacity under pure tension and the calculated concrete breakout load under shear from Equation (2.2). For angles greater than or equal to 45°, the interaction for steel fracture is estimated in accordance with the results of Series 23M54. Therefore, the ratio between the calculated and the measured failure load is (cal F_u / $F_{u,Vers.}$) = 1.01, with a coefficient of variation of 8.4%. This interaction agrees best with the observed behavior.

The interaction according to Equation (2.4) is used, and a exponent of p = 1.8; that is, the failure transition is ignored. This gives (cal F_u / $F_{u,Vers.}$) = 0.95, with a coefficient of variation of 10.2%. This interaction gives the worst description of the test results.

The interaction according to Equation (2.4) is used and the exponent is adjusted. The equation agrees best with the test results using p = 2.5: cal F_u / $F_{u,Vers.}$ = 1.00, and a coefficient of variation is 8.1%. However, this adjustment applies only for a particular combination of parameters. In particular, the exponent depends on the angle at which the transition from concrete breakout to steel failure occurs. This method of adjustment is therefore not suitable for general application. Nevertheless, this description can be used for our present well-defined case in the BDA5 program.

The interaction diagram of forces (Appendix 134) is plotted to compare all the interaction relationships described above. The use of separate interaction relations for steel fracture and concrete breakout best describes the fracture loads, and provides additional information on the expected angle of the failure transition (by the intersection of the curves). This is important if ductile behavior (steel fracture) is required.

Failure loads under pure tension were higher than those in Series 24M54. This means that the edge distance of 5.5 inches (1.57 h_{ef}) in Series 24M54 was not enough to reach the full concrete capacity. The comparison with the interaction for Series 24M54 is shown in Appendix 134. Larger displacements at maximum load were also achieved.

In oblique tension tests at 15°, unfortunately no usable displacement results were obtained, because the bonded Plexiglas plates used as bases broke during the tests.

In the tests at 30°, vertical displacements were larger than under pure tension. The displacements of the tests at 45° are the same as those of Series 23M54 that failed by steel fracture. That interaction of displacements at concrete fracture is approximated by a straight line. It is possible that the displacement values of the oblique tension tests are too high. However, the values agree with Series 23M54, so this is doubtful. Alternatively, the measured displacement values in the pure tension tests might be affected by the scatter. The latter is slightly possible based on the large scatters of these measurements. Correspondingly an estimated straight-line interaction was plotted in the interaction diagram of Appendix 135, with the higher displacements under pure tension. Finally, the mean interaction line is plotted using the displacements of Series 23M54 (steel failure).

3.3.2.3 Mathematical description of load-displacement curves

In the evaluation, the load-displacement curves are mathematically described for the application of the "BDA5" program for computing anchor group behavior under shear and flexural loads. The investigation of average load-displacement curves is required. Both the failure loads and the associated displacements were altered for the determination of average load-displacement curves as described below.

From the data files, the maximum loads were first determined with the load and displacement measured at regular time intervals. The curves were evenly divided into 100 load steps. Within each load step, the associated displacements were obtained by linear interpolation. All load-displacement curves were therefore in the form of a data file of exactly 100 pairs of equal load steps up to the maximum load. For each test series, average load-displacement curves were then calculated by averaging the values of each load step.

The parameters for the mathematical description of curves were then adjusted by eye, using the maximum loads corresponding to the interaction equation and the average failure displacements. In the load-displacement curves (Table 3.10), the mathematical approximation curves are plotted with the designation "curve." The parameters used for each curve equation, and descriptions of the resultant curve group, are plotted in the appendices. Each sub-series is plotted in the appendices given in Table 3.13.

Table 3. 13 *Appendices Where Mathematical Descriptions of Load-Displacement Curves are Given*

Curve Data	Sub-Series							
	23H64	23H74	23M54	23M74	23M53	23M34	24M54	24A54
Curve Parameters	39	56	67	84	95	111	125	136
Plots of Curve Group	40-41	57	68-69	85	96	112	126	137

3.3.2.4 Comparison of the results of sub-series

Figure 3.15 compares the interaction diagram of the failure loads with the mean value curves of all sub-series in Series 2.3. It is apparent from Figure 3.15 that the curves for UC1 (Series 23M54 and 23M53) and the Sleeve Anchor (Series 23H64) are approximately identical. For the tests in concrete of strength 32 N/mm², this expected to the comparable material characteristics of the anchor shanks, and the virtually equal failure displacements under pure tension. In low-strength concrete (f_c = 20.7 N/mm²), however, considerably larger failure displacements occurred, especially under tension. Although this obviously has little influence on the interaction of the failure loads associated with the threaded shank, the displacement behavior under oblique tension is influenced.

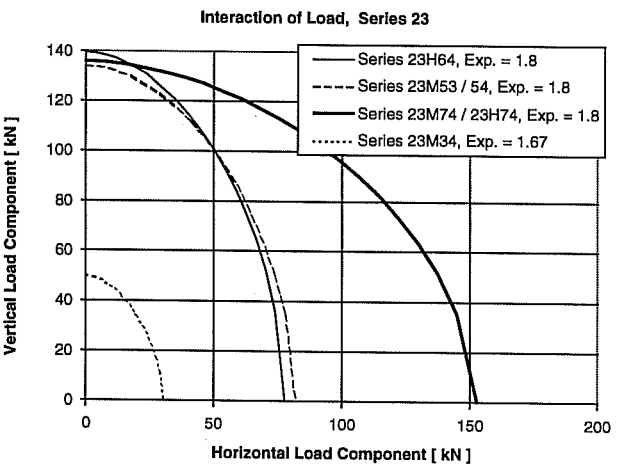

Figure 3. 15 *Interaction diagram of failure loads, Series 2.3, steel fracture*

The average displacement interaction curves of all sub-series in Series 2.3 and 2.4 are shown together in Figure 3.16.

Figure 3.16 shows large displacements in Series 23M53 under tension, approaching the values achieved in higher strength concrete with increased loading angle or increased shear. It also shows good agreement between the values for UC1 and the Sleeve Anchor. On the other hand, essential differences are evident due to the effect of the installation method. Under pure tension, displacements are naturally identical. At small oblique tension angles, the through-sleeve anchor has larger failure displacements than the flush-sleeve anchor. The interaction curve of UC1 of 3/8 inch (Series 23M34, flush-sleeve installation) has generally smaller displacements than UC1 of 5/8 in, but without the distinct maximum displacement at a loading angle of 15°.

Overall, anchors installed with flush sleeves generated smaller shell-shaped concrete spalling in the loading direction in front of anchors. For this reason, they failed under shear and oblique tension by a comparatively small deformation shear fracture of the anchor shank, regardless of the type of anchor. With lower concrete strength, larger displacements was needed at maximum load under tension. These approach the displacements in higher strength concrete with increasing shear. Tests with 3/8-inch anchors showed smaller displacements, and no concrete spalling in front of the anchors, under shear and oblique tension.

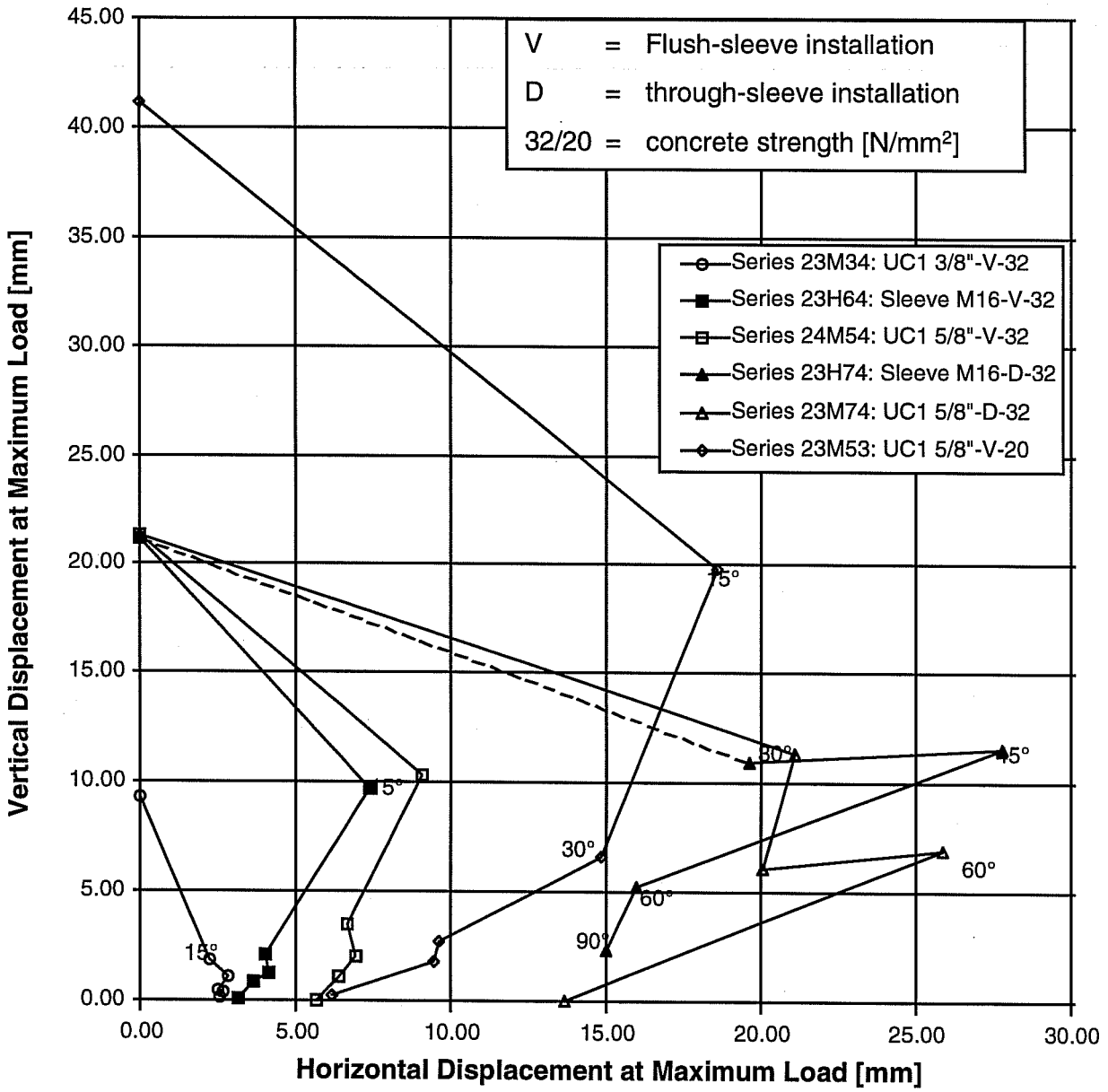

Figure 3. 16 Average displacement interaction curves, Series 2.3

Series 24M54 and 24A54 were evaluated against each other and against Series 2.3 (see Appendices 123,124, 134 and 135).

3.3.2.5 Conclusion of results of Series 2.3 and 2.4

1) The interaction of failure loads for steel failure as well as for concrete failure can be described by an elliptical relation according to Equation (2.4). The exponent for both failure modes lies between p = 1.6 and p = 1.8. In case of different failure modes under tension and shear, the interaction of failure loads can be described very well if the interaction relations for both failure modes are determined separately. The intersection of the interaction curves then denotes the transition angle between the failure modes (Appendix 134).
2) The interaction diagram of displacements as governed by steel failure has a characteristic bulge. Larger horizontal displacements were reached at maximum load under oblique tension than under pure shear (Appendices 38, 55, 66, 83, 94, 110). This is because of the larger shell-shaped spalling that occurs in front of anchors in the loading direction under oblique loading.
3) Depending on concrete strength, anchor size, installation method and loading direction, brittle shear fracture of the anchor shank could occur under load. Lower steel strength, smaller anchor diameter, flush-sleeve installation, and high-strength concrete, all lead to smaller displacements at failure.
4) Ductile fractures are generally achieved if the maximum possible steel strength of the anchor is reached. Therefore, higher-strength, ductile steels and through-sleeve installation are recommended. However, a large edge distance is then required to guarantee sufficient safety against concrete breakout. To achieve ductile failure with smaller edge distances, supplementary hairpins can be used.
5) In tests with steel failure, transverse displacements were smaller in pure shear than under oblique loading, despite the bigger shear force in the pure shear tests.
6) With failure by concrete breakout, interaction of displacements at maximum load can be approximated by a straight line. However, a mathematical interrelation between the loading angles and the position on these straight lines could not be derived from the few test results with concrete breakout.

3.3.3 SERIES 2.5 AND 2.6: LOAD AND DISPLACEMENT BEHAVIOR OF TWO-COMPONENT FASTENINGS UNDER ECCENTRIC SHEAR

In Series 2.5 and 2.6, a two-anchor attachment, with a baseplate that was thick (and therefore presumed rigid), was loaded by eccentric shear. Tests were conducted with eccentricities of 12 in (305 mm) and 18 in (457 mm). To reduce friction, a Teflon sheet was placed between the concrete and the baseplate. In the tests, the horizontal displacement was measured at the back end of the baseplate; vertical displacements were measured at two points. As shown in Figure 3.11 and in Appendices 8 and 9, strain gages were placed at the top and bottom sides of the baseplate in the region between anchors. Key test data and the load and displacement measurements are given in Appendix 145. In Appendix 146 are given the results of the measurement of the shell-shaped concrete spalling in the shear direction in front of the anchors. Table 3.14 is a repetition of the most important results of Series 2.5 and 2.6; the displacement at the center of the baseplate and the rotation were calculated from the vertical displacement

Table 3. 14 Summary of Results of Series 2.5 and 2.6

Test No.	Anchor	Embed Depth, mm	Torque, Nm	Concrete f_c, N/mm^2	Failure F_u[2] kN	H. Displ. $d_{H,u}$, mm	V. Displ. $d_{V,u}$, mm	Rotation deg.	Gaps L[3] mm	Failure[4] mm
25H6421	Sleeve M16	178	203/102	34.9	109.55	5.72	1.65	1.50	1.00	SB
2	Sleeve M16	178	203/102	34.9	110.35	5.31	5.19	2.71	-1.20	SS
3	Sleeve M16	178	203/102	33.8	111.50	5.50	3.19	1.63	0.60	SS
Average					110.46					
25H6481	Sleeve M16	178	203/102	33.8	79.89	5.90	6.56	3.31	1.50	SZ
2	Sleeve M16	178	203/102	33.8	77.93	5.92	5.94	2.95	0.10	SZ
3	Sleeve M16	178	203/102	33.8	77.92	4.18	4.49	2.24	-1.20	SZ
Average					78.58					
25M5421	UC1 5/8	178	244/122	34.9	106.50	7.42	3.35	2.22	1.20	SS
2	UC1 5/8	178	244/122	34.9	110.27	7.01	6.24	2.73	-1.40	SS
3	UC1 5/8	178	244/122	33.8	114.30	9.66	7.77	3.52	1.60	SZ
Average					110.36					
25M5481	UC1 5/8	178	244/122	34.9	78.95	5.13	8.36	3.99	-1.20	SZ
2	UC1 5/8	178	244/122	33.8	78.39	7.95	8.40	4.30	0.60	SZ
3	UC1 5/8	178	244/122	33.8	87.87	6.73	9.79	5.90	-0.20	SZ
Average					81.74					
25M3421	UC1 3/8	89	54/27	34.9	36.16	3.88	0.79	0.48	1.00	SZ
2	UC1 3/8	89	54/27	34.9	35.27	MD[5]	0.89	0.50	-2.00	SS
3	UC1 3/8	89	54/27	34.9	39.45	4.63	1.82	1.10	1.00	SZ
Average					36.96					
25M3481	UC1 3/8	89	54/27	34.9	26.11	2.66	0.40	0.66	1.50	SZ
2	UC1 3/8	89	54/27	34.9	28.07	3.49	1.05	0.48	1.25	SZ
3	UC1 3/8	89	54/27	34.9	28.16	3.28	1.16	0.87	1.00	SZ
Average					27.44					
26M5421	UC1 5/8	89	203/122	41.8	74.22	2.97	1.47	0.42	0.80	BZ
2	UC1 5/8	89	203/123	34.2	69.84	2.74	0.99	0.85	-1.20	BZ
3	UC1 5/8	89	203/124	34.2	69.49	3.61	0.66	0.72	-0.40	BZ
Average					71.18					
26M5481	UC1 5/8	89	203/122	41.8	53.49	2.77	1.36	0.70	-0.30	BZ
2	UC1 5/8	89	203/123	41.8	47.01	2.64	1.44	0.55	0.20	BZ
3	UC1 5/8	89	203/124	34.2	47.71	3.50	0.52	0.50	-1.60	BZ
Average					49.40					

1) UC1 = undercut anchor, sleeve = torque controlled expansion sleeve anchor
2) The values for Series 2.6 with concrete failure were normalized by $\sqrt{f_c}$ (f_c = 32.4 N/mm^2)
3) Gap before installing nuts: (+) for gaps of shear anchors, (-) for gaps of tension anchors
4) SZ = steel fracture at tension anchors, SS = steel fracture at shear anchor, SB = steel fracture at both anchors simultaneously, BZ = concrete fracture at tension anchors
5) Crack occurred at the near-edge shear anchors during application of the torque
6) MD = measurement failure

measurements. Mean failure loads are given. The calculation of mean deformation data was abandoned, because the results for each test depend on the hole tolerances and gaps for that test.

As shown in Table 3.14, despite the differences in gaps between anchors and baseplates among specimens, the failure loads within each single test series showed only a slight scatter. However, considerable scatter was observed in displacements, without any obvious correlation with the measured gaps.

However, the gaps did significantly affect the failure mode. In the tests with an eccentricity of 18 in (457 mm), failure always occurred by fracture at the outermost tension anchor. In the tests with an eccentricity of 12 in (305 mm) in Sub-series 25H642, 25M542, and 25M342, the shear anchors also fractured. In these three sub-series, failure by fracture of the tension anchor occurred only with the largest positive gaps, that is, with maximum gaps of the shear anchors.

Diagrams of the measured displacements, as well as the normal force and bending moment in the baseplate calculated from the strains, are included in Appendices 147 - 164 (Series 2.5) or 165 - 170 (Series 2.6). Post-test photos of the specimen and of the anchors are given in Appendices 171 to 179 for Series 2.5, and in Appendices 180 to 182 for Series 2.6. Table 3.15 shows the Appendices in which results are given for each sub-series.

The graphs of the normal force and bending moment in the baseplate, plotted in the lower diagram in Appendices 147 - 170, were calculated from the results of the strain measurement. Typical results of strain measurement (for Test 25H6423) is plotted in Figure 3.17.

The measurement show that strains are approximately constant over the width of the baseplate, due to its configuration. The large initial strains, of different signs in the top versus the bottom of the baseplate, indicate the bending moment created by the anchor preload. This can be predicted from the strains using Equation (3.3).

$$M = W \cdot \sigma_B = W \cdot E \, (\varepsilon_{top} - \varepsilon_{bottom}) / 2 \qquad (3.3)$$

where W is the section modulus of baseplate, and E is the elastic modulus of steel (2.1×10^6 N/mm^2).

The normal force in the baseplate, equal to the shear in the tension anchor, is given by Equation (3.4):

$$N = A \cdot E \cdot (\varepsilon_{top} + \varepsilon_{bottom}) \qquad (3.4)$$

where A is the cross-sectional area of the baseplate.

Table 3. 15 Contents of Appendices for Different Sub-Series of Series 2.5 and 2.6

	Appendix for Sub-Series							
	25 H642	25 H648	25 M542	25 M548	25 M342	25 M348	26 M542	26 M548
Result Charts	145-146	145-146	145-146	145-146	145-146	145-146	145-146	145-146
Load-displacement curves and force curves	147-149	150-152	153-155	156-158	159-161	162-164	165-167	168-170
Photos of failure states	171	172-173	173-174	174-175	176	176	180-181	181-182
Photos of anchor bolts after tests	177	177	178	178	179	179	182	182

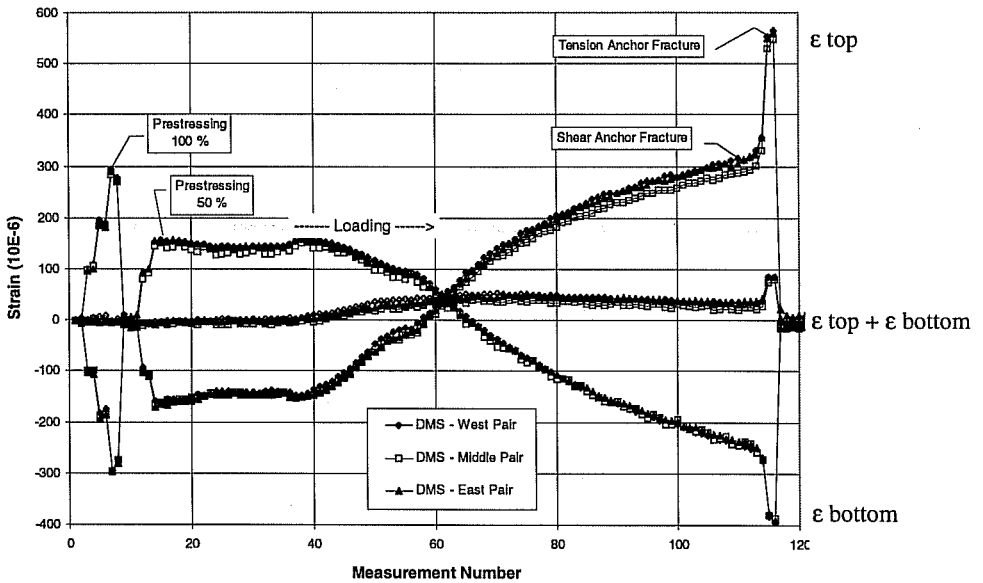

Figure 3. 17 *Strains in Test 25H6423, M16 Sleeve, h_{ef} = 7 in. (178 mm), e = 12 in. (305 mm)*

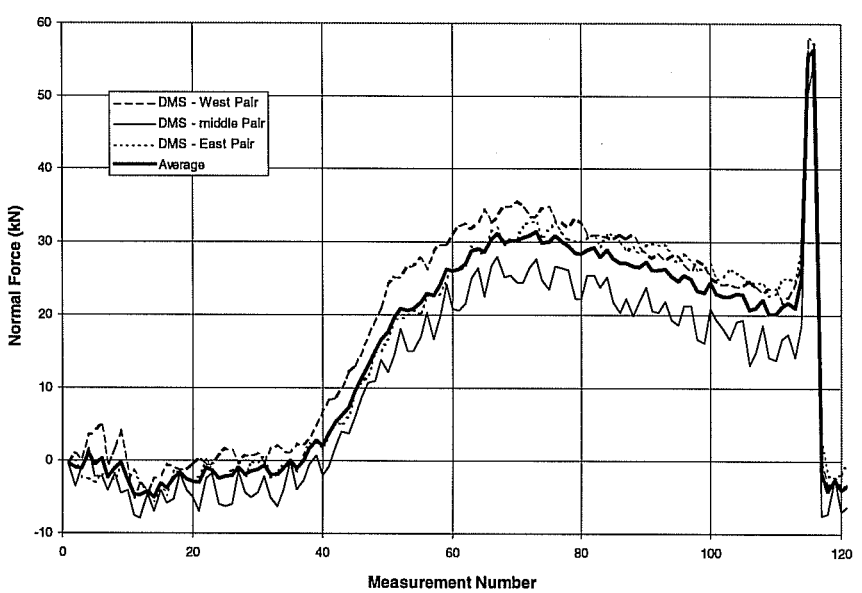

Figure 3. 18 *Normal force in baseplate, calculated separately for each strain-gage pair, Test 25H6423, M16 Sleeve Anchor, h_{ef} = 7 in. (178 mm), e = 12 in. (305 mm)*

The relatively small value of ($\varepsilon_{top} + \varepsilon_{bottom}$) is the summation of the differences between the comparatively large absolute values of the top and the bottom strains. It is therefore sensitive to scatters and inaccuracies of the measured strain value. The normal forces, calculated separately for each of the three pairs of strain gages, have saw-toothed curves and spaced relatively far apart. Figure 3.18 shows this with an example of Test 25H6423. Since all strain-gage pairs provide essentially the same results, the average force (that eliminates the scatter) is only marginally affected.

Figure 3.19 shows the diagram of the forces and bending moment in Test 25H6423, as plotted for each test in the Appendices. The notation "L = + 0.6 mm" denotes a gap of about 0.6 mm in the hole of the baseplate at the shear anchor. As shown in the figure, the normal force in the baseplate (equal to the shear in the tension anchor) increases with the applied load. After the gap at the shear anchor is overcome, this increase slows, and the normal force even decreases at the end. When the shear anchor fractures, the normal force increases abruptly, because the applied shear must then be resisted entirely by the tension anchor.

The hogging bending moment in the baseplate (tension stress on top) decreases with increasing external load, changing finally to a reversed moment caused by a combination of the diagonal compression (at the height of the axis of the shear anchor) and the support reaction from the concrete at the compression edge of the baseplate. The fracture of the shear anchors causes an additional negative moment, which stems from the additional shear force of the tension anchor, applied eccentrically to the bottom edge of the baseplate.

Post-failure photos of the tests of Series 2.5 (Appendices 171 to 176) show generally larger concrete spalling in front of the tension anchors than in front of the shear anchors. This agreed with the results of Series 2.3 overall, in which more spalling was expected at small oblique tension angles. From the photos as well as from measurements of spalling (Appendix 146), the size and depth of the spalling were not

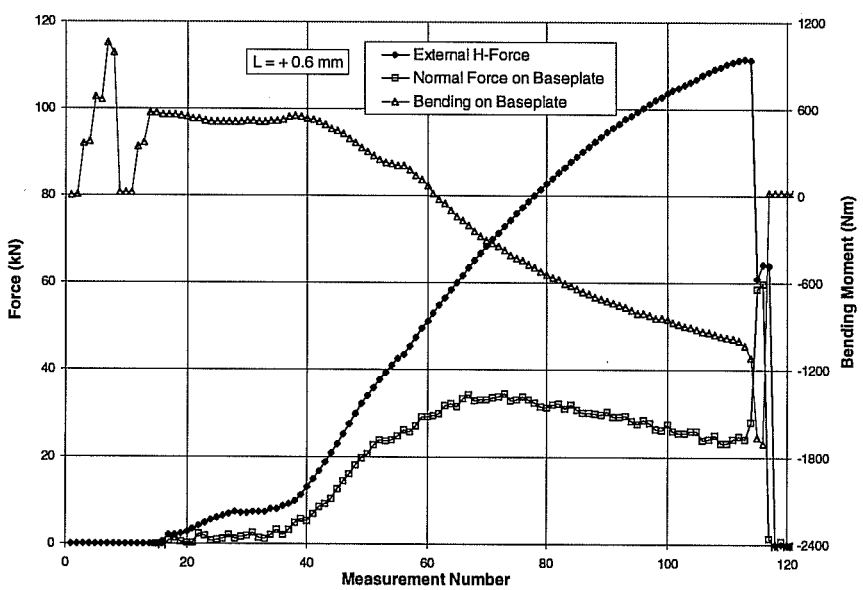

Figure 3. 19 Force and bending moment of Test 23H6423, M16 Sleeve, h_{ef} = 7 in. (178 mm), e = 12 in. (305 mm)

influenced by the load eccentricity nor the anchor type (UC1 versus Sleeve). However, anchor diameter had a significant effect. The 3/8-inch UC1 showed spalling in only two tests, and these spalls were only 3 to 5 mm deep.

In the photos in Appendices 177 to 179, plastic deformation or a fracture necking is clearly visible in almost all shanks of the broken tension anchors. This points out the ductile fracture behavior of these anchors. On the other hand, the shanks of the shear anchors consistently show small-deformation shear fracture. This confirms the results of Series 2.3, in which under pure shear or at an oblique tension angle of greater than 15° to 30°, anchor deformation is small even with steel failure.

The results of Series 2.5 and 2.6 are of additional use both for comparison with the calculation results of the BDA5 program, and for evaluating the comparative merits of elastic and plastic theory as applied to multiple-anchor connections. These are the subjects of the next section of this report.

CHAPTER 4

ADDITIONAL INVESTIGATIONS

4.1 Scope of Additional Investigations

The investigations described below include extensive calculations of the capacity of anchor groups under shear and bending, performed according to the following procedures:

- elastic theory
- plastic theory
- load-displacement curves with the program "BDA5"

These procedures are explained in Chpater 2 of this report. Elastic and plastic methods use approximations of idealized material behavior. The program "BDA5" uses load-displacement curves. How close the results are to the real behavior of anchor groups depends on how accurate the curves are. The extensive tests on single anchors, and the interpretation of Section 3.3 (mathematical description of load-displacement curves) provide a good basis for calculations using those load-displacement curves. All calculations with the BDA5 program are based on the results of Series 2.3 and 2.4 (load-displacement behavior of single anchors).

The tests on two-anchor connections under shear and bending (Series 2.5 and 2.6), carried out under the same conditions as the single-anchor tests, offer the possibility of verifying the calculation results against test data. In those tests the distribution of shear among anchors was inferred from strain measurements on the baseplate. Extensive displacement measurements were also recorded. Those results permit detailed comparison with the calculation results of the BDA5 program. The arrangement of Test Series 2.5 and 2.6 therefore serves as a basis for a clear comparison between test results and computations.

Cook (1989) cites tests on anchor groups with 1 to 3 anchor rows, under eccentric shear. The same type of anchors used in those tests were used in some of the tests described in this report. The tests of Cook could therefore also be compared with BDA5 calculations. The displacement behavior of single anchors must be adjusted only slightly to supply the basis for such computations.

4.2 Calculated results for anchor groups (Series 2.5 and 2.6)

These sections include calculations for the tests of this study on two-anchor connections under shear and bending, as well as additional calculations with other shear eccentricities. By comparing the calculated results with the test results, a secure basis is laid for further investigation.

4.2.1 INPUT PARAMETERS FOR CALCULATION

4.2.1.1 Friction Coefficient

In Series 2.5 and 2.6, a Teflon sheet was laid between the baseplate and the concrete to reduce friction, as in Series 2.3 and 2.4. Friction coefficient (considering the Teflon sheet) must be known for the test computations. To determine this value, the shear tests in Series 2.3 and 2.4 were evaluated. In these tests, the start of baseplate sliding can be inferred from the load-displacement curves. The prestressing force could also be calculated. An average value of $\mu_G = 0.15$ was used for the screw-thread friction. The friction coefficient can then be calculated by:

$$\mu = (\text{load at sliding} / F_V) \tag{4.1}$$

where: the prestressing force $F_V = M_D / (\mu_G \cdot d_G)$; the torque M_D is associated with two prestressing forces, each at 50% of the specified torque); μ_G is the friction coefficient of threads; and d_G is the diameter of the threads

From the 15 tests in which the start of sliding could be read with sufficient accuracy, the mean value was:

$$\mu = 0.10 \tag{4.2}$$

with a coefficient of variation of 38%. This value was used for the calculations with the BDA5 program as well as for the elastic and plastic calculations.

4.2.1.2 Center of rotation of the baseplate

The baseplate used in the tests extends 2 inches (50.8 mm) past the anchor axes at both ends. It was beveled at the compression end over a length of about 42 mm, at an angle of 5°, so that the compression-side anchors would be free of prying tension.

For small rotations, the location of the resultant compression can be assumed at the edge of the bevel. This assumption is correct for baseplate rotation of up to 2.5° (Figure 4.1a). The distance of the compression resultant from the shear anchor is therefore:

$$z_2 = 9 \text{ mm} \tag{4.3}$$

When the baseplate rotation approaches the angle of the bevel, the bearing condition changes. The location of the compression resultant is estimated as shown in Figure 4.1b. In this case, the overall extension length is 52 mm (about 2 in):

$$z_2 \approx 9 \text{ mm} + (51 - 9) / 2 = 30 \text{ mm} \tag{4.4}$$

The rotation of the baseplate reached 5° only in Series 25H648 and 25M548. The calculations for these series were carried out both with the location of the compression resultant according to Figure 4.1a, and with the location according to Figure 4.1b.

For computation with the BDA5 program, the location of the compression edge of the baseplate is required. The program calculated the magnitude of h_D from the compression edge h_D = height of the compression zone. Assuming a triangular stress distribution, the compression resultant is located at distance $h_D/3$ from the compression edge. A clearly defined compression edge does not exist due to the

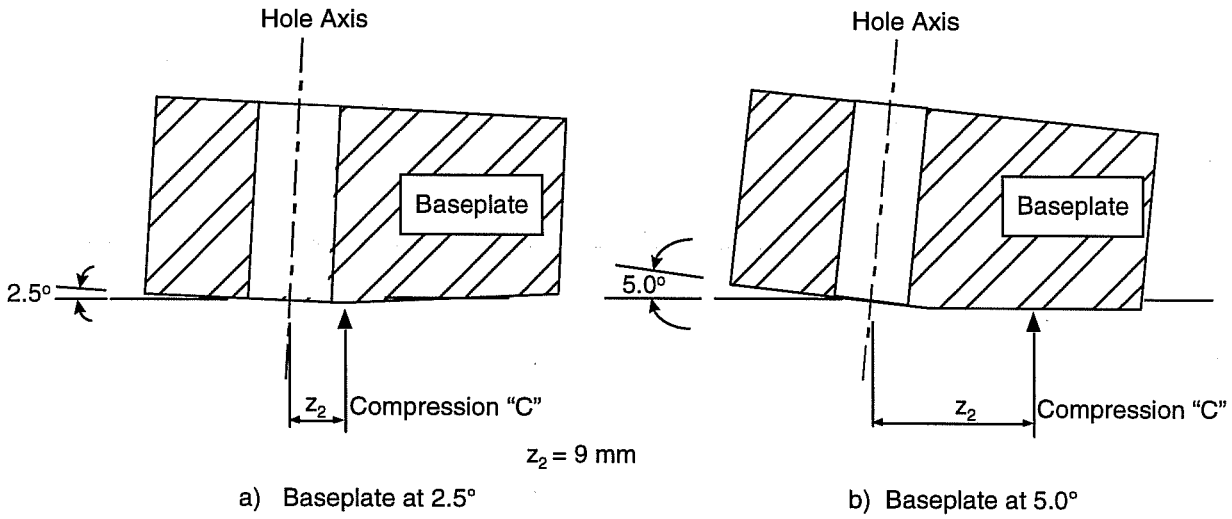

Figure 4. 1 Location of the resultant compression between the baseplate and the concrete

bevel at the end of the baseplate. As a simplification, it is therefore assumed that the compression resultant located in accordance with Figure 4.1, coincides with the compression edge. The internal lever arm of the connection was therefore under-estimated by $h_D/3$.

To get correct values for the vertical displacement at the center of the baseplate in the output of the results of the BDA5 program, the length L_P of the baseplate must be input different from the actual values:

$$L_P = s + 2\, z_2 \qquad (4.5)$$

where: s (anchor spacing) is 10 inches (254 mm). That is, for the extension length on the tension side of the baseplate the same value was input as for the compression side. This influenced only the interpretation of the output data, not the program calculations themselves.

4.2.1.3 Other input parameters

In the BDA5 program, the values in the preceding section were used for the spacing of the anchor from the compression edge on the baseplate. The width of the baseplate in the compression region is:

$$D_P = 8 \text{ inches} = 203.2 \text{ mm}. \qquad (4.6)$$

The values for the interaction of loads and for the load-displacement curves were already specified based on interpretation of tests on single anchors (see Table 3.13 for the appendix assignments).

Appendices 183 and 184 show, for purposes of illustration, the complete input file for the calculation of a connection corresponding to Test Series 25H642, with a gap of 3.0 mm at the shear anchor (L = +3.0 mm). The data are briefly explained in several document lines. Further explanations regarding input and output data files, program control, etc., are included by Li (1994). The basic method of calculation is formulated by Eligehausen and Li (1993).

4.2.2 OVERVIEW OF CALCULATION RESULTS

Results for all tests of Series 2.5 and 2.6 were compared with calculations using elastic theory, plastic theory, and the BDA5 program based on load-displacement curves determined from Series 2.3 and 2.4). The following obervations were made:

1. **Maximum load**: The maximum load was plotted as a function of the loading eccentricity, "e." The plots were first drawn as normalized by the pure tensile strength of a single anchor (V_u /$F_{Z,u,0}$), and then as normalized by the elastically calculated failure load of the group ($V_{u,...}/V_{u,el}$). This permits the results to be compared independent of the actual failure loads of single anchors or anchor groups. To study the influence of loading eccentricity over a large range, the maximum loads for other eccentricities were also calculated. To better determine the discontinuity at the transition of the failure from the shear anchors to the fracture of the tension anchors, calculations in this range were conducted at closer intervals. The graphs also show the test results.
2. **Load distribution**: The distribution of shear influences the bearing behavior of an anchor group mainly by how much shear is carried by the tension anchors, and by the associated reduction in the strength and deformation capacity of those anchors. The loading history of the tension anchor was therefore plotted in the interaction diagram of forces. On the left diagram the test result was plotted; on the right, the results of the BDA5 calculation.
3. **Displacement behavior**: The horizontal and vertical displacements, the rotation of the baseplate, and the vertical displacement at the tension anchor (calculated and observed) were plotted in the form of load-displacement or load-rotation curves.

The results are summarized in Appendices 185 to 214 for all four test series. Table 4.1 gives an overview of those appendices.

Table 4. 1 Assignment of Calculation Results to Appendices and Reference to the Sub-Series of Tests

Diagram Type	Sub-series							
	25 H642	**25 H648**	**25 M542**	**25 M548**	**25 M342**	**25 M348**	**26 M542**	**26 M548**
Relative failure load with "e"	185 - 186		193 - 194		201		208	
Load history of tension anchor	187	190	195	198	202	205	209	212
Load-displacement behavior	188-189	191 -192	196 - 197	199 - 200	203 - 204	206 - 207	210 - 211	213 - 214

4.2.3 LOCATION OF RESULTANT COMPRESSION

The location of the resultant compression between the baseplate and the concrete, together with the anchor layout, determines the internal lever arm of the anchor group under bending moment. For the calculations according to the elastic and plastic theories, the line of action of the resultant is assumed (for simplicity) at the compression edge of the baseplate. On the other hand, in the program BDA5, the

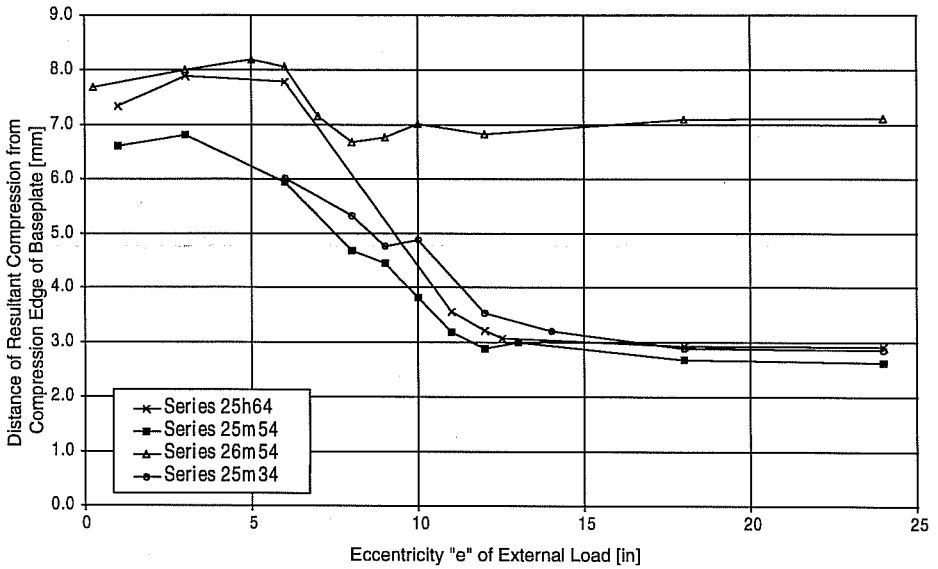

Figure 4. 2 *Distance of the resultant compression from the compression edge of the baseplate at maximum load according to BDA5, z_1 = 263 mm, z_2 = 9 mm*

location was predicted based on the results of the compressive contact area of the concrete (Lieberum, 1987, 1990; Furche, 1992).

For anchor groups in Series 25 and 26, the distance of the compression resultant from the compression edge of the baseplate at maximum load was plotted in Figure 4.2 as a function of the external eccentricity, "e." In Series 25 with steel failure at e > 12 inches (300 mm), the compression resultant from the compression edge was at most 3 mm, about 1.2% of the overall internal lever arm. The expected influence of this distance on the strength of the anchor group is therefore less that 1.5%. At very small eccentricities (e < 5 in, or 125 mm) the distance of the resultant compression from the compression edge is up to 7 mm. However, in these cases the flexural strength of the connection does not govern the maximum load. However, in Series 26 with concrete breakout, the spacing of the resultant compression from the compression edge at e = 25" is also about 7 mm. This signifies an computed strength as much as 3% smaller than that given by elastic or plastic theory. In this case, the program BDA5 program better described the actual situation.

In discussing the input parameters the effect of the bevel of the compression edge of the baseplate, and the effect of large baseplate rotations, should again be noted. The BDA5 program used corrected values for z_2, not just the extension length of the baseplate. Correspondingly, the program calculated a different position of the resultant compression. The discrepancy is tolerable in this case, because it has little influence.

4.2.4 Agreement between Test Results and Calculations with Load-Displacement Curve: Importance of Gaps

The calculations based on load-displacement curves were compared with the individual test results. This is because the results are not restricted to failure loads as with the other procedures, but also include the load distribution among the anchors of the group, the influence of gaps between anchors and the holes in the baseplate, and the deformation history.

In Series 2.5 and 2.6 on two-anchor connectors, despite the use of drilling templates, gaps always existed between the baseplate holes and the anchors. In assessing the agreement between calculations and tests, these gaps are significant. The gaps in the tests were estimated the distance between the hole in the insert and anchor shank, and were documented. Additional gaps between the anchor shank and the anchor sleeve, as well as between the anchor sleeve and wall of the hole in the concrete, could not be determined. The measurements are therefore only an estimate of the actual gaps.

The gap always influences the bearing behavior of anchor groups, if friction is insufficient to transfer shear. The biggest influence of the gap is on near-edge anchors that fail by edge breakout. Therefore, in European design procedure for calculating the capacity of two-anchor connections placed perpendicular to a free edge, the shear capacity of only the near-edge anchor is considered. For anchor groups far from an edge, and failing by fracture of the anchor shank or by concrete breakout of the tension anchor, the influence of the gaps is surely smaller, but still esits. Nevertheless, in European (elastic) design procedures for connections far from an edge, the effect of the gap is neglected. In other words, when using the elastic design approach, plastic deformation capacity is implicitly relied on.

In previous studies of design by plastic theory, the problem of the gap was not addressed. It was assumed that gap effects would be reduced by plastic redistribution. In each case the plastic deformation demand on the anchors is increased by the gap.

In the following investigations, the following limiting cases were considered for the gap between the anchor and the insert:

1) a gap of 3 mm at the tension anchor (L = - 3.0 mm);
2) no gap (L = 0); and
3) a gap of 3 mm at the shear anchor (L = + 3.0 mm).

The estimated gap of 3.0 mm is larger than those measured at the baseplate in tests. This permits the effects of the gap to be clearly evident in the calculation. According to UEAtc (1992), the maximum allowable gap between the anchor shank and the hole in the baseplate is 2.0 mm (for anchor diameters of 10 to 24 mm). Considering the possible gap between the anchor shank and the anchor sleeve, as well as between the anchor sleeve and the concrete, the assumed 3.0-mm gap is a reasonable upper limit

In Table 4.2, the test results are arranged according to the gaps measured in the tests, and effect of gaps on the calculation results is assessed.

Table 4.2 shows that the maximum loads achieved in tests coincide very well with the values calculated by the BDA5 program, especially when the mean test value is compared with the calculated value for the average situation (L = 0), thereby neglecting the extreme deviations caused by large gaps. The use of a greater length of the baseplate (z_1 = 284 mm, z_2 = 30 mm instead of z_1 = 263 mm, z_2 = 9 mm) leads to

higher calculated failure loads under the same conditions. This proves meaningful for Series 25H648 and 25M548, which had larger rotations of the baseplate, and observed capacities closer to the values calculated with the larger extension length. In tests with UC1 (25M548), even the rotation of 5° was exceeded, and so was the calculated failure load.

The influence of gaps on the distribution of forces in the connection can be better followed using the measured strains in the baseplate. Using those strains, the normal force and the bending moment in the baseplate, and the load on the tension anchor, can be calculated. The development of the tension force was plotted in the force interaction diagram. The plots for the tests as well as for the calculated results are included in Appendices 187, 190, 195, 198, 202, 205, 209, and 212 (see Table 4.1).

The load history of the tension anchor calculated using the large gap values clarifies tendencies which can already be observed from the test results themselves. This leads to the following conclusions:

- If there is little or no difference between the gaps in front of anchors, the loading curves are virtually straight. In other words, there is little or no load redistribution even near yield.

- Gaps at the tension anchors first keep those anchors free of shear. After the gaps close, the tension anchor takes on shear relatively quickly. Depending on the size of the gap, the initial deviation is thereby partially eliminated.

- Positive gap (that is, a gap at the shear anchor) causes first of all a clearly flatter loading curve (that is, more shear is carried by the tension anchor). After the gap closes, the tension anchor is released from incremental increases in shear by the relatively stiff behavior of shear anchors (steep slope of the load-displacement curve near the origin). With a sufficiently large difference between the initial gaps and failure displacement, compensation is largely made for the effect of the gap.

- In the calculations for Series 25M34 with UC1 of 3/8 inch (approximately M10), the anchors with an assumed 3-mm gap are not activated in shear at any time, because the displacements at failure in shear are less than 3 mm. This confirmed analytically the very significant influence of the gap on the failure loads. In the tests, the influence of the gap is clearly evident. However, the effects are less pronounced than in the calculation because the gap is smaller.

- In the calculations for Series 26M54 (UC1 of 5/8 inch failing by concrete breakout), because the failure displacements are relatively small, the effect of initial gaps cannot be as extensively compensated for as in the test series with steel fracture. However, before failure, all anchors carry shear. This is basically because failure occurs by concrete breakout of the tension anchor rather than by concrete edge breakout due to shear of the near-edge anchor, in calculations as well as in tests. The tests show only modest gap differences. Nevertheless, the observed trends confirm the calculation results.

The loading curves clearly show the effect of the gap on the distribution of shear within the connection. The calculation based on load-displacement curves of single anchors impressively confirms that a good description of the behavior of an anchor group is possible, and therefore suitable for parametric studies of the maximum loads and load distribution.

Table 4. 2 *Comparison of Failure Load Displacement at Failure and Failure Mode in Calculation Tests*

Test No.	Anchor [1]	Test Results						Calculation Results					
		Gap [2] mm	Failure F_u [3] kN	Hor. Dspl. $d_{H,u}$ [4] mm	Ver. Dspl. $d_{V,u}$ mm	Rot. Deg.	Failure Mode [5]	Gap [6] mm	Failure F_u kN	Hor. Dspl. $d_{H,u}$. mm	Ver. Dspl. $d_{V,u}$ mm	Rot.. deg.	Failure Mode [5]
25H6422	Sleeve M16	-1.20	110.4	5.31	5.19	2.71	SS	-3	90.6	3.18	4.10	1.88	SS
3	Sleeve M16	0.60	111.5	5.50	3.19	1.63	SS	0	108.5	3.28	6.76	3.07	SS
1	Sleeve M16	1.00	109.6	5.72	1.65	1.50	SB	+3	108.1	5.47	6.10	2.78	SZ
Ave.			**110.5**	5.51					**102.4**				
25H6483	Sleeve M16	-1.20	77.9	4.18	4.49	2.24	SZ	-3	79.5	2.53	10.59	4.76	SZ
2	Sleeve M16	0.10	77.9	5.92	5.94	2.95	SZ	0	77.0	1.80	8.90	4.01	SZ
		Calculation with z2 = 30 mm:						0	86.4	2.62	8.83	3.5	SZ
1	Sleeve M16	1.50	79.9	5.90	6.56	3.31	SZ	+3	74.0	4.16	7.21	3.27	SZ
Ave.			**78.6**						**76.8**				
25M5422	UC1 5/8	-1.40	110.3	7.01	6.24	2.73	SS	-3	107.0	5.88	6.82	3.15	SS
1	UC1 5/8	1.20	106.5	7.42	3.35	2.22	SS	0	107.9	4.91	7.33	3.38	SZ
3	UC1 5/8	1.60	114.3	9.66	7.77	3.52	SZ	+3	105.2	6.83	6.31	2.92	SZ
Ave.			**110.4**						**106.7**				
25M5481	UC1 5/8	-1.20	79.0	5.13	8.36	3.99	SZ	-3	75.8	3.35	10.02	4.58	SZ
3	UC1 5/8	-0.20	87.9	6.73	9.79	5.90	SZ	0	74.1	2.54	8.74	4.01	SZ
		Calculation with z2 = 30 mm:						0	83.0	3.68	8.86	3.5	SZ
2	UC1 5/8	0.60	78.4	7.95	8.40	4.30	SZ	+3	72.1	4.81	7.46	3.44	SZ
Ave.			**81.7**						**74.0**				
25M3422	UC1 3/8	-2.00	35.4	n.g.	0.89	0.50	SS	-3	34.0	2.57	0.73	0.36	SS
3	UC1 3/8	1.00	39.5	4.63	1.82	1.10	SZ	0	38.7	1.73	1.97	0.92	SZ
1	UC1 3/8	1.00	36.2	3.88	0.79	0.48	SZ	+3	25.0	2.69	0.39	0.19	SZ
Ave.			**37.0**						**32.6**				
25M3483	UC1 3/8	1.00	28.2	3.28	1.16	0.87	SZ	-3	28.6	1.64	5.04	2.29	SZ
2	UC1 3/8	1.25	28.1	3.49	1.05	0.48	SZ	0	27.1	0.94	3.38	1.55	SZ
1	UC1 3/8	1.50	26.1	2.66	0.40	0.66	SZ	+3	20.9	2.73	0.71	0.34	SZ
Ave.			**27.4**						**25.5**				
26M5422	UC1 5/8	-1.20	69.8	2.74	0.99	0.85	BZ	-3	76.4	3.48	0.80	0.40	BZ
3	UC1 5/8	-0.40	69.5	3.61	0.66	0.72	BZ	0	75.3	2.10	0.87	0.43	BZ
1	UC1 5/8	0.80	74.2	2.97	1.47	0.42	BZ	+3	71.4	3.79	0.85	0.42	BZ
Ave.			**71.2**						**74.4**				
26M5483	UC1 5/8	-1.60	47.7	3.50	0.52	0.50	BZ[7]	-3	50.9	1.70	0.80	0.40	BZ
1	UC1 5/8	-0.30	53.5	2.77	1.36	0.70	BZ	0	50.8	1.24	0.80	0.40	BZ
2	UC1 5/8	0.20	47.0	2.64	1.44	0.55	BZ	+3	48.5	3.15	0.81	0.40	BZ
Ave.			**49.4**						**50.1**				

[1] UC1 = undercut anchor, Sleeve = torque-controlled expansion sleeve anchor

[2] Visible gap between anchor shank and baseplate before mounting of nuts: (+) for gap of the shear anchor, (-) for gap of the tension anchor; the current anchor is different because of the walls of hole

[3] The values for the Series 2.6 with concrete failure were normalized by $\sqrt{f_c}$ to f_c = 32.4 N/mm².

[4] The test value included additional displacements from regular gaps of both anchors; the calculation value did not include them.

[5] SZ = steel fracture at tension anchor, SS = steel fracture at shear anchor, SB = steel fracture at both anchor simultaneously, BZ = concrete fracture at tension anchor

[6] overall gaps. For sign, see [2]

[7] During the prestressing of the near-edge shear anchor, a splitting crack appeared; failure was still by concrete breakout of the tension anchor.

The deformations at failure (Table 4.1) are quite variable, and are of limited usefulness in evaluating the effects of gaps. This is because of the high scatter, the small numbers of tests, and the inexact gap measurements in the tests.

For better studies of the deformation of anchor groups, the calculated and measured load-displacement curves for the horizontal and vertical displacement and the rotation of the baseplate as well as the vertical displacement at the tension anchor, are therefore plotted in the Appendices as listed in Table 4.1.

The horizontal displacements measured in the tests are expected to exceed the calculated ones. This is because the calculations did not include the case in which gaps appeared at both anchors. According to the experiences of Series 2.3 and 2.4, and based on the evaluation of the load versus horizontal displacement curves of Series 2.5 and 2.6, gaps did exist at both anchors in most tests. However, the most significant possibility is gaps between the anchor shank and the anchor sleeve, and between the anchor sleeve and the concrete, in addition to the observed gap between the anchors and the walls of the holes in the baseplate.

For the vertical displacements and the rotations of the baseplate, good agreement exists between the measured and the calculated load-displacement curves. However, the scatter was considerable, especially in Series 25H64 and 25M54 with anchor sizes of 5/8 inch (M16) and steel failure. This was due to the large scatters in the displacements of single anchors, the uncertain influence of the shell-shaped spalling, and the extreme dependence of the displacement on the loading angle in the range of 0° to 30° from the anchor axis.

In summary, calculation based on load-displacement curves provides a very good description of the bearing behavior of anchor groups, and provides a way to investigate the influence of factors thus far neglected, such as unequal gaps at individual anchors.

The calculations and tests show that with the anchor sizes of 5/8" (M16) and failure by steel fracture, the effects of initial gap are overcome. With concrete failure, and for small diameter anchors failing by concrete or steel, this effects of gaps can conceivably not be overcome, due to the small displacements at failure. Regulations regarding the maximum permissible gap must therefore address the effect of anchor diameters, and must treat near-edge anchors separately.

4.2.5 MAXIMUM LOAD AT VARIOUS LOADING ECCENTRICITIES "E:" CALCULATIONS VERSUS TEST RESULTS

The results of calculations are plotted in Appendices 185 through 186, 193 through 194, 201, and 208 for each individual test series. The plots of normalized maximum loads ($V_u/F_{Z,u,0}$ or $V_{u,...}/V_{u,el}$) over the range of loading eccentricities, e, permits comparisons among test series independent of the failure load of the anchors used.

Besides the calculations of the tests, calculations were carried out with many values of eccentricity "e," using especially fine increments of "e" to better show discontinuities in the region of transition from the failure of shear anchors to the fracture of tension anchors.

First of all, some common characteristics of results are discussed:

The failure load V_u of the group increases at small eccentricities from that corresponding to pure shear (e = 0). This is due to friction between the baseplate and the concrete. The additional shear transferred by friction initially exceeds the reduction in shear strength of anchors caused by the additional tension. With further increases in eccentricity, however, the external shear capacity clearly decreases, because the tension anchors resist less shear. In this region the failure loads estimated by plastic theory clearly exceed those calculated by elastic theory. The difference between the two theoretical curves is greatest at moderate eccentricity of about 12 inches (300 mm), and decreases to zero at very large eccentricities. This becomes clear in the lower diagrams in Appendices 185, 186, 193, 194, 201, and 208, in which the failure loads, normalized by the elastically calculated values, are plotted as a function of the eccentricity "e." Within the tested anchor groups, shear redistribution is possible. However, tension load redistribution was obviously precluded because only one anchor was present in the tension zone. When the anchor group is loaded predominantly by moment, the calculation procedures give approximately the same failure loads.

The tests were conducted in the region where the maximum shear redistribution occurred, that is, at eccentricities where the differences between the failure loads by elastic theory and by plastic theory were comparatively large. The maximum loads measured in tests generally lay between these extreme values, as did the calculation results achieved by applying load-displacement curves (BDA5), which coincide well with the observed failure loads.

The location of the line of action of the compression resultant between the baseplate and the anchor base has a significant influence on the internal lever arm, and therefore on the failure load of the anchor group. As explained in Section 4.2.1.2, at rotation angles of the baseplate greater than 2.5°, the compression resultant moves quickly to the edge of the baseplate, increasing the internal lever arm of the connection. Baseplate rotations exceeding 2.5° were reached only in Series 25H64 and 25M54, and always with the larger loading eccentricity of 18 inches (457.2 mm). For those test series, additional plots were made of the tested and calculated values with the lever arm magnified by rotation (z_1 = 284 mm, z_2 = 30 mm, Appendices 186 and 194). The maximum loads at e = 12 inches (305 mm) calculated with enlarged lever arm was clearly overestimated, as expected. The calculated results at e = 18 inches (457.2 mm) agree well with the maximum loads of the tests of Series 25M548 overall, in which rotations of about 5° were reached. The maximum loads of the tests of Series 25H648 (e = 18 inches, or 457.2 mm) lie only slightly above the values calculated with the small lever arm, and clearly lie below those calculated using the large lever arm. This outcome was expected, based on the observed rotation of about 3°. The calculated rotations agree well with those occurring in the tests (Appendices 192 and 200).

In evaluating the maximum loads calculated with the BDA5 program, the distinct maximum and the irregular form of the curves have to be noticed, especially at eccentricities smaller than values which give the maximum ratio of $V_{u,BDA5}/V_{u,el}$. The reason for this becomes clear when the failure mode of the tension anchors is considered in the interaction diagram of displacements and loads. Figures 4.3 and 4.4 show an example of Test Series 25M54 (UC1), calculated with a normal lever arm.

If failure occurs by fracture of the shear anchors, the horizontal displacement of the group is limited by the failure displacement of the shear anchors, and so is the maximum displacement of the tension anchor. In the interaction diagram of displacements, this is recognizable by the approximately vertical line (Figure 4.3). The spacing of this line from the interaction curve is irregular due to the back-and-forth nature of the interaction. This leads to a continuous change in the extent to which the tension anchors are used (Figure 4.4), and to a corresponding irregularity in the plot of failure loads as a function of the loading eccentricity "e."

The calculated results in Figures 4.3 and 4.4 also explain the small difference between the failure loads calculated according to plastic theory and with the BDA5 program near the failure transition between the shear anchor and the tension anchors. The bulged form of the displacement interaction diagram is the

reason that a region exists in which the shear anchor governs failure of the group. In the region of the failure transition, the strength of both anchors is fully utilized. At this point, the load distribution therefore agrees with the ideal assumptions of plastic theory. It therefore gives equal failure loads, except for the above-mentioned discrepancies due to differences in the internal lever arm.

Results of individual sub-series are given below:

Series 25h64 and 25m54:

The results of Series 25H64 (Sleeve Anchor, flush-sleeve installation, failing by steel fracture) and 25M54 (UC1, flush sleeve installation, failing by steel fracture) show consistent behavior despite some differences in the load-displacement behavior of single anchors. Consequently, similar results were achieved for the two-anchor connections with both anchor systems, in tests and also in calculations. These are therefore discussed together.

For both anchor systems, Appendices 185 and 186 (Sleeve Anchor) or 193 and 194 (UC1) show analytical failure loads about 18% higher according to plastic theory than according to elastic theory. The maximum occurred at a loading eccentricity of about 12 to 14 inches (305 to 355 mm). The calculated results from load-displacement curves (Program BDA5) show a distinct maximum, in which the failure load is about 15% to 18% higher than that of the elastic calculation. This maximum marks the failure transition from shear to tension anchors. In this transition region, both anchors of the group are fully utilized. This was achieved at somewhat larger eccentricities "e" with the Sleeve Anchor than with UC1, due to the smaller ratio between the failure load of shear and pure tension of the Sleeve Anchor compared to UC1 is ($\gamma = F_{S,u,0}/F_{Z,u,0} = 0.558$, compared to 0.607 for the UC1).

For both anchor systems, when an increased length of the baseplate is used in the calculations ($z_1 = 284$ mm, $z_2 = 30$ mm), the failure loads calculated with the BDA5 program are closer to the fracture loads calculated according to plastic theory, although the increased length was used consistently in all calculations. The curves are closest at relatively large eccentricities, if the tension anchors govern the failure of the group. With e = 21 inches (533 mm) the results most closely approach those of the plastic calculation. For this eccentricity, the loading curve of the anchor is plotted in Figure 4.5. It shows that in calculation with the BDA5 program using the greater length of the baseplate, the compression-side anchors are in tension. This is not possible according to either elastic or plastic theory, because the compression-side anchors are defined as pure shear anchors. The tension in the shear anchor requires (by equilibrium) an increase of the support force at the compression edge of the baseplate. Thereby more of the shear could be transferred by friction, increasing the tensile strength of the tension anchor and the failure load of the group. Despite their considerable tension, the moment contribution of the compression anchors is negligible because of their small lever arm.

In Table 4.3 and 4.4, the ratios of the failure loads in tests versus calculations are given. At e = 12 inches (305 mm), the test results agree well with the results of the calculation according to BDA5 (test/calculation $\approx$ 1.02) and according to plastic theory (test/calculation $\approx$ 0.98), while elastic theory underestimates the failure load by about 15%.

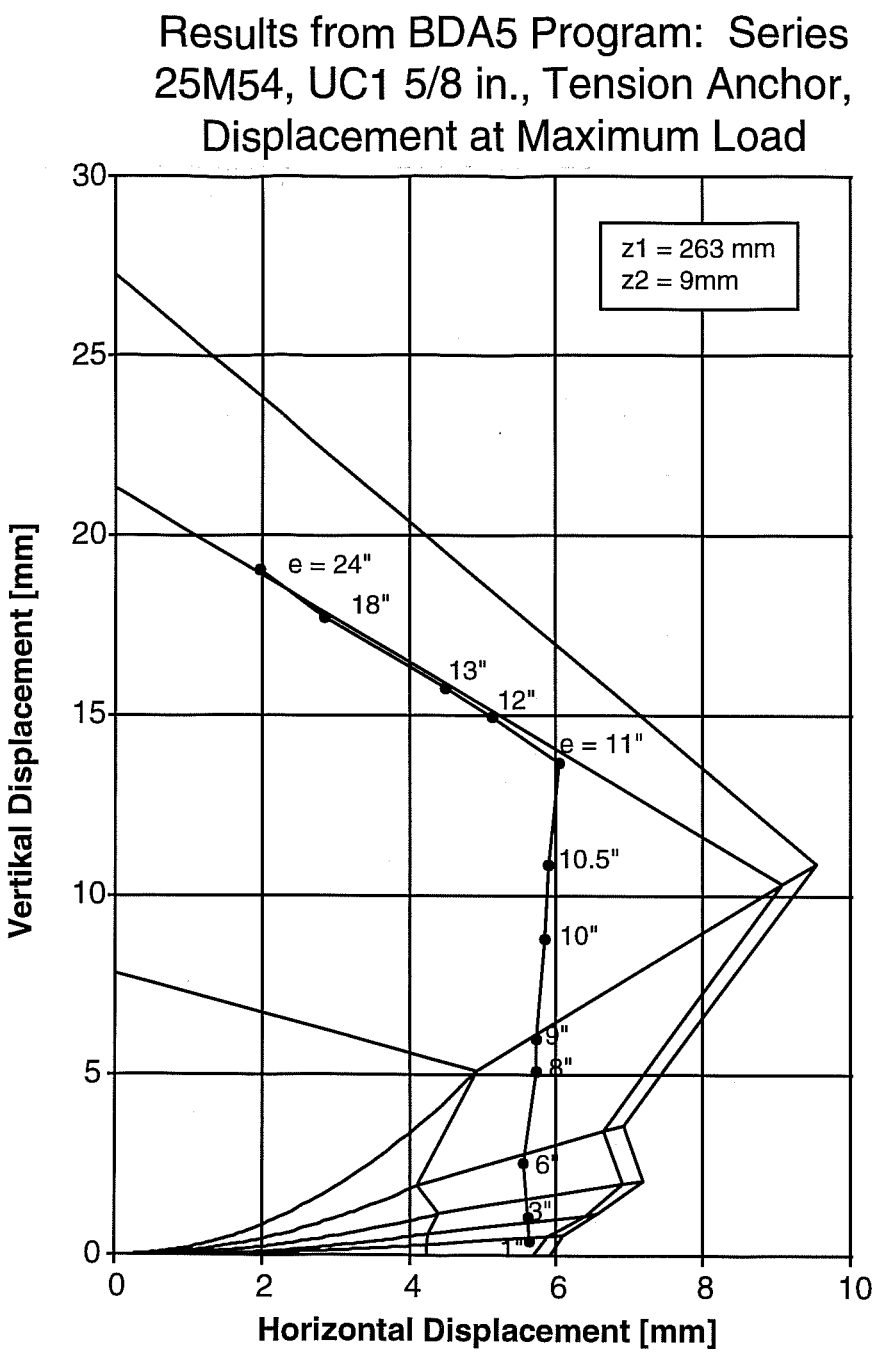

Figure 4. 3 *Fracture states of tension anchors in the displacement interaction diagram of Series 25M54*

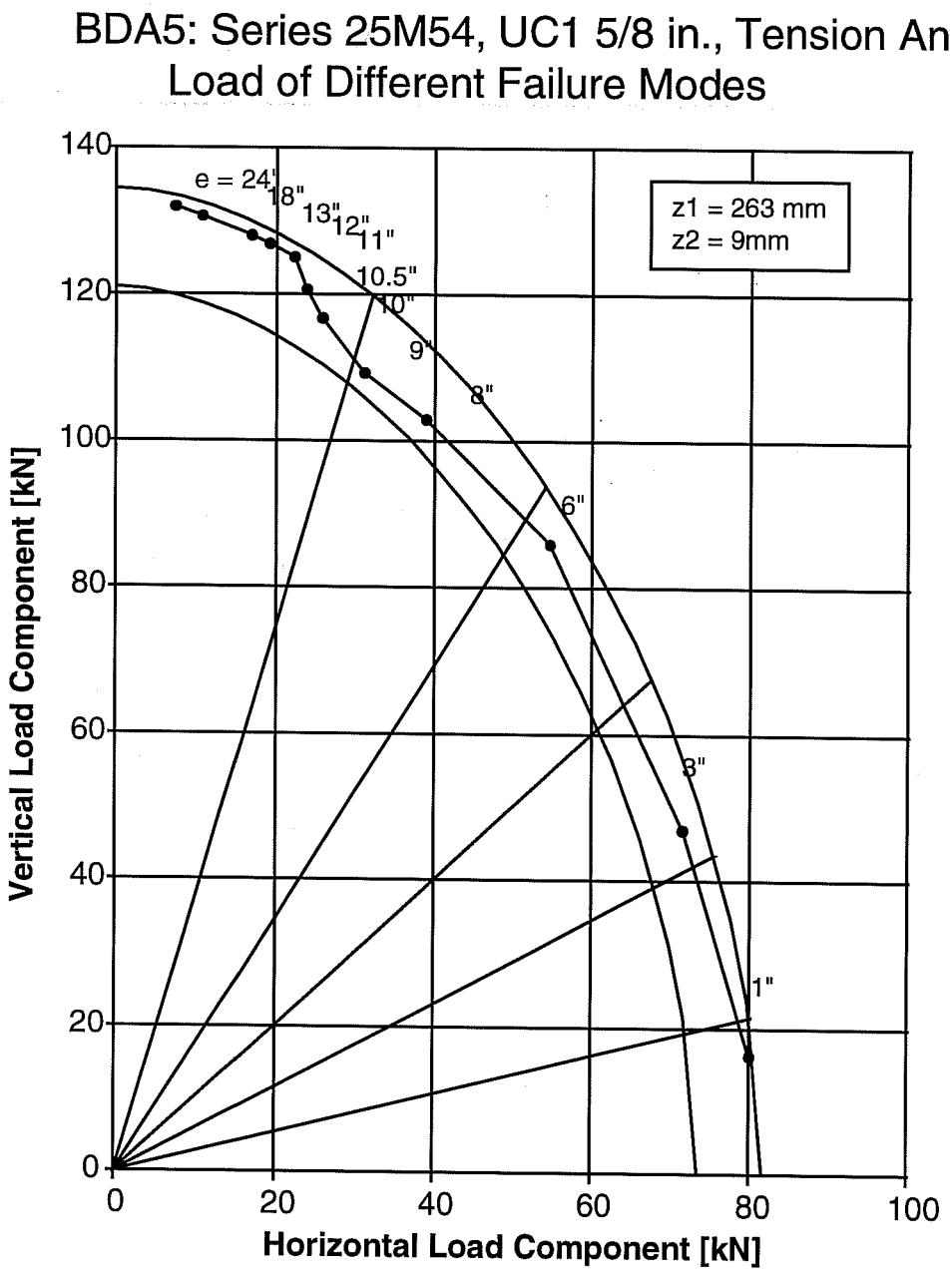

Figure 4. 4 Load interaction diagram for Series 25M54

Table 4. 3 Comparison of Failure Load in Calculation and Test, Series 25h65

Calculation according to:	Average Value of Test/Calculation for:		
	e = 12 in. (304.8 mm)	e = 18 in. (457.2 mm)	
	z_1 = 263 mm, z_2 = 9 mm	z_1 = 263 mm, z_2 = 9 mm	z_1 = 284 mm, z_2 = 30 mm
Elastic Theory	1.150	1.090	1.030
BDA5	1.018	1.021	0.909
Plastic Theory	0.974	0.978	0.906

At e = 18 inches (457 mm), calculations were carried out with both the original and the increased length of the baseplate. With the Sleeve Anchor (Series 25H64), good agreement exists between tests and calculations according to BDA5, or plastic theory using the small baseplate length. The test value exceeds the calculated value by about 2%. The average observed rotation of the baseplate at maximum load is 2.83°, also slightly greater than the value of 2.5° which corresponds to the small baseplate extension length (Section 4.2.1.2). The failure load according to elastic theory is about 9% below the tests. Assuming an increased baseplate length, the failure loads calculated according to BDA5 and plastic theory exceed the test values by about 10%. According to elastic theory the failue loads calculated using the increased baseplate length is still about 3% lower than those measured in tests. However, the use of a magnified extension length is not justified by the observed rotations.

For UC1 (Series 25M54) at e = 18 inches (457 mm), the expected good agreement between tests and calculations was achieved using the increased baseplate length. The 2 to 3% shortfall of calculated values could be explained in terms of the mean observed rotation of 4.73°, compared with the calculated rotation angles of 5°.

Overall, it can be concluded that when reasonable values are used for the extension length of the baseplate the test values lie between the calculated results from plastic theory and from the BDA5 program.

In comparing plastic calculations and tests, internal assumptions of the method of calculations affect the failure load. By assuming an ideal load distribution on the ductile anchors investigated in these series, the failure load was overestimated. This effect is, however, balanced by the neglect of the tension in the shear anchors. The magnitude of the deviations in all cases studied here leads to the conclusion that an extensive parameter study is required for a sufficiently safe design. This can be done using calculations based on load-displacement curves.

Series 25M34:

The results of Series 25M35 are very similar to those of Series 25M54 and 25H64. However, the computed failure transition from the shear to the tension anchor (BDA5) occurred at e = 10 inches (254 mm). The maximum increase in the failure load according to plastic theory, over that calculated by elastic theory, occurred at an eccentricity of about 12 inches (305 mm), and is about 20%. The ratios between measured and calculated failure loads at the tested eccentricities are summarized in Table 4.5. The table shows that the calculation according to plastic theory overestimates the actual failure loads by up to 11%, although the failure was governed by steel fracture and a ductile material was used for the

Table 4. 4 Calculated Versus Observed Loads, Series 25M54

Calculation	Average Value of Test/Calculation for:		
according to:	e = 12 in. (304.8 mm)	e = 18 in. (457.2 mm)	
	z_1 = 263 mm, z_2 = 9 mm	z_1 = 263 mm, z_2 = 9 mm	z_1 = 284 mm, z_2 = 30 mm
Elastic Theory	1.154	1.154	1.085
BDA5	1.022	1.103	0.985
Plastic Theory	0.979	1.050	0.972

Table 4. 5 Calculated Versus Observed Failure Load in Calculation and Test, Series 25M34, z_1 = 263 mm, z_2 = 9 mm

Calculation according to:	Average Value of Test/Calculation for:	
	e = 12 in. (304.8 mm)	e = 18 in. (457.2 mm)
Elastic Theory	1.071	1.062
BDA5	0.955	1.011
Plastic Theory	0.892	0.945

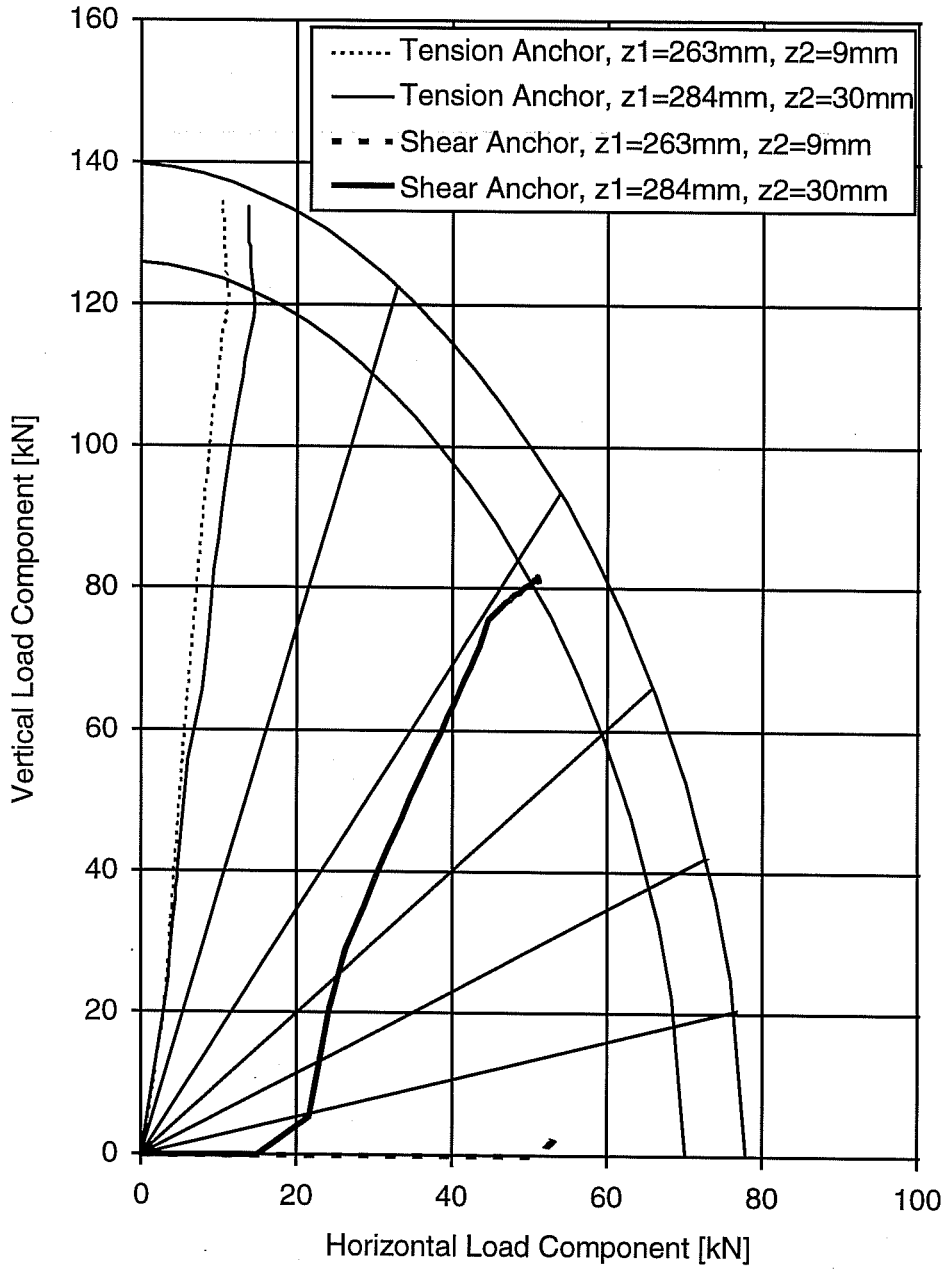

Figure 4. 5 *Loading curves for tension and shear anchors according to BDA5, sleeve anchor M16, e = 21 inches (533 mm). Based on Series 25H64, influence of extension length of baseplate.*

anchors. This is because of the generally smaller failure displacements of the smaller diameter anchors (3/8 inch or M9.5), compared to the larger anchors (5/8 inch or M16) used in Series 25H64 and 25M54.

Series 26M54:

The line for the failure load according to elastic theory is horizontal for small loading eccentricities (Appendix 208). In this region, the failure load according to elastic theory is limited by the shear strength of the shear anchors because the strength of the shear anchor is affected by edge effects. This does not happen when both anchors are of equal strength, because then with even distribution of shear on both anchors (according to elastic theory) plus the superimposed tension, combined failure of the tension anchor always governs failure of the group.

In the eccentricity range between 3 and 7 inches (75 and 178 mm), the maximum load according to the BDA5 program is smaller than that according to elastic theory. Figure 4.6 shows the reason for this in terms of the shear versus transverse displacement curve for the shear anchor under pure shear, and for the tension anchor (c_1 = 11inches or 280 mm) at various loading directions.

The load-displacement curves for the horizontal components of loads and displacements under oblique tension are flatter than for pure shear. The tension anchor therefore takes less shear than the shear anchor. Therefore, the failure load of the group is smaller than twice the shear strength of the shear anchors (which would be the failure load according to elastic theory). This ratio, plotted in the form of $V_{u,pl}/V_{u,el}$ and $V_{u,BDA5}/V_{u,el}$ has a minimum of 0.95 at e = 6 inches (150 mm). The maximum is then reached at about 9 to 10 in, where the BDA5 program shows failure transition from the shear anchor to the tension anchors. However the maximum value is only $V_{u,BDA5}/V_{u,el}$ = 1.03. At larger eccentricities,

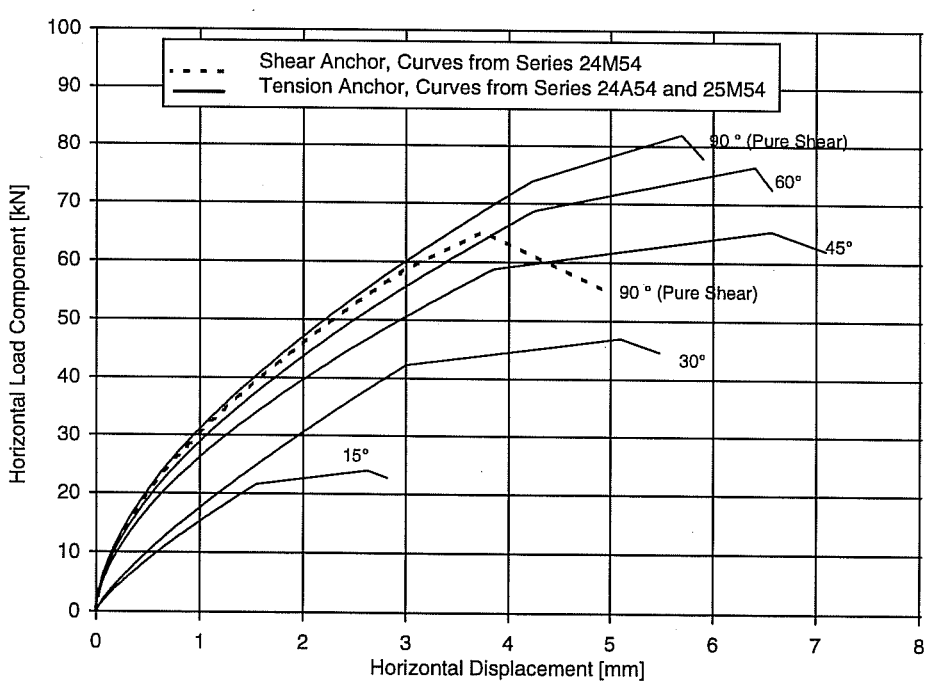

Figure 4. 6 *Comparison of shear versus horizontal displacement curve for shear and tension anchors*

the calculated values according to the BDA5 program again lie beneath the elastically calculated values. However, based on the assumption of the line of action of the resultant compression at the edge of the baseplate that was used in calculation according to elastic and plastic theory, the failure load was already overestimated by about 3% (see Figure 4.2).

The comparison of test versus calculation in Table 4.6 shows that calculated maximum loads are generally somewhat higher than the test values. This can be due to the possible overestimation of the strength of the tension anchor based on the very low numbers of tests in Series 24A54.

Furthermore, the differences between the calculation procedures are smaller than for the other configurations. According to plastic theory the shear anchors are most completely utilized. The real behavior, and similarly the other calculation procedures comes relatively closer to this assumption because of the low strength of the near-edge shear anchors compared to the tension anchors.

4.3 Investigations of Anchor Groups with 2 and 3 Anchor Rows based on the Test Results of Cook (1989)

Cook (1989) reports tests on anchor groups under eccentric shear with loading eccentricities of 6 inches (152.4 mm), 18 inches (457 mm, 2 and 3 anchor rows), and 36 inches (914 mm, 1 anchor row). He used adhesive, headed, and undercut anchors. The undercut system was the same as those used in the present investigation, for which load-displacement curves were determined in Series 23M54. It is now possible to compare the results of Cook (1989) with calculations based on those curves, and to carry out calculations at other eccentricities as well. However, differences in the quality of steel used must be considered in discussing the maximum loads.

In the following, the tests of Cook (1989) are first described. Subsequently, the input parameters for the capacity calculations were derived from the combination of the tests of Cook (1989) with results of this study. Finally, the results of the tests and calculations as well as those of the continued investigations of this study, are plotted and discussed.

4.3.1 Description of Tests

The test setup used by Cook (1989) is schematically shown in Figure 4.7. Two metal plates were welded on a baseplate with dimensions of 18 x 12 x 2 inches (457 x 253 x 51 mm), on which a tensioning device could be pin-connected at different heights. The baseplate was sufficiently thick that it could be assumed

Table 4. 6 *Calculated Versus Observed Failure Loads in Calculation and Test, Series 26M54, z_1 = 263 mm, z_2 = 9 mm*

Calculation according to:	Average Value of Test/Calculation for:	
	e = 12 in. = 304.8 mm	e = 18 in. = 457.2 mm
Elasticity Theory	0.945	0.954
BDA5	0.945	0.973
Plasticity Theory	0.903	0.941

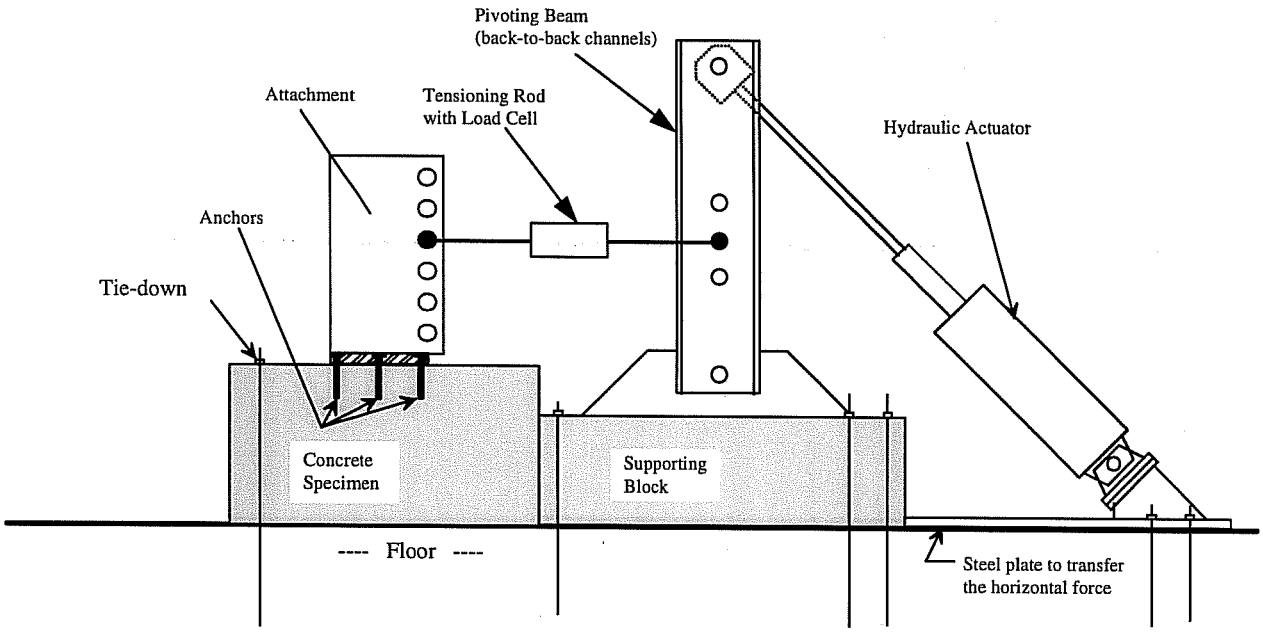

Figure 4. 7 Test setup of Cook (1989) for tests on anchor groups

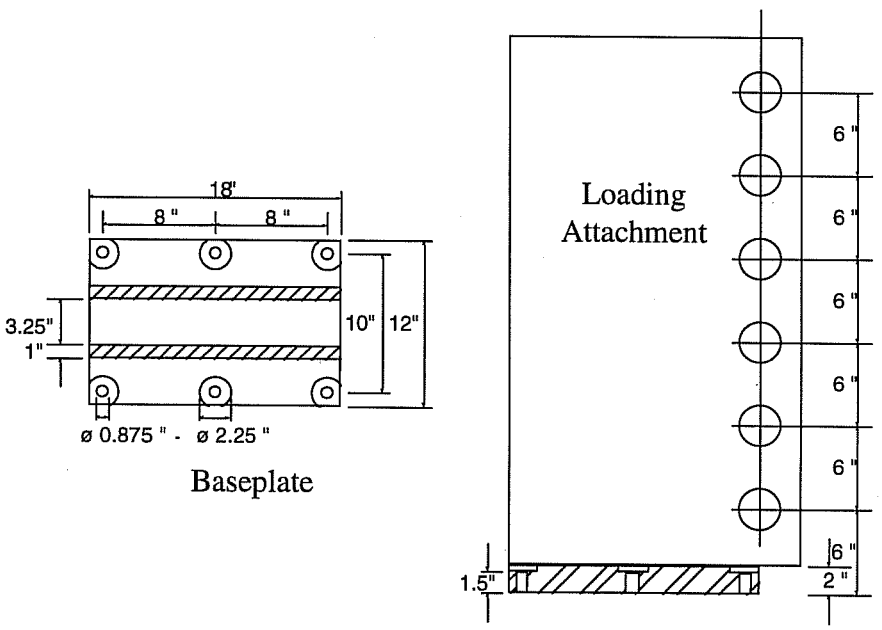

Figure 4. 8 Loading apparatus used by Cook (1989)

stiff. The locations of the holes in the baseplate are shown in Figure 4.8. The diameter of holes was 7/8 inch (22.2 mm). With a nominal anchor shank diameter of 5/8 inch (15.9 mm), there was a very big gap of 1/4 inch (6.3 mm). The locations of anchors in these oversized holes were unfortunately not stated in the test report. The outer holes were always used for tests with fewer than 3 anchor rows.

The anchors were installed according to the manufacturer's instruction with the manufacturer's setting tools. In contrast to the tests of this report, the anchor prestressing force was applied by hydraulic ram rather than by a torque wrench. With an anchor tension of 80% of nominal yield, the nut was hand-tightened, and then the force was released. The remaining prestressing force was measured with load cells between washers and the baseplate, which were also used during the tests. It amounted to about 40% to 70% of the nominal yield, slightly higher than in the tests described here.

The load was applied with a hydraulic actuator, in 40 to 50 approximately equal steps of monotonically increasing displacement up to fracture. Each step lasted about 30 seconds. The total loading duration was therefore about 20 to 30 minutes.

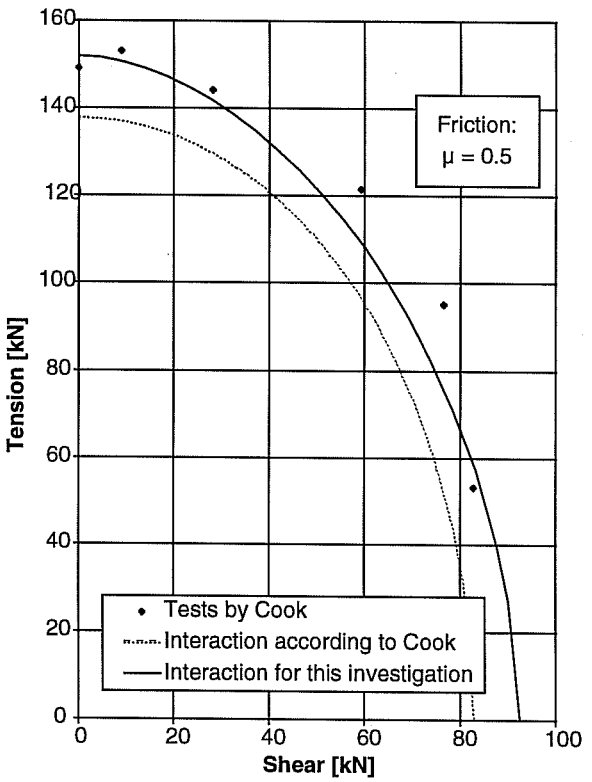

Figure 4. 9 *Interaction of forces for the undercut anchors used by Cook (1989), determined from tets with an anchor row*

4.3.2 Input Parameters for Calculations

Cook (1989) conducted some tests with only one anchor row to determine the friction coefficient and the interaction relationship of the anchors used. It is important to use the same friction coefficient for the calculation of the tests and the investigation of the interaction. Cook evaluated the test results both with a friction coefficient determined individually for each test, and with uniform friction coefficient of $\mu = 0.5$. The latter is beneficial for calculations on the basis of tests. In Figure 4.9, the test results of Cook are plotted with $\mu = 0.5$ in the interaction diagram. Also plotted is the comparatively conservative interaction relationship used by Cook for his calculations, as well as the interaction used in the following for calculations based on the results of Cook ($F_{Z,u,0} = 304$ kN for each series, $\gamma = 0.608$, exponent of interaction $p = 1.8$).

Corresponding to the determination of the interaction relationship, a friction coefficient of $\mu = 0.5$ is used in all further calculations, based on the tests of Cook.

The cylinder compressive strength of the concrete was between 4500 and 6500 psi (31 and 45 N/mm²) in the tests by Cook (1989). Cylinder strengths were not given for individual specimens. It is therefore not useful to re-compute the displacements measured in the single-anchor tests of this study to compensate

for differences in concrete strength before using them in the calculations with BDA5 for the tests of Cook. No sure method is available for such a recomputation, and the strength differences are not very large in any event.

The concrete strength is also needed in the BDA5 program to determine the crushing of the concrete at the compression edge of the baseplate. However, this has only a slight influence on the results. Therefore the concrete strength of the tests of this study was used throughout (f_c = 32.4 N/mm²).

The shank of the anchor used in the tests of Cook (1989) was made of material meeting the same specification as in the tests of this study. However, the work of Cook included no information on the actual fracture elongation of the material.

In general, based on the above-mentioned facts, it seems reasonable to assume the displacement values unchanged from those of Series 23M54; that is, only the maximum loads of the load-displacement curves in the interaction relationship were adjusted according to Figure 4.9. Both the dimensions of the baseplate and the anchor group could be input as described in Section 4.3.1.

4.3.3 Calculation Results and Comparison with Test Results

The investigation based on the results of Cook (1989) is limited basically to comparing of the maximum loads with the results of different calculation procedures, as well as with the present test results.

The calculation results were plotted as in the preceding sections in the form of relative maximum loads, in terms of the loading eccentricity "e." Plots are given in Appendix 215 for the connection with 4 anchors (2 rows), and in Appendix 216 for the connection with 6 anchors (3 rows). The test results of Cook (1989) are also plotted.

Cook (1989) reported each test at eccentricities of 6 inches (152.4 mm), 12 inches (304.8 mm) and 18 inches (457.2 mm) on anchor groups with 2 and 3 rows (2 anchors each row) and with undercut anchors. Calculations were conducted according to elastic and plastic theory in the range from e = 0 to e = 25 inches (635 mm). Calculations with the BDA5 program were limited to e = 6 inches (150 mm) to e = 18 inches (457 mm) corresponding to the test range. Appendices 215 and 216 include diagrams of the relative failure loads over the eccentricity "e."

For the connection with two rows, Appendix 215 shows that the results of the plastic calculation and the results of the calculation with load-displacement curves are closer together than in the calculations described earlier in this report. The reason for this is the higher friction coefficient and the longer extension length (by 1.0 in, or 25.4 mm) of the baseplate at the compression zone. The longer extension length causes the compression anchor to lie in the tension zone. With the higher friction coefficient considerable shear could thereby be transferred. To illustrate this effect, computations are conducted with the BDA5 program, with the compression anchors placed at z_2 = 9 mm from the compression edge of the baseplate, instead of at the actual 25.4 mm. The results are plotted in the lower diagram of Appendix 215. In the plastic calculation, tension in the compression-zone anchor was not considered.

Agreement between the test results and the BDA5 calculation results is good. Only at e = 6 inches (152.4 mm) is the test value lower than the calculation value, by about 4%. This difference can be caused by the unconsidered gaps. The failure loads calculated according to plastic theory were not reached in tests, although the interaction relationship used in the comparison to the results obtained from the tests with

one anchor row was still considered as conservative. The results according to elastic theory lie consistently on the safe side.

In these calculations and tests, the plastic redistribution of only the shear could be investigated, because there was only one anchor row in the tension zone. The plastic redistribution of tension, which is analogous to that used in calculating the plastic moment in steel members, is now investigated by calculation, based on the tests by Cook (1989) on connections with three rows of two anchors each.

The calculation results for the 3-row connection are plotted in Appendix 216, and are compared with the test results of Cook (1989). The maximum test loads scatter around the BDA5 curve. The results of the plastic calculation lie above, and those of the elastic calculation lie under, the test results. Anticipating the proposed modification of plastic design as discussed in Chapter 5 of this report, a new curve was also plotted, according to plastic theory, though without plastic redistribution of shear. This curve agrees well with the test results overall. Ductile behavior of anchors is still required for this restricted application of plastic theory.

4.4 Investigations of the Influence of Installation Method, Concrete Strength and Friction Coefficient

For the investigations accomplished so far, direct comparison of calculations and test results for anchor groups was always possible with at least 2 values of loading eccentricity, "e." The following section contains analytical investigation, for which the load-displacement curves of Series 2.3 or 2.4 exist, but for which no test results are available.

Based on the good agreement between tests and (BDA5) calculations from load-displacement curves, the following calculations are considered reliable.

4.4.1 Influence of Installation Method in Anchors with Through-Sleeve Installation

Through-sleeve installation implies that the anchor is installed with the sleeve through the baseplate hole, so that the sleeve helps transfer shear. This installation method was used in Series 23M74 and 23H74 with single anchors. The shear strength and the failure displacements under shear and oblique tension were considerably increased compared to anchors whose sleeves stopped at the concrete surface, leaving only the threads in the critical shear plane.

Calculations were carried out for the bearing behavior of two-anchor attachments using the load-displacement curve of Series 23M74 and 23H74. Other aspects of the connections were assumed identical to those of Series 25.

The results of the calculation are again plotted in the form of normalized failure loads ($V_u/F_{Z,u,0}$ or $V_u/V_{u,el}$) in Appendices 217 and 218 for undercut anchors and torque-controlled expansion sleeve anchors. The results show no significant differences between the two anchor systems.

For comparison, the BDA5 results for flush-sleeve installations were plotted with the curves of $V_u/F_{Z,u,0}$ in terms of "e." Under predominant shear, the strength of the connection almost doubled as a result of the anchor sleeve. With increasing eccentricity, the curves approach each other. At "e" greater than 15

inches (about 380 mm), failure loads are essentially identical for flush-sleeve versus through-sleeve installations.

The maximum of the ratio $V_{u,BDA5}/V_{u,el}$ or $V_{u,pl}/V_{u,el}$ is achieved at e ≈ 6 inches (152 mm), based on higher shear strength of anchors relative to the tensile strength, compared to e ≈ 12 inches (305 mm) for flush-sleeve installation. For both installation methods, the calculated BDA5 failure loads clearly lie below the values estimated according to plastic theory. In spite of the larger shear deformation capacity of the through-sleeve anchors, the results of calculations with load-displacement curves are not closer to the values predicted by plastic theory than in the calculations described earlier in this study.

4.4.2 Influence of Concrete Strength

In Series 23M53, single anchors in low-strength concrete (f_c = 20.7 N/mm²) were tested to study the influence of the concrete strength on load-displacement behavior at different loading directions. The results of these tests provided the basis for BDA5 calculations. All input parameters were the same as in the previous calculations (Appendices 183 - 184), with the exception of the load-displacement curves and the concrete strength. Results are plotted in Appendix 219. For comparison, the BDA5 results for f_c = 32.4 N/mm² are also plotted. The results according to plastic and elastic theory are independent of concrete strength.

The results of calculation with load-displacement curves shows a massive influence of concrete strength in the range of small eccentricity of shear load; that is, on failure of the shear anchors. As already explained in Section 4.2.3 (Figures 4.3 and 4.4), the bulged form of the displacement interaction curve also has an influence, because at small shear eccentricity, failure occurs by fracture of the shear anchor, the tension anchors do not reach their maximum strength. The bulged form of the interaction diagram for anchors in low-strength concrete is more distinct than in higher strength concrete. Under tension and oblique tension, considerably larger displacements were reached at maximum load, while under pure shear the restraint by the baseplate of shell-shaped spalling in front of the anchor only permits a small increase in displacements.

Figure 4.10 shows the deformation of the tension anchor at maximum load of the group plotted with the displacement interaction diagram. The region to the right of the line of tension anchor displacements could not be used. Figure 4.11 shows the associated load states of the tension anchor at maximum load of the group, plotted

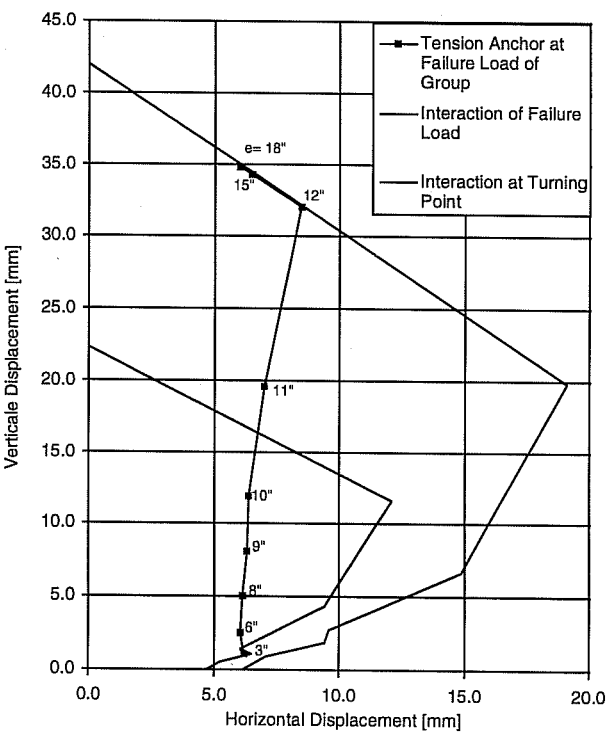

Figure 4. 10 *Deformation state of the tension anchor at maximum load of the group, plotted on the displacement interaction diagram*

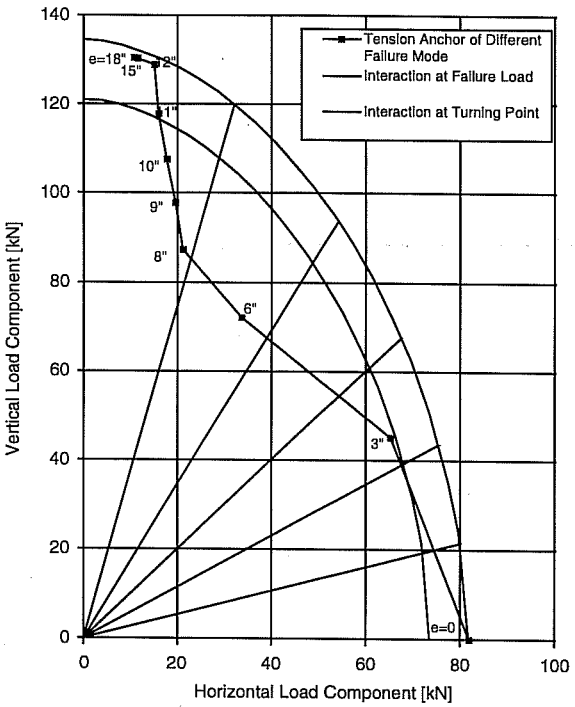

Figure 4. 11 *Load state of tension anchors at the maximum load of the group, plotted on the force interaction diagram*

against the force interaction diagram. Contrary to the assumptions of plastic theory, the tension anchors could not be fully utilized for small loading eccentricities. Figure 4.12 illustrates the influence of concrete strength on this effect, with a plot of the utilization factor of the tension anchors depending on the eccentricity of external shear for f_c = 20.7 N/mm² and for f_c = 32.4 N/mm². The inferior utilization with the lower concrete strength is obvious.

Therefore, larger deformation does not automatically cause the actual behavior to approach that predicted by plastic theory. On the contrary, the graph in Appendix 219 shows that for f_c = 20.7 N/mm² and steel failure, not even the calculated *elastic* failure loads were achieved. However, the discrepancy is comparatively small, about 10%.

Altogether, it is concluded that the bulged form of the displacement interaction diagram for single anchors results in incomplete utilization of the tension anchors in the range of small eccentricity of shear. Consequently, the failure load of the group can be considerably smaller than that load calculated according to plastic theory.

4.4.3 INFLUENCE OF FRICTION

The calculation procedure used here considers that under eccentric shear, part of the shear is transferred through friction between the baseplate and the concrete on the compression side of the baseplate. The tests described in this report were conducted with a Teflon sheet between the baseplate and the concrete to reduce the test scatter as well as for technical testing reasons. The friction coefficient between the baseplate and the concrete was $\mu \approx 0.1$ in test, rather than the value of $\mu \approx 0.5$ that would exist without the Teflon sheet. To confirm the applicability of these results in practice, the influence of the friction coefficient is now examined, with special attention to the effect of concrete strength.

Capacities of the familiar two-anchor connections with undercut anchors of 5/8-inch (16-mm) diameter at an embedment depth of 7 inches (178 mm) were predicted with μ = 0.1 and μ = 0.5. The results are plotted in Appendix 220 for low-strength concrete (f_c = 20.7 N/mm²) and in Appendix 221 for higher strength concrete (f_c = 32.4 N/mm²).

The plot shows that the maximum calculated capacity of the group, normalized by the tensile strength of a single anchor, is clearly higher with μ = 0.5 than with μ = 0.1. Plots of the ratio of $V_{u,pl}/V_{u,el}$ or $V_{u,BDA5}/V_{u,el}$ in the lower diagram show only a compression of the curves in direction of x axis, that is, they have about equally large minima and maxima for μ = 0.5 as for μ = 0.1, but at smaller eccentricities.

For the-low strength concrete (f_c = 20.7 N/mm²), according to the BDA5 results calculated with $\mu = 0.5$, elastic theory overestimates the maximum capacity by up to 10%. Plastic theory overestimates the maximum capacity by up to 25%. For f_c = 32.4 N/mm², the maximum BDA5 capacities exceeded those from elastic theory. Maximum loads were overestimated by plastic theory by about 10%.

All calculation procedures show approximately the same increase in absolute failure loads with increasing friction coefficient at small eccentricities. Based on these results, different friction coefficients between the baseplate and the concrete do not produce qualitative changes in the results corresponding to a friction coefficient of $\mu \approx 0.1$.

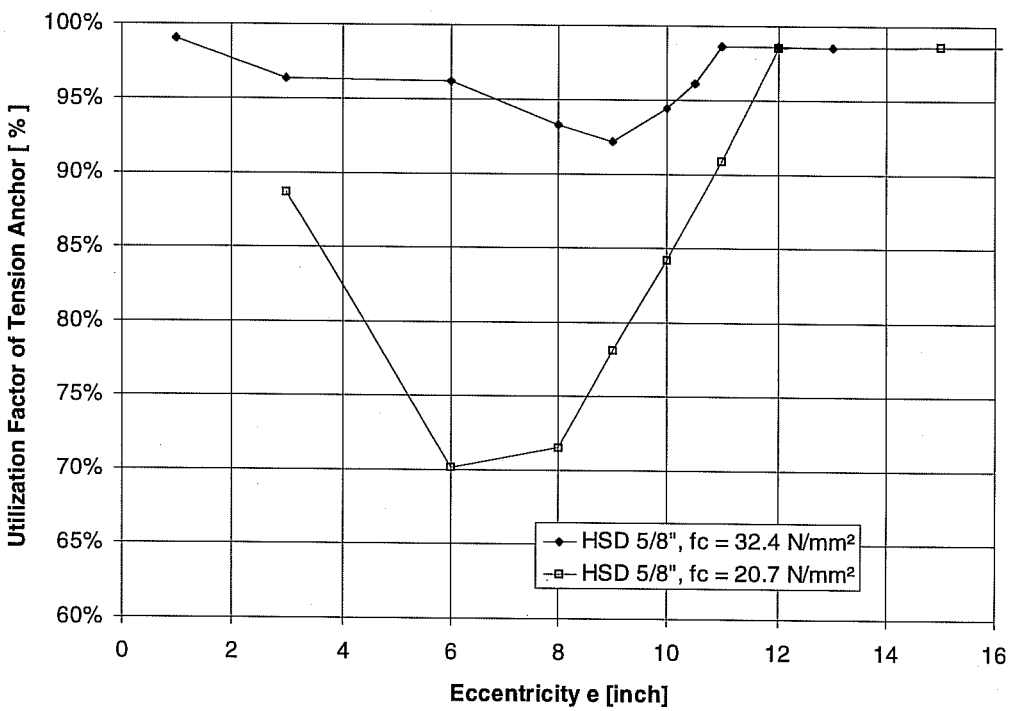

Figure 4. 12 *Utilization factor of tension anchors of a two-anchor connection (UC1, 5/8-inch, h_{ef} = 7 inches, $F_{S,u,o}/F_{Z,u,o} = \gamma = 0.60.8$, $\mu = 0.1$*

CHAPTER 5

IMPROVED DESIGN ACCORDING TO PLASTIC THEORY

The results of the tests and calculations of this study, as well as the results of the latest calculations of the tests by Cook (1989), show that the plastic theory provides a good description of the behavior of anchor groups at large eccentricities of the external shear ($e > e_2$) and given ductile fracture of the anchors. The assumption of elasto-plastic behavior of the tension anchor is an idealization of the actual load-displacement behavior. However, under these conditions, the use of real load-displacement curves does not lead to significantly different tensile elongations of single anchors.

At medium eccentricities ($e_1 < e < e_2$), design according to plastic theory assumes that the compression-side anchors (shear anchors) alone resist all external shear exceeding the friction, and that the tensile strength of the tension anchors is not affected. This assumption requires that the tension anchors deform in shear up to the failure displacement of the shear anchors, without any reduction in their tensile strength. Based on the present test results, this prerequisite is not satisfied. However, the shear stiffness of the tension anchor is much smaller than that of the shear anchor. The overestimation of the failure load in calculation according to plastic theory is therefore also comparatively small in this range (< 10%).

At smaller eccentricity of the external shear ($e < e_1$), design according to plastic theory assumes first of all that the compression-zone anchors reach their full shear strength. This assumption is justified. In the tests, failure occurred in this range by shear fracture of the compression anchors. It is further assumed that the tension zone anchors, under oblique tension, reach their maximum strength in accordance with the developed force interaction curve. This assumption is not justified by the present results, because the shear deformation of the tension zone anchors could not be significantly larger than that of the compression- zone anchors. The "belly" in the force interaction diagram was not reached (see Figures 4.3, 4.4, 4.10, 4.11 and 4.12). As a result, the failure load of the group can be overestimated by as much as 25% (Appendix 220). A modification of the plastic design method is therefore presented.

The results of calculation with the load-displacement curves of Series 23M53 (f_c = 20.7 N/mm², Appendix 220) also show that the failure load is overestimated by less than 10%, if the shear is assumed to be distributed even on all anchors (for the two-anchor connection investigated, this agrees with the calculation according to elastic theory).

Calculation of the anchor group with 6 anchors (3 rows) tested by Cook (1989), assuming even distribution of the shear exceeding friction on all anchors of the group, also shows a good agreement between calculations and tests. The results of tests, as well as the calculations with different procedures, are plotted in Figure 4.13 and are also compared with the failure loads of elastic calculation. Figure 4.13 shows that the advantages of the plastic design can also be used in calculations without shear redistribution, and that the above-mentioned unsafe regions are eliminated.

The conversion of the modified procedure to the framework of the design of anchor groups under shear and bending is now described briefly. For the design procedure, it is assumed that the anchor pattern and the geometry of the baseplate are already fixed because these parameters are limited by the attachment.

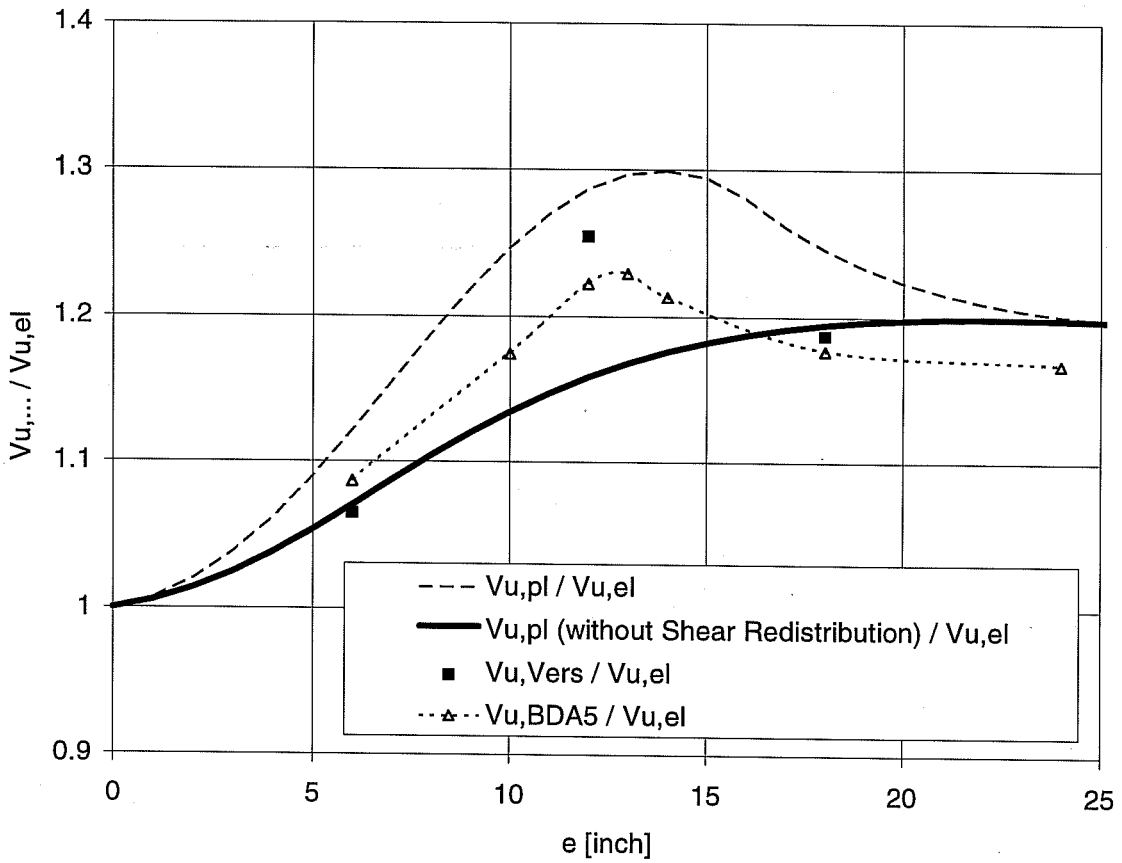

Figure 5. 1 *Comparison of results of different calculation methods with test results of an anchor group with six anchors (three rows) and stiff baseplates tested by Cook (1989)*

However, the number of anchor rows can vary. The size and eccentricity of the load are given. The first step in design is the calculation of the anchor tension force $F_{Z,i}$ ($F_{Z,1} = F_{Z,2} = ... = F_{Z,n}$):

$$\Sigma M=0: \; V \cdot e = F_{Z,i} \cdot \Sigma(z_i) \tag{5.1}$$

$$\text{So that } F_{Z,i} = V \cdot e / \Sigma(z_i) \tag{5.2}$$

$$\Sigma V=0: \; C = \mu \cdot n \cdot F_{Z,i} \tag{5.3}$$

$$\Sigma H=0: \; F_{S,i} = \frac{V - C}{n} = \frac{V}{n} - \mu \cdot F_{Z,i} \tag{5.4}$$

The selection of the anchor depends on the forces $F_{S,i}$ and $F_{Z,i}$. If no matching anchor is found, the calculation can be repeated with new $\Sigma(z_i)$ and n.

With even distribution of anchors over the length of the baseplate instead of "$\Sigma(z_i)$" the value

$$n/2 \cdot z_1 \text{ can be used,} \tag{5.5}$$

where: z_1 = spacing of the outer most anchor row and n = number of anchors in the tension zone.

So $F_{Z,i}$ depends on z_1 and n:

$$F_{Z,i} = (V \cdot e) / (n/2 \cdot z1) \tag{5.6}$$

$$C = 2 \cdot \mu \cdot e \cdot V / z1 \tag{5.7}$$

$$F_{S,i} = A \cdot V / n \tag{5.8}$$

where: $A = 1 - \frac{2\mu e}{z_1}$

The design should proceed as follows:

1) calculate the coefficient A;
2) assume the number of anchor rows;
3) calculate $F_{Z,i}$ according to Equation (5.6), and $F_{S,i}$ according to Equation (5.8);
4) select of a suitable anchor for the calculated oblique tension; and
5) Repeat steps (2) through (4) as required.

This design procedure is no more complicated than that proposed by Cook and Klingner (1989, 1992-1, 1992-2). The design leads to higher anchor requirements only in the region of small eccentricity of the shear. A region of unconservatism is eliminated by these newly discovered research results.

CHAPTER 6

SUMMARY

In this report, theoretical and experimental investigations of the bearing behavior of multiple-anchor connections to concrete are described. The research was carried out at the Phil. M. Ferguson Structural Engineering Laboratory of The University of Texas at Austin. The following problems were investigated:

1) Load-displacement behavior of two-anchor connections under pure tension with high loading rates, and failing by concrete breakout;

2) Load-displacement behavior of single anchors at various loading directions as a basis for the calculation of the behavior of multiple-anchor connections; and

3) Bearing behavior, displacement behavior and load distribution of anchor groups under shear and bending.

To investigate the influence of higher loading rates on two-anchor connections under pure tension, failing by concrete breakout, undercut anchors and torque-controlled expansion sleeve anchors of 3/4 inch (approximately M20) were tested statically (about 2-4 minutes to fracture) and dynamically (about 0.1 seconds to fracture). The following conclusions are summarized from the results of Series 2.1 and 2.2:

1) With undercut anchors (UC1), an increase in the loading rate by a factor of 10^3 to 10^4 leads to an increase in the concrete breakout load of two-anchor groups by about 15% to 25%. This value agrees well overall with the results of investigations of single anchors (Eibl, Keintzel, 1989; Rodriguez, 1995).

2) The influence of anchor spacing on the ultimate load of the group follows the well-known rules for static loading (Figure 3.14). It suggests no increase in the critical spacing.

3) Measurement of the fracture cone contour in some tests (Appendices 25 and 26) also suggests no enlargement of the fracture cone under dynamic loading. In fact, steeper fracture cones were measured. This result requires additional confirmation due to the large scatter.

4) Torque-controlled expansion sleeve anchors, the expansion sleeve configuration had a considerable influence on test result, as noted from the load-displacement curves (Appendices 13 - 20) and the load-time curves (Appendices 21 - 24). In particular, the sudden stopping of the cone at a lip in the sleeve led to a sudden increase in the instantaneous loading rate, to about twice the nominal value. Failure loads in the dynamic tests were about 42% - 45% higher than in the static tests. The almost doubled loading rate is not enough by itself to substantiate the larger failure load increase, compared to the tests with undercut anchors. Instead, the results indicate that the effect of change of loading rate is intensified through the high strain gradients in the region of the crack tip, in combination with the crack propagation.

5) The load-displacement behavior of anchors was independent of loading rate. The larger displacements at failure in the dynamic tests result from higher failure loads. However, the flattened form of the load-displacement curve for the undercut anchor near maximum dynamic capacity, as well as the fact that the cone was drawn into the sleeve in these tests, suggests that the local strength of the concrete in the load transfer region does not increase as much as the concrete breakout load.

The load-displacement behavior of anchors at various loading directions was investigated with torque-controlled expansion sleeve anchors (Sleeve Anchors) and undercut anchors (UC1) of 3/8 inch (about M10) and 5/8 inch (about M16). In these tests, the embedment depth and edge distance were varied to achieve the expected failure mode (steel fracture or concrete breakout). Furthermore, in the tests with steel fracture some anchor were installed with flush sleeves, and others with through sleeves. The results of Series 2.3 and 2.4 as well as the conclusions from these can be summarized as follows:

1) The interaction of forces is well described by an elliptical interaction equation (Eq. 2.4). Based on the present test results, the exponent is $p \approx 1.67 - 1.80$ for steel failure and $p \approx 1.6$ for concrete fracture. A higher value for the exponents p is required for different failure modes under tension and shear. However, this depends on the angles at which the failure transition occurs. In this case, the use of distinct interaction equations for each failure mode best describes the test results. The smaller of the calculated failure loads always governs. The change of failure mode occurs at the loading angle at which the interaction curves intersect (Appendix 134).

2) The displacement interaction diagram for steel fracture has a bulbous form; that is, the shearing displacement at failure under oblique tension is larger than under pure shear. This is due to larger spalling under oblique tension in the direction of the shear, in front of the anchor (Appendices 38, 55, 66, 83, 94, 110).

3) In failure by concrete breakout, displacement interaction at maximum load can be approximated by a straight line (Appendix 124). The relation between positions on these straight lines and the loading angles obeys a nonlinear rule, and cannot be specified here based on the small number of tests with concrete breakout.

4) Failure by steel fracture and ductile behavior of the steel of anchor shank do not by themselves guarantee ductile behavior of a connection. Brittle fractures of the anchor shank can occur, depending on concrete strength, anchor size, installation method and loading direction, especially under predominant shear. Low steel strength, small anchor diameters, flush-sleeve installation, and high-strength concrete all lead to small deformation capacity.

5) Ductile fractures will be achieved, in principle, if the maximum possible steel strength of the anchor is reached. Therefore, connections with large edge distance, with higher strength yet ductile steels, and with through-sleeve installation (sleeve extending to the top surface of baseplate) are recommended.

6) At smaller edge distances, ductile failure is possible using supplementary hairpin reinforcement. This increases the strength of the concrete edge. Furthermore, the formation of cracks in the concrete is necessary to activate the reinforcement. This causes an increase in the measured deformation.

The experimental phase of the investigation of the bearing behavior of multiple-anchor connections included tests on two-anchor connections with sleeve and undercut anchors under shear and bending. In the tests, the eccentricity of the shear was varied, along with the type of anchor, the anchor diameter, and the failure mode (steel or concrete governing) through corresponding selection of the embedment depth and edge distance. In addition to the external load and the displacements of the baseplate, the strain distributions in the baseplate were measured between the anchors, to determine the distribution of shear on the anchors. Finally, before each test, the gap between the anchor shank and the hole in the baseplate were documented.

In the theoretical phase of the research, the load-displacement curves for single anchors (that had been determined in Series 2.3 and 2.4) were used for the load-displacement calculations of groups, by means of the BDA5 program (Li 1994). The calculations included the configuration of the tests of Series 2.5 and 2.6, as well as those of Cook (1989). Good agreement was achieved between computer calculations and tests.

From the results of the experimental and theoretical investigations of the bearing behavior of anchor groups under shear and bending, the following key conclusions are drawn:

1) The BDA5 calculations based on load-displacement curves provided a very good description of the bearing behavior of anchor groups. These even permitted the prediction of load-displacement behavior for cases that were not directly tested, such as those involving unequal gaps of the individual anchors of a connection.

2) For large eccentricity in shear (that is, at failure by fracture of the tension anchor), only small differences exist between the actual failure load of the connection and the values calculated according to plastic theory. For the connections studied here ($z_2/z_1 \geq 0.5$), differences are small between the assumed and the actual distributions of tension and shear on the anchors or anchor rows of the group.

3) The bulbous shape of the displacement interaction curve also causes a failure transition from the tension anchor to the shear anchor at a certain eccentricity of shear (Sections 4.3, 4.4 and 4.10 through 4.12). At this point, both the shear anchors and the tension anchors are fully utilized, and the assumptions of the plastic theory agree with the actual fracture state of the connections.

4) Except as a result of unequal gaps, the transverse displacement of the tension anchor cannot exceed the transverse displacement of the shear anchor. For that reason, the tension anchors of the group cannot reach the fracture states in the "bulge" of the displacement interaction curve. Contrary to the assumptions of plastic theory, this causes the strength of the tension anchor to not be fully utilized at small loading eccentricities (Sections 4.3, 4.4, and 4.10 through 4.12). Depending on how pronounced the "bulge" of the interaction curve is, the calculated capacity of the group can be considerably overestimated by plastic theory, or even by elastic theory.

5) These results clearly show that even given ductile failure of individual anchors, actual group capacities can be considerably overestimated by plastic theory. This leads to the conclusion that an adjustment of the plastic design method is required. Therefore, Section 5 of this report proposes an improvement of design by plastic theory, based on the assumption of an

even distribution of shear to all anchors. For the connections tested in this study, as well as those tested by Cook (1989), the modified design procedure provides good results.

Further results and conclusions from the tests on multiple-anchor connections, and from the continuing theoretical investigations, are summarized below:

- The loading history of the tension anchors of two-anchor connections under shear and bending, plotted on the force interaction diagram, is approximately straight, provided that there are no differences in gaps between both anchors. Shear does not redistribute from the tension anchor to the shear anchor in the fracture region. This is shown by the test results as well as the test calculations (Appendices 187, 190, 195, 198, 202, 205, 209, and 212).

- The calculations and tests show that with the anchor sizes of 5/8 inch (M16), failing by steel fracture, the effects of the gaps were partially compensated by the high shear stiffness of the anchor which is first not loaded in shear (Appendices 187, 190, 195, and 198). With concrete failure (Appendices 209, 212), as well as for steel failure with smaller anchor diameters (Appendices 202, 205), this compensation is conceivably not possible, due to the smaller displacements at failure. Regulations regarding the limit of the gaps must therefore include the anchor diameter, and must treat near-edge anchors separately.

- Depending on the baseplate extension length, anchors on the compression side resist considerable tension near failure (Figure 4.5), due to prying. This increases the transferable friction forces, though the shear in the anchors decreases. The net result is a small increase in the failure load.

- The calculation according to plastic theory leads to an overestimation of the failure load by 2% to 11% for the tested connection, based on the actual strength of each single anchor. Elastic theory underestimates the failure loads by up to 15%. Calculations based on load-displacement curves differ by at most 5% from the measured values, using a reasonable assumption of the internal lever arm.

- The results of Cook (1989) were suitably described by calculations based on load-displacement curves. The application of plastic theory leads to an overestimate of the failure load based on the actual strength of single anchors. Through application of plastic theory only for bending, without considering the redistribution of shear, the failure loads of the anchor groups tested by Cook can be approximately correctly estimated (Appendices 215, 216). However, the under-utilization of the second anchor row in tension then leads to about 3% smaller failure loads than projected according to plastic theory.

- With decreasing eccentricity of the applied shear, the ductility of the anchor group decreases. The shear deformation decreases the failure deformation of the tension anchors.

- In low-strength concrete, the failure displacements of individual anchors increase. However, this increase is much smaller under shear than under pure or oblique tension. The displacement interaction curve of single anchors is more bulbous than in higher strength concrete, even further reducing the extent to which the tension anchors are utilized (see Figure 4.12). The failure loads calculated from load-displacement curves for anchors in low-strength concrete fall below even the calculated values from elastic theory (Appendix 220).

- Anchors installed with through sleeves (anchor sleeve up to the top surface of the baseplate), failing by steel fracture, have higher failure loads and displacements than anchors installed with flush sleeves (anchor sleeve flush with surface of concrete). Calculations by plastic theory also lead in this case to an overestimation of the failure loads.

- Friction plays an essential role in the transfer of eccentric shear in multiple-anchor connections. At medium eccentricities, higher friction coefficients lead to higher failure loads. From comparisons between tests and calculations of investigations without Teflon sheets (Cook, 1989) and with Teflon sheets (Series 2.5 and 2.6 of this report), it is concluded that the relationship between calculations and tests is independent of the friction coefficient. In other words, whether friction is included or neglected, the effects are essentially the same for elastic theory, plastic theory, or computer calculations.

CHAPTER 7

OPEN QUESTIONS

The results of these theoretical and experimental investigations provide valuable bases for the application of plastic theory to multiple-anchor connections under shear and moment. However, to determine the necessary boundary conditions (such as failure displacement, or the utilization factor of a given anchor row depending on the shape of the load-displacement curves and the interaction of displacements), more investigation is required. The following paragraphs are offered by the author as means of processing questions and proposing possible solutions.

1) Load-Displacement Behavior of Single Anchors

   Some basic mechanisms of the dependence of the load-displacement behavior of single anchors on the loading direction could be clarified by this study. However, the number of tests and the parameters varied were not sufficient. It would be useful to conduct complementary finite-element calculations, especially to investigate the influences on the size and form of the shell-shaped spalling in the loading direction in front of the anchors under shear for a quantitative description. The loading direction and the confinement of the spalling by an baseplate are already established as essential influencing factors.

2) Parameter Studies

   The calculations carried out here provide information over a comparatively small range. Therefore, additional parameter studies are required, in which (besides the many influences on the form of the load-displacement curves and the interaction of displacements), the geometry of the baseplate and the attachment member, the concrete quality and strength, the gap and the location of the connection in relation to the member edge are varied. The presently available program BDA5 is not suitable for such extensive parameter studies. However, using the available results for the interaction of displacements, it can offer a basis for the development of a program to calculate the fracture load of a given connection for all geometrically possible fracture states. The results can then be plotted over the eccentricity of shear, as in this report.

   Figure 7.1 illustrates the proposed procedure in the form of a displacement interaction diagram for a connection with three anchor rows. For a given horizontal displacement, the maximum possible vertical displacement (at failure) of the outermost anchor can now be predicted. Based on a stiff baseplate and axis of rotation at the compression edge, the deformation of each anchor of the group at failure is well known. Given the load-displacement curves, the anchor forces and the size and eccentricity of the external load can be predicted. In a computer-aided calculation, the horizontal displacement must be used as the control dimension. This is maximized until the state described as "Case 2" in Figure 7.1 is reached. Then the horizontal displacement is again reduced (preferably in smaller steps), to predict the deformation state of the connection now governed by the failure of Anchor Row 1.

   With these simplifications, a closed-form solution of the problem is possible over a large range. Iteration is required only to approximate the failure transition from Row 1 to Row 3 (Case 2 in

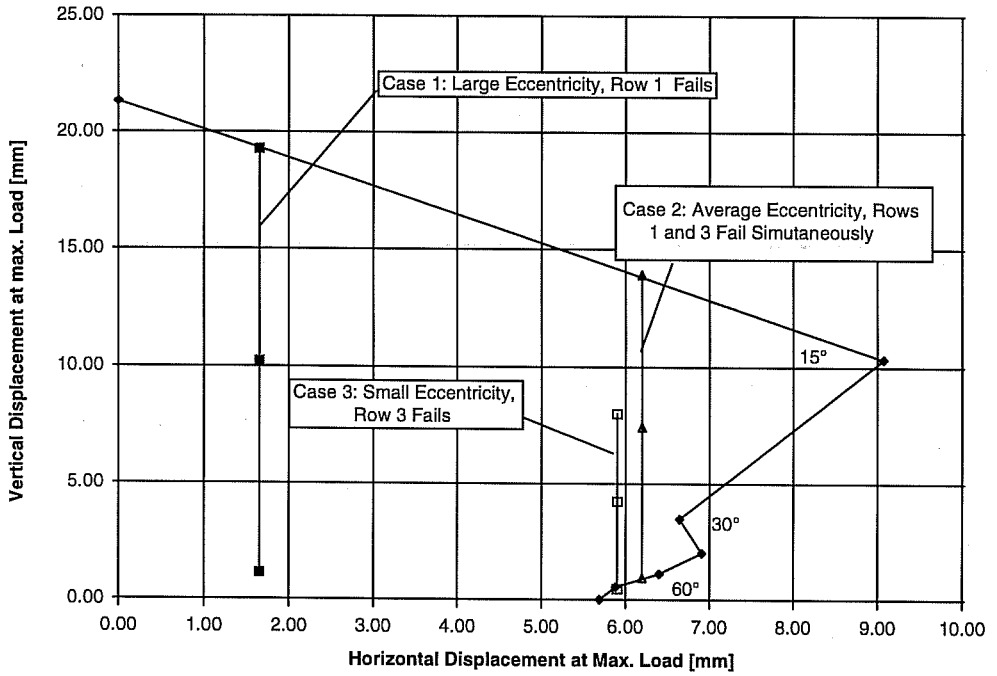

Figure 7. 1 *Proposed procedure for investigation of the possible failure states of a connection in the context of a calculation program*

Figure 7.1). The curves of failure load and failure deformation of the connection as functions of the eccentricity of the external shear could be computed very quickly for each parameter combination. By applying iterative solution methods, this procedure could be extended to address the gradual yielding of baseplates, and the crushing of the compression edge of the baseplate into the concrete. Gaps can easily be addressed as a constant difference of the horizontal displacement between anchor rows.

3. Development of General Rules of Application for the Plastic Design Procedure

Based on connection configuration and on the load-displacement behavior of the individual anchors of a connection, it is possible to derive general rules of application for plastic design. It is possible to develop rules in terms of the ratio z_{min}/z_n, in which z_n is the spacing of the outermost tension-zone anchor from the compression edge of the baseplate, and z_{min} is the least required spacing from the compression edge, so an anchor will reach its maximum strength.

Each of these three questions deals with research tasks of considerable sophistication and extensive scope. Nevertheless, it appears possible and meaningful to clarify these open questions, so that the plastic design approach can be developed into an efficient and simple procedure for the economic design of ductile baseplate connections.

CHAPTER 8

REFERENCES

Bode, H. And Roik, K. (1987): Headed Studs - Embedded in Concrete and Loaded in Tension. Anchorage to Concrete, American Concrete Institute, SP-103, Detroit, 1987, S. 61 - 89

CEB (1991): Fastenings to Reinforced Concrete and Masonry Structures, Bulletin D'Information No. 206 and 207, Comité Euro-International du Beton, 1991

Collins, D.M., Klingner, R. E., and Polyzois, D. (1989): Load-Deflection Behavior of Cast-in-Place and Retrofit Concrete Anchors Subjected to Static, Fatigue and Impact Tensile Loads. *Research Report No. 1126-1*, Center for Transportation Research, University of Texas, Austin, Texas, February 1989

Cook, R. A., and Klingner, R. E. (1989): "Behavior and Design of Ductile Multiple-Anchor Steel-To-Concrete Connections." *Research Report No. 1126-3*, Center for Transportation Research, University of Texas, Austin, Texas, March 1989

Cook, R. A., Doerr, G. T., and Klingner, R. E. (1989): "Design Guide for Steel-to-Concrete Connections." *Research Report No. 1126-4*, Center for Transportation Research, University of Texas, Austin, Texas, March 1989

Cook, R. A., and Klingner, R. E. (1992-1): "Ductile Multiple-Anchor Steel-To-Concrete Connections." *Journal of Structural Engineering*, Vol. 118, No. 6, June, 1992, S.1645-1665

Cook, R. A., and Klingner, R. E. (1992-2): "Behavior of Ductile Multiple-Anchor Steel-To-Concrete Connections with Surface-Mounted Baseplates." *Special Publication No.130-4*, Journal of the American Concrete Institute, 1992

Dieterle, H., Bozenhardt, A., Hirth, W., and Opitz V. (1989): "Tragverhalten von nicht generell zugzonentauglichen Dübeln, Teil 4: Verhalten im unbewegten Parallelriß unter Schrägzugbelastung." *Bericht Nr.* 1/45 - 89/19, Institut für Werkstoffe im Bauwesen, Universität Stuttgart 1989

Eibl, J., and Keintzel, E. (1989): "Zur Beanspruchung von Befestigungsmitteln bei dynamischen Lasten." *Forschungsbericht* T2169, Institut für Massivbau und Baustofftechnologie, Universität Karlsruhe, 1989.

Eligehausen, R., Fuchs, W., Lotze, D., and Reuter, M. (1989): "Befestigungen in der Betonzugzone." *Beton- und Stahlbetonbau Nr.*1/1989 S.27-32, Nr.2/1989 S.71-74

Fuchs, W.: (1990): "Tragverhalten von Befestigungen unter Querlast in ungerissenem Beton", Dissertation, Universität Stuttgart, 1990

Furche, J. (1994): "Zum Trag- und Verschiebungsverhalten von Kopfbolzen bei zentrischem Zug." Dissertation, Universität Stuttgart, 1994

Johnson, M., and Lew, H. (1990): "Experimental Study of Post-Installed Anchors under Combined Shear and Tension Loading." ACI Symposium "Anchorage to Concrete", Toronto, 1990

Klingner, R. E., Eligehausen, R., and Balogh, T. (1992): "The Role of Plastic Design Approaches For Single- And Multiple-Anchor Connections To Concrete." *Bericht Nr.* 12/19-92/13, Institut für Werkstoffe im Bauwesen, Universität Stuttgart, 1992

Lehmann, R. (1994): "Tragverhalten von Metallspreizdübeln im ungerissenen und gerissenen Beton bei der Versagensart Herausziehen." Dissertation, Universität Stuttgart, 1994

Li, L., and Eligehausen, R. (1993): "Tragverhalten von Gruppenbefestigungen unter kombinierter Schrägzug- und Momentenbeanspruchung." *Forschungsbericht* des Instituts für Werkstoffe im Bauwesen, Universität Stuttgart, August 1993

Li, L. (1994): "BDA5: Programm zur Berechnung des Trag- und Verformungsverhaltens von Gruppenbefestigungen unter kombinierter Schrägzug- und Momentenbeanspruchung." *Bericht* des Instituts für Werkstoffe im Bauwesen, Universität Stuttgart, August 1994

Lieberum, K.-H. (1987): "Das Tragverhalten von Beton bei extremer Teilflächenbelastung." Dissertation, Technische Hochschule Darmstadt, 1987

Lieberum, K.-H. (1990): "Lokal hohe Pressungen - Einfluß der Betonzusammensetzung und der Belastungsgeometrie auf das Last - Verformungsverhalten." *Darmstädter Massivbau-Seminar*, Band 5, Verankerungen in Beton, TH Darmstadt, 1990

Lotze, D. (1986): "Tragverhalten von Dübeln unter nicht vorwiegend ruhender Belastung, Tragverhalten von Gruppenbefestigungen." *Bericht Nr.* 11/3 - 86/11, Institut für Werkstoffe im Bauwesen, Universität Stuttgart, 1986

Lotze, D. (1989): "Tragverhalten von Dübeln unter nicht vorwiegend ruhender Belastung - Stand der Kenntnisse und mögliche Perspektiven." *Bericht Nr.* 11/7 - 89/14, Institut für Werkstoffe im Bauwesen, Universität Stuttgart, 1989

Lotze, D. (1989): "Beeinflussung der Trag- und Gebrauchsfähigkeit von Stahlbetonbauteilen durch Spaltkräfte von Befestigungen." *Werkstoff und Konstruktion II* (Prof. Dr.-Ing. Dr.-Ing. E. h. Gallus Rehm zum 65. Geburtstag) S.169 - 178, Otto-Graf-Institut, Oktober, 1989

Lotze, D. (1992): "Tragverhalten und Anwendung von Dübeln unter oftmals wiederholter Belastung." Dissertation, Universität Stuttgart, 1993

PCI (1985): *PCI Design Handbook*, Precast and Prestressed Concrete, Third Edition, 1985

Rehm, G., Eligehausen, R., and Mallée, R. (1992): "Befestigungstechnik." *Betonkalender 1992*, S.569 - 663

Rodriguez, M. (1995): "Behavior of Anchors in Uncracked Concrete under Static and Dynamic Tensile Loading." Master Thesis, University of Texas at Austin, 1995

Shaikh, A., and Whayong, Y. (1985): "In-place Strength of Welded Headed Studs." *Journal* of the Prestressed Concrete Institute 1985 S. 56 - 81

UEAtc (1992): UEAtc Technical Guide on Anchors for Use in Cracked and Non-cracked Concrete, Union Européenne Pour L'agrément Technique Dans La Construction, 1992.

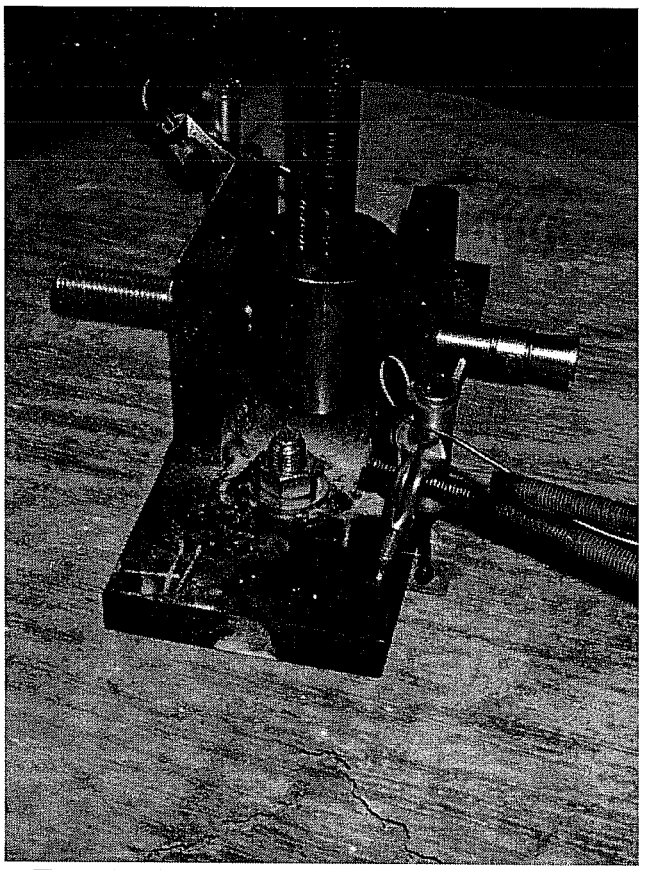

Pure Tension Test on Two-Anchor Connections, Baseplate with Connection to Threaded Rod and Displacement Measurement

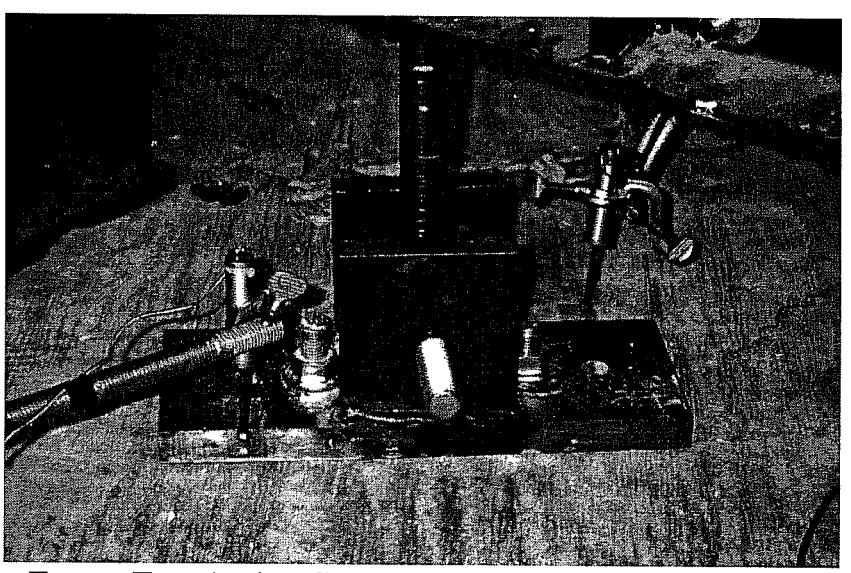

Pure Tension Test on Two-Anchor Connections, Baseplate with Connection to Threaded Rod and Displacement Measurement

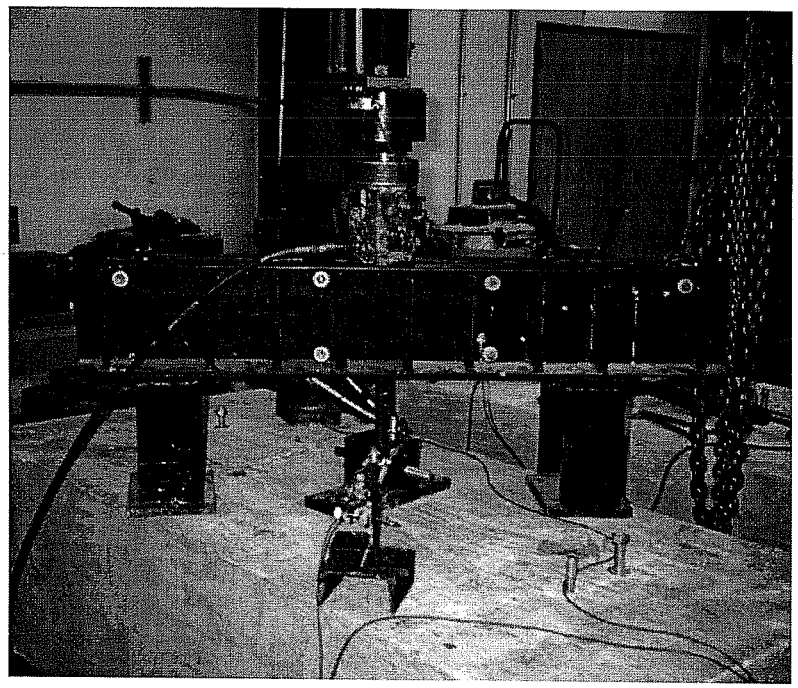

Test Setup of Series 2.1, Pure Tension Tests on Two-Anchor Connections, Static Loading

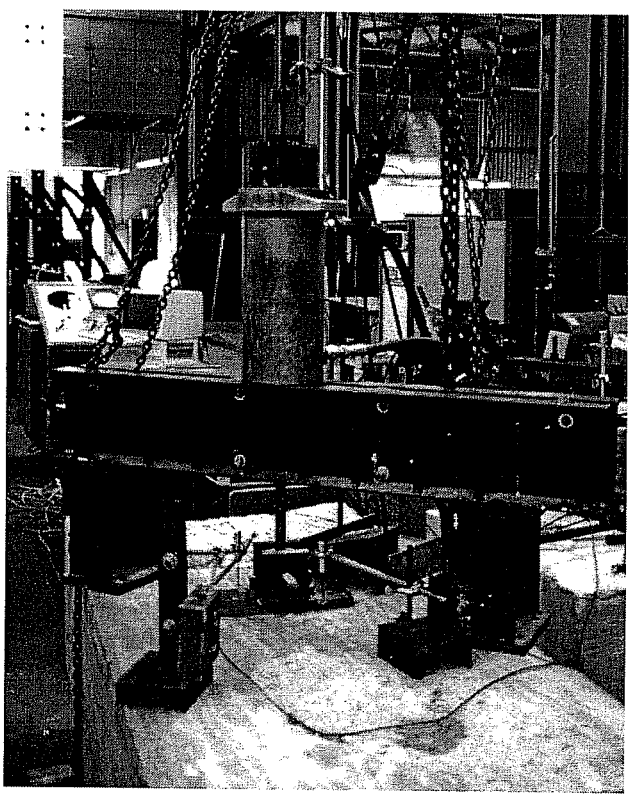

Test Setup of Series 2.2, Pure Tension Tests on Two-Anchor Connections, Dynamic Loading

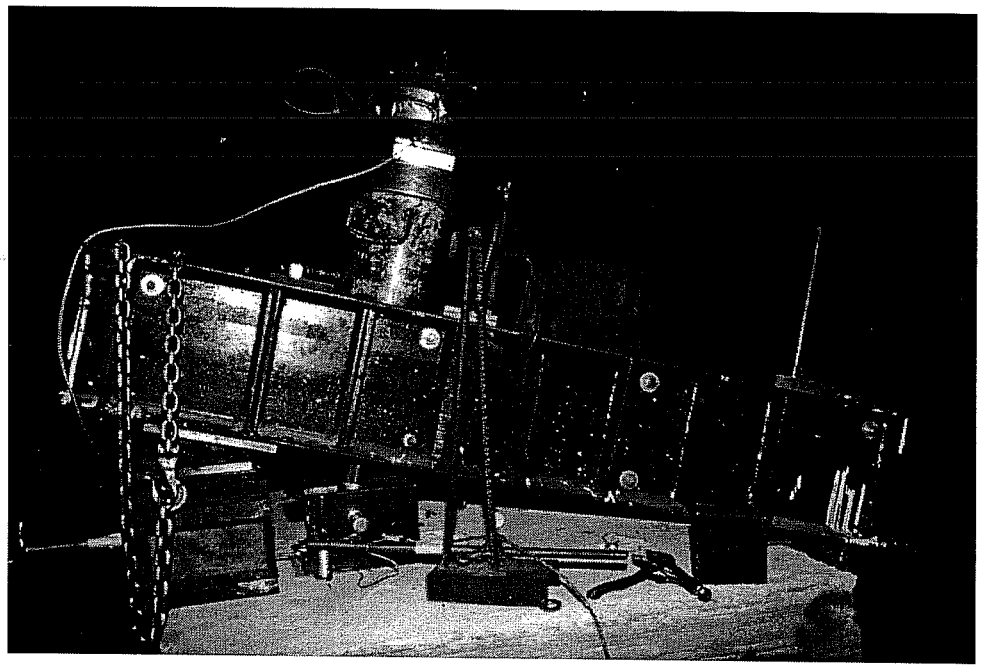

Test Setup of Series 2.3, Oblique Tension Tests at 15° with Steel Failure

Bearing Support of Series 2.3, Oblique Tension Tests at 15° with Steel Failure

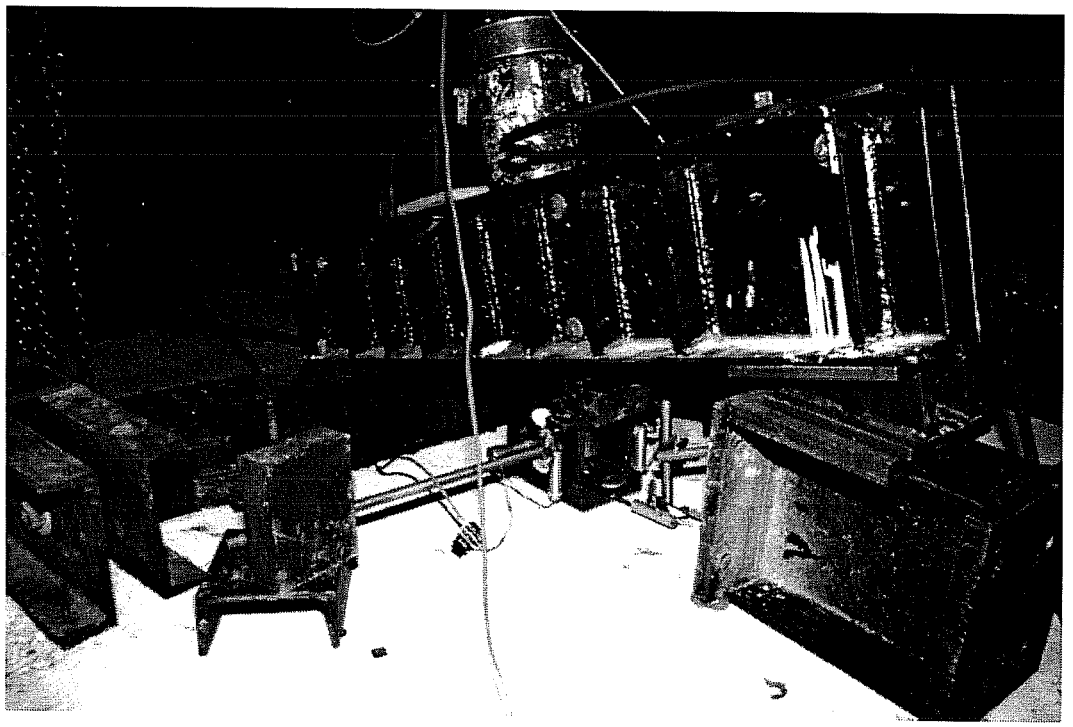

Test Setup of Series 2.4, Oblique Tension Tests at 15° with Concrete Failure Breakout

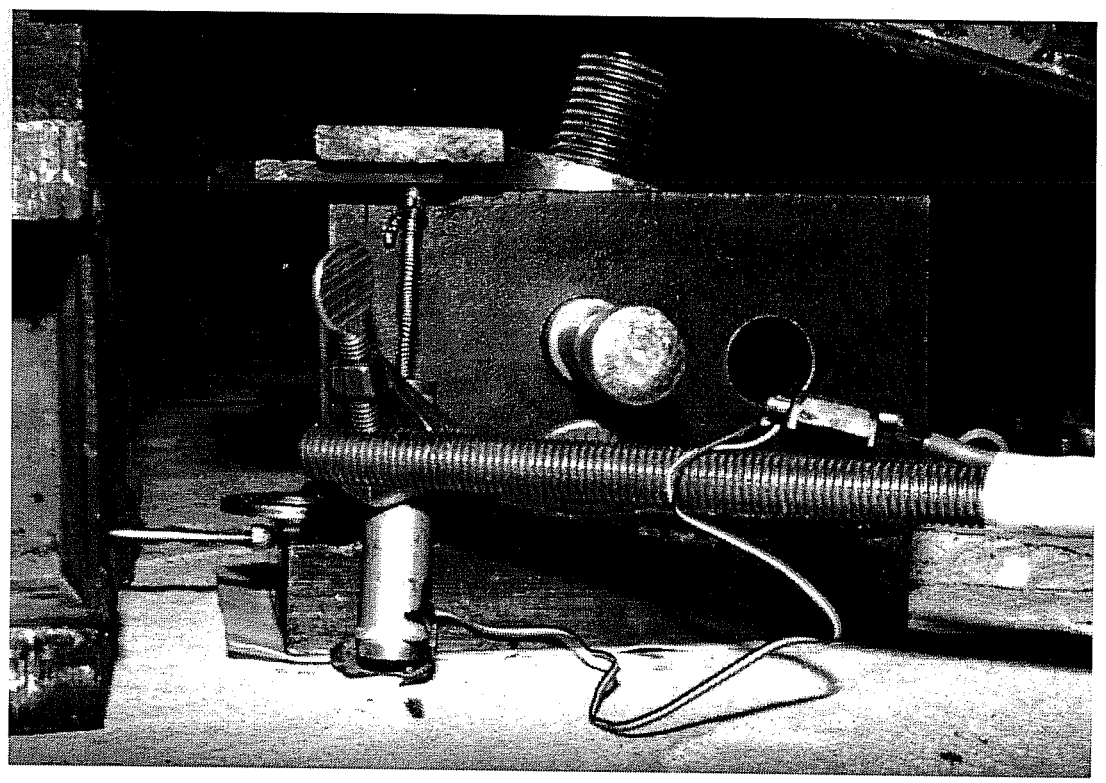

Loading Shoe with Displacement Measurement, Oblique Tension Tests at 15°

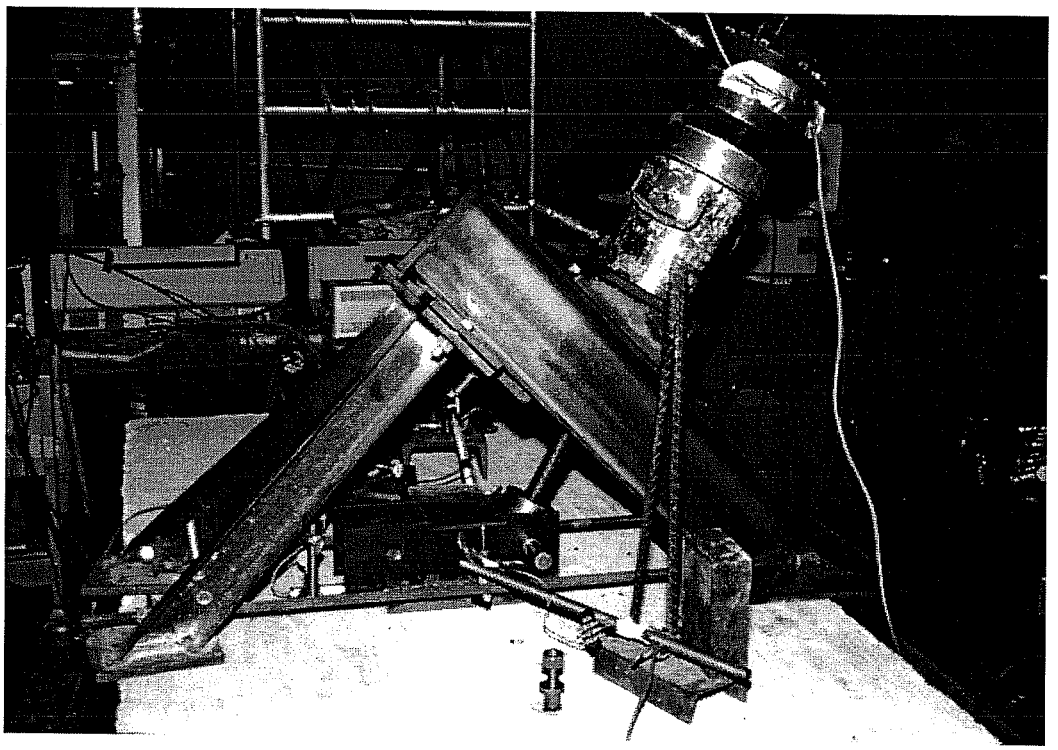

Test Setup of Series 2.3, Oblique Tension Tests at 30° - 60° (here 30°) with Steel Failure

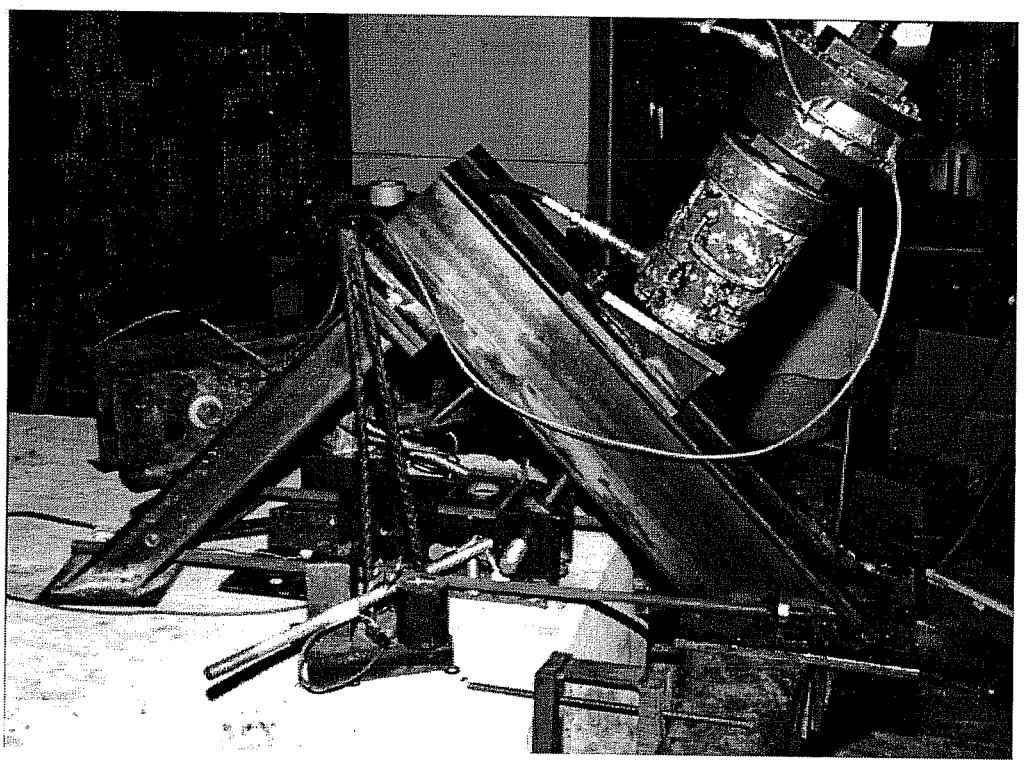

Test Setup of Series 2.4, Oblique Tension Tests at 30° - 60° (here 30°) with Concrete Failure

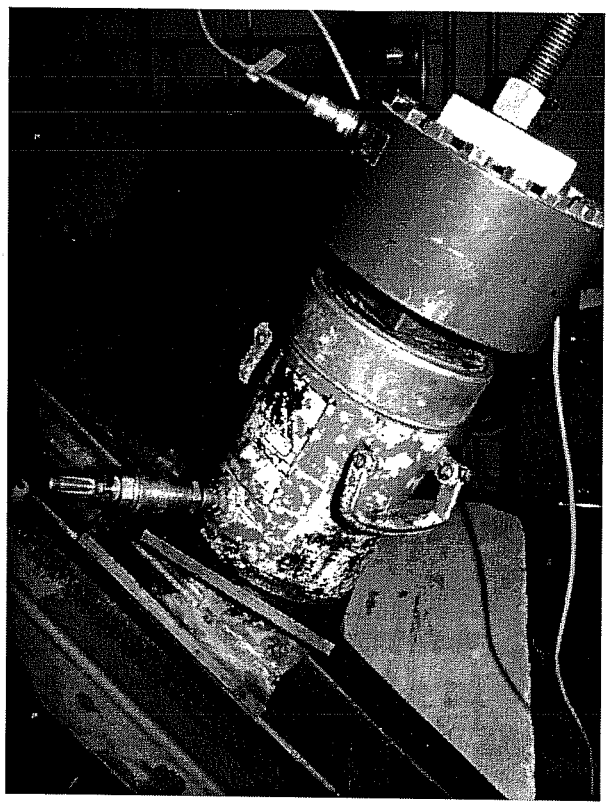

Hydraulic Ram with Load Cell Mounted on 15° Wedge Element and 45° Frame for Oblique Tension Tests at 30°, Series 2.3 or 2.4

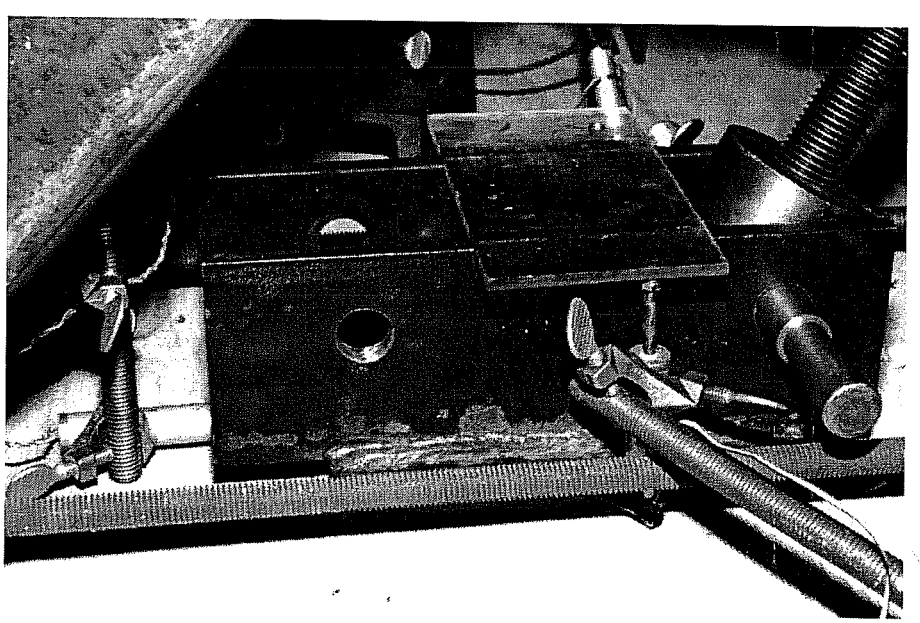

Loading Shoe for Oblique Tension Tests of Series 2.3 and 2.4 at 30° or 60° (here 30°) with Threaded Rod Connection and Displacement Measurement

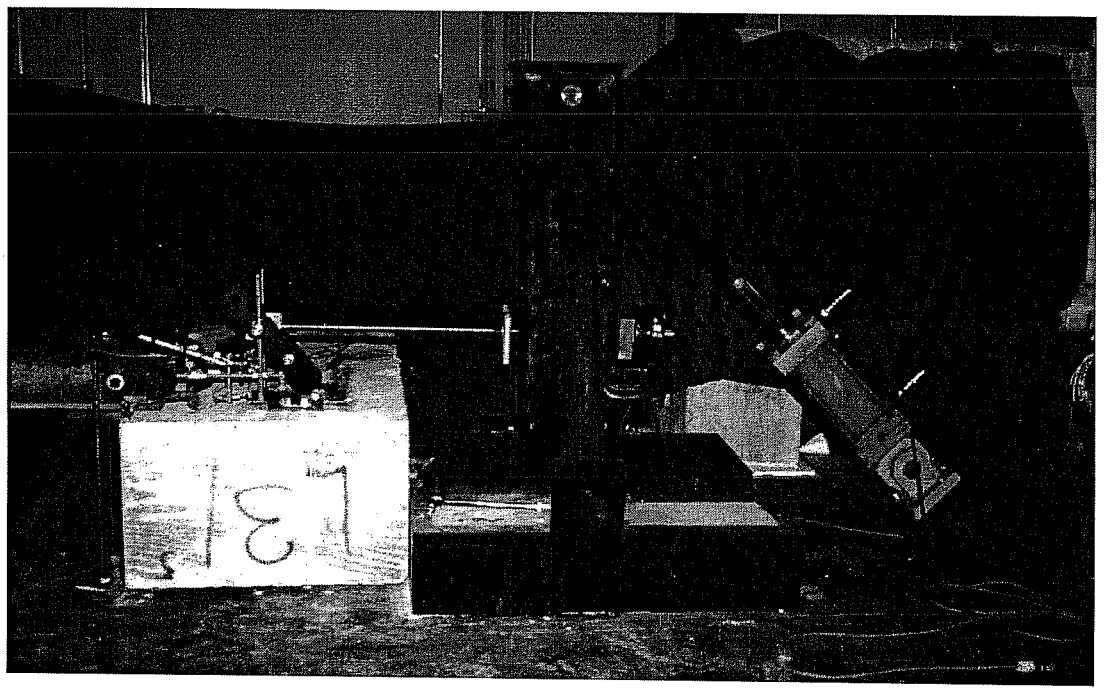

Test Setup of Series 2.5 and 2.6, Two-Anchor Connections under Shear and Bending

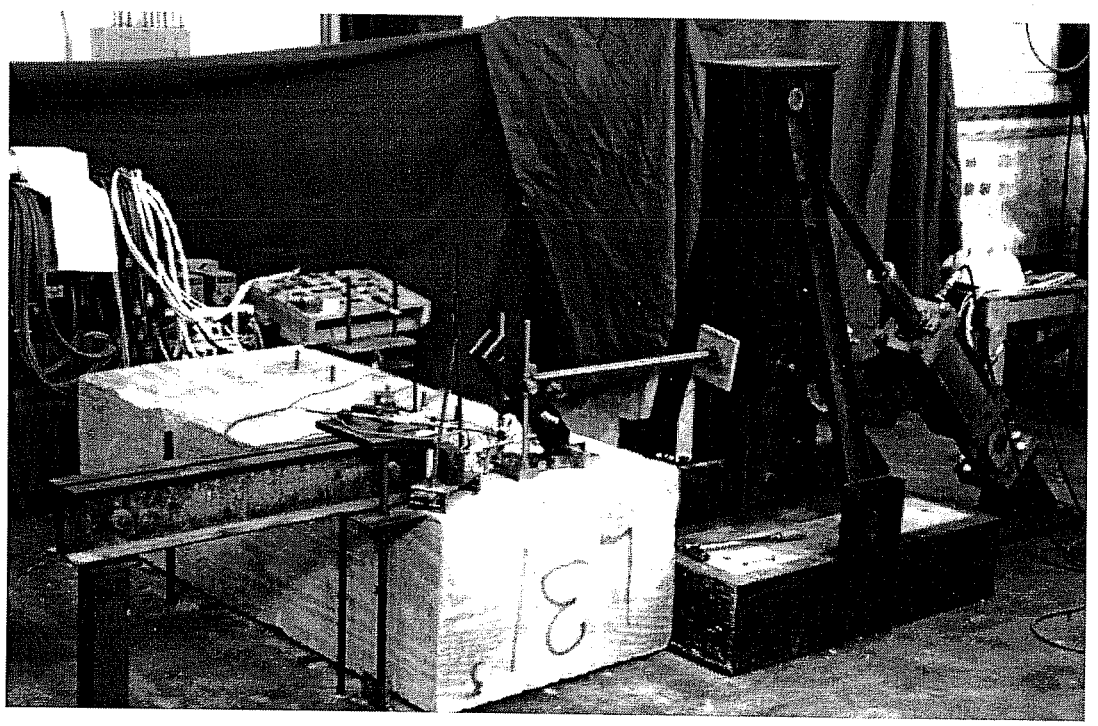

Test Setup of Series 2.5 and 2.6, Two-Anchor Connections under Shear and Bending

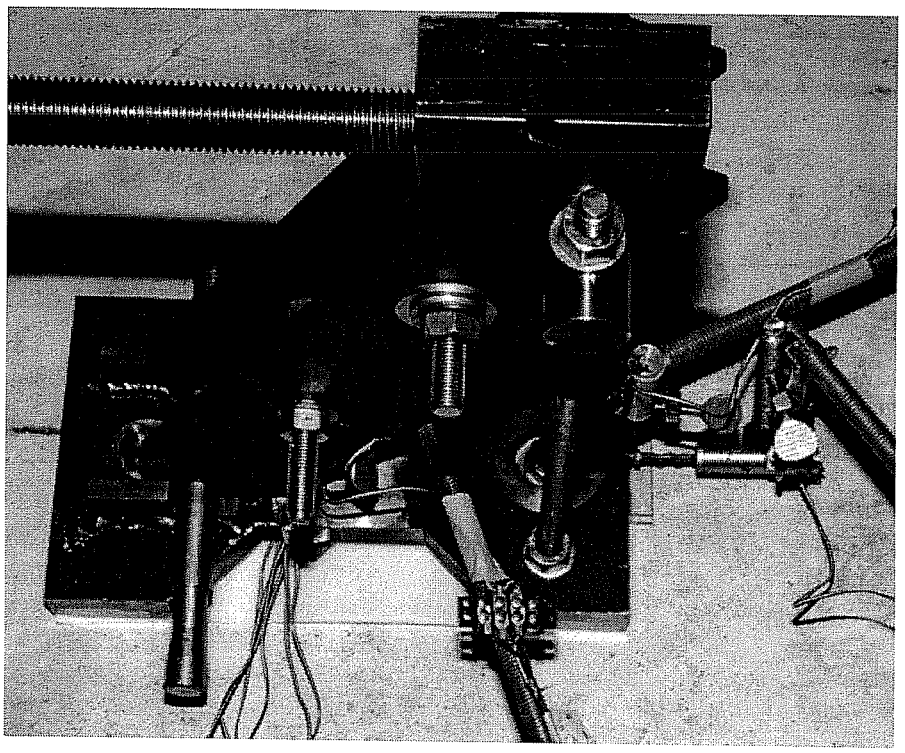

Test Setup of Series 2.5 and 2.6, Two-Anchor Connections under Shear and Bending, Load Transfer to Baseplate and Measurement Setup (Plan View)

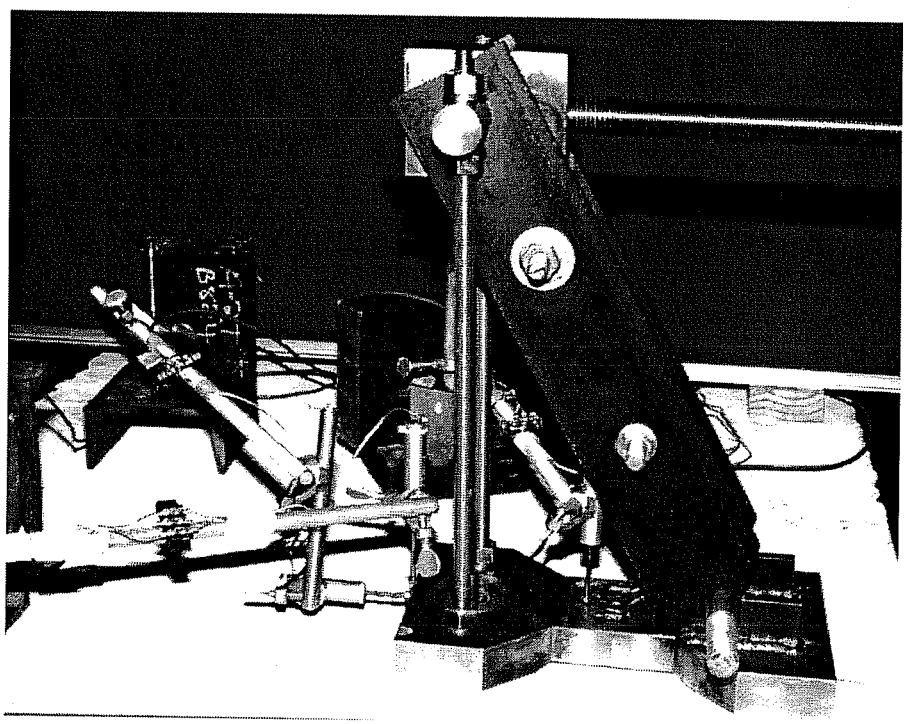

Test Setup of Series 2.5 and 2.6, Two-Anchor Connections under Shear and Bending, Load Transfer to Baseplate and Measurement Setup (Elevation)

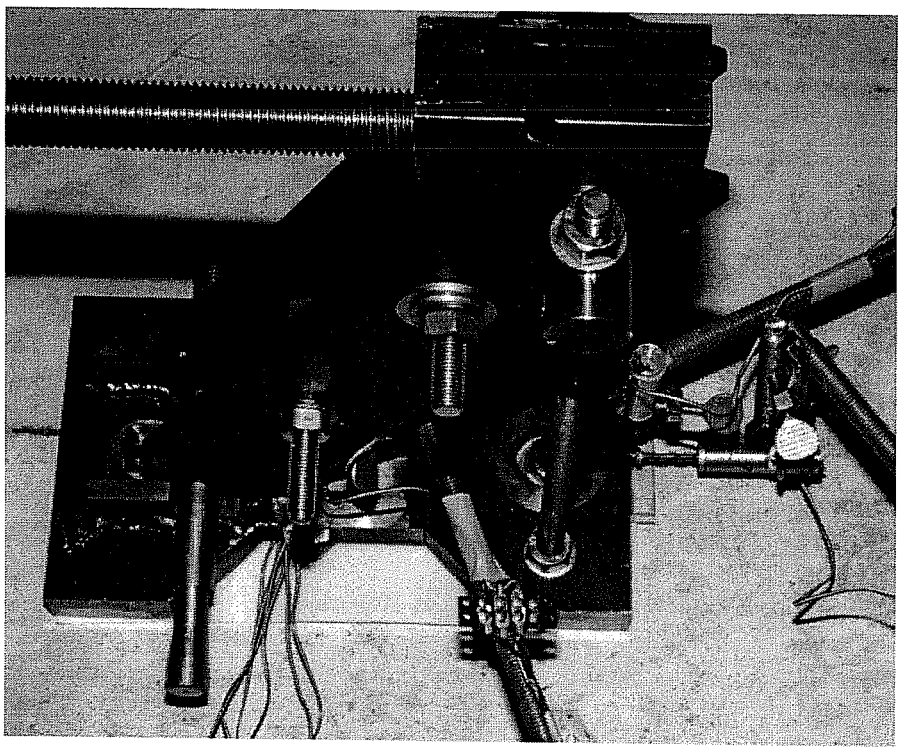

Test Setup of Series 2.5 and 2.6, Two-Anchor Connections under Shear and Bending, Load Applied to Baseplate and Measurement Setup (Plan View)

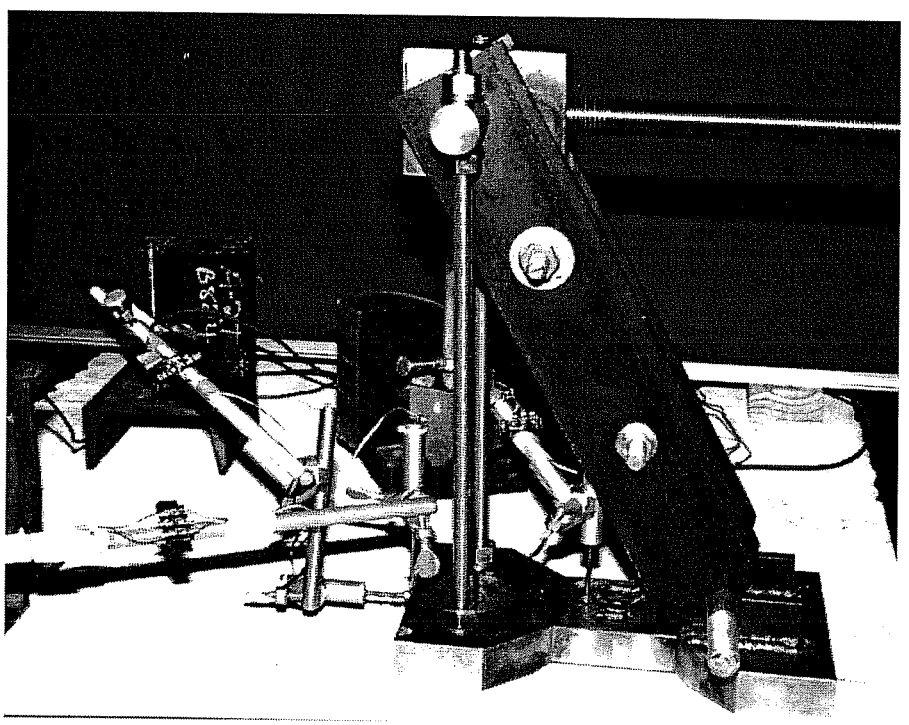

Test Setup of Series 2.5 and 2.6, Two-Anchor Connections under Shear and Bending, Load Applied to Baseplate and Measurement Setup (Elevation)

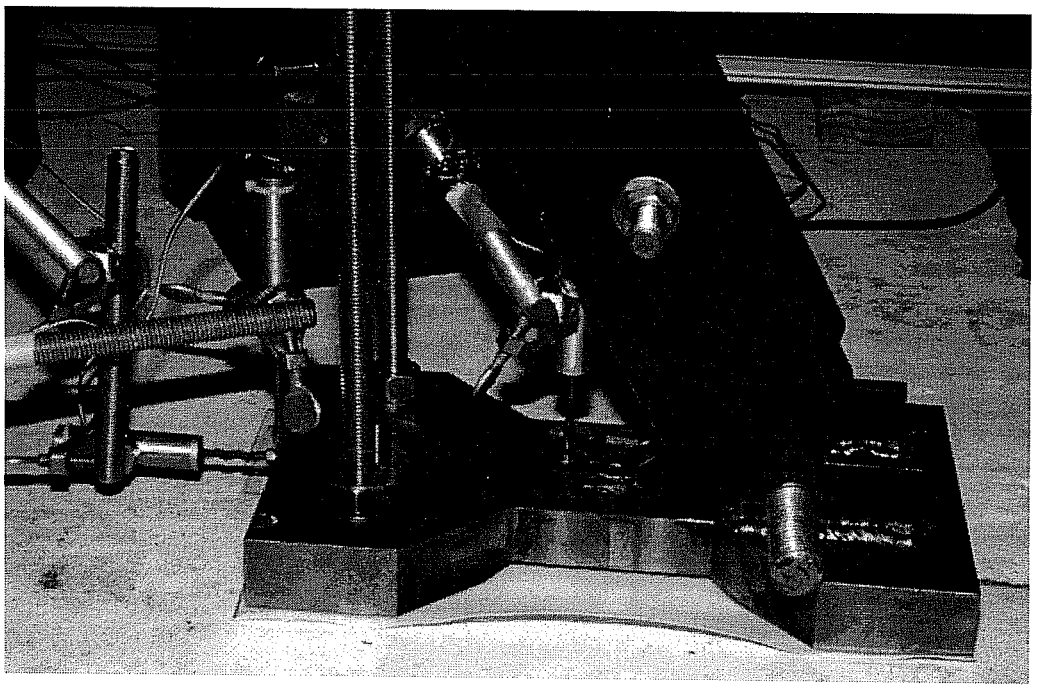

Test Setup of Series 2.5 and 2.6, Two-Anchor Connections under Shear and Bending, Baseplate Details

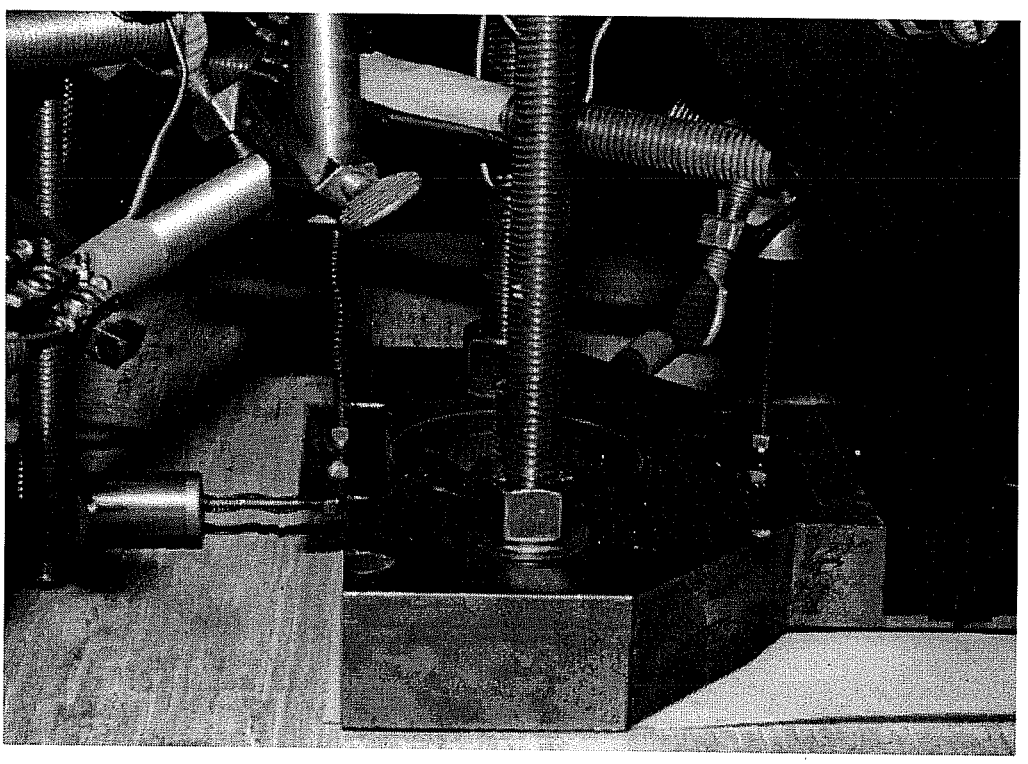

Test Setup of Series 2.5 and 2.6, Two-Anchor Connections under Shear and Bending, Details of Measurement Setup at Tension Side of Baseplate

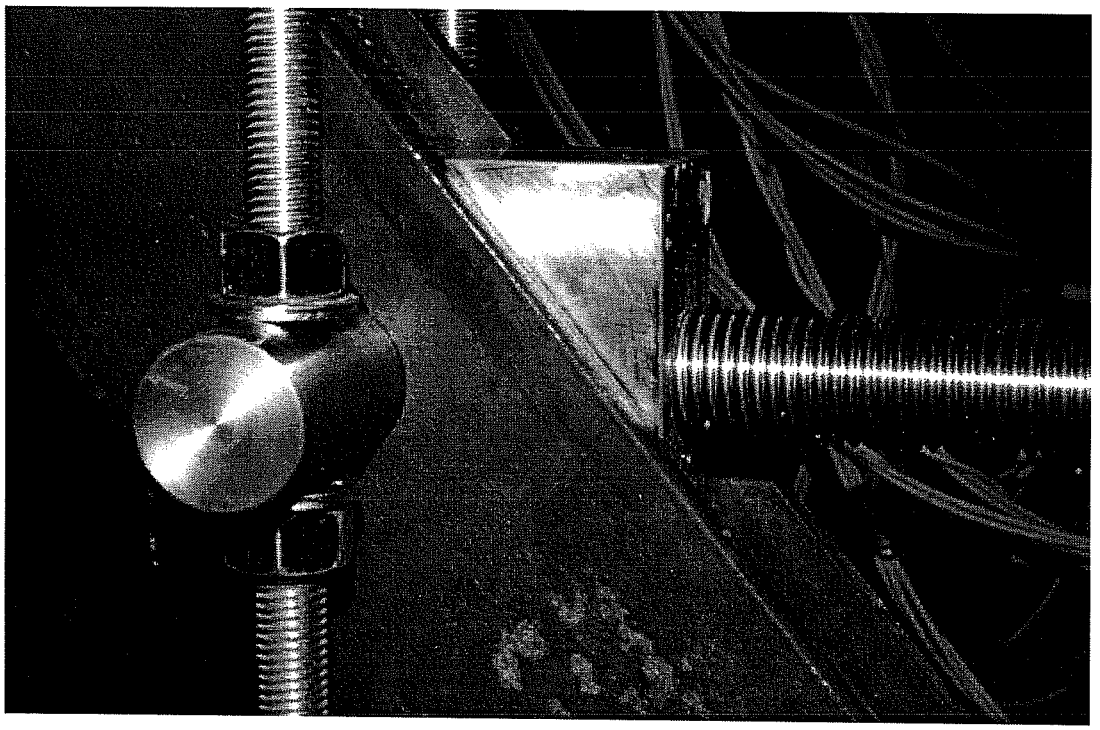

Test Setup of Series 2.5 and 2.6, Two-Anchor Connections under Shear and Bending, Details of the Upper Joint Connection

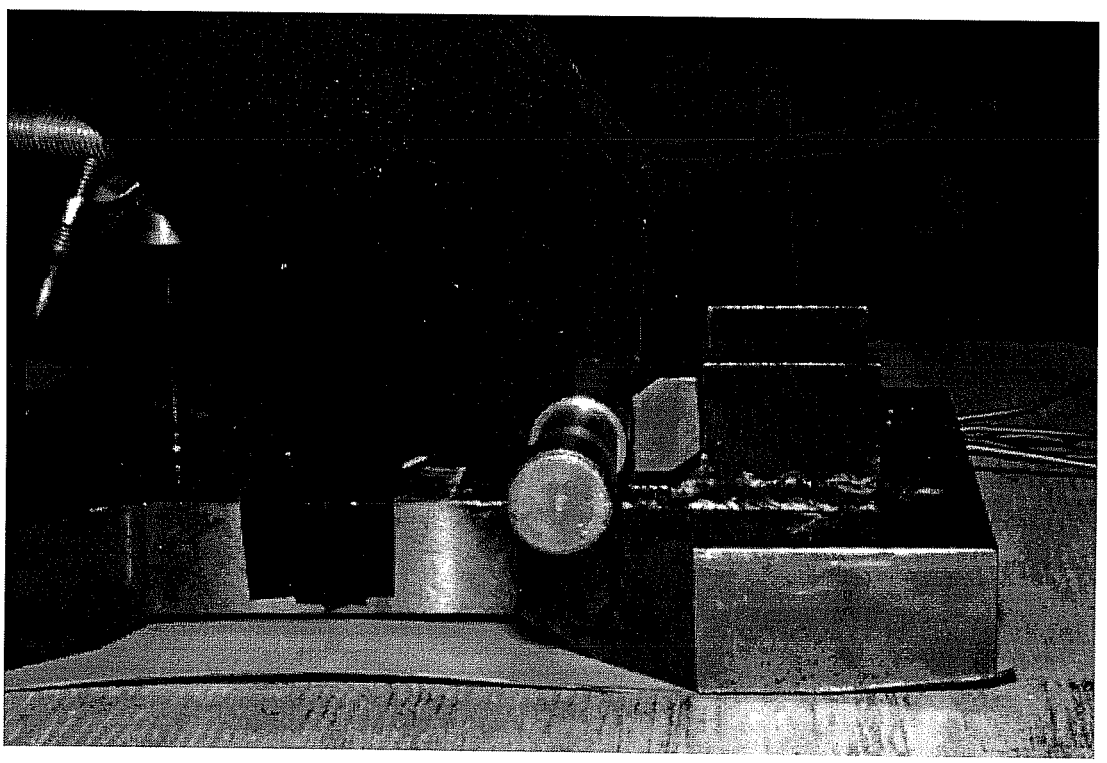

Test Setup of Series 2.5 and 2.6, Two-Anchor Connections under Shear and Bending, Details of Compression Side of Baseplate

Test No.	Anchor	Spacing s / h_{ef}	Torque Nm	Loading Time min:sec	Block No.	Concrete Strength f_c [N/mm²]	Failure Load F_u kN	Displ. at Failure d_u mm	F_u (f_c = 32,4) kN	Failure Mode 1)	Location of Fastening 2)	Note
21SM2501	UC1 3/4 in.	2.5	271/136	3:10	L29-T	25.9	169.5	(2.12)	189.5	1 BA	M	
2	UC1 3/4 in.	2.5	271/136	3:15	L28-T	25.9	177.9	0.660	198.9	2 BA/Sp	E	
3	UC1 3/4 in.	2.5	271/136	3:20	L28-T	25.9	188.2	0.406	210.3	2 BA	E	
4	UC1 3/4 in.	2.5	271/136	3:20	L29-B	25.9	190.8	1.003	213.3	1 BA	M	
5	UC1 3/4 in.	2.5	271/136	3:20	L28-B	25.9	192.2	0.648	214.8	1 BA/Sp	E	
Ave. [kN]							**183.7**	**0.679**	**205.4**			
COV [%]							**5.29**	**36.13**	**5.29**			
21SM1501	UC1 3/4 in.	1.5	271/136	3:05	L29-T	25.9	172.1	0.521	192.4	2 BA/Sp	E	
2	UC1 3/4 in.	1.5	271/136	3:00	L29-T	25.9	163.7	(0.2159)	183.0	2 BA/Sp	E	
3	UC1 3/4 in.	1.5	271/136	1:30	L28-T	25.9	159.7	(0.1905)	178.5	2 BA	M	4)
4	UC1 3/4 in.	1.5	271	2:35	L29-B	25.9	149.5	1.270	167.1	2 BA	E	
5	UC1 3/4 in.	1.5	271/136	2:45	L29-B	25.9	150.3	0.851	168.1	2 BA/Sp	E	
Ave. [kN]							**159.1**	**0.881**	**177.8**			
COV [%]							**5.97**	**42.65**	**5.97**			
21SH2501	Sleeve M20	2.5	258/129	2:45	L1-T	28.3	152.1	2.248	162.7	1 BA	M	
2	Sleeve M20	2.5	258	3:00	L1-T	28.3	168.6	1.651	180.3	2 BA	E	
3	Sleeve M20	2.5	258/129	3:15	L1-B	28.3	190.8	2.845	204.0	Splitting	E	
4	Sleeve M20	2.5	258/129	2:45	L1-B	28.3	158.8	(5.41)	169.8	2 BA	M	
5	Sleeve M20	2.5	258/129	2:30	L1-B	28.3	140.1	2.616	149.8	Splitting	E	
Ave. [kN]							**162.1**	**2.340**	**173.3**			
COV [%]							**11.79**	**22.27**	**11.79**			
21SH1501	Sleeve M20	1.5	258/129	2:30	L3-T	28.3	139.2	1.257	148.9	Splitting	E	
2	Sleeve M20	1.5	258/129	2:45	L2-T	28.3	149.5	1.473	159.8	1 BA	M	3)
3	Sleeve M20	1.5	258/129	2:00	L3-B	28.3	128.5	(5.45)	137.5	2 BA/Sp	E	
4	Sleeve M20	1.5	258/129	2:30	L3-B	28.3	129.4	3.099	138.4	2 BA/Sp	E	
5	Sleeve M20	1.5	258/129	2:45	L3-B	28.3	140.1	1.499	149.8	2 BA	M	
Ave. [kN]							**137.4**	**1.832**	**146.9**			
COV [%]							**6.28**	**46.48**	**6.28**			

1) 1 BA = Concrete breakout at an anchor
2 BA = Concrete breakout at both anchors
Sp = Splitting at specimen end

2) E = Fastening installed at the end of the specimen ($c1 > 350$ mm), M = Fastening installed in the middle of the specimen

3) Only 1 displacement measured

4) Fastening without displacement measured up to 138 [kN], then unloaded and loaded again with displacement measurement

Test Results of Series 21: Two-Anchor Connections under Pure Tension, Enbedment Depth h_{ef} = 101.6 mm, Static Load = 2 - 4 Minutes until Failure

Testing Period: Jul. 1, 94 - Jul. 7, 94 (UC1), Mar. 3, 94 - Mar. 10, 94 (Sleeve)

Test No.	Anchor	Spacing s / h_{ef}	Torque Nm	Loading Time sec	Block	Concrete Strength f_c [N/mm²]	Failure Load F_u kN	Displ. at Failure d_u mm	F_u (f_c=32,4) kN	Failure Mode 1)	Location of Fastening 2)	Note
22DM2501	UC1 3/4 in.	2.5	271/136	0.1	L28-B	27.7	205.9	4.775	222.6	1-2 BA	M	
2	UC1 3/4 in.	2.5	271/136	0.1	L30-T	27.7	199.7	4.191	215.8	2 BA	E	
3	UC1 3/4 in.	2.5	271/136	0.1	L30-B	27.7	218.4	2.794	236.0	2 BA	E	
4	UC1 3/4 in.	2.5	271/136	0.1	L30-B	27.7	235.7	2.819	254.8	1-2 BA	E	
Ave.							**214.9**	**3.645**	**232.3**			
COV [%]							**7.39**	**27.35**	**7.39**			
22DM1501	UC1 3/4 in.	1.5	271/136	0.1	L28-B	27.7	197.0	1.295	213.0	2 BA/Sp	E	
2	UC1 3/4 in.	1.5	271/136	0.1	L30-T	27.7	187.3	1.143	202.4	2 BA/Sp	E	
3	UC1 3/4 in.	1.5	271/136	0.1	L30-T	27.7	197.0	1.219	213.0	2 BA	M	
4	UC1 3/4 in.	1.5	271/136	0.1	L30-B	27.7	183.3	1.524	198.1	2 BA/Sp	E	
Ave. [kN]							**191.2**	**1.295**	**206.6**			
COV [%]							**3.66**	**12.71**	**3.66**			
22DH2501	Sleeve M20	2.5	258/129	0.1	L4-T	29.5	225.5	2.946	236.2	2 BA/Sp	E	
2	Sleeve M20	2.5	258	0.1	L4-T	29.5	238.0	2.6035	249.2	1-2 BA	M	3)
3	Sleeve M20	2.5	258/129	0.1	L2-B	29.5	226.8	2.570	237.6	2 BA	E	
4	Sleeve M20	2.5	258/129	0.1	L4-B	29.5	250.4	2.329	262.2	2 BA	E	
Ave. [kN]							**235.2**	**2.612**	**246.3**			
COV [%]							**4.93**	**9.74**	**4.93**			
22DH1501	Sleeve M20	1.5	258/129	0.1	L2-T	29.5	214.8	3.734	225.0	2 BA/Sp	E	
2	Sleeve M20	1.5	258/129	0.1	L4-T	29.5	213.1	1.803	223.1	2 BA	E	
3	Sleeve M20	1.5	258/129	0.1	L2-B	29.5	205.1	4.495	214.7	2 BA/Sp	E	
4	Sleeve M20	1.5	258/129	0.1	L2-B	29.5	181.5	4.751	190.0	2 BA	M	
5	Sleeve M20	1.5	258/129	0.1	L4-B	29.5	203.3	3.294	212.9	2 BA	M	
Ave. [kN]							**203.5**	**3.615**	**213.1**			
COV [%]							**6.53**	**32.33**	**6.53**			

1) 1 BA = Concrete breakout at an anchor
2 BA = Concrete breakout at both anchors
Sp = Splitting at specimen end
2) E = Fastening installed at the end of the specimen (c1 > 350 mm), M = Fastening installed in the middle of the specimen
3) Only 1 displacement measured

Test Results of Series 22: Two-Anchor Connections under Pure Tension, Embedment Depth h_{ef} = 101.6 mm, Dynamic Loading = 0.1 sec. until Failure

Testing Period: Jul. 28, 94 - Aug. 1, 94 (UC1), Aug. 3, 94 - Aug. 9, 94 (Sleeve)

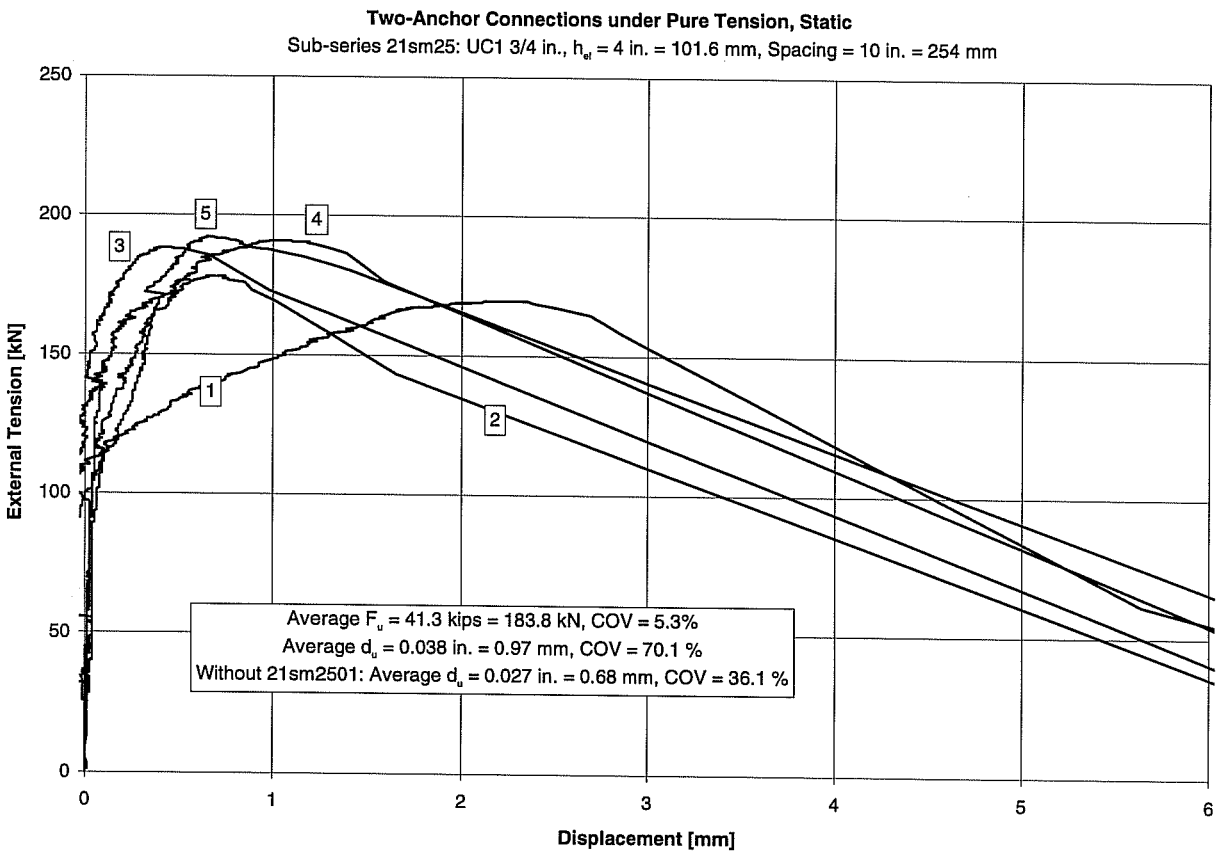
Two-Anchor Connections under Pure Tension, Static
Sub-series 21sm25: UC1 3/4 in., h_{ef} = 4 in. = 101.6 mm, Spacing = 10 in. = 254 mm
External Tension [kN]
Displacement [mm]
250
200
150
100
50
0
0
1
2
3
4
5
6
1
2
3
4
5
Average F_u = 41.3 kips = 183.8 kN, COV = 5.3%
Average d_u = 0.038 in. = 0.97 mm, COV = 70.1 %
Without 21sm2501: Average d_u = 0.027 in. = 0.68 mm, COV = 36.1 %

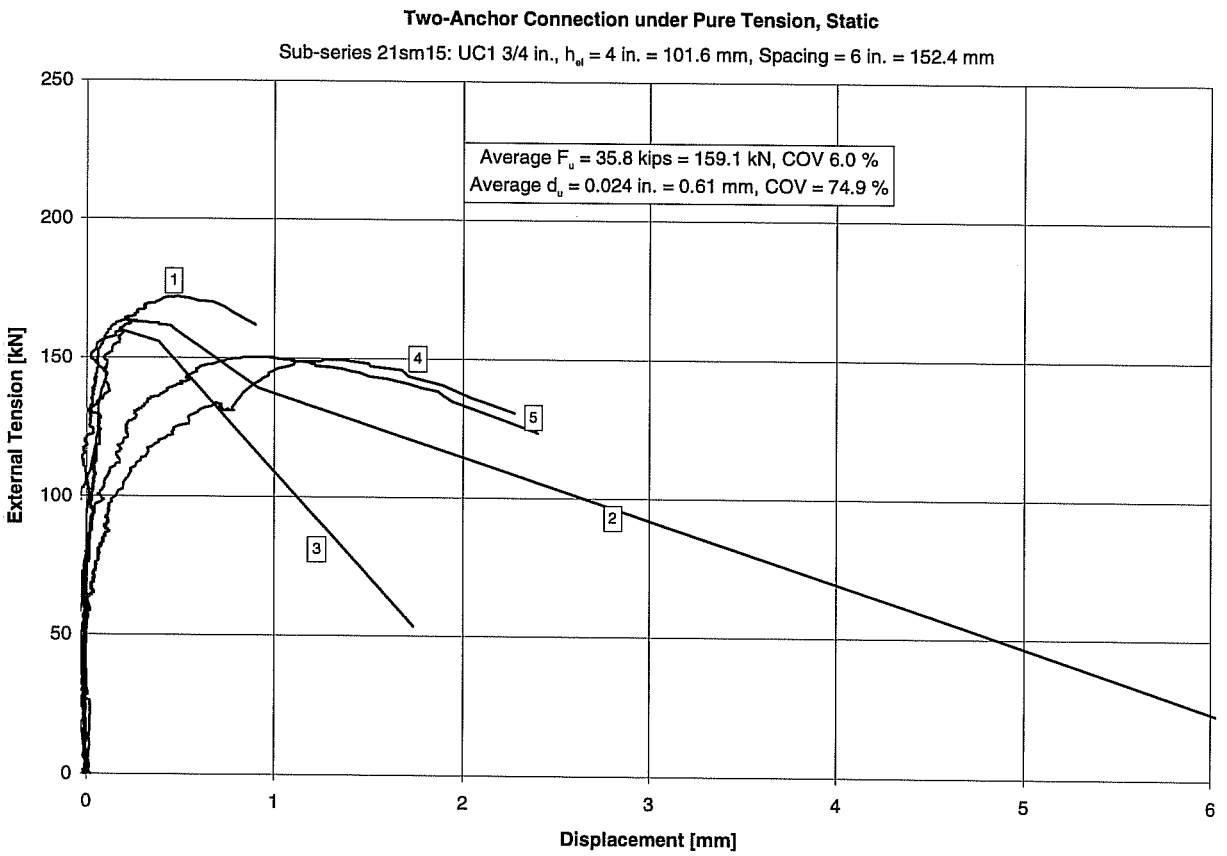
Two-Anchor Connection under Pure Tension, Static
Sub-series 21sm15: UC1 3/4 in., h_{el} = 4 in. = 101.6 mm, Spacing = 6 in. = 152.4 mm
Average F_u = 35.8 kips = 159.1 kN, COV 6.0 %
Average d_u = 0.024 in. = 0.61 mm, COV = 74.9 %
External Tension [kN]
Displacement [mm]
250
200
150
100
50
0
0
1
2
3
4
5
6
1
2
3
4
5

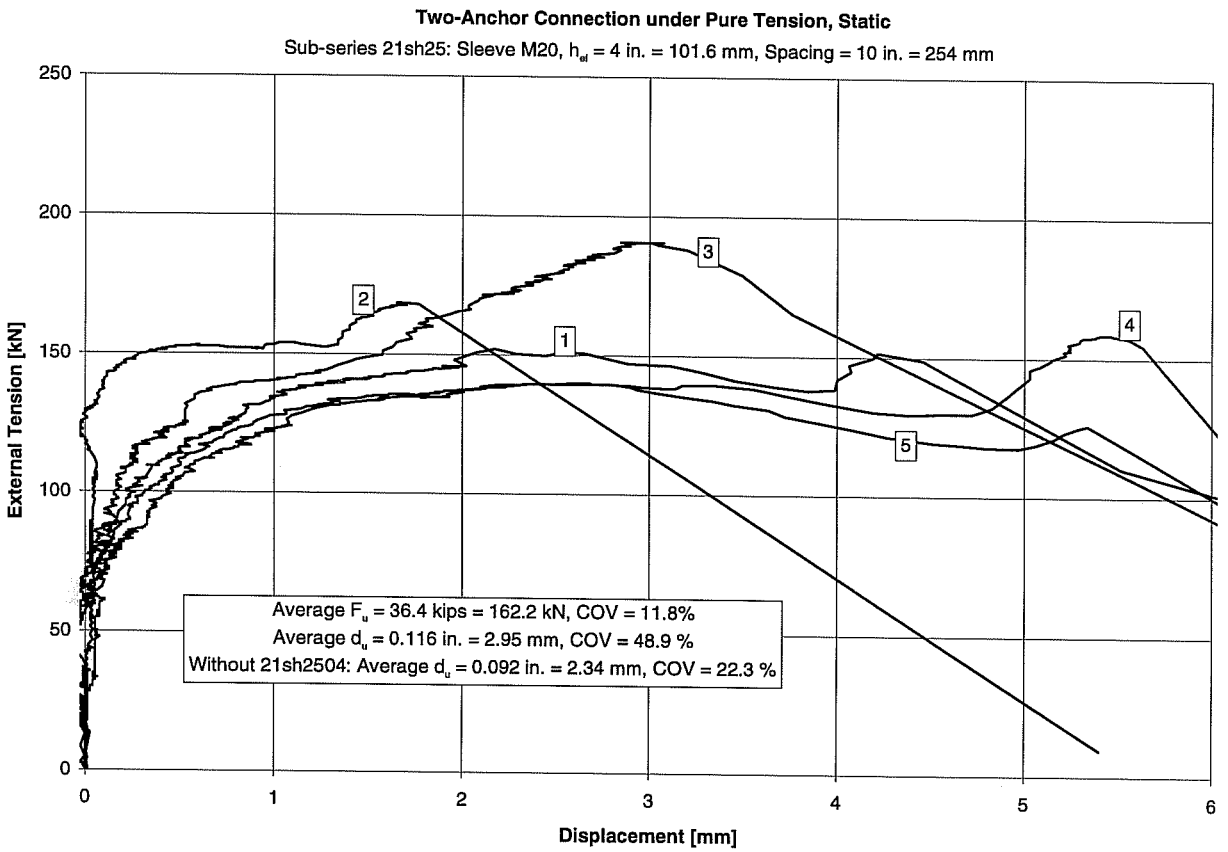
Two-Anchor Connection under Pure Tension, Static
Sub-series 21sh25: Sleeve M20, h_{ef} = 4 in. = 101.6 mm, Spacing = 10 in. = 254 mm
External Tension [kN]
250
200
150
100
50
0
0
1
2
3
4
5
6
Displacement [mm]
1
2
3
4
5
Average F_u = 36.4 kips = 162.2 kN, COV = 11.8%
Average d_u = 0.116 in. = 2.95 mm, COV = 48.9 %
Without 21sh2504: Average d_u = 0.092 in. = 2.34 mm, COV = 22.3 %

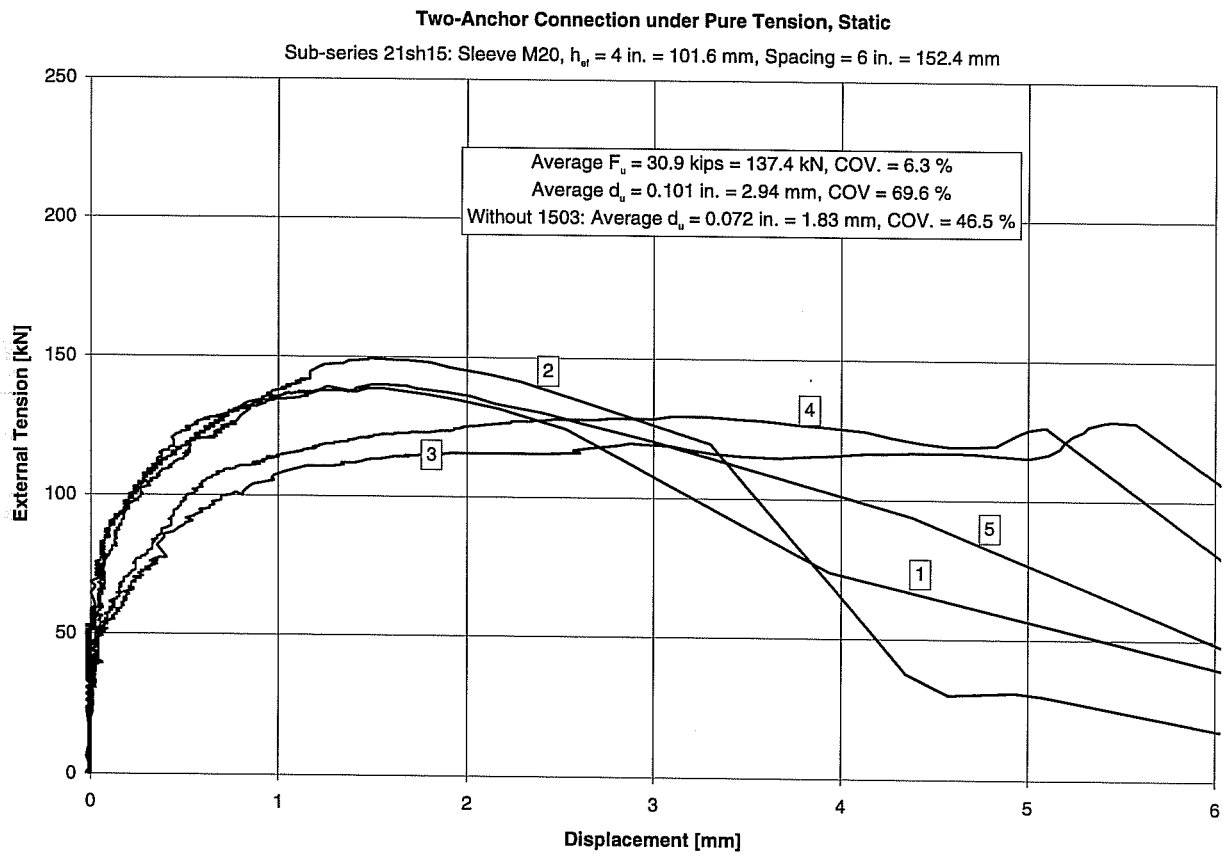
Two-Anchor Connection under Pure Tension, Static
Sub-series 21sh15: Sleeve M20, h_{ef} = 4 in. = 101.6 mm, Spacing = 6 in. = 152.4 mm
Average F_u = 30.9 kips = 137.4 kN, COV. = 6.3 %
Average d_u = 0.101 in. = 2.94 mm, COV = 69.6 %
Without 1503: Average d_u = 0.072 in. = 1.83 mm, COV. = 46.5 %
External Tension [kN]
Displacement [mm]
250
200
150
100
50
0
0
1
2
3
4
5
6
1
2
3
4
5

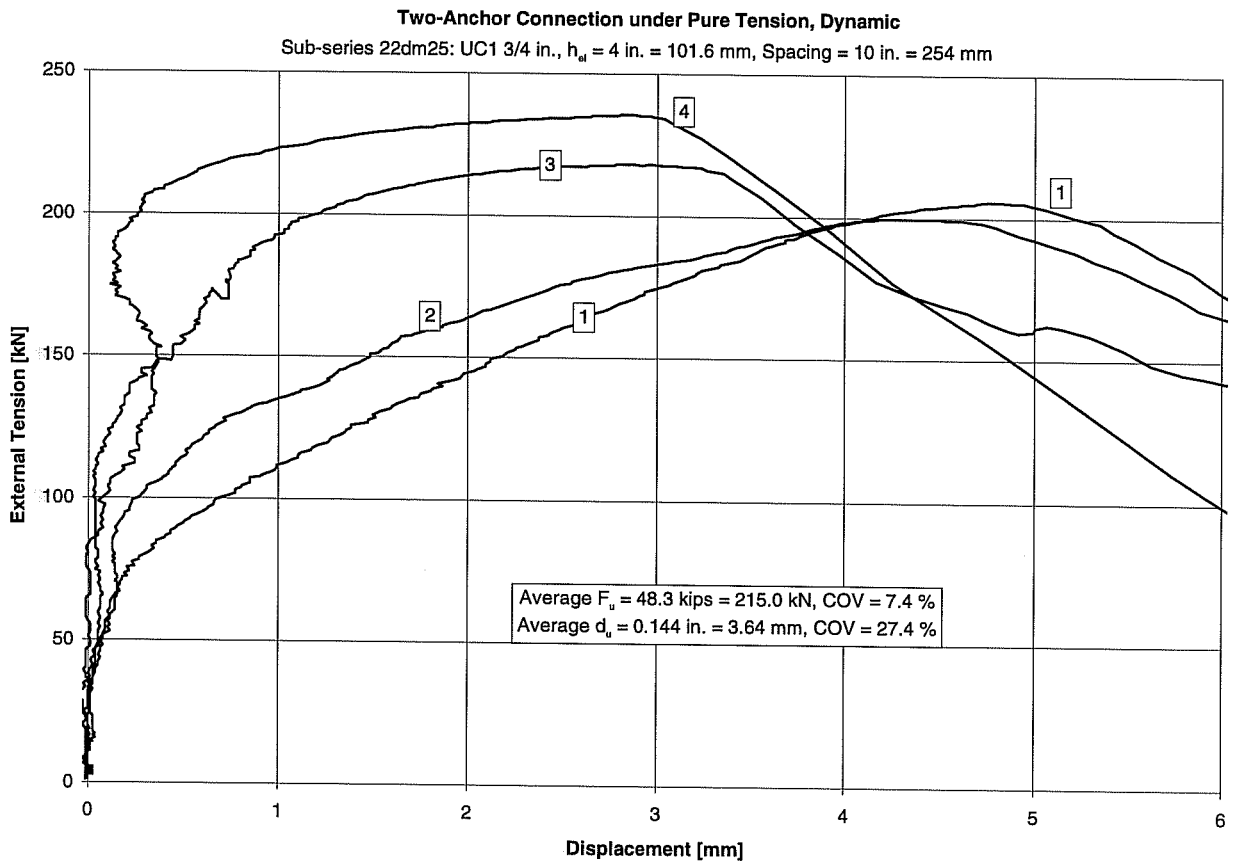
Two-Anchor Connection under Pure Tension, Dynamic
Sub-series 22dm25: UC1 3/4 in., h_{ef} = 4 in. = 101.6 mm, Spacing = 10 in. = 254 mm
External Tension [kN]
250
200
150
100
50
0
0
1
2
3
4
5
6
Displacement [mm]
4
3
2
1
1
Average F_u = 48.3 kips = 215.0 kN, COV = 7.4 %
Average d_u = 0.144 in. = 3.64 mm, COV = 27.4 %

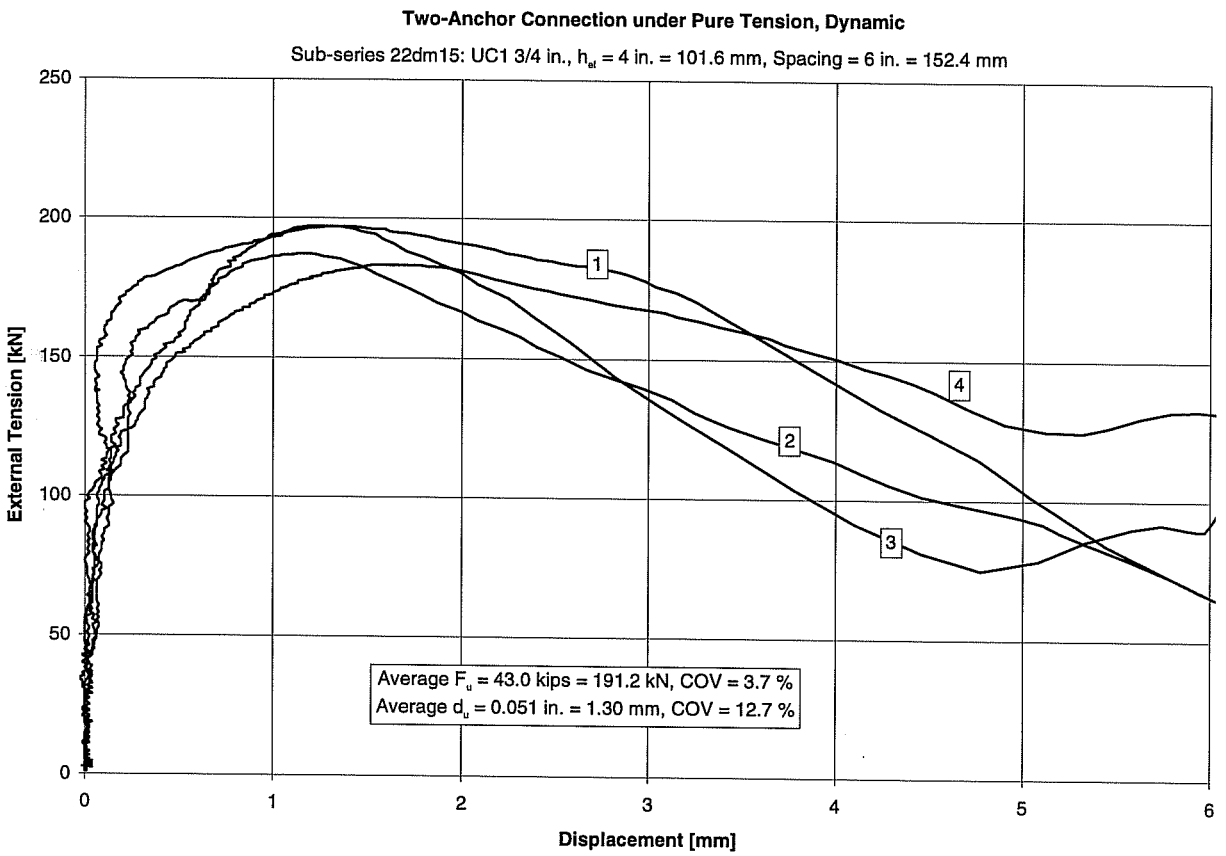
Two-Anchor Connection under Pure Tension, Dynamic
Sub-series 22dm15: UC1 3/4 in., h_{ef} = 4 in. = 101.6 mm, Spacing = 6 in. = 152.4 mm
External Tension [kN]
250
200
150
100
50
0
0
1
2
3
4
5
6
Displacement [mm]
1
2
3
4
Average F_u = 43.0 kips = 191.2 kN, COV = 3.7 %
Average d_u = 0.051 in. = 1.30 mm, COV = 12.7 %

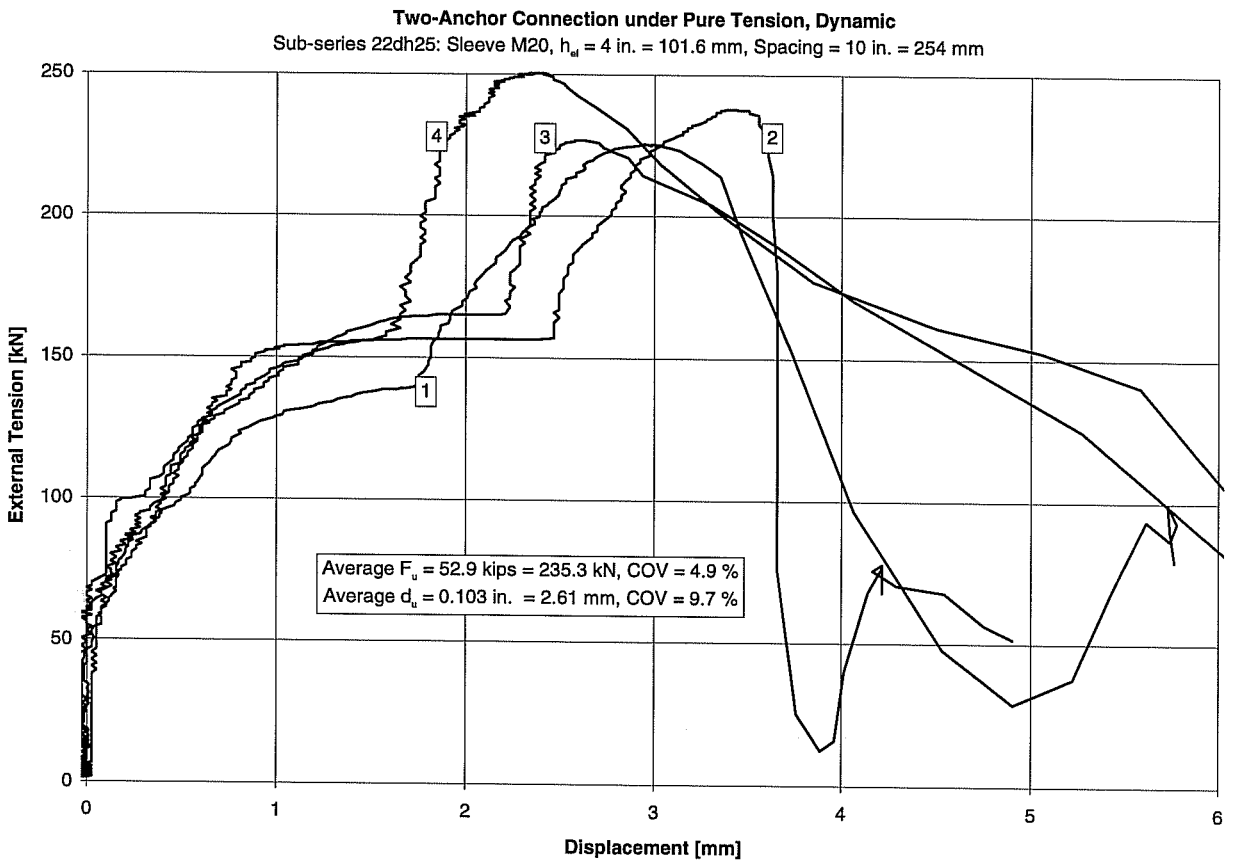
Two-Anchor Connection under Pure Tension, Dynamic
Sub-series 22dh25: Sleeve M20, h_{ef} = 4 in. = 101.6 mm, Spacing = 10 in. = 254 mm
External Tension [kN]
Displacement [mm]
250
200
150
100
50
0
0
1
2
3
4
5
6
1
2
3
4
Average F_u = 52.9 kips = 235.3 kN, COV = 4.9 %
Average d_u = 0.103 in. = 2.61 mm, COV = 9.7 %

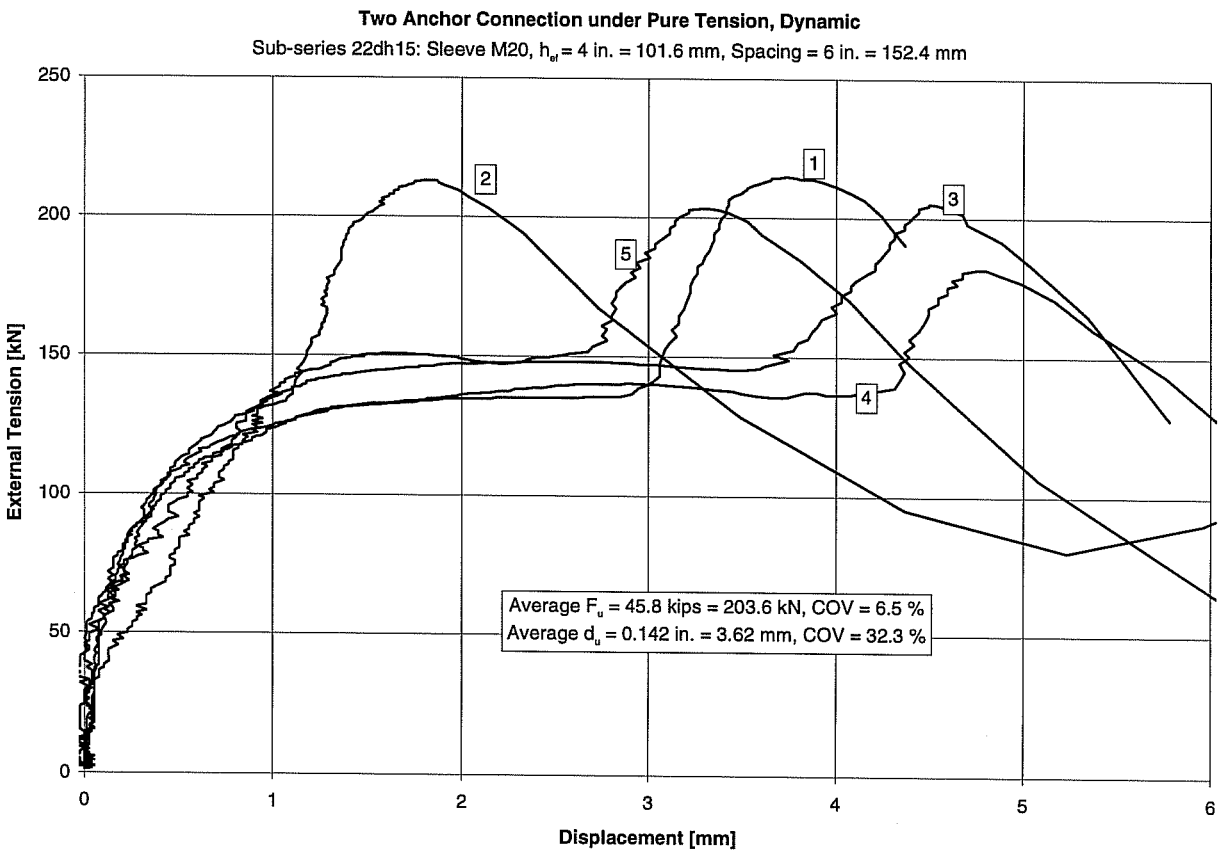
Two Anchor Connection under Pure Tension, Dynamic
Sub-series 22dh15: Sleeve M20, h_{ef} = 4 in. = 101.6 mm, Spacing = 6 in. = 152.4 mm
External Tension [kN]
Displacement [mm]
250
200
150
100
50
0
0
1
2
3
4
5
6
1
2
3
4
5
Average F_u = 45.8 kips = 203.6 kN, COV = 6.5 %
Average d_u = 0.142 in. = 3.62 mm, COV = 32.3 %

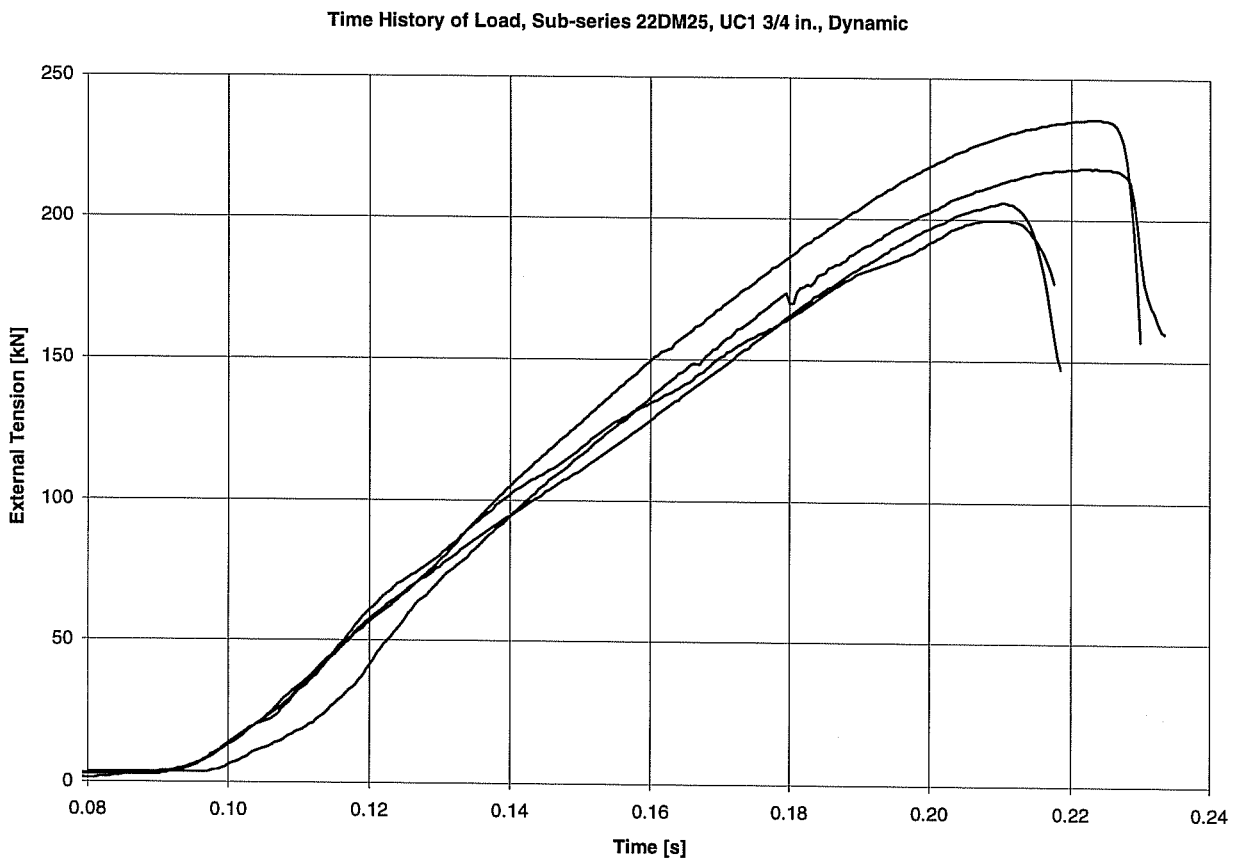
Time History of Load, Sub-series 22DM25, UC1 3/4 in., Dynamic
External Tension [kN]
250
200
150
100
50
0
0.08
0.10
0.12
0.14
0.16
0.18
0.20
0.22
0.24
Time [s]

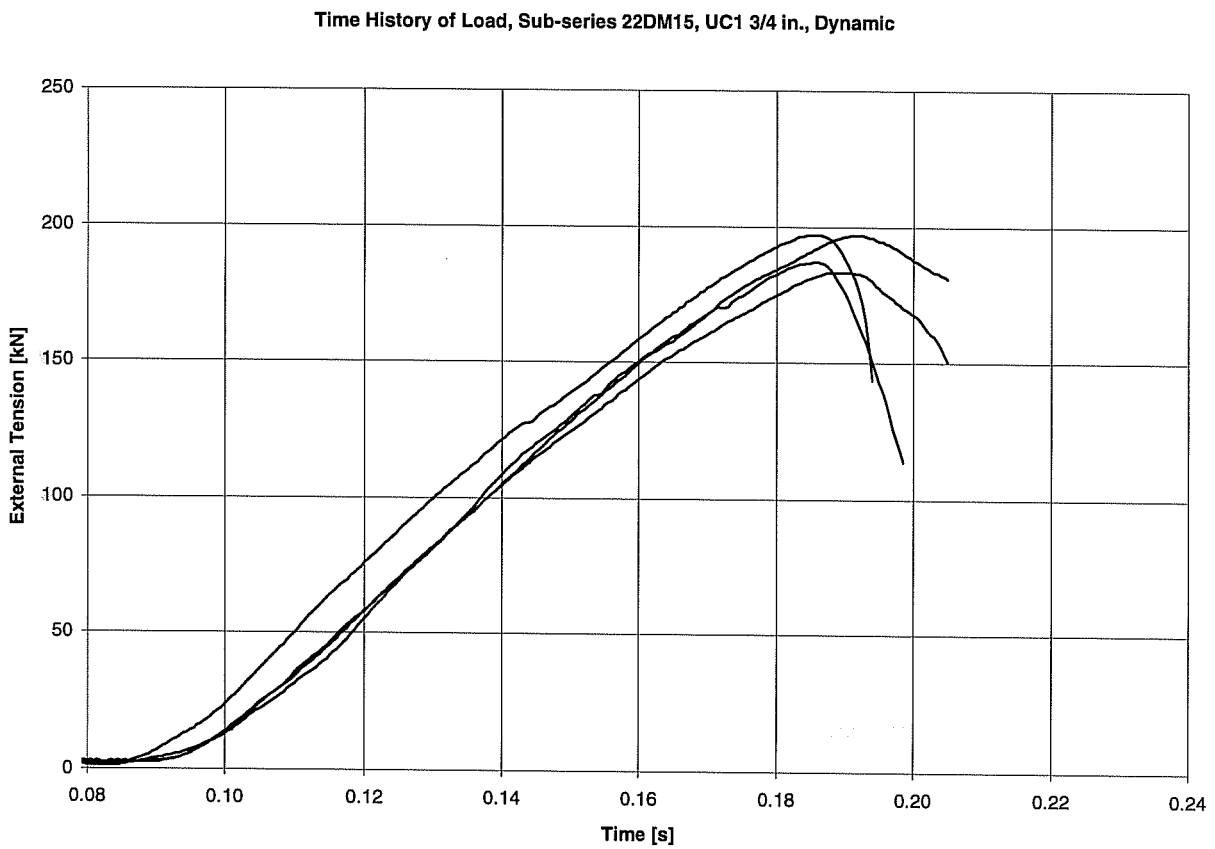
Time History of Load, Sub-series 22DM15, UC1 3/4 in., Dynamic
External Tension [kN]
250
200
150
100
50
0
0.08
0.10
0.12
0.14
0.16
0.18
0.20
0.22
0.24
Time [s]

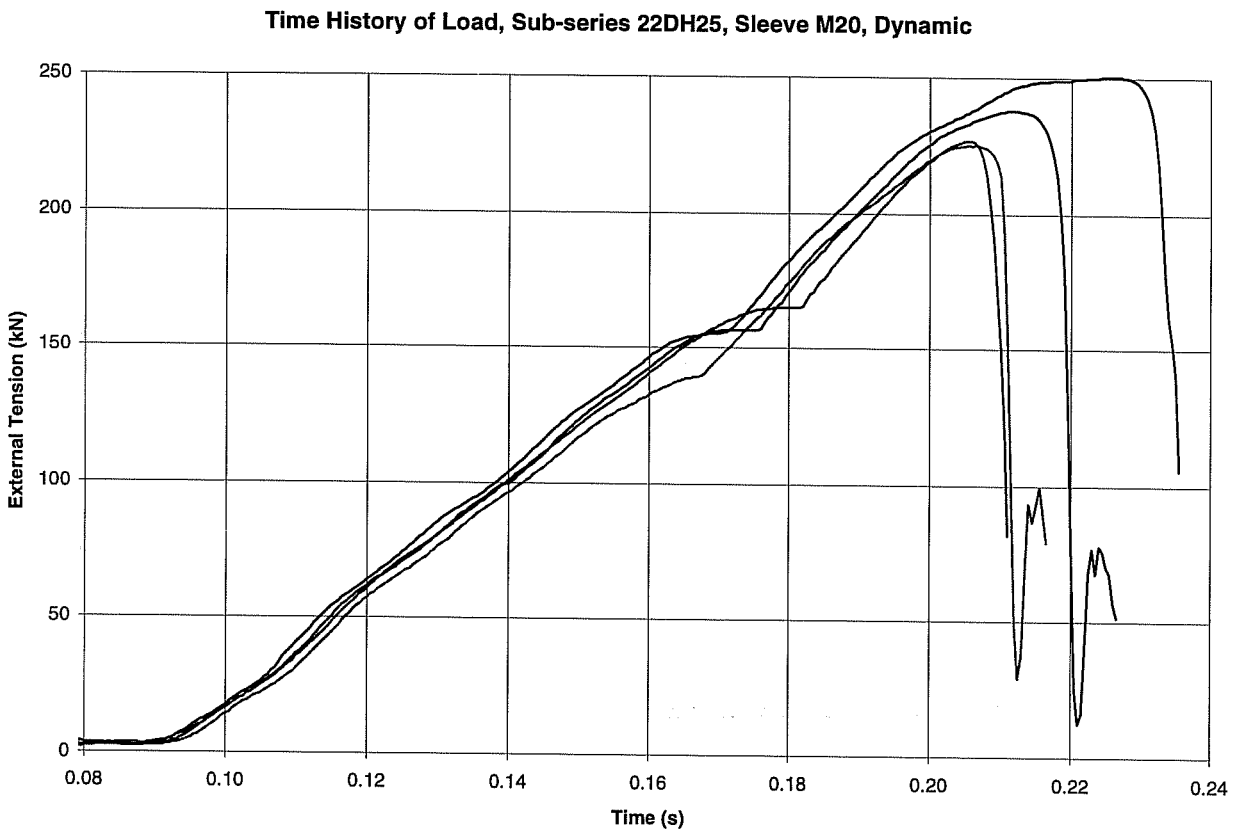
Time History of Load, Sub-series 22DH25, Sleeve M20, Dynamic
External Tension (kN)
250
200
150
100
50
0
0.08
0.10
0.12
0.14
0.16
0.18
0.20
0.22
0.24
Time (s)

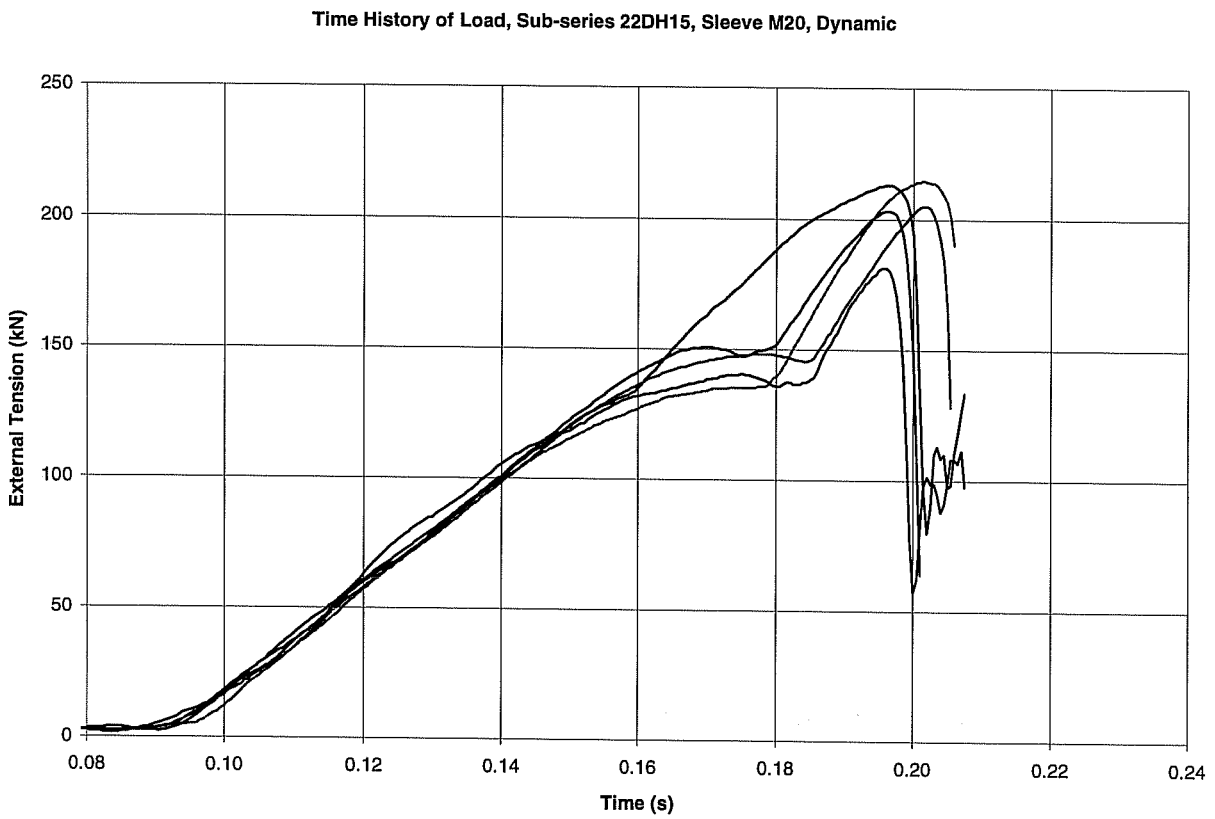
Time History of Load, Sub-series 22DH15, Sleeve M20, Dynamic
External Tension (kN)
250
200
150
100
50
0
0.08
0.10
0.12
0.14
0.16
0.18
0.20
0.22
0.24
Time (s)

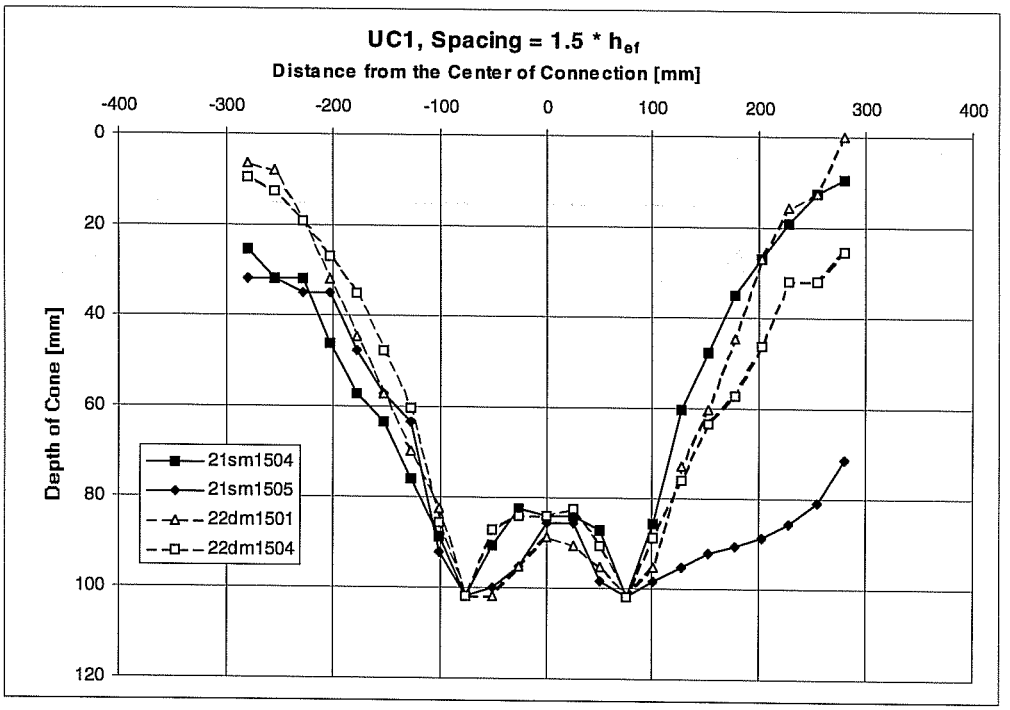

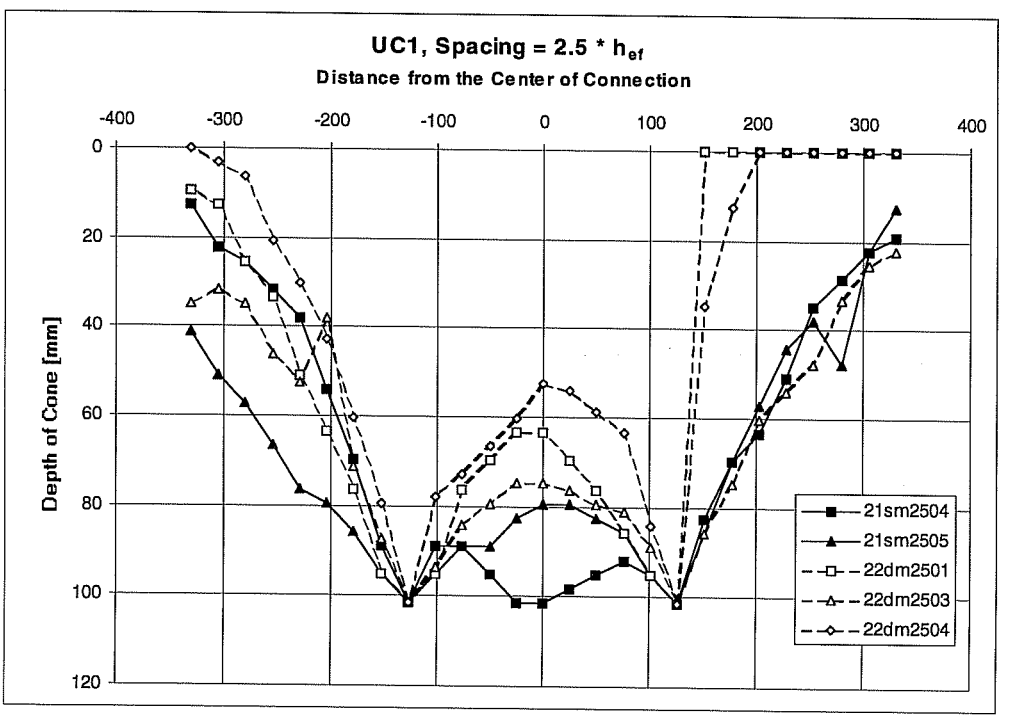

Results of Breakout Cone Measurement

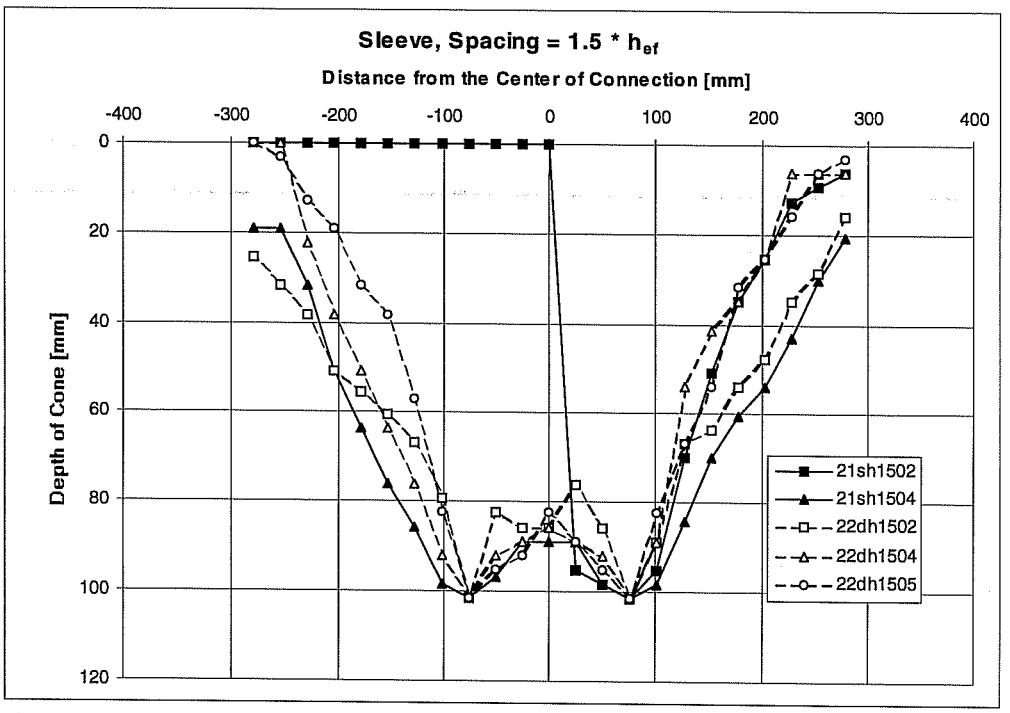

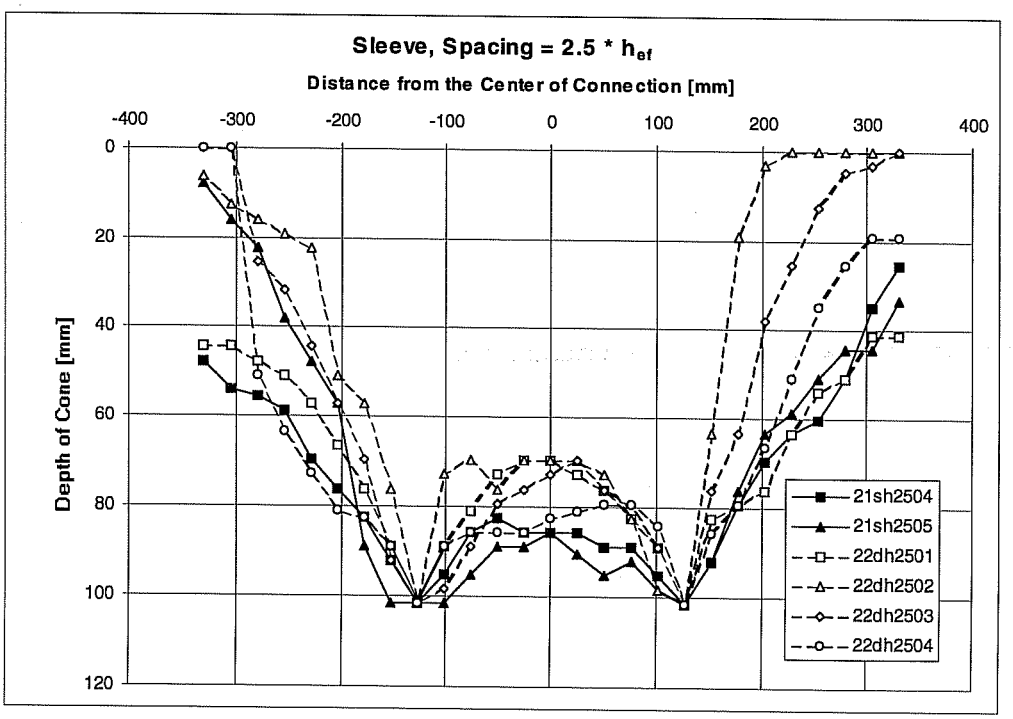

Results of Breakout Cone Measurement

Failure Picture of Test 21SM2501, Spacing of 2.5 * h_{ef}, UC1, Static, Concrete Breakout at Anchor

Failure Picture of Test 21SM2502, Spacing of 2.5 * h_{ef} , UC1, Static, Concrete Failure at Both Anchors of Group and Splitting of End of Specimen

Failure Picture of Test 21SM2503, Spacing of 2.5 * h_{ef}, UC1, Static, Concrete Failure at Both Anchors of Group

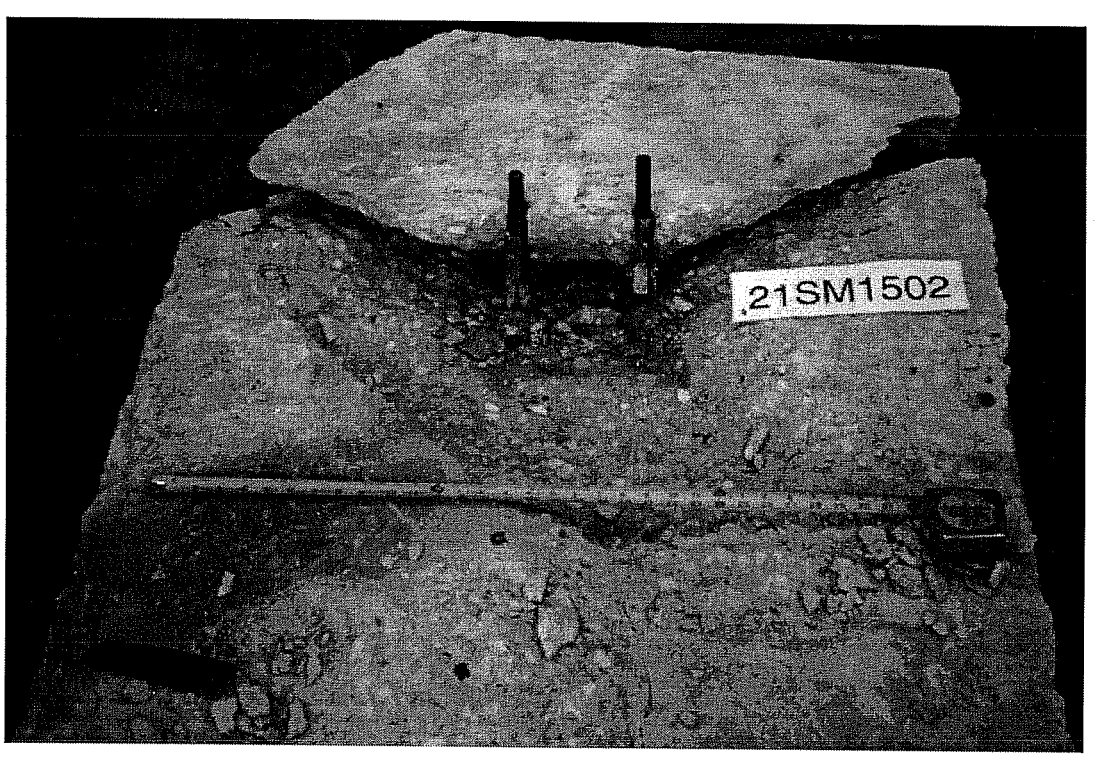

Failure Picture of Test 21SM1502, Spacing of 1.5 * h_{ef}, UC1, Static, Concrete Failure at Both Anchors of Group and Splitting of End of Specimen

Failure Picture of Test 21SM1503, Spacing of 1.5 * h_{ef} , UC1, Static, Concrete Failure at Both Anchors of Group

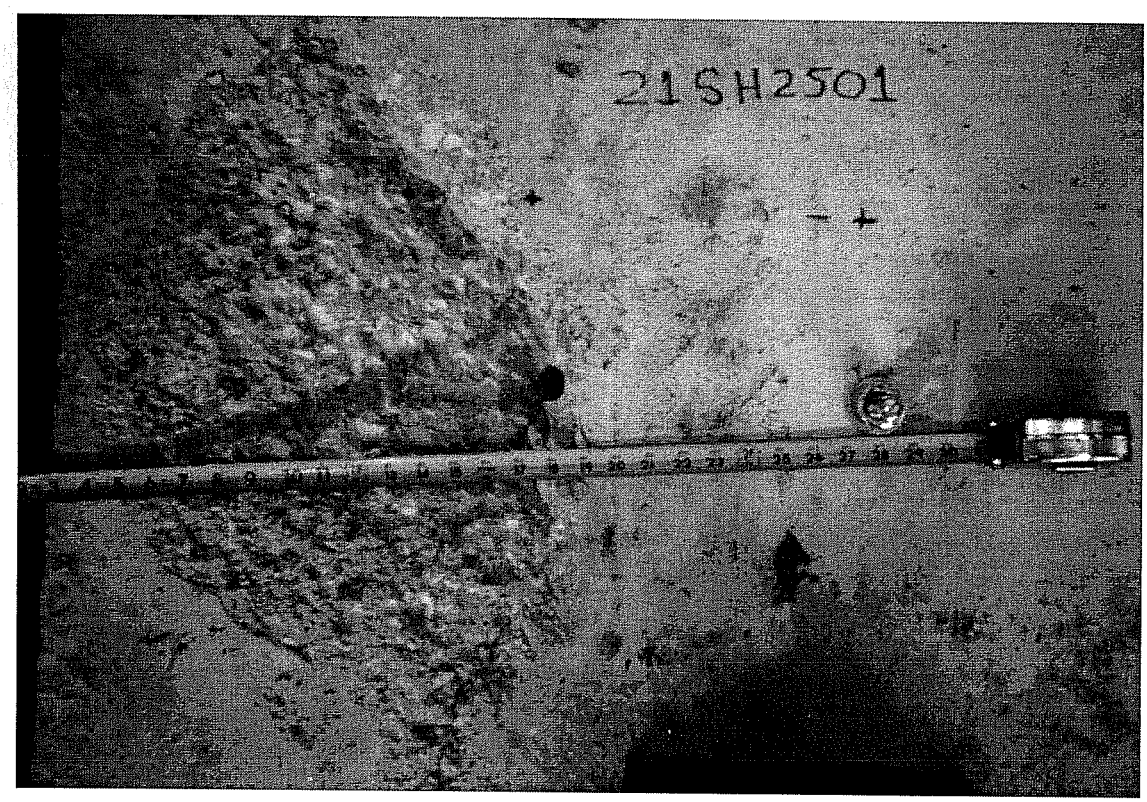

Failure Picture of Test 21SH2501, Spacing of 2.5 * h_{ef} , Sleeve, Static, Concrete Failure at Anchor

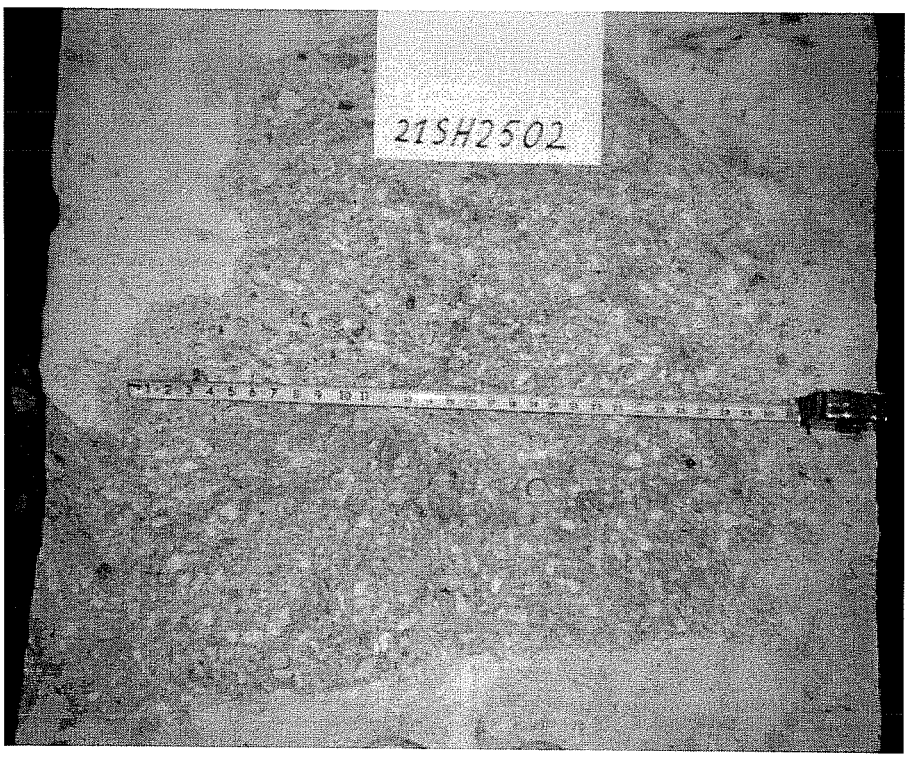

Failure Picture of Test 21SH2502, Spacing of 2.5 * h_{ef} , Sleeve, Static, Concrete Failure at Both Anchors of Group

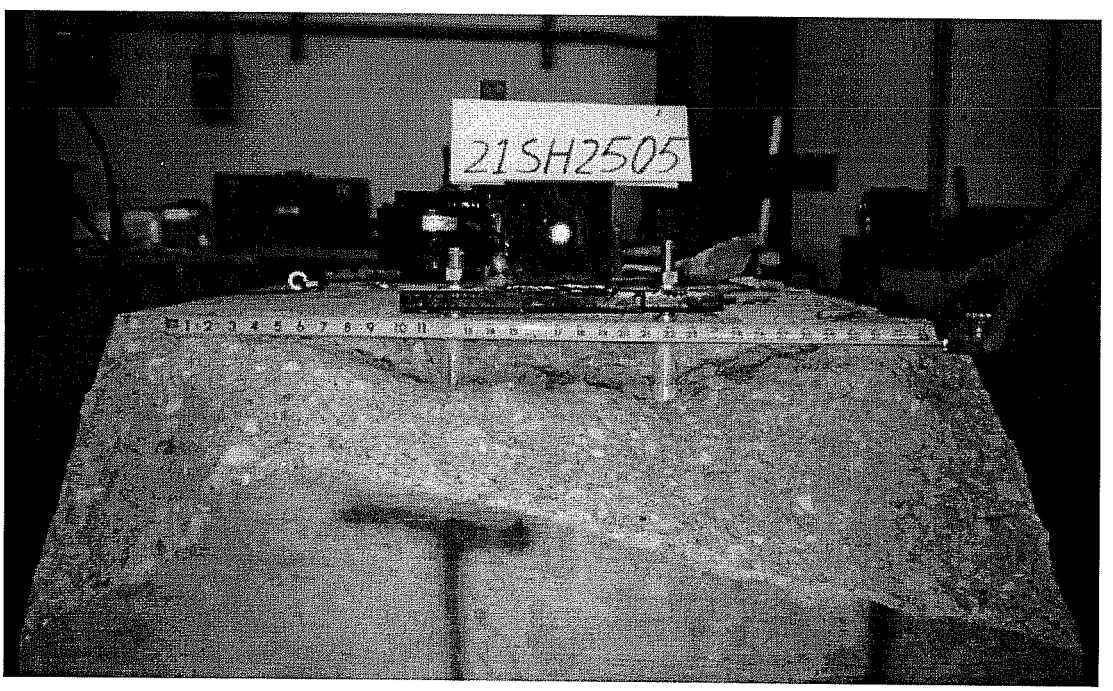

Failure Picture of Test 21SH2505, Spacing 2.5 * h_{ef} , Sleeve, Static, Concrete Failure at Both Anchors of Group and Splitting of End of Specimen

Failure Picture of Test 21SH1502, Spacing of 1.5 * h_{ef} , Sleeve, Static, Concrete Failure at Anchor

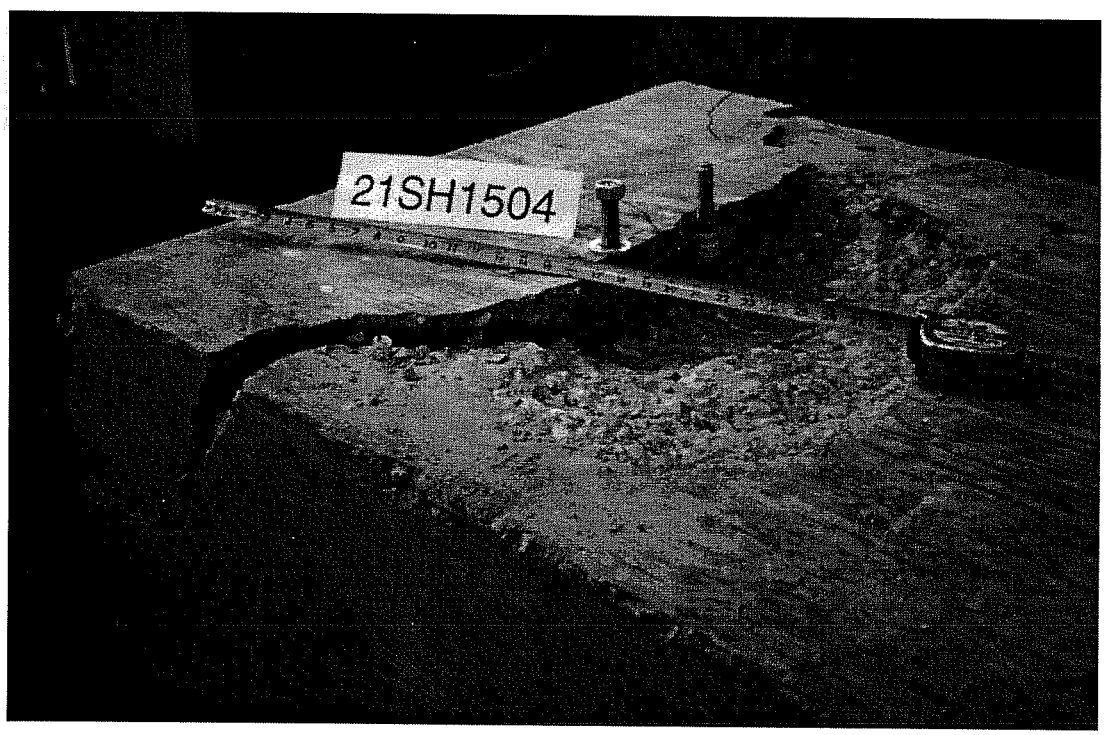

Failure Picture of Test 21SH1504, Spacing of 1.5 * h_{ef} , Sleeve, Static, Concrete Failure at Both Anchors of Group and Splitting of End of Specimen

Failure Picture of Test 22DM2503, Spacing of 2.5 * h_{ef} , UC1, Dynamic, Concrete Failure at Both Anchors of Group

Failure Picture of Test 22DM1502, Spacing of 1.5 * h_{ef} , UC1, Dynamic, Concrete Failure at Both Anchors of Group and Splitting of End of Specimen

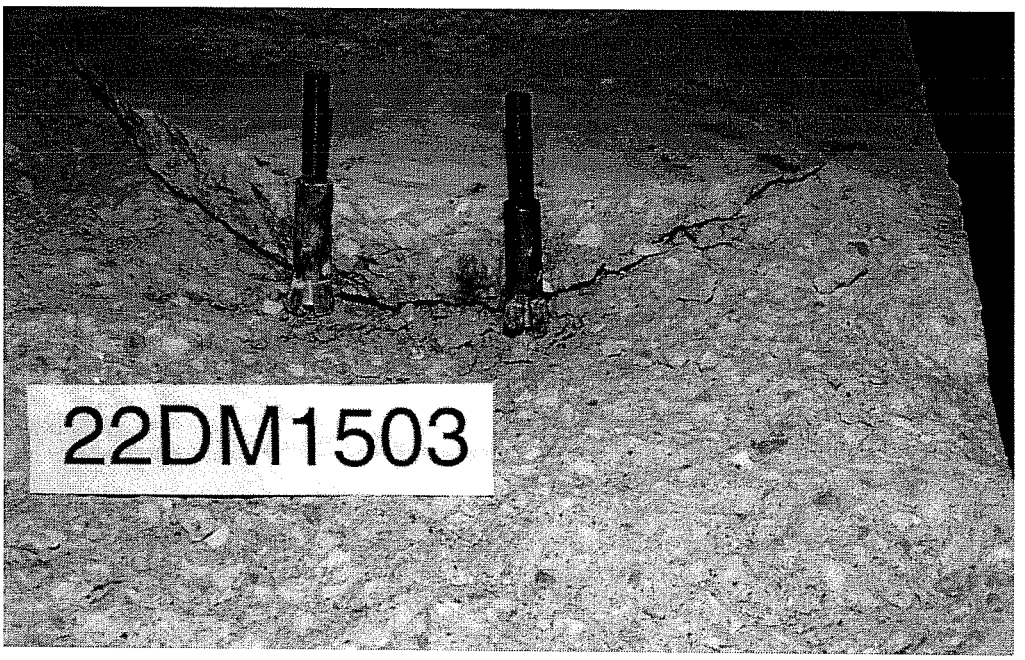

Failure Picture of Test 22DM1503, Spacing of 1.5 * h_{ef} , UC1, Dynamic, Concrete Failure at Both Anchors of Group

Failure Picture of Test 22DM1504, Spacing of 1.5 * h_{ef} , UC1, Dynamic, Concrete Failure at Both Anchors of Group and Splitting of End of Specimen

Failure Picture of Test 22DM2504, Spacing of 2.5 * h_{ef} , UC1, Dynamic, Concrete Failure at Both Anchors of Group

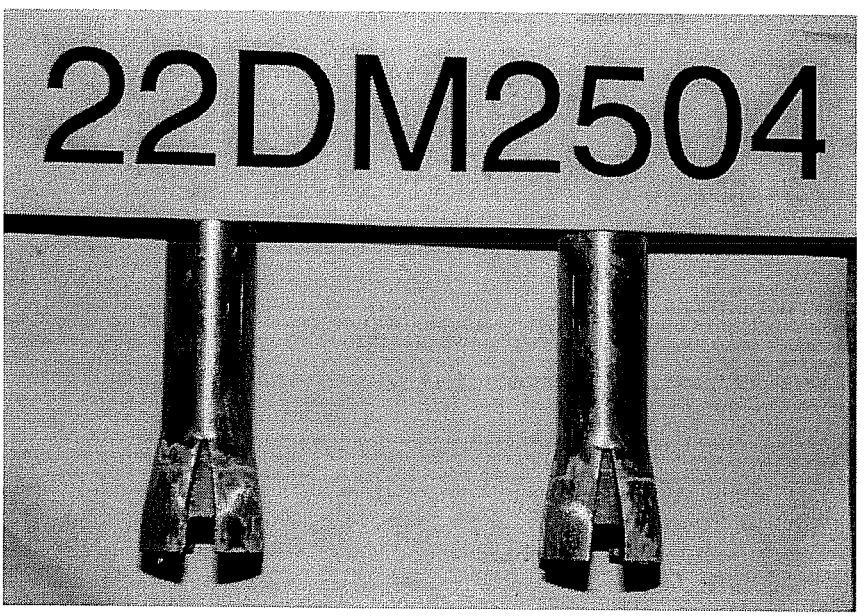

Undercut Anchors after Dynamic Test 22DM2504

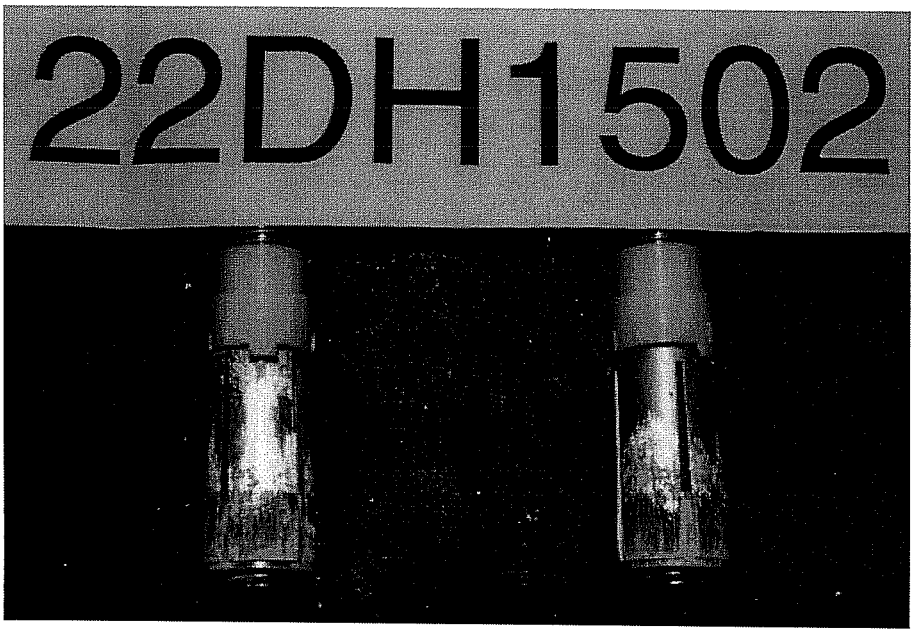

Torque-Controlled Expansion Sleeve Anchors after Dynamic Test 22DH1502, Cones Stopped by Steps on Interior Surfaces of Sleeves

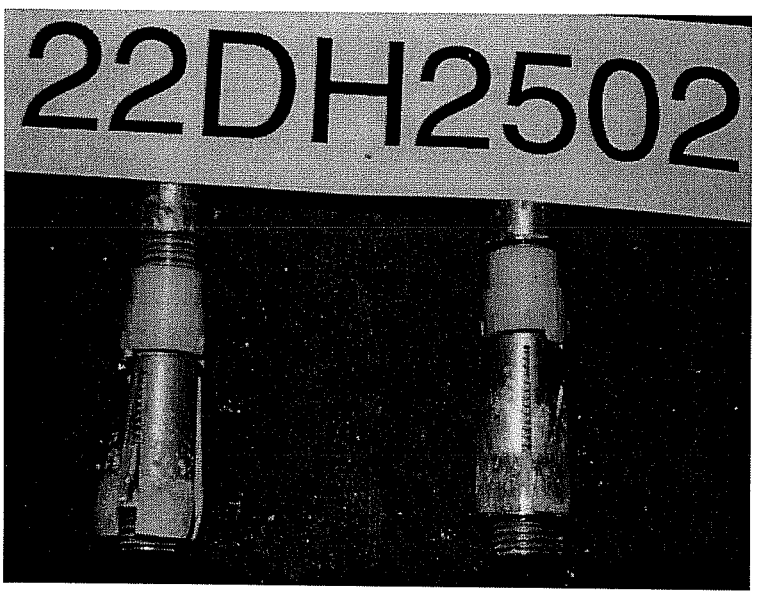

Torque-Controlled Expansion Sleeve Anchors after Dynamic Test 22DH2502, 1 Cone Stopped by Step, 1 Cone Pulled into Sleeve

Test No.	Loading Angle degrees	Torque Nm	Block No.	Concrete f_c N/mm²	Failure Load F_u kN	Hor. Displ. $d_{H,u}$ mm	Corr. c(H) mm	Vert. Displ. $d_{V,u}$ mm	Spalling Depth t mm	Note
23H64T1	Tension	203/102	L36-T	~32.4	121.875	-	-	15.82	-	1)
2	Tension	203/102	L36-T	~32.4	115.648	-	-	23.86	-	1)
3	Tension	203/102	L36-B	~32.4	127.213	-	-	23.27	-	1)
4	Tension	203/102	L36-B	~32.4	140.112	-	-	21.84		2)
Ave.					**126.212**			**21.20**		
COV [%]					**8.24**			**17.37**		
23H6431	15	203/102	L35-T	~32.4	126.323	6.81	0.25	10.45	25	
2	15	203/102	L35-T	~32.4	128.547	8.49	0.00	11.60	29	
3	15	203/102	L35-B	~32.4	127.658	6.72	1.30	6.97	29	
Ave.					**127.509**	**7.34**		**9.67**	**27.67**	
COV [%]					**0.88**	**13.54**		**24.89**	**8.35**	
23H6431	30	203/102	L36-B	~32.4	108.086	4.26	0.50	2.32	13	
2	30	203/102	L36-B	~32.4	108.086	3.66	0.75	1.85	6	
3	30	203/102	L35-T	~32.4	103.638	4.13	1.00	2.06	13	
Ave.					**106.604**	**4.02**		**2.08**	**10.67**	
COV [%]					**2.41**	**7.76**		**11.34**	**37.89**	
23H6441	45	203/102	L36-T	~32.4	91.6288	4.76	2.05	1.45	n.g.	3)
2	45	203/102	L36-T	~32.4	89.4048	4.18	2.30	1.47	n.g.	
3	45	203/102	L35-B	~32.4	88.0704	3.50	1.80	0.85	6	
Ave.					**89.7013**	**4.14**		**1.26**	**6.00**	
COV [%]					**2.00**	**15.21**		**28.00**		
23H6461	60	203/102	L36-T	~32.4	83.6224	3.68	2.80	0.53	0	
2	60	203/102	L36-T	~32.4	84.512	3.24	0.00	0.57	0	
3	60	203/102	L36-B	~32.4	82.7328	3.33	0.50	0.99	3	
4	60	203/102	L36-B	~32.4	81.8432	4.39	0.00	1.31	6	
Ave.					**83.1776**	**3.66**		**0.85**	**2.25**	
COV [%]					**1.38**	**14.32**		**43.31**	**127.66**	
23H64S1	Shear	203/102	L36-T	~32.4	79.1744	3.66	0.25	0.15	n.g.	
2	Shear	203/102	L36-T	~32.4	77.84	3.18	0.25	0.10	n.g.	
3	Shear	203/102	L36-B	~32.4	76.9504	2.77	0.25	0.03	0	
4	Shear	203/102	L36-B	~32.4	77.84	2.95	0.25	0.08	0	
Ave.					**77.9512**	**3.14**		**0.09**	**0.00**	
COV [%]					**1.18**	**12.26**		**59.48**		

1) failure: cones pulled through sleeve

2) 2 x nut thread stripped, load-displacement curves composed from 3 loads

3) only 1 displacement measured for vertical displacement dV

Test Results of Series 23H64: Flush-sleeve installation

hef = 178 mm (7 in.), fc = 32.4 N/mm² (4700 psi), Failing by Steel Fracture

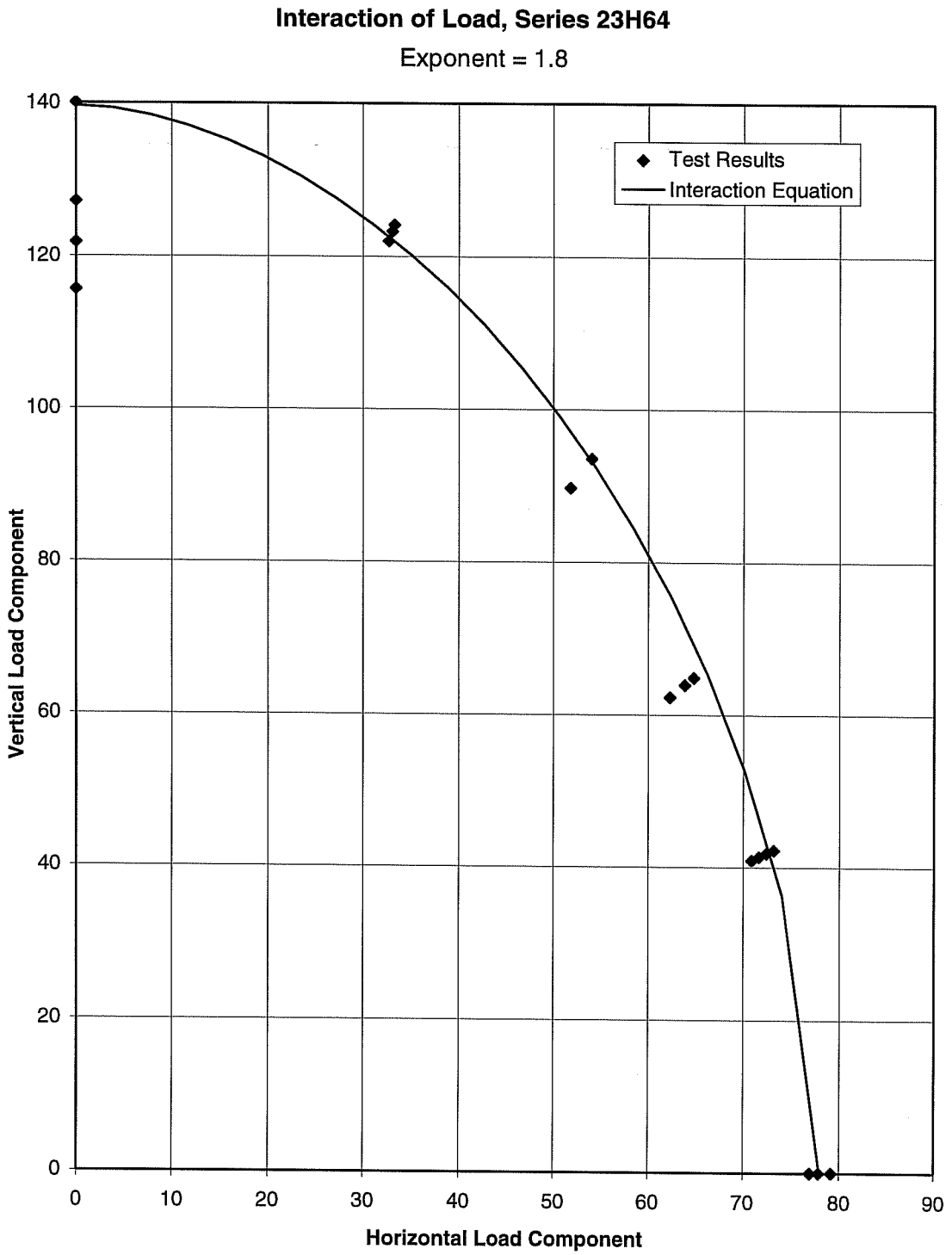
Interaction of Load, Series 23H64
Exponent = 1.8
Test Results
Interaction Equation
Vertical Load Component
Horizontal Load Component
140
120
100
80
60
40
20
0
0
10
20
30
40
50
60
70
80
90

Interaction of Displacement at Max. Load

Series 23H64, Sleeve M16, h_{ef} = 7 inches (178 mm), f_c = 4700 psi (32.4 N/mm²)

Installation with Threaded Bolt (Flush-sleeve installation)

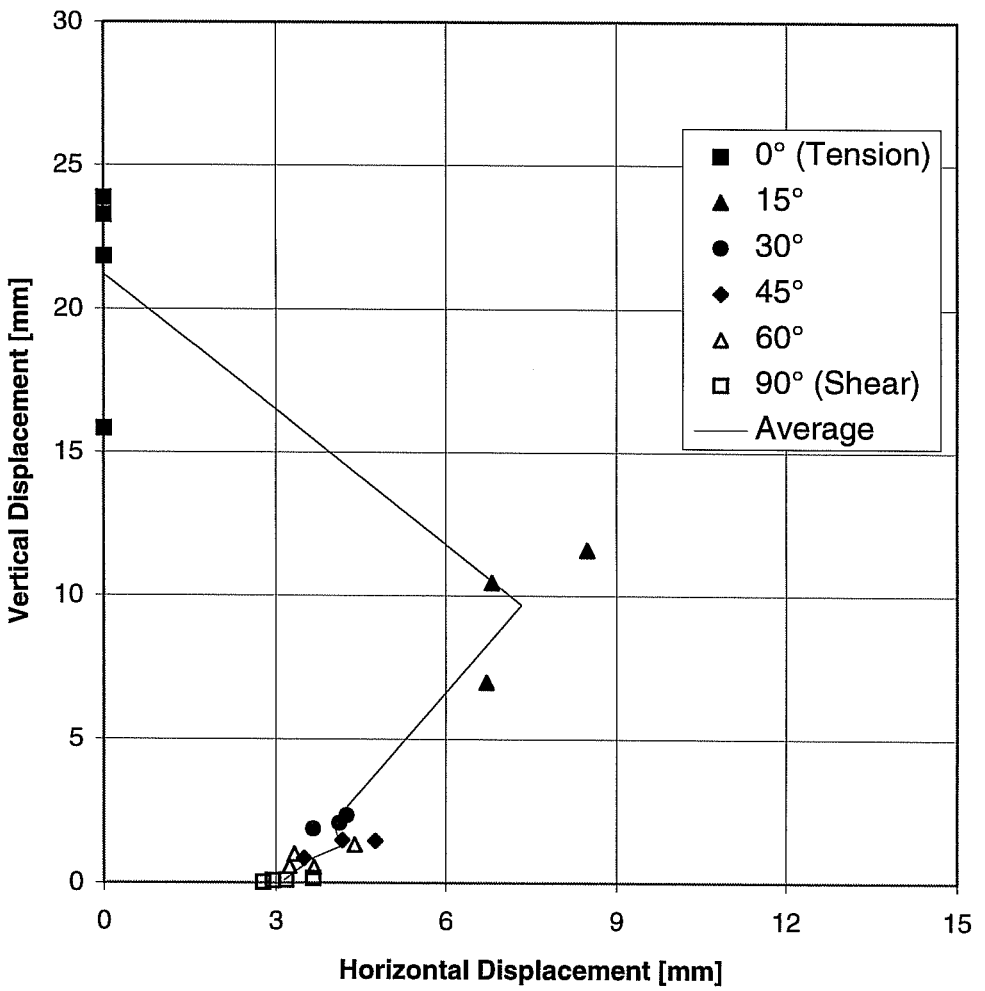

Part 1: Interaction of Force	**Interaction Exponent**	σ_Z	σ_S	
Breaks of Curves	1.80	800.8	446.9	
Max. Load	1.80	889.8	496.5	
Remaining Load	1.80	845.3	471.7	
Part 2: Load-Displacement Curves	**Angle** d_{knick}	d_u	d_{Rest}	**Curvature Exponent**
Angle	0			
d_{Ver}	15.06	21.20	25.47	0.30
Angle	15			
d_{Hor}	4.19	7.34	7.80	0.50
d_{Ver}	6.33	9.67	10.06	0.25
Angle	30			
d_{Hor}	2.19	4.02	4.54	0.50
d_{Ver}	1.06	2.08	2.23	0.25
Angle	45			
d_{Hor}	2.67	4.14	4.49	0.60
d_{Ver}	0.77	1.26	1.37	0.25
Angle	60			
d_{Hor}	2.44	3.66	4.15	0.60
d_{Ver}	0.50	0.85	0.94	0.25
Angle	75			
d_{Hor}	2.38	3.28	3.56	0.60
d_{Ver}	0.24	0.42	0.46	0.25
Angle	90			
d_{Hor}	2.36	3.14	3.34	0.60

Displacement in mm, Angle in degrees

Mathematical Description of the Results of Series 23H64 Sleeve Anchors (h_{ef} = 7 inches, c1 ≥ 11 inches) in flush-sleeve installation for Program BDA5 (75° interpolated), f_c = 32.4 N/mm²

Mathematical Description of Load-Displacement Curves of Series 23H64

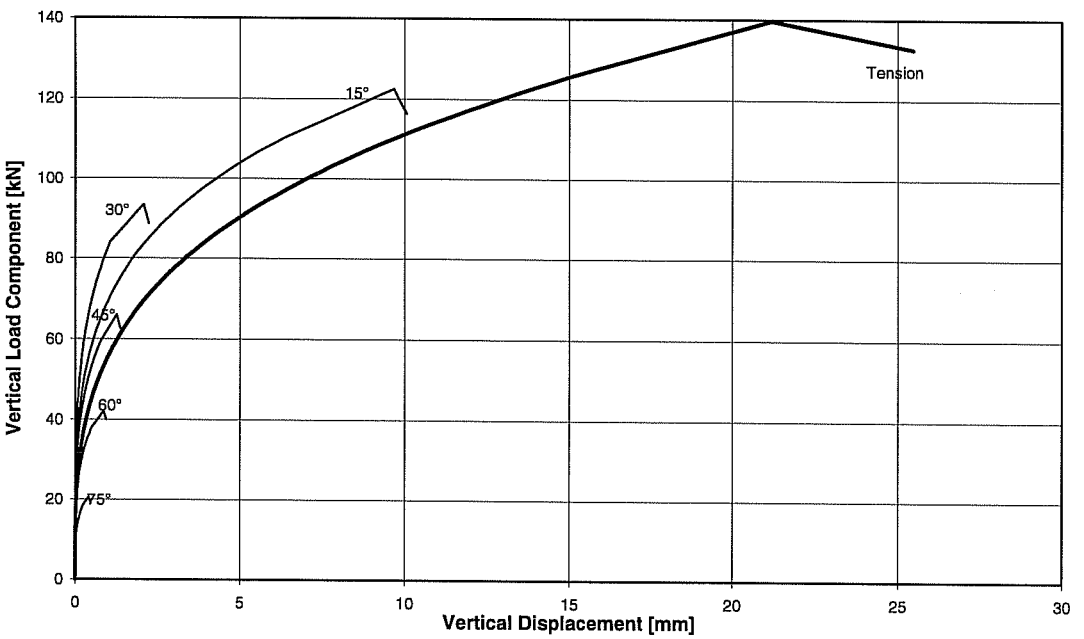

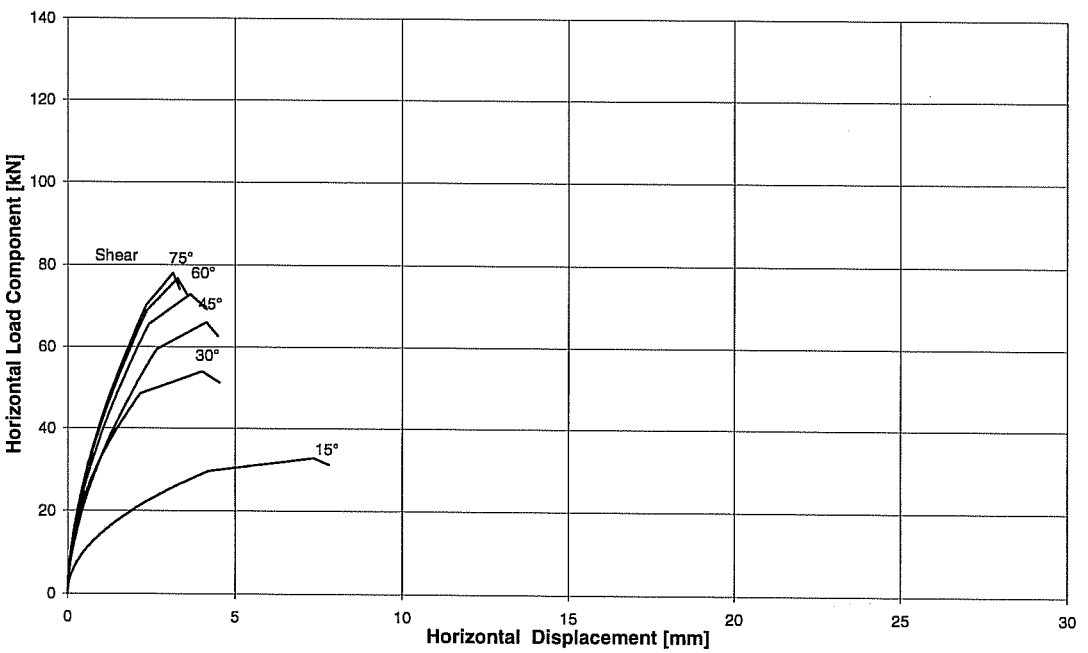
Horizontal Load Component [kN]
140
120
100
80
60
40
20
0
0
5
10
15
20
25
30
Horizontal Displacement [mm]
Shear
75°
60°
45°
30°
15°

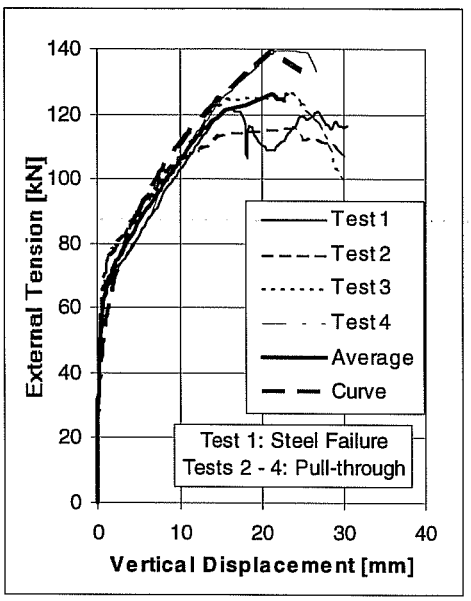

Pure Tension

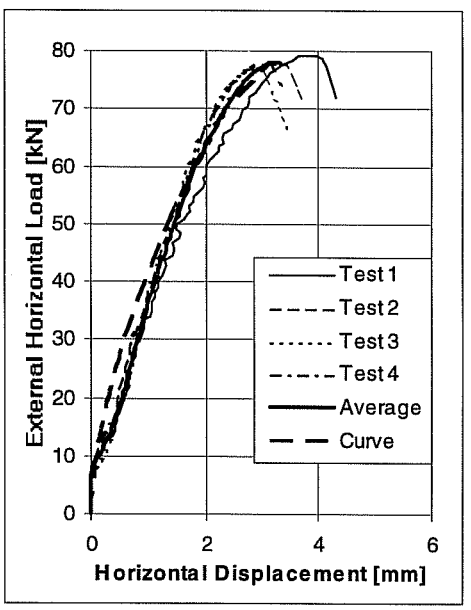

Pure Shear

Load-Displacement Curves of Series 23h64T (Tension) and 23h64S (Shear) Sleeve Anchors M16,
h_{ef} = 7 inches (178 mm), c1 ≥ 11 inches (279 mm), f_c = 32.4 N/mm²

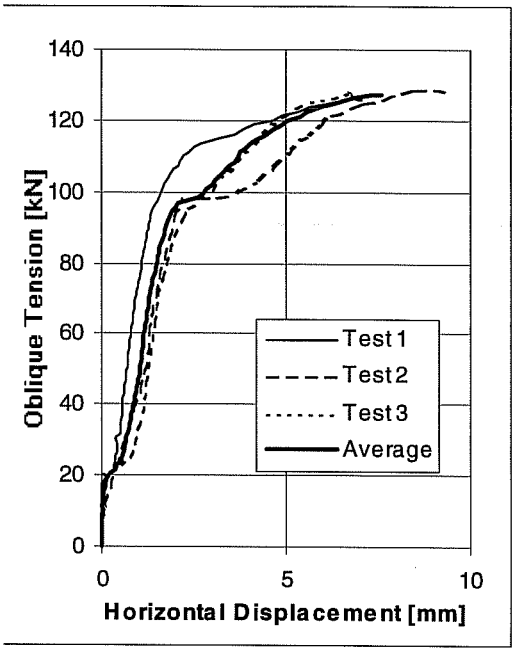

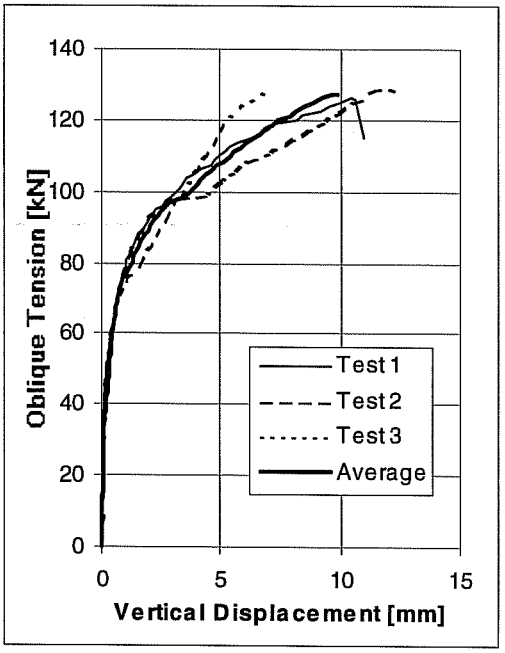

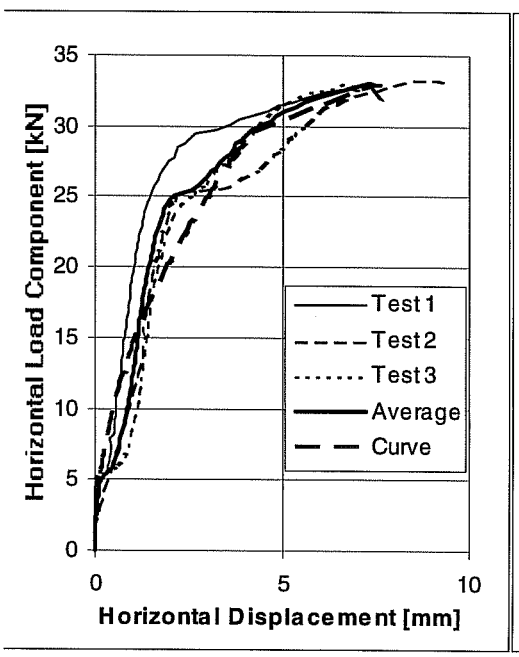

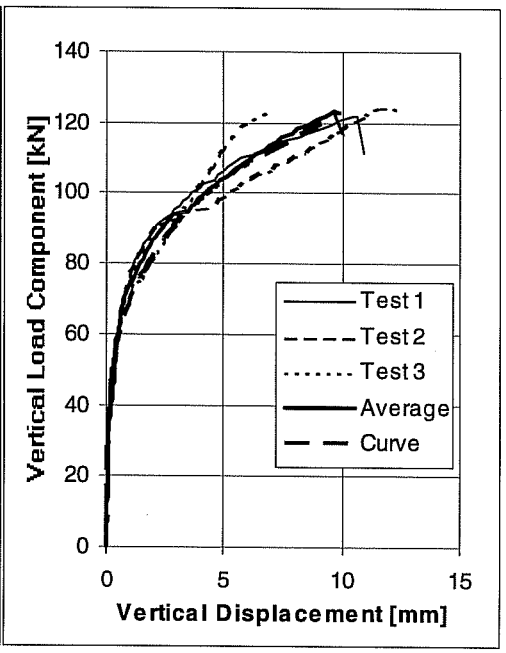

Load-Displacement Curves of Series 23h641,
Sleeve M16, h_{ef} = 7 inches (178 mm), ar ≥ 11 inches (279 mm),
f_c = 32.4 N/mm², Loading Angle 15° from Anchor Axis

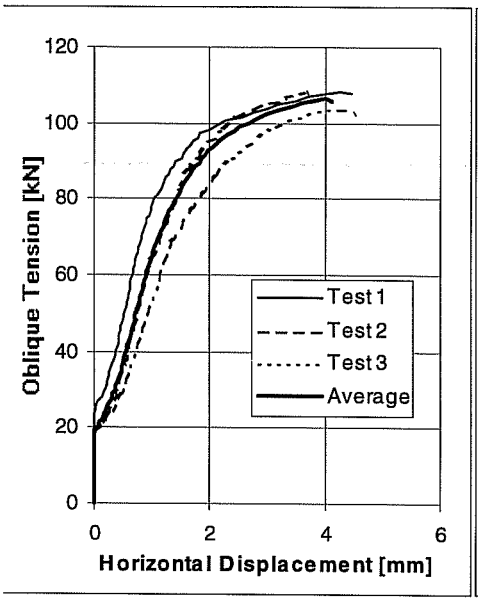

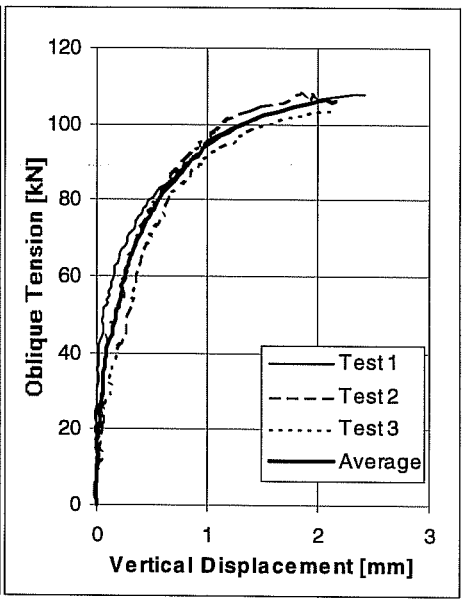

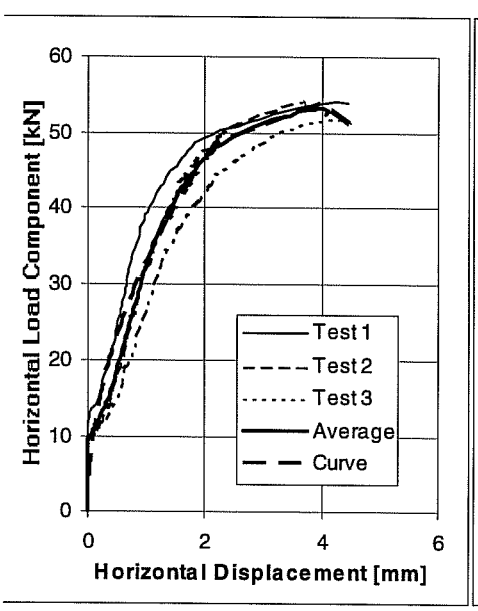

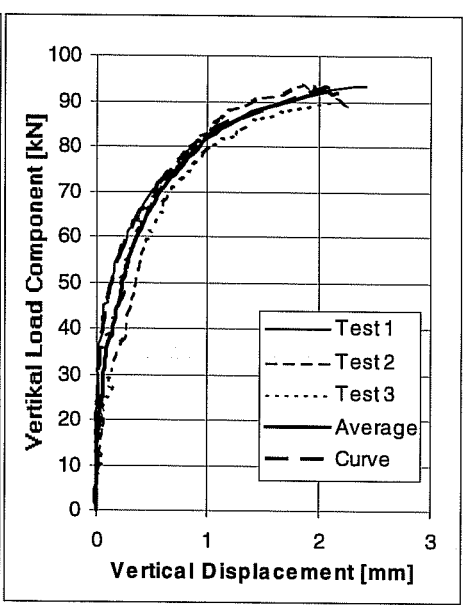

Load-Displacement Curves of Series 23h643,
Sleeve M16, h_{ef} = 7 inches (178 mm), c1 ≥ 11 inches (279 mm),
f_c = 32.4 N/mm², Loading Angle 30° from Anchor Axis

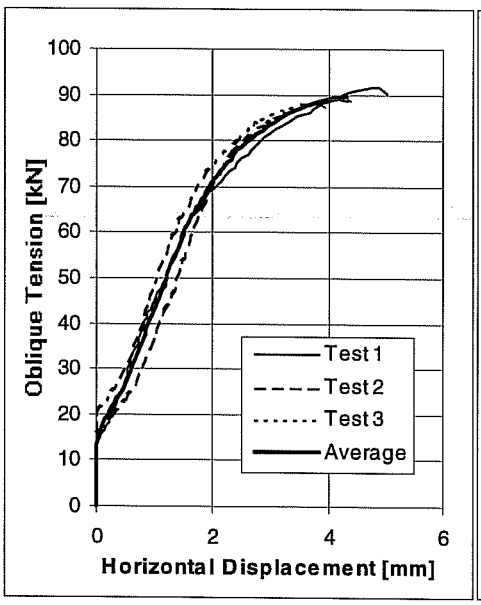

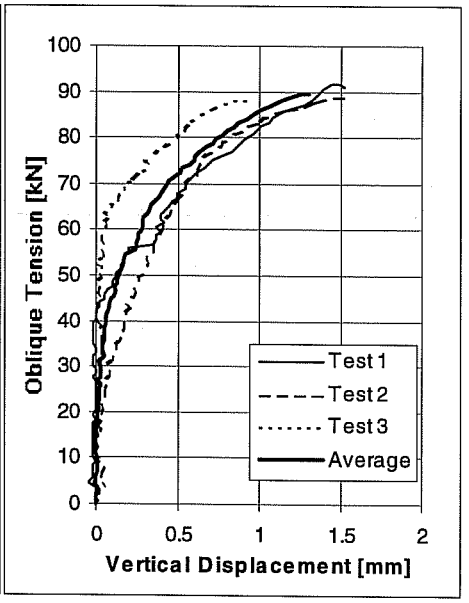

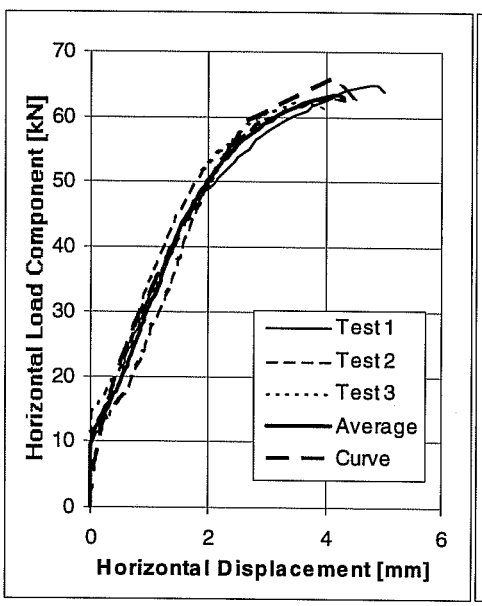

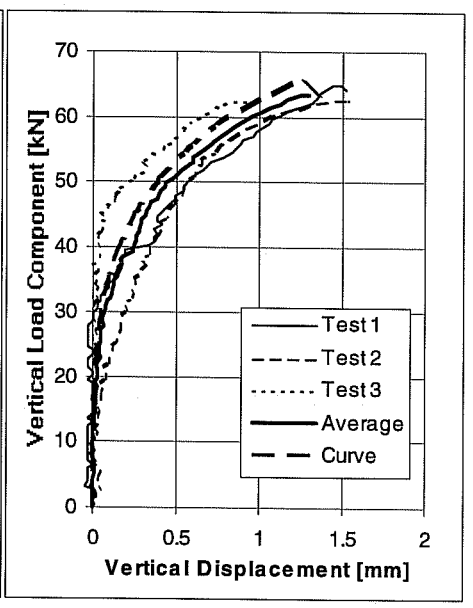

Load-Displacement Curves of Series 23h644,
Sleeve M16, h_{ef} = 7 inches (178 mm), c1 ≥ 11 inches (279 mm),
f_c = 32.4 N/mm², Loading Angle 45° from Anchor Axis

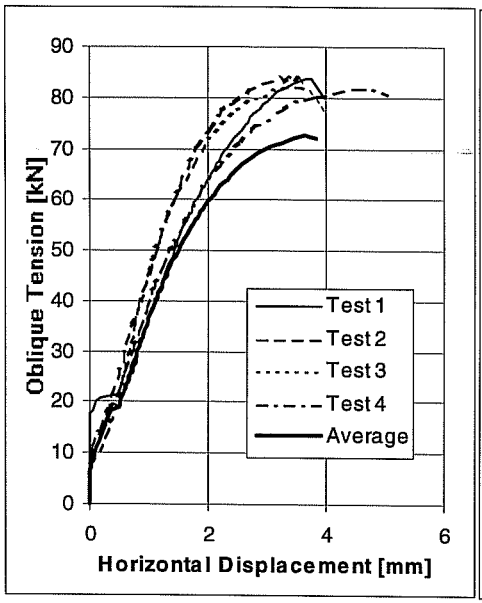

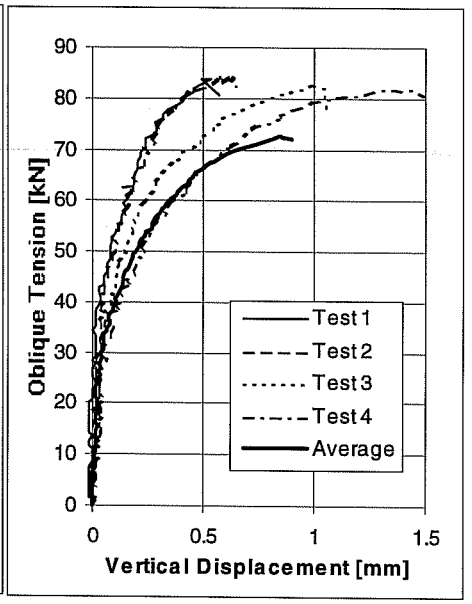

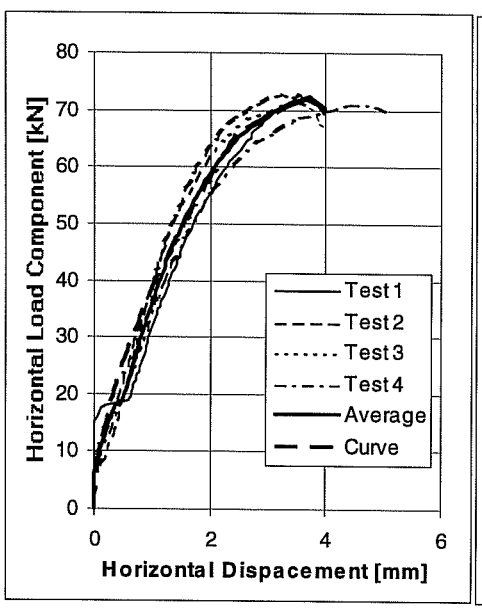

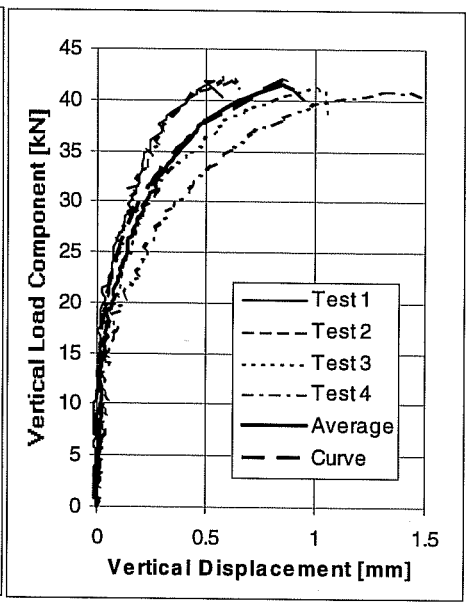

Load-Displacement Curves of Series 23h646,
Sleeve M16, h_{ef} = 7 inches (178 mm), c1 ≥ 11 inches (279 mm),
f_c = 32.4 N/mm², Loading Angle 60° from Anchor Axis

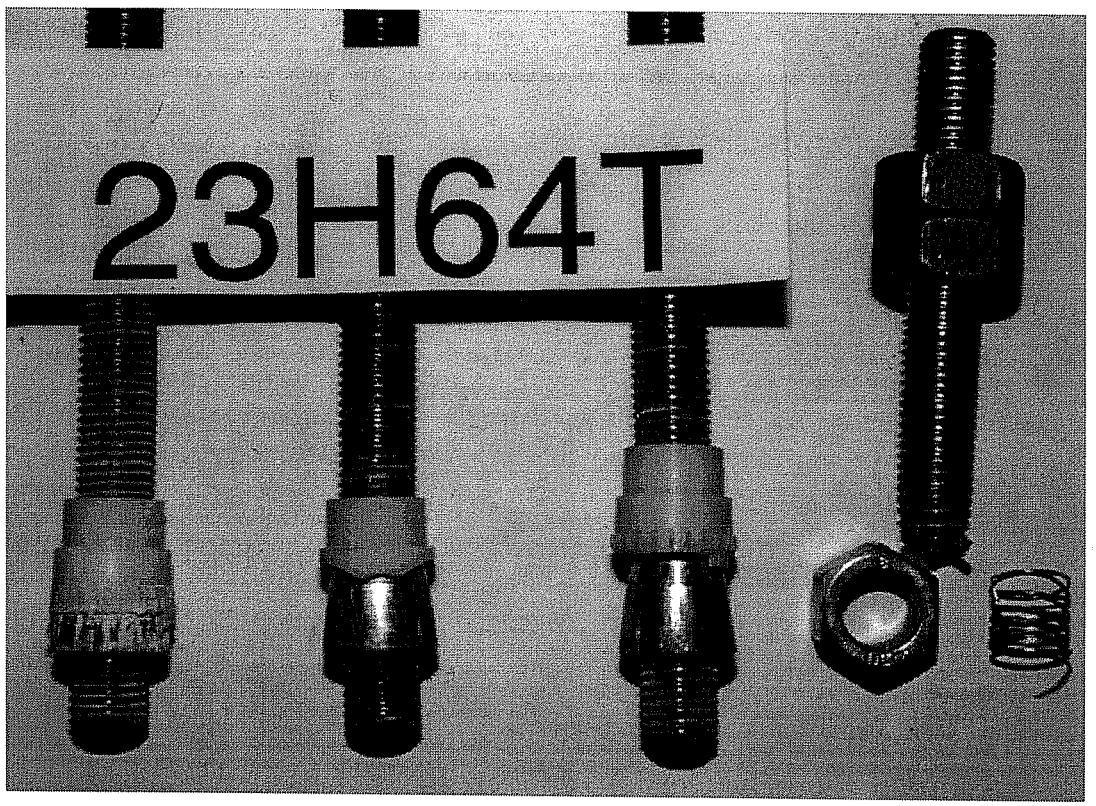

Series 23H64T, Sleeve M16, Pure Tension, Anchor Shanks after Test

Failure Picture of Test 23H6411, Sleeve M16, Oblique Tension 15°

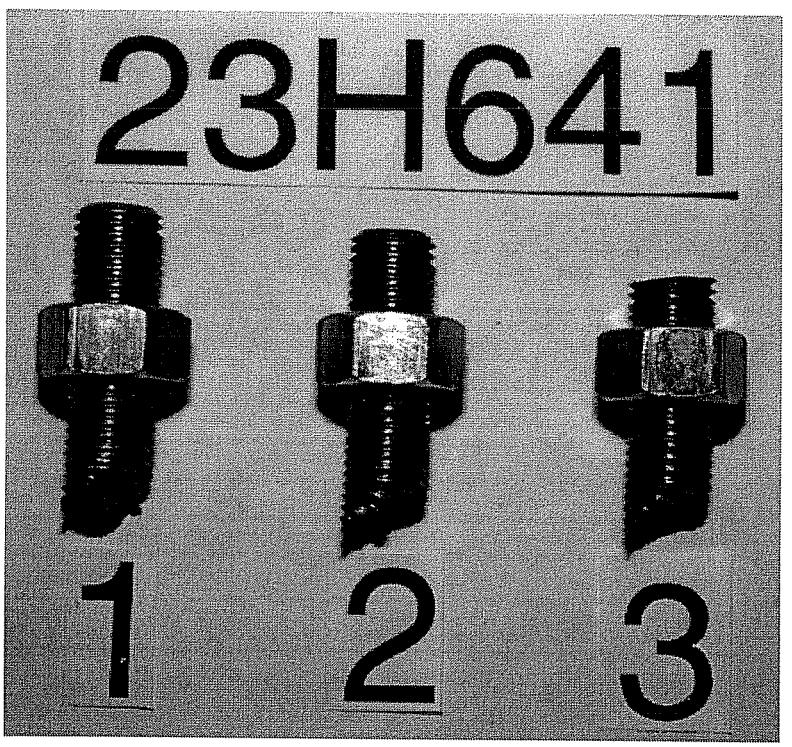

Series 23H641, Sleeve M16, Oblique Tension 15°, Fractured Anchor Shanks

Failure Picture of Test 23H6431, Sleeve M16, Oblique Tension 30°

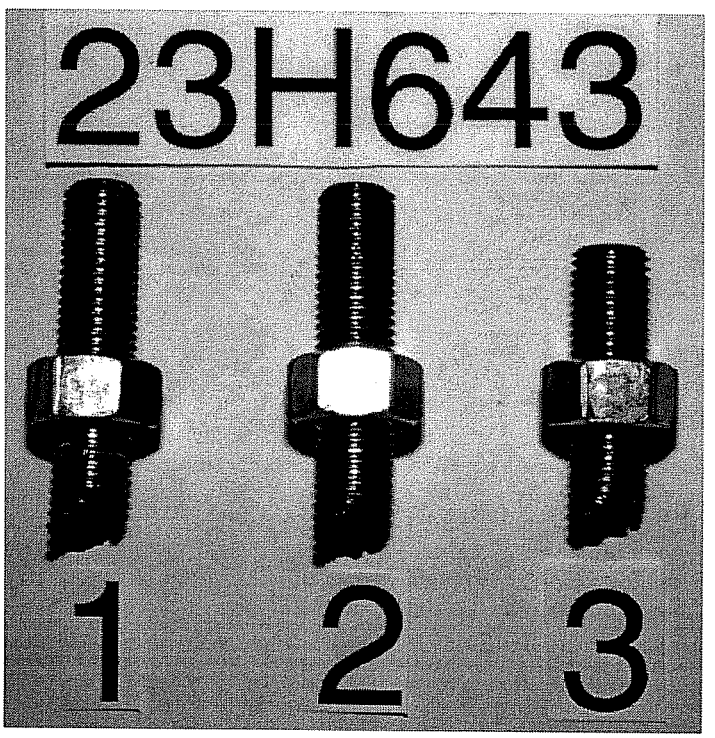

Series 23H643, Sleeve M16, Oblique Tension 30°, Fractured Anchor Shanks

Failure Picture of Test 23H6442, Sleeve M16, Oblique Tension 45°

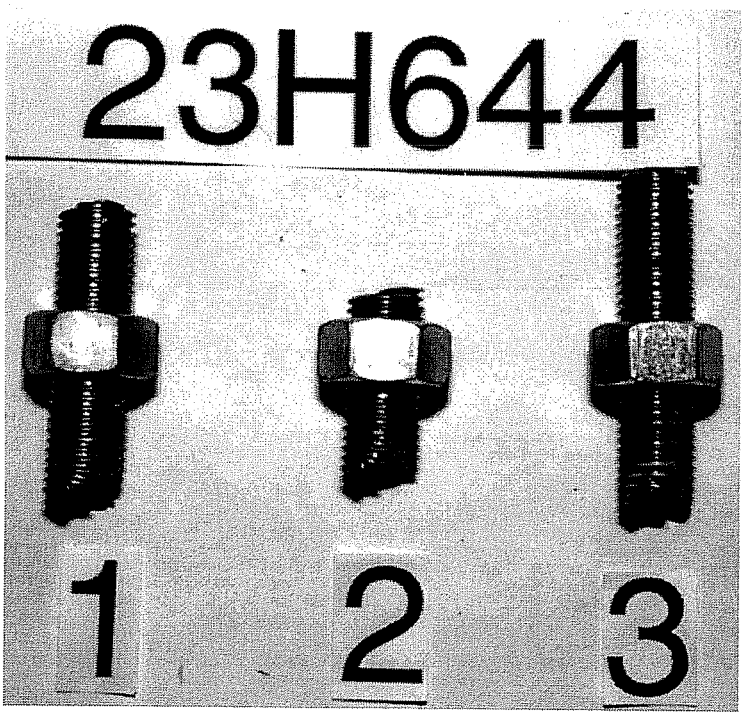

Series 23H644, Sleeve M16, Oblique Tension 45°, Fractured Anchor Shanks

Failure Picture of Test 23H6464, Sleeve M16, Oblique Tension 60°

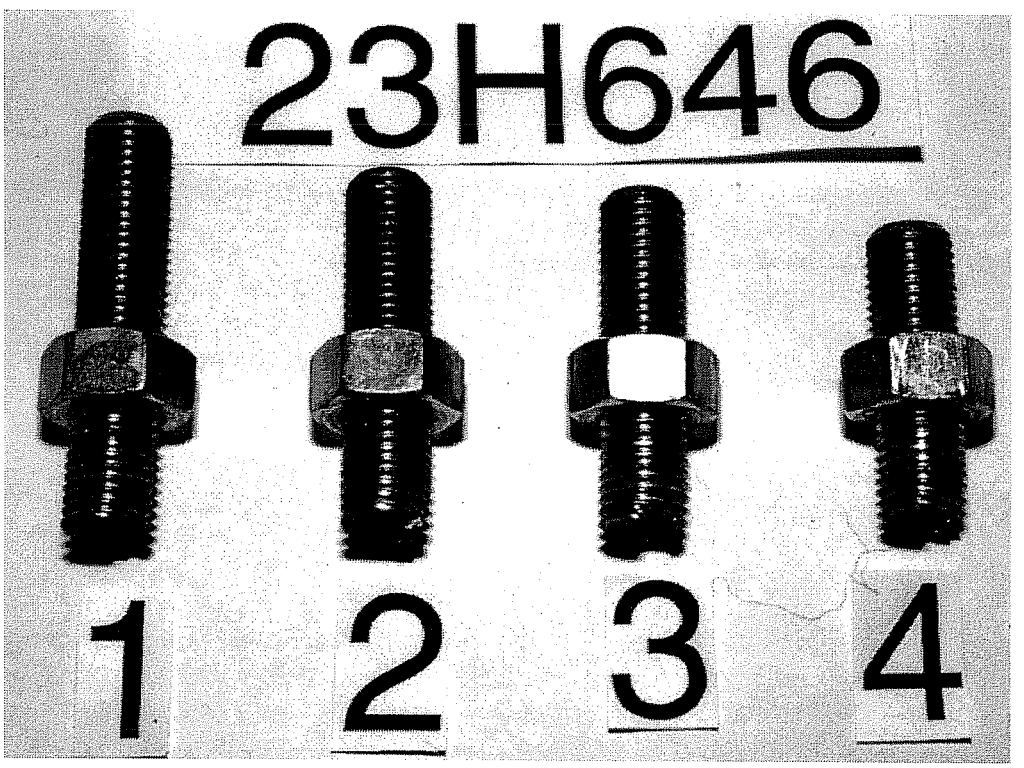

Series 23H646, Sleeve M16, Oblique Tension 60°, Fractured Anchor Shanks

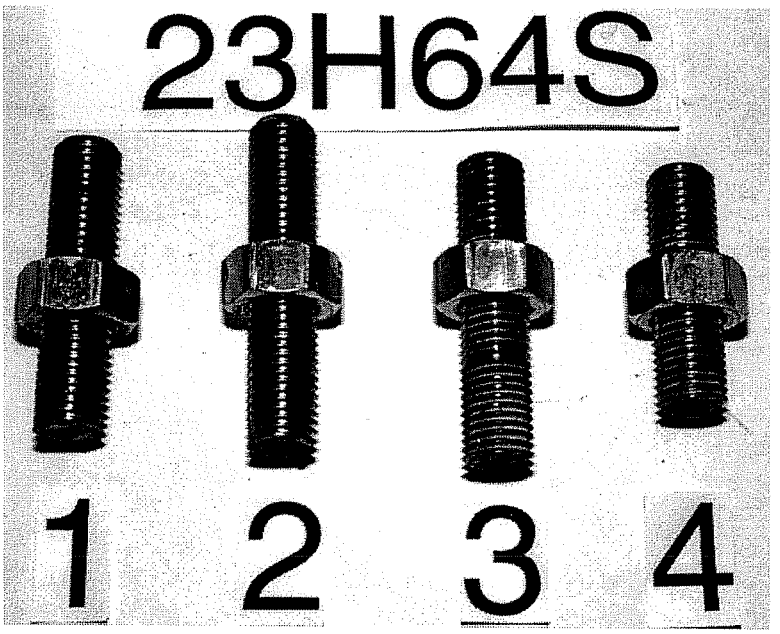

Series 23H64S, Sleeve M16, Shear, Fractured Anchor Shanks

Test No.	Loading Angle	Torque Nm	Block No. -	Concrete f_c N/mm²	Failure Load F_u kN	Hor. Displ. $d_{H,u}$ mm	Corr. c(H) mm	Vert. Displ. $d_{V,u}$ mm	Spalling Depth t mm	Note
23H7431	30	203/102	L36-B	~32.4	131.216	15.55	0.00	7.71	25	
2	30	203/102	L35-T	~32.4	142.336	23.74	0	14.21	51	
Ave.					**136.776**	**19.65**		**10.96**	**38.00**	
23H7441	45	203/102	L36-T	~32.4	142.336	30.64	1.30	12.70	41	1)
2	45	203/102	L35-B	~32.4	131.6608	24.90	0	10.41	44	
Ave.					**136.998**	**27.77**		**11.56**	**42.50**	
23H7461	60	203/102	L36-T	~32.4	128.992	16.88	0.00	5.23	38	
2	60	203/102	L36-B	~32.4	147.2288	15.04	0.00	5.21	32	
Ave.					**138.11**	**15.96**		**5.22**	**35.00**	
23H74S1	Querzug	203/102	L36-B	~32.4	156.5696	13.79	0.00	2.41	9	
2	Querzug	203/102	L35-T	~32.4	142.7808	16.26	0.00	2.29	16	
Ave.					**149.675**	**15.02**		**2.35**	**12.50**	

1) displacement measurement slid, therefore extrapolated to about 0.98*F_u

Test Data of Series 23H74: Sleeve Anchors M16,
through-sleeve installation
h_{ef} = 178mm (= 7 in.), f_c = 32.4 N/mm² (= 4700 psi), Failing by Steel Fracture

Test No.	Loading Angle	Torque Nm	Block No. -	Concrete f_c N/mm²	Failure Load F_u kN	Hor. Displ. $d_{H,u}$ mm	Corr. c(H) mm	Vert. Displ. $d_{V,u}$ mm	Spalling Depth t mm	Note
23H7431	30	203/102	L36-B	~32.4	131.216	15.55	0.00	7.71	25	
2	30	203/102	L35-T	~32.4	142.336	23.74	0	14.21	51	
Ave.					**136.776**	**19.65**		**10.96**	**38.00**	
23H7441	45	203/102	L36-T	~32.4	142.336	30.64	1.30	12.70	41	1)
2	45	203/102	L35-B	~32.4	131.6608	24.90	0	10.41	44	
Ave.					**136.998**	**27.77**		**11.56**	**42.50**	
23H7461	60	203/102	L36-T	~32.4	128.992	16.88	0.00	5.23	38	
2	60	203/102	L36-B	~32.4	147.2288	15.04	0.00	5.21	32	
Ave.					**138.11**	**15.96**		**5.22**	**35.00**	
23H74S1	Querzug	203/102	L36-B	~32.4	156.5696	13.79	0.00	2.41	9	
2	Querzug	203/102	L35-T	~32.4	142.7808	16.26	0.00	2.29	16	
Ave.					**149.675**	**15.02**		**2.35**	**12.50**	

1) displacement measurement of slid, therefore extraploated to about $0.98*f_u$

Test Data of Series 23H74: Sleeve Anchors M16, through-sleeve installation
h_{ef} = 178mm (= 7 in.), f_c = 32.4 N/mm² (= 4700 psi), Failing by Steel

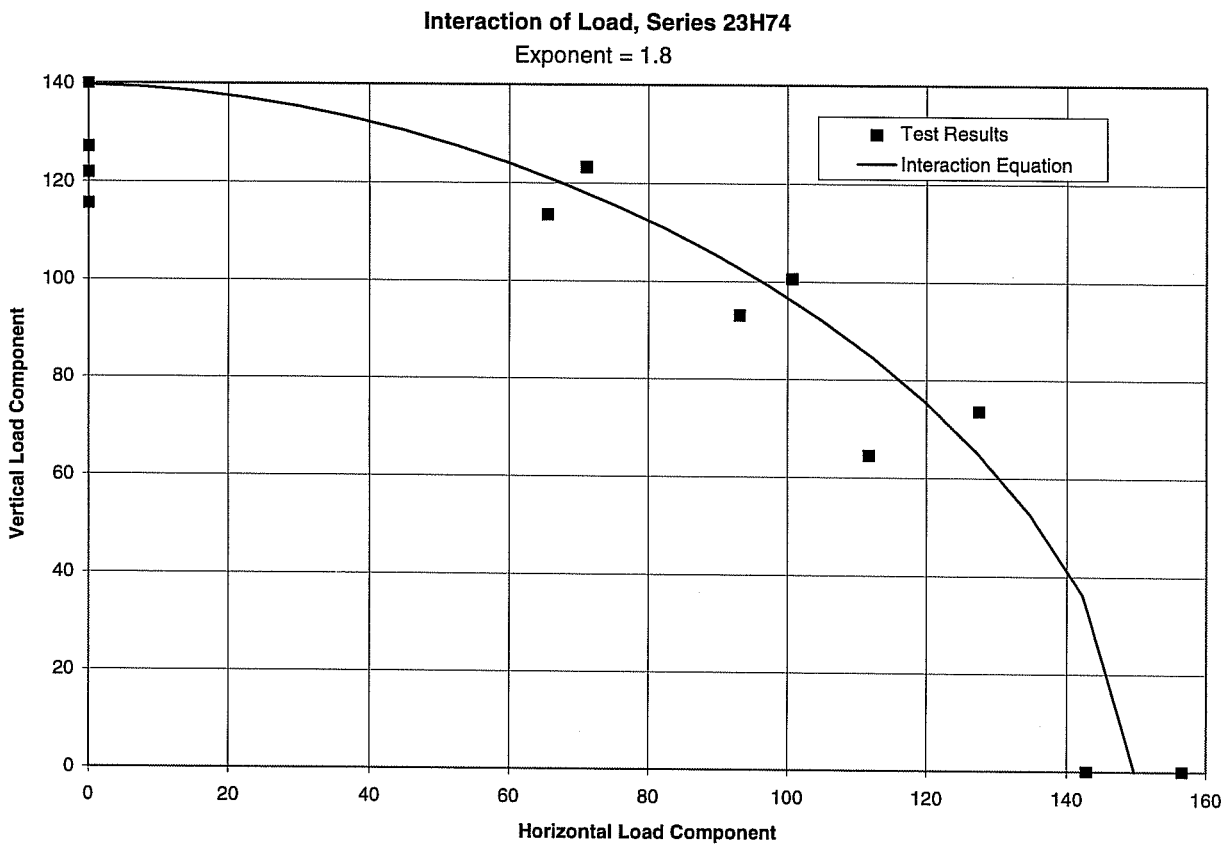
Interaction of Load, Series 23H74
Exponent = 1.8
Test Results
Interaction Equation
Vertical Load Component
Horizontal Load Component
0
20
40
60
80
100
120
140
160

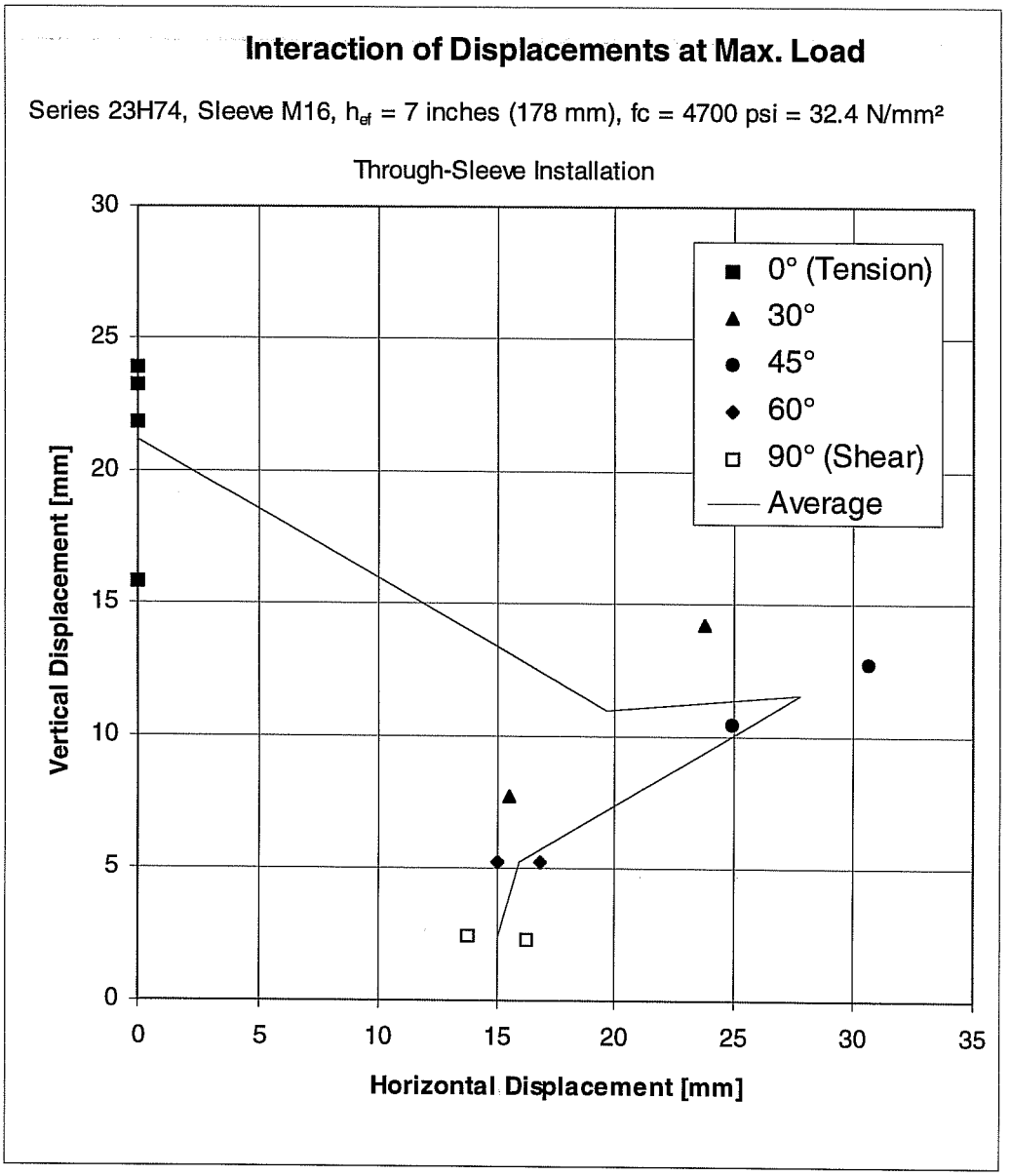
Interaction of Displacements at Max. Load
Series 23H74, Sleeve M16, h_{ef} = 7 inches (178 mm), fc = 4700 psi = 32.4 N/mm²
Through-Sleeve Installation
Vertical Displacement [mm]
Horizontal Displacement [mm]
0° (Tension)
30°
45°
60°
90° (Shear)
Average
0
5
10
15
20
25
30
35

Part 1: Interaction of Force	**Interactions Exponent**	σ_Z	σ_S	
Break of Curve	1.80	711.8	762.7	
Maxi. Load	1.80	889.8	953.3	
Remnant Load	1.80	845.3	905.7	
Part 2: Load-Displacement Curves	**Angle d_{knick}**	**d_u**	**d_{Rest}**	**Curvature Exponent**
Angle	0			
d_{Ver}	9.53	21.84	26.67	0.25
Angle	15			
d_{Hor}	5.06	10.22	10.55	0.40
d_{Ver}	8.74	18.63	22.48	0.25
Angle	30			
d_{Hor}	9.73	19.65	20.28	0.40
d_{Ver}	6.86	10.96	12.46	0.25
Angle	45			
d_{Hor}	13.83	27.77	28.45	0.40
d_{Ver}	6.97	11.56	12.32	0.25
Angle	60			
d_{Hor}	5.16	15.96	22.41	0.50
d_{Ver}	1.59	5.22	6.74	0.25
Angle	75			
d_{Hor}	6.78	15.31	17.49	0.50
d_{Ver}	0.85	2.78	3.60	0.30
Angle	90			
d_{Hor}	7.49	15.02	15.32	0.50

Displacement in mm, Angle in degrees

Mathematical Description of Results of Series 23H74 with Sleeve Anchors (h_{ef} = 7 inches, c1 ≥ 11 inches) Through-Sleeve Installation for Program BDA5 (0° from Series 23H64, 15° and 75° interpolated), f_c = 32.4 N/mm²

Mathematical Description of Load-Displacement Curves of Series 23M74

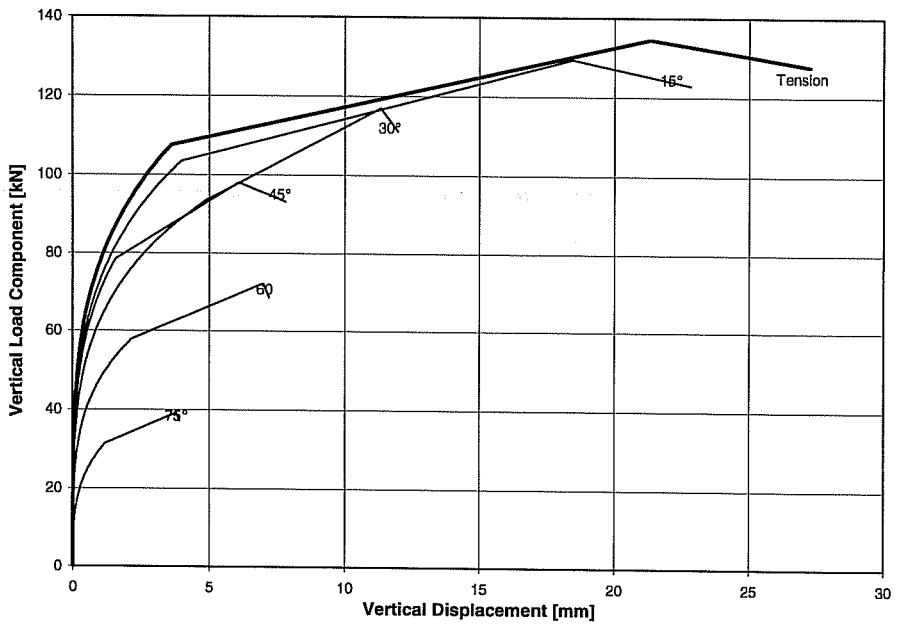

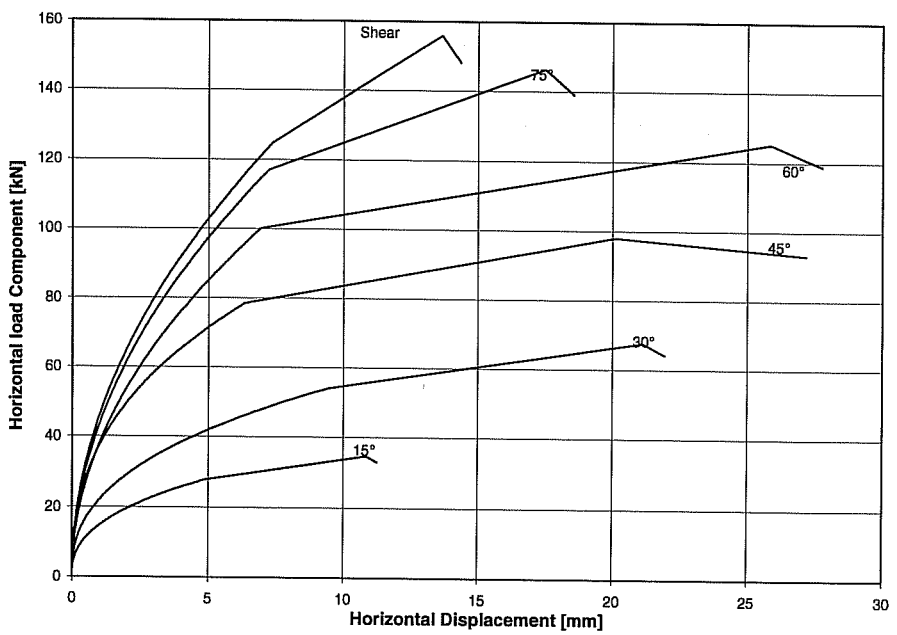

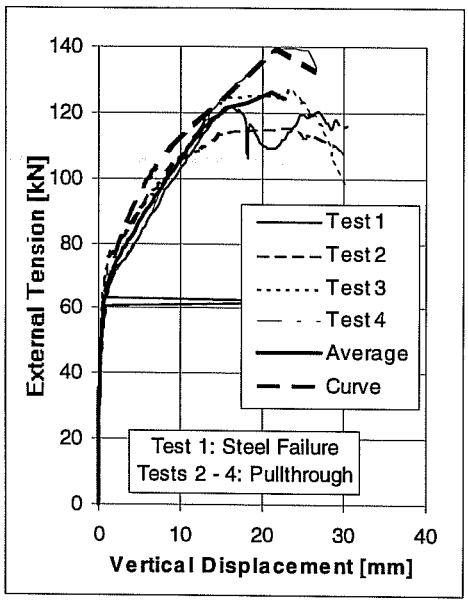

Pure Tension

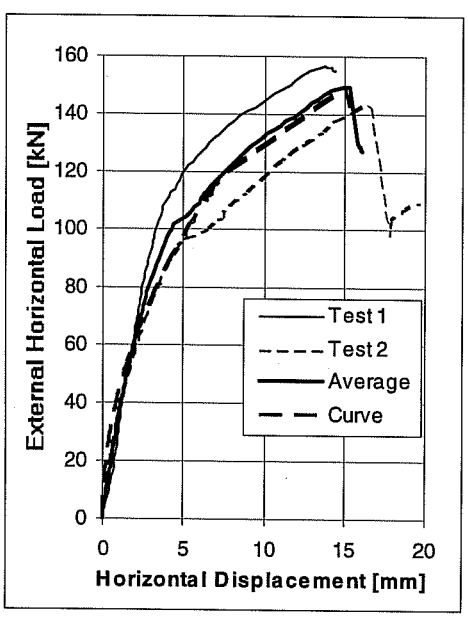

Pure Shear

Load-Displacement Curves of Series 23h64T (Tension) and 23h74S (Shear)
Sleeve Anchor M16, h_{ef} = 7 inches (178 mm),
c1 ≥ 11 inches (279 mm), f_c = 32.4 N/mm²
Shear with Through-Sleeve Installation

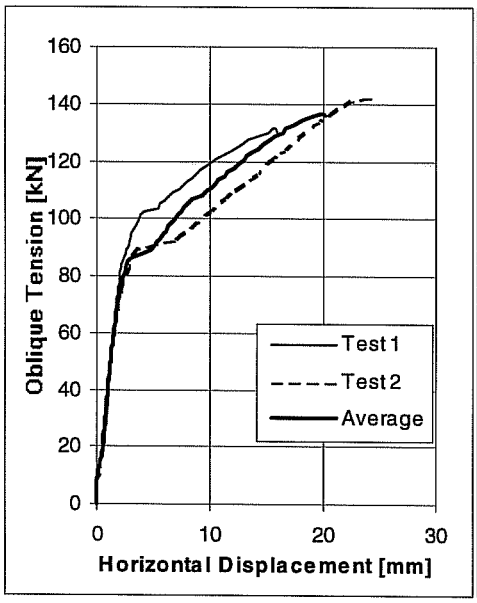

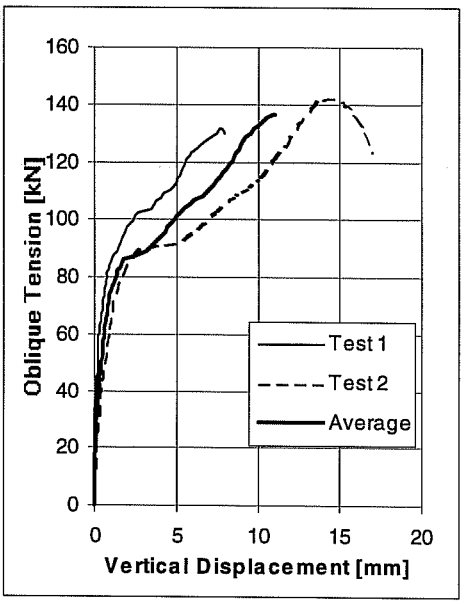

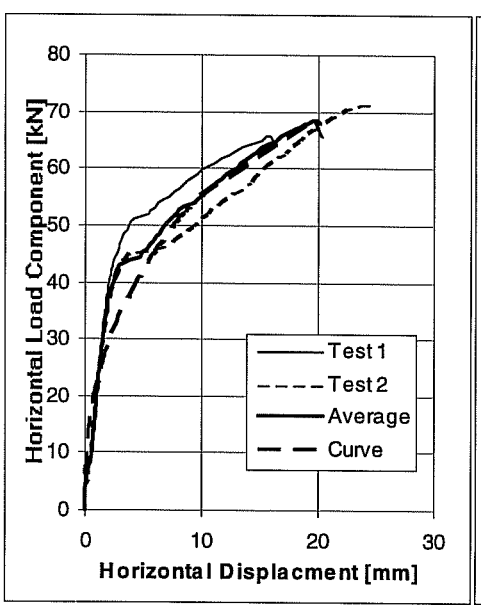

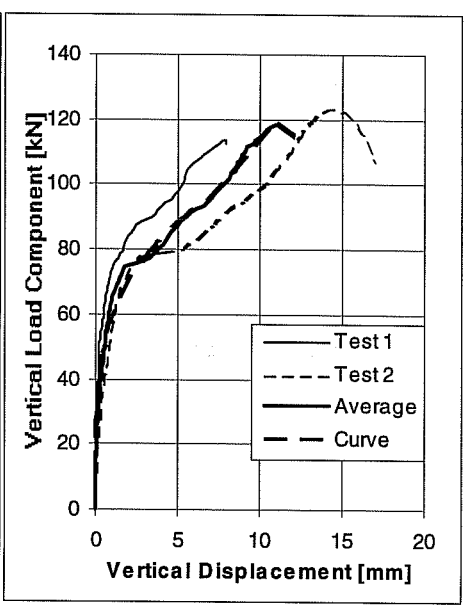

Load-Displacement Curves of Series 23h743,
Sleeve Anchors M16, h_{ef} = 7 inches (178 mm)
c1 ≥ 11 inches (279 mm), f_c = 32.4 N/mm², Loading Angle 30° from Anchor Axis
Through-Sleeve Installation

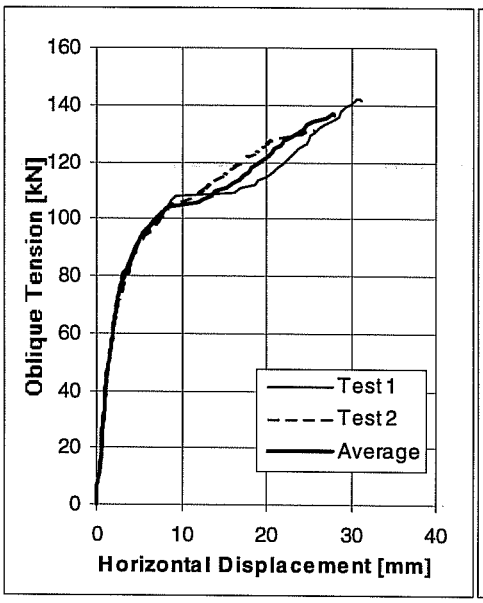

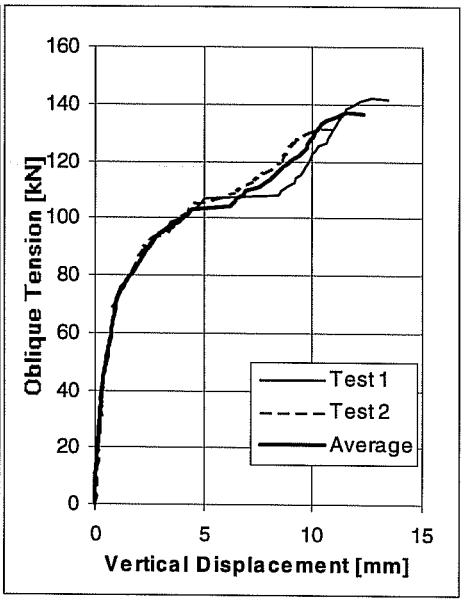

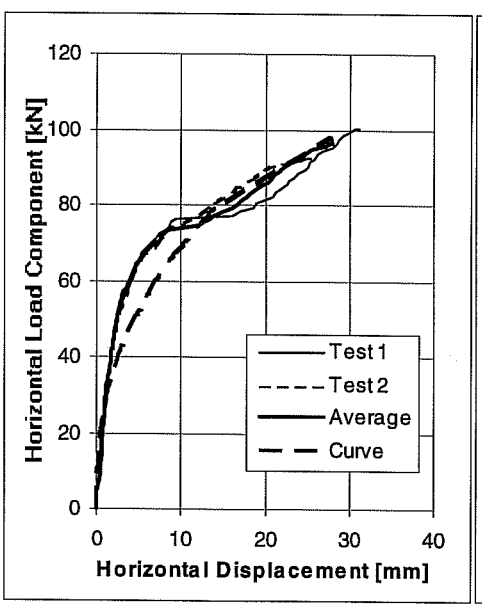

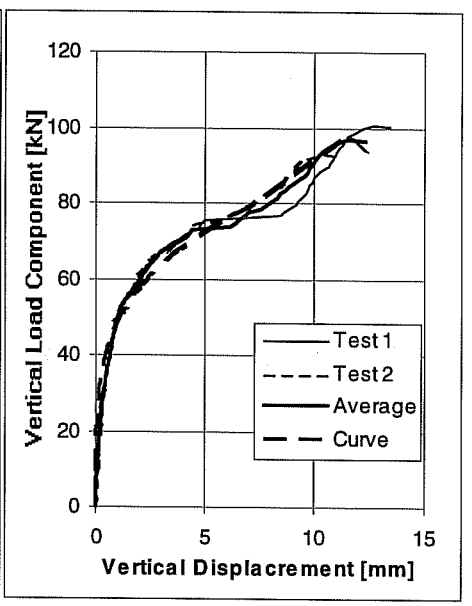

Load-Displacement Curves of Series 23h744,
Sleeve Anchors M16, h_{ef} = 7 inches (178 mm)
c1 ≥ 11 inches (279 mm), f_c = 32.4 N/mm², Loading Angle 45° from Anchor Axis
Through-Sleeve Installation

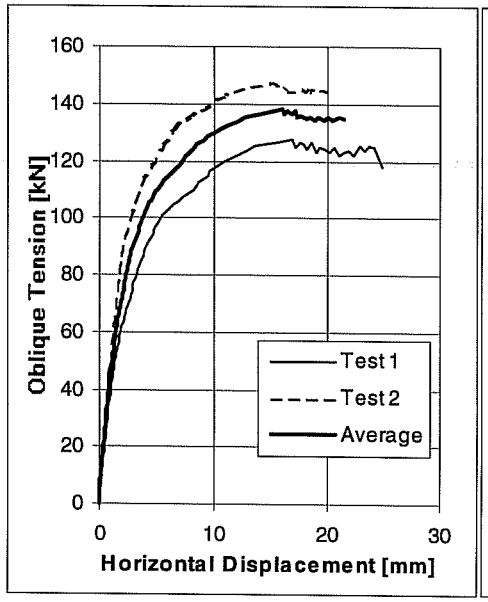

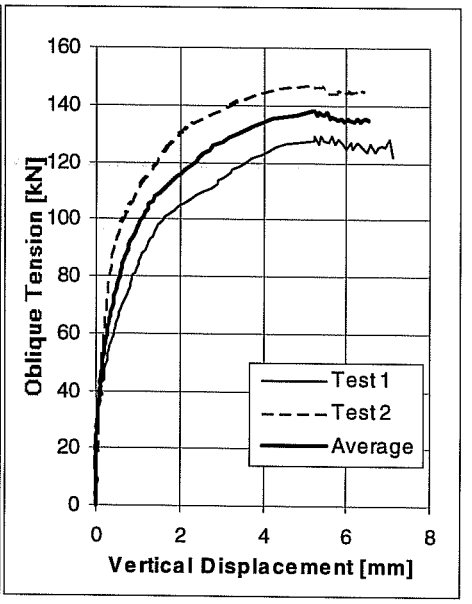

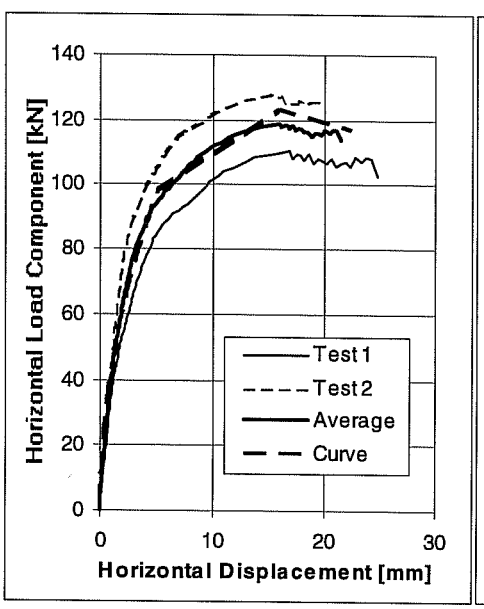

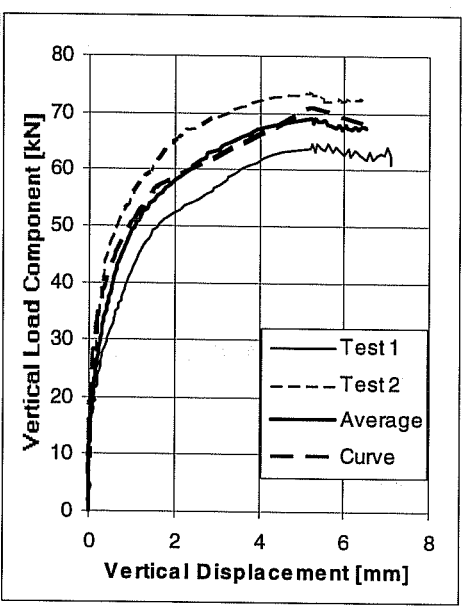

Load-Displacement Curves of Series 23h746,
Sleeve Anchors M16, h_{ef} = 7 inches (178 mm)
c1 ≥ 11 inches (279 mm), f_c = 32.4 N/mm², Loading Angle 60° from Anchor Axis
Through-Sleeve Installation

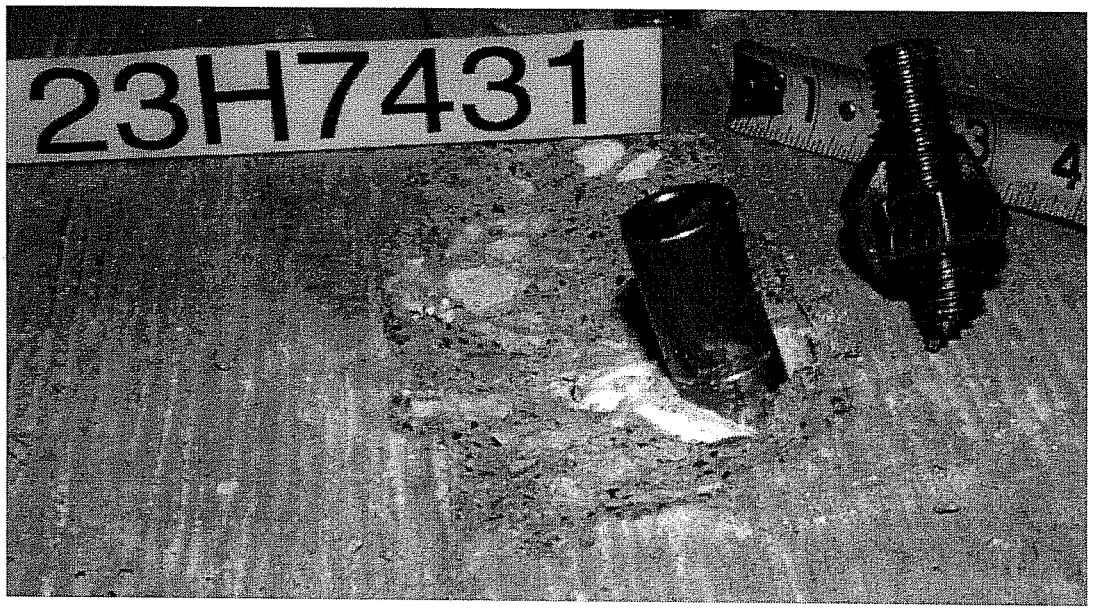

Failure Picture of Test 23H7431, Sleeve M16, Oblique Tension 30°

Failure Picture of Test 23H7442, Sleeve M16, Oblique Tension 45°

Failure Picture of Test 23H7462, Sleeve M16, Oblique Tension 60°

Failure Picture of Test 23H74S2, Sleeve M16, Shear

Test No.	Loading Angle degrees	Torque Nm	Block No.	Concrete f_c N/mm²	Failure Load F_u kN	Hor. Displ. $d_{H,u}$ mm	Corr. c(H) mm	Vert. Displ. $d_{V,u}$ mm	Spalling Depth t mm	Note
23M54T1	Tension	244/122	L36-T	~ 32.4	135.66	-	-	28.52	-	
2	Tension	244/122	L36-T	~ 32.4	131.22	-	-	17.81	-	
3	Tension	244	L36-B	~ 32.4	137.89	-	-	22.33	-	1)
4	Tension	244/122	L36-B	~ 32.4	136.55	-	-	16.69	-	
Ave.					**135.33**			**21.34**		
COV [%]					**2.14**			**25.20**		
23M5411	15	244/122	L35-T	~ 32.4	128.55	13.47	1.30	14.69	32	
2	15	244/122	L35-B	~ 32.4	123.65	6.63	0.75	7.21	16	
3	15	244/122	L35-B	~32.4	127.66	7.11	1.30	9.07	16	
Ave.					**126.62**	**9.07**		**10.33**	**21.33**	
COV [%]					**2.06**	**42.05**		**37.73**	**43.30**	
23M5431	30	244/122	L36-B	~32.4	112.53	6.56	2.00	3.29	13	
2	30	244/122	L36-B	~32.4	115.65	5.98	1.50	3.43	13	
3	30	244/122	L35-T	~32.4	108.53	7.39	2.00	3.66	13	
Ave.					**112.24**	**6.65**		**3.46**	**13.00**	
COV [%]					**3.18**	**10.69**		**5.38**	**0.00**	
23M5441	45	244/122	L36-T	~32.4	92.52	7.36	0.00	2.24	n.g.	
2	45	244/122	L36-T	~32.4	91.18	6.45	1.30	1.84	n.g.	
3	45	244/122	L36-T	~32.4	96.52	7.74	2.00	2.37	n.g.	
4	45	244/122	L36-B	~32.4	93.85	6.10	1.50	1.54	9	
Ave.					**93.52**	**6.91**		**2.00**	**9.00**	
COV [%]					**2.44**	**11.04**		**19.08**		
23M5461	60	244/122	L36-T	~32.4	83.18	6.94	0.00	1.32	n.g.	
2	60	244/122	L36-T	~32.4	85.40	6.59	0.50	1.27	n.g.	
3	60	244/122	L36-B	~32.4	84.96	6.13	0.30	0.84	6	2)
4	60	244/122	L36-B	~32.4	91.18	5.96	0.00	1.02	6	
Ave.					**86.18**	**6.40**		**1.11**	**6.00**	
COV [%]					**4.03**	**6.96**		**20.31**		
23M54S1	Shear	244/122	L36-T	~32.4	80.95	6.35	1.30	0.00		
2	Shear	244/122	L36-T	~32.4	81.84	5.54	0.00	0.00	n.g.	3)
3	Shear	244/122	L36-T	~32.4	80.51	5.64	0.00	0.00	n.g.	4)
4	Shear	244/122	L36-B	~32.4	84.96	6.16	0.80	0.00	3	
5	Shear	244/122	L36-B	~32.4	82.73	4.78	0.00	0.00	0	
Ave.					**82.20**	**5.69**		**0.00**	**1.50**	
COV [%]					**2.14**	**10.81**				

1) Torque was not reduced.

2) only 1 displacement measured for vertical displacement d_V

3) The displacement measurement for d_V slid against loading plate.

4) Load cell rubbed on base

Results of Series 23M54: UC1Anchors of 5/8",
Flush-Sleeve Installation
h_{ef} = 178mm (7 in.), f_c = 32.4 N/mm² (4700 psi), Failing by Steel Fracture

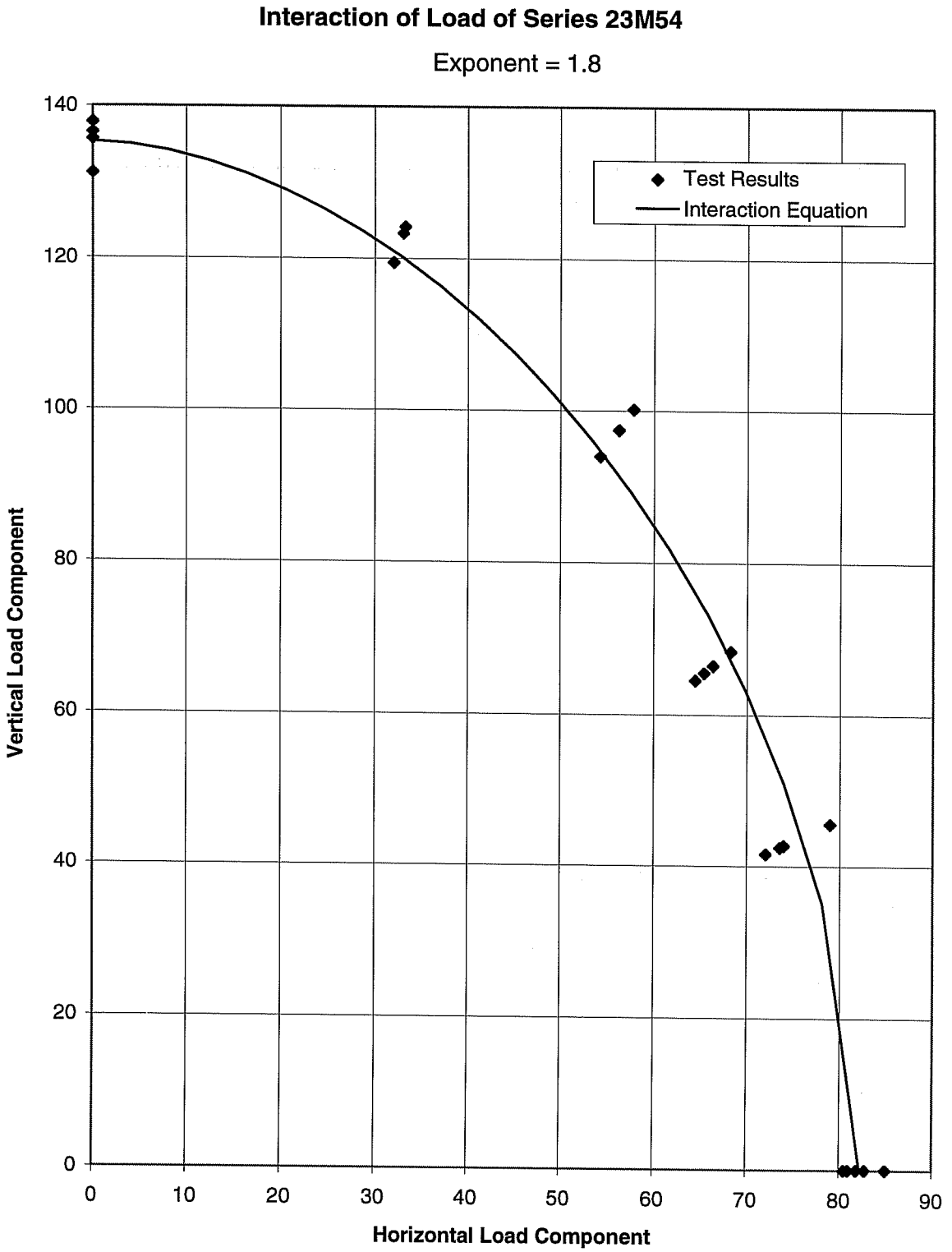
Interaction of Load of Series 23M54
Exponent = 1.8
Test Results
Interaction Equation
Vertical Load Component
Horizontal Load Component
0
20
40
60
80
100
120
140
0
10
20
30
40
50
60
70
80
90

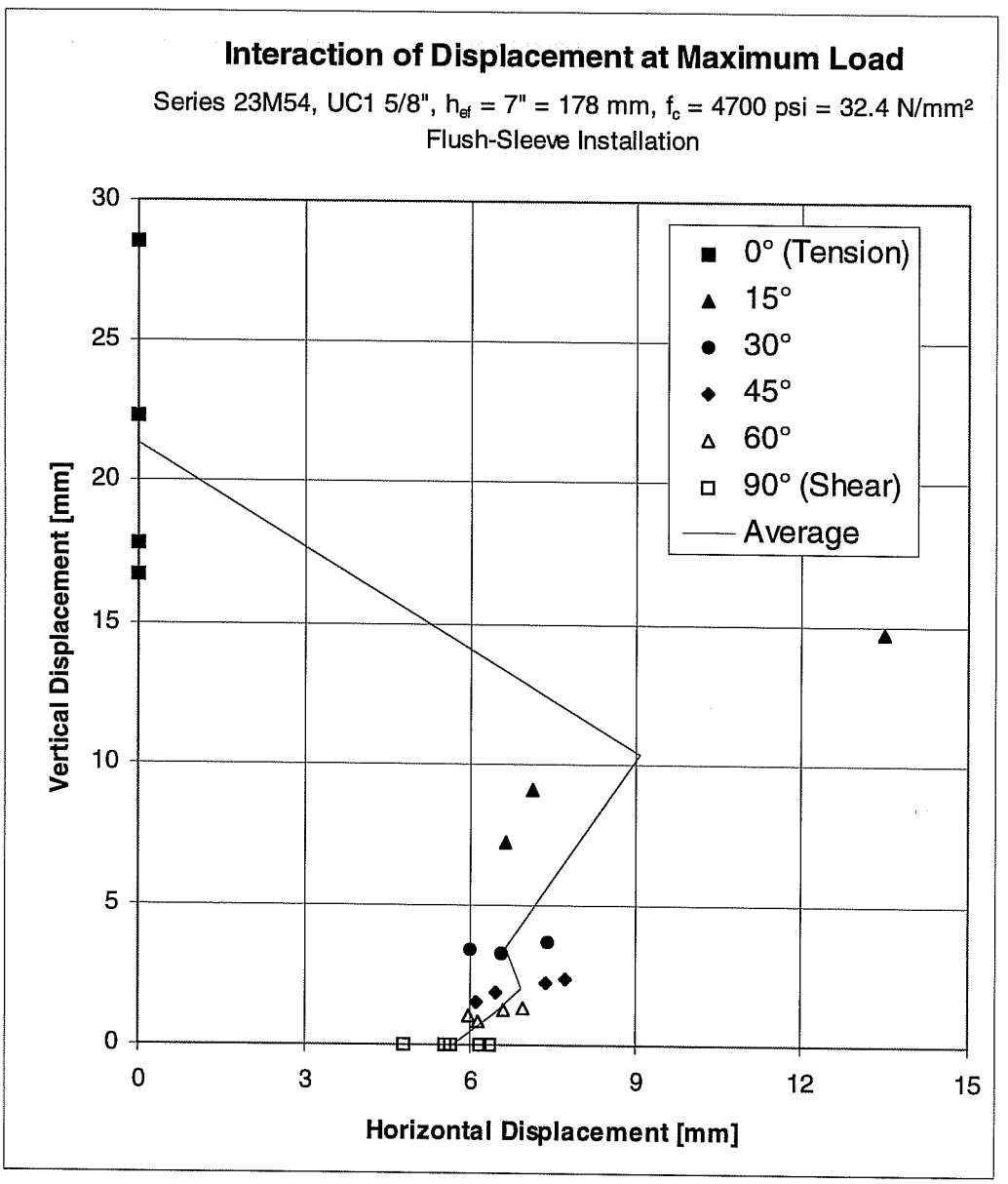
Interaction of Displacement at Maximum Load
Series 23M54, UC1 5/8", h_{ef} = 7" = 178 mm, f_c = 4700 psi = 32.4 N/mm²
Flush-Sleeve Installation
Vertical Displacement [mm]
Horizontal Displacement [mm]
0
5
10
15
20
25
30
0
3
6
9
12
15
0° (Tension)
15°
30°
45°
60°
90° (Shear)
Average

Part 1: Interaction of Force	**Interaction Exponent**	σ_Z	σ_S	
Break of Curve	1.80	829.8	504.5	
max. Load	1.80	922.0	560.5	
Remnant Load	1.80	875.9	532.5	
Part 2: Load-Displacement Curves	**Angle d_{knick}**	**d_u**	**d_{Rest}**	**Curvature Exponent**
Angle	0			
d_{Ver}	7.83	21.34	27.26	0.17
Angle	15			
d_{Hor}	4.92	9.07	9.55	0.40
d_{Ver}	5.11	10.33	10.88	0.20
Angle	30			
d_{Hor}	4.11	6.65	6.92	0.50
d_{Ver}	1.93	3.46	3.60	0.25
Angle	45			
d_{Hor}	4.40	6.91	7.18	0.50
d_{Ver}	1.15	2.00	2.06	0.25
Angle	60			
d_{Hor}	4.25	6.40	6.57	0.60
d_{Ver}	0.60	1.11	1.15	0.25
Angle	75			
d_{Hor}	4.23	5.89	6.09	0.60
d_{Ver}	0.29	0.55	0.57	0.25
Angle	90			
d_{Hor}	4.23	5.69	5.90	0.60

Displacement in mm, Angle in degrees

Mathematical Descrpition of Results of Series 23M54 with UC1 Anchors (h_{ef} = 7 inches, c1 ≥ 11 inches) in Flush-Sleeve Installation for Program BDA5 (75° interpolated) f_c = 32.4 N/mm²

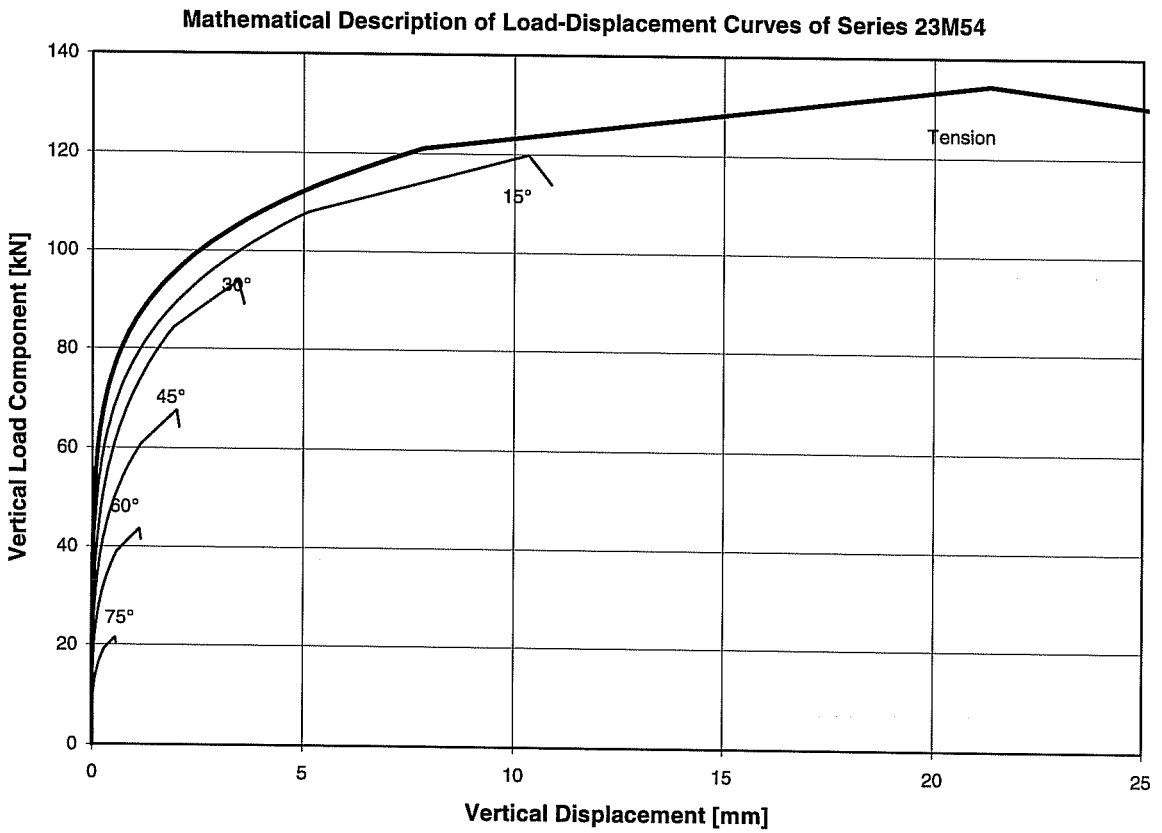
Mathematical Description of Load-Displacement Curves of Series 23M54
Vertical Load Component [kN]
Vertical Displacement [mm]
140
120
100
80
60
40
20
0
0
5
10
15
20
25
Tension
15°
30°
45°
60°
75°

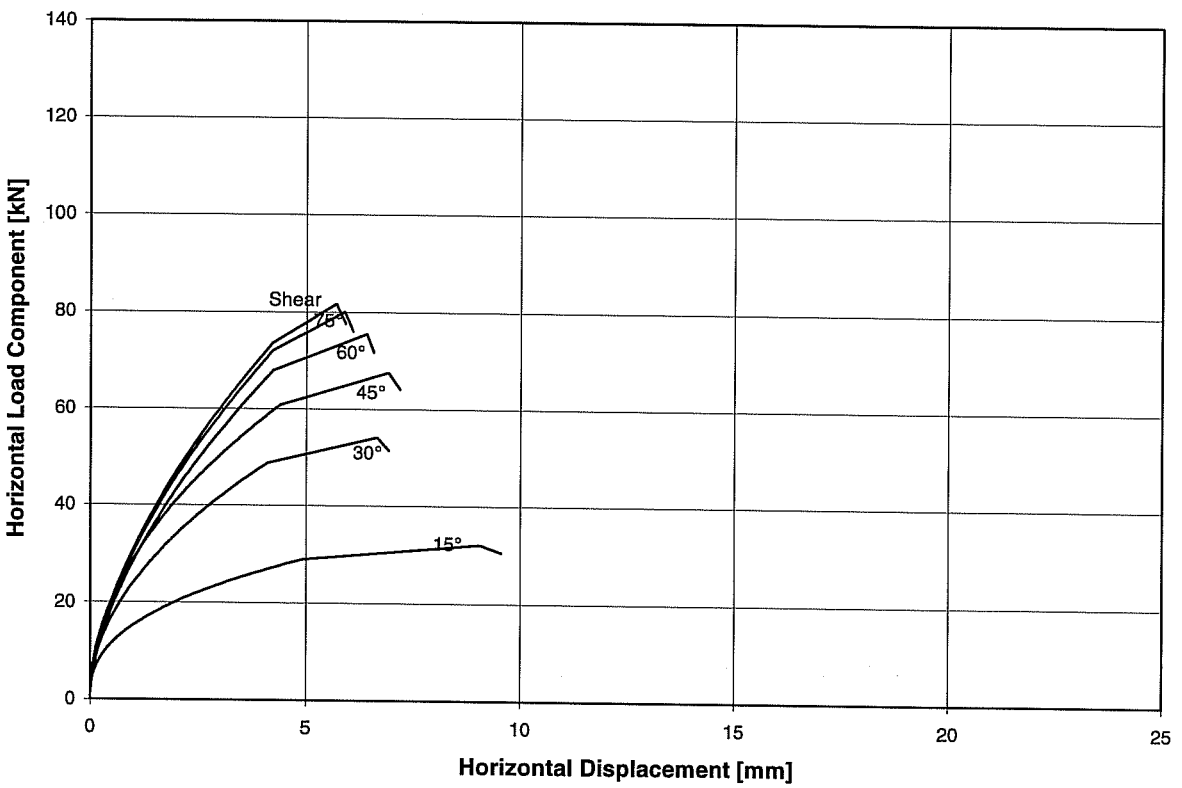
Horizontal Load Component [kN]
140
120
100
80
60
40
20
0
0
5
10
15
20
25
Horizontal Displacement [mm]
Shear
75°
60°
45°
30°
15°

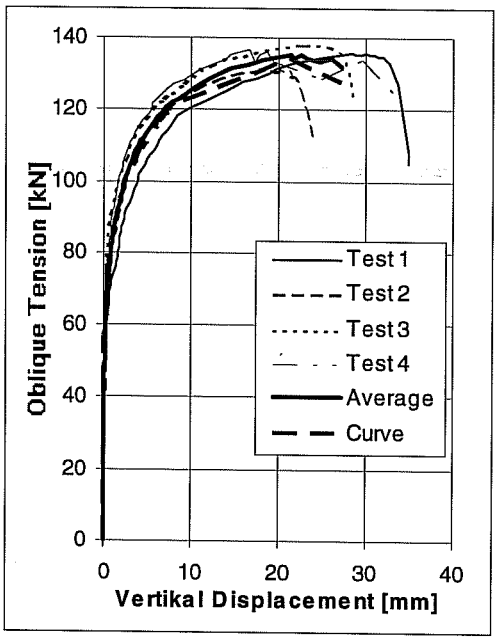

Pure Tension

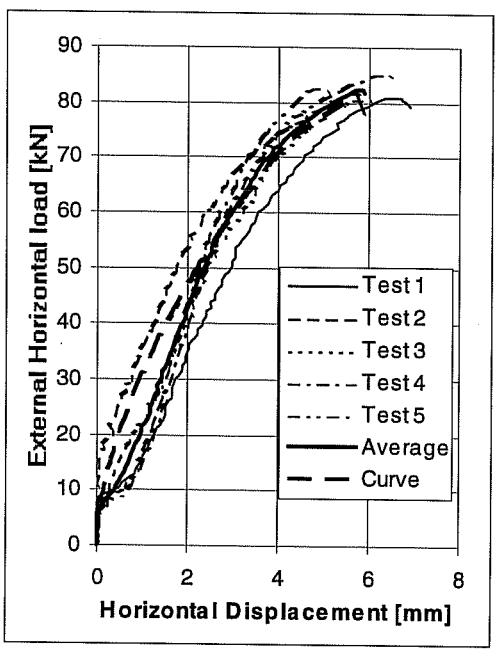

Pure Shear

Load-Displacement Curves of Series 23m54T (Tension) and 23m54S (Shear)
UC1 Anchors 5/8-inch, h_{ef} = 7 inches (178 mm), c1 ³ 11 inches (279 mm), f_c = 32.4 N/mm²

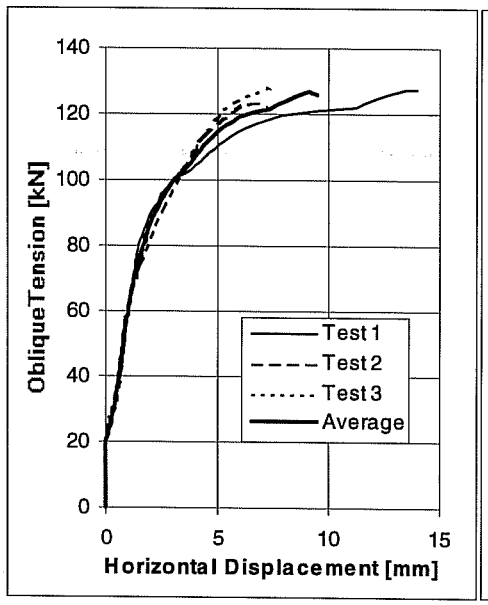

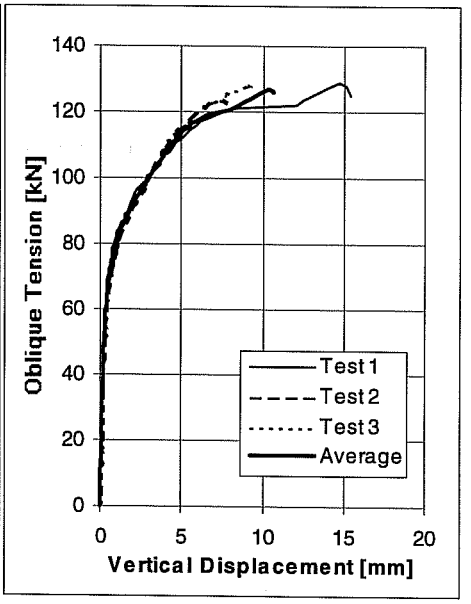

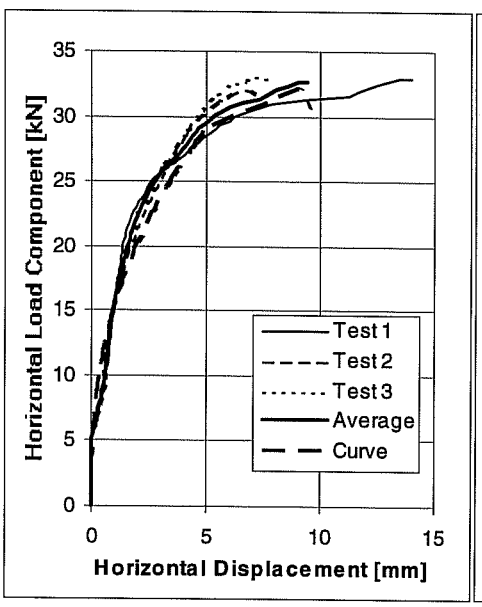

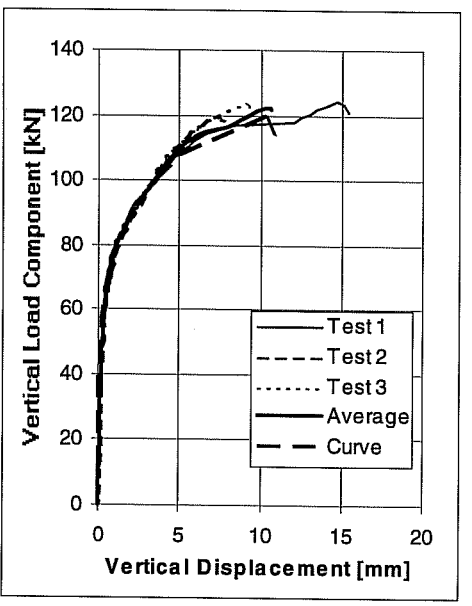

Load-Displacement Curves of Series 23m541,
UC1Anchor 5/8", h_{ef} = 7 inches (178 mm), c1 ≥ 11 inches (279 mm),
f_c = 32.4 N/mm², Loading Angle 15° from Anchor Axis

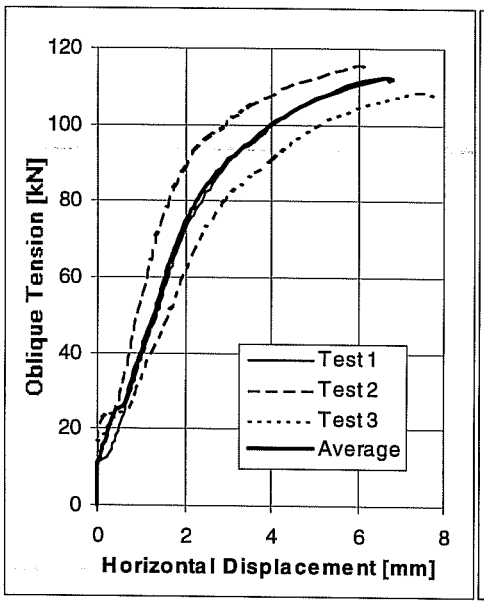

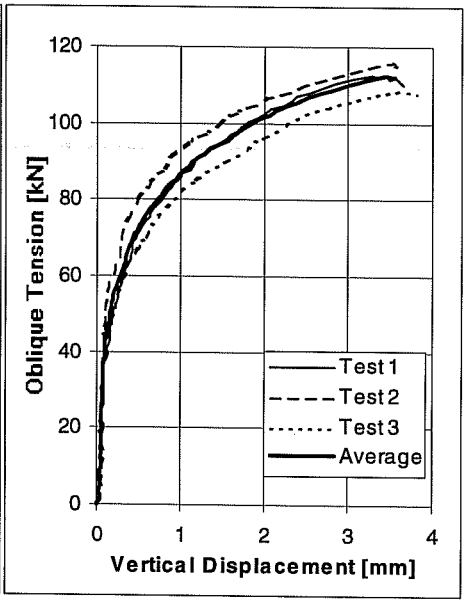

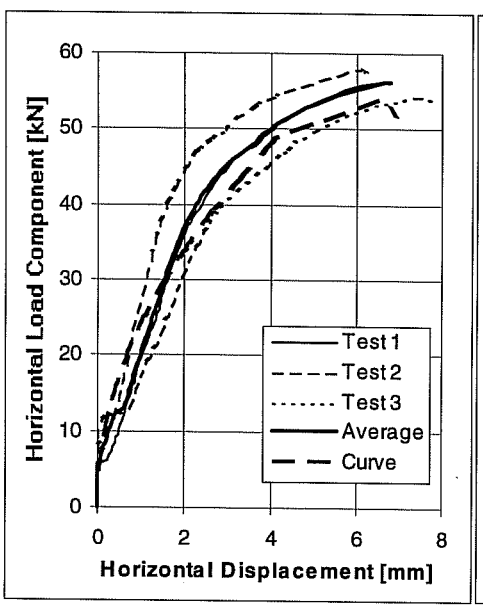

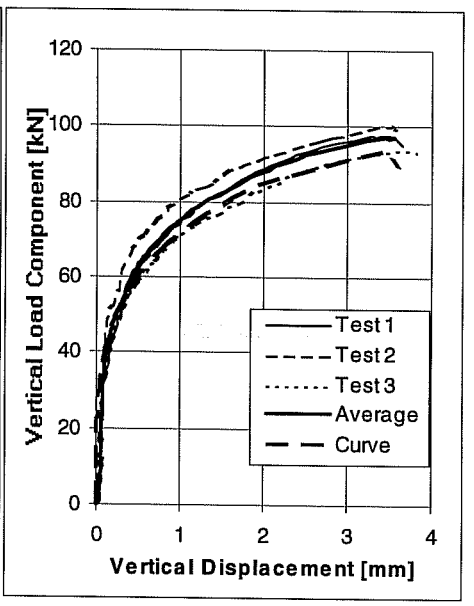

Load-Displacement Curves of Series 23m543,
UC1 Anchors 5/8 inches, hef = 7 inches (178 mm), c1 ³ 11 inches (279 mm),
f_c = 32.4 N/mm², Loading Angle 30° from Anchor Axis

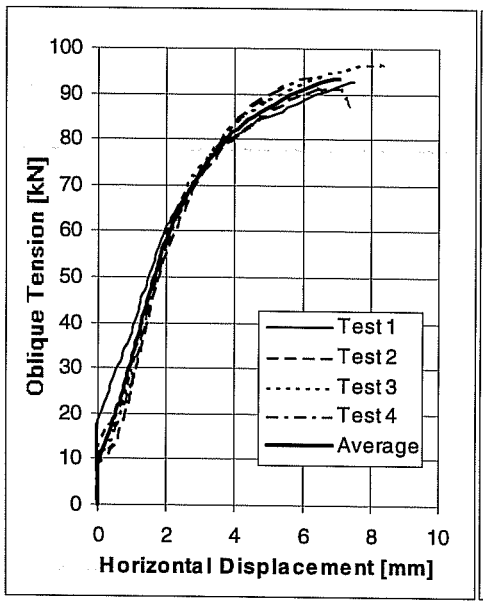

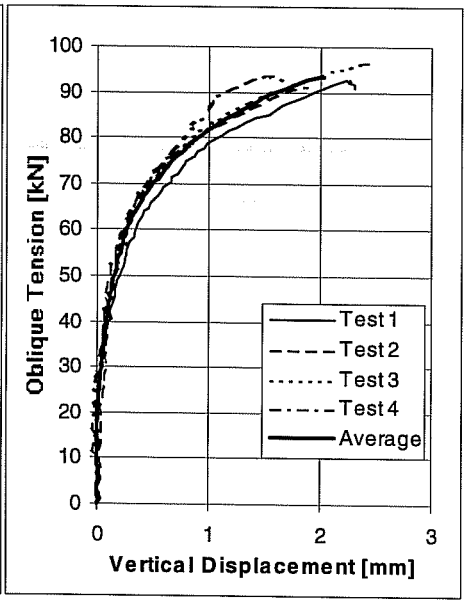

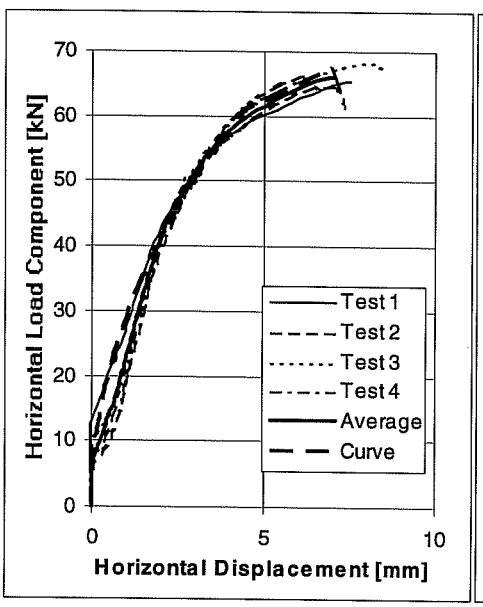

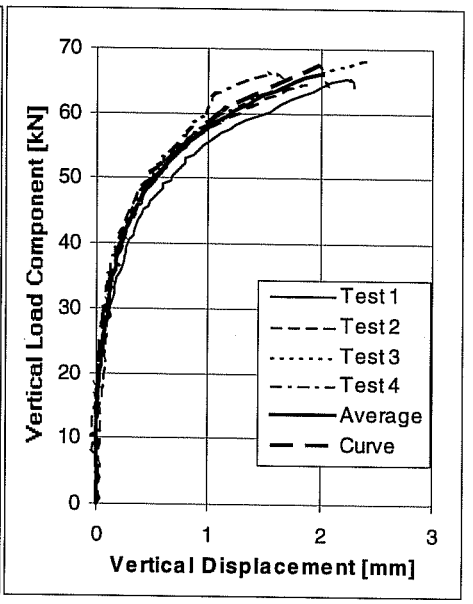

Load-Displacement Curves of Series 23m544,
UC1 Anchors 5/8 inches, hef = 7 inches (178 mm), c1 ³ 11 inches (279 mm),
f_c = 32.4 N/mm², Loading Angle 45° from Anchor Axis

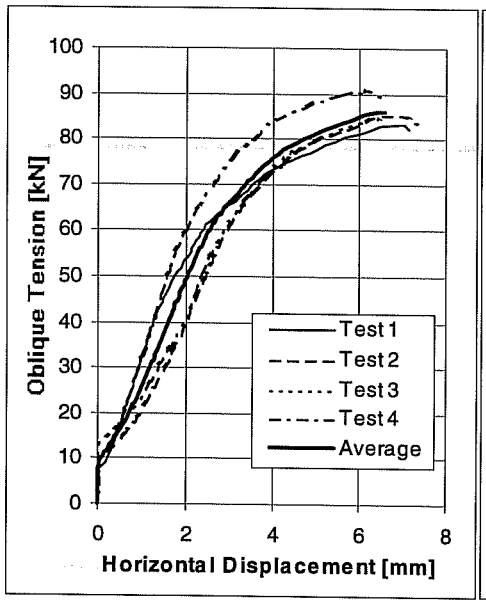

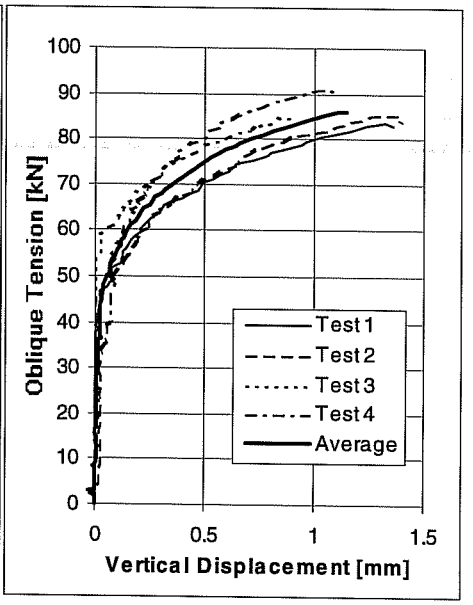

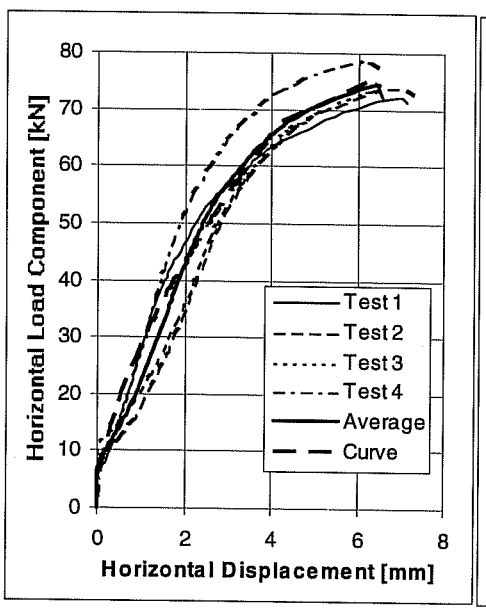

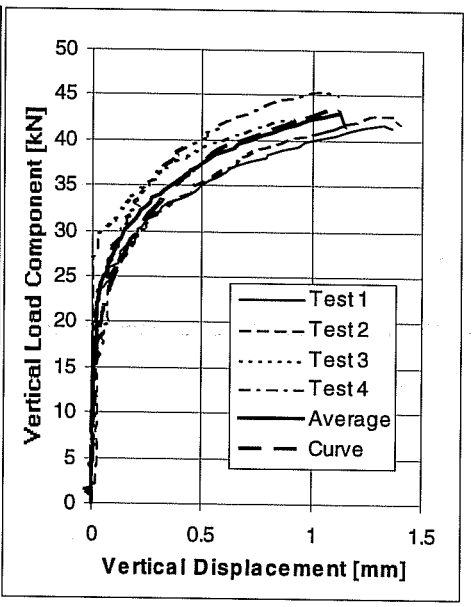

Load-Displacement Curves of Series 23m546,
UC1 Anchors 5/8 inches, hef = 7 inches (178 mm), c1 ³ 11 inches (279 mm),
f_c = 32.4 N/mm², Loading Angle 60° from Anchor Axis

Failure Picture of Test 23M54T4, UC1 5/8", Pure Tension

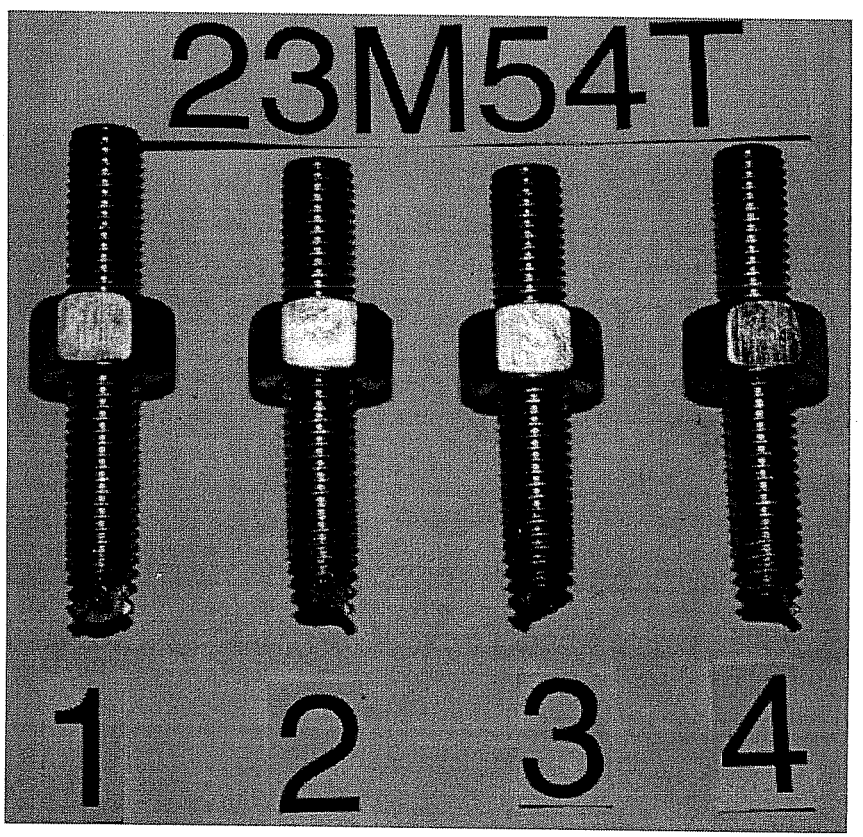

Series 23M541, UC1 5/8", Pure Tension, Fractured Anchor Shanks

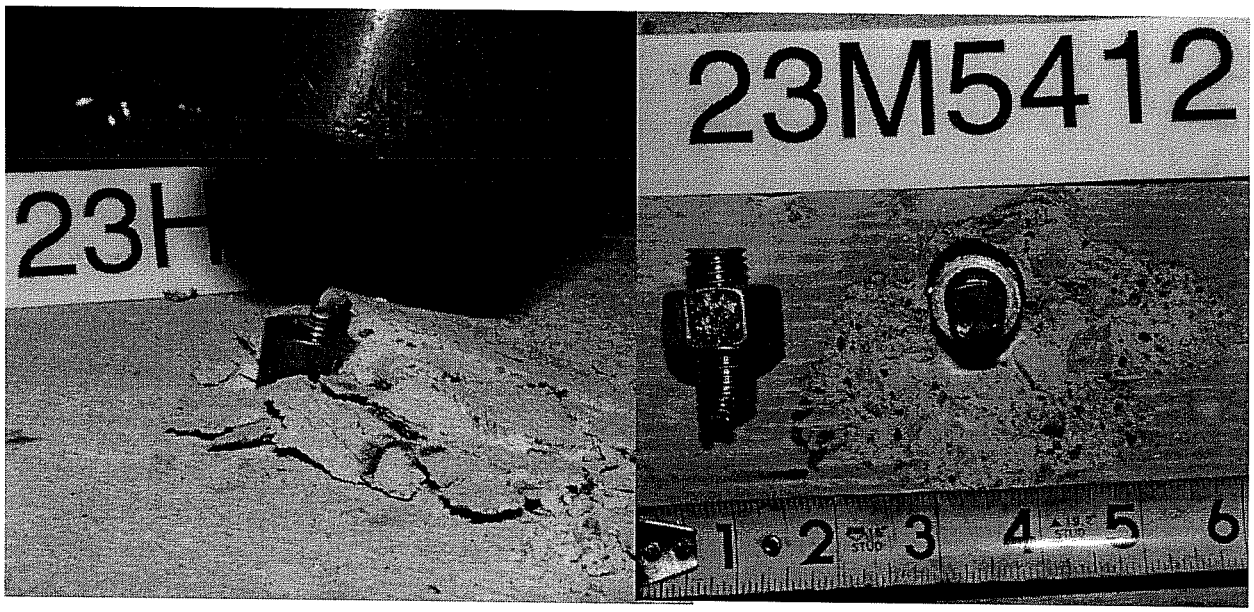

Failure Picture of Test 23M5411 and 23M5412, UC1 5/8", Oblique Tension 15°

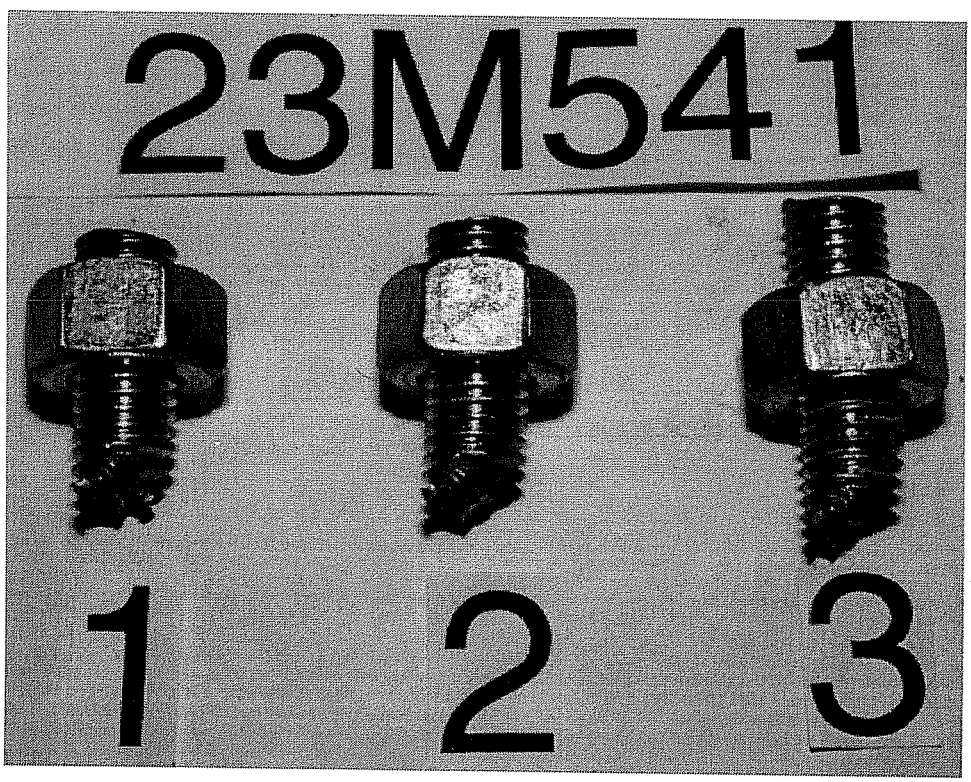

Series 23M541, , UC1 5/8", Oblique Tension 15°, Fractured Anchor Shanks

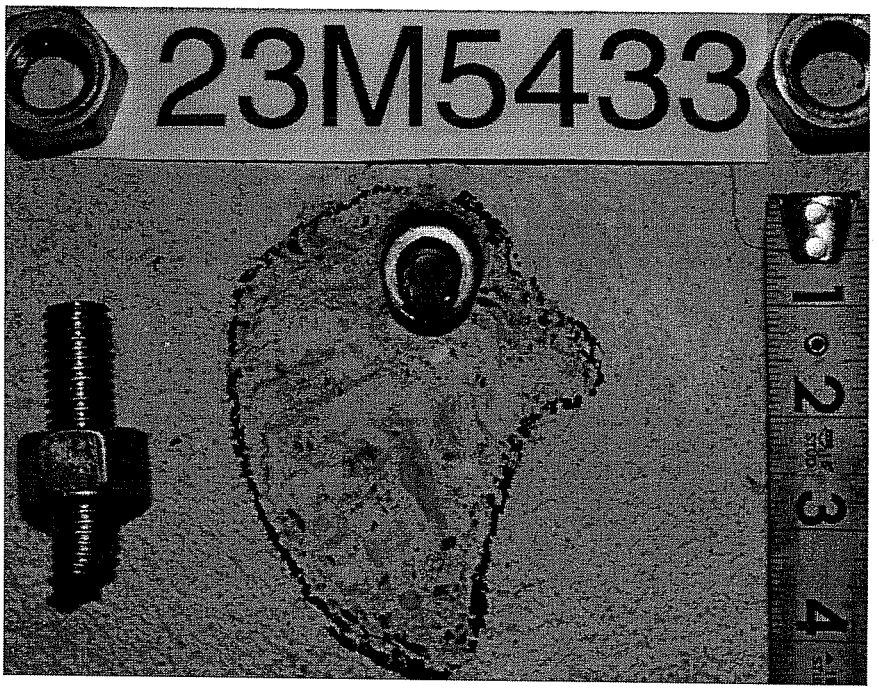

Failure Picture of Test 23M5433, UC1 5/8", Oblique Tension 30°

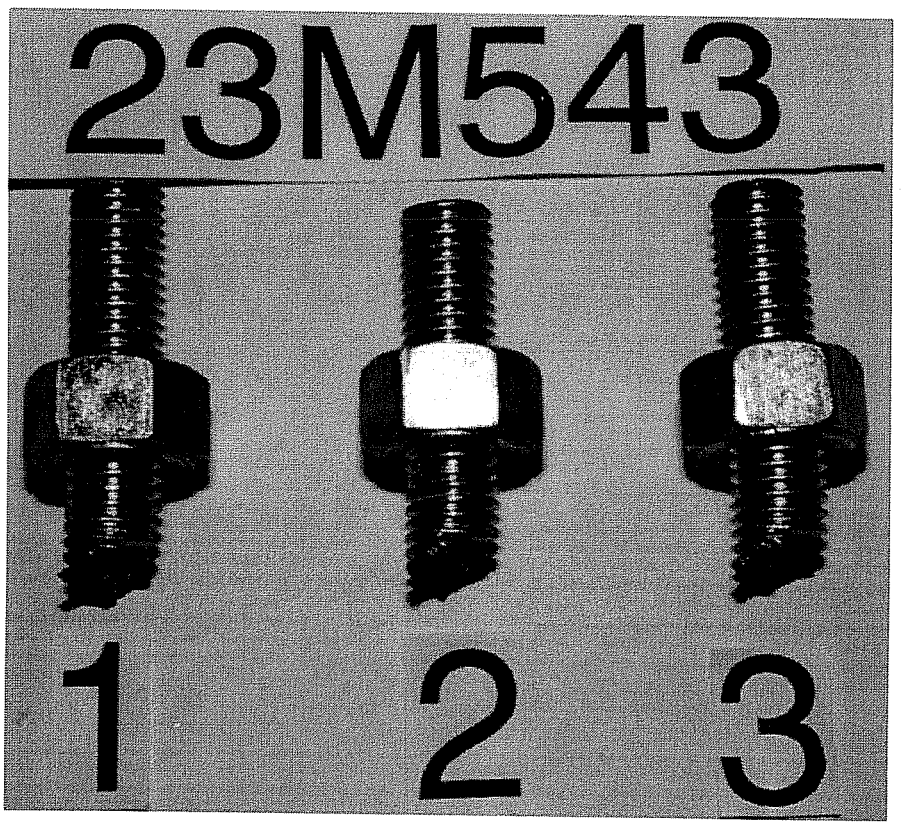

Series 23M543, , UC1 5/8", Oblique Tension 30°, Fractured Anchor Shanks

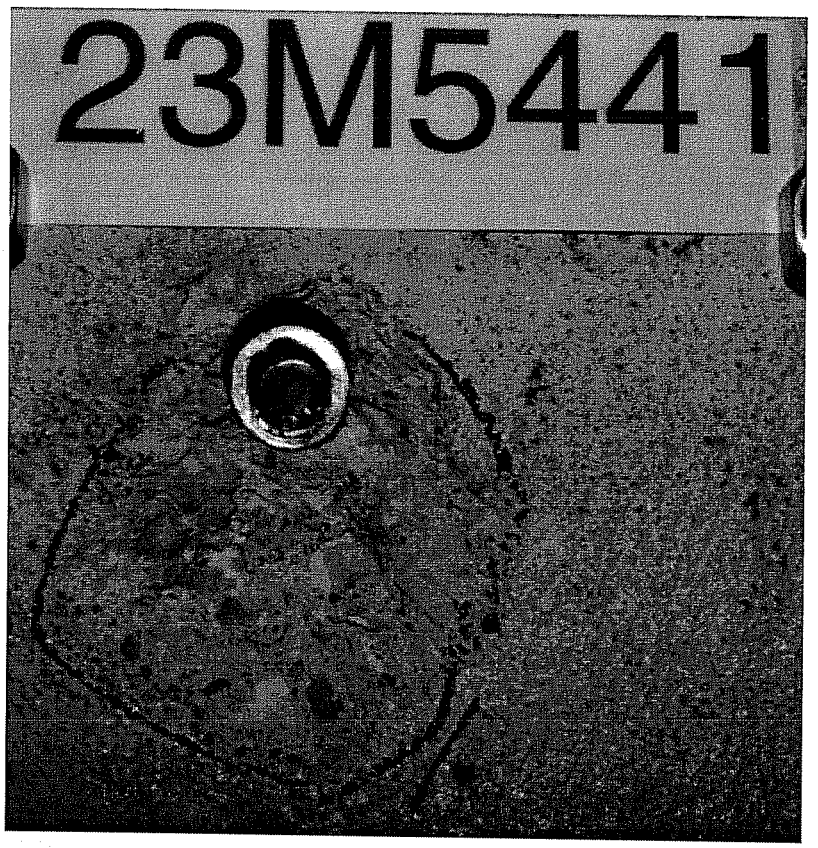

Failure Picture of Test 23M5441, UC1 5/8", Oblique Tension 45°

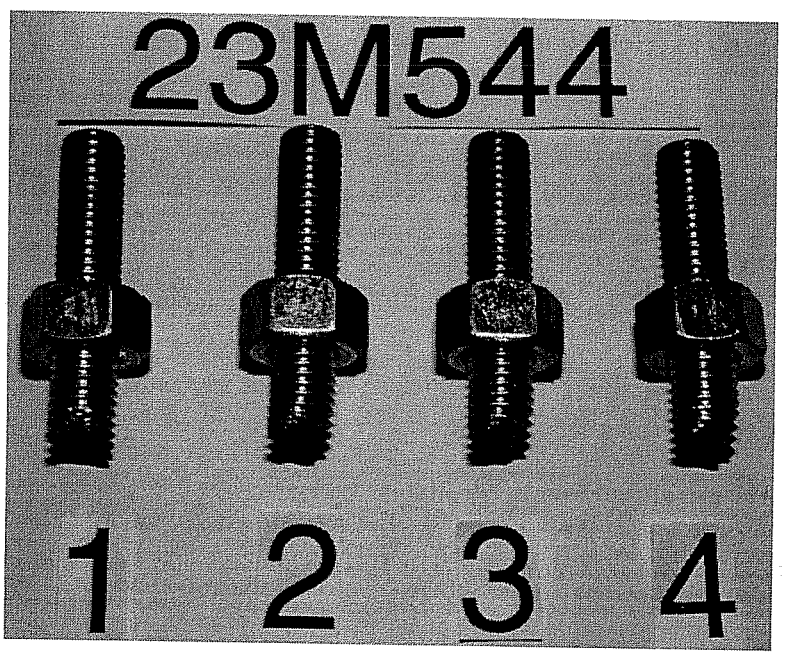

Series 23M544, , UC1 5/8", Oblique Tension 45°, Fractured Anchor Shanks

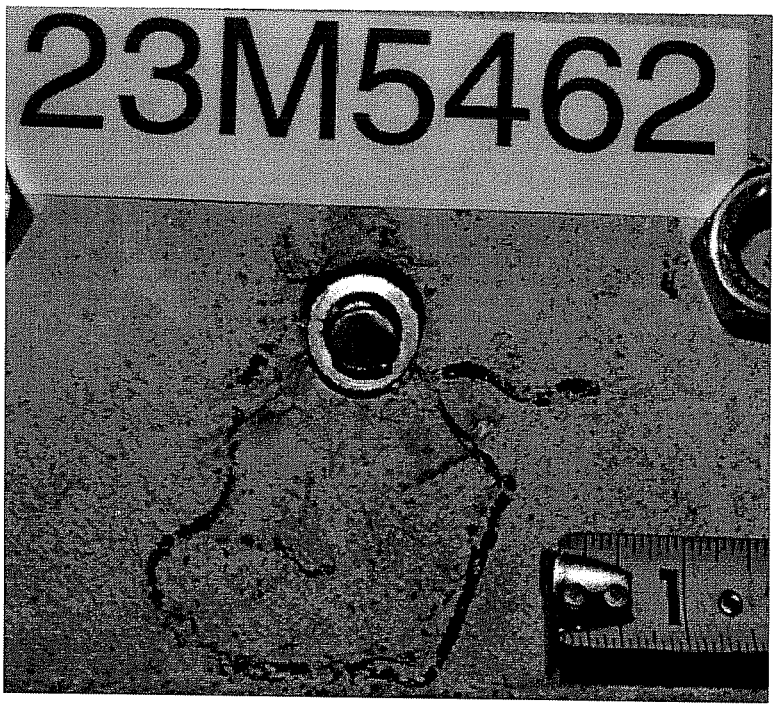

Failure Picture of Test 23M5462, UC1 5/8", Oblique Tension 60°

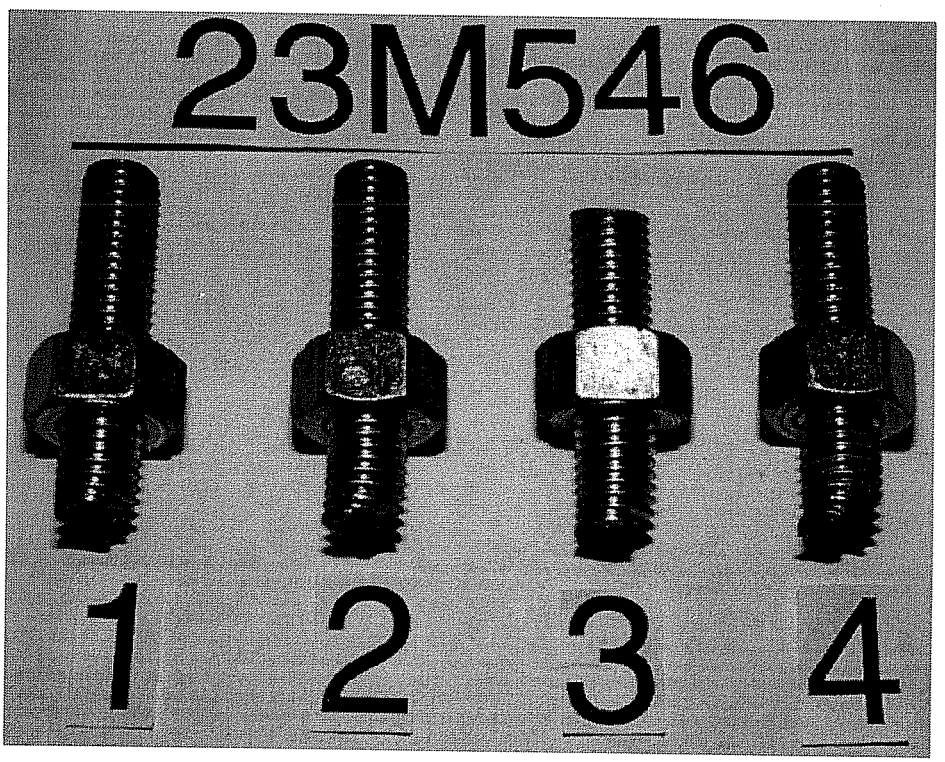

Series 23M546, , UC1 5/8", Oblique Tension 60°, Fractured Anchor Shanks

Failure Picture of Test 23M54S2, UC1 5/8", Shear

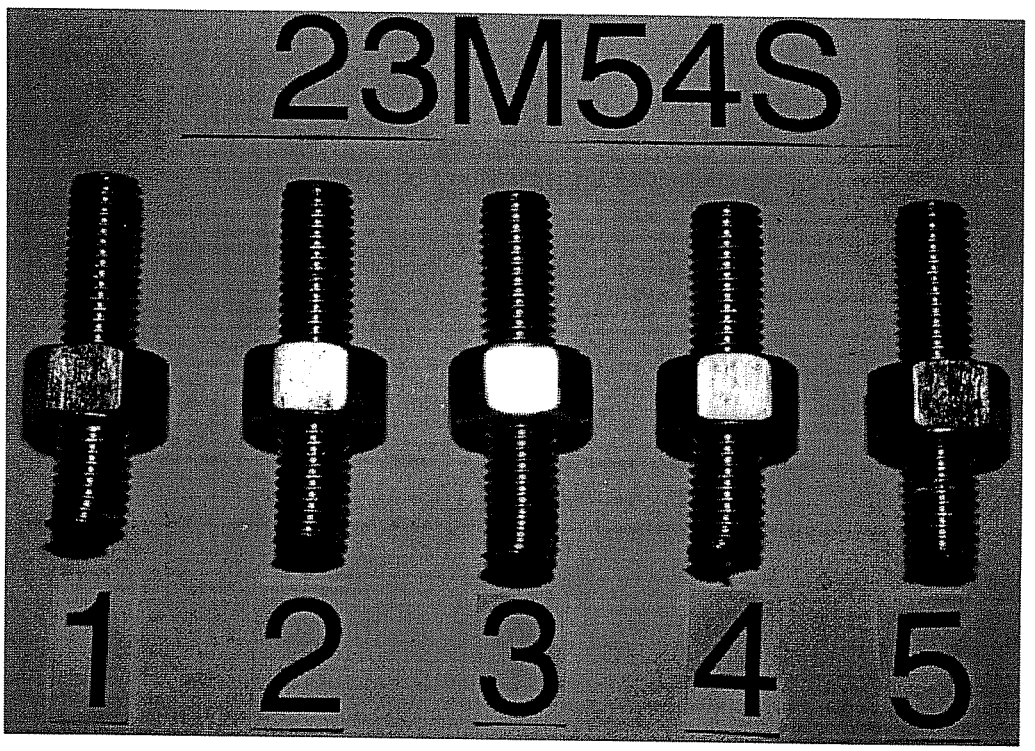

Series 23M54S, UC1 5/8", Shear, Fractured Anchor Shanks

Test No.	Loading Angle degrees	Torque Nm	Block No.	Concrete f_c N/mm²	Failure Load F_u kN	Hor. Displ. $d_{H,u}$ mm	Corr. c(H) mm	Vert. Displ. $d_{V,u}$ mm	Spalling Depth t mm	Note
23m7431	30	244/122	L36-B	~32.4	145.005	19.44	0.50	10.05	51	
2	30	244/122	L35-T	~32.4	145.005	22.79	0.00	12.64	51	1)
Ave.					**145.005**	**21.11**		**11.34**	**51.00**	
23M7441	45	244/122	L36-T	~32.4	130.326	27.03	0.00	9.54	32	
2	45	244/122	L36-B	~32.4	136.109	13.15	1.30	2.60	38	2)
Ave.					**133.218**	**20.09**		**6.07**	**35.00**	
23m7461	60	244/122	L36-T	~32.4	136.554			6.76	38	3)
2	60	244/122	L36-B	~32.4	127.213	25.85	0.00	7.18	38	
Ave.					**131.883**	**25.85**		**6.97**	**38.00**	
23m74s1	Shear	244/122	L36-B	~32.4	157.459	11.86	0.00	0.00	6	
2	Shear	244/122	L35-T	~32.4	154.346	15.43	1.00	0.00	9	
Ave.					**155.902**	**13.65**		**0.00**	**7.50**	

1) 15° wedge element slided; load-displacement curves composed from 3
2) shell-shaped concrete spalling immediately after maximum load
3) measurement failed on Hd

Test Results of Series 23M74: UC1 Anchor Bolts 5/8", Through-Sleeve Installation
h_{ef} = 178mm (7 in.), f_c = 32.4 N/mm² (4700 psi), Failing by Steel Fracture

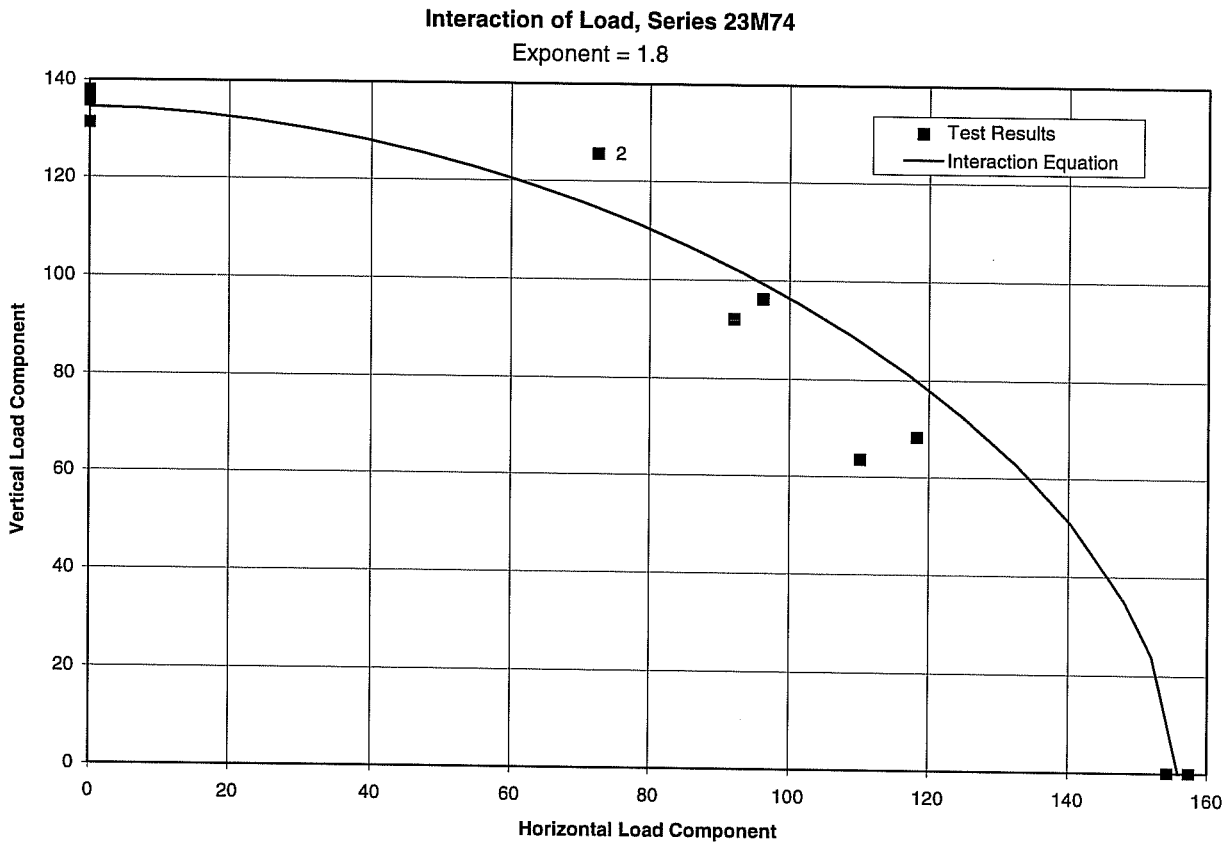
Interaction of Load, Series 23M74
Exponent = 1.8
Test Results
Interaction Equation
2
Vertical Load Component
Horizontal Load Component
0
20
40
60
80
100
120
140
160

Interaction of Displacements at Maximum Load

Series 23M74, UC1 5/8", h_{ef} = 7 inches (178 mm), fc = 4700 psi = 32.4 N/mm²
Through-Sleeve Installation

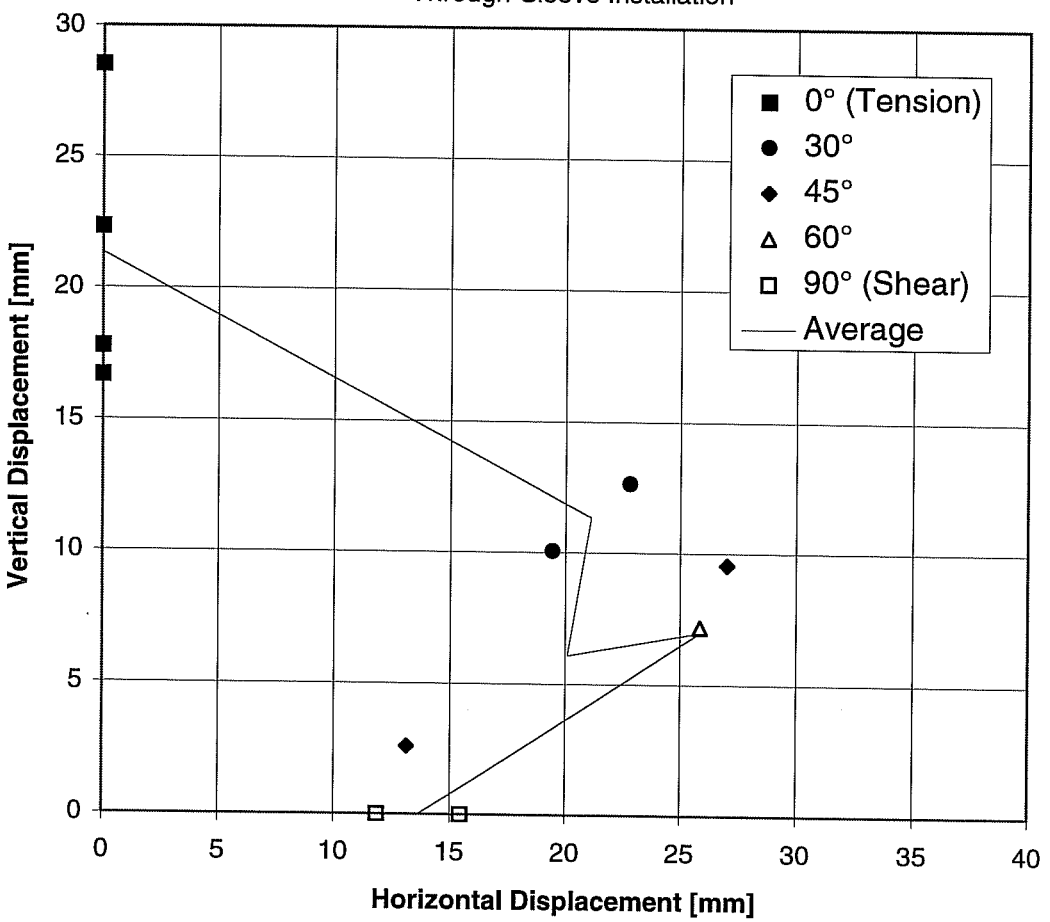

Teil 1: Interaction of Force	**Interaction Exponent**	σ_Z	σ_S	
Break of Curve	1.80	737.6	855.4	
Max. Load	1.80	922.0	1069.3	
Remaining Load	1.80	875.9	1015.8	
Part 2: Load-Displacement Curves	**Angle** d_{knick}	d_u	d_{Rest}	**Curvature Exponent**
Angle	0			
d_{Ver}	3.62	21.34	27.26	0.25
Angle	15			
d_{Hor}	4.84	10.84	11.26	0.40
d_{Ver}	3.99	18.44	22.83	0.25
Angle	30			
d_{Hor}	9.43	21.11	21.94	0.40
d_{Ver}	4.90	11.34	11.96	0.25
Angle	45			
d_{Hor}	6.32	20.09	27.19	0.40
d_{Ver}	1.54	6.07	7.81	0.25
Angle	60			
d_{Hor}	6.92	25.85	27.77	0.50
d_{Ver}	2.13	6.97	7.19	0.25
Angle	75			
d_{Hor}	7.21	17.48	18.56	0.50
d_{Ver}	1.16	3.78	3.90	0.30
Angle	90			
d_{Hor}	7.35	13.65	14.35	0.50

Displacement in mm, Angle in degrees

Mathematic Description of Results of Series 23M74 with UC1 Anchors 5/8 inches (h_{ef} = 7 inches, c1 ≥ 11 inches) in Through-Sleeve Installation for Program BDA5 (0° from Series 23M64, 15° and 75° interpolated), f_c = 32.4 N/mm²

Mathematical Description of Load-Displacement Curves of Series 23M74

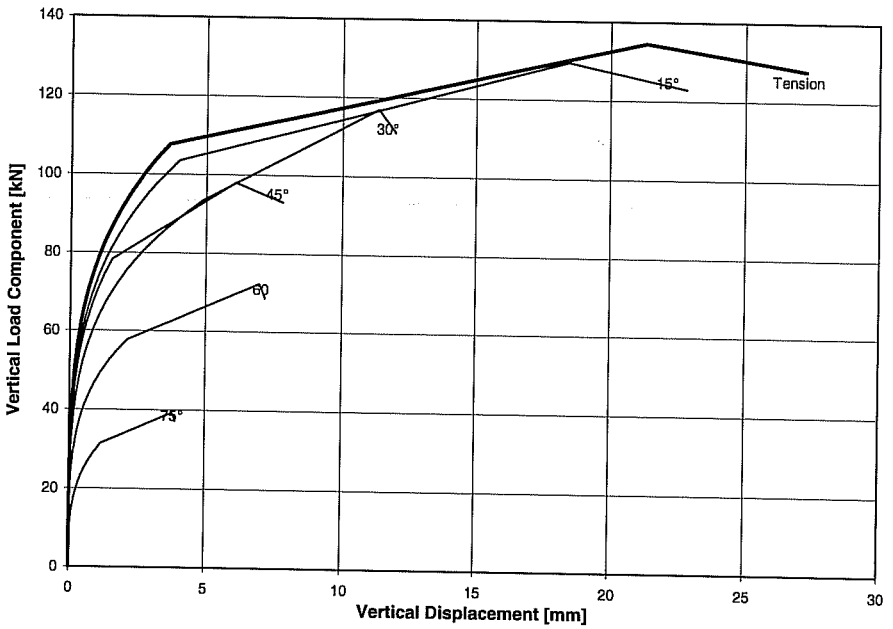

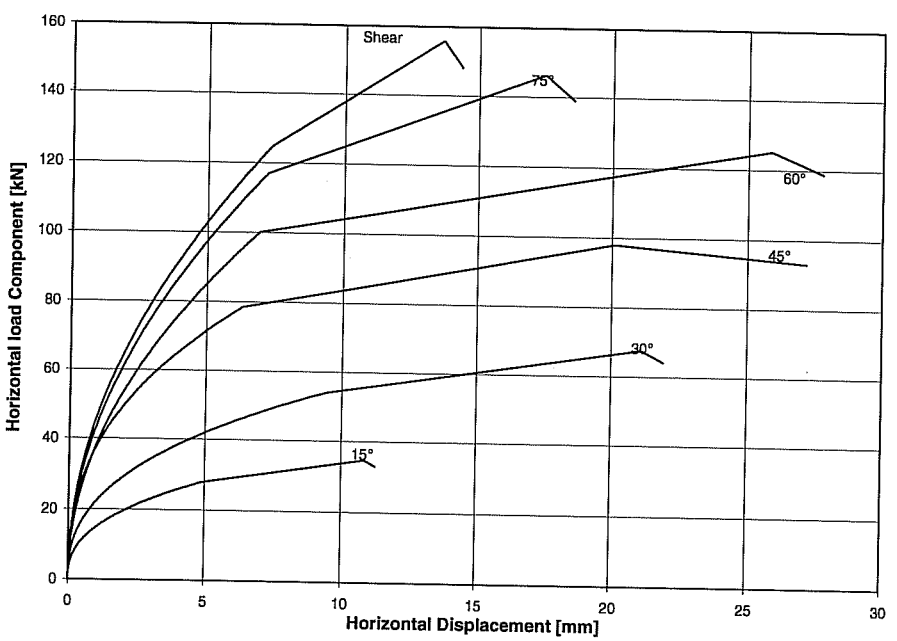

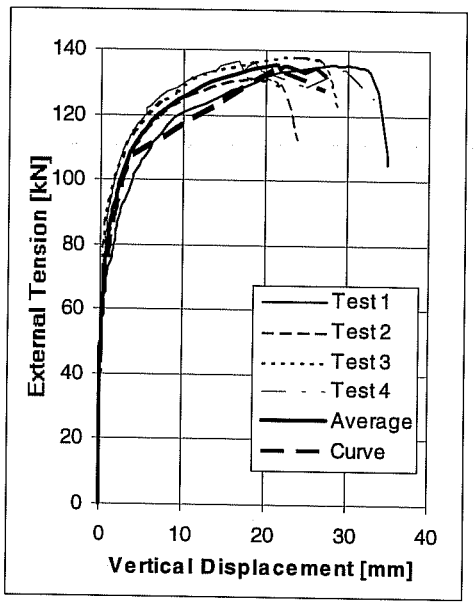

Pure Tension

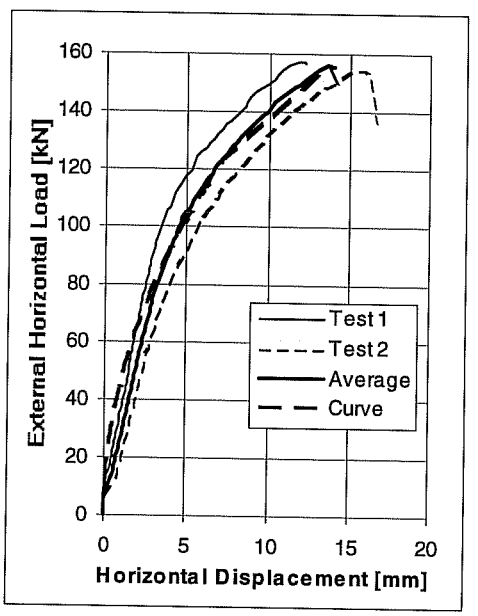

Pure Shear

Load-Displacement Curves of Series 23m54T (Tension) and 23m74S (Shear)
UC1 Anchor 5/8 inches, hef = 7 inches (178 mm), c1 ³ 11 inches (279 mm), fc = 32.4 N/mm²
Shear with Through-Sleeve Installation

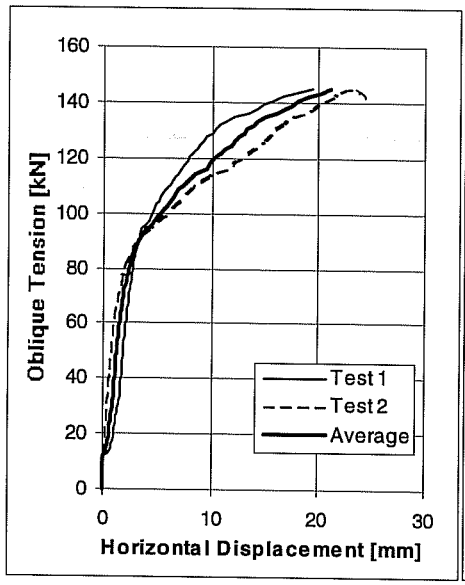

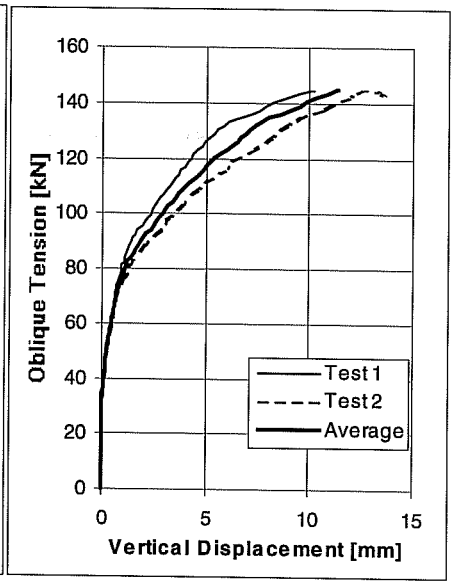

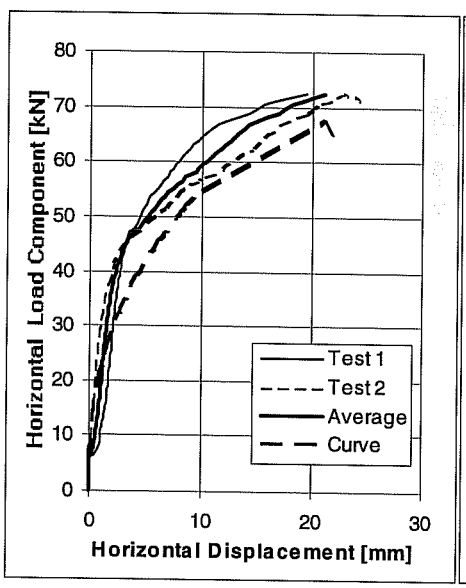

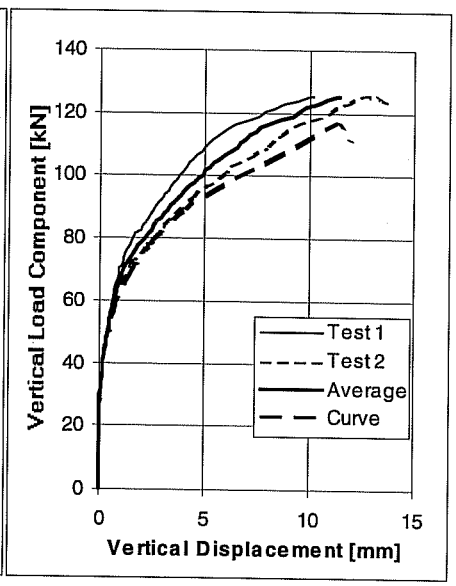

Load-Displacement Curves of Series 23m743,
UC1 Anchor 5/8 inches, hef = 7 inches (178 mm), c1 ³ 11 inches (279 mm),
f_c = 32.4 N/mm², Loading Angle 30° from Anchor Axis
Through-Sleeve Installation

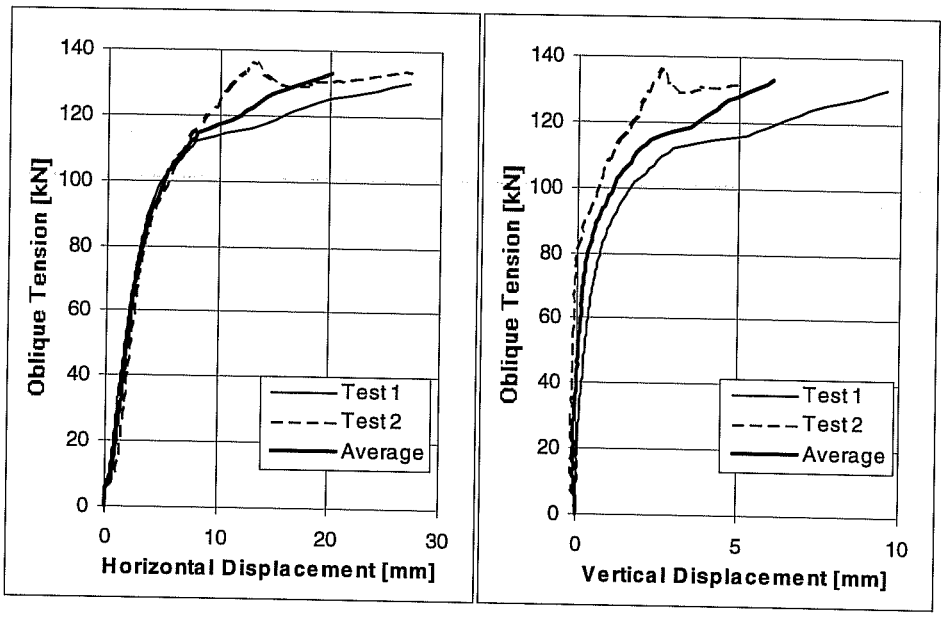

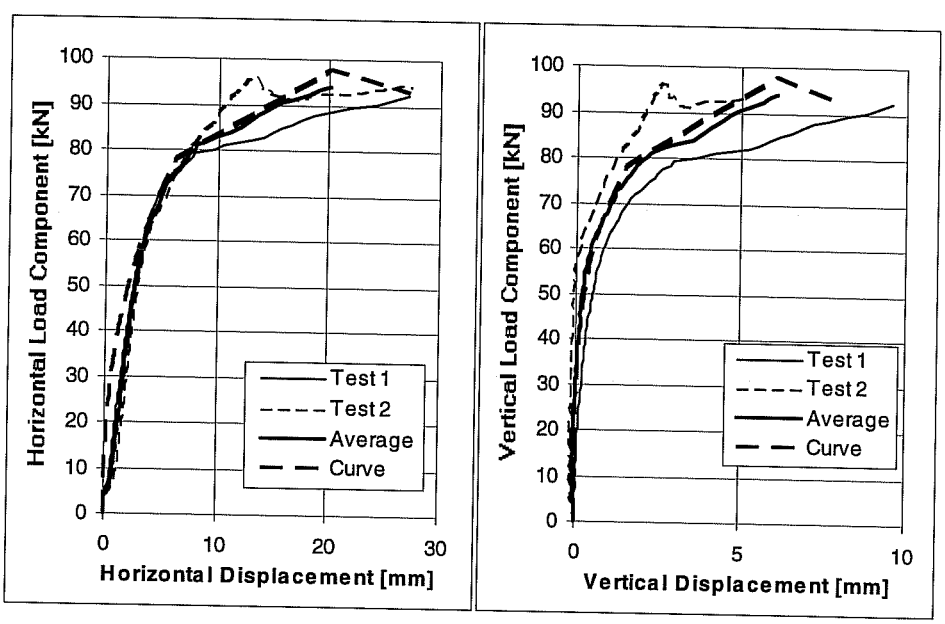

Load-Displacement Curves of Series 23m744,
UC1 Anchor 5/8 inches, hef = 7 inches (178 mm), c1 ³ 11 inches (279 mm),
f_c = 32.4 N/mm², Loading Angle 45° from Anchor Axis
Through-Sleeve Installation

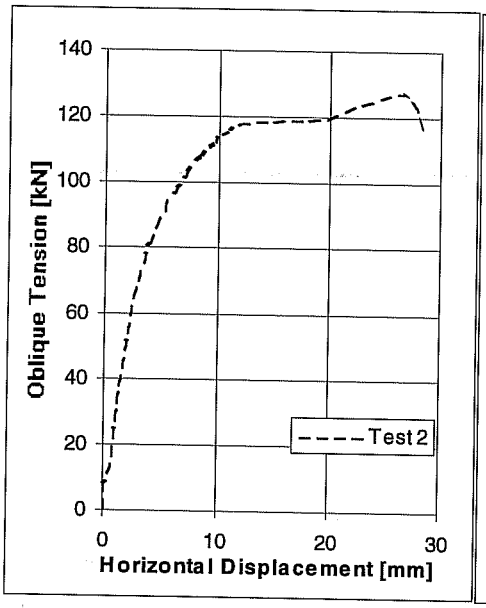

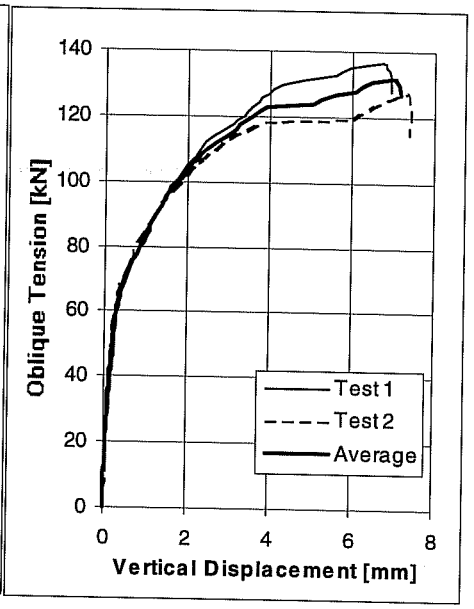

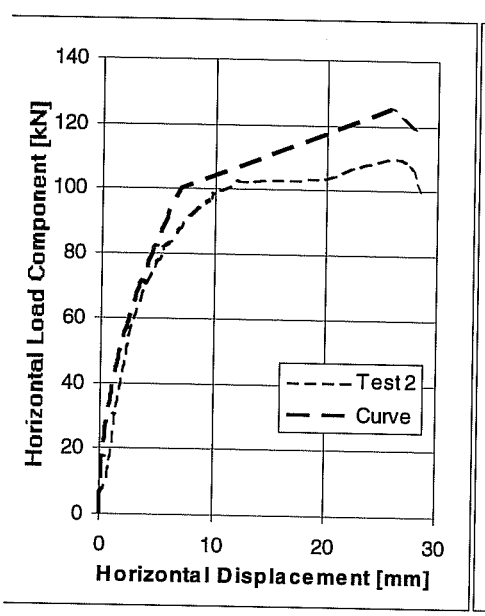

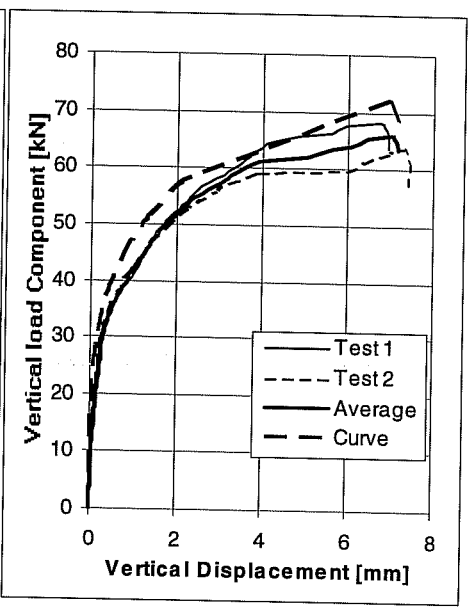

Load-Displacement Curves of Series 23m746,
UC1 Anchor 5/8 inches, hef = 7 inches (178 mm), c1 ³ 11 inches (279 mm),
f_c = 32.4 N/mm², Loading Angle 60° from Anchor Axis
Through-Sleeve Installation

Failure Picture of Test 23M7431, UC1 5/8", Oblique Tension 30°

Failure Picture of Test 23M7441, UC1 5/8", Oblique Tension 45°

Failure Picture of Test 23M7462, UC1 5/8", Oblique Tension 60°

Failure Picture of Test 23M74S2, UC1 5/8", Shear

Test No.	Loading Angle degrees	Torque Nm	Block No.	Concrete f_c N/mm²	Failure Load F_u kN	Hor. Displ. $d_{H,u}$ mm	Corr. c(H) mm	Vert. Displ. $d_{V,u}$ mm	Spalling Depth t mm	Note
23M53T1	Tension	244/122	54-T	21.1	126.768	-	-	43.69	-	1)
2	Tension	244/122	54-T	21.1	136.109	-	-	41.86	-	
3	Tension	244/122	54-B	21.1	133.44	-	-	40.40	-	
Ave.					**134.8**			**41.13**		2)
COV [%]					**3.57**			**4.01**		
23M5311	15	244/122	54-T	21.1	131.216	16.84	0.75	19.58	35	3)
2	15	244/122	54-T	21.1	132.106	23.94	1.50	25.02	38	
3	15	244/122	54-B	21.1	127.213	15.05	0.50	14.86	32	
Ave.					**130.2**	**18.61**		**19.82**	**35.00**	
COV [%]					**2.00**	**25.26**		**25.65**		
23M5331	30	244/122	54-T	21.1	108.086	14.51	0.75	5.64	25	
2	30	244/122	54-T	21.1	104.973	20.30	0.25	8.86	n.g.	
3	30	244/122	54-B	21.1	107.197	9.77	2.00	5.38	25	4)
Ave.					**106.8**	**14.86**		**6.63**	**25.00**	
COV [%]					**1.50**	**35.49**		**29.26**		
23M5341	45	244/122	54-T	21.1	93.408	9.53	1.80	2.48	18	
2	45	244/122	54-T	21.1	93.408	10.82	1.30	3.43	18	
3	45	244/122	54-B	21.1	98.7456	8.49	0.00	2.20	18	
Ave.					**95.1872**	**9.61**		**2.70**	**18.00**	
COV [%]					**3.24**	**12.14**		**23.91**	**0.00**	
23M5361	60	244/122	54-T	21.1	83.6224	10.42	1.30	2.07	18	
2	60	244/122	54-T	21.1	83.1776	9.28	2.00	1.96	11	
3	60	244/122	54-T	21.1	86.2912	8.55	0.75	1.35	13	
Ave.					**84.3637**	**9.42**		**1.79**	**14.00**	
COV [%]					**2.00**	**10.05**		**21.73**	**25.75**	
23M53S1	Shear	244/122	54-T	21.1	76.9504	6.76	0.50	0.48	9	
2	Shear	244/122	54-T	21.1	77.3952	6.27	1.30	0.15	6	
3	Shear	244/122	54-B	21.1	86.736	5.51	0.00	0.00	0	
Ave.					**80.3605**	**6.18**		**0.21**	**5.00**	
COV [%]					**6.88**	**10.21**		**116.55**	**91.65**	

1) failing by pullout with subsequent concrete breakout

2) average value for test 2 and 3 with steel failure

3) curves composed from 2 loading

4) only 1 displacement measured for vertical displacement d_V

Test Results of Series 23M53: UC1 Anchors 5/8", Flush-Sleeve Installation hef = 178mm (7 in.), fc = 21,1 N/mm² (3056 psi), Failing by Steel Fracture

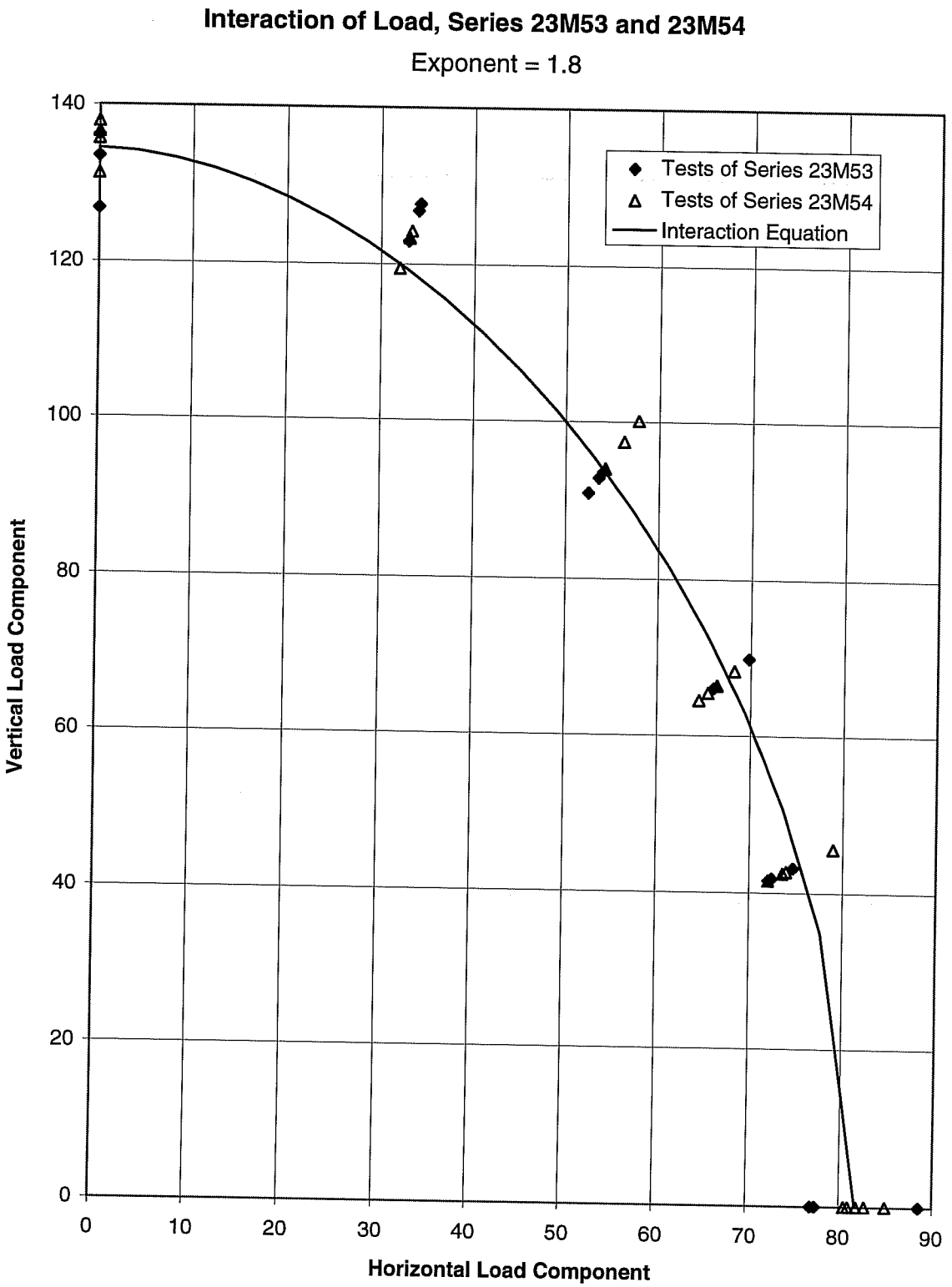
Interaction of Load, Series 23M53 and 23M54
Exponent = 1.8
Tests of Series 23M53
Tests of Series 23M54
Interaction Equation
Vertical Load Component
Horizontal Load Component
0
20
40
60
80
100
120
140
0
10
20
30
40
50
60
70
80
90

Interaction of Displacement at Max. Load

Series 23M53, UC1 5/8", h_{ef} = 7 inches = 178 mm, f_c = 3000 psi = 20.7 N/mm²
Flush-Sleeve Installation

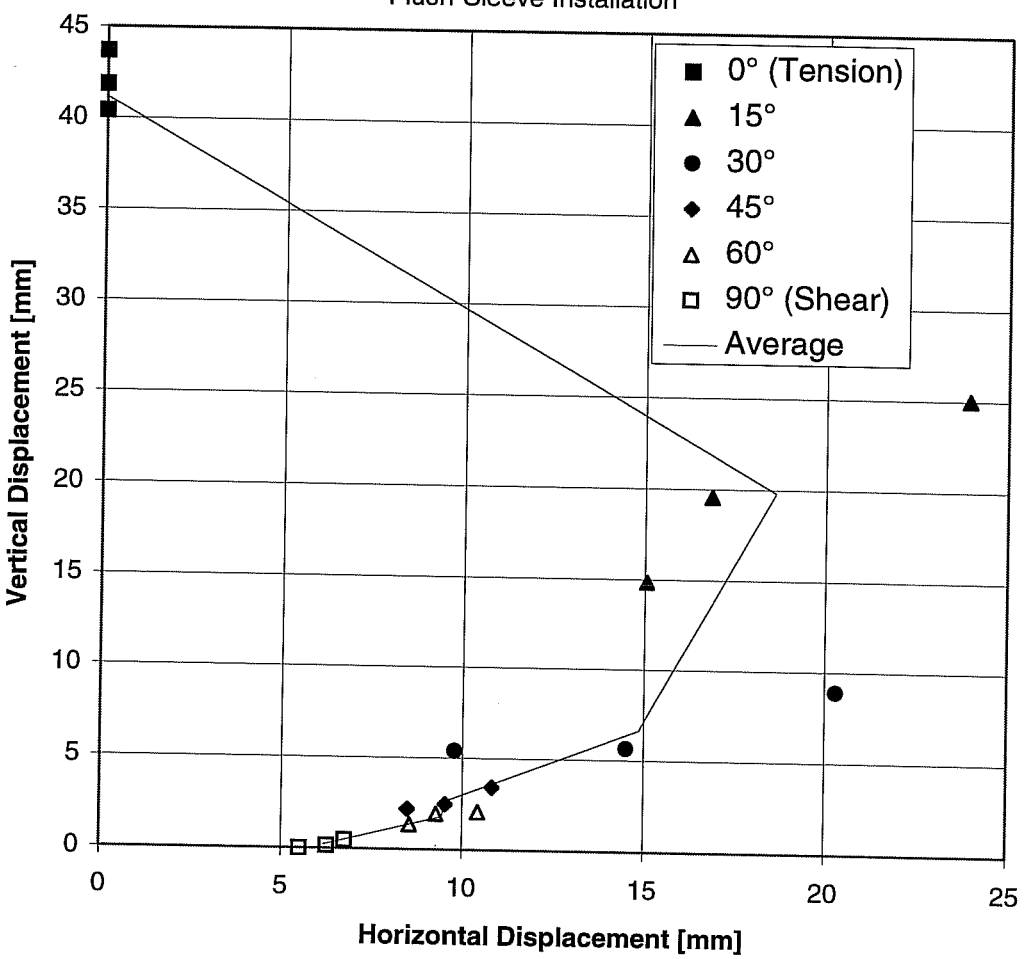

Part 1: Interaction of Force	**Interaction Exponent**	σ_Z	σ_S	
Break of Curve	1.80	829.8	504.5	
Max. Load	1.80	922.0	560.5	
Remaining Load	1.80	875.9	532.5	
Part 2: Load-Displacement Curves	**Angle** d_{knick}	d_u	d_{Rest}	**Curvature Exponent**
Angle	0			
d_{Ver}	22.31	41.98	43.99	0.25
Angle	15			
d_{Hor}	12.08	19.11	20.55	0.40
d_{Ver}	11.61	19.82	21.01	0.25
Angle	30			
d_{Hor}	9.41	14.86	15.40	0.50
d_{Ver}	4.31	6.63	6.85	0.25
Angle	45			
d_{Hor}	6.06	9.61	10.17	0.60
d_{Ver}	1.37	2.70	2.87	0.25
Angle	60			
d_{Hor}	6.49	9.42	10.32	0.60
d_{Ver}	1.07	1.79	1.98	0.25
Angle	75			
d_{Hor}	5.22	7.06	7.67	0.60
d_{Ver}	0.53	0.88	0.97	0.25
Angle	90			
d_{Hor}	4.74	6.18	6.67	0.60

Displacement in mm, Angle in degrees

Mathematic Description of Results of Series 23M53 with UC1 Anchors 5/8 inches (h_{ef} = 7 inches, c1 ≥ 11 inches) in Flush-Sleeve Installations for Program BDA5 (75° interpolated), f_c = 20.7 N/mm²

Mathematical Description of Load-Displacement Curves of Series 23M53

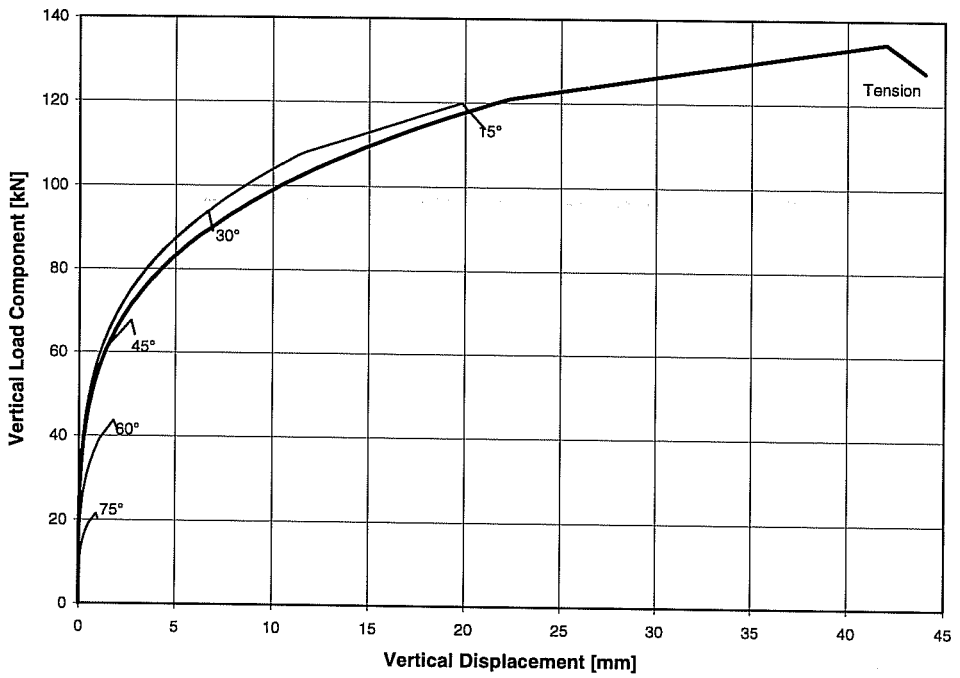

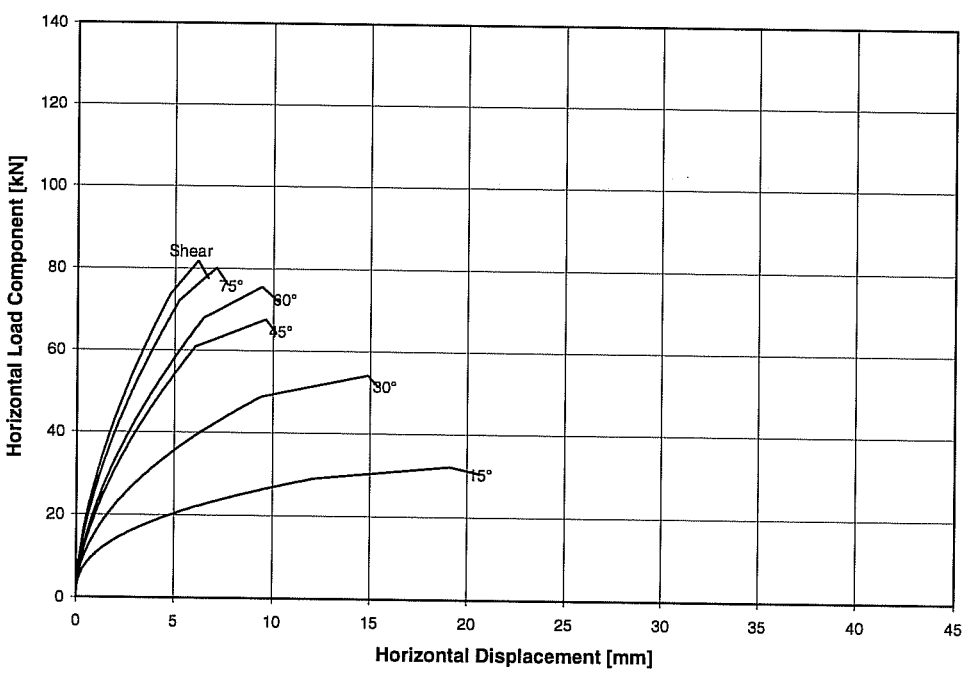

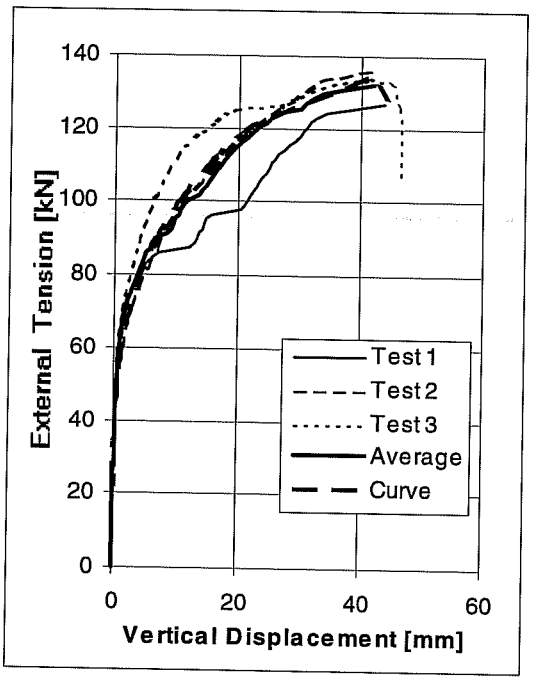

Pure Tension

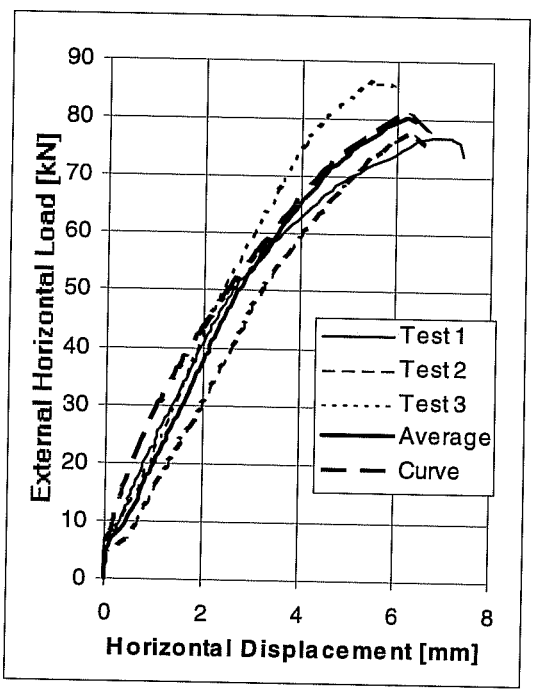

Pure Shear

Load-Displacement Curves of Series 23m53T (Tension) and 23m53S (Shear)
UC1 Anchors 5/8 inches, hef = 7 inches (178 mm), c1 ³ 11 inches (279 mm), fc = 20.7 N/mm²

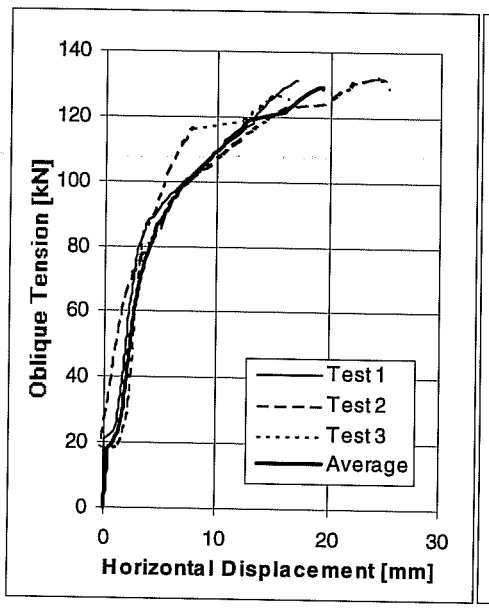

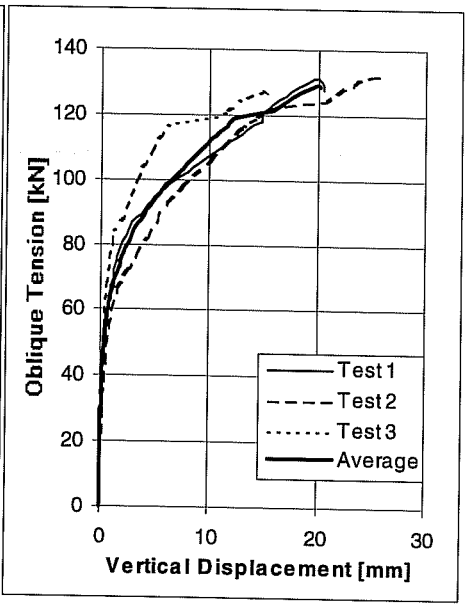

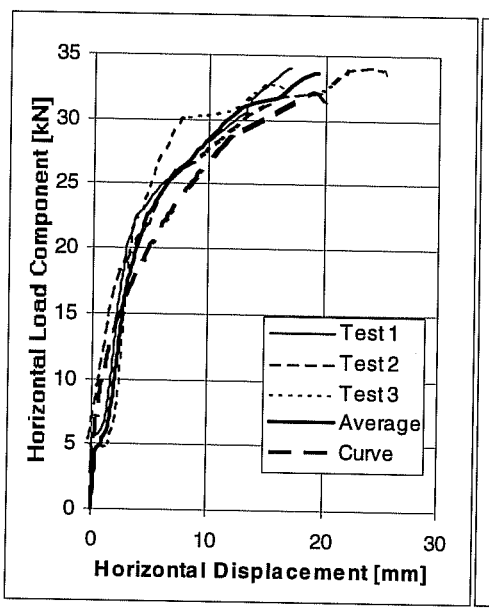

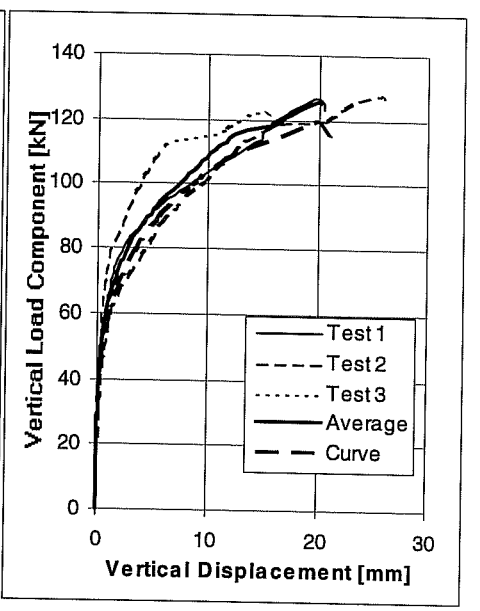

Load-Displacement Curves of Series 23m531,
UC1 Anchors 5/8 inches, hef = 7 inches (178 mm), c1 ³ 11 inches (279 mm),
f_c = 20.7 N/mm², Loading Angle 15° from Anchor Axis

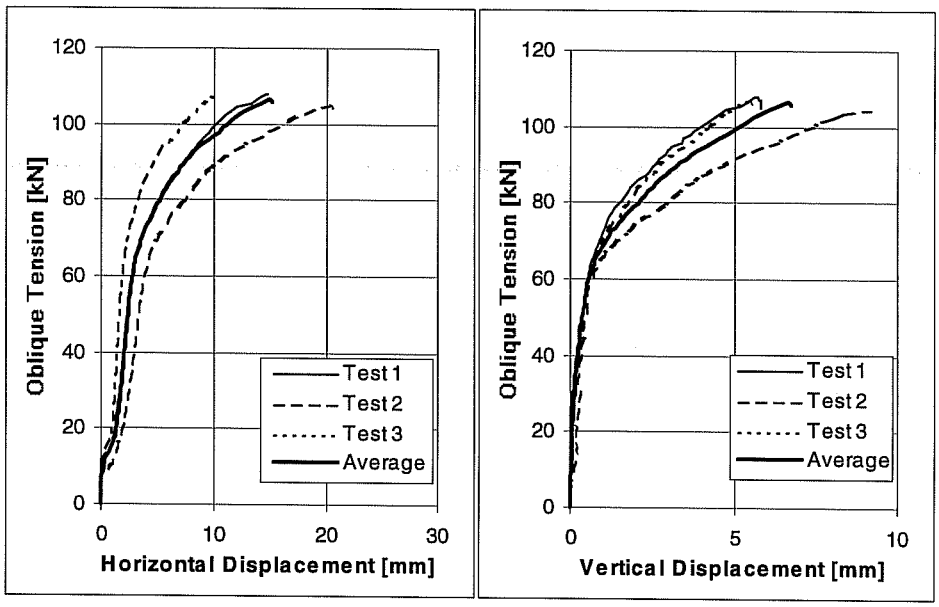

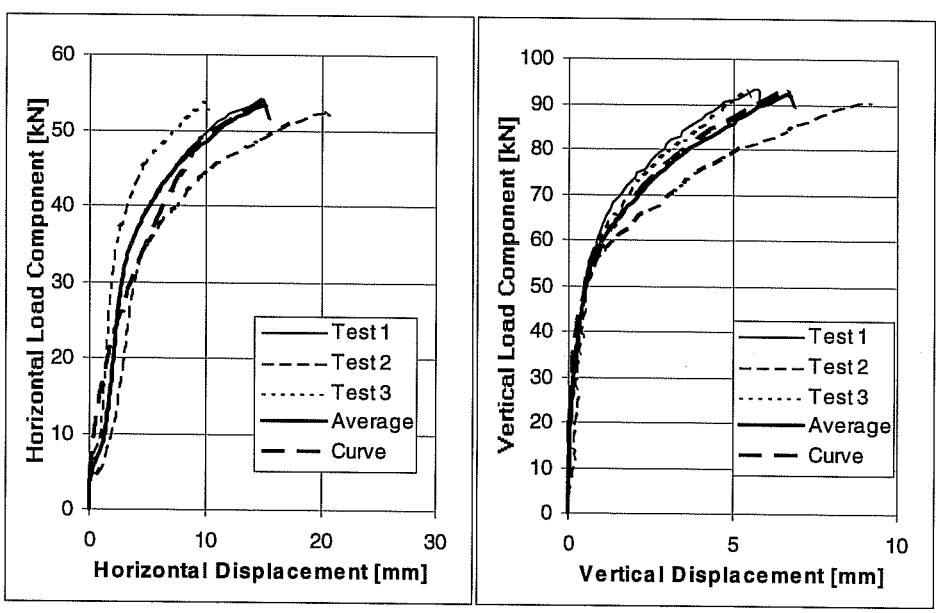

Load-Displacement Curves of Series 23m533,
UC1 Anchors 5/8 inches, hef = 7 inches (178 mm), c1 ³ 11 inches (279 mm),
f_c = 20.7 N/mm², Loading Angle 30° from Anchor Axis

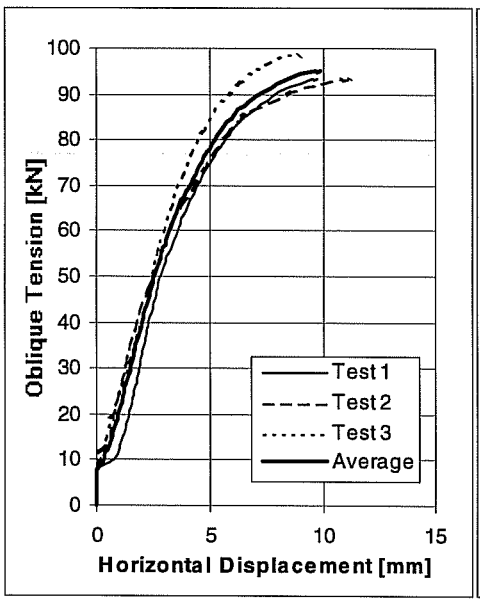

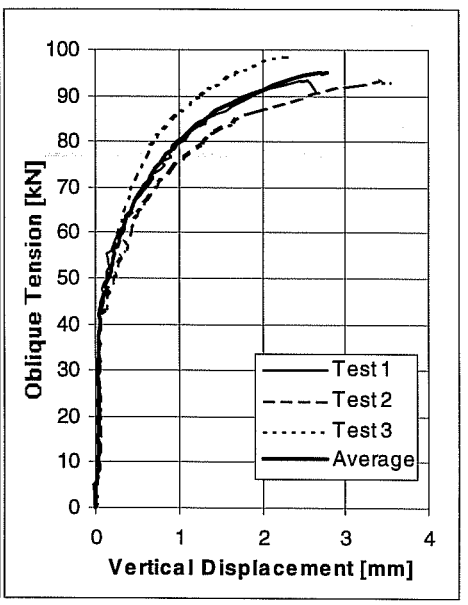

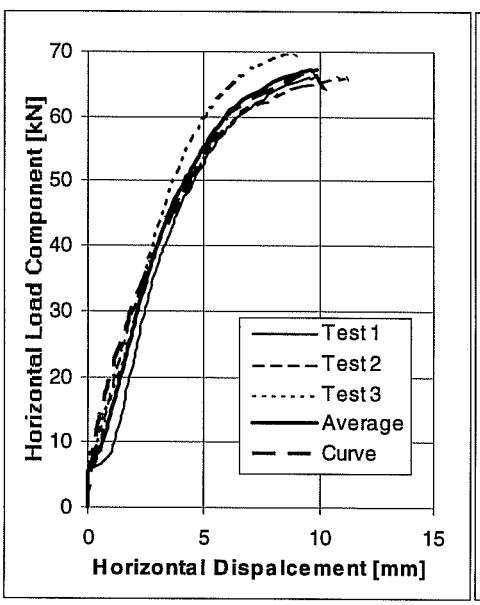

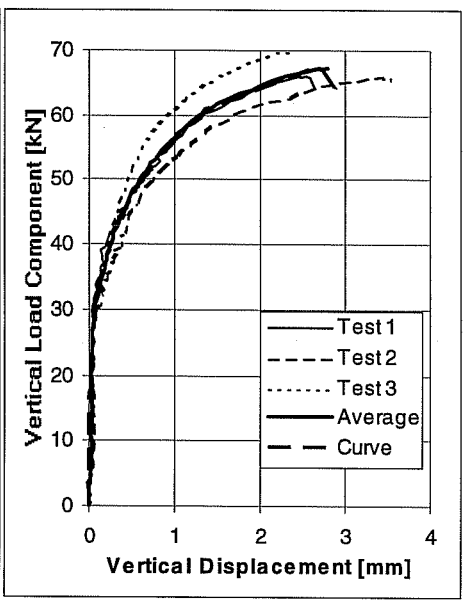

Load-Displacement Curves of Series 23m534,
UC1 Anchors 5/8 inches, hef = 7 inches (178 mm), c1 ³ 11 inches (279 mm),
f_c = 20.7 N/mm², Loading Angle 45° from Anchor Axis

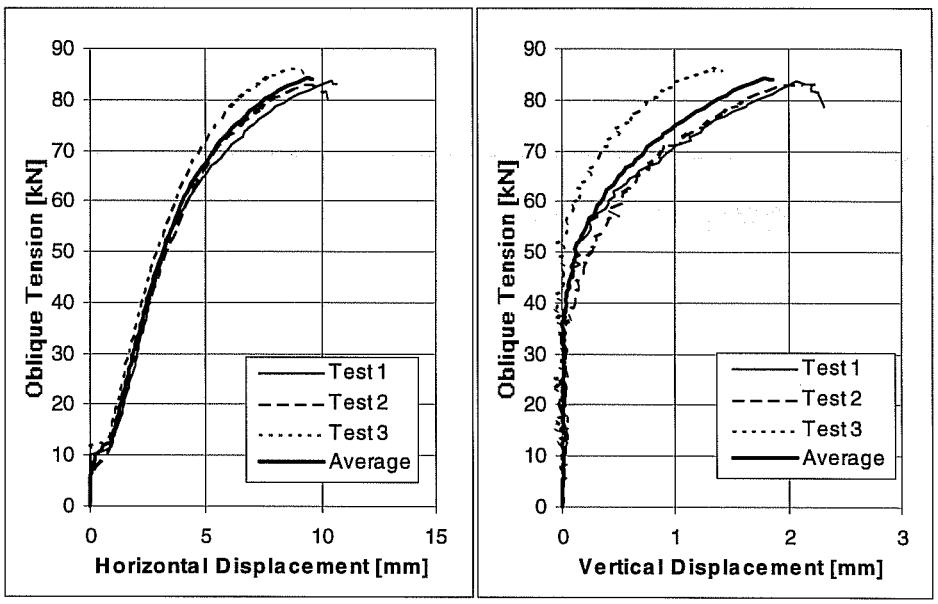

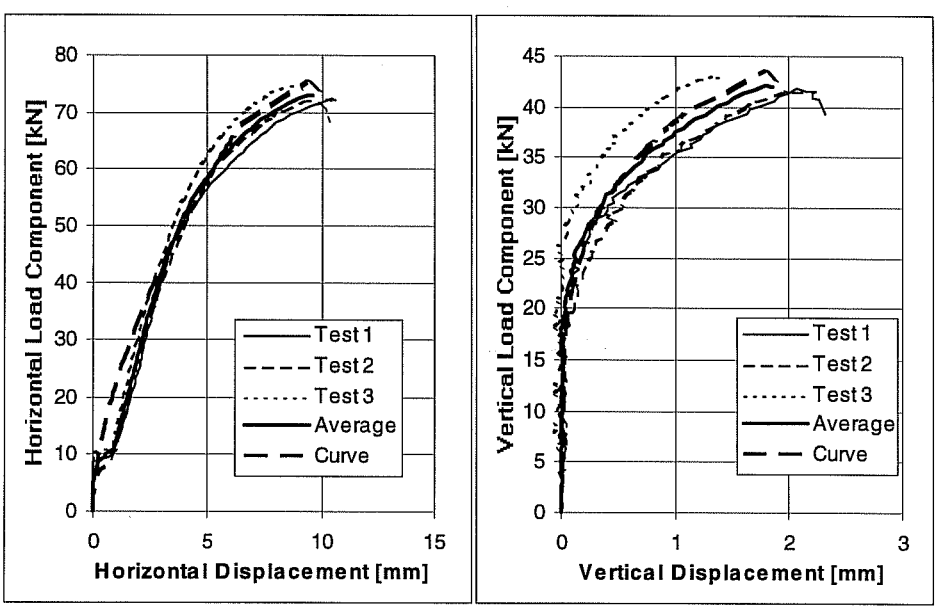

Load-Displacement Curves of Series 23m536,
UC1 Anchors 5/8 inches, hef = 7 inches (178 mm), c1 ³ 11 inches (279 mm),
f_c = 20.7 N/mm², Loading Angle 60° from Anchor Axis

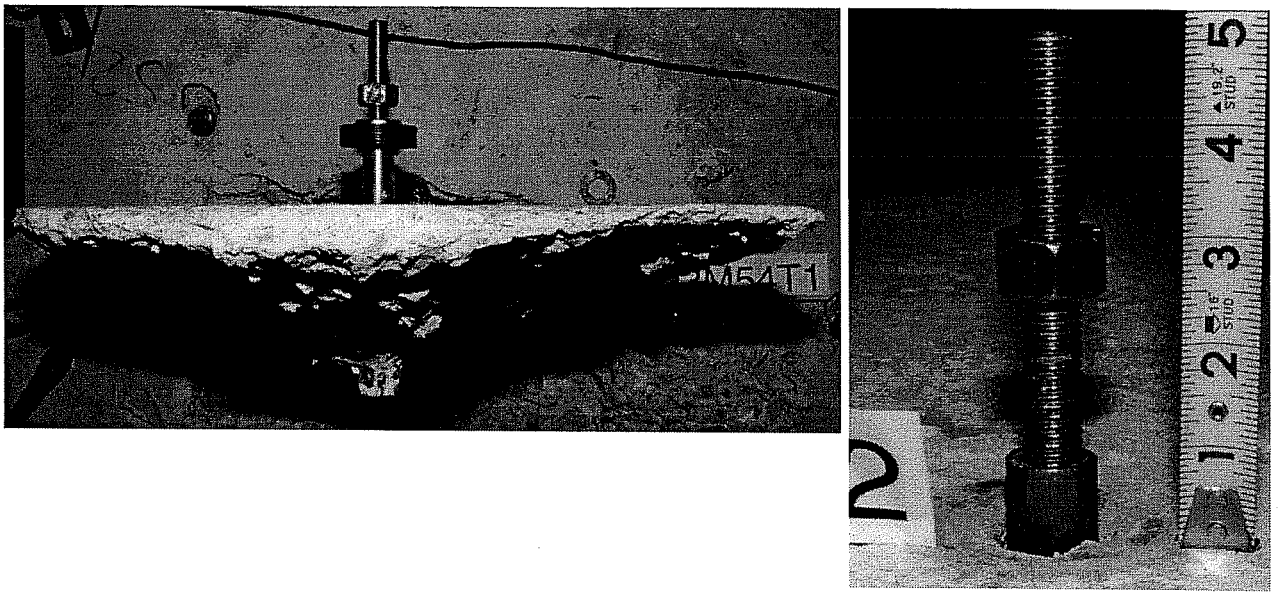

Failure Picture of Test 23M53T1 (Left) and 23M53T2 (right), UC1 5/8", Pure Tension

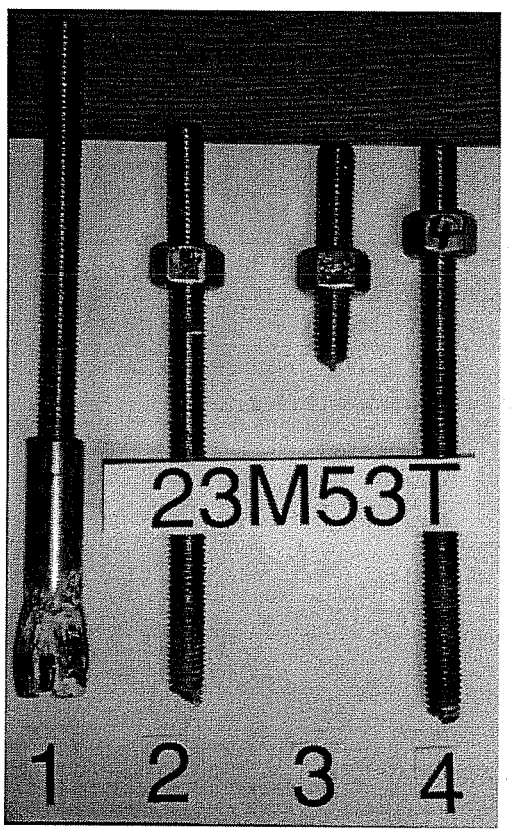

Series 23M53T, UC1 5/8", Pure Tension, Anchor Shanks after Tests

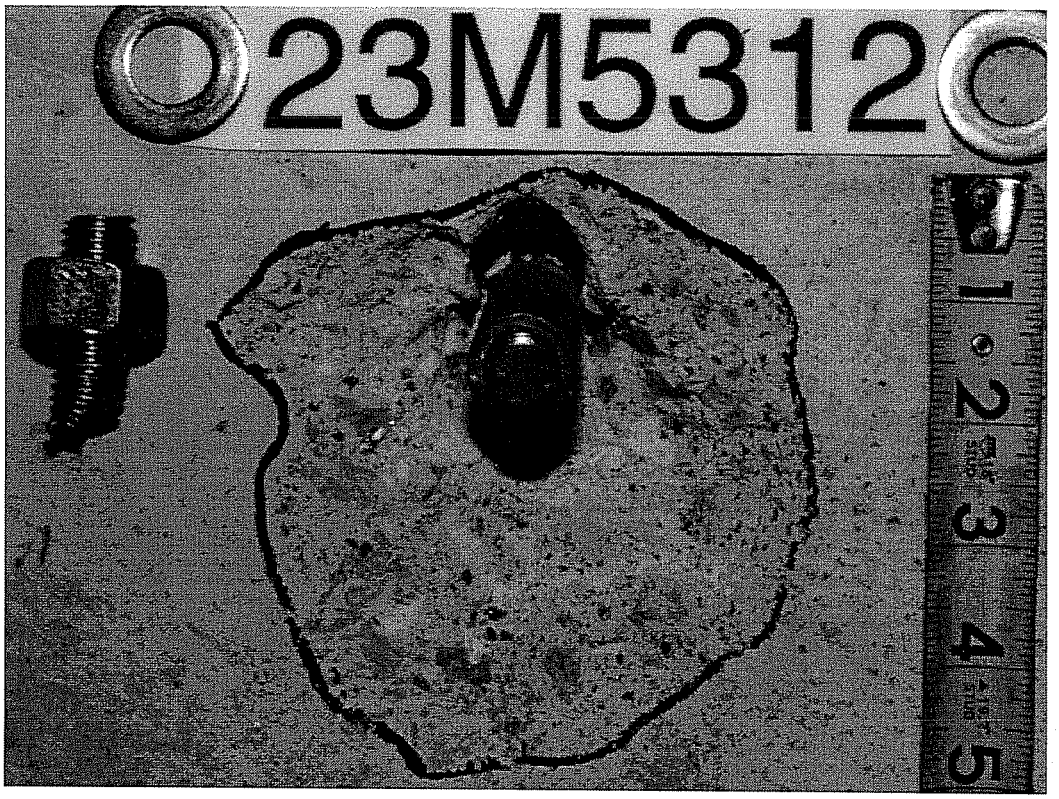

Failure Picture of Test 23M5312, UC1 5/8", Oblique Tension 15°

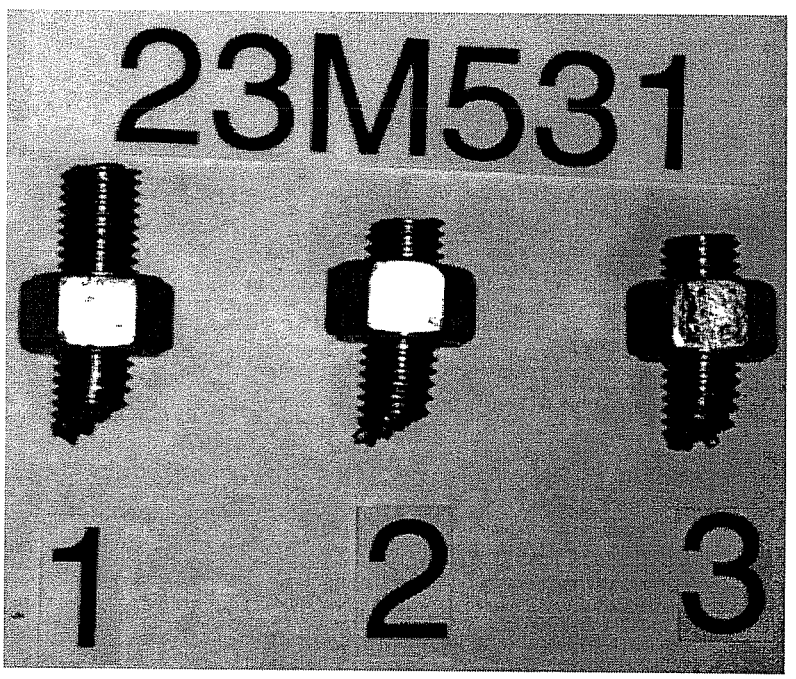

Series 23M531, UC1 5/8", Oblique Tension 15°, Fractured Anchor Shanks

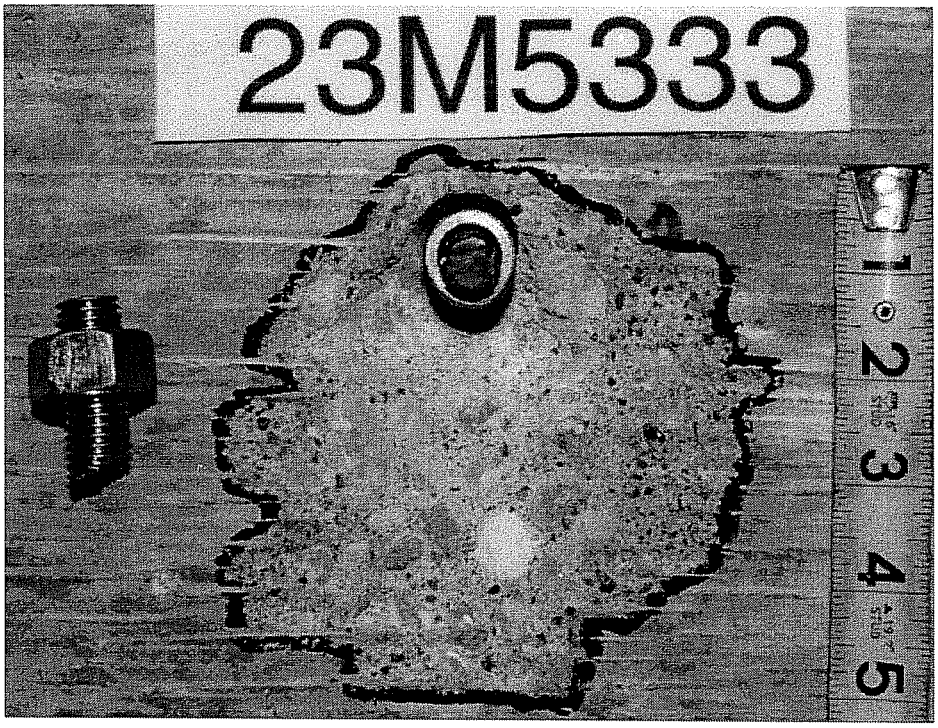

Failure Picture of Test 23M5333, UC1 5/8", Oblique Tension 30°

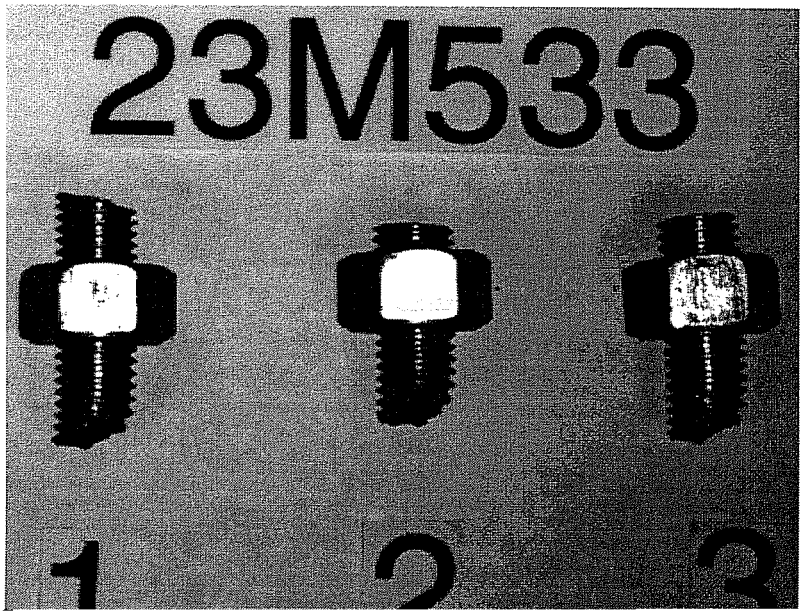

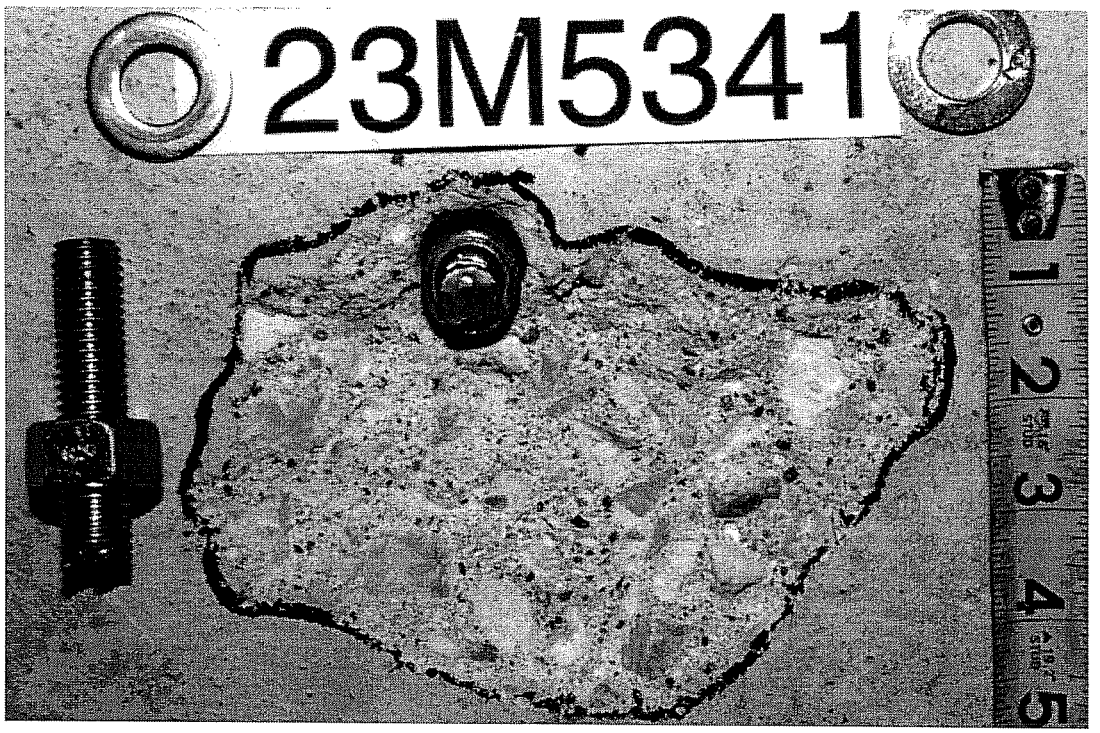

Failure Picture of Test 23M5341, UC1 5/8", Oblique Tension 45°

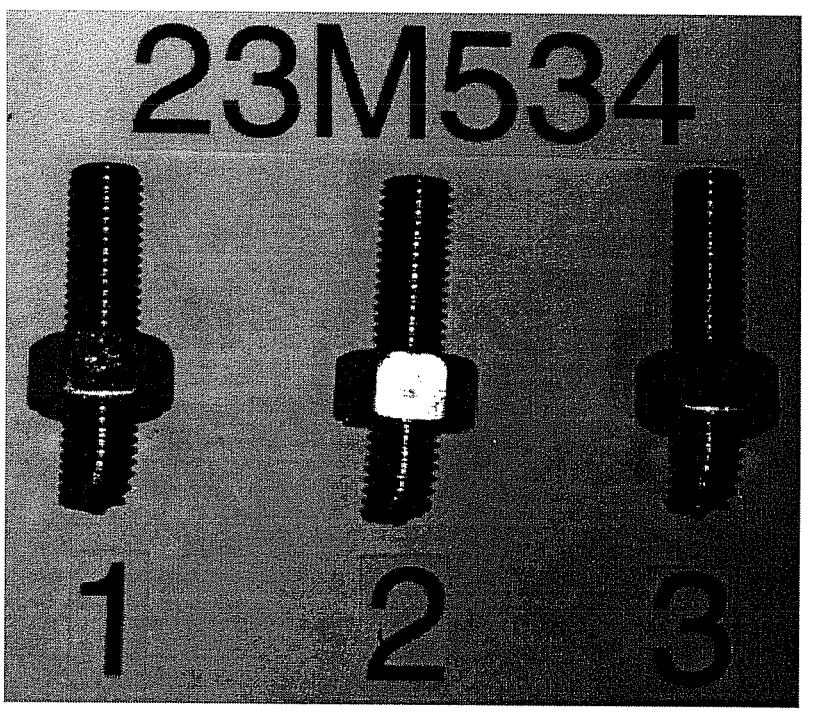

Series 23M534, UC1 5/8", Oblique Tension 45°, Fractured Anchor Shanks

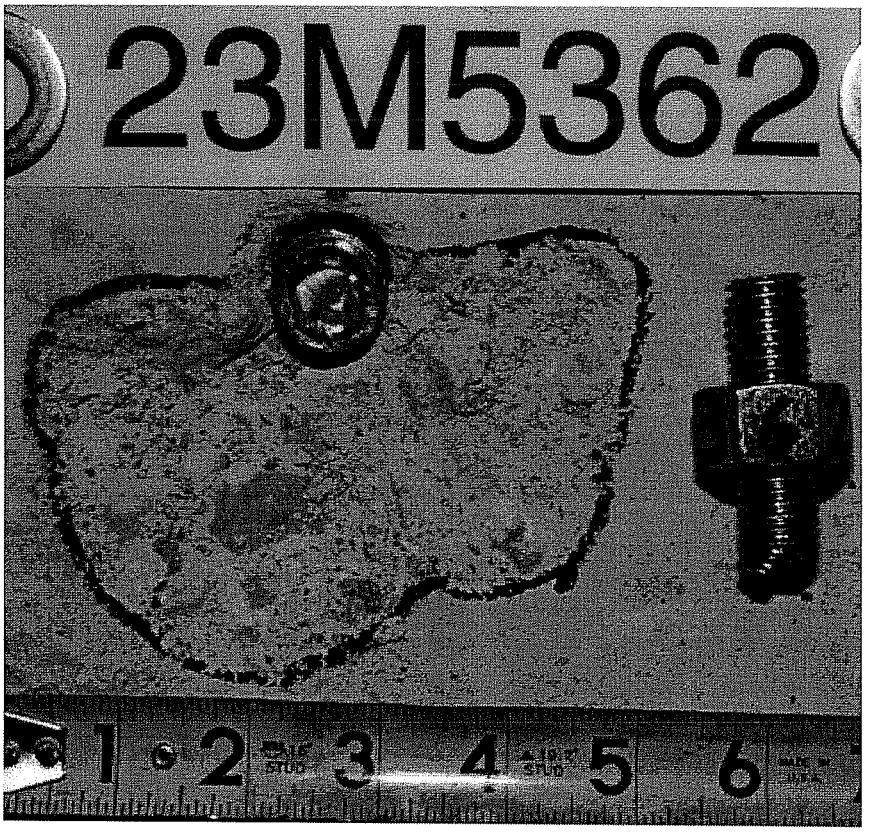

Failure Picture of Test 23M5362, UC1 5/8", Oblique Tension 60°

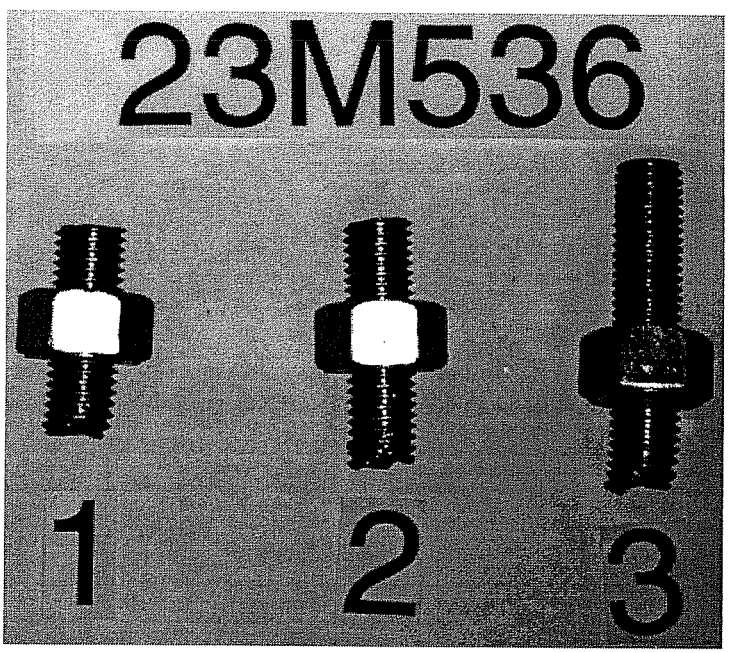

Series 23M536, UC1 5/8", Oblique Tension 60°, Fractured Anchor Shanks

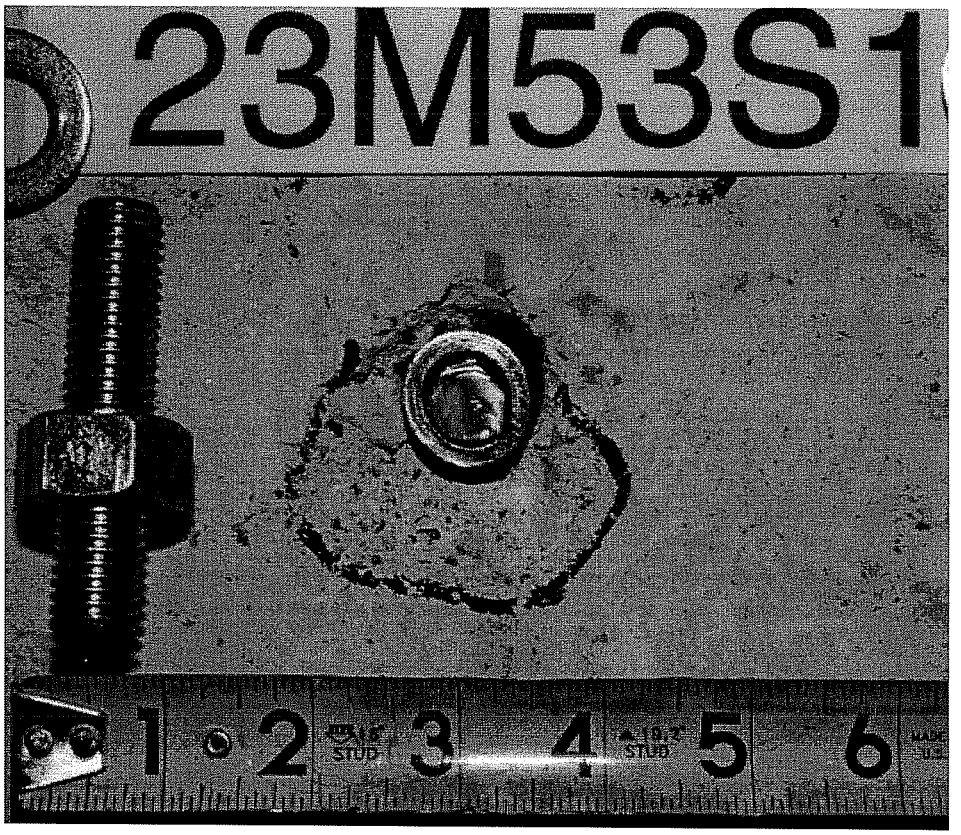

Failure Picture of Test 23M53S1, UC1 5/8", Shear

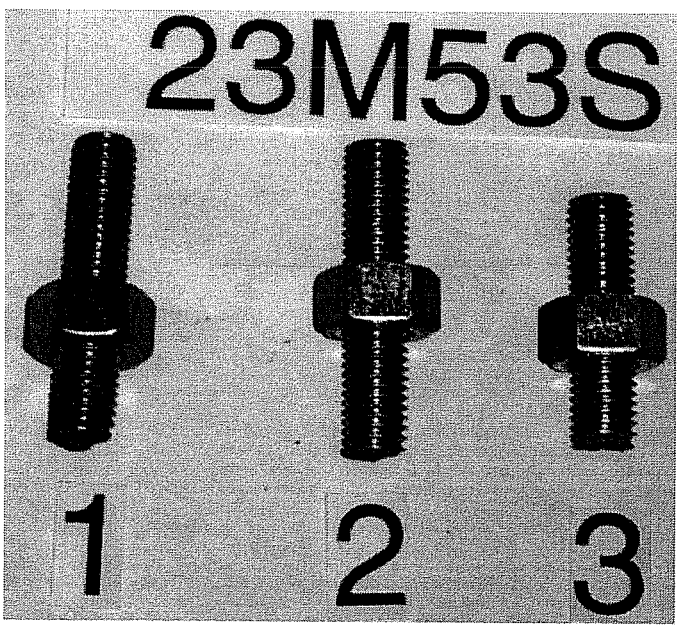

Series 23M53S, UC1 5/8", Shear, Fractured Anchor Shanks

Test No.	Loading Angle degrees	Torque Nm	Block No.	Concrete f_c N/mm²	Failure Load F_u kN	Hor. Displ. $d_{H,u}$ mm	Corr. c(H) mm	Vert. Displ. $d_{V,u}$ mm	Spalling Depth t mm	Note
23M34T1	Tension	54/27	L36-T	~32.4	50.2624	-	-	8.50	-	1)
2	Tension	54/27	L36-T	~32.4	51.152	-	-	6.74	-	1)
3	Tension	54/27	L36-B	~32.4	50.2624	-	-	12.78	-	
4	Tension	54/27	L36-B	~32.4	50.2624	-	-	14.11	-	2)
Ave.					**50.5589**			**9.34**		3)
COV [%]					**0.88**			**37.26**		
23M3411	15	54/27	L35-T	~32.4	45.3696	2.08	0	1.59	0	
2	15	54/27	L35-B	~32.4	39.5872	2.25	0.25	1.79	0	
3	15	54/27	L35-B	~32.4	48.928	2.44	0.50	2.16	0	
Ave.					**44.6283**	**2.26**		**1.85**		
COV [%]					**10.56**	**7.94**		**15.70**		
23M3431	30	54/27	L36-B	~32.4	40.4768	2.45	0.25	0.66	0	
2	30	54/27	L36-B	~32.4	36.4736	2.58	0.00	0.98	0	
3	30	54/27	L35-T	~32.4	39.1424	3.56	0.00	1.70	0	
Ave.					**38.6976**	**2.86**		**1.11**		
COV [%]					**5.27**	**21.21**		**47.94**		
23M3441	45	54/27	L36-T	~32.4	32.9152	2.53		0.33	0	4)
2	45	54/27	L36-T	~32.4	37.3632	2.15		0.41	0	
3	45	54/27	L36-T	~32.4	37.808	2.00	1.30	0.58	0	
4	45	54/27	L36-T	~32.4	36.0288	2.72	0.25	0.55	0	
5	45	54/27	L36-B	~32.4	32.0256	3.15	2.00	0.58	0	
Ave.					**35.2282**	**2.51**		**0.49**		
COV [%]					**8.41**	**23.06**		**4.49**		
23M3461	60	54/27	L36-T	~32.4	30.6912	2.38	0.00	0.19	0	
2	60	54/27	L36-T	~32.4	30.6912	2.85	0.00	0.42	0	
3	60	54/27	L36-B	~32.4	30.6912	2.60	0.00	0.33	0	
4	60	54/27	L36-B	~32.4	31.136	2.80	0.00	0.50	0	
Ave.					**30.8024**	**2.66**		**0.36**		
COV [%]					**0.83**	**4.89**		**23.03**		
23M34S1	Shear	54/27	L36-T	~32.4	31.5808	3.20	0.00	0.00	0	
2	Shear	54/27	L36-T	~32.4	27.5776	2.53	0.75	0.10	0	
3	Shear	54/27	L36-B	~32.4	31.136	2.17	0.75	0.15	0	
4	Shear	54/27	L36-B	~32.4	29.8016	2.42	0.40	0.36	0	
Ave.					**30.024**	**2.58**		**0.15**		
COV [%]					**5.99**	**7.07**		**88.19**		

1) insert too thick

2) failed by concrete fracture; presumably through other tests

3) for the average value, only Tests 1 - 3 with steel failure were considered

4) initially loaded at about 14 kN, then released due to measurement failure

Test Results of Series 23M34: UC1 of 3/8", Flush-Sleeve Installation hef = 89 mm (3.5 in), fc = 32.4 N/mm² (4700 psi), Failing by Steel Fracture

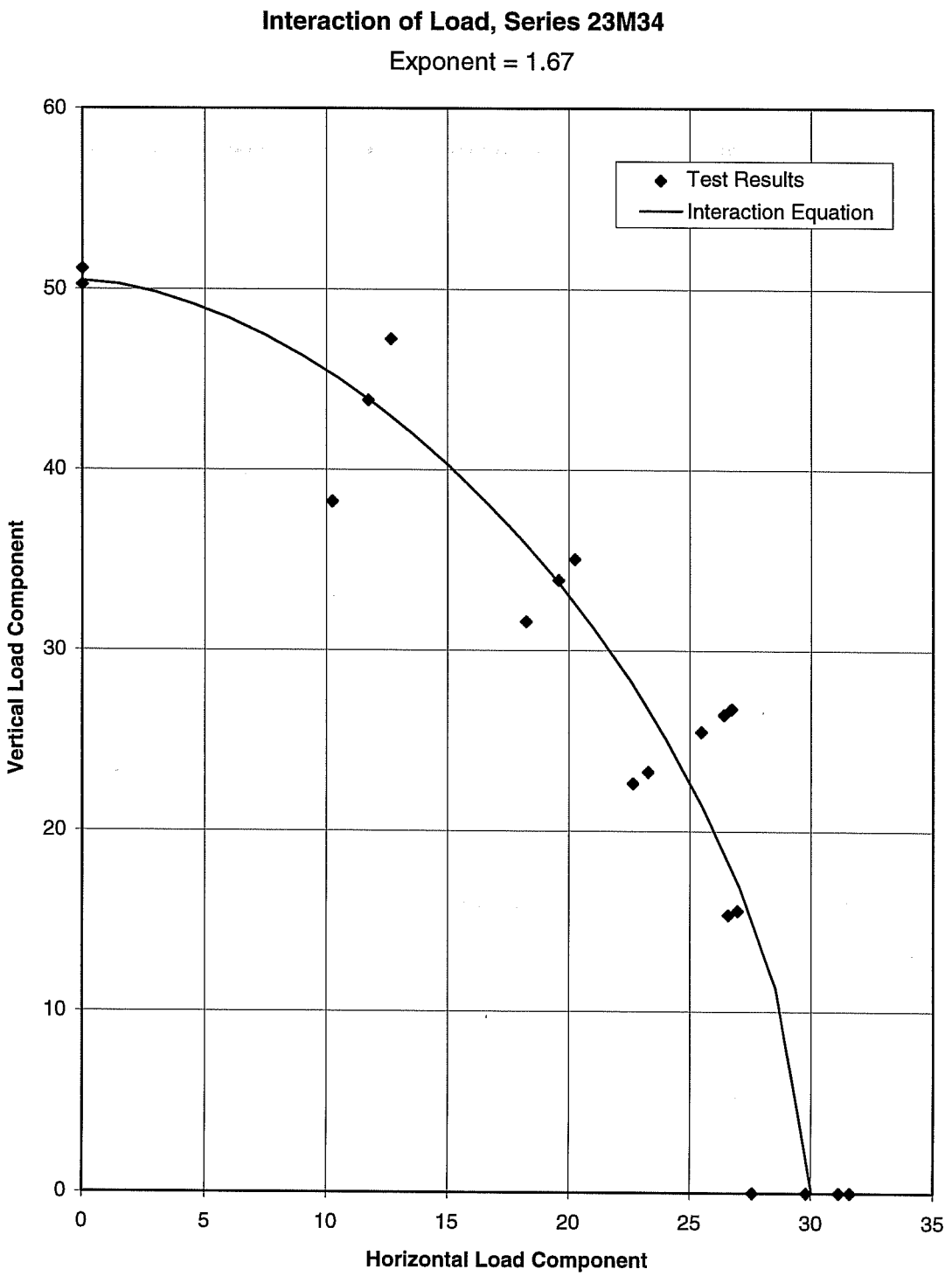
Interaction of Load, Series 23M34
Exponent = 1.67
Test Results
Interaction Equation
Vertical Load Component
Horizontal Load Component
60
50
40
30
20
10
0
0
5
10
15
20
25
30
35

Interaction of Displacement at Max. Load

Series 23M34, UC1 3/8", h_{ef} = 3.5 inches = 89 mm, f_c = 4700 psi = 32.4 N/mm²
Flush-Sleeve Installation

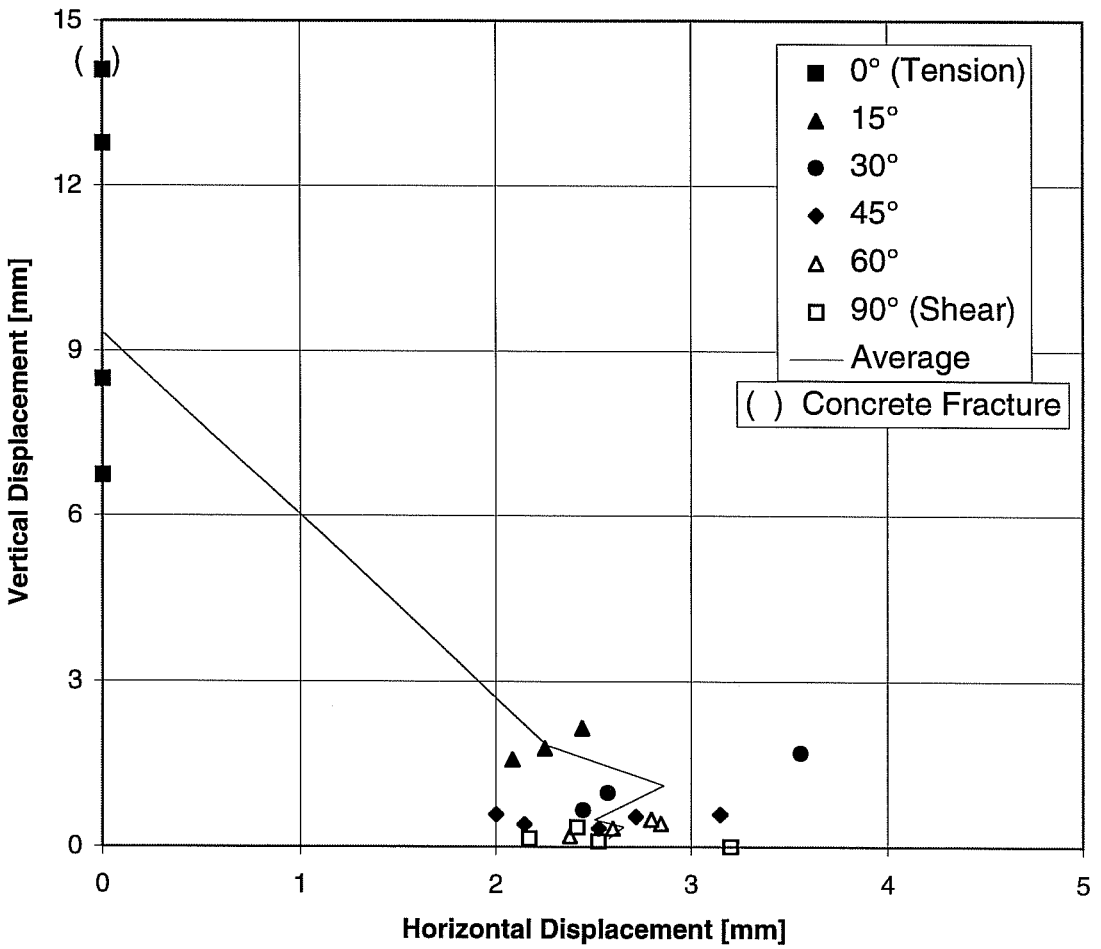

Part 1: Interaction of Force	**Interaction Exponent**	σ_Z	σ_S	
Break of Curve	1.67	903.0	537.0	
Max. Load	1.67	1003.3	596.7	
Remaining Load	1.67	973.2	578.8	
Part 2: Load-Displacement Curves	**Angle** d_{knick}	d_u	d_{Rest}	**Curvature Exponent**
Angle	0			
d_{Ver}	2.77	10.53	10.94	0.20
Angle	15			
d_{Hor}	1.41	2.26	2.72	0.60
d_{Ver}	1.01	1.85	2.32	0.25
Angle	30			
d_{Hor}	1.98	2.86	3.23	0.60
d_{Ver}	0.60	1.11	1.31	0.25
Angle	45			
d_{Hor}	1.74	2.51	2.79	0.60
d_{Ver}	0.16	0.49	0.60	0.25
Angle	60			
d_{Hor}	1.96	2.66	2.81	0.60
d_{Ver}	0.22	0.36	0.39	0.25
Angle	75			
d_{Hor}	1.95	2.60	2.93	0.60
d_{Ver}	0.11	0.18	0.20	0.25
Angle	90			
d_{Hor}	1.94	2.58	2.99	0.60
Displacement in mm, Angle in degrees				

Mathematic Description of Results of Series 23M34 with UC1 Anchors 3/8 inches (h_{ef} = 3.5 inches, c1 ≥ 5,5 inches) in Flush-Sleeve Installation for Program BDA5 (75° Interpolated), f_c = 32.4 N/mm²

Mathematical Description of Load-Displacement Curves of Series 23M34

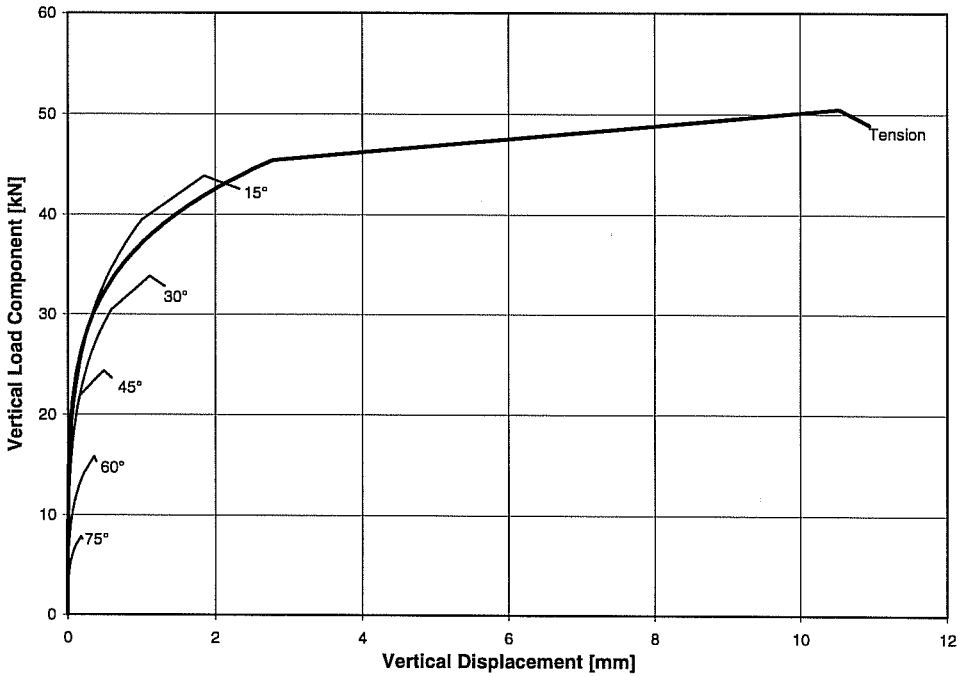

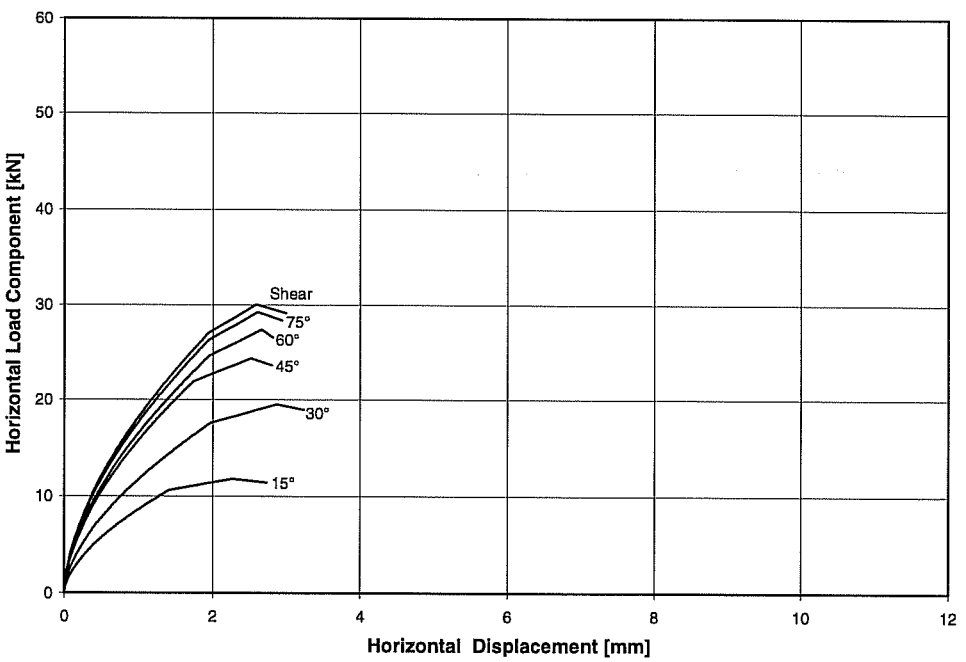

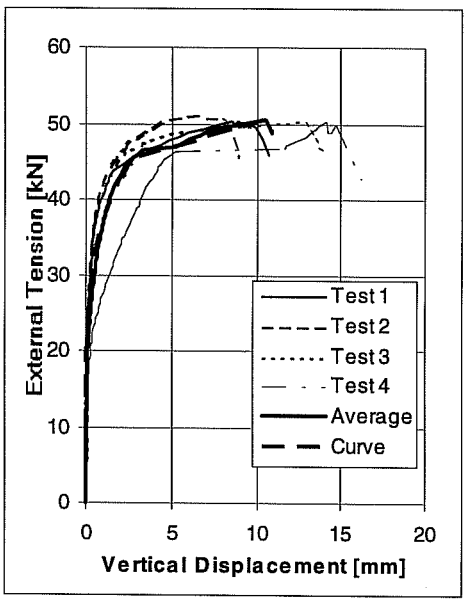

Pure Shear

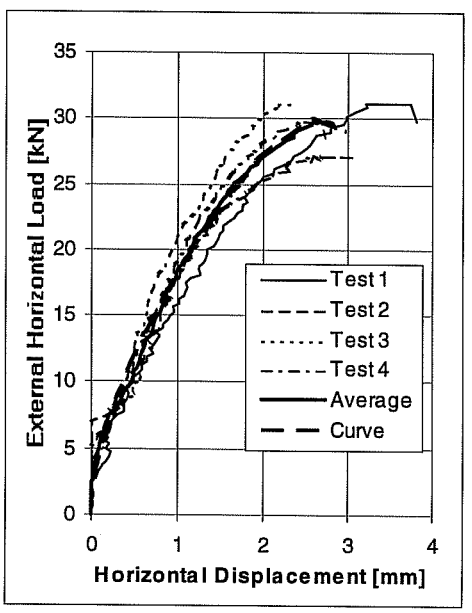

Pure Shear

Load-Displacement Curves of Series 23m34T (Tension) and 23m34S (Shear)
UC1 Anchors 5/8 inches, hef = 7 inches (178 mm), c1 ³ 11 inches (279 mm), fc = 32.4 N/mm²

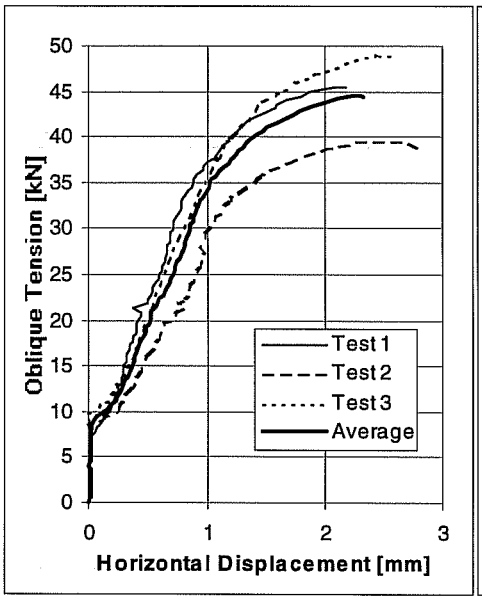

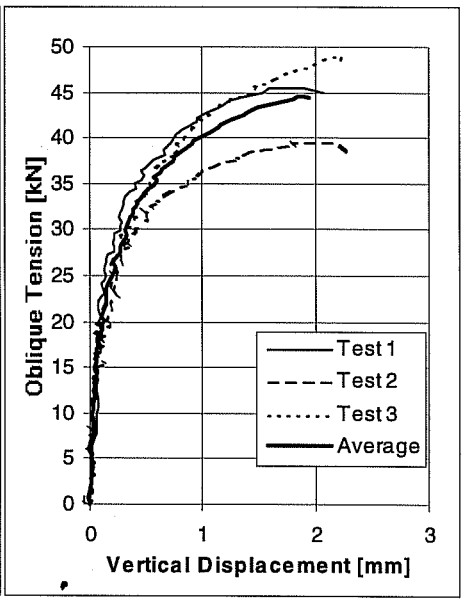

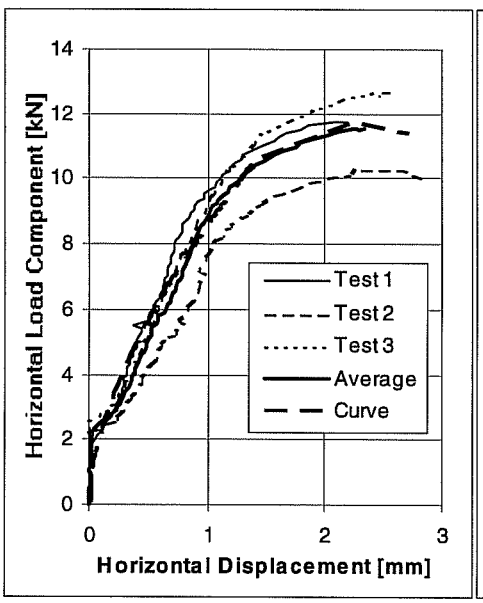

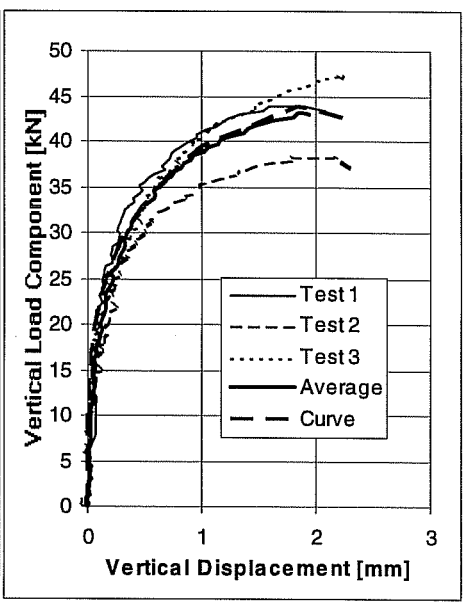

Load-Displacement Curves Series 23m341,
UC1 Anchors 3/8 inches, hef = 7 inches (178 mm), c1 ³ 11 inches (279 mm),
f_c = 32.4 N/mm², Loading Angle 15° from Anchor Axis

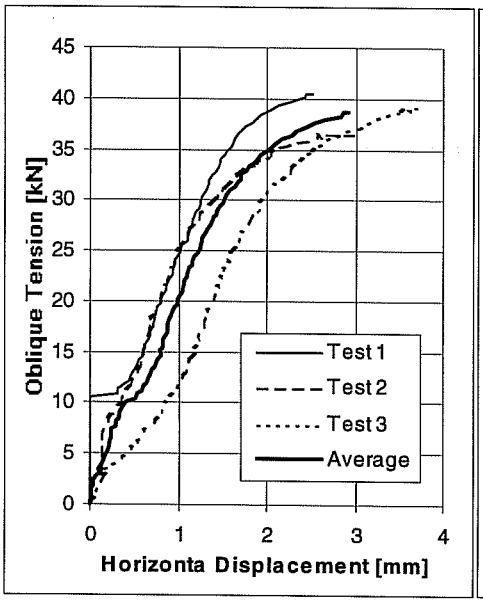

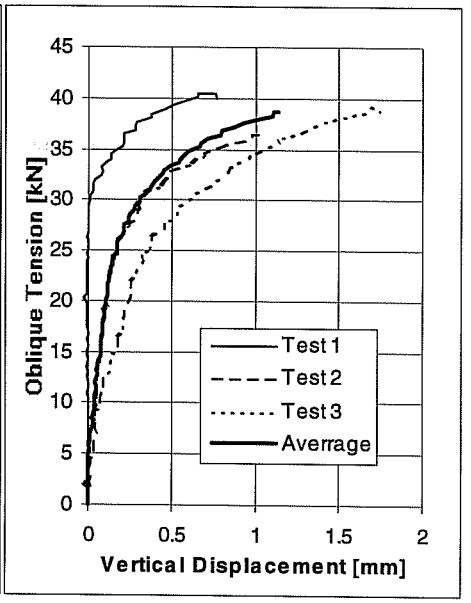

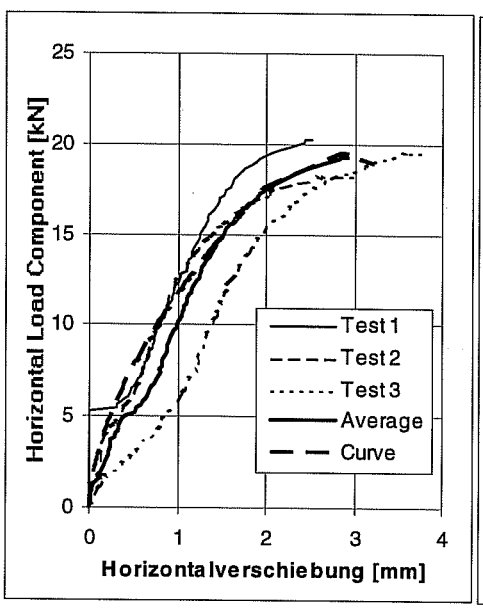

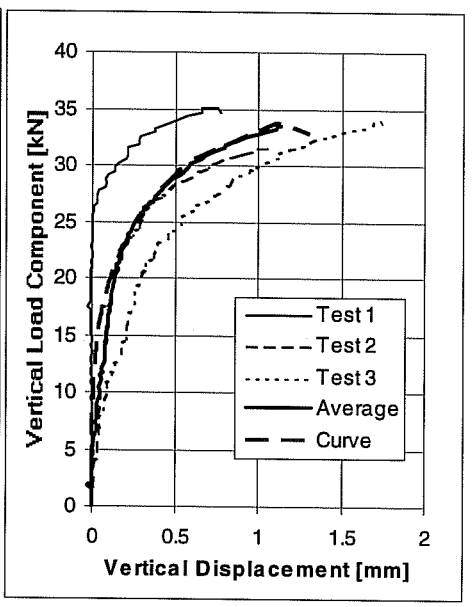

Load-Dispalcement Curves of Series 23m343,
UC1 3/8 inches, hef = 7 inches (178 mm), c1 ³ 11 inches (279 mm),
f_c = 32.4 N/mm², Loading Angle 30° from Anchor Axis

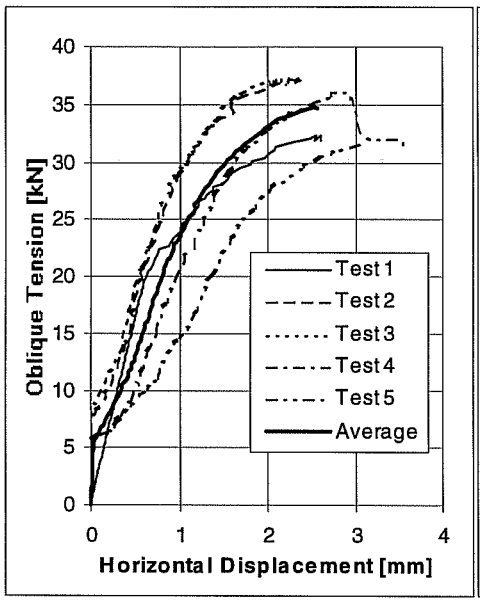

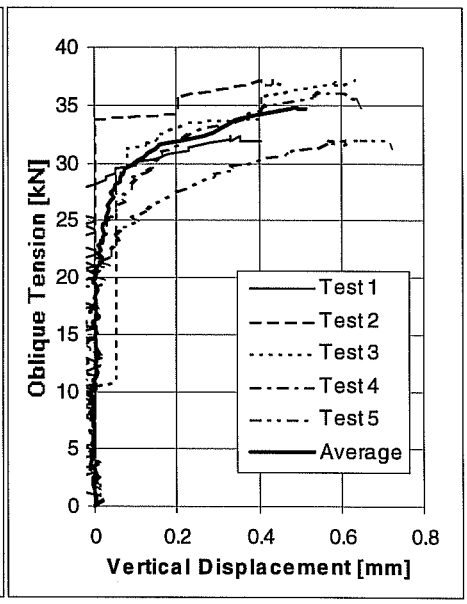

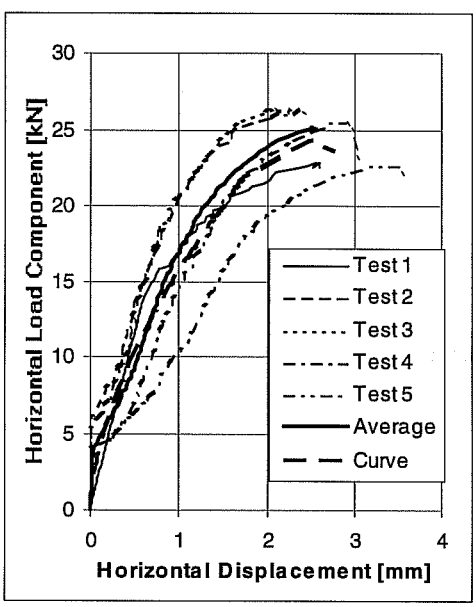

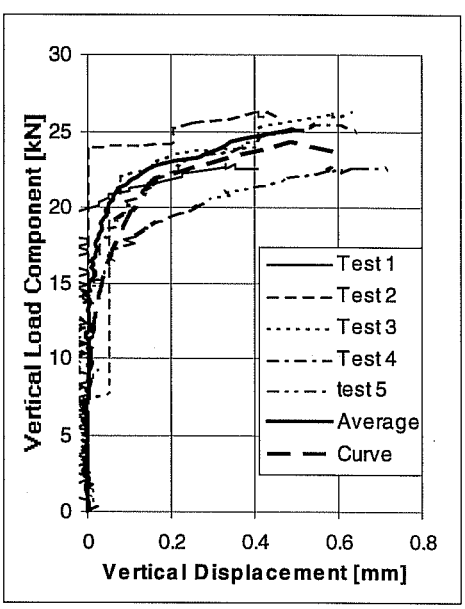

Load-Displacement Curves of Series 23m344,
UC1 Anchors 3/8 inches, hef = 7 inches (178 mm), c1 ³ 11 inches (279 mm),
$f_{c.}$ = 32.4 N/mm², Loading Angle 45° from Anchor Axis

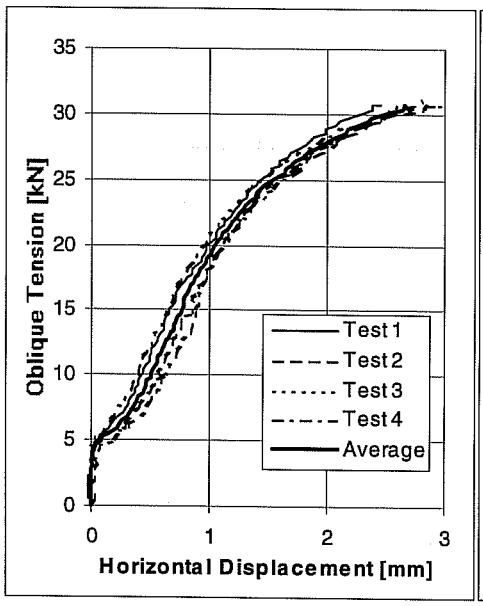

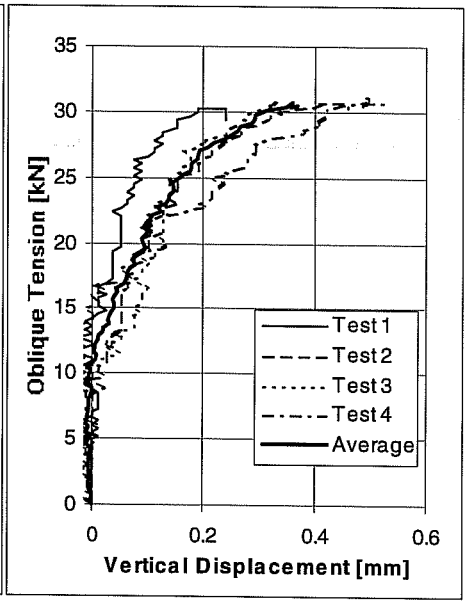

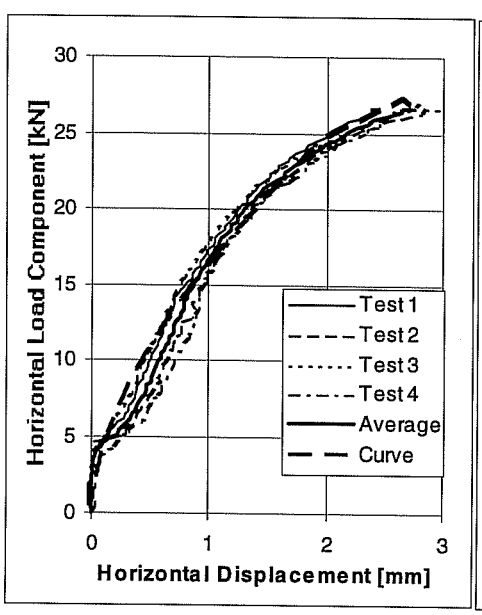

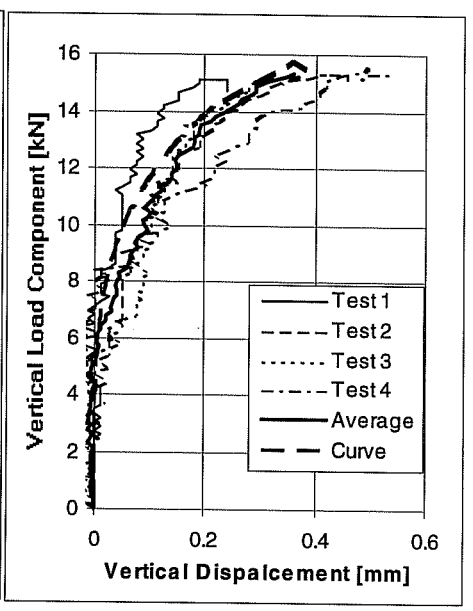

Load-Displacement Curves of Series 23m346,
UC1 Anchors 3/8 inches, hef = 7 inches (178 mm), c1 ³ 11 inches (279 mm),
f_c = 32.4 N/mm², Loading Angle 60° from Anchor Axis

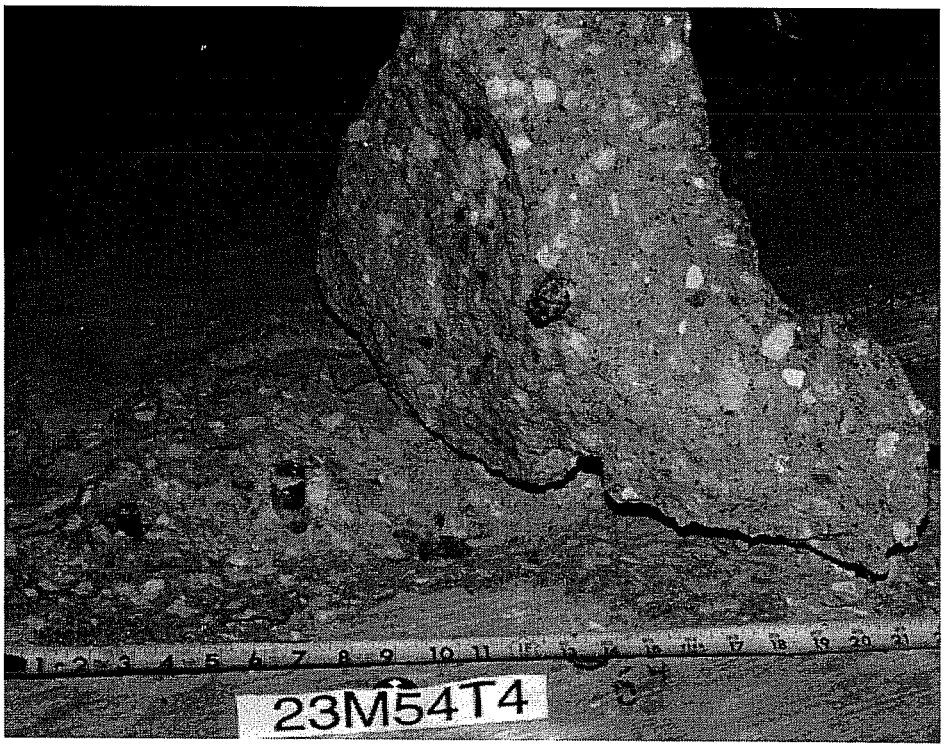

Failure Picture of Test 23M34T4, UC1 3/8", Pure Tension

Failure Picture of Test 23M34T4, UC1 3/8", Pure Tension, Details of Expansion Elements

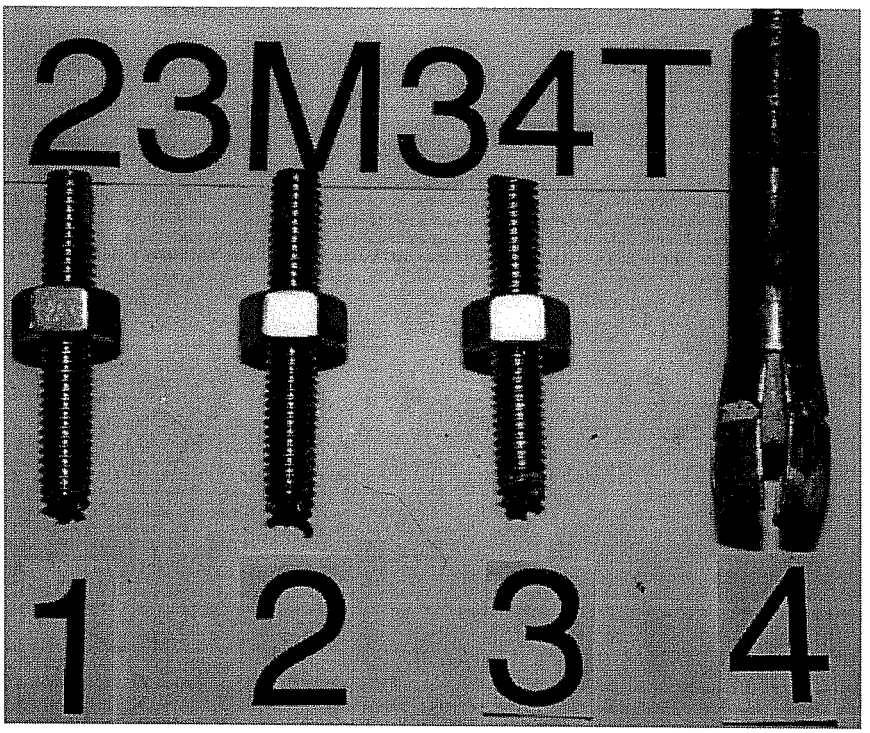

Series 23M34T, UC1 3/8V, Pure Tension, Anchor Shanks after Tests

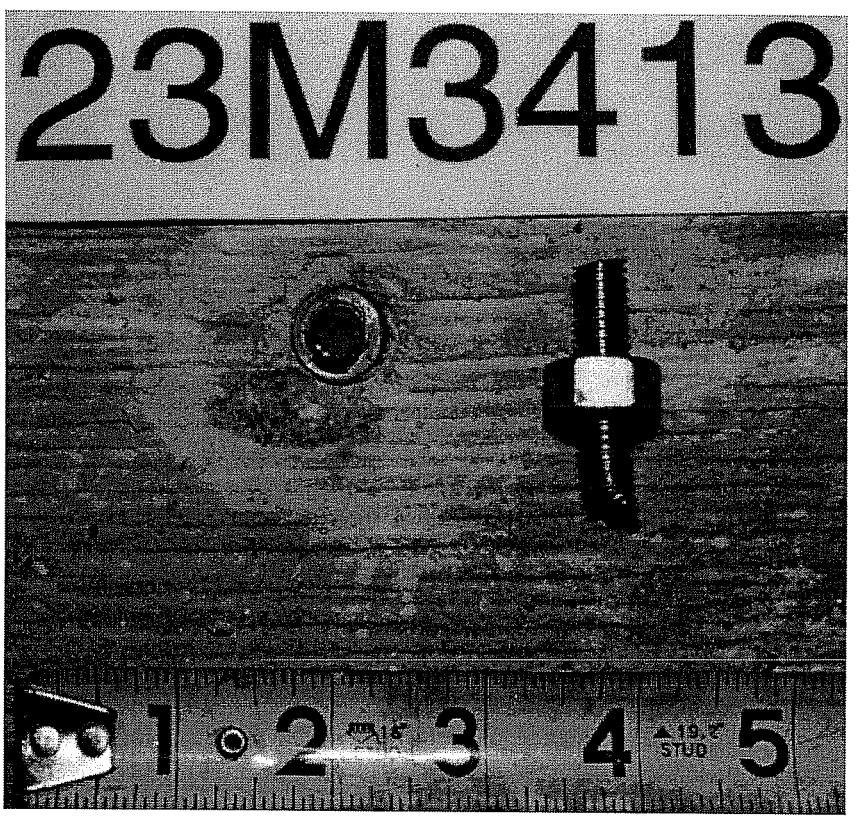

Failure Picture of Test 23M3413, UC1 3/8", Oblique Tension 15°

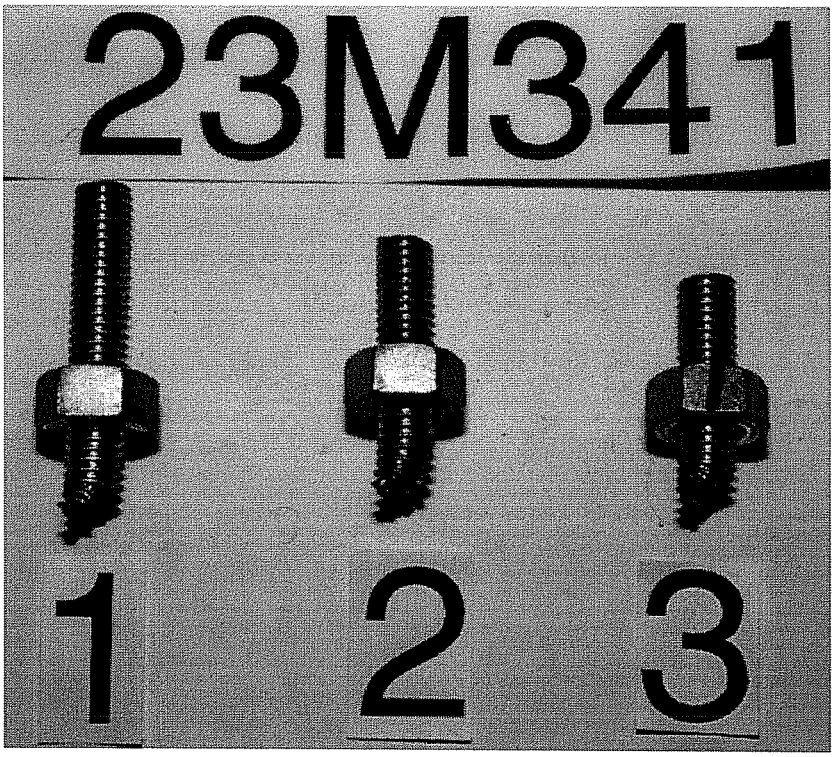

Series 23M341, UC1 3/8", Oblique Tension 15°, Fractured Anchor Shanks

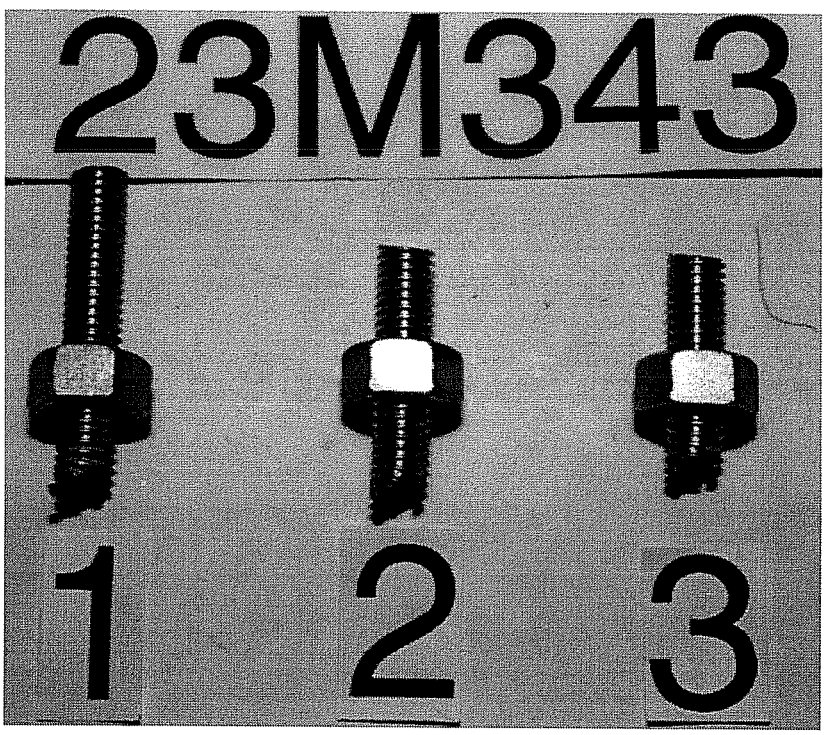

Series 23M343, UC1 3/8", Oblique Tension 30°, Fractured Anchor Shanks

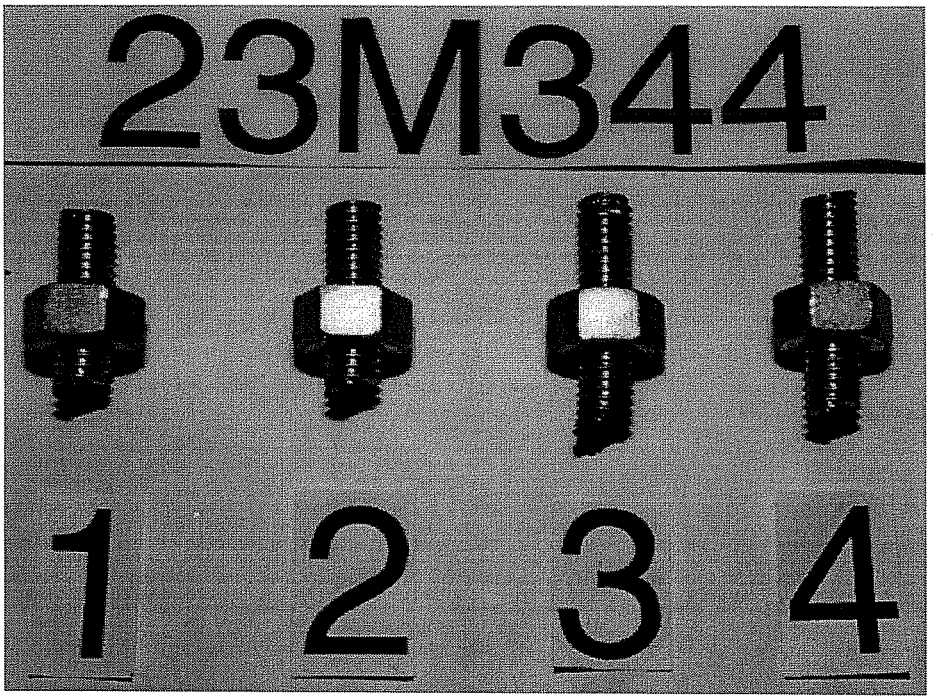

Series 23M344, UC1 3/8", Oblique Tension 45°, Fractured Anchor Shanks

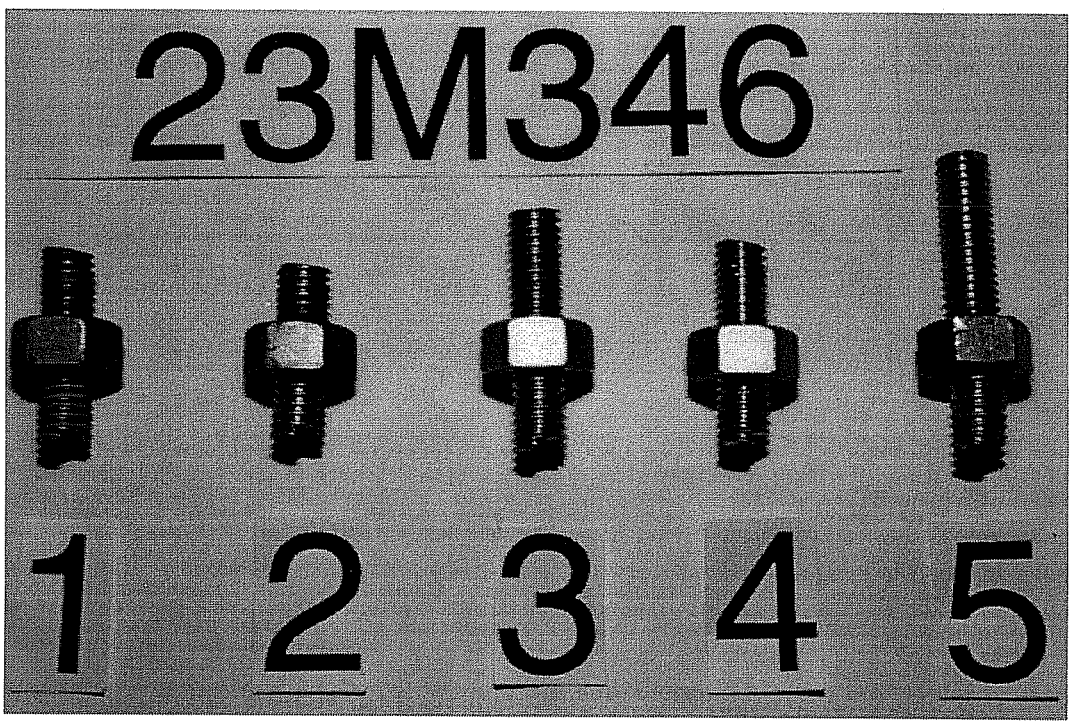

Series 23M346, UC1 3/8", Oblique Tension 60°, Fractured Anchor Shanks

Test No.	Loading Angle degrees	Edge Distance c1 mm	Torque Nm	Block No.	Concrete Strength N/mm²	Failure Load F_u kN	F_u (f_c=32.4) kN	Hor. Displ. $d_{H,u}$ mm	Corr. c(H) mm	Vert. Displ. $d_{V,u}$ mm	Frac. Cone Height h mm	Note
		25										
24M54T4	Tension	140	244/122	L33-B	31.5	74.3	75.3	0.00	-	1.71	-	
5	Tension	140	203/122	L34-T	29.6	72.9	76.4	0.00	-	0.67	-	
Ave.						**73.6**	**75.9**	**0.00**		**1.19**		
24M5431	30	143	244/122	L33-T	33.9	78.3	76.6	1.98	0.25	0.38	190.5	1)
2	30	137	244/122	L33-T	33.9	68.5	67.0	1.79	0	0.36	171.45	
3	30	141	203/122	L33-B	31.5	60.9	61.8	1.89	0		228.6	2)
4	30	140	203/122	L33-B	31.5	70.3	71.3	2.10	0.5	0.48	152.4	
Ave.						**69.5**	**69.2**	**1.94**		**0.41**	**185.74**	
COV [%]								**6.81**		**22.10**	**21.35**	
24M5441	45	130	244/122	L33-T	33.9	77.8	76.1	3.53	0	0.61	273.05	
2	45	140	244/122	L33-T	33.9	70.7	69.2	2.19	1	0.37	171.45	
3	45	140	203/122	L33-B	31.5	64.5	65.4	2.21	0	0.57	184.15	
Ave.						**71.0**	**70.2**	**2.64**		**0.52**	**209.55**	
COV [%]								**29.14**		**27.82**	**4.29**	
24M5461	60	137	244/122	L33-T	33.9	57.8	56.6	2.30	0.25	0.28	177.8	
2	60	146	203/122	L33-B	31.5	54.7	55.5	1.68	0.75		203.2	2)
3	60	143	203/122	L33-B	31.5	58.7	59.5	2.75	0	0.22	139.7	
Ave.						**57.1**	**57.2**	**2.24**		**0.25**	**173.57**	
COV [%]								**23.94**			**18.41**	
24M54S1	Shear	140	244/122	L33-T	33.9	61.4	60.0	3.38	0.25	0.00	228.6	
2	Shear	140	244/122	L33-T	33.9	72.5	70.9	4.63	0.75	0.00	254	
3	Shear	140	203/122	L34-T	29.6	61.4	64.3	3.21	0.5	0.00	279.4	
Ave						**65.1**	**65.1**	**3.74**			**254.00**	
COV [%]								**20.80**			**10.00**	

1) only 1 displacement measured for vertical displacement d_V

2) vertical displacement not measured (failure of both dispacement measurements)

Test Results of Series 24M54: UC1 5/8 inches, hef = 89 mm (3.5 inches), Edge Distance c1 = 140 mm (5.5 inches), Failing by Concrete Fracture fc = 32.4 N/mm² (4700 psi), Flush-Sleeve Installation

Test No.	Loading Angle degrees	Edge Distance c1 mm	Torque mm	Block No.	Concrete Strength N/mm²	Failure Load F_u kN	F_u (f_c=32.4) kN	Hor. Displ. $d_{H,u}$ mm	Corr. c(H) mm	Vert. Displ. $d_{V,u}$ mm	Note
24M54T1	Tension	> 278	244/122	L33-T	33.9	101.0	98.8	0.00	-	3.07	
2	Tension	> 279	244/122	L33-T	33.9	98.7	96.6	0.00	-	0.65	
3	Tension	> 280	244/122	L33-B	31.5	77.4	78.5	0.00	-	1.45	
Ave.						**92.4**	**91.3**	**0.00**		**1.72**	
COV [%]										**32.84**	
24A5411	15	279	244/122	L34-T	29.6	88.5	92.7	MD		MD	1)
24A5431	30	279	244/122	L34-T	29.6	95.2	99.7	5.10	0	2.02	
24A5441	45	279	244/122	L33-T	33.9	93.4	89.4	6.28	0	1.96	2)
2	45	279	244/122	L34-T	29.6	87.6	91.8	6.84	0	1.87	
Ave.						**90.5**	**90.6**	**6.6**		**1.9**	

1) MD = measurement failure

2) failure by steel fracture

Test Results of Series 24A54: UC1 5/8 inches, hef = 89 mm (3.5 inches), Edge Distance c1 ³ 279mm, Failing by Concrete Fracture fc = 32.4 N/mm² (4700 psi), Flush-Sleeve Installation

Interaction of Load, Series 24M54

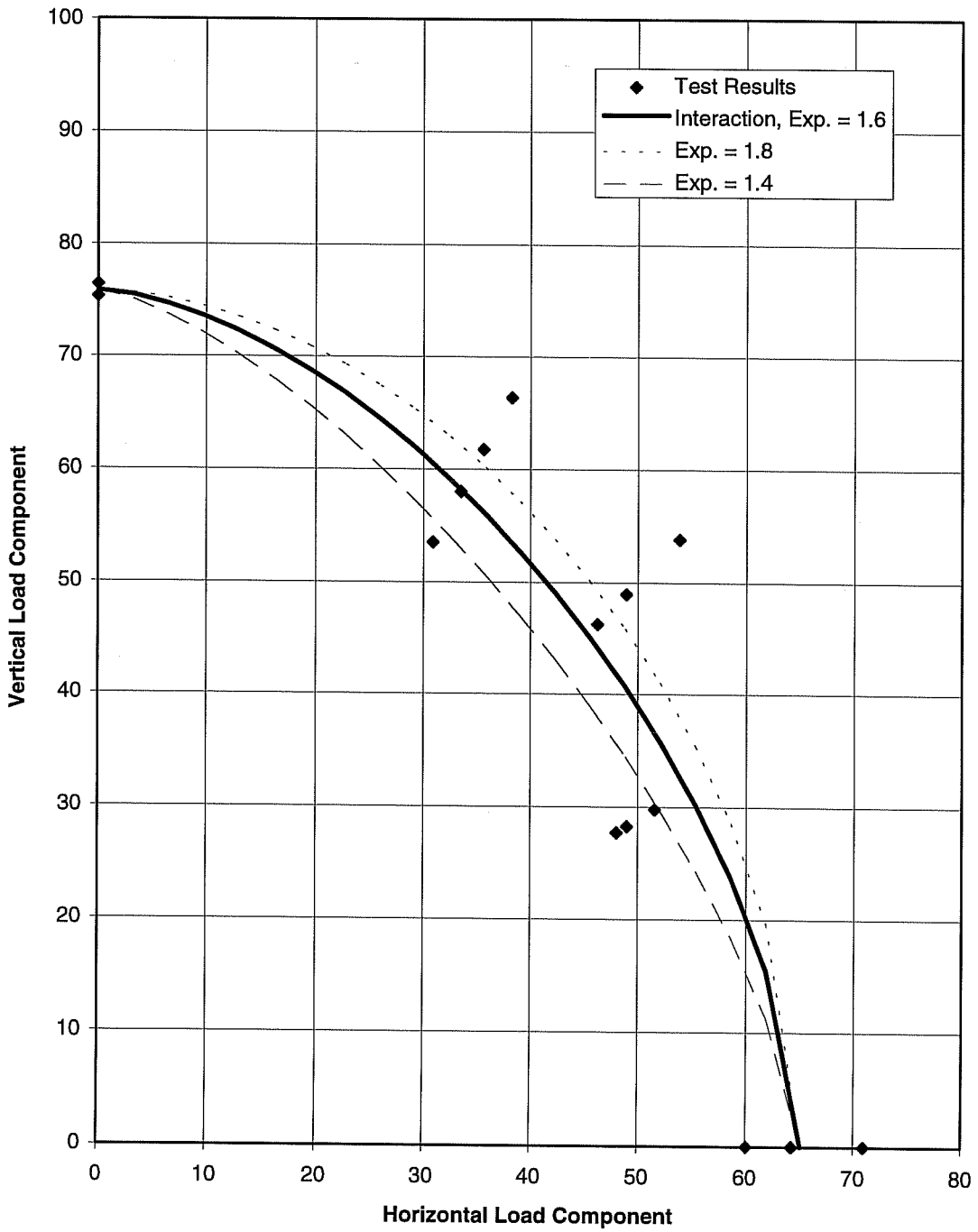

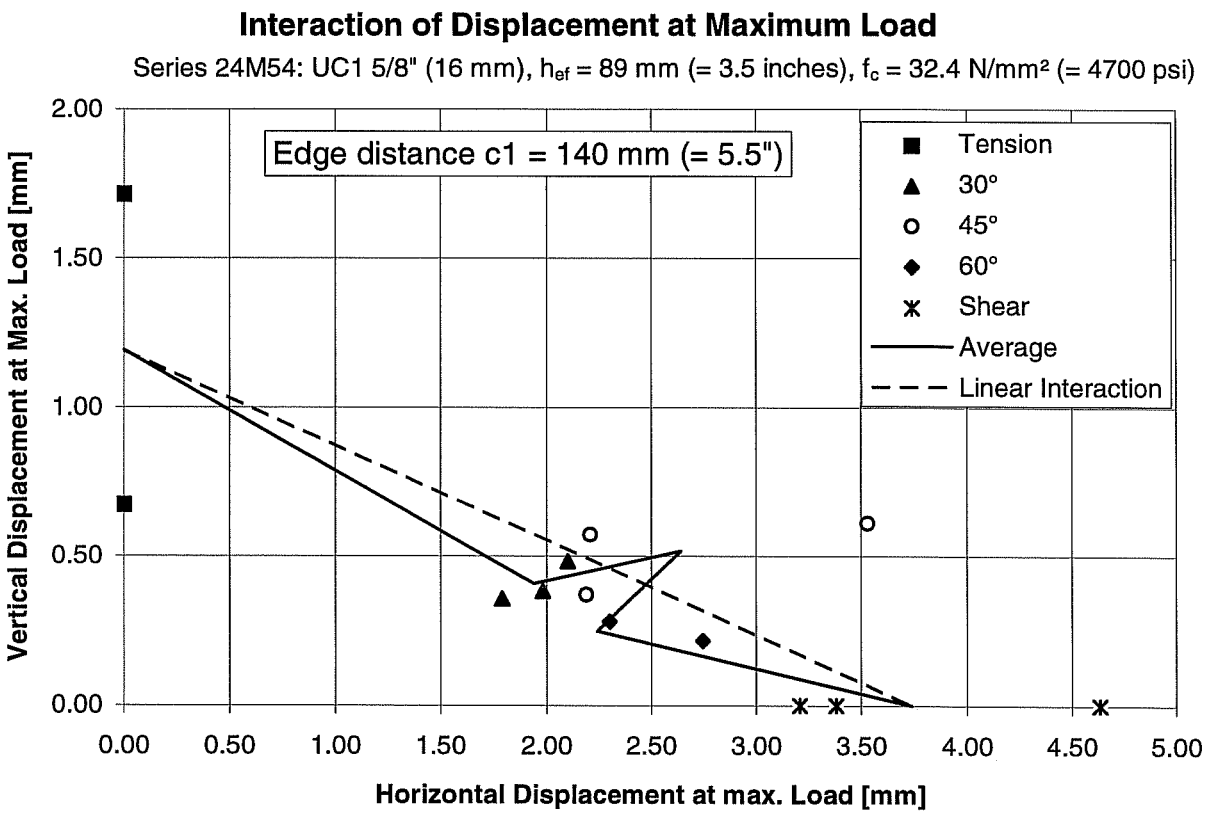
Interaction of Displacement at Maximum Load
Series 24M54: UC1 5/8" (16 mm), h_{ef} = 89 mm (= 3.5 inches), f_c = 32.4 N/mm² (= 4700 psi)
Edge distance c1 = 140 mm (= 5.5")
Tension
30°
45°
60°
Shear
Average
Linear Interaction
Vertical Displacement at Max. Load [mm]
Horizontal Displacement at max. Load [mm]
2.00
1.50
1.00
0.50
0.00
0.00
0.50
1.00
1.50
2.00
2.50
3.00
3.50
4.00
4.50
5.00

Part 1: Interaction of Force	**Interaction Exponent**	σ_Z	σ_S	
Break of Curve	1.60	482.7	402.1	
Höchstlast	1.60	536.4	446.8	
Restlast	1.60	455.9	379.8	
Part 2: Load-Displacement Curves	**Angle** d_{knick}	d_u	d_{Rest}	**Curvature Exponent**
Angle	0			
d_{Ver}	0.69	1.19	1.98	0.25
Angle	15			
d_{Hor}	0.81	0.97	1.07	0.80
d_{Ver}	0.47	0.80	1.24	0.25
Angle	30			
d_{Hor}	1.62	1.94	2.13	0.80
d_{Ver}	0.25	0.41	0.85	0.25
Angle	45			
d_{Hor}	1.92	2.23	3.15	0.80
d_{Ver}	0.21	0.30	0.69	0.25
Angle	60			
d_{Hor}	2.24	2.80	3.50	0.70
d_{Ver}	0.24	0.38	0.58	0.25
Angle	75			
d_{Hor}	2.73	3.43	4.46	0.63
d_{Ver}	0.07	0.12	0.31	0.25
Angle	90			
d_{Hor}	2.98	3.74	4.94	0.60
Displacement in mm, Angle in degrees				

Mathematical Description of Results of Series 24M54 with UC1 5/8 inches (h_{ef} = 3.5 inches, c1 = 5.5 inches) in Flush-Sleeve Installations for Program BDA5 (75° Interpolated), f_c = 32.4 N/mm²

Mathematical Description of Load-Displacement Curves of Series 24M54

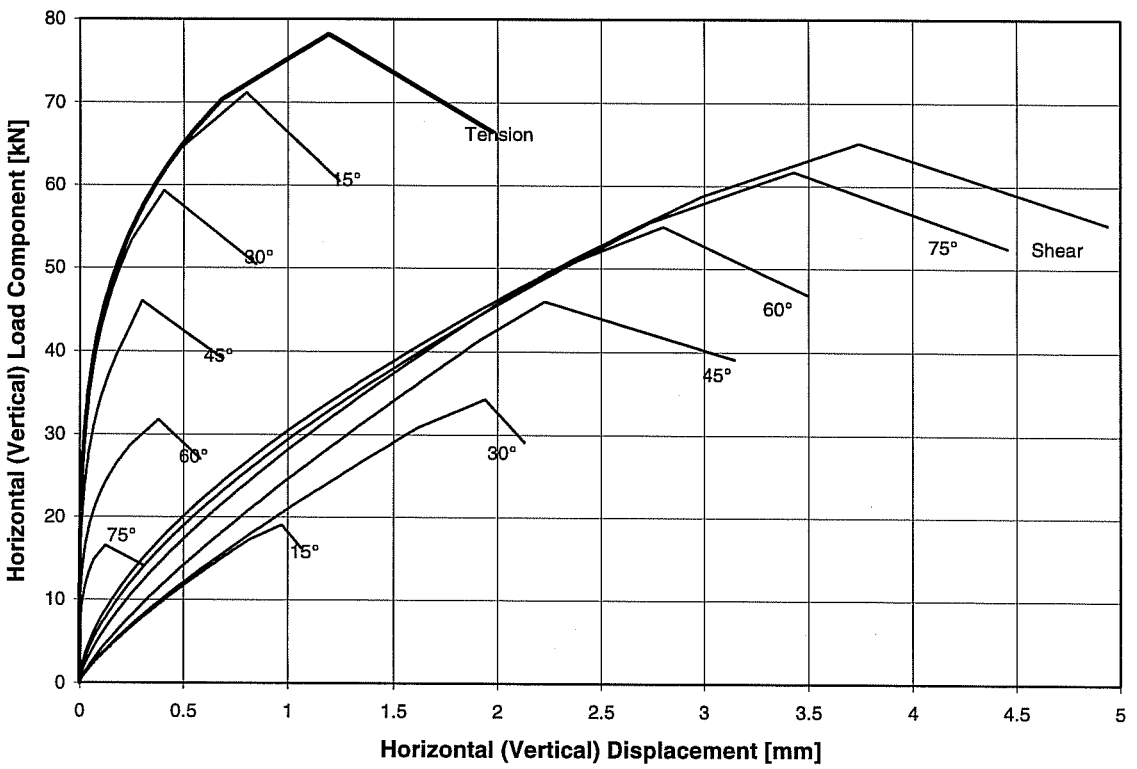

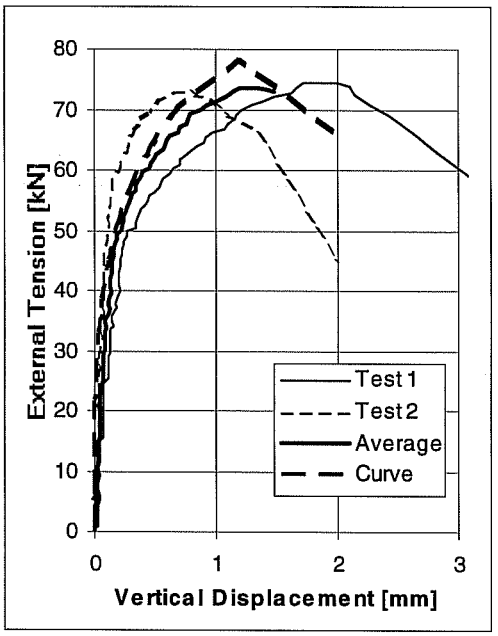

Pure Tension

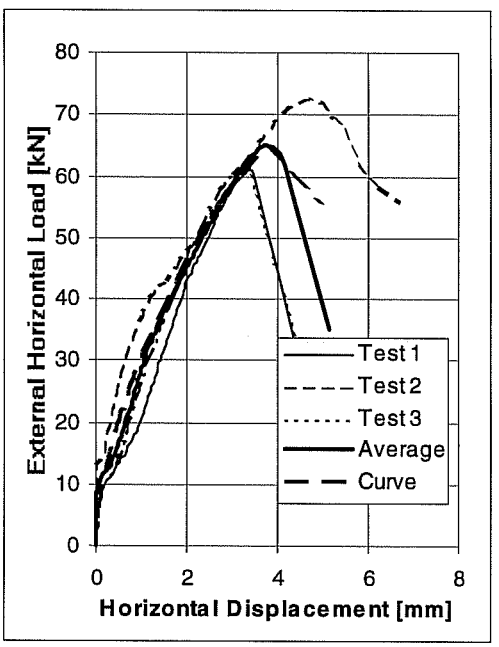

Pure Shear

Load-Displacement Curves of Series 24m54T (Tension) and 24m54S (Shear)
UC1 Anchors 5/8 inches, hef = 3.5 inches (89 mm), c1 = 5.5 inches (140 mm), fc = 32.4 N/mm²

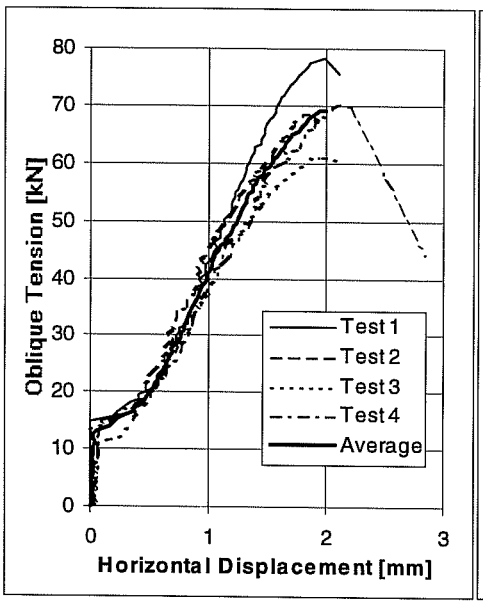

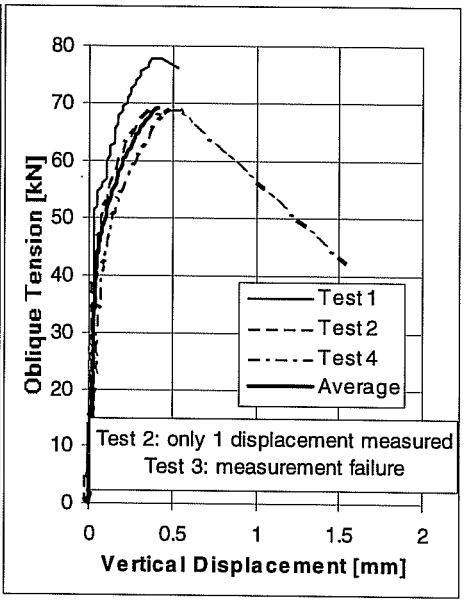

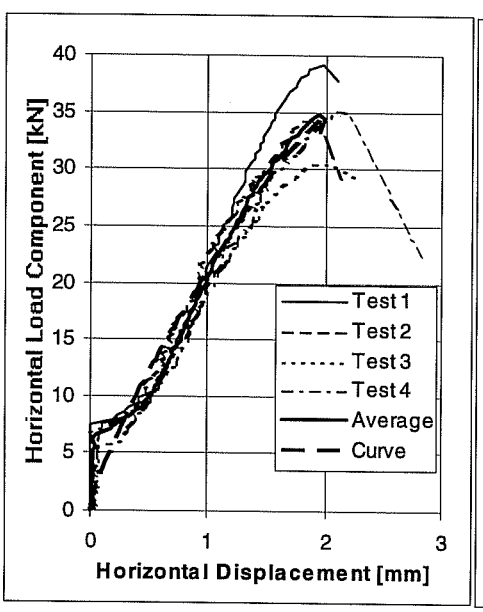

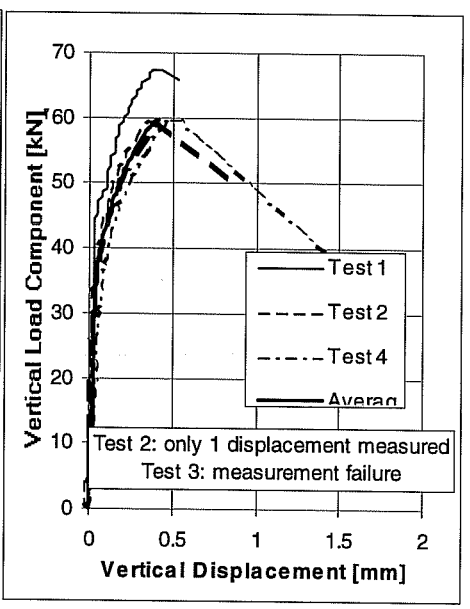

Load-Displacement Curves of Series 24m543,
UC1 Anchors 5/8 inches, hef = 3.5 inches (89 mm), c1 = 5.5 inches (140 mm),
f_c = 32.4 N/mm², Loading Angle 30° from Anchor Axis

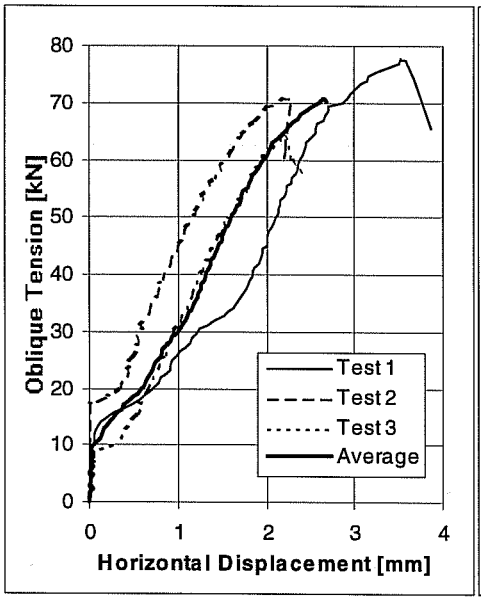

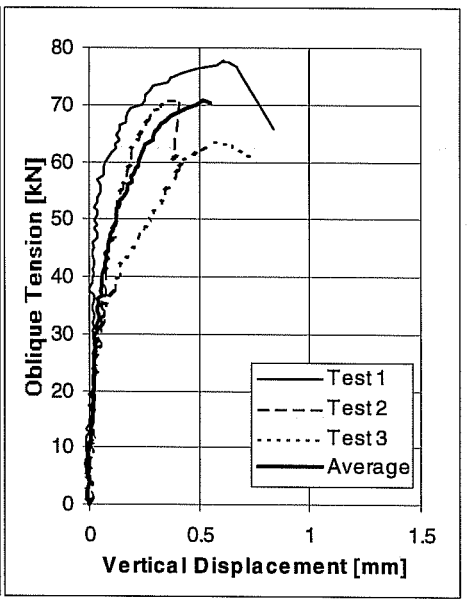

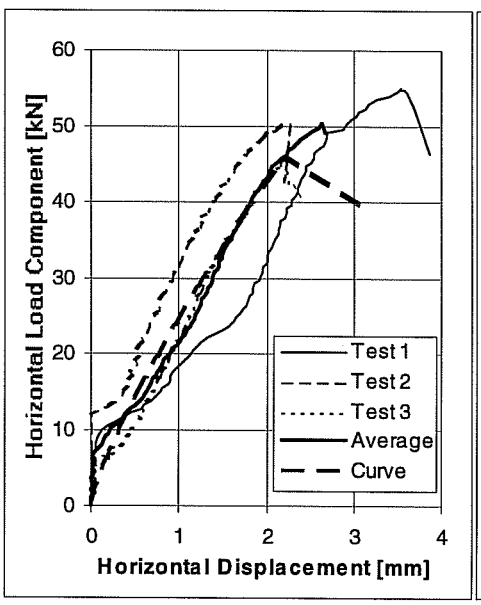

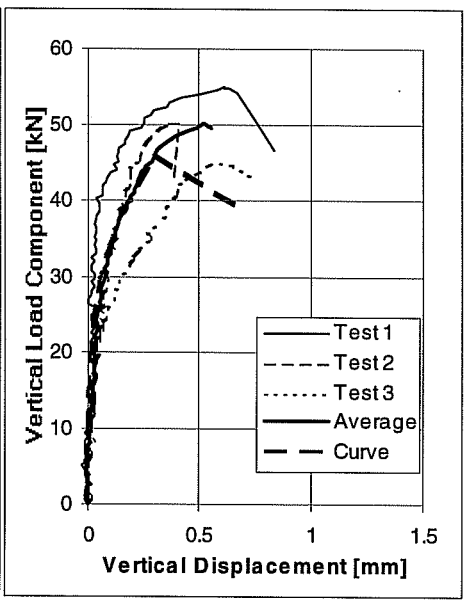

Load-Displacement Curves of Series 24m544,
UC1 5/8 inches, hef = 3.5 inches (89 mm), c1 = 5.5 inches (140 mm),
f_c = 32.4 N/mm², Loading Angle 45° from Anchor Axis

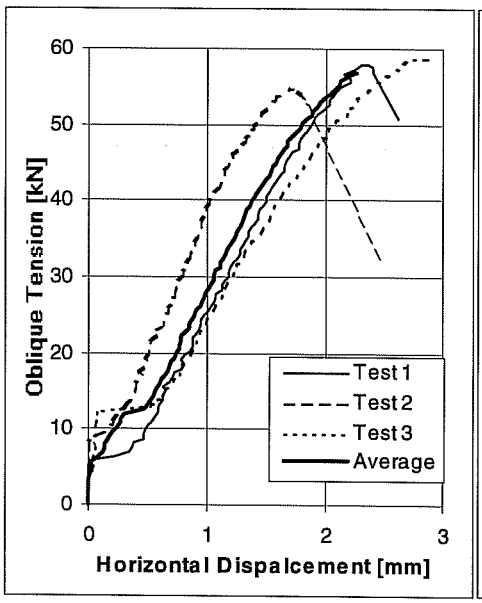

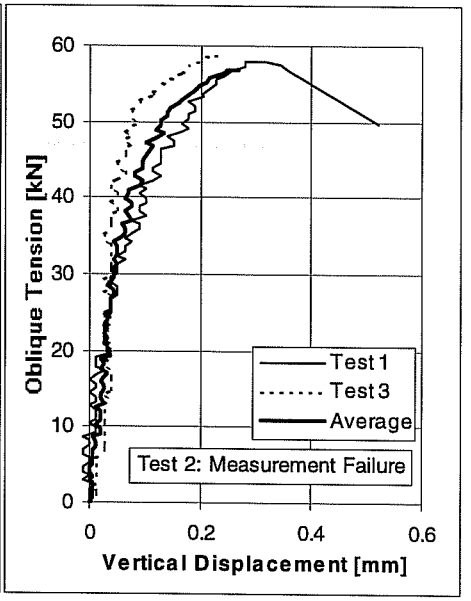

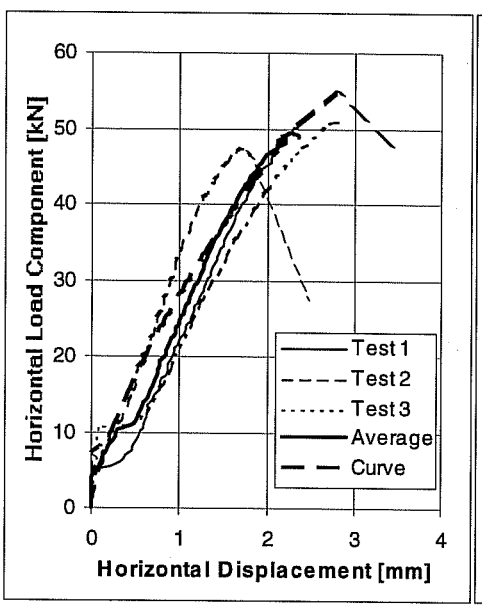

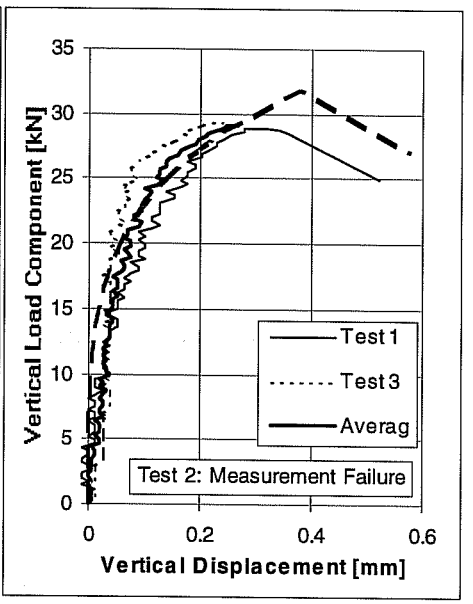

Load-Displacement Curves of Series 24m546,
UC1 5/8 inches, hef = 3.5 inches (89 mm), c1 = 5.5 inches (140 mm),
f_c = 32.4 N/mm², Loading Angle 60° from Anchor Axis

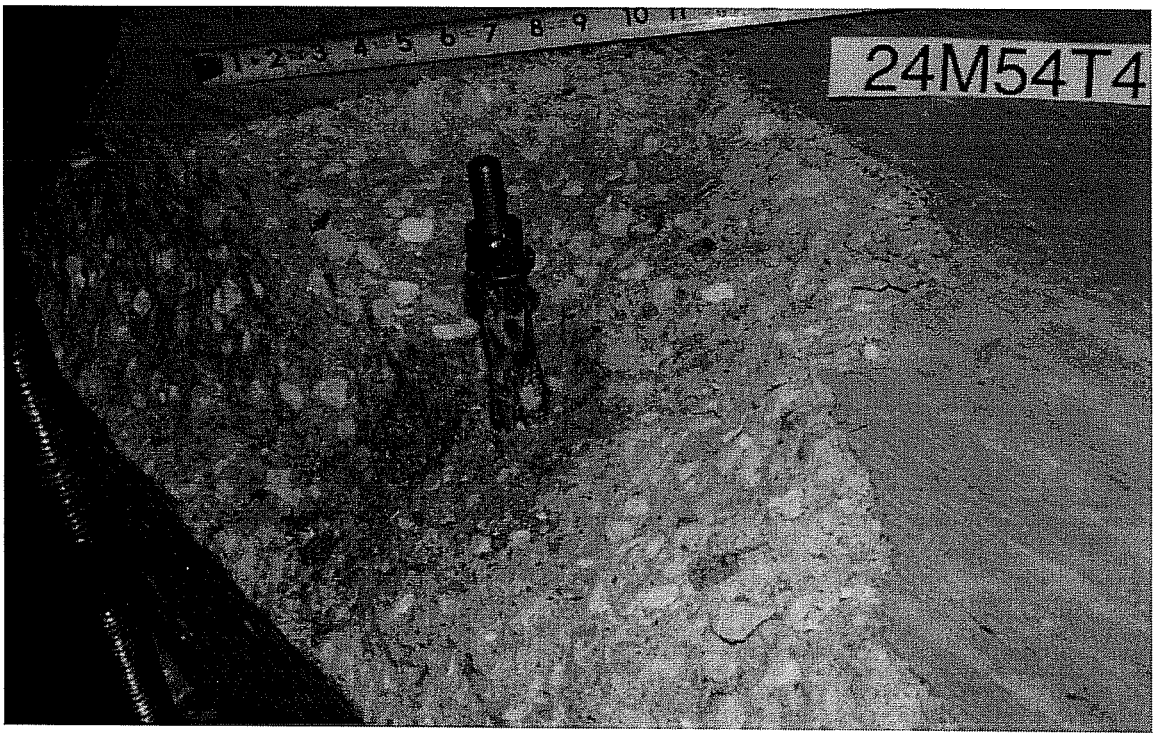

Failure Picture of Test 24M54T4, UC1 5/8", h_{ef} = 89 mm, c1 = 140 mm, Pure Tension

Failure Picture of Test 24M5433, UC1 5/8", h_{ef} = 89 mm, c1 = 140 mm, Oblique Tension 30°

Failure Picture of Test 24M5442, UC1 5/8", h_{ef} = 89 mm, c1 = 140 mm, Oblique Tension 45°

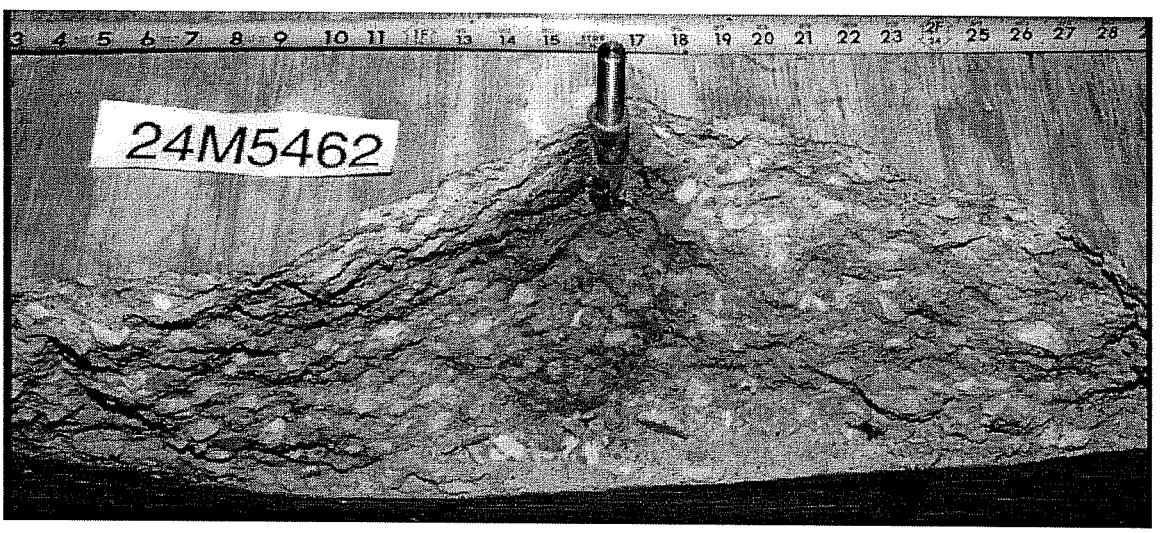

Failure Picture of Test 24M5462, UC1 5/8", h_{ef} = 89 mm, c1 = 140 mm, Oblique Tension 60°

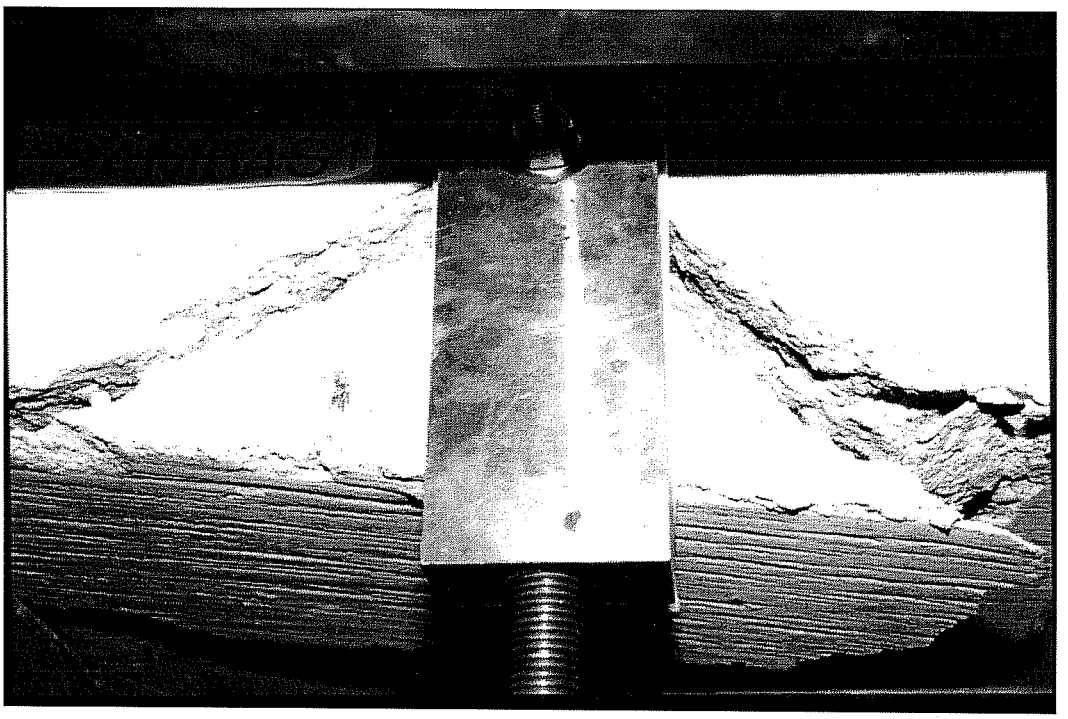

Failure Picture of Test 24M54S1, UC1 5/8", h_{ef} = 89 mm, c1 = 140 mm, Shear

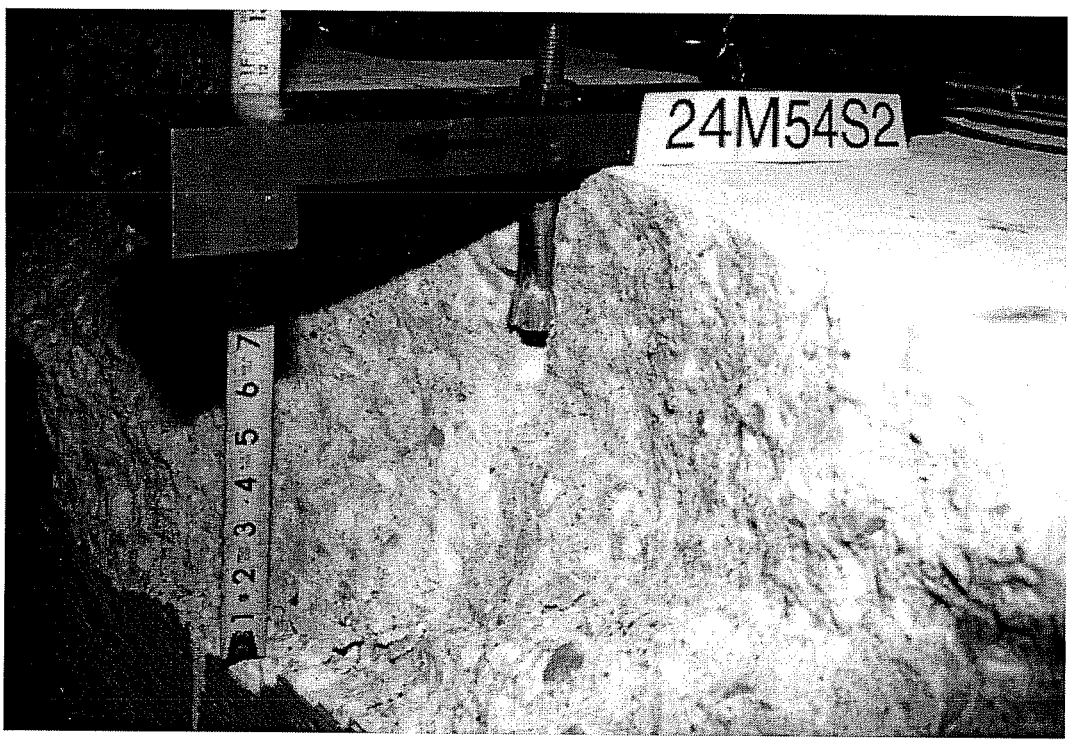

Failure Picture of Test 24M54S2, UC1 5/8", h_{ef} = 89 mm, c1 = 140 mm, Shear

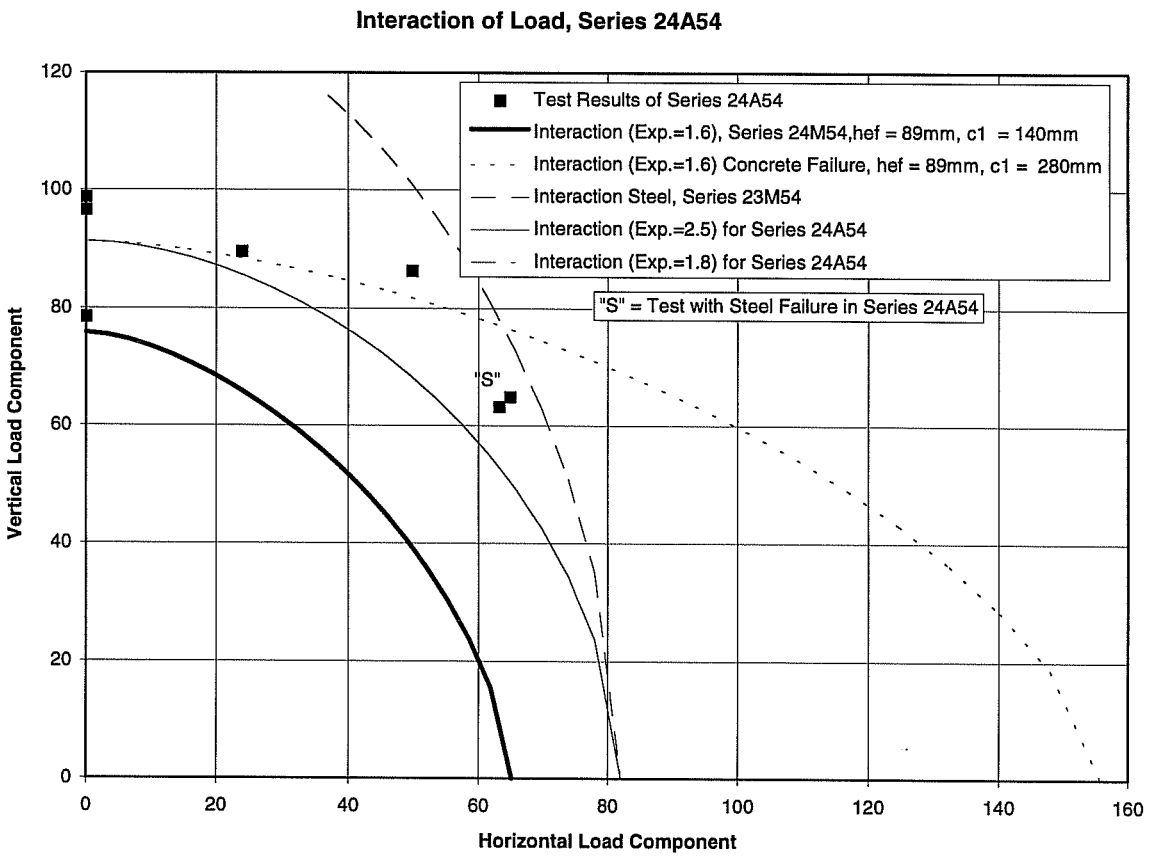
Interaction of Load, Series 24A54
Test Results of Series 24A54
Interaction (Exp.=1.6), Series 24M54,hef = 89mm, c1 = 140mm
Interaction (Exp.=1.6) Concrete Failure, hef = 89mm, c1 = 280mm
Interaction Steel, Series 23M54
Interaction (Exp.=2.5) for Series 24A54
Interaction (Exp.=1.8) for Series 24A54
"S" = Test with Steel Failure in Series 24A54
"S"
Vertical Load Component
Horizontal Load Component
0
20
40
60
80
100
120
140
160

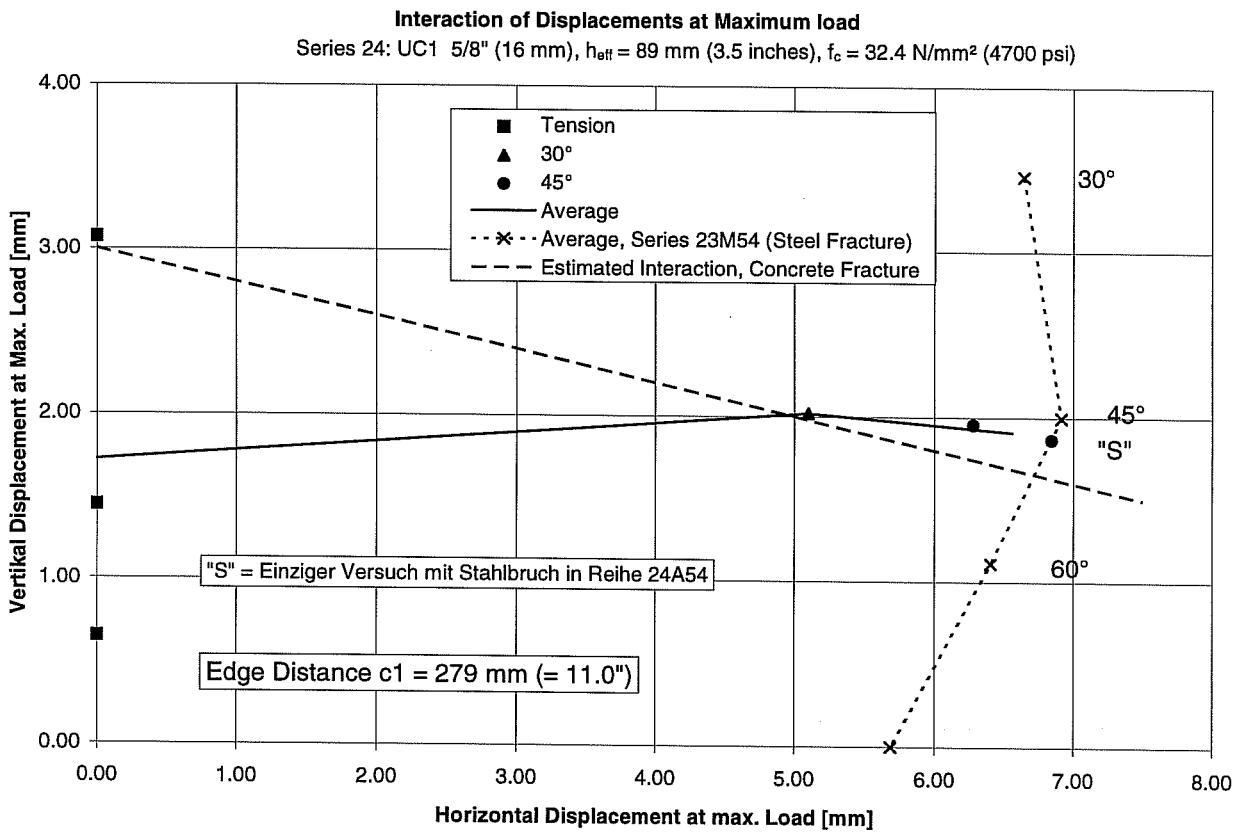
Interaction of Displacements at Maximum load
Series 24: UC1 5/8" (16 mm), h_{eff} = 89 mm (3.5 inches), f_c = 32.4 N/mm² (4700 psi)
Tension
30°
45°
Average
Average, Series 23M54 (Steel Fracture)
Estimated Interaction, Concrete Fracture
"S" = Einziger Versuch mit Stahlbruch in Reihe 24A54
Edge Distance c1 = 279 mm (= 11.0")
30°
45°
"S"
60°
Vertikal Displacement at Max. Load [mm]
Horizontal Displacement at max. Load [mm]
0.00
1.00
2.00
3.00
4.00
5.00
6.00
7.00
8.00

Part 1: Interaction of Force	**Interaction Exponent**	σ_Z	σ_S	
Break of Curve	2.50	563.5	506.2	
Max. Load	2.50	626.1	562.4	
Remaining Load	2.50	594.8	534.3	
Part 2: Load-Displacement Curves	**Angle d_{knick}**	**d_u**	**d_{Rest}**	**Curvature Exponent**
Angle	0			
d_{Ver}	0.77	1.72	2.01	0.25
Angle	15			
d_{Hor}	1.55	2.63	2.82	0.80
d_{Ver}	0.76	1.77	2.09	0.25
Angle	30			
d_{Hor}	3.00	5.10	5.47	0.80
d_{Ver}	0.67	2.02	2.49	0.25
Angle	45			
d_{Hor}	3.85	6.56	7.09	0.60
d_{Ver}	0.89	1.91	2.11	0.25
Angle	60			
d_{Hor}	4.25	6.40	6.57	0.60
d_{Ver}	0.60	1.11	1.15	0.25
Angle	75			
d_{Hor}	4.23	5.81	6.01	0.60
d_{Ver}	0.29	0.55	0.57	0.25
Angle	90			
d_{Hor}	4.23	5.69	5.90	0.60

Displacement in mm, Angle in degrees

Mathematical Description of Results of Series 24A54 with UC1 Anchors 5/8 inches (h_{ef} = 3.5 inches, c1 ≥ 11 inches) in Flush-Sleeve Anchor for Program BDA5 (15° Interpolated, 60° to 90° from Series 23M54), f_c = 32.4 N/mm²

Mathematical Description of Load-Displacement Curves of Series 24A54

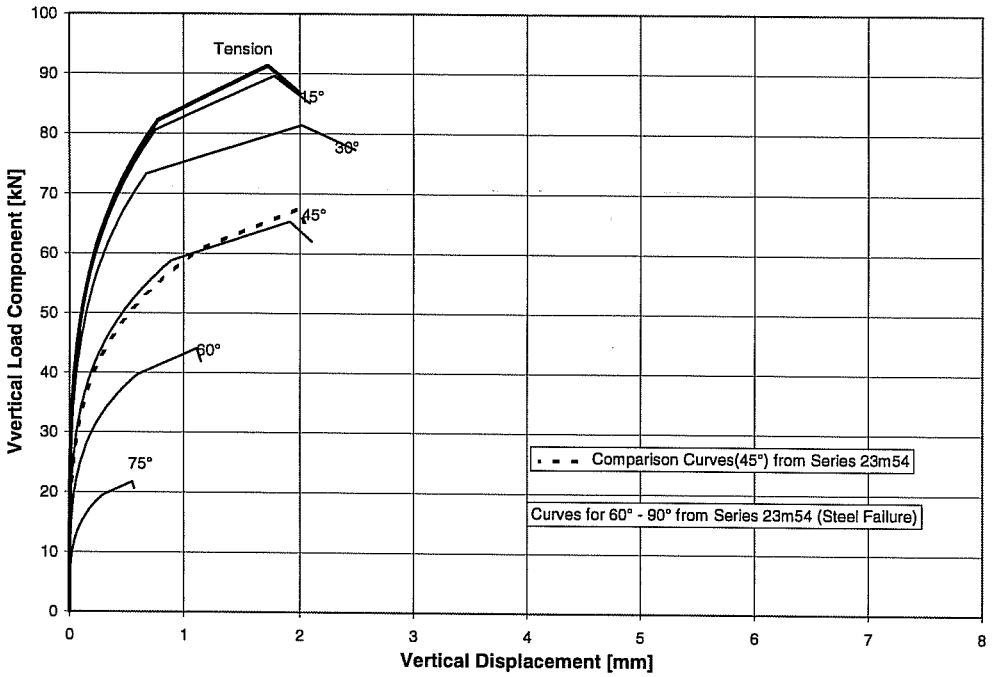

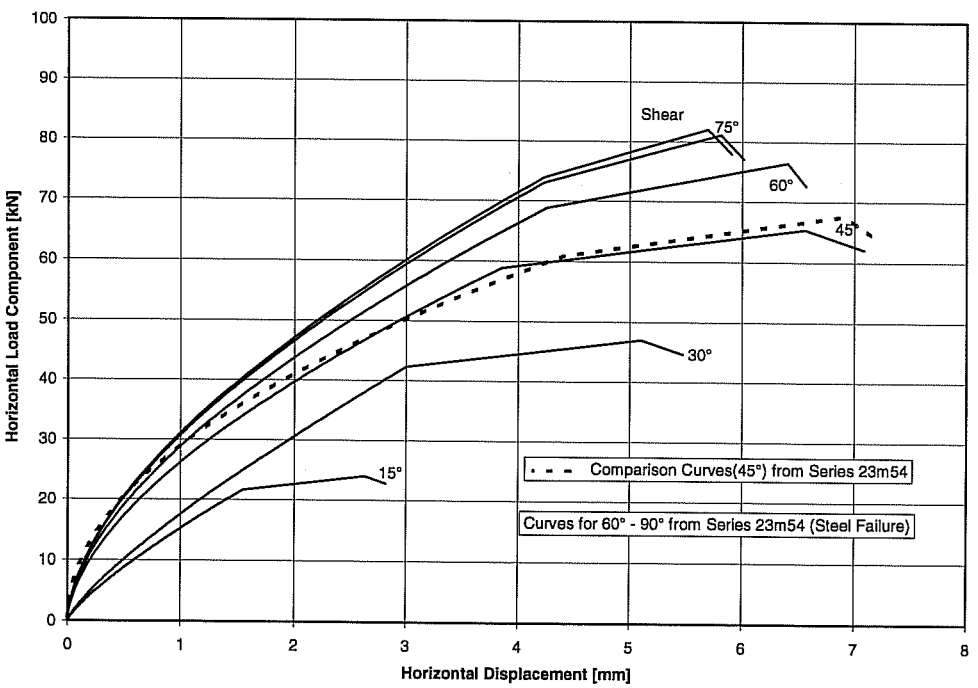

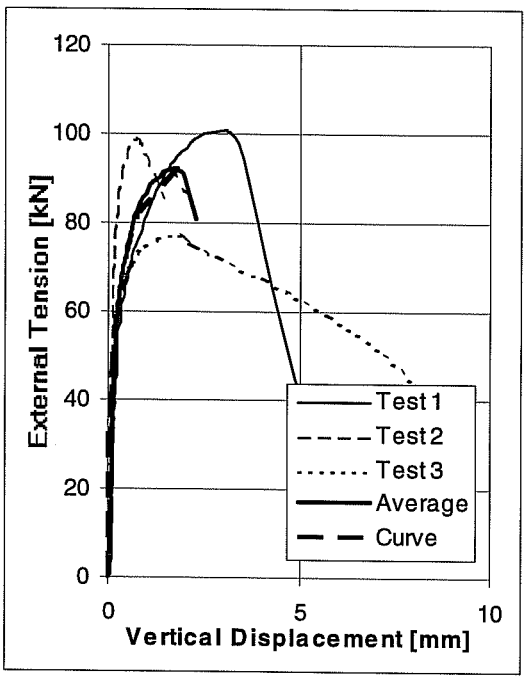

Load-Displacement Curves of Series 24a54T (Tension), Failing by Concrete Breakout UC1 5/8", h_{ef} = 3.5 inches (178 mm), c1 ≥ 11 inches (279 mm), f_c = 32.4 N/mm²

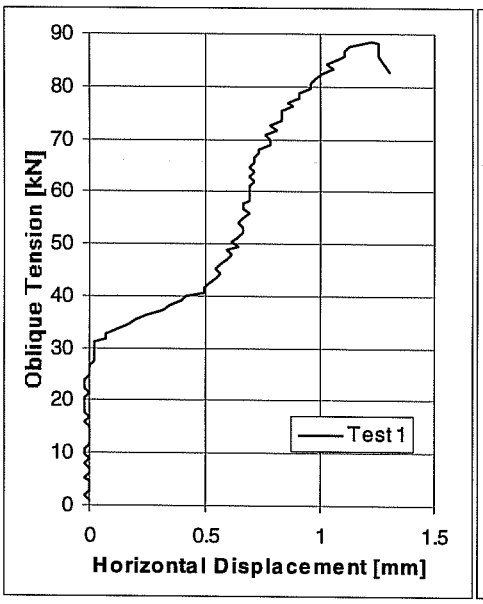

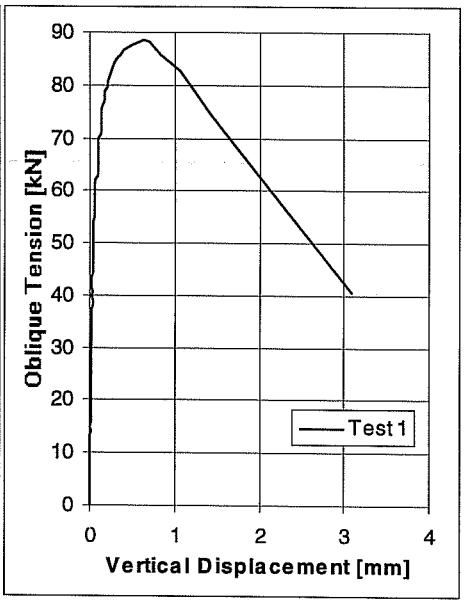

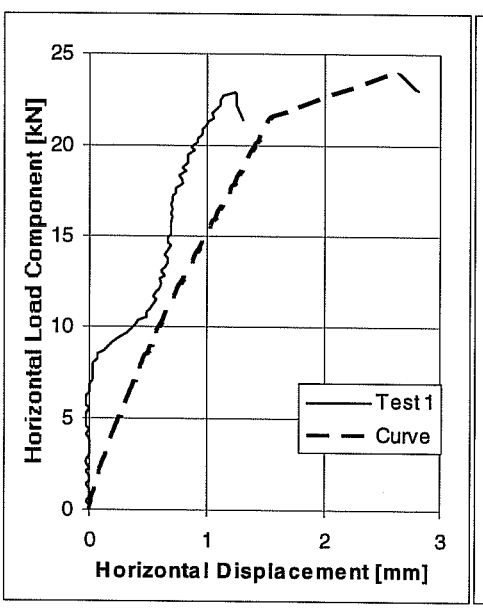

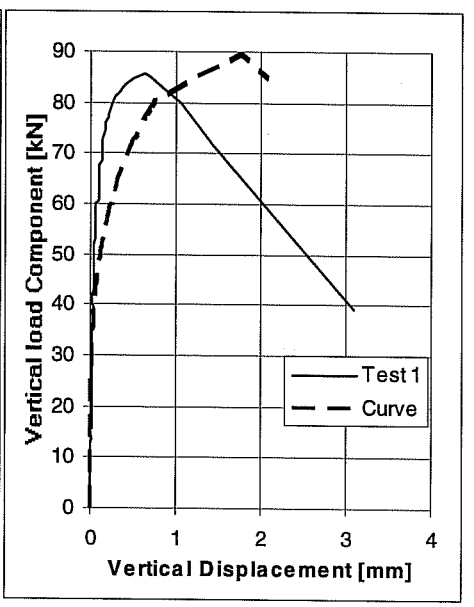

Load-Displacement Curves of Series 24a541,
UC1 5/8 inches, hef = 3.5 inches (178 mm), c1 ³ 11 inches (279 mm),
f_c = 32.4 N/mm², Loading Angle 15° from Anchor Axis

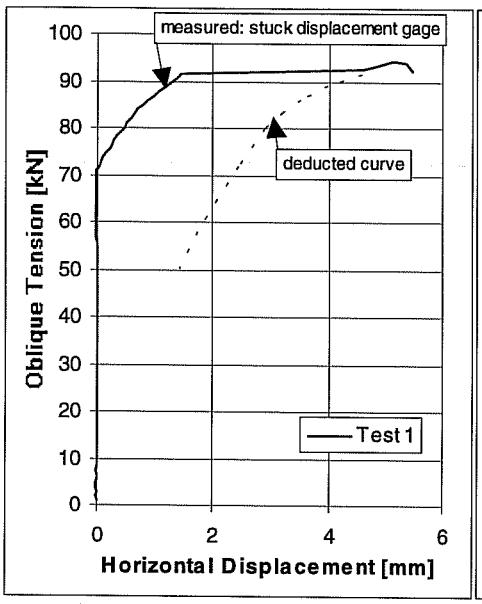

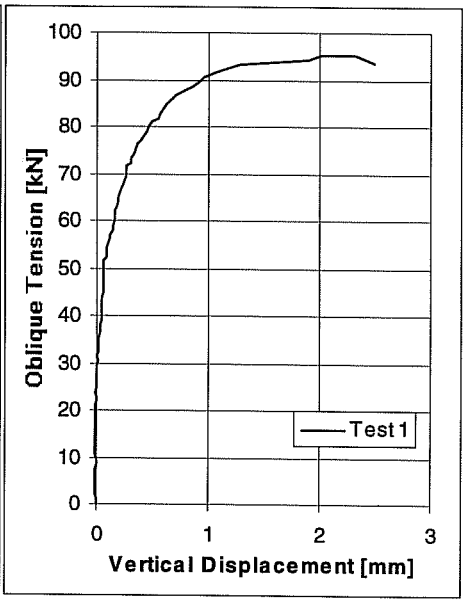

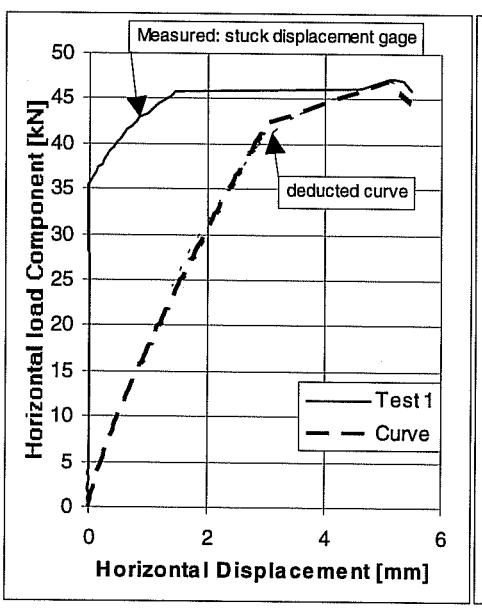

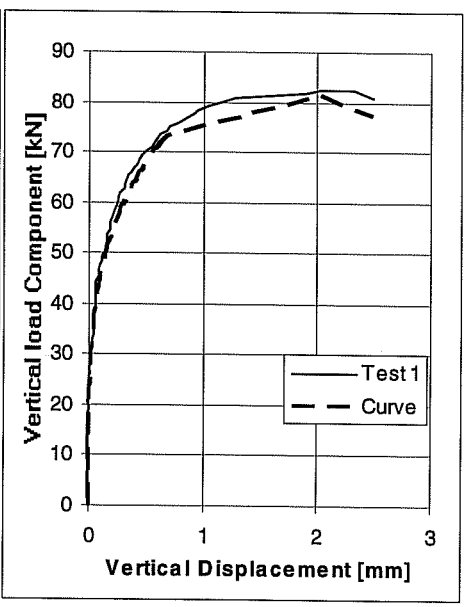

Load-Displacement Curves of Series 24a543,
UC1 5/8 inches, hef = 3.5 inches (178 mm), c1 ³ 11 inches (279 mm),
f_c = 32.4 N/mm², Loading Angle 30° from Anchor Axis

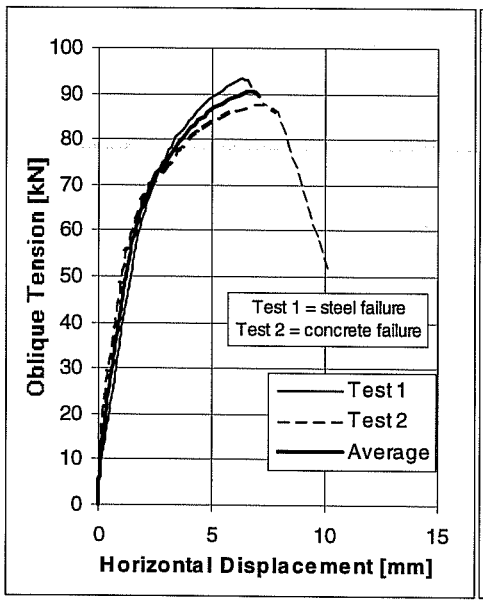

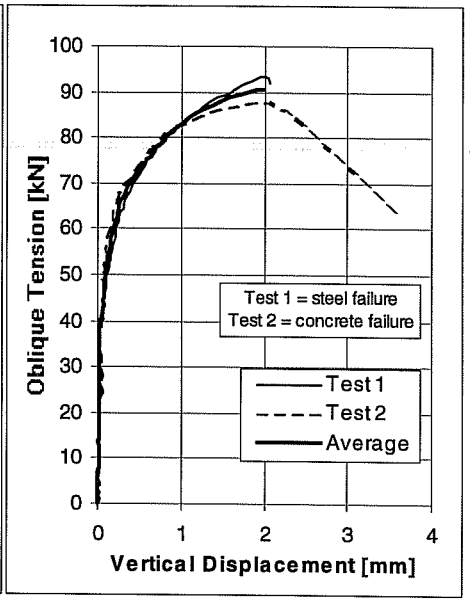

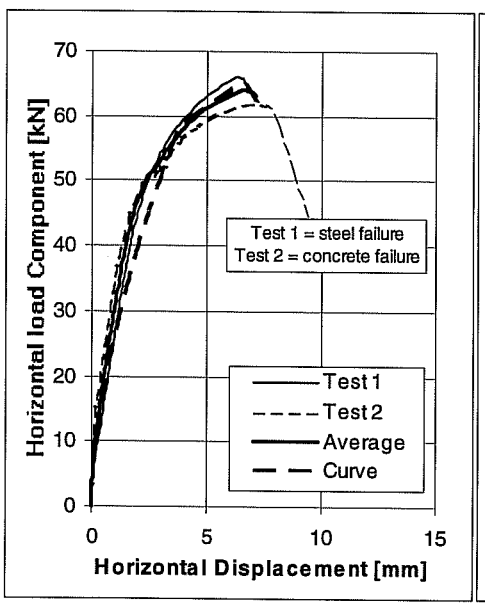

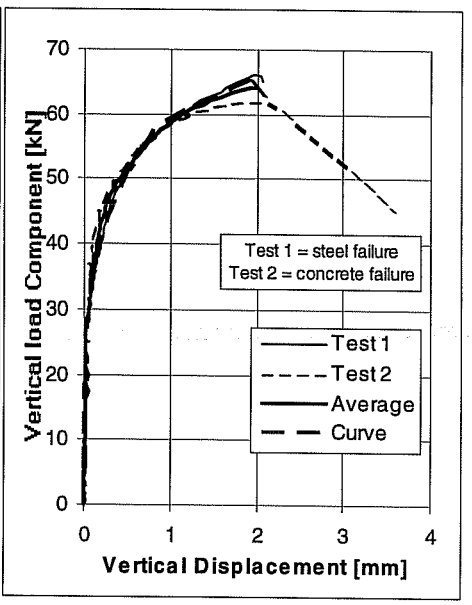

Load-Displacement Curves of Series 24a544,
UnUC1 5/8 inches, hef = 3.5 inches (89 mm), c1 ³ 11 inches (279 mm),
f_c = 32.4 N/mm², Loading Angle 45° from Anchor Axis

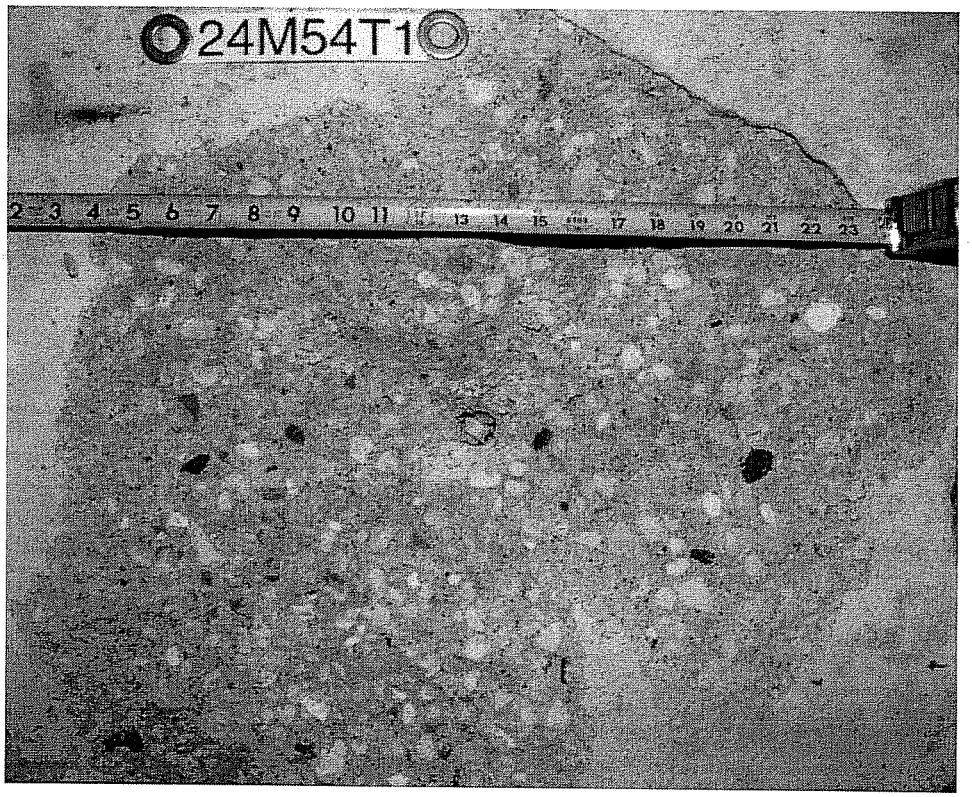

Failure Picture of Test 24M54T1 (Series 24A54), UC1 5/8", h_{ef} = 89 mm, c1 ≥ 279 mm, Pure Tension

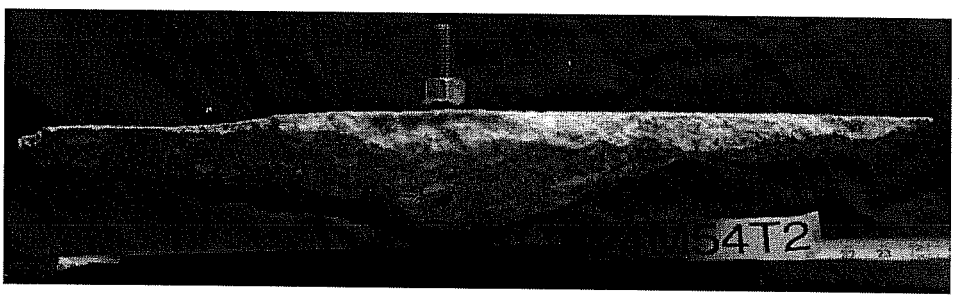

Failure Picture of Test 24M54T1 (Series 24A54), UC1 5/8", h_{ef} = 89 mm, c1 ≥ 279 mm, Pure Tension

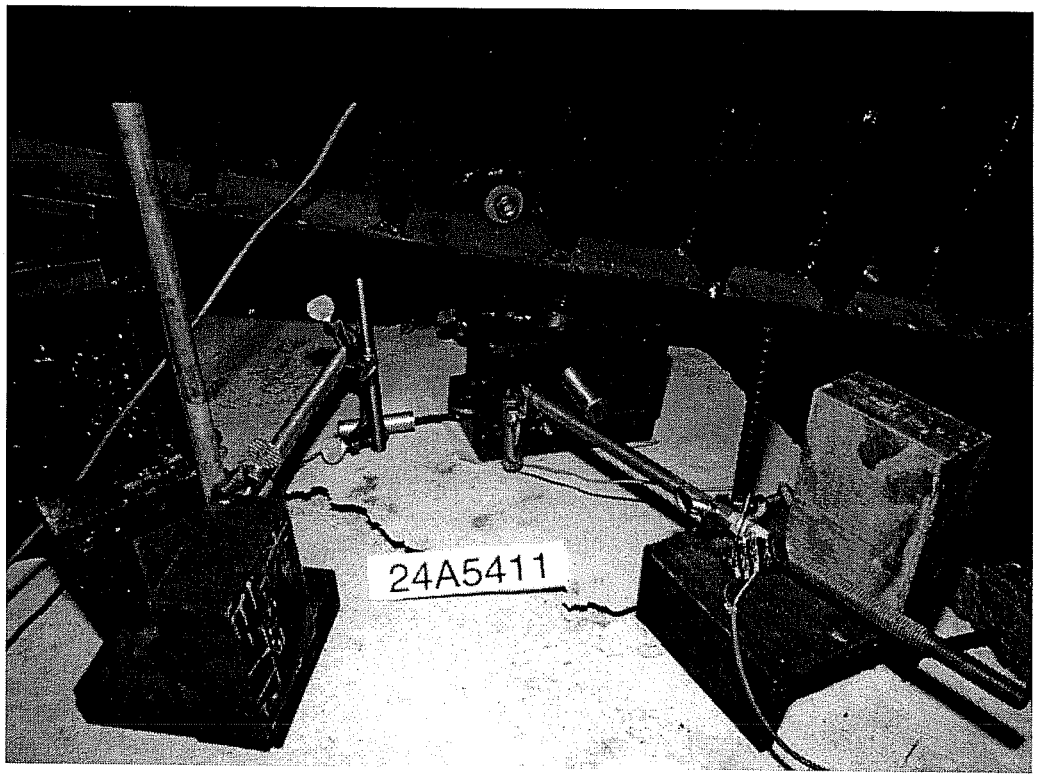

Failure Picture of Test 24A5411, UC1 5/8", h_{ef} = 89 mm, c1 ≥ 279 mm, Oblique Tension 15°

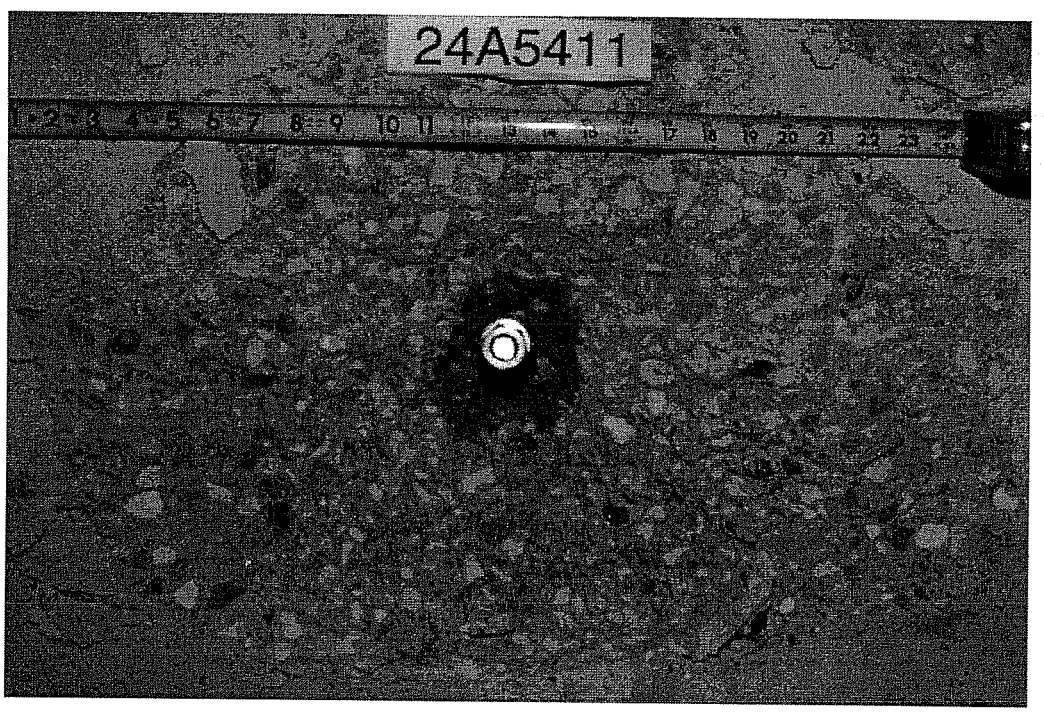

Failure Picture of Test 24A5411, UC1 5/8", h_{ef} = 89 mm, c1 ≥ 279 mm, Oblique Tension 15°

Failure Picture of Test 24A5431, UC1 5/8", h_{ef} = 89 mm, c1 ≥ 279 mm, Oblique Tension 30°

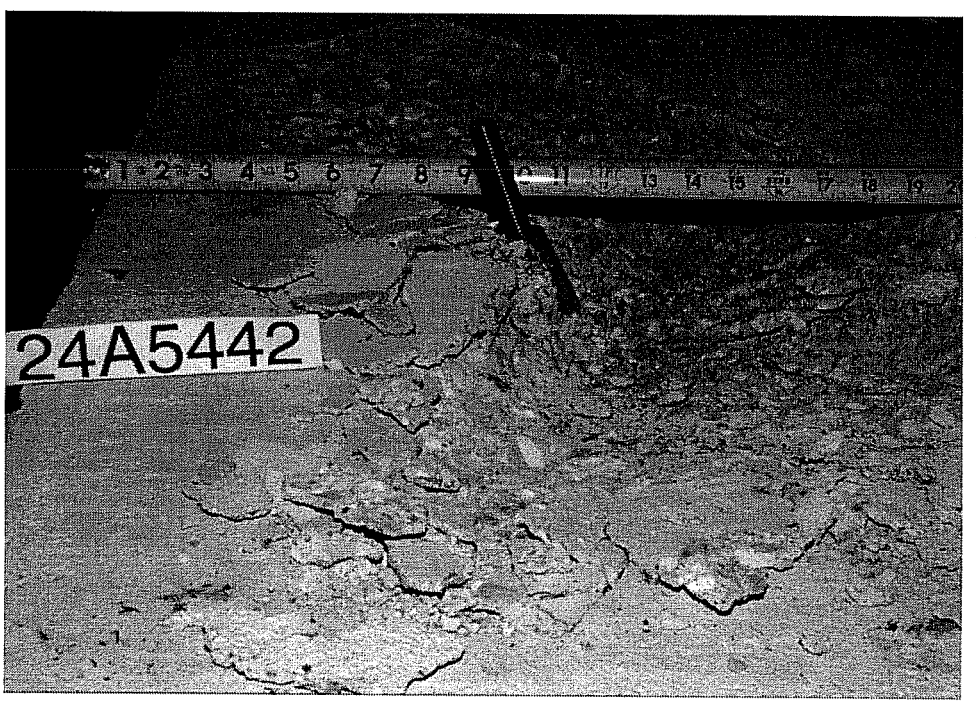

Failure Picture of Test 24A5442, UC1 5/8", h_{ef} = 89 mm, c1 ≥ 279 mm, Oblique Tension 45°

Test No.	Anchor 1)	Diameter mm / in	Embed. h_{ef} mm	Torque Nm	Block No. 2)	Concrete Strength f_c N/mm²	Failure Load F_u [kN]	F_u (f_c=32.4) kN	Hor. Displ. $d_{H,u}$ 3) mm	Vert. Displ. 3) 4) $d_{V,7,u}$ mm	$d_{V,t2,u}$ mm	Gap L 5) mm	Failure Mode 6)	Note
25H6421	Sleeve	M16	177.8	203/102	L31-T	34.9	109.55	-	5.72	2.98	6.29	1.00	SB	
2	Sleeve	M16	177.8	203/102	L31-T	34.9	110.35	-	5.31		12.46	-1.20	SS	
3	Sleeve	M16	177.8	203/102	L31-B	33.8	111.50	-	5.50	4.64	8.25	0.60	SS	
Ave.							110.46							
25H6481	Sleeve	M16	177.8	203/102	L31-B	33.8	79.89	-	5.90	9.50	16.86	1.50	SZ	
2	Sleeve	M16	177.8	203/102	L31-B	33.8	77.93	-	5.92	8.55	15.10	0.10	SZ	
3	Sleeve	M16	177.8	203/102	L31-B	33.8	77.92	-	4.18	6.47	11.44	-1.20	SZ	
Ave.							78.58							
25M5421	UC1	0.75 "	177.8	244/122	L31-T	34.9	106.50	-	7.42	5.32	10.25	1.20	SS	
2	UC1	0.75 "	177.8	244/122	L31-T	34.9	110.27	-	7.01	8.67	14.73	-1.40	SS	
3	UC1	0.75 "	177.8	244/122	L31-B	33.8	114.30	-	9.66	10.90	18.72	1.60	SZ	
Ave.							110.36							
25M5481	UC1	0.75 "	177.8	244/122	L31-T	34.9	78.95	-	5.13	11.91	20.77	-1.20	SZ	
2	UC1	0.75 "	177.8	244/122	L31-B	33.8	78.39	-	7.95	12.22	21.78	0.60	SZ	
3	UC1	0.75 "	177.8	244/122	L31-B	33.8	87.87	-	6.73	15.04	28.17	-0.20	SZ	
Ave.							81.74							
25M3421	UC1	0.375 "	88.9	54/27	L31-T	34.9	36.16	-	3.88	1.22	2.29	1.00	SZ	
2	UC1	0.375 "	88.9	54/27	L31-T	34.9	35.27	-	n.g.	1.34	2.45	-2.00	SZ	
3	UC1	0.375 "	88.9	54/27	L31-T	34.9	39.45	-	4.63	2.80	5.23	1.00	SZ	
Ave.							36.96							
25M3481	UC1	0.375 "	88.9	54/27	L31-T	34.9	26.11	-	2.66	0.98	2.44	1.50	SZ	
2	UC1	0.375 "	88.9	54/27	L31-T	34.9	28.07	-	3.49	1.48	2.55	1.25	SZ	
3	UC1	0.375 "	88.9	54/27	L31-T	34.9	28.16	-	3.28	1.94	3.87	1.00	SZ	
Ave.							27.44							
26M5421	UC1	0.75 "	88.9	203/122	L32-T	41.8	84.30	74.22	2.97	1.85	2.78	0.80	BZ	
2	UC1	0.75 "	88.9	203/123	L32-B	34.2	71.76	69.84	2.74	1.75	3.64	-1.20	BZ	
3	UC1	0.75 "	88.9	203/124	L32-B	34.2	71.39	69.49	3.61	1.30	2.90	-0.40	BZ	
Ave.								71.18						
26M5481	UC1	0.75 "	88.9	203/122	L32-T	41.8	60.76	53.49	2.77	1.67	3.53	-0.30	BZ	7)
2	UC1	0.75 "	88.9	203/123	L32-T	41.8	53.40	47.01	2.64	1.68	3.13	0.20	BZ	7)
3	UC1	0.75 "	88.9	203/124	L32-B	34.2	49.02	47.71	3.50	0.96	2.07	-1.60	BZ	Splitting 8)
Ave.								49.40						

1) UC1 = Undercut anchor, Sleeve = Torque-controlled expansion sleeve anchor
2) T =Top =top surface of concrete specimen, B = Bottom = bottom surface of concrete specimen
3) displacement at maximum load
4) $d_{V,nu}$: n gives the spacing [inch] from the axis of shear anchor.
5) Gap before the montage of the nut: (+) for gap of the shear anchor, () for gap of the tension anchor; the presently different anchor is because of the wall of hole
6) SZ = Steel fracture of tension anchor, SS = Steel fracture of shear anchor, SB = Steel fracture zt both anchors simutaneously, BZ = Concrete failure at tension anchor
7) Vertical displacement measured at distanceof 6 in. from shear anchor ($d_{V,6}$) and corrected as follows: $d_{V,7} = d_{V,6} + (d_{V,t2}-d_{V,6})/6$
8) During installation of edge-close shear anchor, concrete splitting occurred.

Test Data and Results of Series 2.5 and 2.6: Two-Anchor Connection under Shear and Bending

Test No.	Anchor 1)	Diameter mm / "	Embed. Depth mm	Block No. 2)	Dimension of Shell-Shaped Concrete Spalling 3)					
					Tension Anchor (Z)			Shear Anchor (Q)		
					Lm (mm)	Bm (mm)	Tm (mm)	Lm (mm)	Bm (mm)	Tm (mm)
25H6421	Sleeve	M16	177.8	L31-T	95.3	139.7	22.2	38.1	25.4	3.2
2	Sleeve	M16	177.8	L31-T	88.9	88.9	12.7	-	-	-
3	Sleeve	M16	177.8	L31-B	63.5	88.9	15.9	44.5	25.4	3.2
25H6481	Sleeve	M16	177.8	L31-B	177.8	228.6	31.8	-	-	-
2	Sleeve	M16	177.8	L31-B	82.6	139.7	12.7	-	-	-
3	Sleeve	M16	177.8	L31-B	31.8	38.1	6.4	-	-	-
25M5421	UC1	0.75 "	177.8	L31-T	127.0	203.2	25.4	-	-	-
2	UC1	0.75 "	177.8	L31-T	76.2	88.9	15.9	69.9	63.5	6.4
3	UC1	0.75 "	177.8	L31-B	82.6	127.0	15.9	-	-	-
25M5481	UC1	0.75 "	177.8	L31-T	38.1	50.8	6.4	-	-	-
2	UC1	0.75 "	177.8	L31-B	101.6	127.0	25.4	50.8	76.2	9.5
3	UC1	0.75 "	177.8	L31-B	50.8	76.2	15.9	63.5	63.5	15.9
25M3421	UC1	0.375 "	88.9	L31-T	-	-	-	-	-	-
2	UC1	0.375 "	88.9	L31-T	38.1	31.8	3.2	-	-	-
3	UC1	0.375 "	88.9	L31-T	38.1	38.1	4.8	-	-	-
25M3481	UC1	0.375 "	88.9	L31-T	-	-	-	-	-	-
2	UC1	0.375 "	88.9	L31-T	-	-	-	-	-	-
3	UC1	0.375 "	88.9	L31-T	-	-	-	-	-	-

1) UC1 = Undercut anchor, Sleeve = Torque-controlled expansion sleeve anchor

2) T =Top = top surface of concrete specimen, B = Bottom = bottom surface of concrete specimen

3) Lm = length at load direction, Bm = width, Tm = depth

Sizes of the Shell-Shaped Concrete Spalling at Shear Direction in Front of the Anchor, Series 2.5 and 2.6: Two-Anchor Connections under Shear and Bending

Test 25H6421, Sleeve M16, e = 12 inches (304.8 mm)
Steel Failure of Both Anchors
- Results of Displacement Measurement -

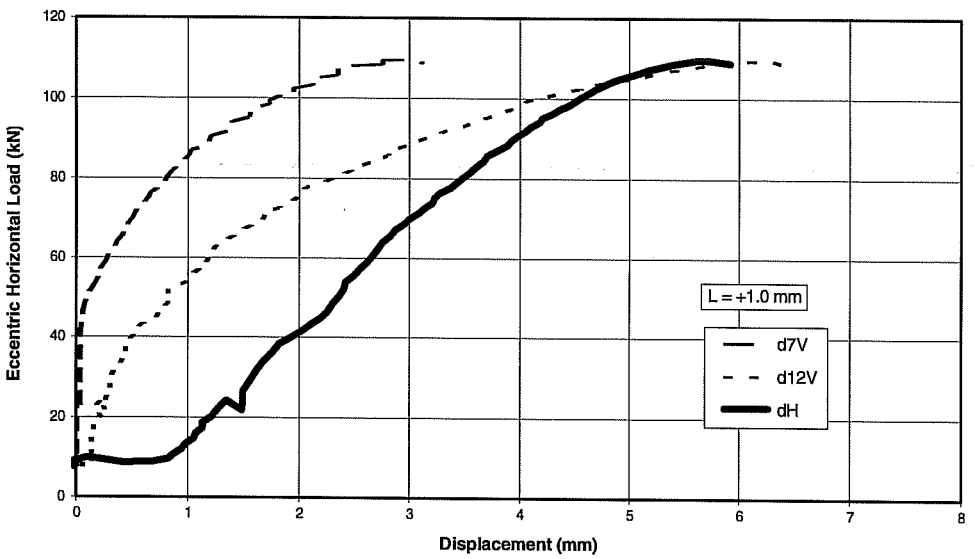

- Force and Bending Moment -

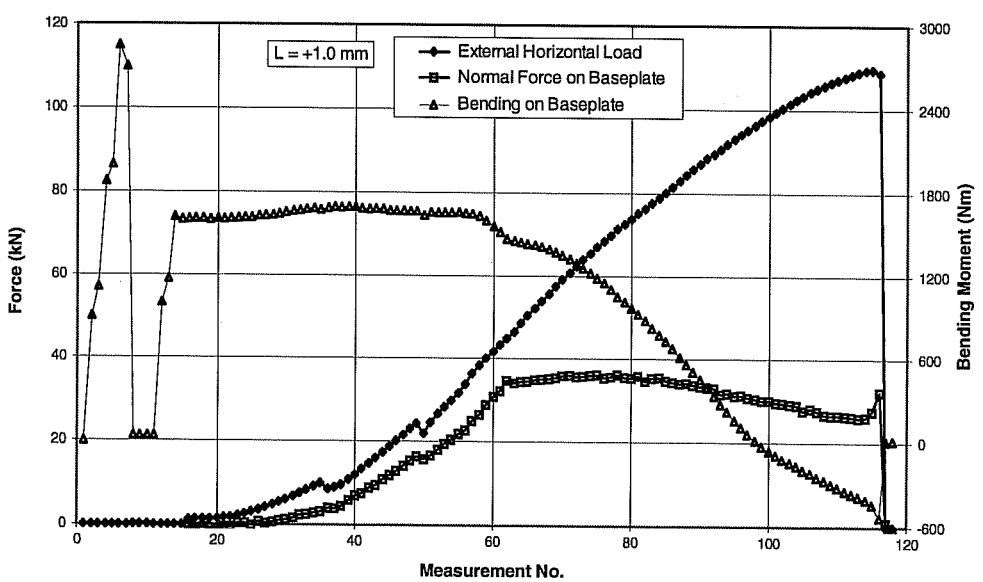

Test 25H6422, Sleeve M16, e = 12 inches (304.8 mm), Steel Failure of Shear Anchor

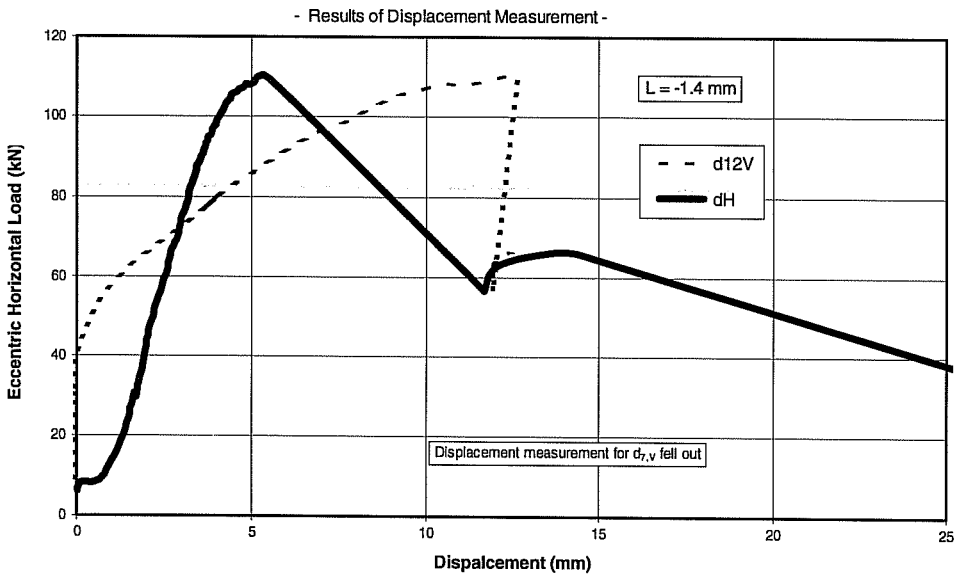

- Force and Bending Moment -

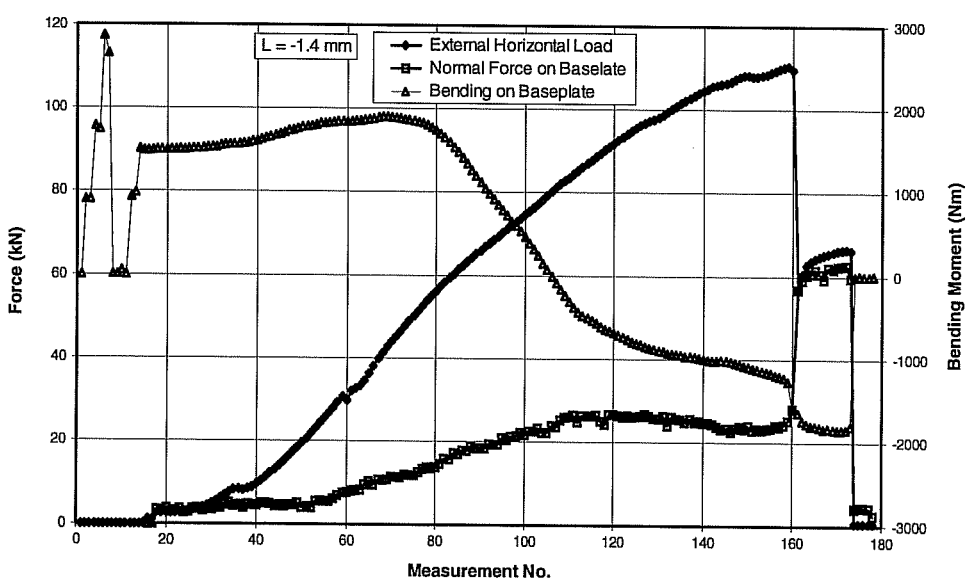

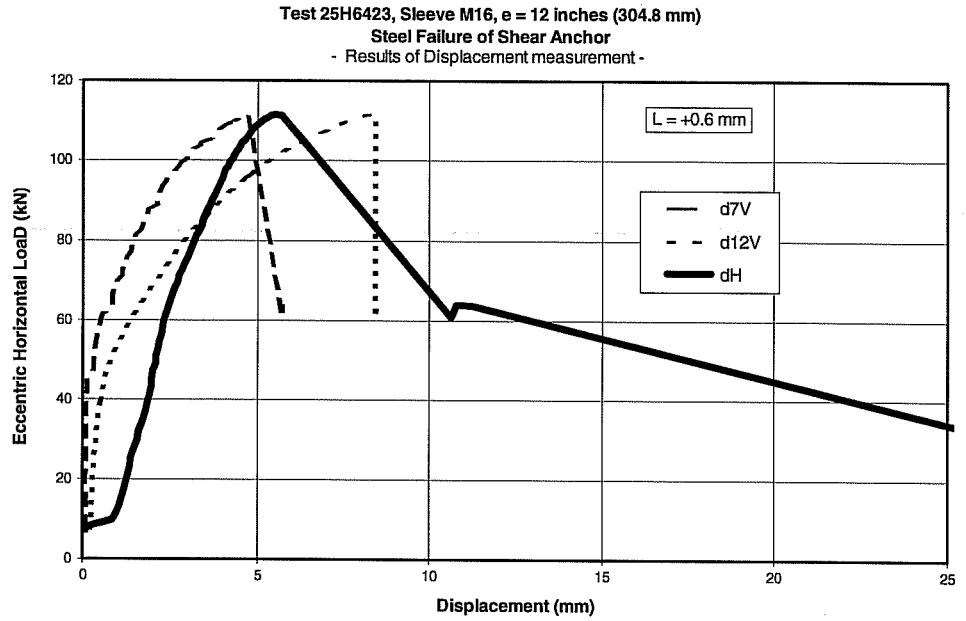
Test 25H6423, Sleeve M16, e = 12 inches (304.8 mm)
Steel Failure of Shear Anchor
- Results of Displacement measurement -
L = +0.6 mm
d7V
d12V
dH
Eccentric Horizontal LoaD (kN)
Displacement (mm)
0
20
40
60
80
100
120
0
5
10
15
20
25

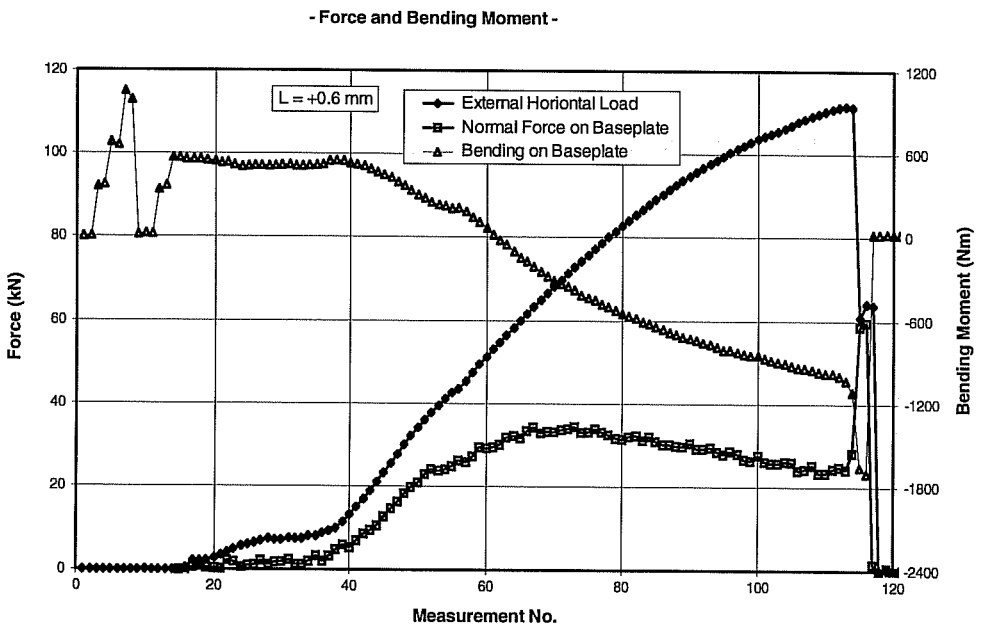
- Force and Bending Moment -
L = +0.6 mm
External Horiontal Load
Normal Force on Baseplate
Bending on Baseplate
Force (kN)
Bending Moment (Nm)
Measurement No.
0
20
40
60
80
100
120
1200
600
0
-600
-1200
-1800
-2400

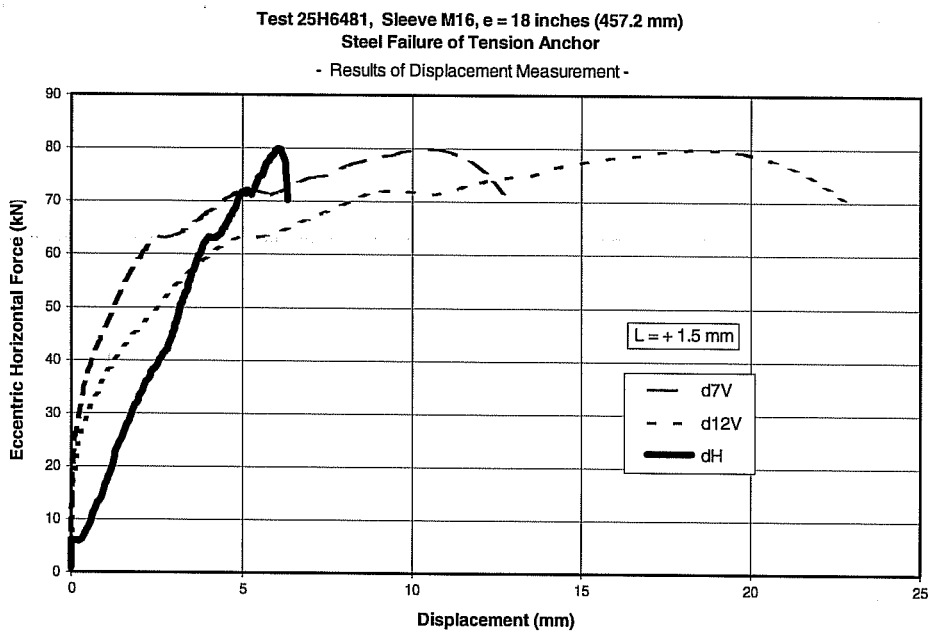
Test 25H6481, Sleeve M16, e = 18 inches (457.2 mm)
Steel Failure of Tension Anchor
- Results of Displacement Measurement -
Eccentric Horizontal Force (kN)
Displacement (mm)
L = + 1.5 mm
d7V
d12V
dH

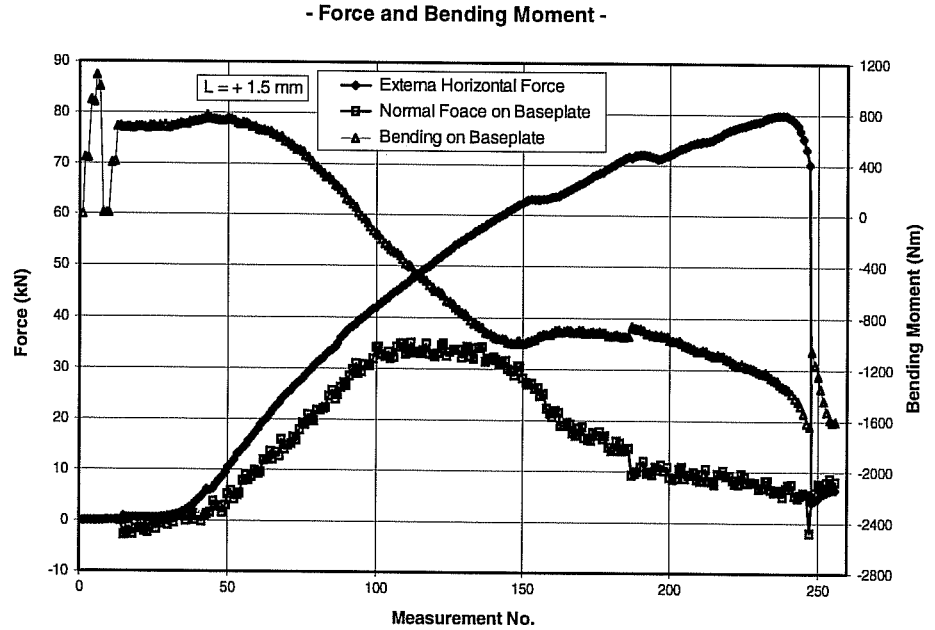
- Force and Bending Moment -
L = + 1.5 mm
Externa Horizontal Force
Normal Foace on Baseplate
Bending on Baseplate
Force (kN)
Bending Moment (Nm)
Measurement No.

Test 25H6482, Sleeve M16, e = 18 inches (457.2 mm)
Steel Failure of Tension Anchor

- Results of Displacement Measurement -

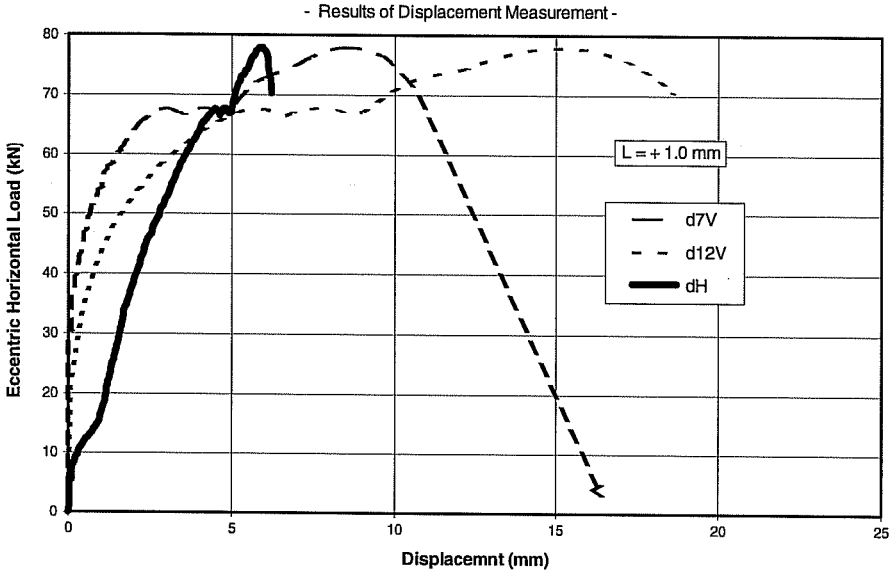

- Force and Bending Moment -

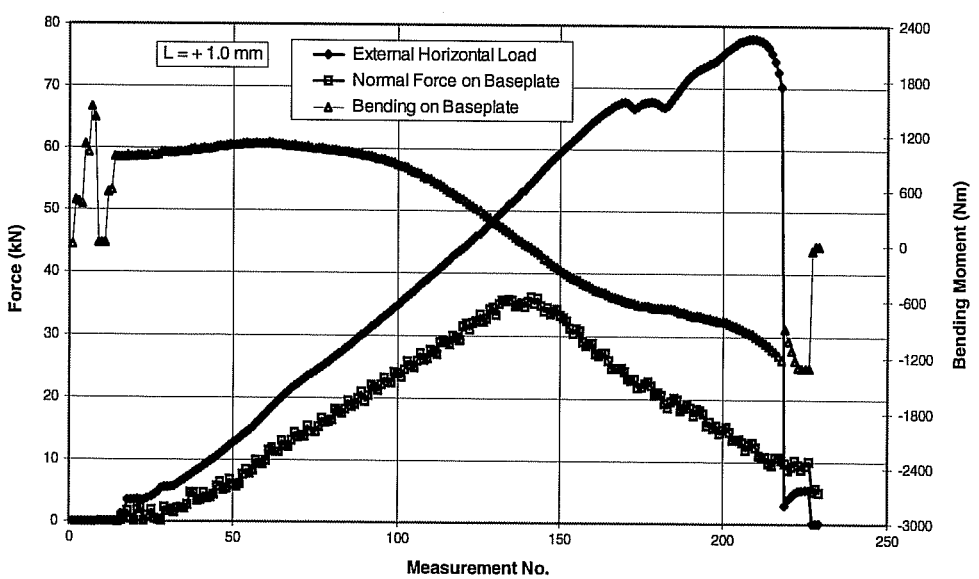

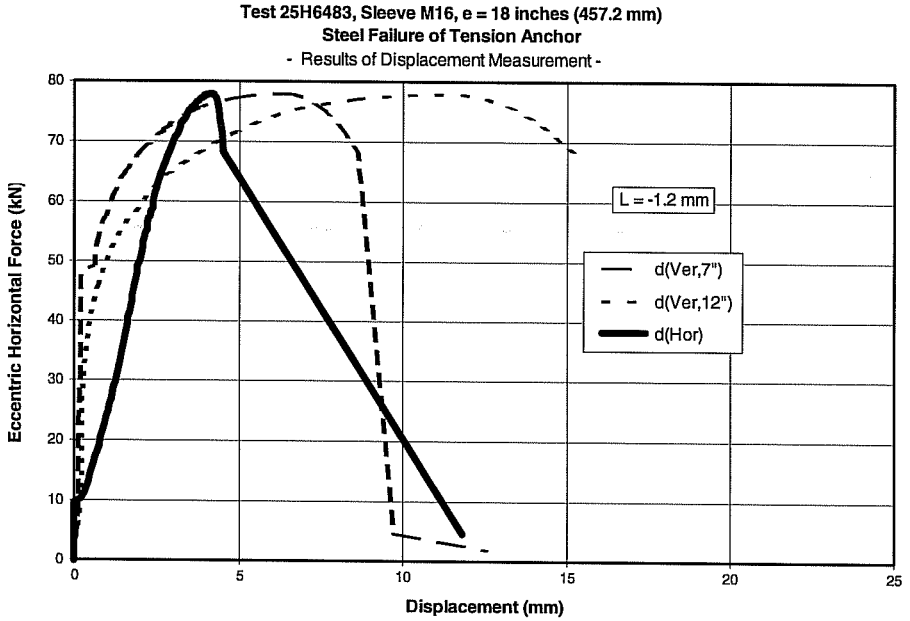
Test 25H6483, Sleeve M16, e = 18 inches (457.2 mm)
Steel Failure of Tension Anchor
- Results of Displacement Measurement -
Eccentric Horizontal Force (kN)
Displacement (mm)
L = -1.2 mm
d(Ver,7")
d(Ver,12")
d(Hor)
0
10
20
30
40
50
60
70
80
0
5
10
15
20
25

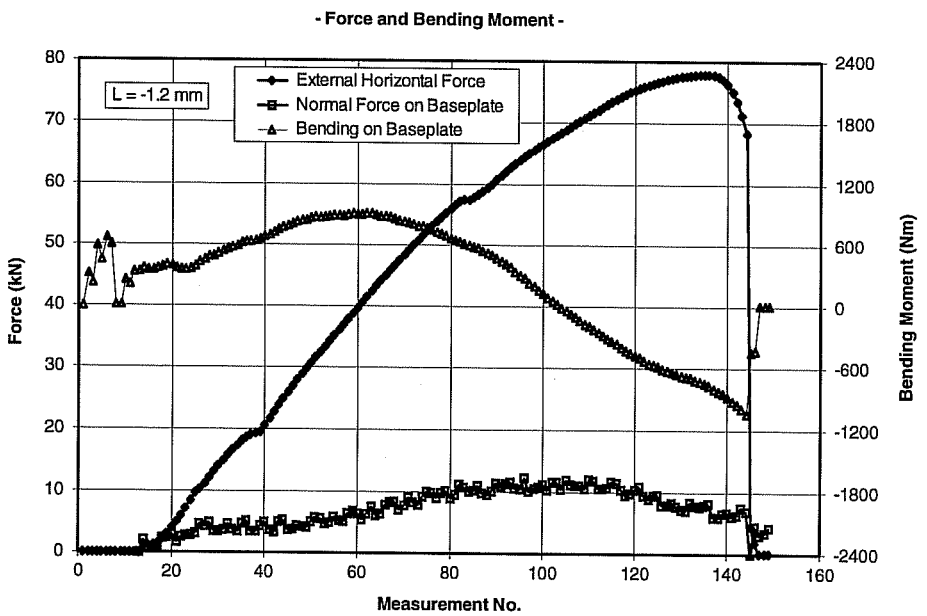
- Force and Bending Moment -
L = -1.2 mm
External Horizontal Force
Normal Force on Baseplate
Bending on Baseplate
Force (kN)
Bending Moment (Nm)
Measurement No.
0
10
20
30
40
50
60
70
80
2400
1800
1200
600
0
-600
-1200
-1800
-2400
0
20
40
60
80
100
120
140
160

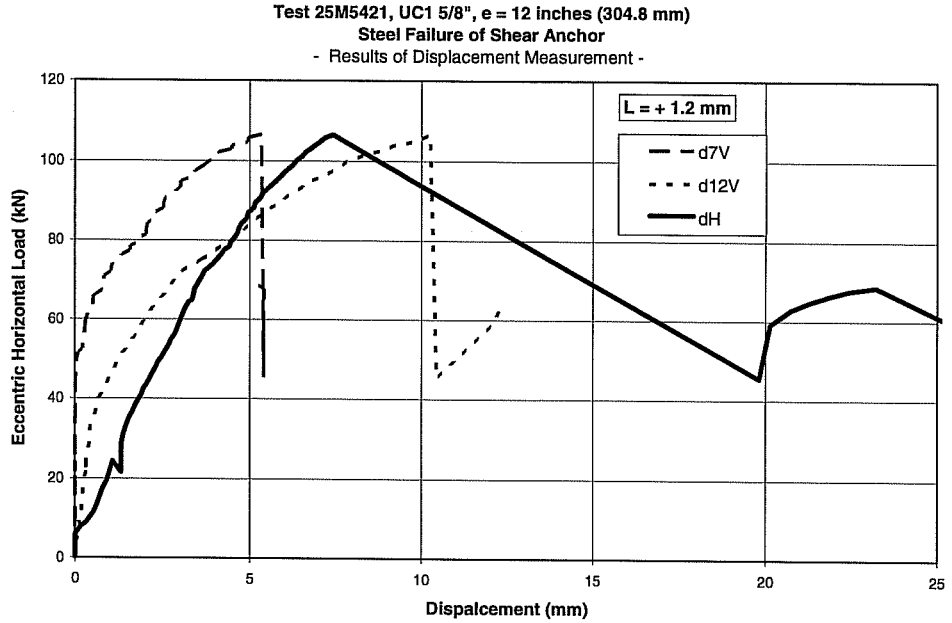
Test 25M5421, UC1 5/8", e = 12 inches (304.8 mm)
Steel Failure of Shear Anchor
- Results of Displacement Measurement -
L = + 1.2 mm
d7V
d12V
dH
Eccentric Horizontal Load (kN)
Dispalcement (mm)
0
20
40
60
80
100
120
0
5
10
15
20
25

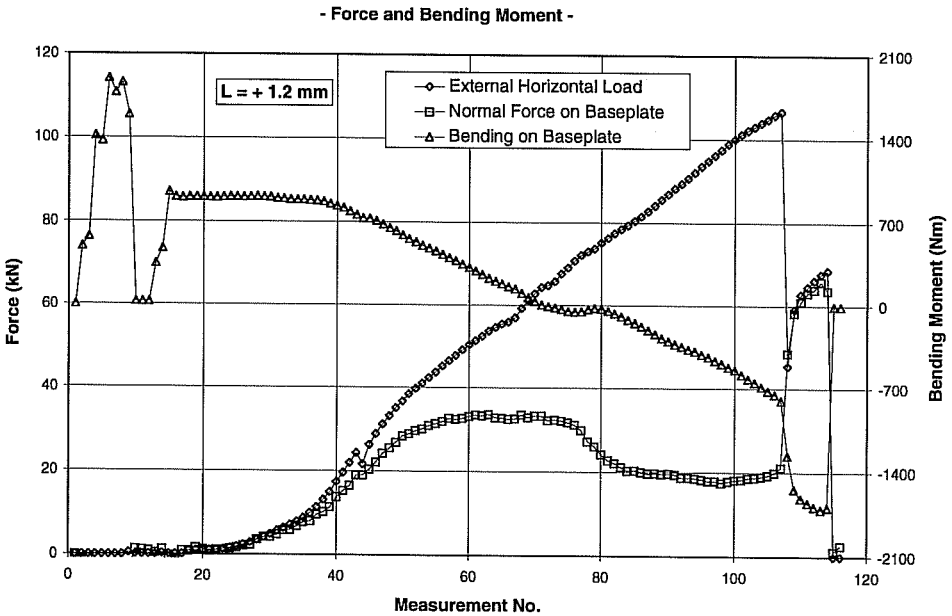
- Force and Bending Moment -
L = + 1.2 mm
External Horizontal Load
Normal Force on Baseplate
Bending on Baseplate
Force (kN)
Bending Moment (Nm)
Measurement No.
0
20
40
60
80
100
120
2100
1400
700
0
-700
-1400
-2100

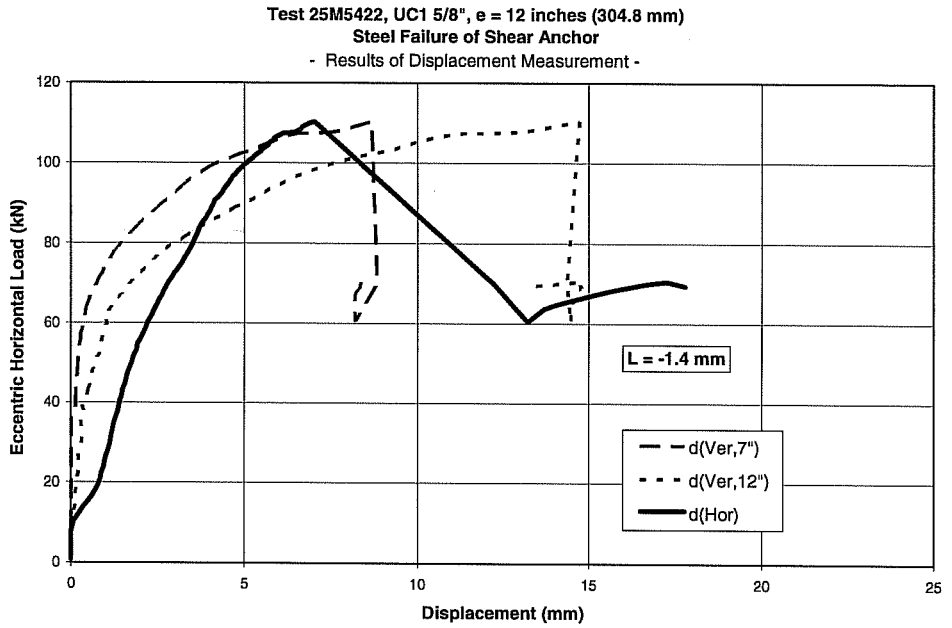
Test 25M5422, UC1 5/8", e = 12 inches (304.8 mm)
Steel Failure of Shear Anchor
- Results of Displacement Measurement -
Eccentric Horizontal Load (kN)
Displacement (mm)
L = -1.4 mm
d(Ver,7")
d(Ver,12")
d(Hor)

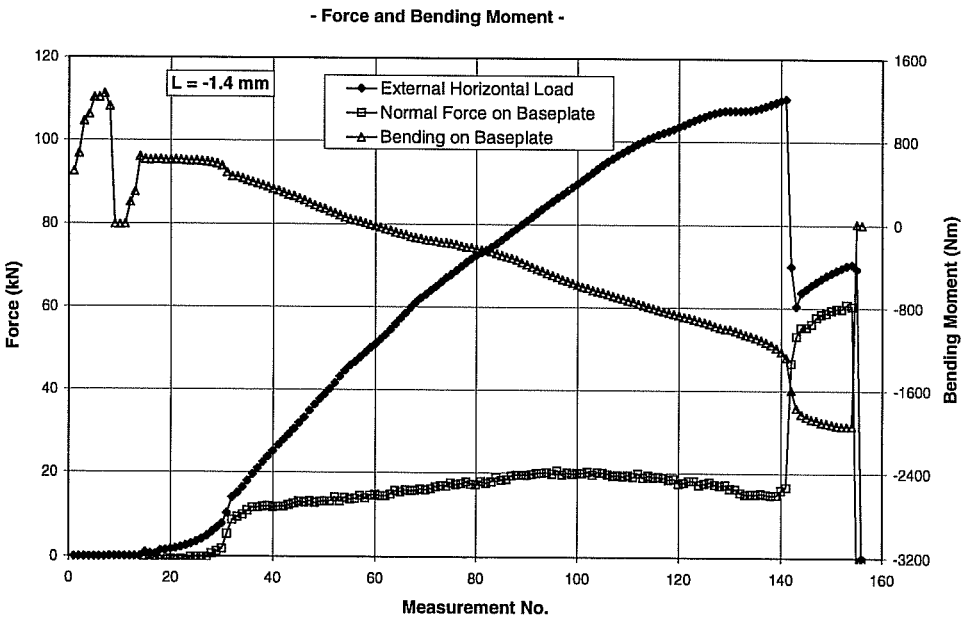
- Force and Bending Moment -
L = -1.4 mm
External Horizontal Load
Normal Force on Baseplate
Bending on Baseplate
Force (kN)
Bending Moment (Nm)
Measurement No.

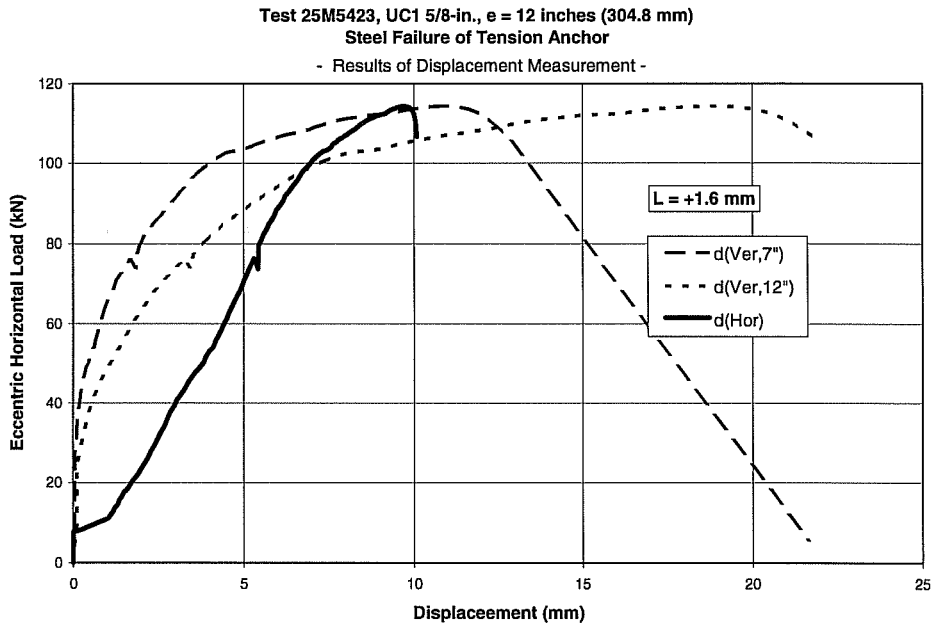
Test 25M5423, UC1 5/8-in., e = 12 inches (304.8 mm)
Steel Failure of Tension Anchor
- Results of Displacement Measurement -
Eccentric Horizontal Load (kN)
Displaceement (mm)
L = +1.6 mm
d(Ver,7")
d(Ver,12")
d(Hor)
0
20
40
60
80
100
120
0
5
10
15
20
25

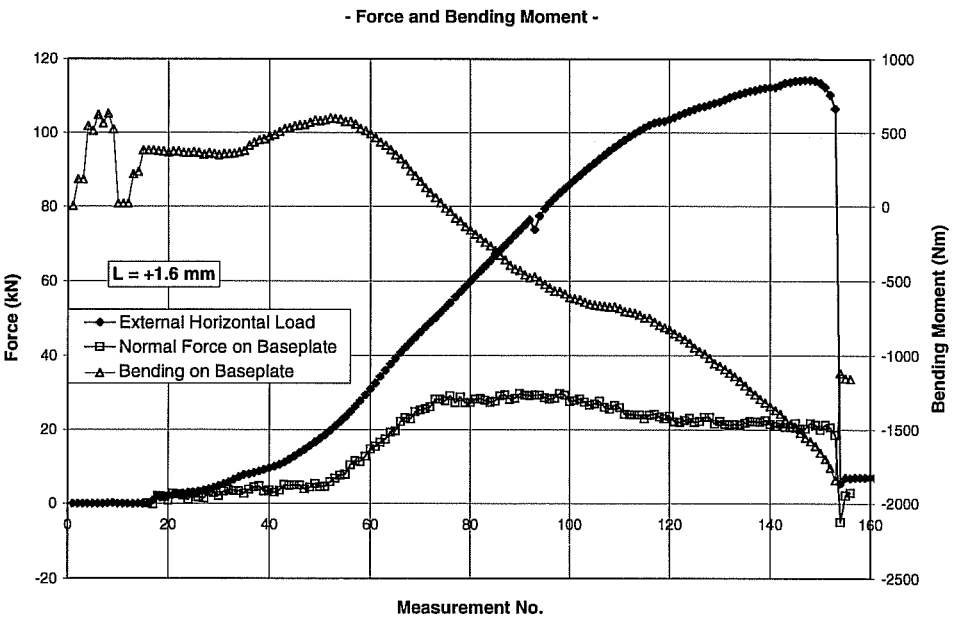
- Force and Bending Moment -
Force (kN)
Bending Moment (Nm)
Measurement No.
L = +1.6 mm
External Horizontal Load
Normal Force on Baseplate
Bending on Baseplate
120
100
80
60
40
20
0
-20
1000
500
0
-500
-1000
-1500
-2000
-2500
0
20
40
60
80
100
120
140
160

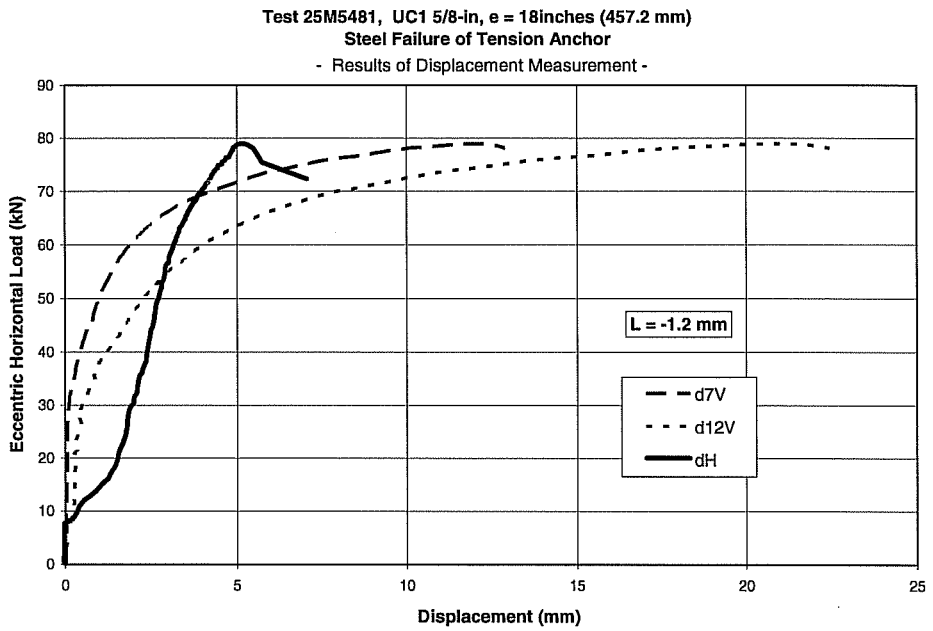
Test 25M5481, UC1 5/8-in, e = 18inches (457.2 mm)
Steel Failure of Tension Anchor
- Results of Displacement Measurement -
Eccentric Horizontal Load (kN)
Displacement (mm)
L = -1.2 mm
d7V
d12V
dH

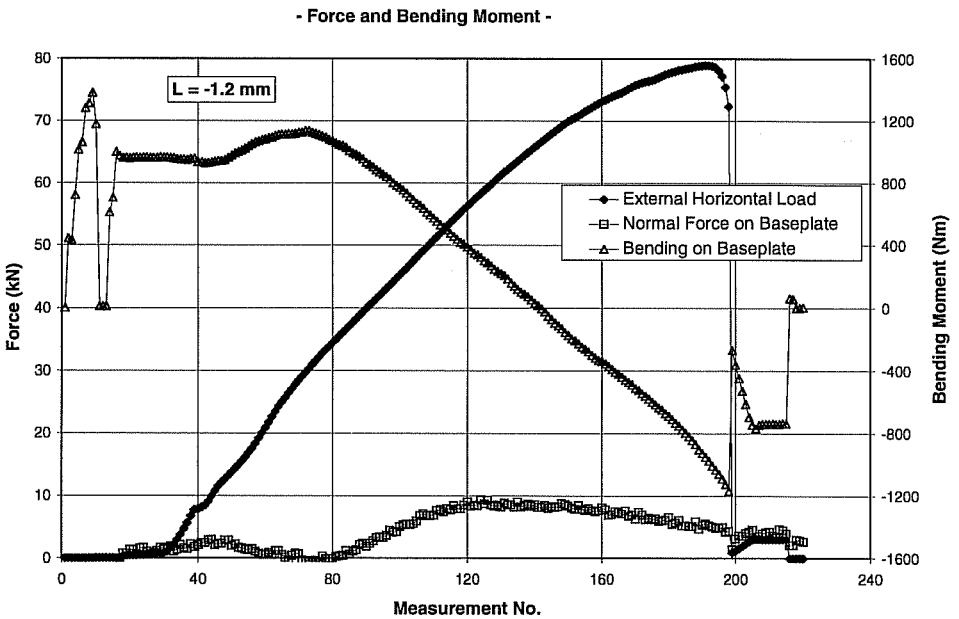
- Force and Bending Moment -
L = -1.2 mm
External Horizontal Load
Normal Force on Baseplate
Bending on Baseplate
Force (kN)
Bending Moment (Nm)
Measurement No.

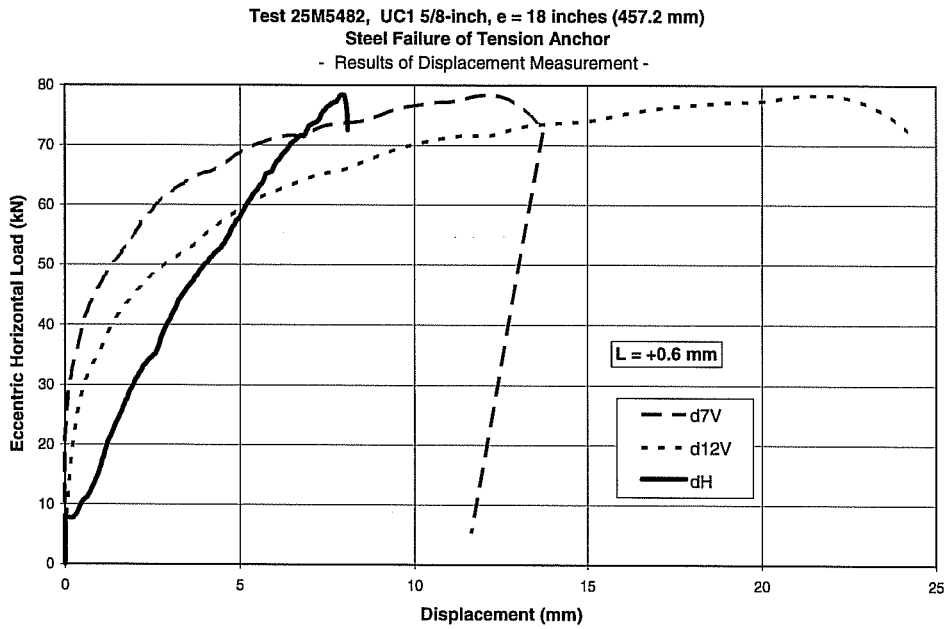
Test 25M5482, UC1 5/8-inch, e = 18 inches (457.2 mm)
Steel Failure of Tension Anchor
- Results of Displacement Measurement -
Eccentric Horizontal Load (kN)
Displacement (mm)
L = +0.6 mm
d7V
d12V
dH

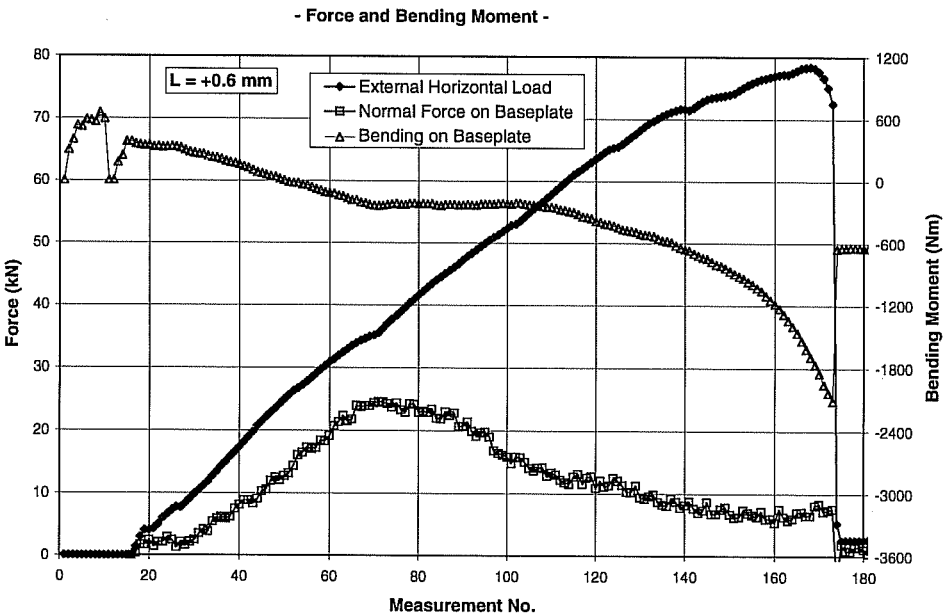
- Force and Bending Moment -
L = +0.6 mm
External Horizontal Load
Normal Force on Baseplate
Bending on Baseplate
Force (kN)
Bending Moment (Nm)
Measurement No.

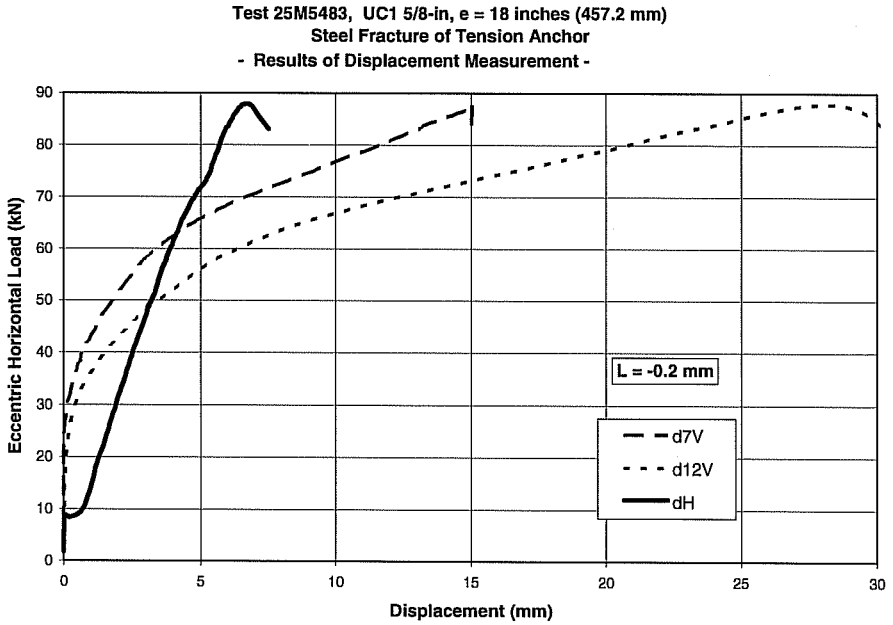
Test 25M5483, UC1 5/8-in, e = 18 inches (457.2 mm)
Steel Fracture of Tension Anchor
- Results of Displacement Measurement -
Eccentric Horizontal Load (kN)
Displacement (mm)
L = -0.2 mm
d7V
d12V
dH

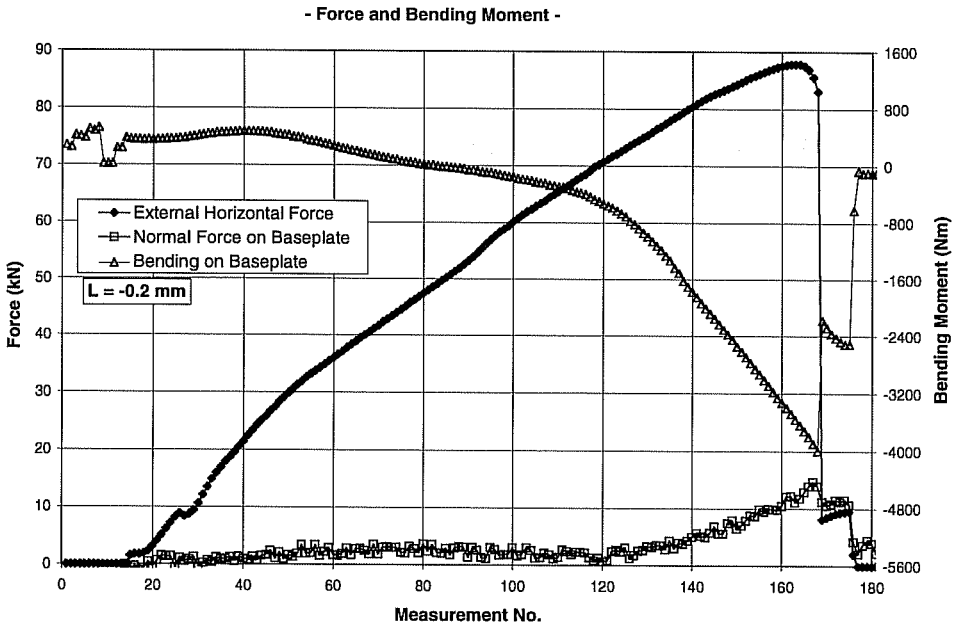
- Force and Bending Moment -
Force (kN)
Bending Moment (Nm)
Measurement No.
External Horizontal Force
Normal Force on Baseplate
Bending on Baseplate
L = -0.2 mm

Test 25M3421, UC1 3/8-in, e = 12 inches (304.8 mm)
Steel Failure of Tension Anchor
- Results of Displacement Measurement -

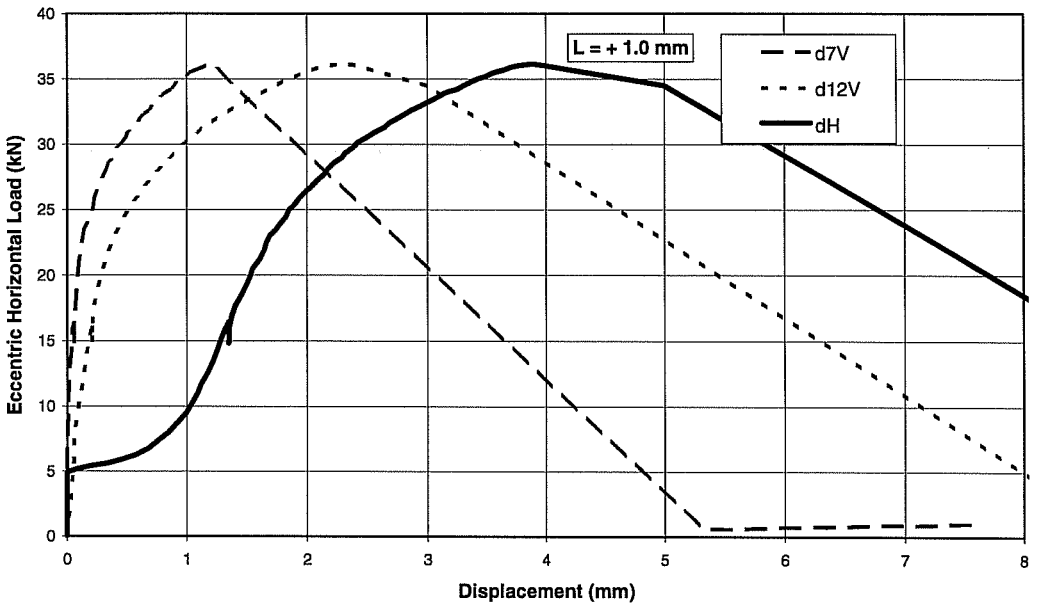

- Force and Bending Moment -

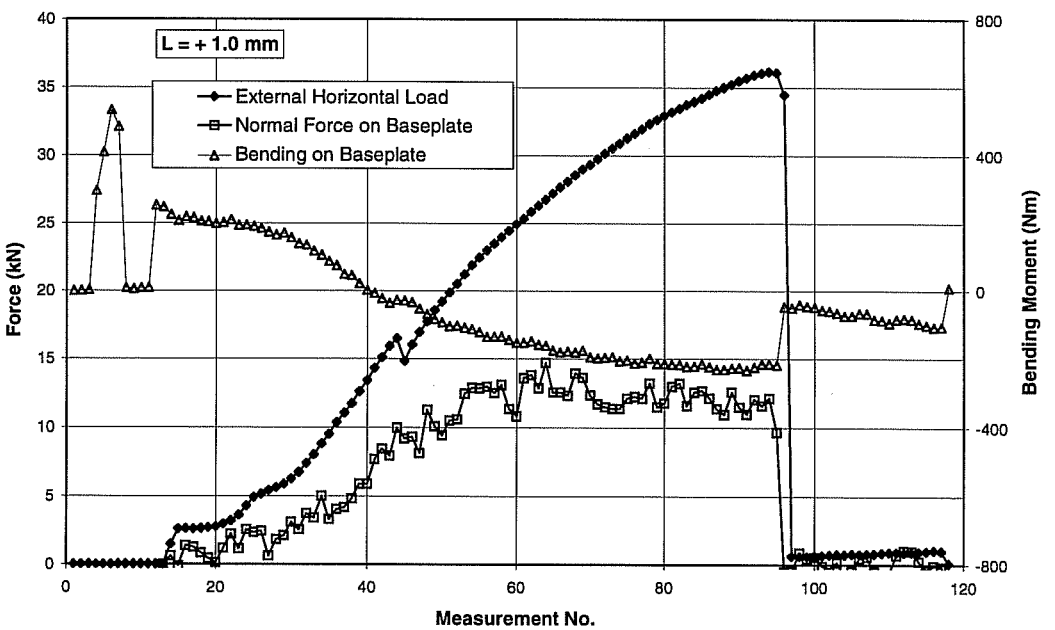

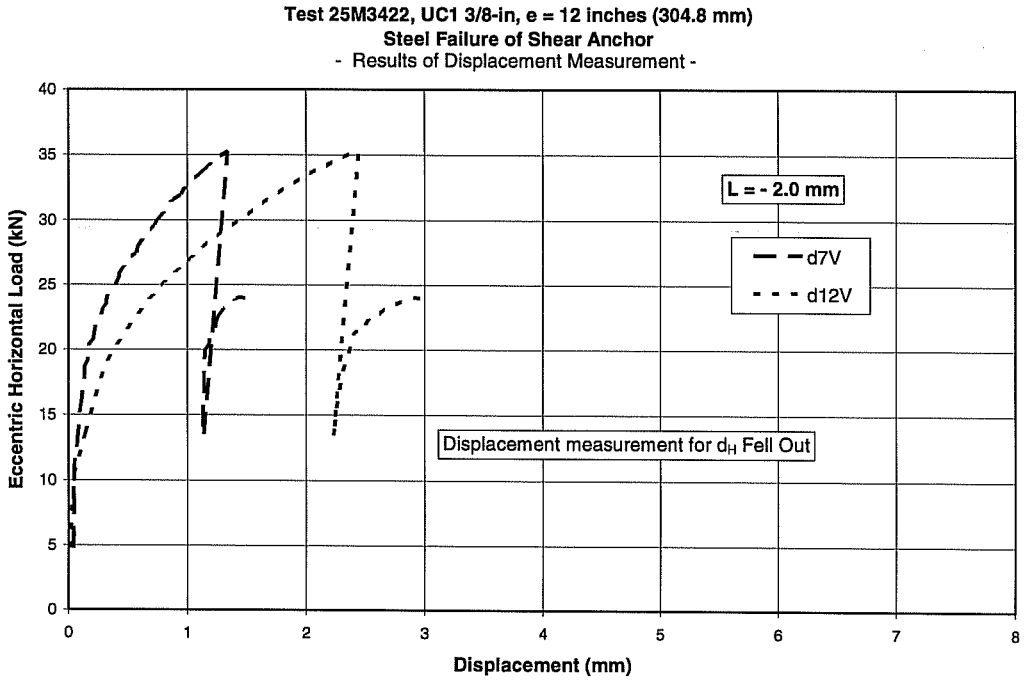
Test 25M3422, UC1 3/8-in, e = 12 inches (304.8 mm)
Steel Failure of Shear Anchor
- Results of Displacement Measurement -
Eccentric Horizontal Load (kN)
Displacement (mm)
L = - 2.0 mm
d7V
d12V
Displacement measurement for d_H Fell Out

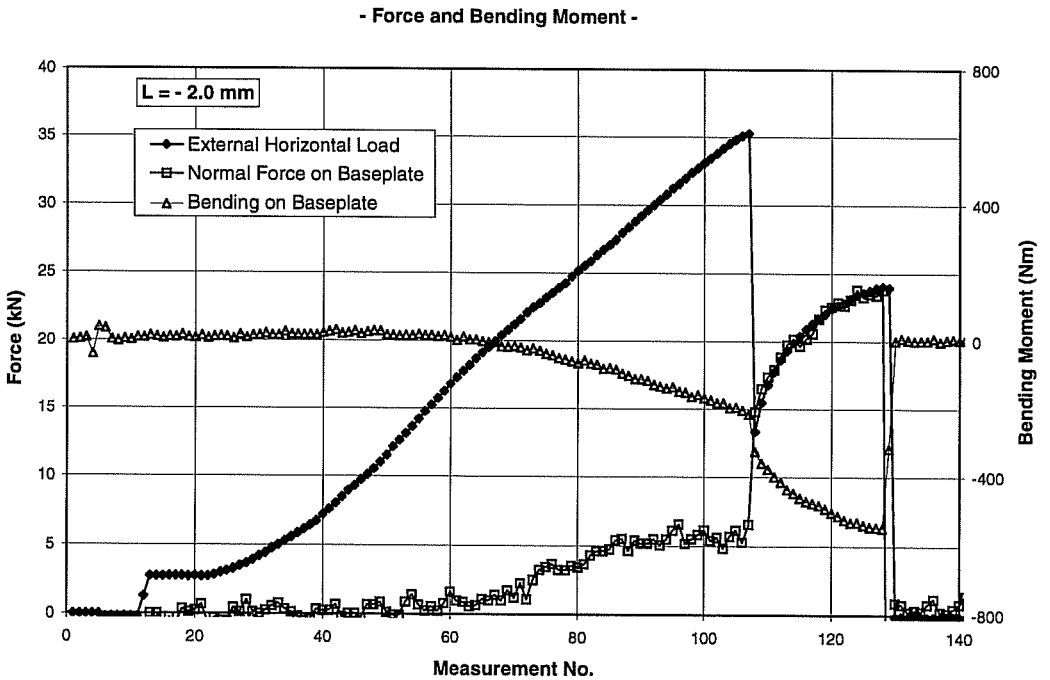
- Force and Bending Moment -
L = - 2.0 mm
External Horizontal Load
Normal Force on Baseplate
Bending on Baseplate
Force (kN)
Bending Moment (Nm)
Measurement No.

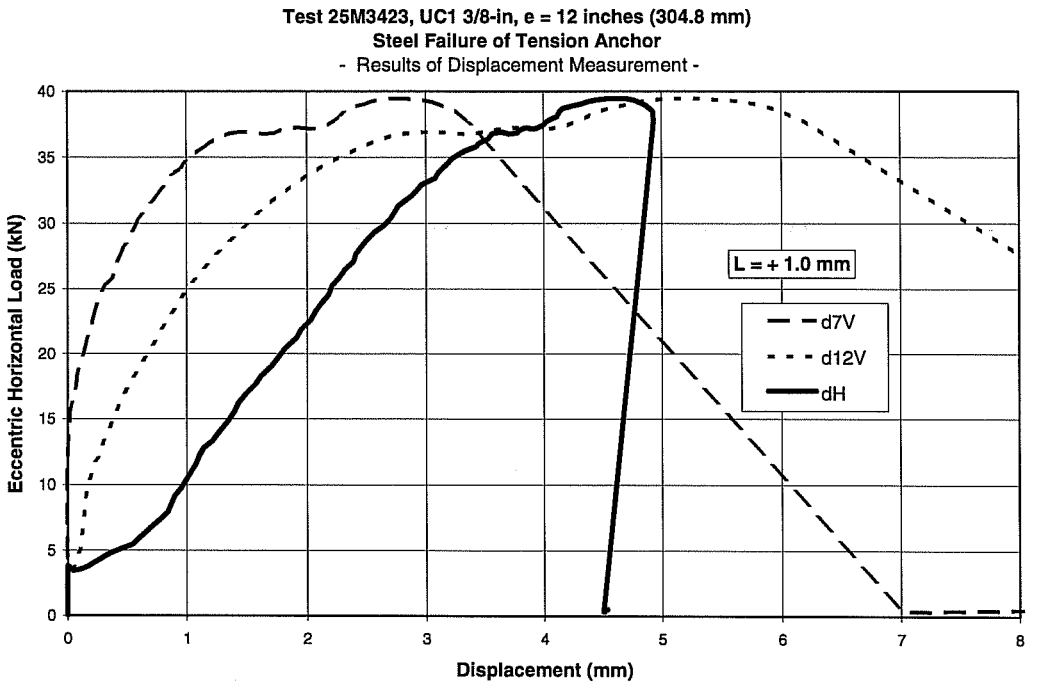
Test 25M3423, UC1 3/8-in, e = 12 inches (304.8 mm)
Steel Failure of Tension Anchor
- Results of Displacement Measurement -
Eccentric Horizontal Load (kN)
Displacement (mm)
L = + 1.0 mm
d7V
d12V
dH

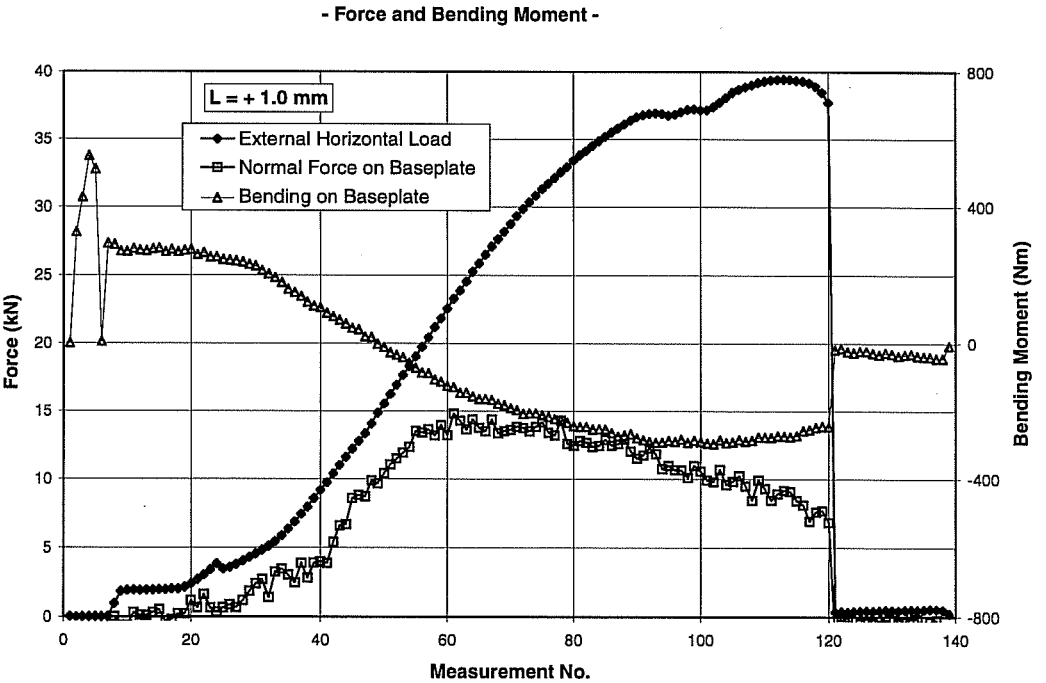
- Force and Bending Moment -
L = + 1.0 mm
External Horizontal Load
Normal Force on Baseplate
Bending on Baseplate
Force (kN)
Bending Moment (Nm)
Measurement No.

Test 25M3481, UC1 3/8", e = 18 inches (457.2 mm), Steel Failure at Tension Anchor

- Results of Displacement Measurement -

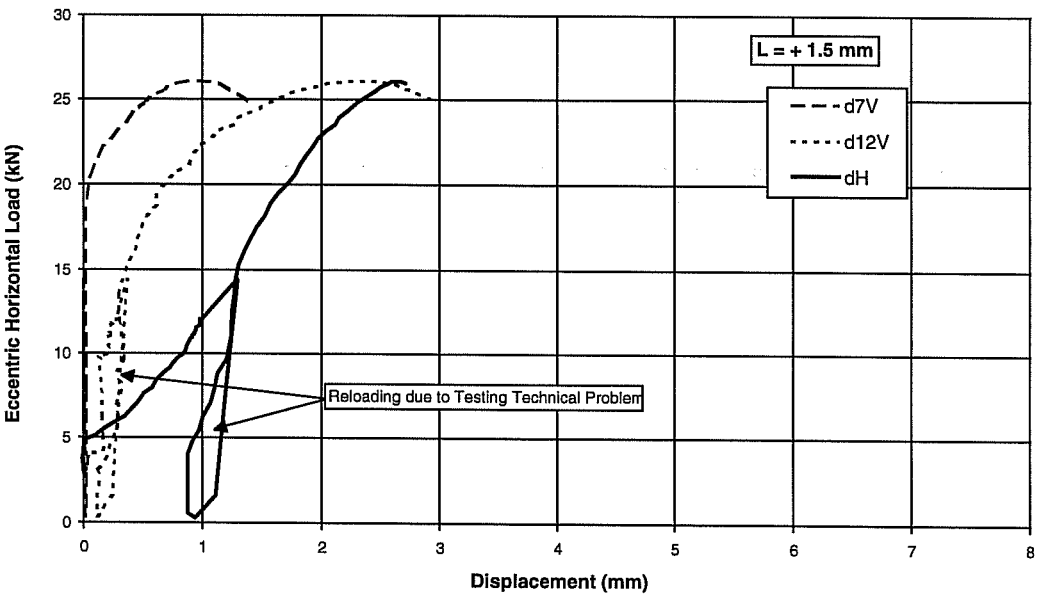

- Force and Bending Moment -

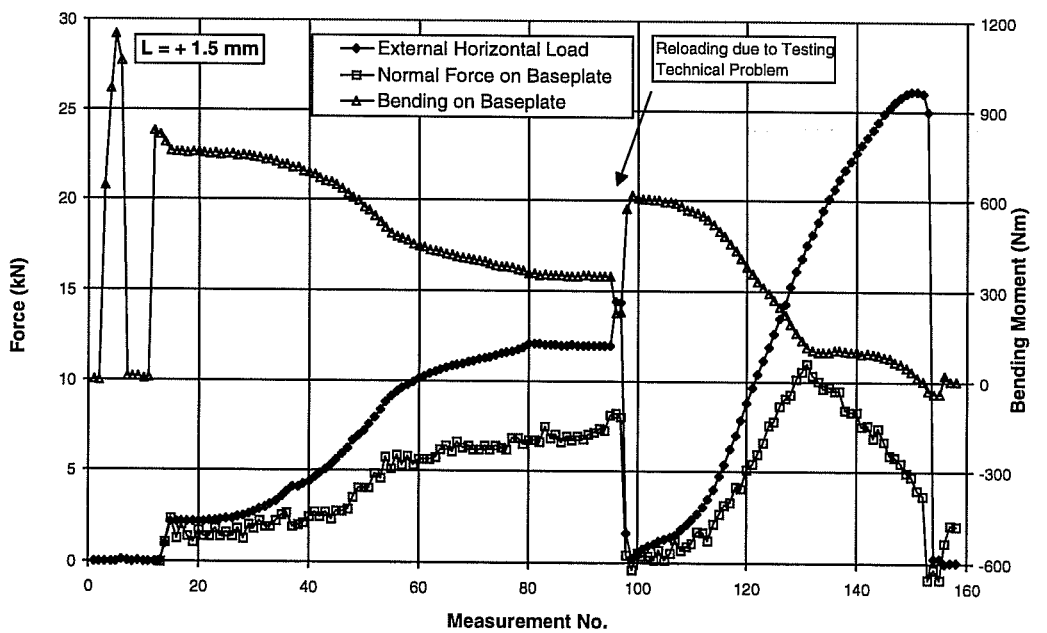

Test 25M3482, HSD 3/8", e = 18" = 457.2 mm, Steel Failure at Tension Anchor

- Results of Displacement Measurement -

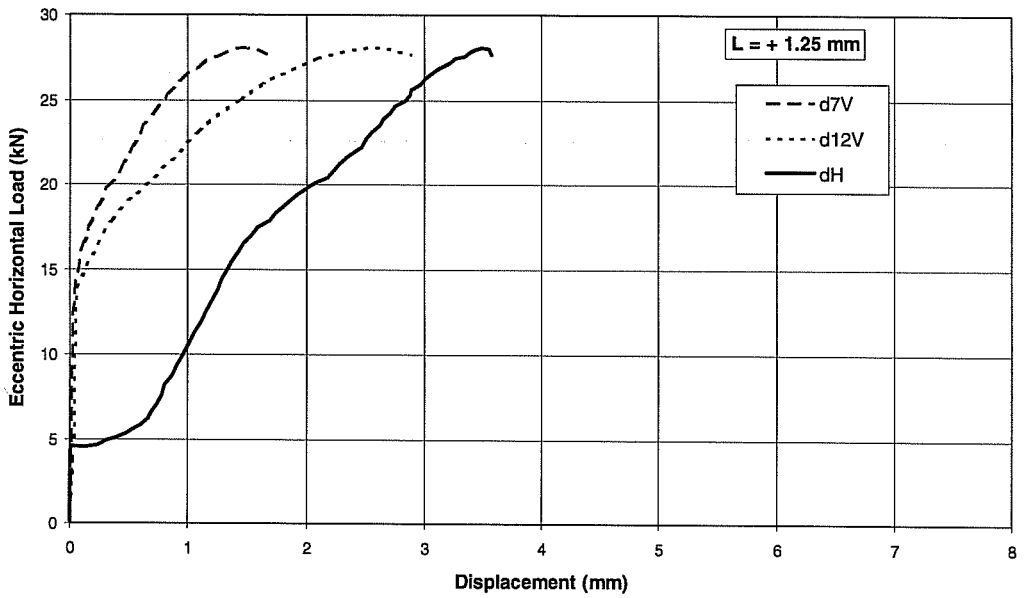

- Force and Bending Moment -

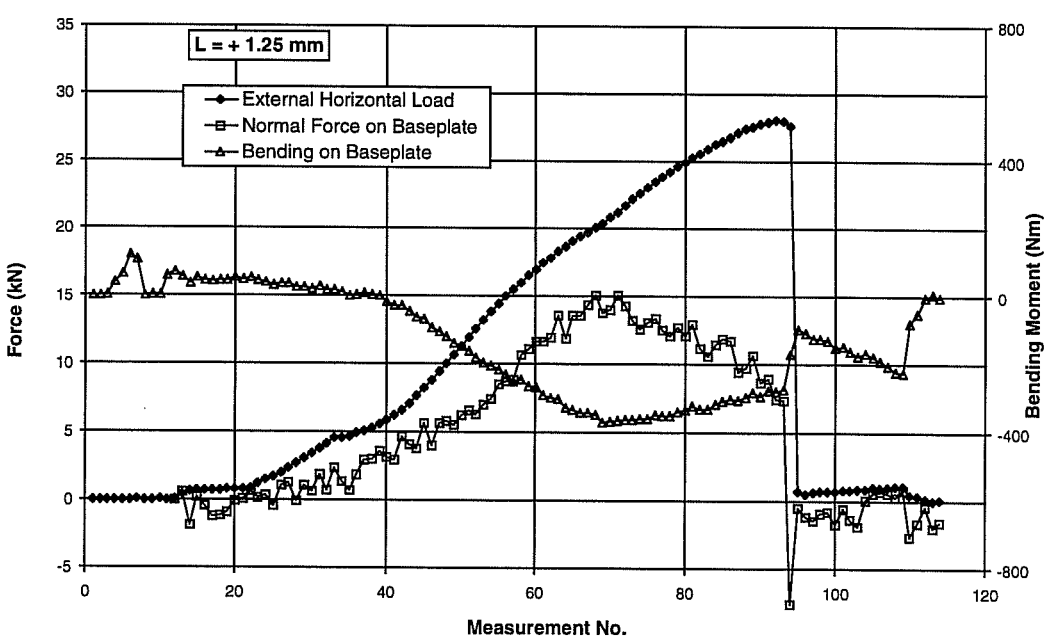

Versuch 25M3482, HSD 3/8", e = 18" = 457.2 mm, Stahlbruch am Zuganker

- Ergebnisse der Verschiebungsmessung -

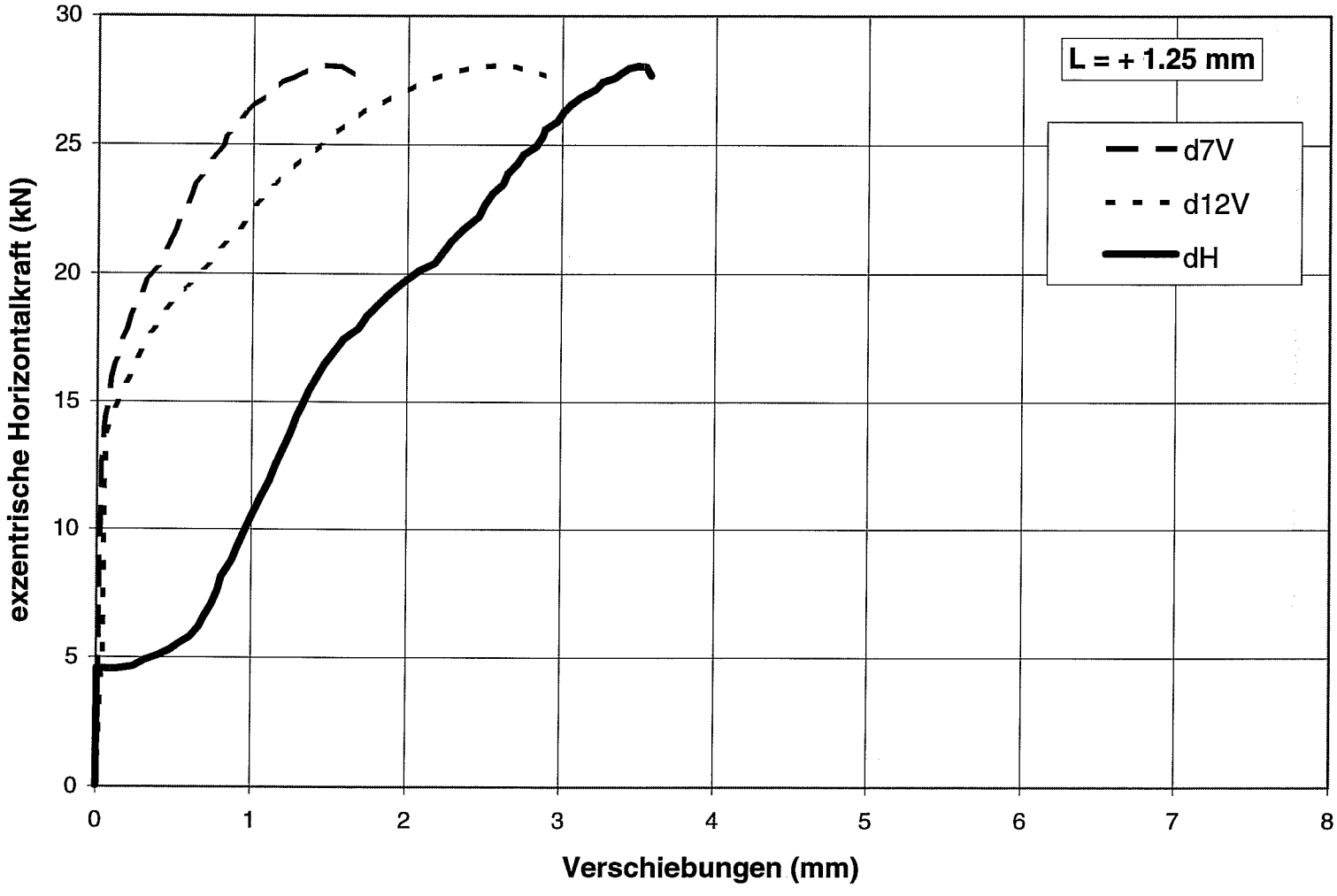

Test 25M3483, HSD 3/8", e = 18" = 457.2 mm, Steel Failure at Tension Anchor

- Results of Displacement Measurement -

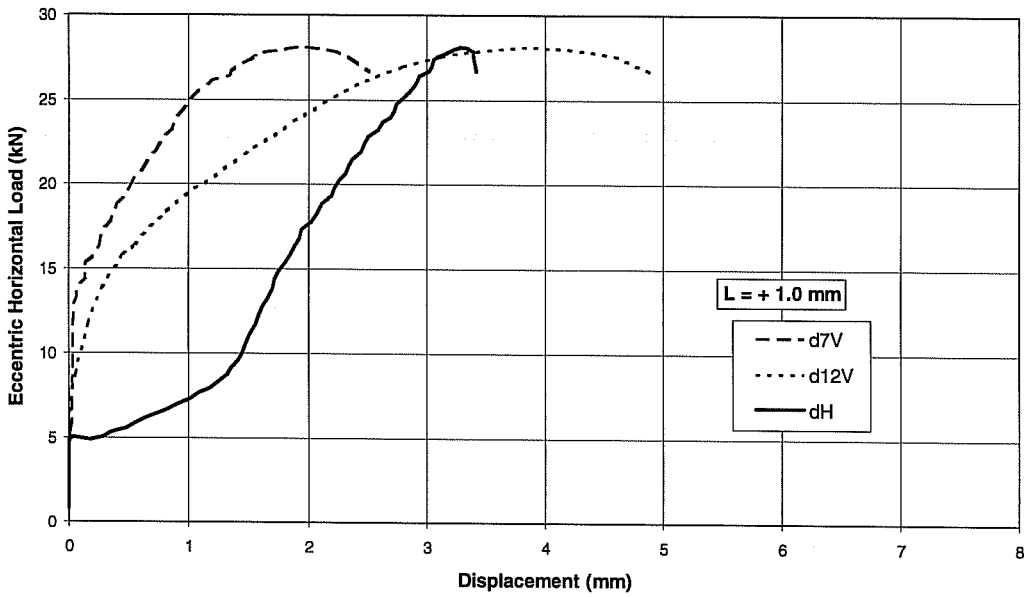

- Force and Bending Moment -

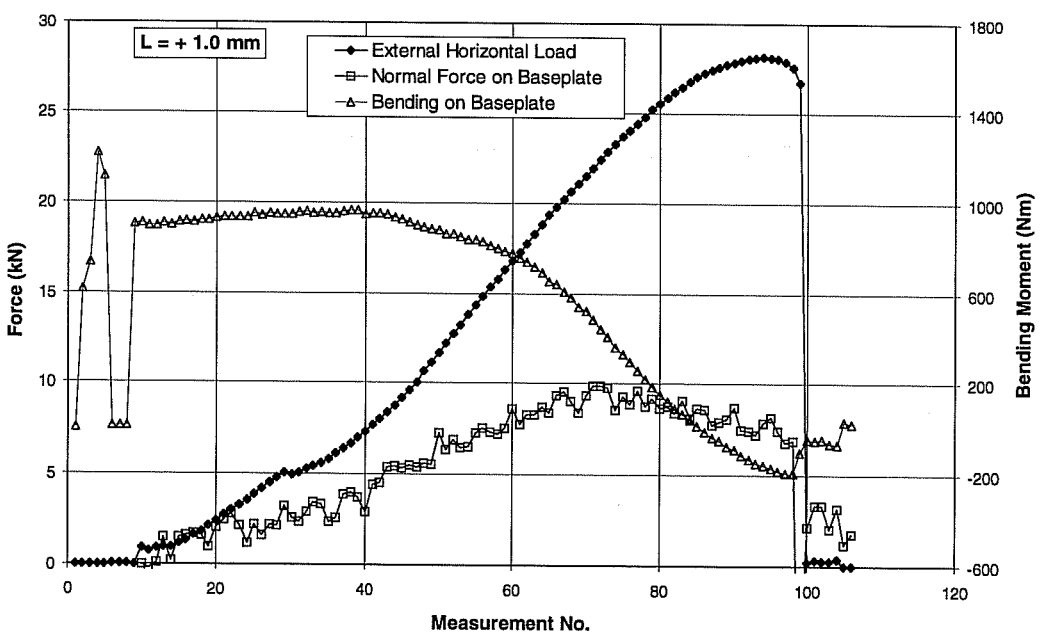

Versuch 25M3483, HSD 3/8", e = 18" = 457.2 mm, Stahlbruch am Zuganker

- Ergebnisse der Verschiebungsmessung -

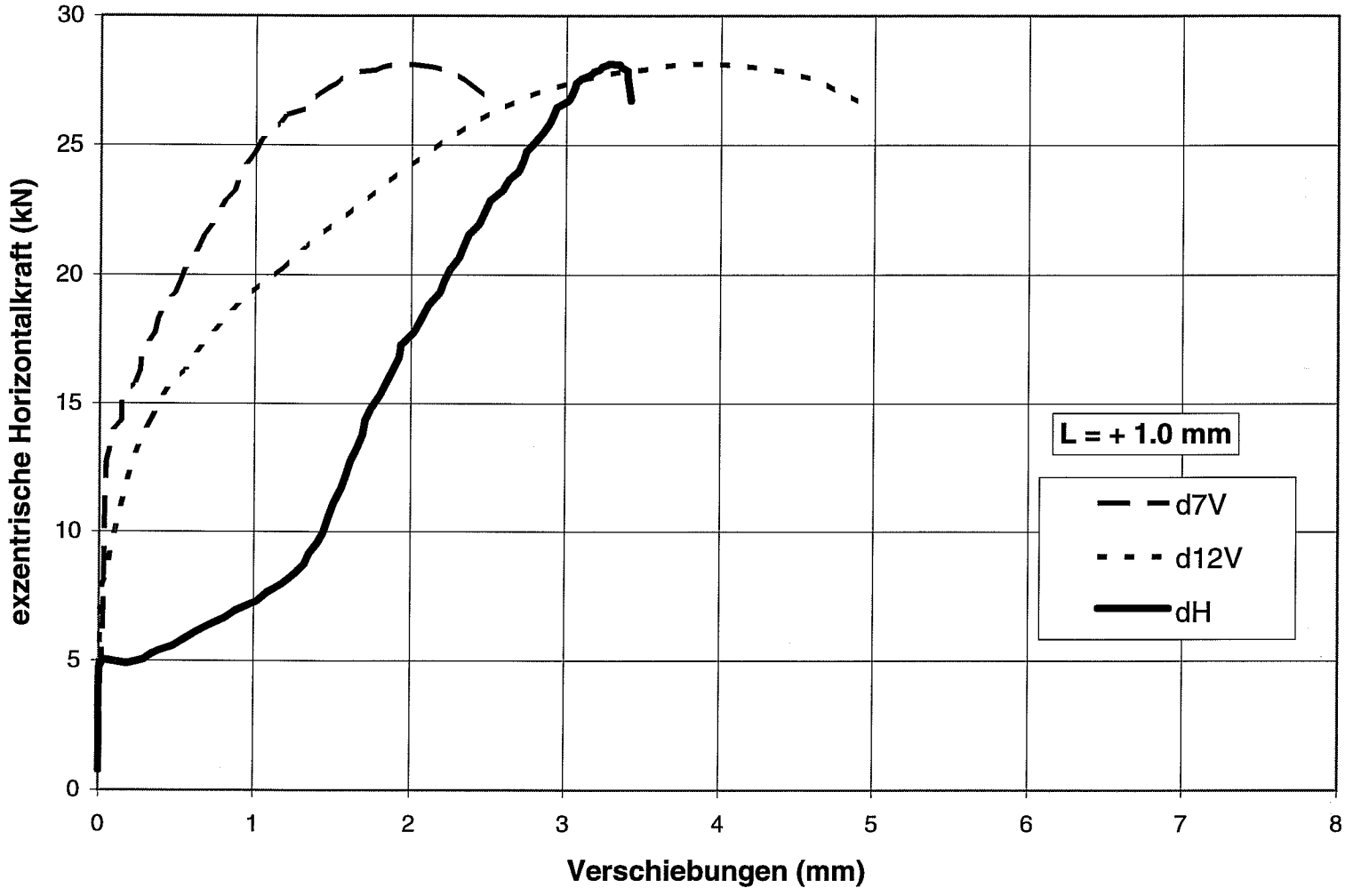

Test 26M5421, UC1 5/8", e = 12 inches (304.8 mm), Concrete Failure of Tension Anchor

- Results of Displacement Measurement -

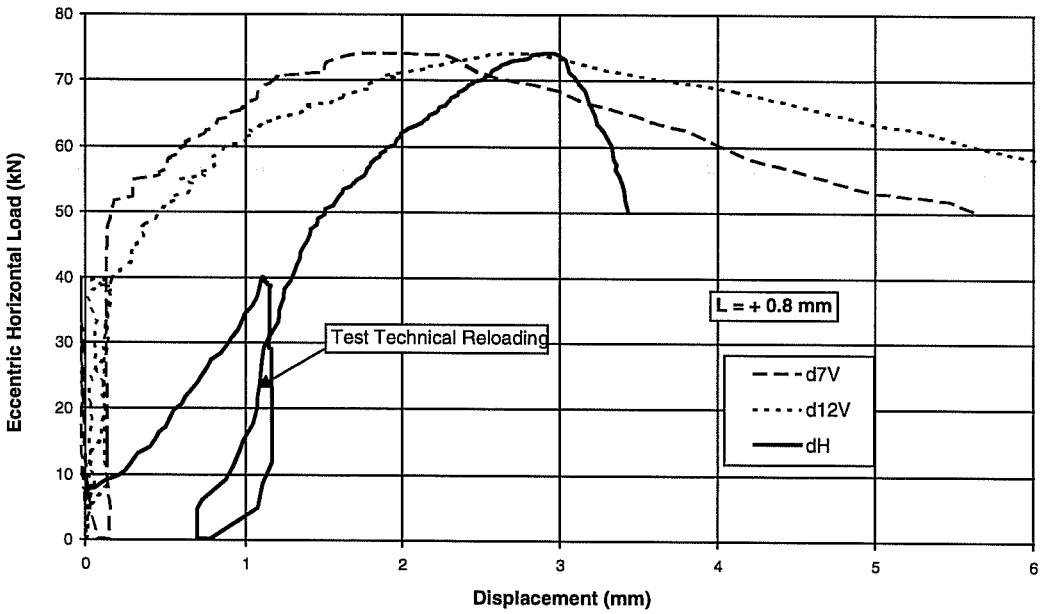

- Force and Bending Moment -

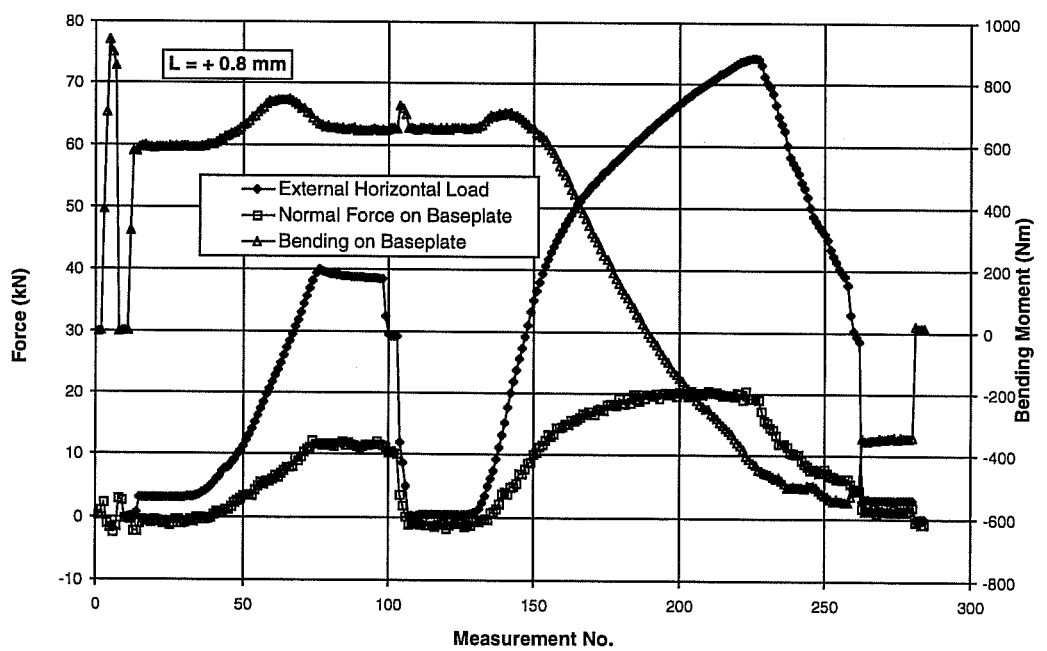

Test 26M5422, UC1 5/8", e = 12 inches (304.8 mm), Concrete Failure of Tension Anchor

- Results of Displacement Measurement -

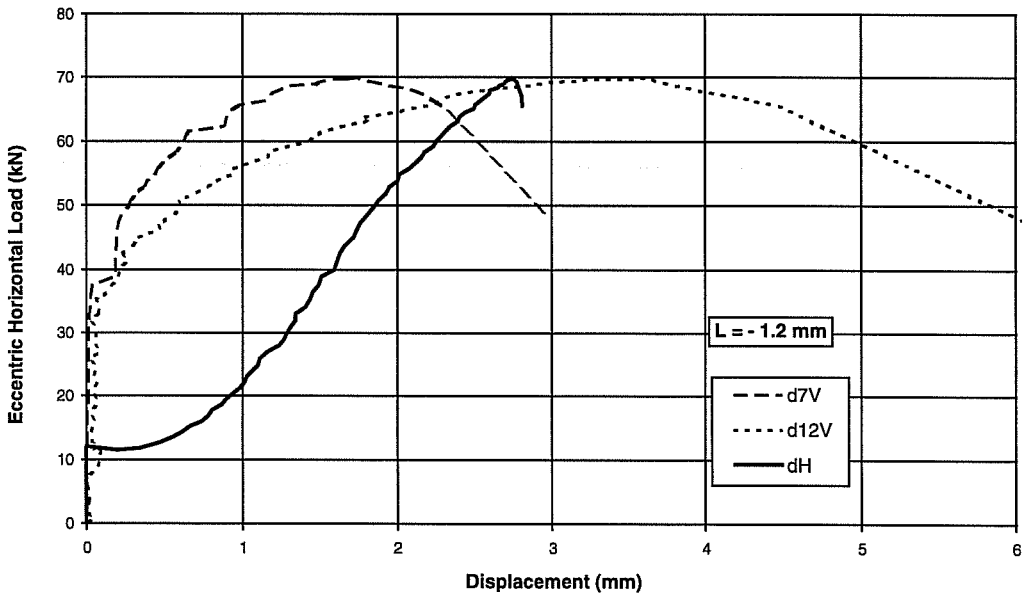

- Force and Bending Moment -

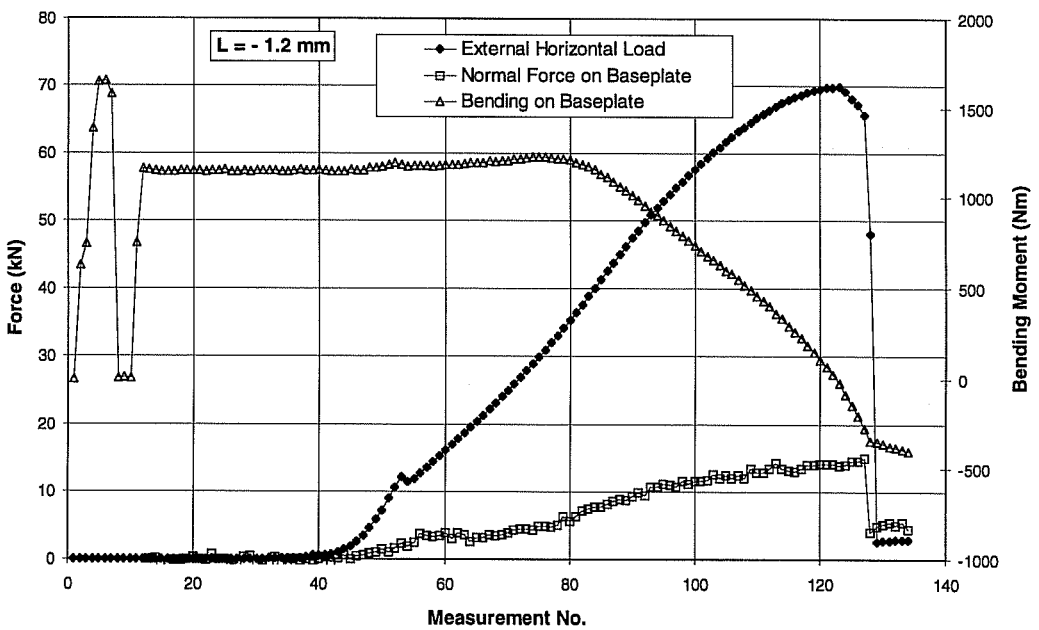

Test 26M5423, UC1 5/8", e = 12 inches (304.8 mm), Concrete Failure of Tension Anchor

- Results of Displacement Measurement -

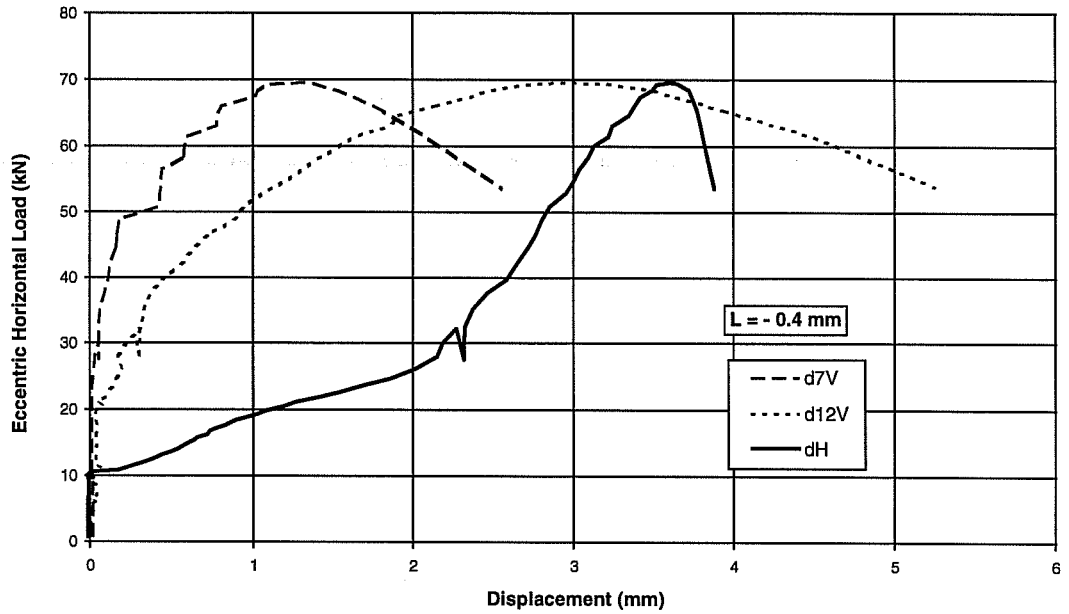

- Force and Bending Moment -

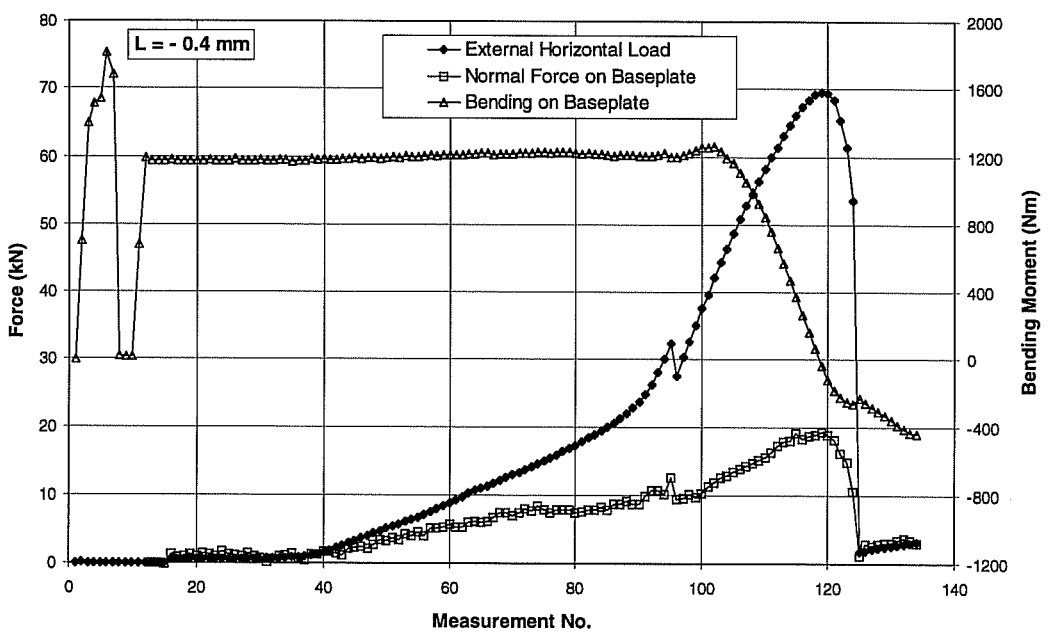

Test 26M5481, UC1 5/8", e = 12 inches (304.8 mm), Concrete Failure of Tension Anchor

- Results of Displacement Measurement -

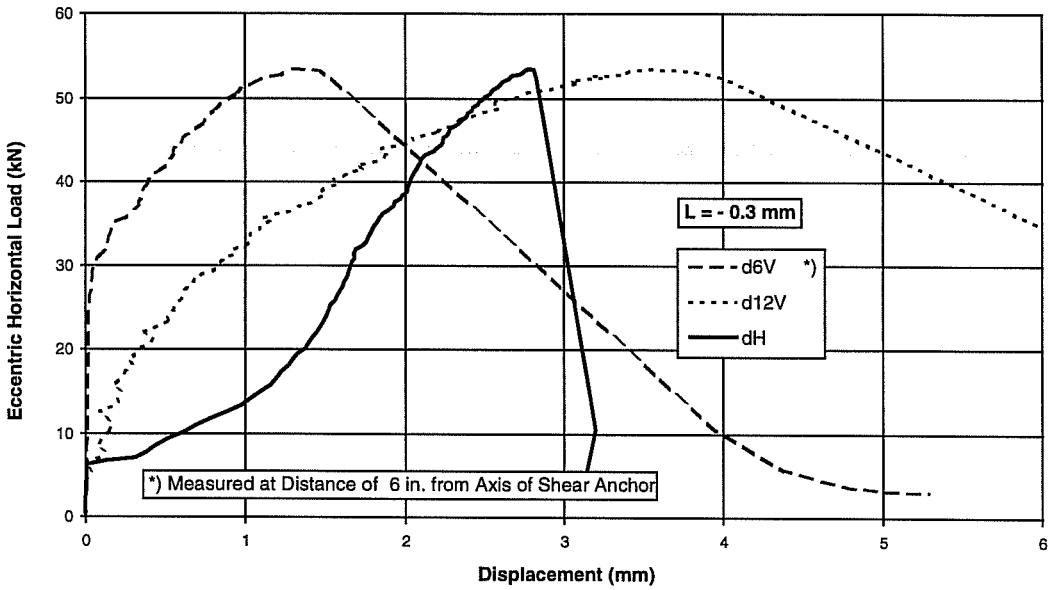

- Force and Bending Moment -

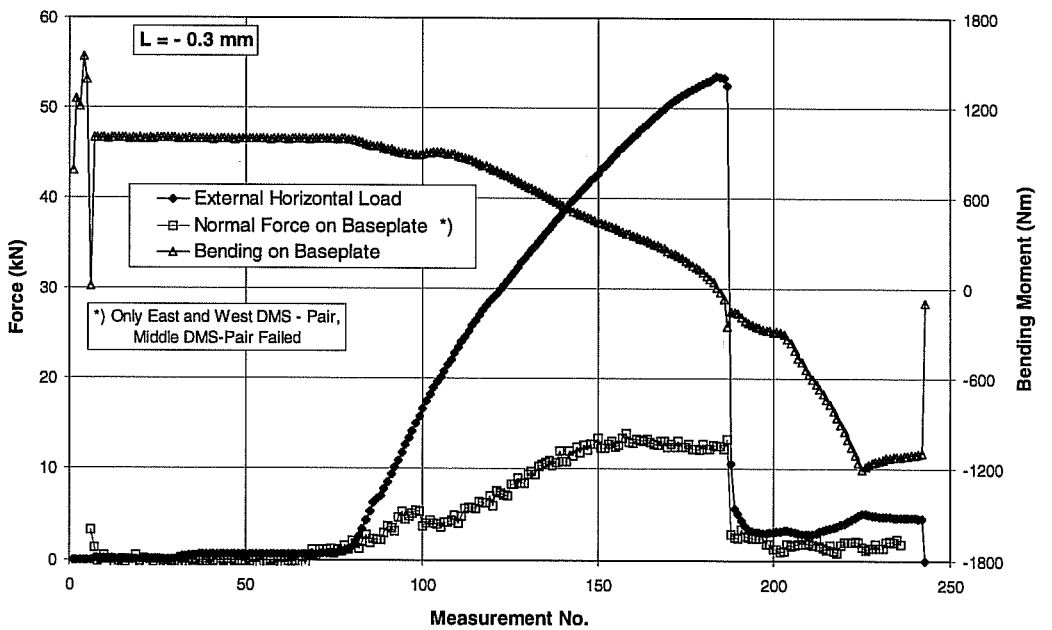

Test 26M5482, UC1 5/8", e = 12 inches (304.8 mm), Concrete Failure of Tension Anchor

- Results of Displacement Measurement -

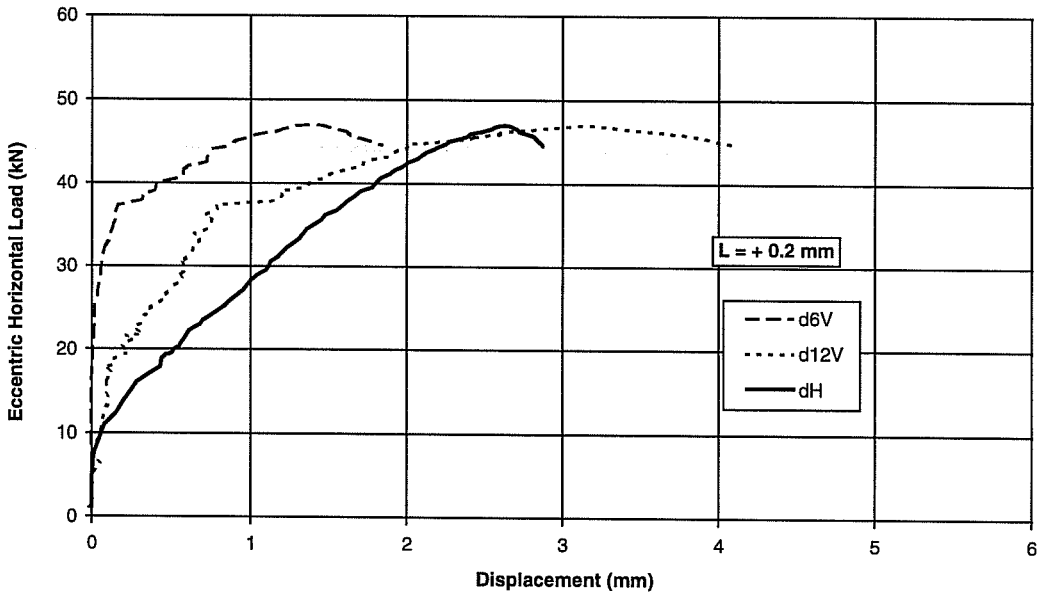

- Force and Bending Moment -

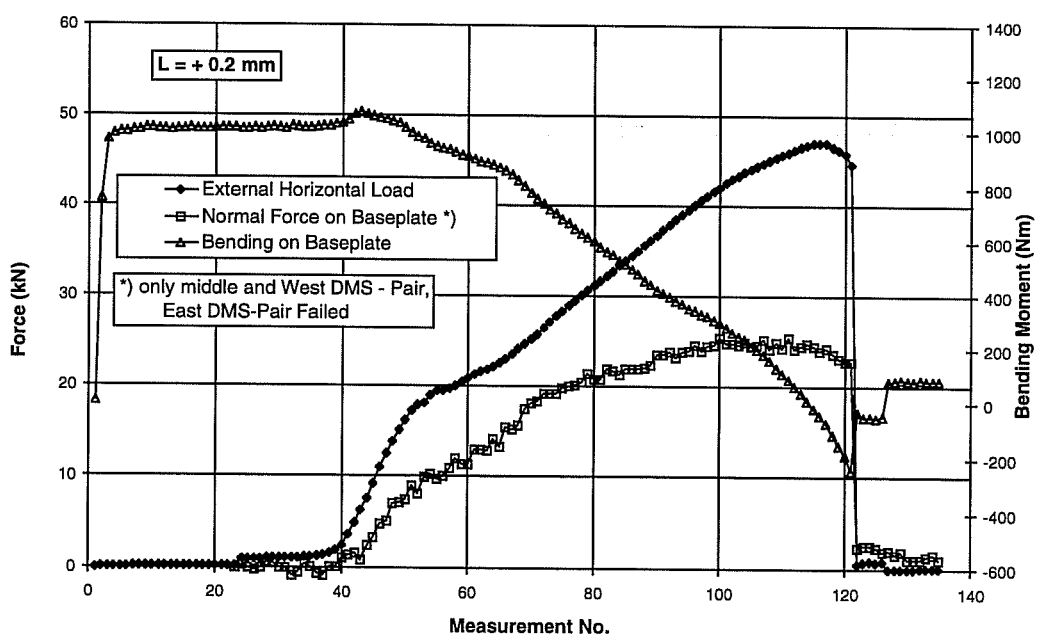

Test 26M5483, UC1 5/8", e = 12 inches (304.8 mm), Concrete Failure of Tension Anchor

- Results of Displacement Measurement -

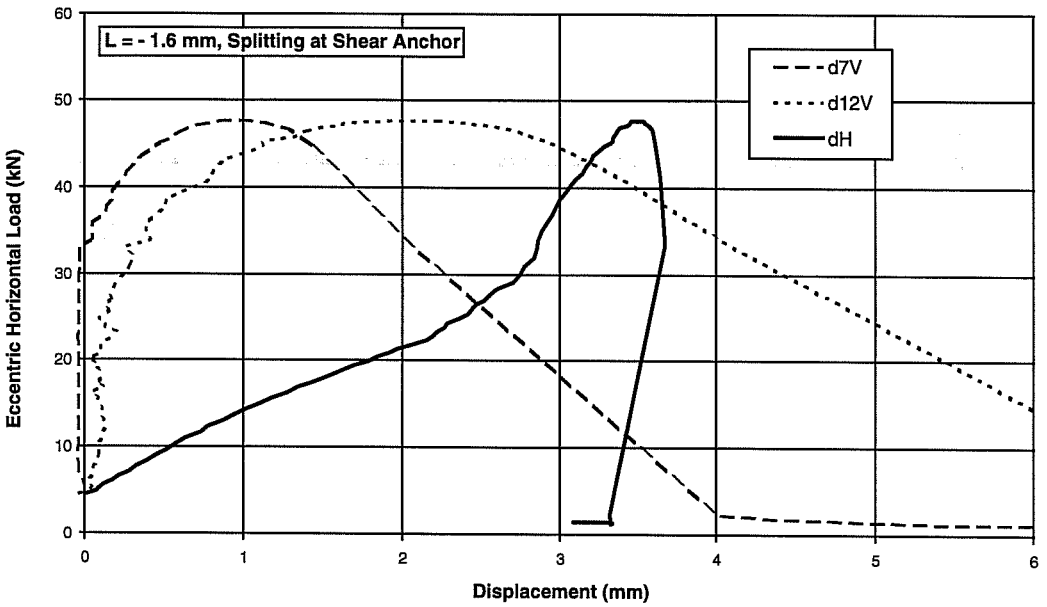

- Force and Bending Moment -

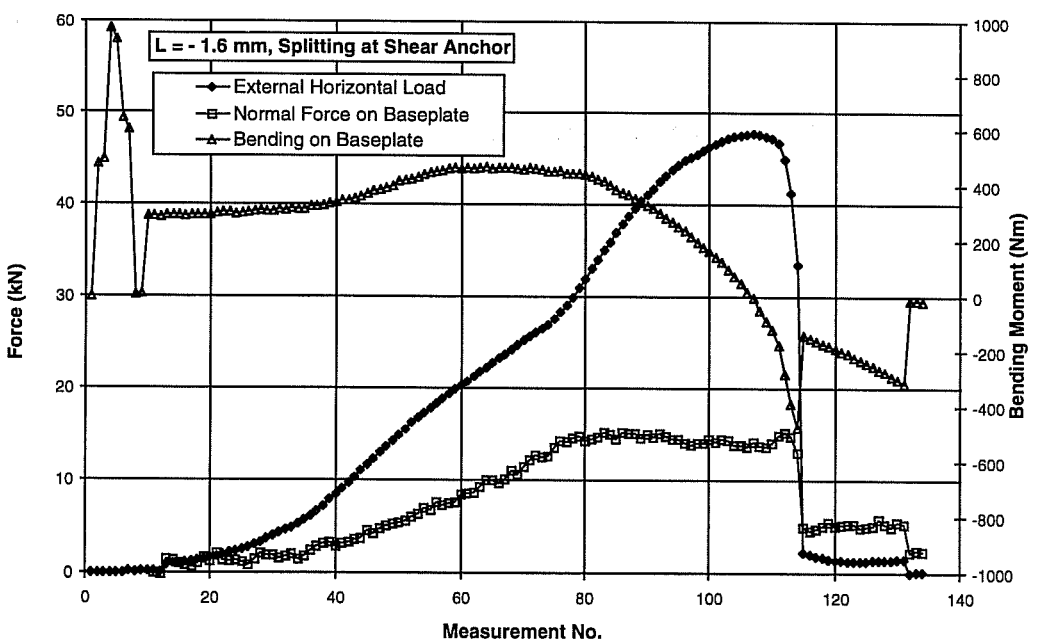

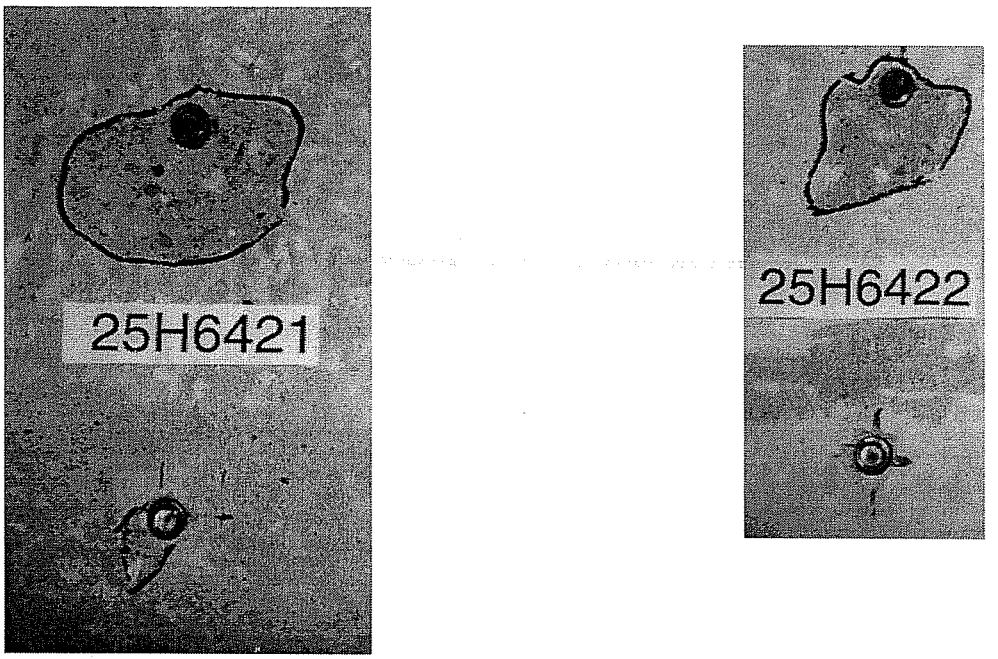

Failure Picture of Test 25H6421 (Both Anchors Failed Together) and 25H6422 (Shear Anchor Failed First), Sleeve M16, h_{ef} = 7 inches (178 mm), e = 12 inches (304.8 mm)

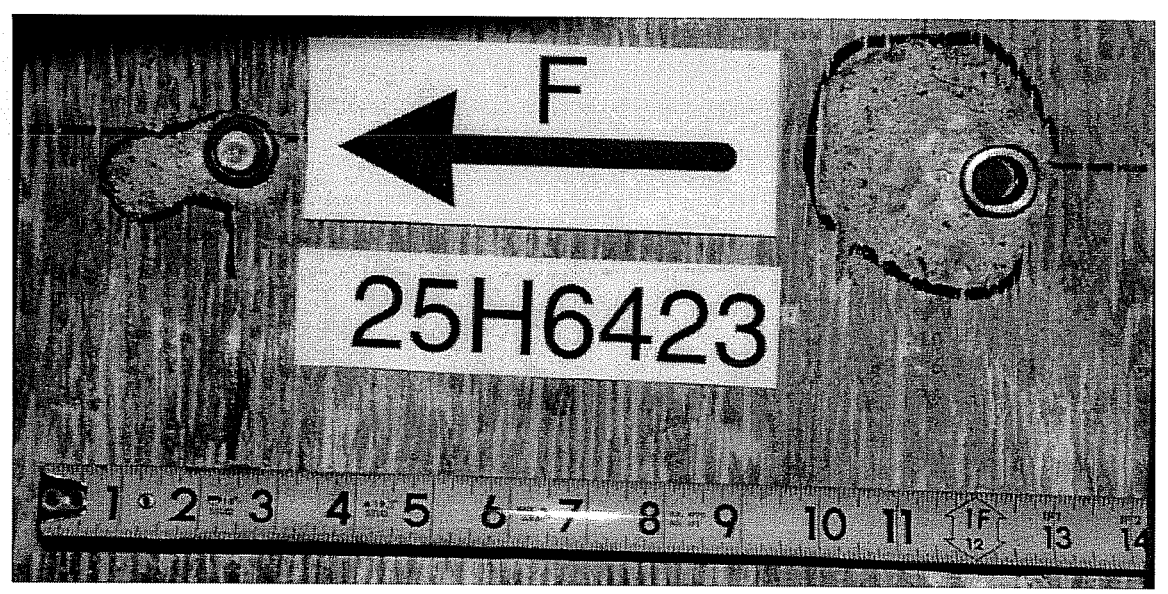

Failure Picture of Test 25H6423 (Shear Anchor Failed First), Sleeve M16, h_{ef} = 7 inches (178 mm), e = 12 inches (304.8 mm)

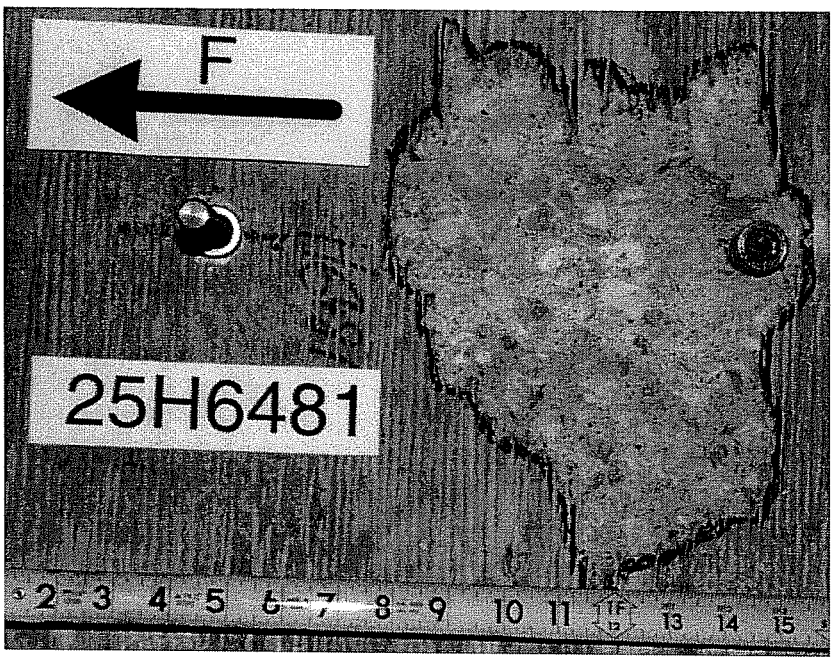

Failure Picture of Test 25H6481 (Failure of Tension Anchor), Sleeve M16, h_{ef} = 7 inches (178 mm), e = 18 inches (457.2 mm)

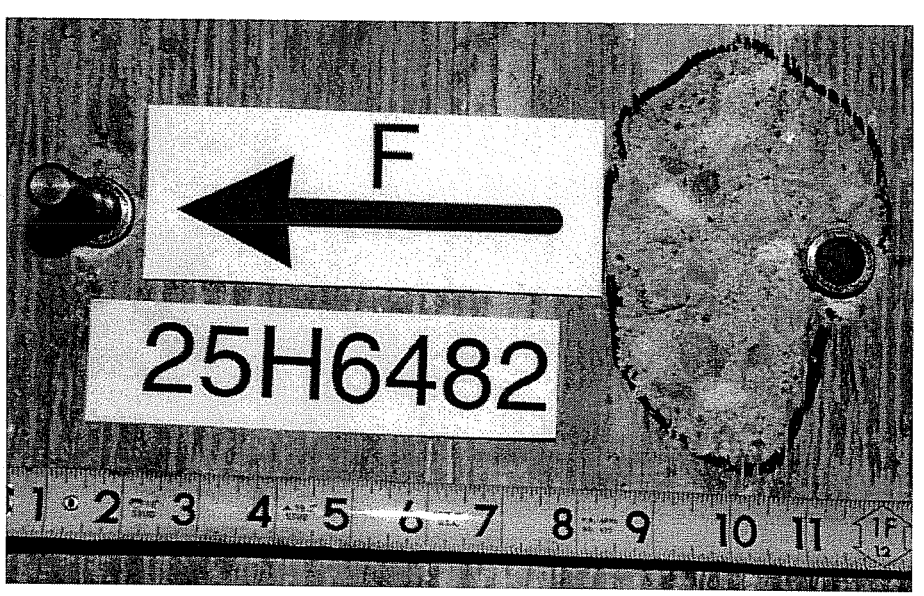

Failure Picture of Test 25H6482 (Failure of Tension Anchor), Sleeve M16, h_{ef} = 7 inches (178 mm), e = 18 inches (457.2 mm)

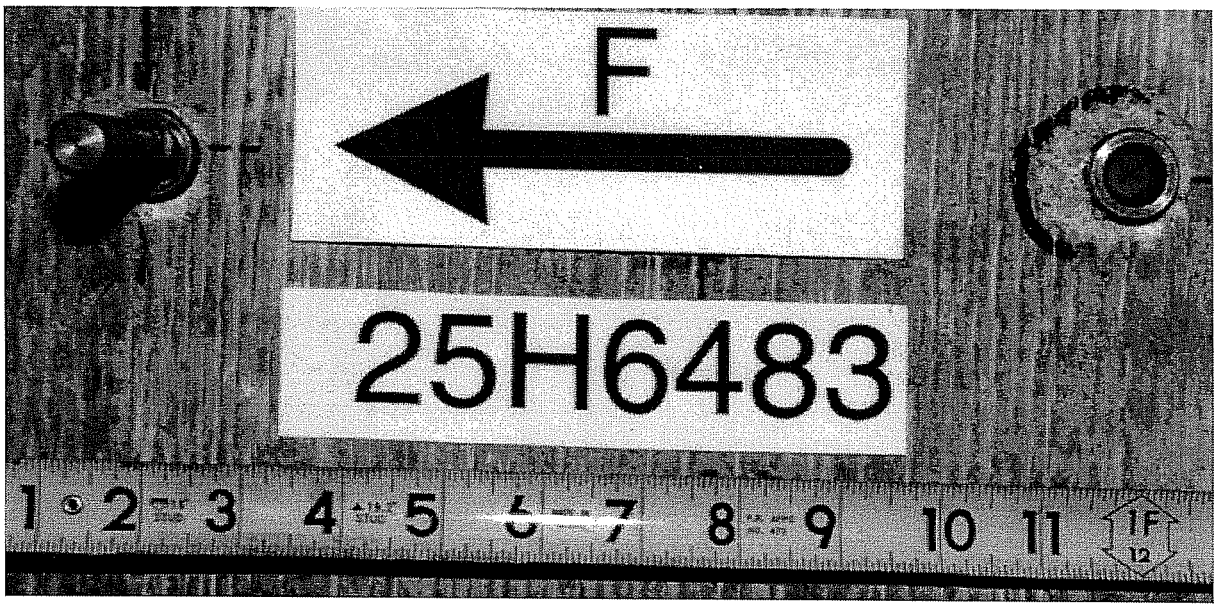

Failure Picture of Test 25H6483 (Failure of Tension Anchor), Sleeve M16, h_{ef} = 7 inches (178 mm), e = 18 inches (457.2 mm)

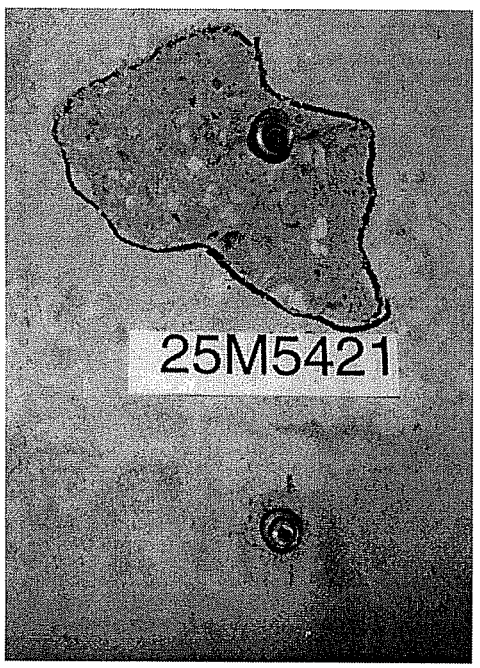

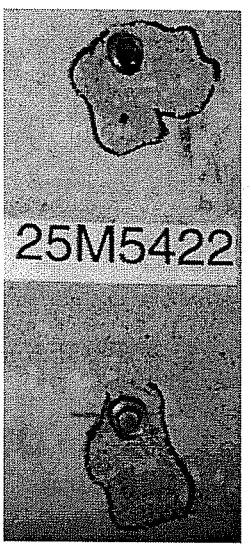

Failure Picture of Test 25M5421 (Shear Anchor Failed First) and 25M5422 (Shear Anchor Failed First), UC1 5/8", h_{ef} = 7 inches (178 mm), e = 12 inches (304.8 mm)

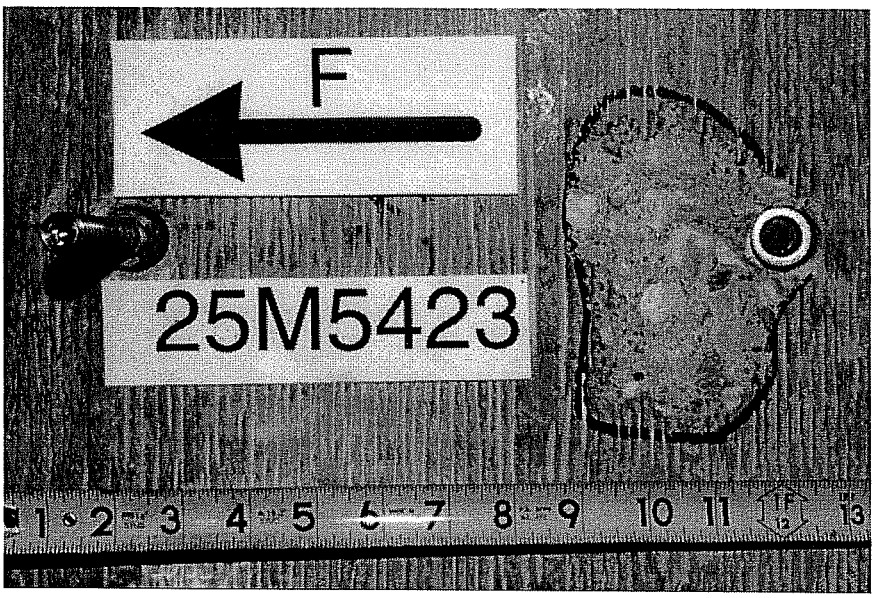

Failure Picture of Test 25M5423 (Tension Anchor Failed First), UC1 5/8", h_{ef} = 7 inches (178 mm), e = 12 inches (304.8 mm)

Failure Picture of Test 25M5481 (Failure of Tension Anchor), UC1 5/8", h_{ef} = 7 inches (178 mm), e = 18 inches (457.2 mm)

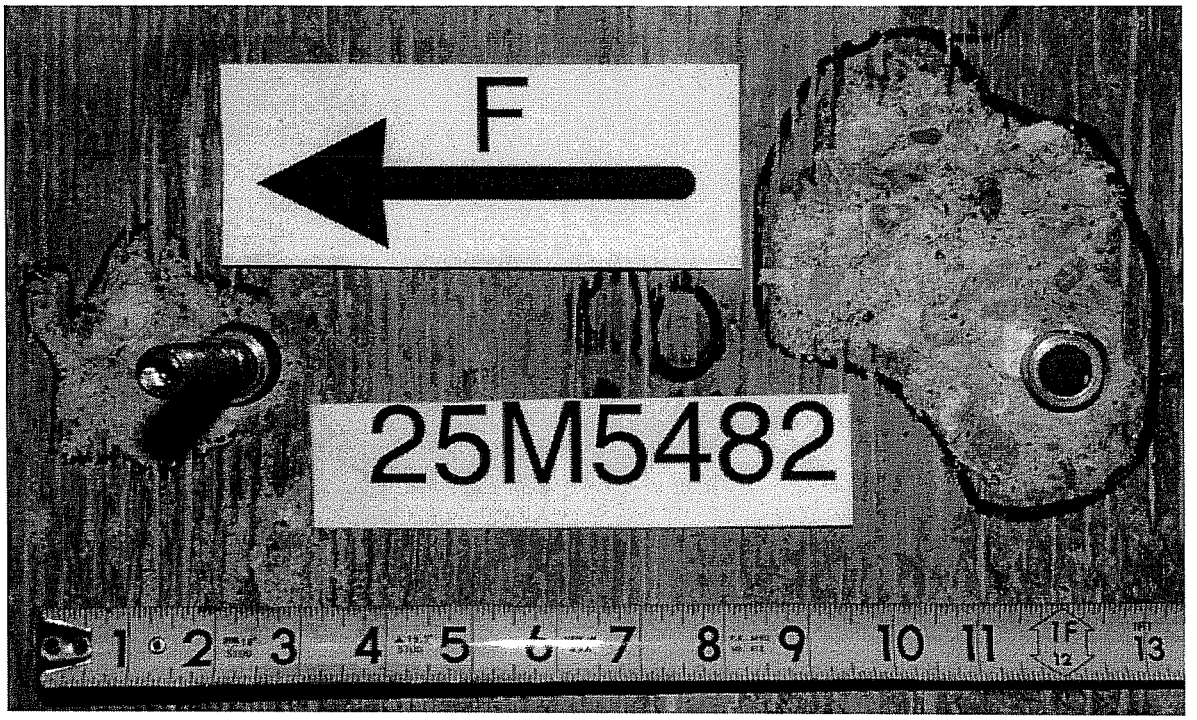

Failure Picture of Test 25M5482 (Failure of Tension Anchor), UC1 5/8", h_{ef} = 7 inches (178 mm), e = 18 inches (457.2 mm)

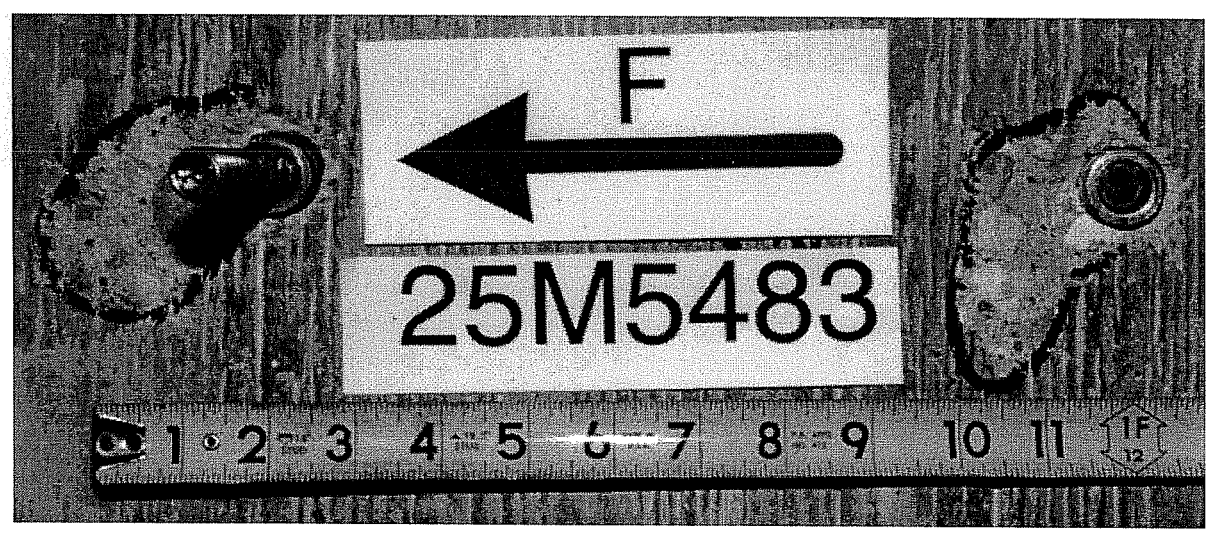

Failure Picture of Test 25M5483 (Failure of Tension Anchor), UC1 5/8", h_{ef} = 7 inches (178 mm), e = 18 inches (457.2 mm)

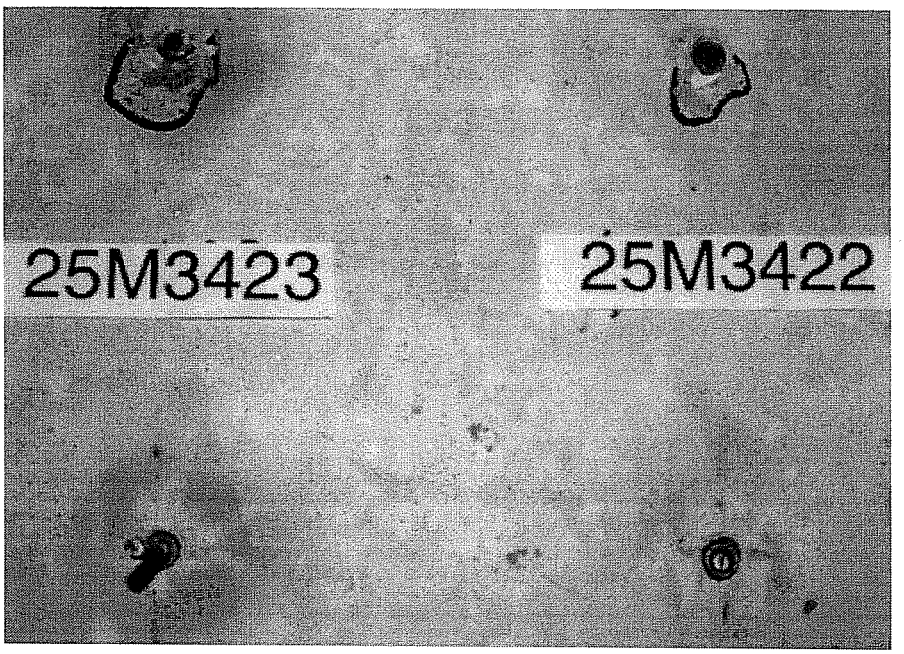

Failure Picture of Test 25M3422 (Shear Anchor Failed First) and 25M3423 (Failure of Tension Anchor), UC1 3/8", h_{ef} = 3.5 inches (89 mm), e = 12 inches (304.8 mm)

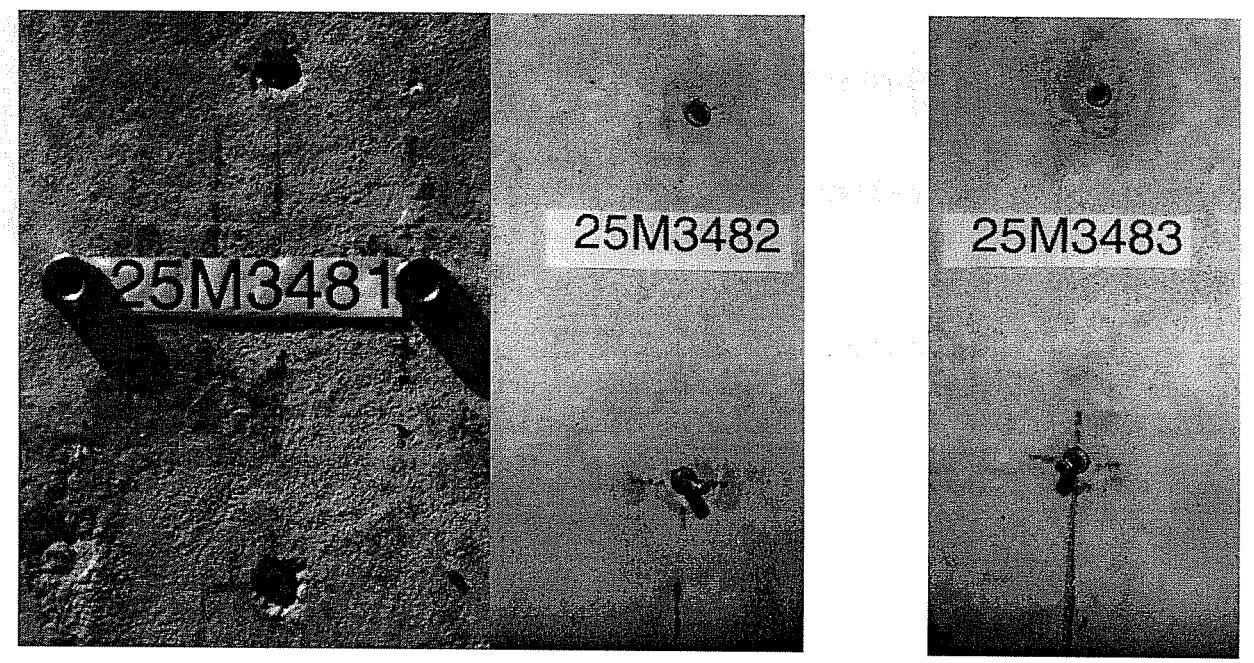

Failure Picture of Test 25M3483 (Failure of Tension Anchor), 25M3482 (Shear Anchor Failed First) and 25M3483 (Failure of Tension Anchor), UC1 3/8", h_{ef} = 3.5 inches (89 mm), e = 18 inches (457.2 mm)

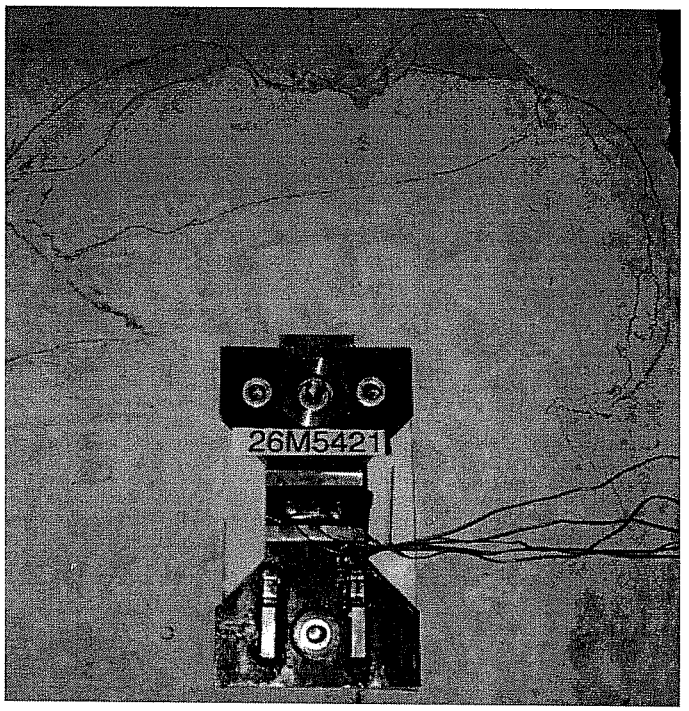

Failure Picture of Test 26M5421 (Concrete Failure at Tension Anchor), Right after Test, UC1 5/8", h_{ef} = 3.5 inches (89 mm), e = 12 inches (304.8 mm)

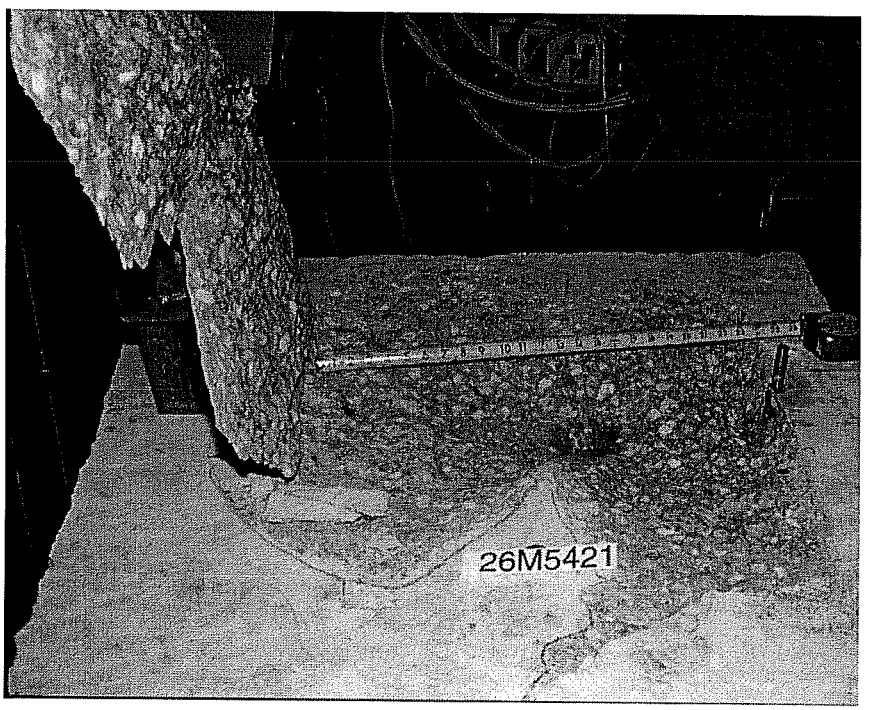

Failure Picture of Test 26M5421 (Concrete Failure at Tension Anchor), Breakout Cone, UC1 5/8", h_{ef} = 3.5 inches (89 mm), e = 12 inches (304.8 mm)

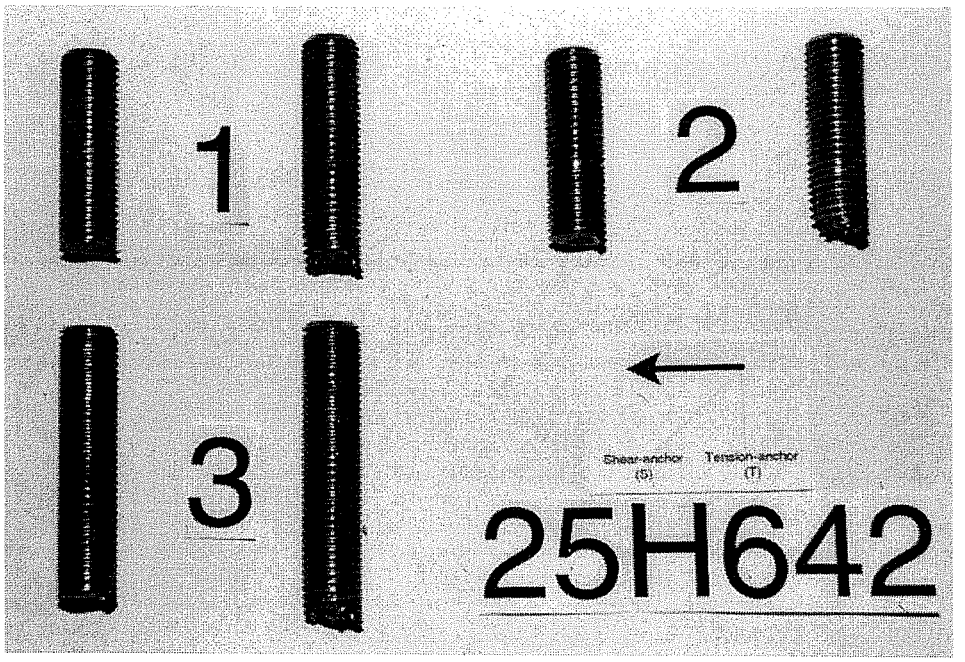

Fractured Anchor Shanks of Series 25H642, Sleeve M16, h_{ef} = 7 inches (178 mm), e = 12 inches (304.8 mm)

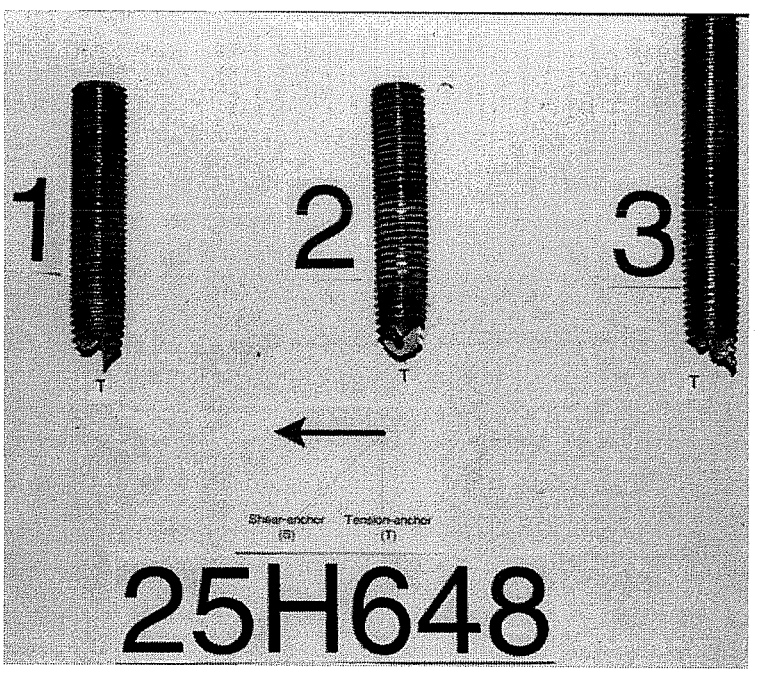

Fractured Anchor Shanks of Series 25H648, Sleeve M16, h_{ef} = 7 inches (178 mm), e = 18 inches (457.2 mm)

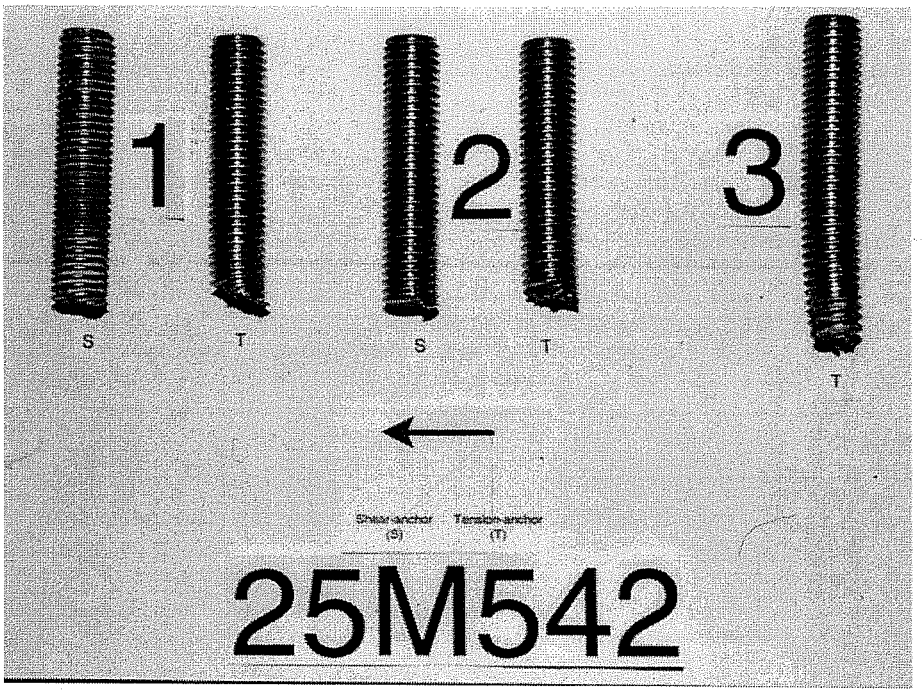

Fractured Anchor Shanks of Series 25M542, UC1 5/8", h_{ef} = 7 inches (178 mm), e = 12 inches (304.8 mm)

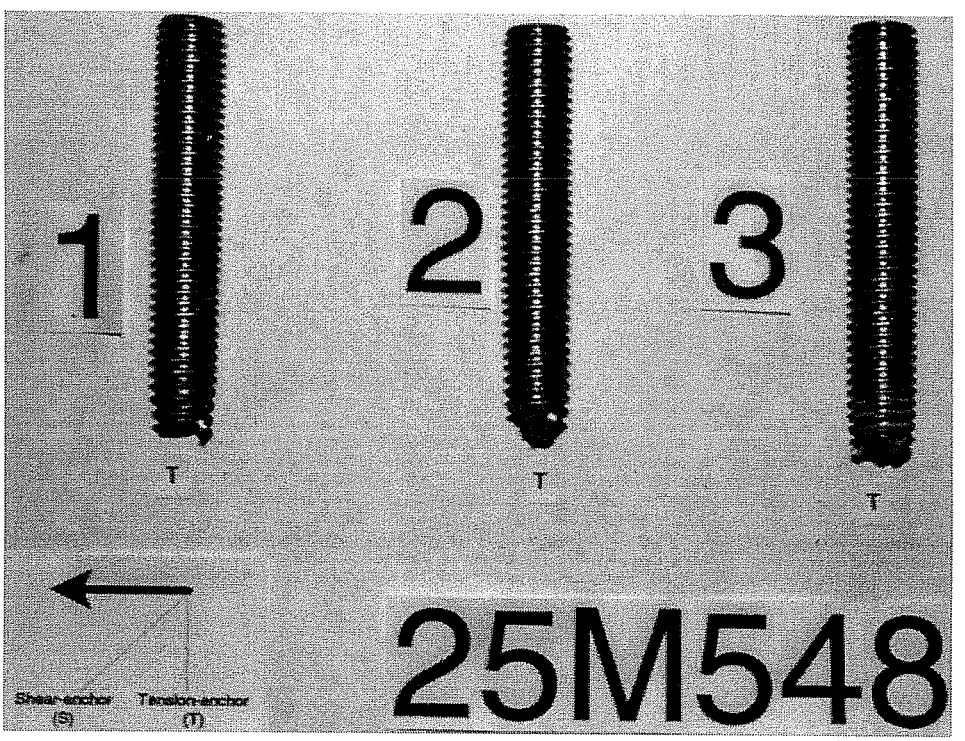

Fractured Anchor Shanks of Series 25M548, UC1 5/8", h_{ef} = 7 inches (178 mm), e = 18 inches (457.2 mm)

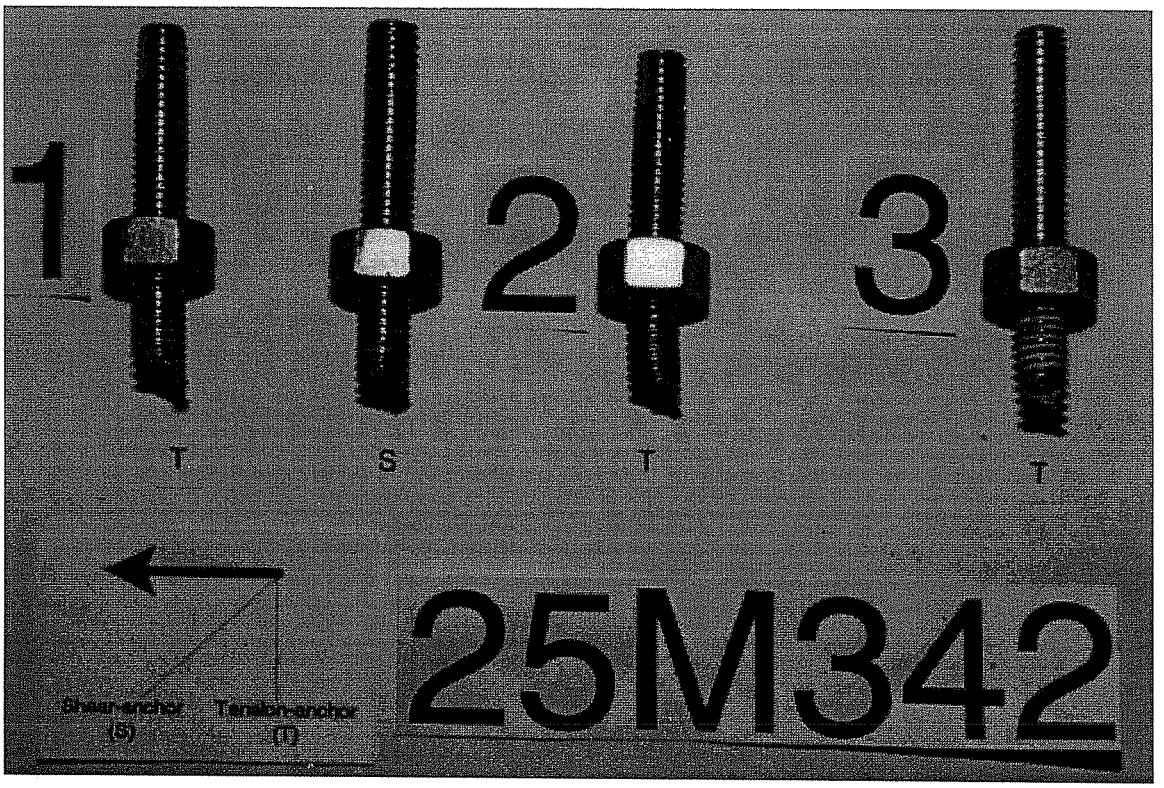

Fractured Anchor Shanks of Series 25M342, UC1 3/8", h_{ef} = 3.5 inches (89 mm), e = 12 inches (304.8 mm)

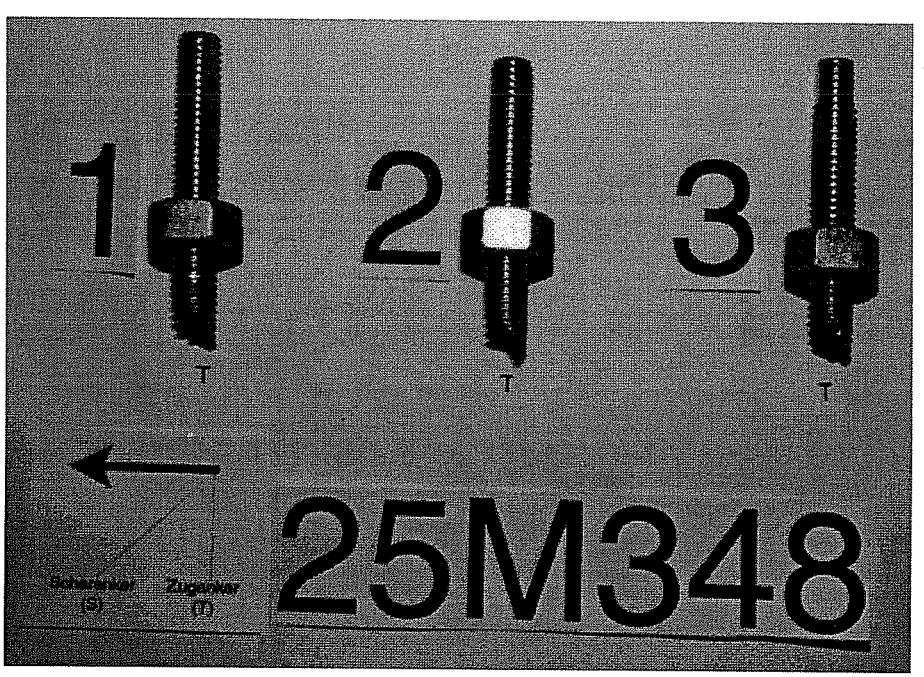

Fractured Anchor Shanks of Series 25M348, UC1 3/8", h_{ef} = 3.5 inches (89 mm), e = 18 inches (457.2 mm)

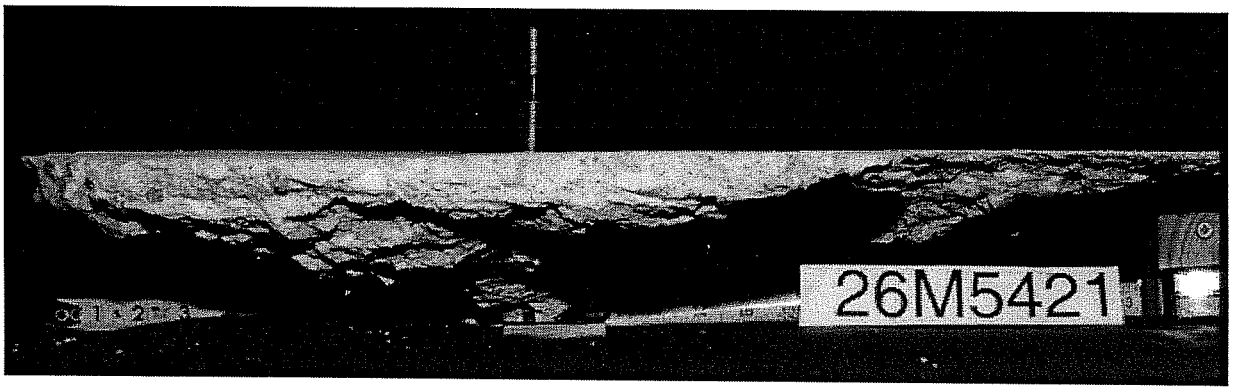

Cone of Test 26M5421 (Concrete Failure at Tension Anchor), UC1 5/8", h_{ef} = 3.5 inches (89 mm), e = 12 inches (304.8 mm)

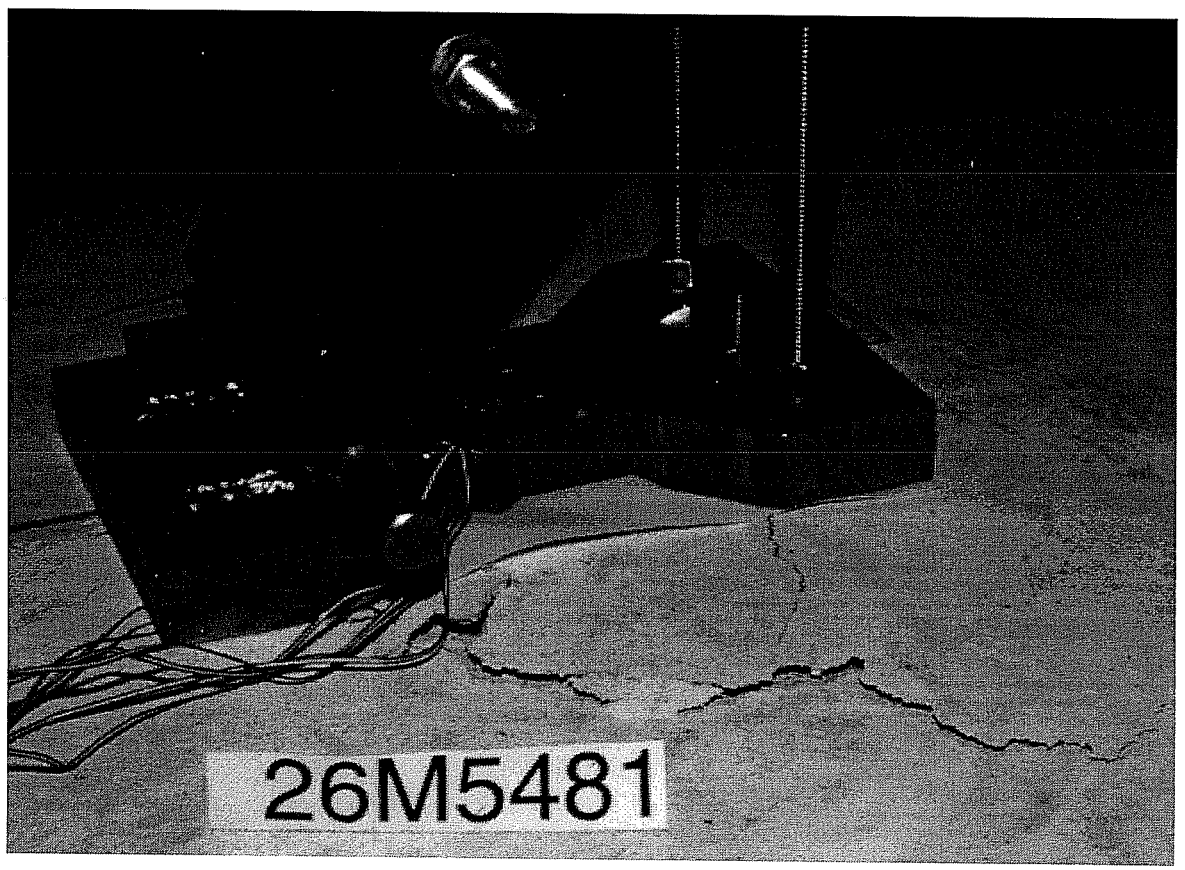

Failure Picture Right after Test 26M5481 (Concrete Failure at Tension Anchor), UC1 5/8", h_{ef} = 3.5 inches (89 mm), e = 18 inches (457.2 mm)

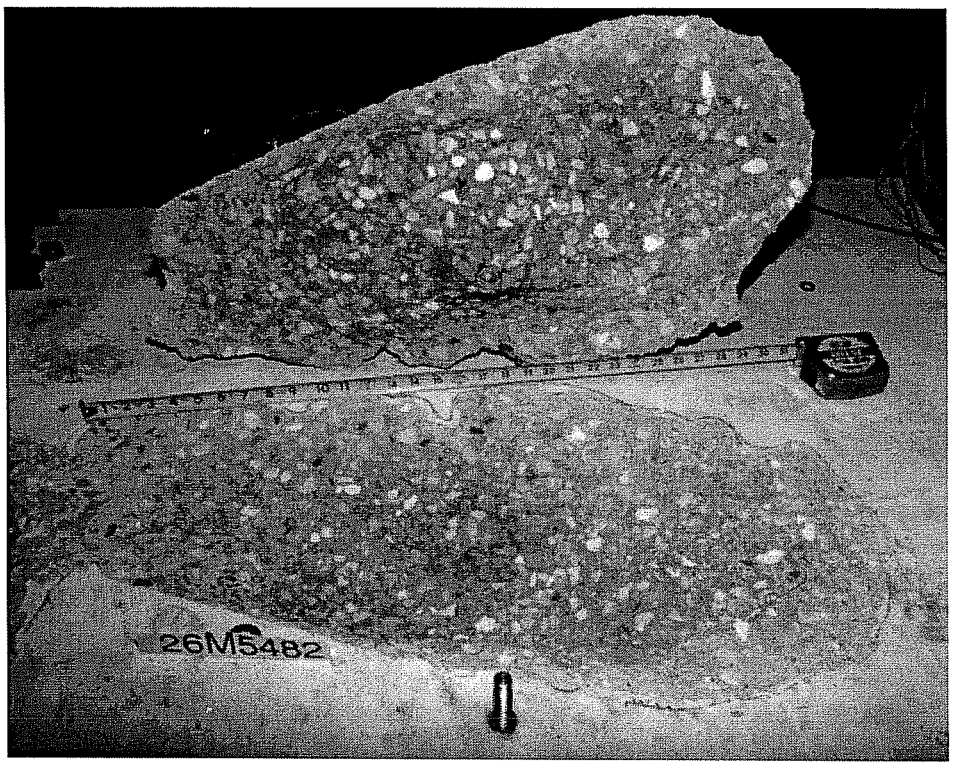

Failure Picture of Test 26M5482 (Concrete Failure at Tension Anchor), Breakout Cone, UC1 5/8", h_{ef} = 3.5 inches (89 mm), e = 18 inches (457.2 mm)

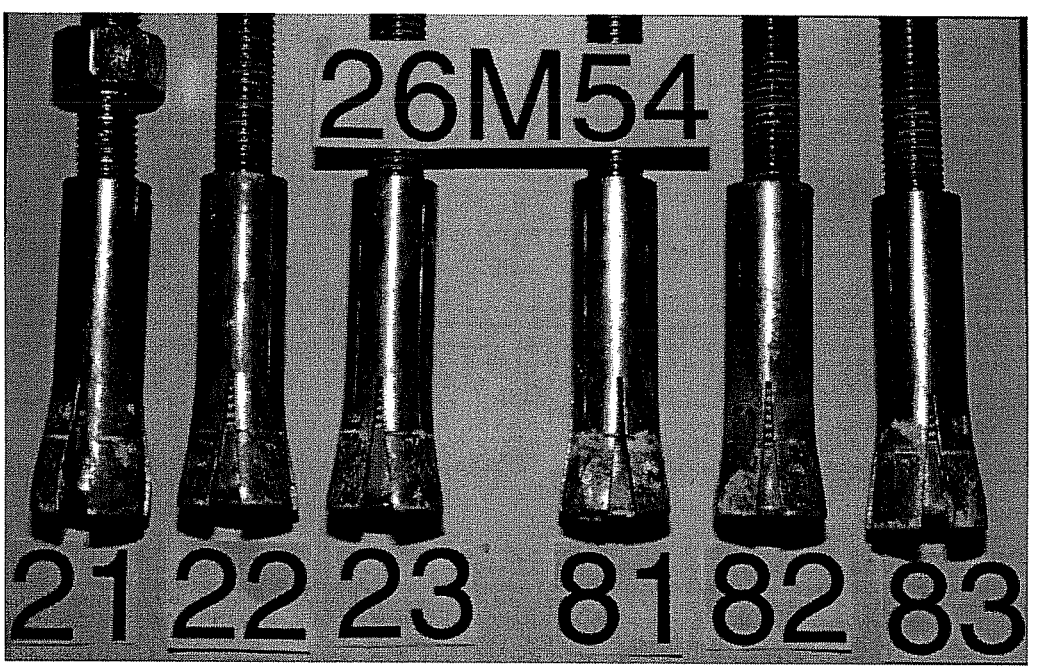

Tested Anchors, Series 2.6, UC1 5/8", h_{ef} = 3.5 inches (89 mm), e = 18 inches (457.2 mm)

EXAMPLE INPUT FILE TO BDA5 PROGRAM

(SERIES 23H642, L = +3 MM)

```
PLASTIC DESIGN OF FASTENINGS OF ANCHOR BOLTS
90.0     304.8   0.0                  loading angle [°], eccentricity [mm], weight of fastening
1,1,                                  type of  baseplate (1 = rectangular), stratum height calculated compression zone
272.0  203.2                          length of baseplate [mm], width of baseplate [mm]
  2                                   number of rows of anchors
9.0,157.0,3.                          1st anchor row: distance from compression edge, cross-sectional area, gap
263.0,157.0,0.                        2nd anchor row: distance from compression edge, cross-sectional area, gap
  2                                   number of load-displacement curves (= number of rows of anchors)
  1                                   control number for force interaction (1 = using interaction equation)
  1.80000   800.83   446.85           exponent of interaction, tension, shear at turning point of curve
  1.80000   889.81   496.50           exponent of interaction, tension, shear of maximum load
  1.80000   845.32   471.68           exponent of interaction, tension, shear of residual load
  7                                   number of curve given curves (program interpolate between curves)
  0.00000                                 loading angle of the following curve ([°], 0 = tension)
 15.06220  21.19900  25.46700  0.30000  vertical displacement at turning point, maximum, and residual load
 15.00000                                loading angle of the following curve
  4.19300   7.34000   7.79800  0.50000  transverse displacement at turning point, maximum, and residual load
  6.32900   9.67300  10.05800  0.25000  vertical displacement at turning point, maximum, and residual load
 30.00000                                loading angle of the following curve
  2.18516   4.01656   4.53637  0.50000  transverse displacement at turning point, maximum, and residual load
  1.06300   2.07900   2.23100  0.25000  vertical displacement at turning point, maximum, and residual load
 45.00000                                loading angle of the following curve
  2.66731   4.14407   4.48509  0.60000  transverse displacement at turning point, maximum, and residual load
  0.77100   1.25700   1.36600  0.25000  vertical displacement at turning point, maximum, and residual load
 60.00000                                loading angle of the following curve
  2.43719   3.65745   4.15414  0.60000  transverse displacement at turning point, maximum, and residual load
  0.49500   0.85100   0.94300  0.25000  vertical displacement at turning point, maximum, and residual load
 75.00000                                loading angle of the following curve
  2.38080   3.28018   3.56233  0.60000  transverse displacement at turning point, maximum, and residual load
  0.24154   0.41525   0.46014  0.25000  vertical displacement at turning point, maximum, and residual load
 90.00000                                loading angle of the following curve
  2.36000   3.14100   3.34400  0.60000  transverse displacement at turning point, maximum, and residual load

  1                                   Beginning of input data for 2nd curve group (2nd anchor row),
  1.80000   800.83   446.85           refer to the 1st curve group
  1.80000   889.81   496.50
  1.80000   845.32   471.68
  7
```

```
 0.00000
15.06220 21.19900 25.46700  0.30000
15.00000
 4.19300  7.34000  7.79800  0.50000
 6.32900  9.67300 10.05800  0.25000
30.00000
 2.18516  4.01656  4.53637  0.50000
 1.06300  2.07900  2.23100  0.25000
45.00000
 2.66731  4.14407  4.48509  0.60000
 0.77100  1.25700  1.36600  0.25000
60.00000
 2.43719  3.65745  4.15414  0.60000
 0.49500  0.85100  0.94300  0.25000
75.00000
 2.38080  3.28018  3.56233  0.60000
 0.24154  0.41525  0.46014  0.25000
90.00000
 2.36000  3.14100  3.34400  0.60000
32.400   0.10                cylinder compressive strength fc of concrete, friction coefficient μ
0.15E-4  1.00                relative crushing s/d, relative compression σ / fc (Li, 1994)
0.1E-8   1.00     1.00       allowable tolerance of the displacement in iteration
1.0E1    1.0E1    1.0E1      allowable equilibrium tolerance
0.70     0.50     0.50       iteration constant 0 < ωI < 1.0
1.0E-3   1.0E-3   1.0E1      step size δx for differential calculation
  3  10.                     control number 3 = rotation, termination at load decrease > 10%
  4                          4 calculation step size of increase of control number
1.E-3      10                size and number of steps of the control number
3.75E-2    40                      "          "
1.E-2       2                      "          "
1.E-1     100                      "          "
```

Comparison Among Plasticity Theory, ElasticTheory, Calculation with BDA5, and Test Results of Connections of Series 25h64

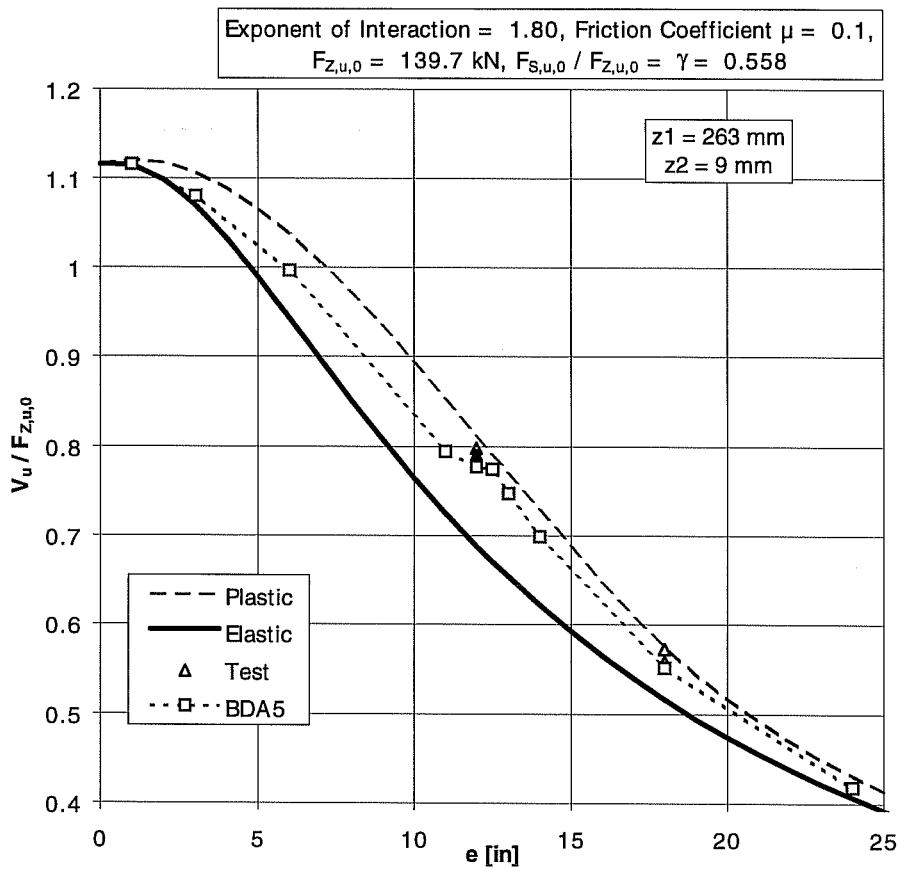

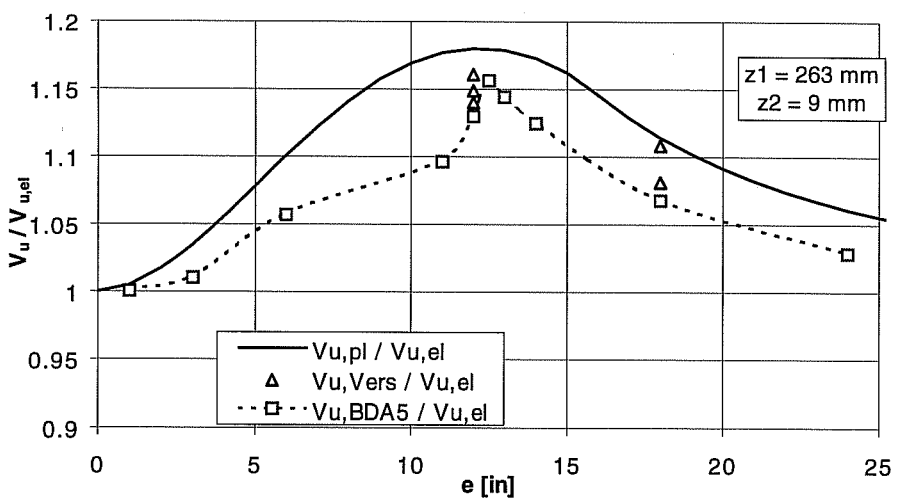

Comparison Among Plasticity Theory, Elastic Theory, Calculation with BDA5, and Test Results of Connections of Series 25h64

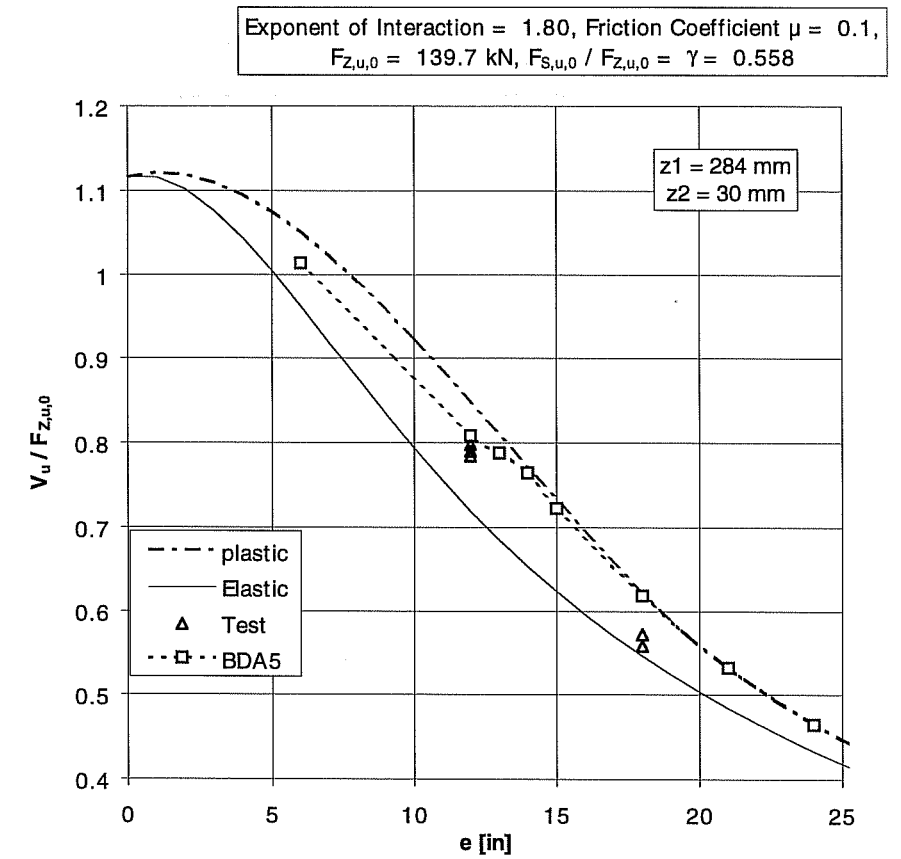

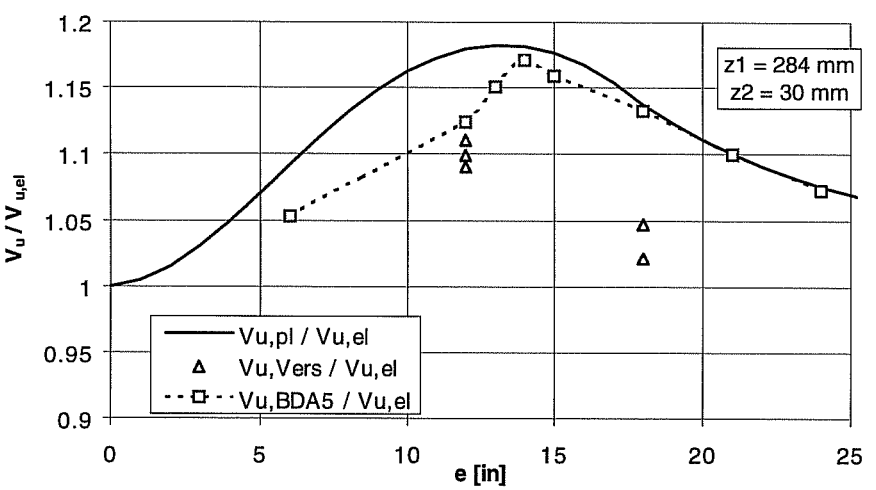

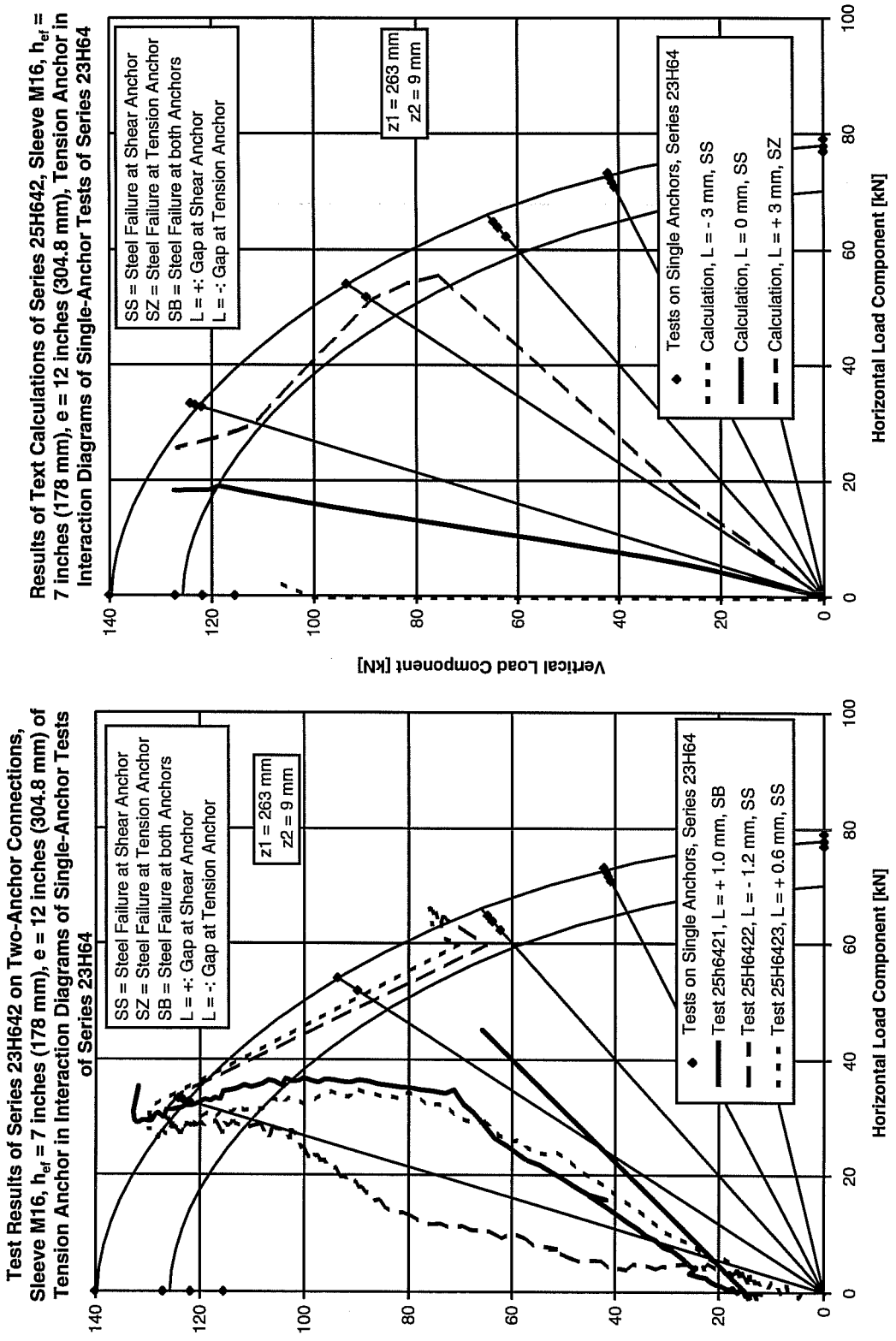
Test Results of Series 23H642 on Two-Anchor Connections, Sleeve M16, h_{ef} = 7 inches (178 mm), e = 12 inches (304.8 mm) of Tension Anchor in Interaction Diagrams of Single-Anchor Tests of Series 23H64
SS = Steel Failure at Shear Anchor
SZ = Steel Failure at Tension Anchor
SB = Steel Failure at both Anchors
L = +: Gap at Shear Anchor
L = -: Gap at Tension Anchor
z1 = 263 mm
z2 = 9 mm
Tests on Single Anchors, Series 23H64
Test 25h6421, L = + 1.0 mm, SB
Test 25H6422, L = - 1.2 mm, SS
Test 25H6423, L = + 0.6 mm, SS
Vertical Load Component [kN]
Horizontal Load Component [kN]
0
20
40
60
80
100
120
140
Results of Text Calculations of Series 25H642, Sleeve M16, h_{ef} = 7 inches (178 mm), e = 12 inches (304.8 mm), Tension Anchor in Interaction Diagrams of Single-Anchor Tests of Series 23H64
SS = Steel Failure at Shear Anchor
SZ = Steel Failure at Tension Anchor
SB = Steel Failure at both Anchors
L = +: Gap at Shear Anchor
L = -: Gap at Tension Anchor
z1 = 263 mm
z2 = 9 mm
Tests on Single Anchors, Series 23H64
Calculation, L = - 3 mm, SS
Calculation, L = 0 mm, SS
Calculation, L = + 3 mm, SZ
Vertical Load Component [kN]
Horizontal Load Component [kN]

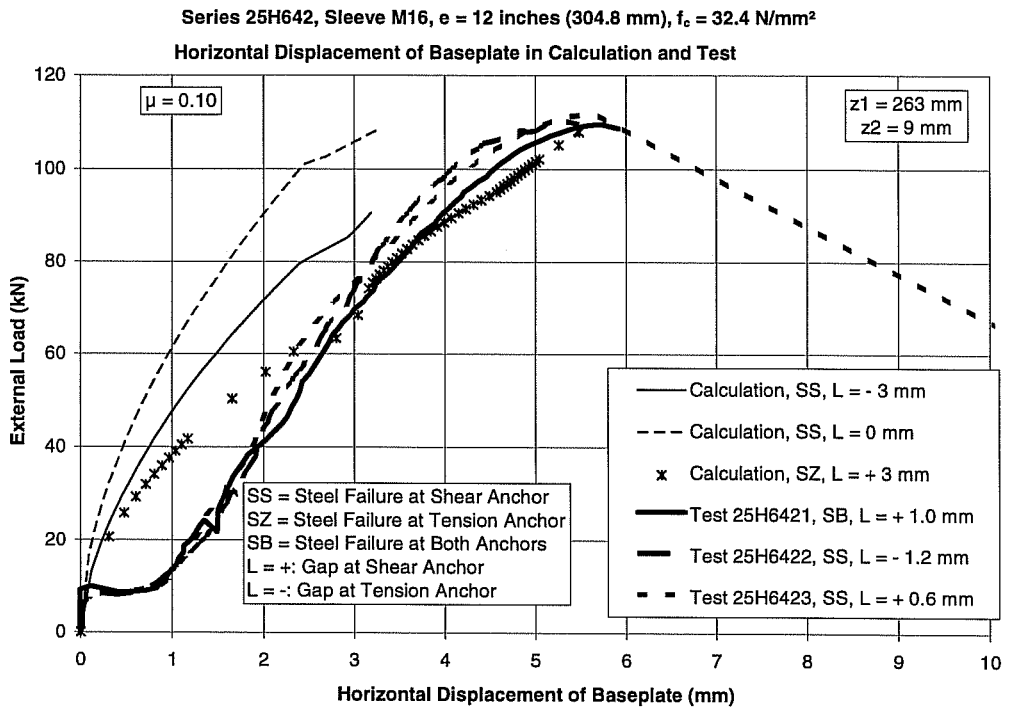
Series 25H642, Sleeve M16, e = 12 inches (304.8 mm), f_c = 32.4 N/mm²
Horizontal Displacement of Baseplate in Calculation and Test
μ = 0.10
z1 = 263 mm
z2 = 9 mm
SS = Steel Failure at Shear Anchor
SZ = Steel Failure at Tension Anchor
SB = Steel Failure at Both Anchors
L = +: Gap at Shear Anchor
L = -: Gap at Tension Anchor
Calculation, SS, L = - 3 mm
Calculation, SS, L = 0 mm
Calculation, SZ, L = + 3 mm
Test 25H6421, SB, L = + 1.0 mm
Test 25H6422, SS, L = - 1.2 mm
Test 25H6423, SS, L = + 0.6 mm
External Load (kN)
Horizontal Displacement of Baseplate (mm)
0
20
40
60
80
100
120
0
1
2
3
4
5
6
7
8
9
10

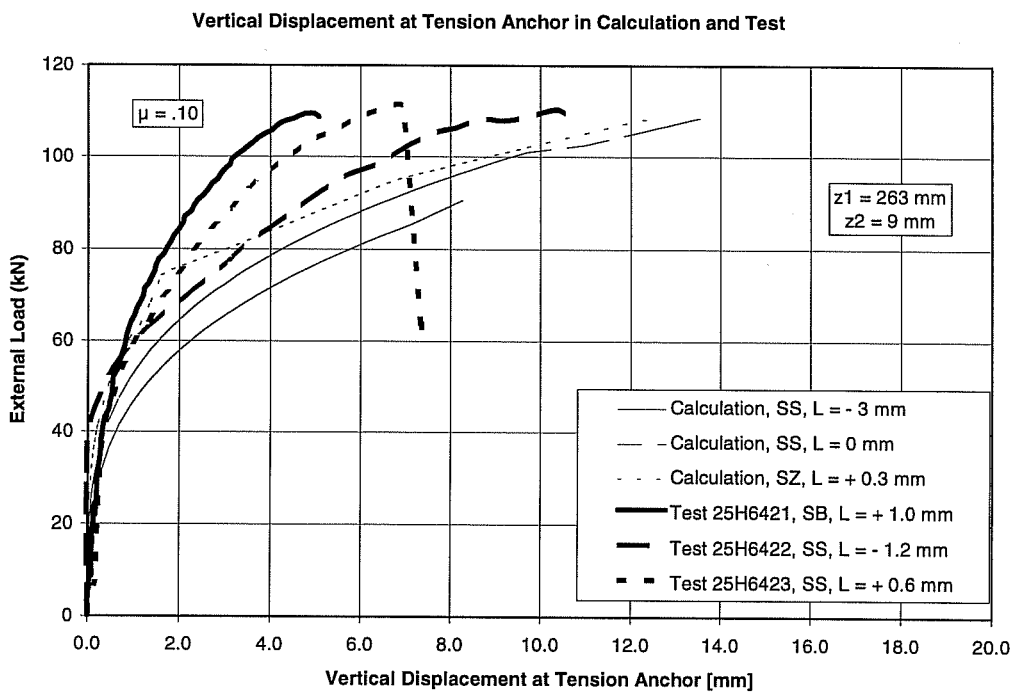
Vertical Displacement at Tension Anchor in Calculation and Test
μ = .10
z1 = 263 mm
z2 = 9 mm
Calculation, SS, L = - 3 mm
Calculation, SS, L = 0 mm
Calculation, SZ, L = + 0.3 mm
Test 25H6421, SB, L = + 1.0 mm
Test 25H6422, SS, L = - 1.2 mm
Test 25H6423, SS, L = + 0.6 mm
External Load (kN)
Vertical Displacement at Tension Anchor [mm]
0
20
40
60
80
100
120
0.0
2.0
4.0
6.0
8.0
10.0
12.0
14.0
16.0
18.0
20.0

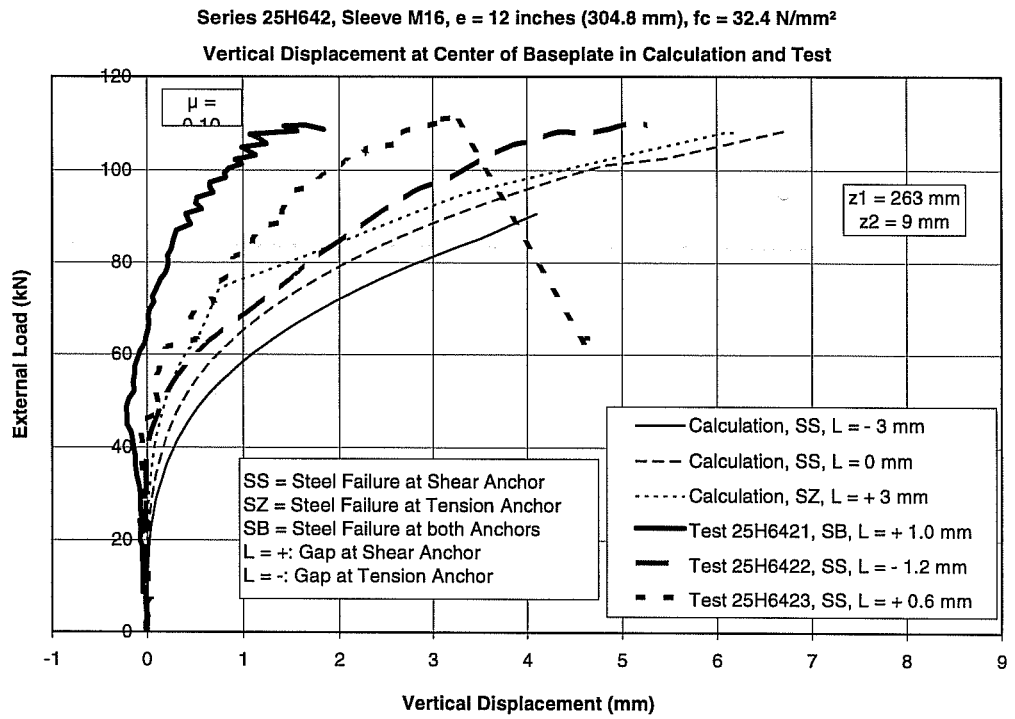
Series 25H642, Sleeve M16, e = 12 inches (304.8 mm), fc = 32.4 N/mm²
Vertical Displacement at Center of Baseplate in Calculation and Test
μ =
z1 = 263 mm
z2 = 9 mm
SS = Steel Failure at Shear Anchor
SZ = Steel Failure at Tension Anchor
SB = Steel Failure at both Anchors
L = +: Gap at Shear Anchor
L = -: Gap at Tension Anchor
Calculation, SS, L = - 3 mm
Calculation, SS, L = 0 mm
Calculation, SZ, L = + 3 mm
Test 25H6421, SB, L = + 1.0 mm
Test 25H6422, SS, L = - 1.2 mm
Test 25H6423, SS, L = + 0.6 mm
External Load (kN)
Vertical Displacement (mm)
120
100
80
60
40
20
0
-1
0
1
2
3
4
5
6
7
8
9

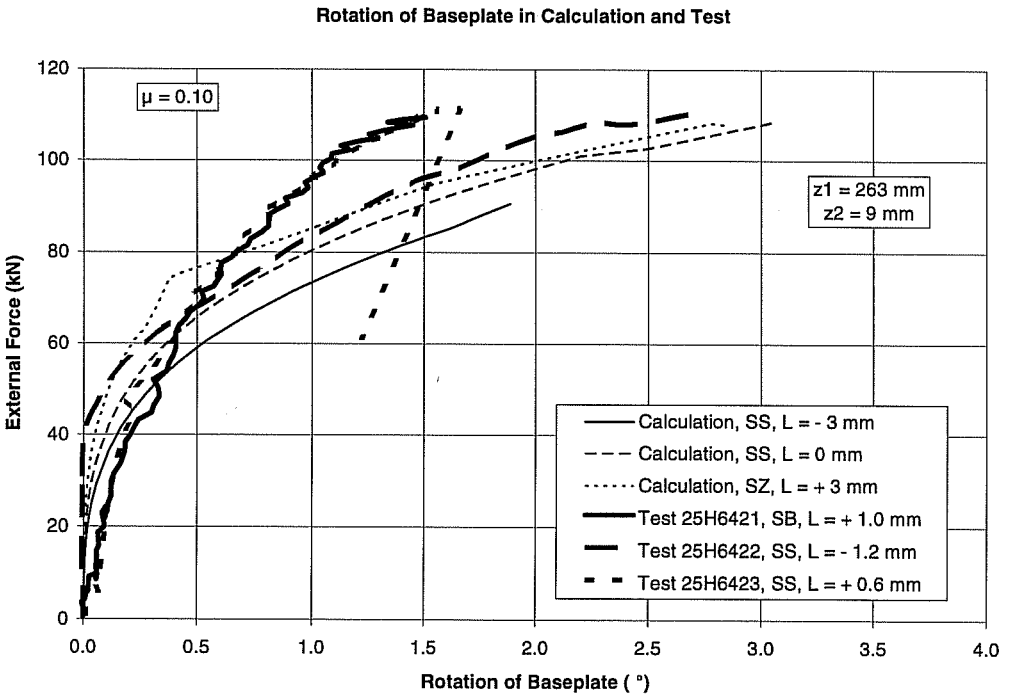
Rotation of Baseplate in Calculation and Test
μ = 0.10
z1 = 263 mm
z2 = 9 mm
Calculation, SS, L = - 3 mm
Calculation, SS, L = 0 mm
Calculation, SZ, L = + 3 mm
Test 25H6421, SB, L = + 1.0 mm
Test 25H6422, SS, L = - 1.2 mm
Test 25H6423, SS, L = + 0.6 mm
External Force (kN)
Rotation of Baseplate (°)
120
100
80
60
40
20
0
0.0
0.5
1.0
1.5
2.0
2.5
3.0
3.5
4.0

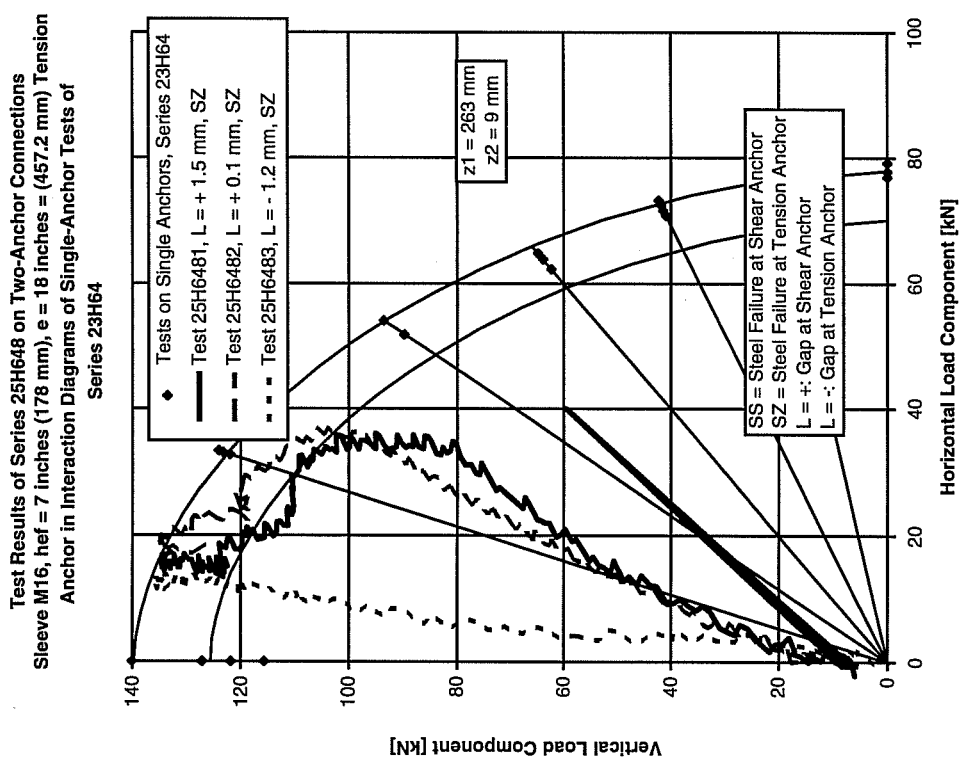
Test Results of Series 25H648 on Two-Anchor Connections
Sleeve M16, hef = 7 inches (178 mm), e = 18 inches = (457.2 mm) Tension
Anchor in Interaction Diagrams of Single-Anchor Tests of
Series 23H64
Tests on Single Anchors, Series 23H64
Test 25H6481, L = + 1.5 mm, SZ
Test 25H6482, L = + 0.1 mm, SZ
Test 25H6483, L = - 1.2 mm, SZ
z1 = 263 mm
z2 = 9 mm
SS = Steel Failure at Shear Anchor
SZ = Steel Failure at Tension Anchor
L = +: Gap at Shear Anchor
L = -: Gap at Tension Anchor
Vertical Load Component [kN]
Horizontal Load Component [kN]
0
20
40
60
80
100
120
140

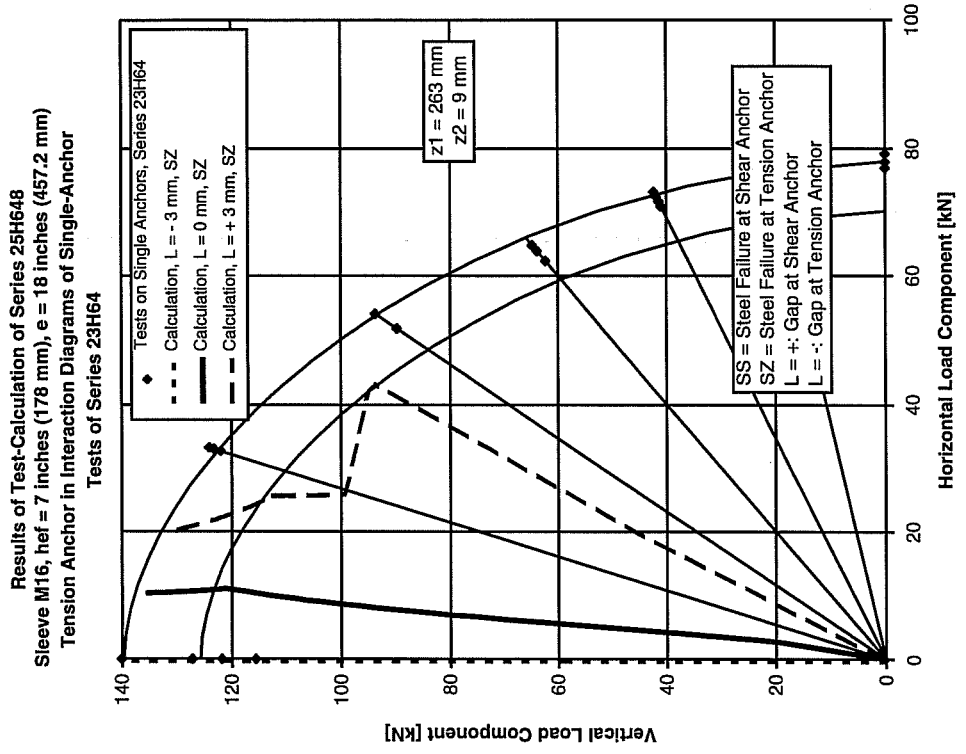
Results of Test-Calculation of Series 25H648
Sleeve M16, hef = 7 inches (178 mm), e = 18 inches (457.2 mm)
Tension Anchor in Interaction Diagrams of Single-Anchor
Tests of Series 23H64
Tests on Single Anchors, Series 23H64
Calculation, L = - 3 mm, SZ
Calculation, L = 0 mm, SZ
Calculation, L = + 3 mm, SZ
z1 = 263 mm
z2 = 9 mm
SS = Steel Failure at Shear Anchor
SZ = Steel Failure at Tension Anchor
L = +: Gap at Shear Anchor
L = -: Gap at Tension Anchor
Vertical Load Component [kN]
Horizontal Load Component [kN]
0
20
40
60
80
100
120
140

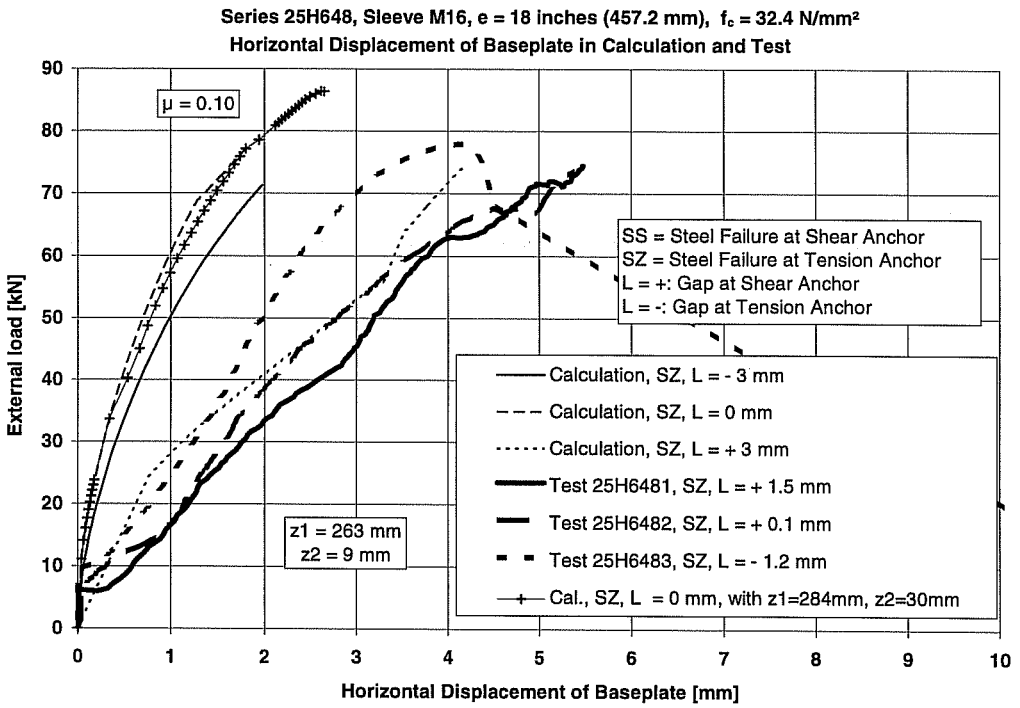
Series 25H648, Sleeve M16, e = 18 inches (457.2 mm), f_c = 32.4 N/mm²
Horizontal Displacement of Baseplate in Calculation and Test
μ = 0.10
z1 = 263 mm
z2 = 9 mm
SS = Steel Failure at Shear Anchor
SZ = Steel Failure at Tension Anchor
L = +: Gap at Shear Anchor
L = -: Gap at Tension Anchor
Calculation, SZ, L = - 3 mm
Calculation, SZ, L = 0 mm
Calculation, SZ, L = + 3 mm
Test 25H6481, SZ, L = + 1.5 mm
Test 25H6482, SZ, L = + 0.1 mm
Test 25H6483, SZ, L = - 1.2 mm
Cal., SZ, L = 0 mm, with z1=284mm, z2=30mm
External load [kN]
Horizontal Displacement of Baseplate [mm]
0
10
20
30
40
50
60
70
80
90
0
1
2
3
4
5
6
7
8
9
10

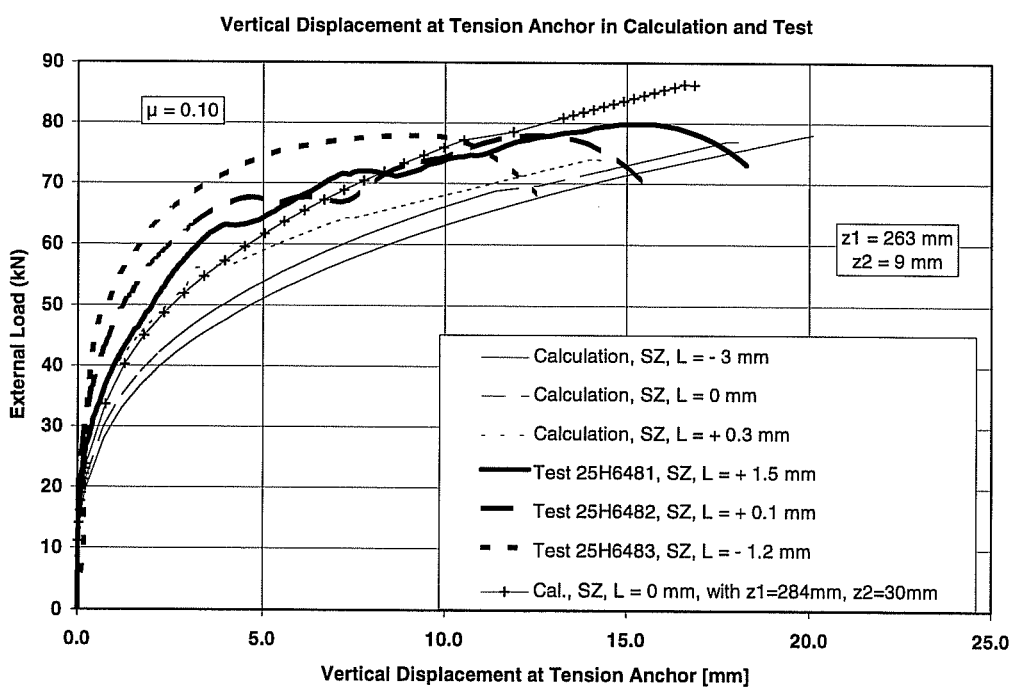
Vertical Displacement at Tension Anchor in Calculation and Test
μ = 0.10
z1 = 263 mm
z2 = 9 mm
Calculation, SZ, L = - 3 mm
Calculation, SZ, L = 0 mm
Calculation, SZ, L = + 0.3 mm
Test 25H6481, SZ, L = + 1.5 mm
Test 25H6482, SZ, L = + 0.1 mm
Test 25H6483, SZ, L = - 1.2 mm
Cal., SZ, L = 0 mm, with z1=284mm, z2=30mm
External Load (kN)
Vertical Displacement at Tension Anchor [mm]
0
10
20
30
40
50
60
70
80
90
0.0
5.0
10.0
15.0
20.0
25.0

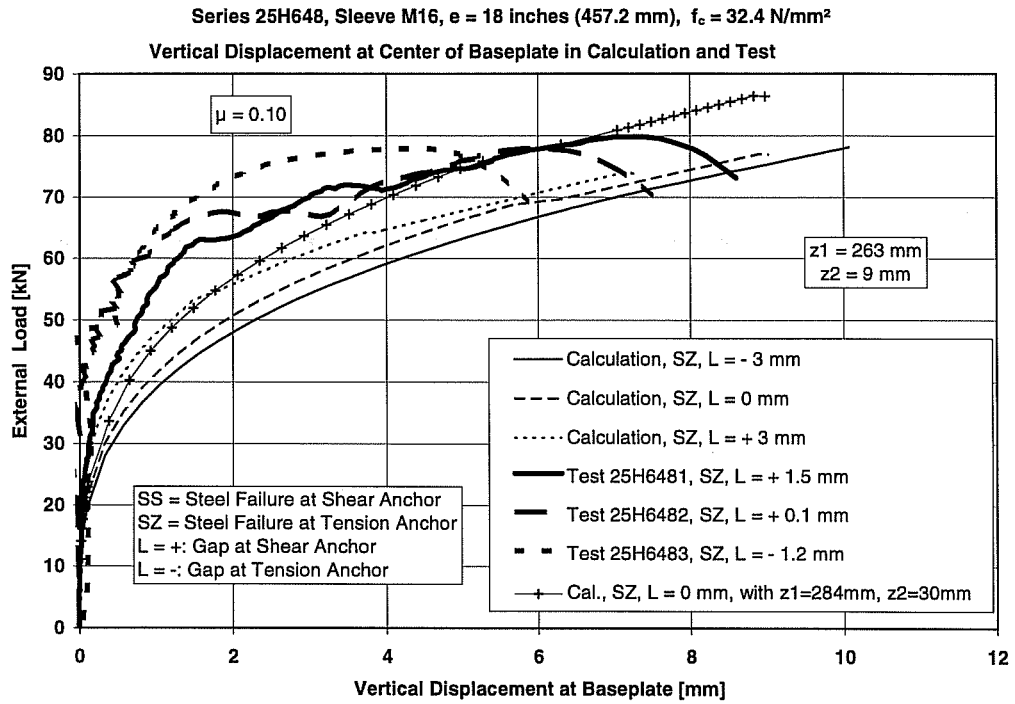
Series 25H648, Sleeve M16, e = 18 inches (457.2 mm), f_c = 32.4 N/mm²
Vertical Displacement at Center of Baseplate in Calculation and Test
μ = 0.10
z1 = 263 mm
z2 = 9 mm
SS = Steel Failure at Shear Anchor
SZ = Steel Failure at Tension Anchor
L = +: Gap at Shear Anchor
L = -: Gap at Tension Anchor
Calculation, SZ, L = - 3 mm
Calculation, SZ, L = 0 mm
Calculation, SZ, L = + 3 mm
Test 25H6481, SZ, L = + 1.5 mm
Test 25H6482, SZ, L = + 0.1 mm
Test 25H6483, SZ, L = - 1.2 mm
Cal., SZ, L = 0 mm, with z1=284mm, z2=30mm
External Load [kN]
Vertical Displacement at Baseplate [mm]
0
10
20
30
40
50
60
70
80
90
0
2
4
6
8
10
12

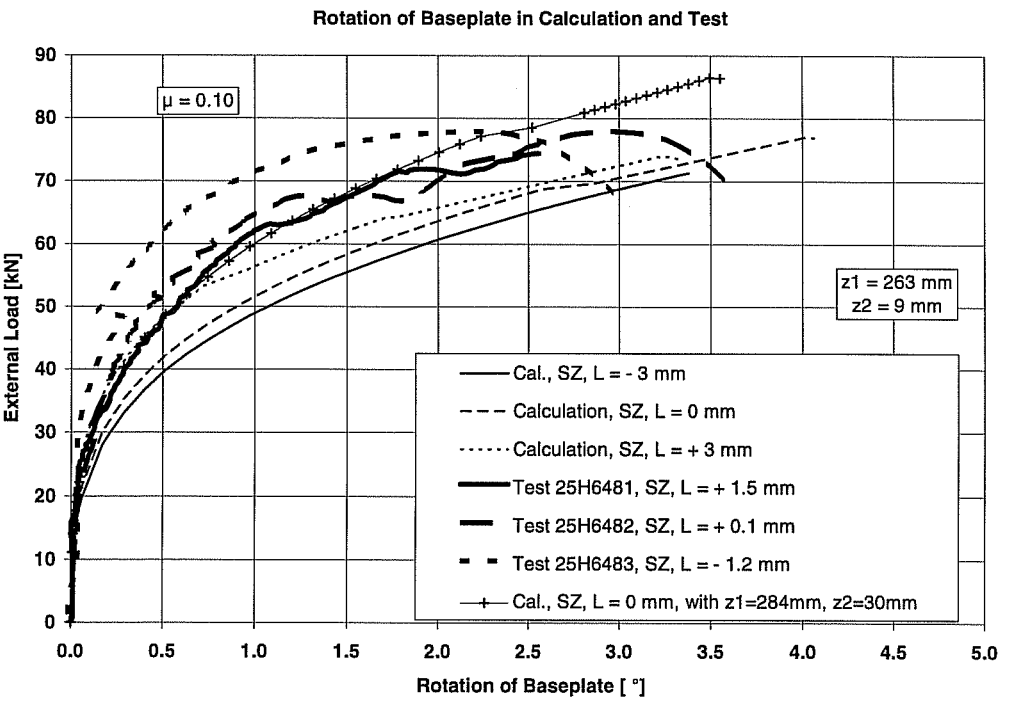
Rotation of Baseplate in Calculation and Test
μ = 0.10
z1 = 263 mm
z2 = 9 mm
Cal., SZ, L = - 3 mm
Calculation, SZ, L = 0 mm
Calculation, SZ, L = + 3 mm
Test 25H6481, SZ, L = + 1.5 mm
Test 25H6482, SZ, L = + 0.1 mm
Test 25H6483, SZ, L = - 1.2 mm
Cal., SZ, L = 0 mm, with z1=284mm, z2=30mm
External Load [kN]
Rotation of Baseplate [°]
0
10
20
30
40
50
60
70
80
90
0.0
0.5
1.0
1.5
2.0
2.5
3.0
3.5
4.0
4.5
5.0

Comparison Among Plastic Theory, Elastic Theory, Calculation with BDA5, and Test Results of Connections of Series 25M54

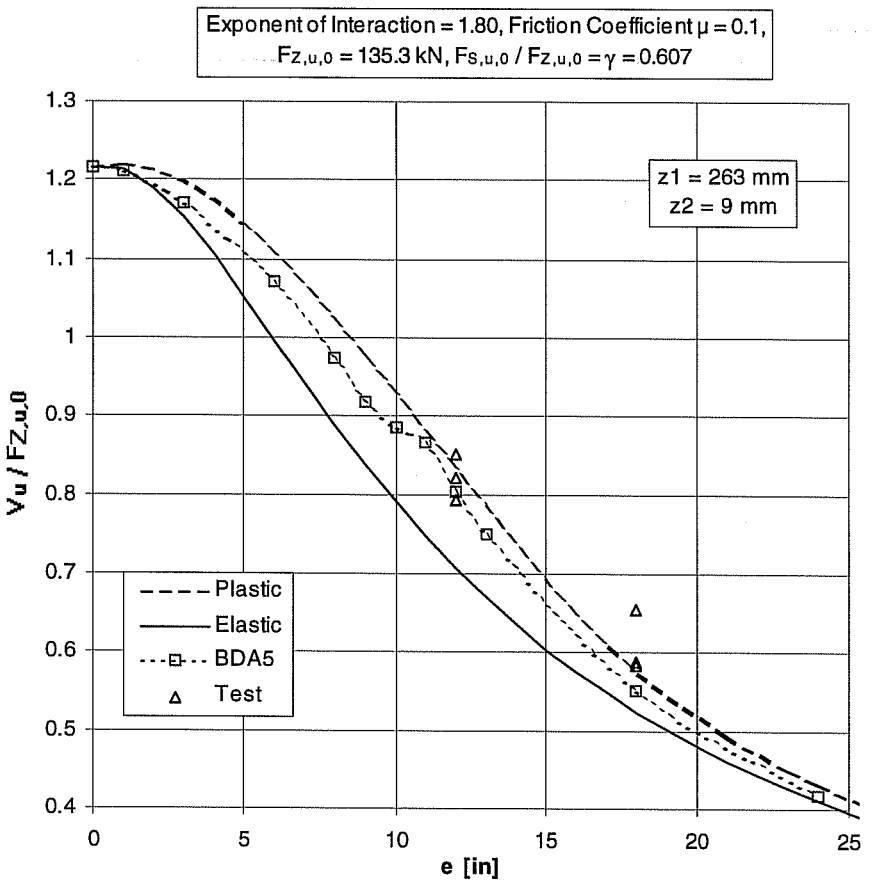

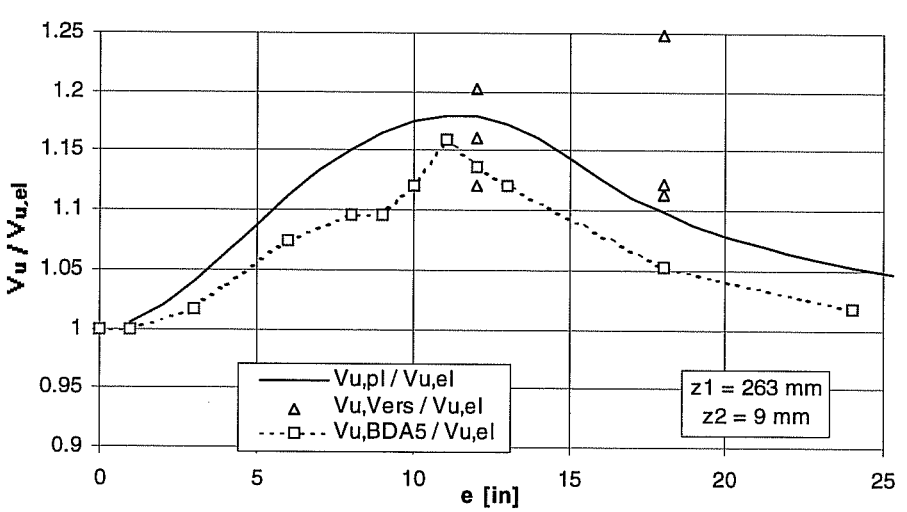

Comparison Among Plastic Theory, Elastic Theory, Calculation with BDA5, and Test Results of Connections of Series 25M54

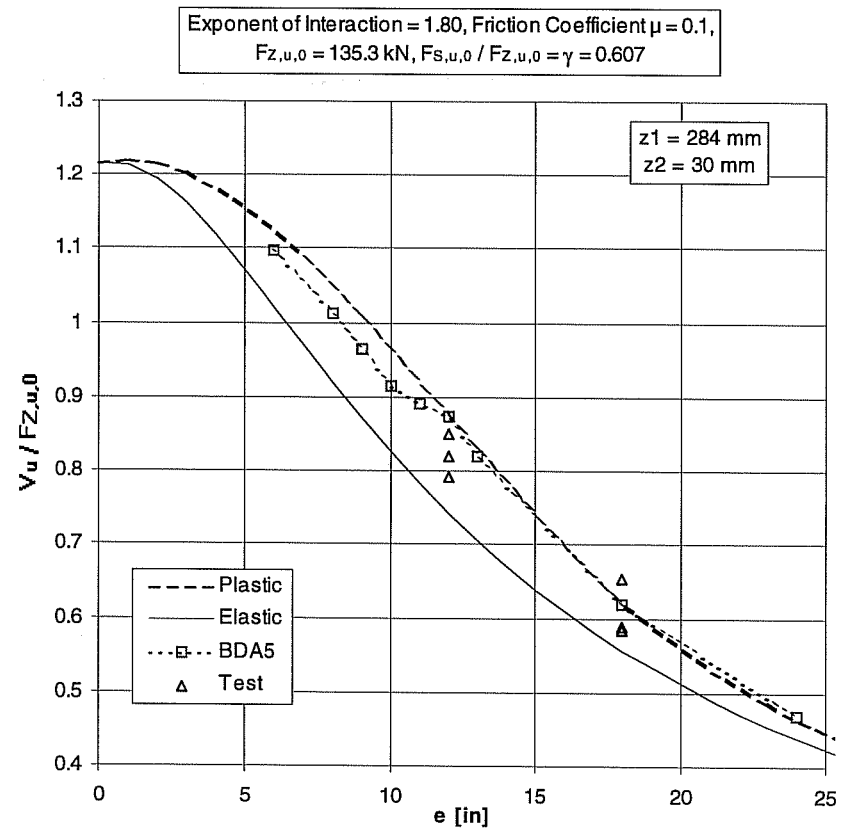

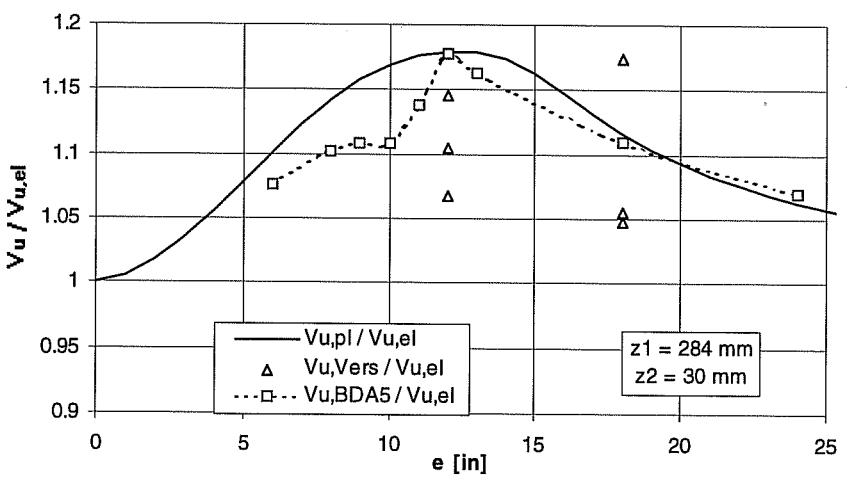

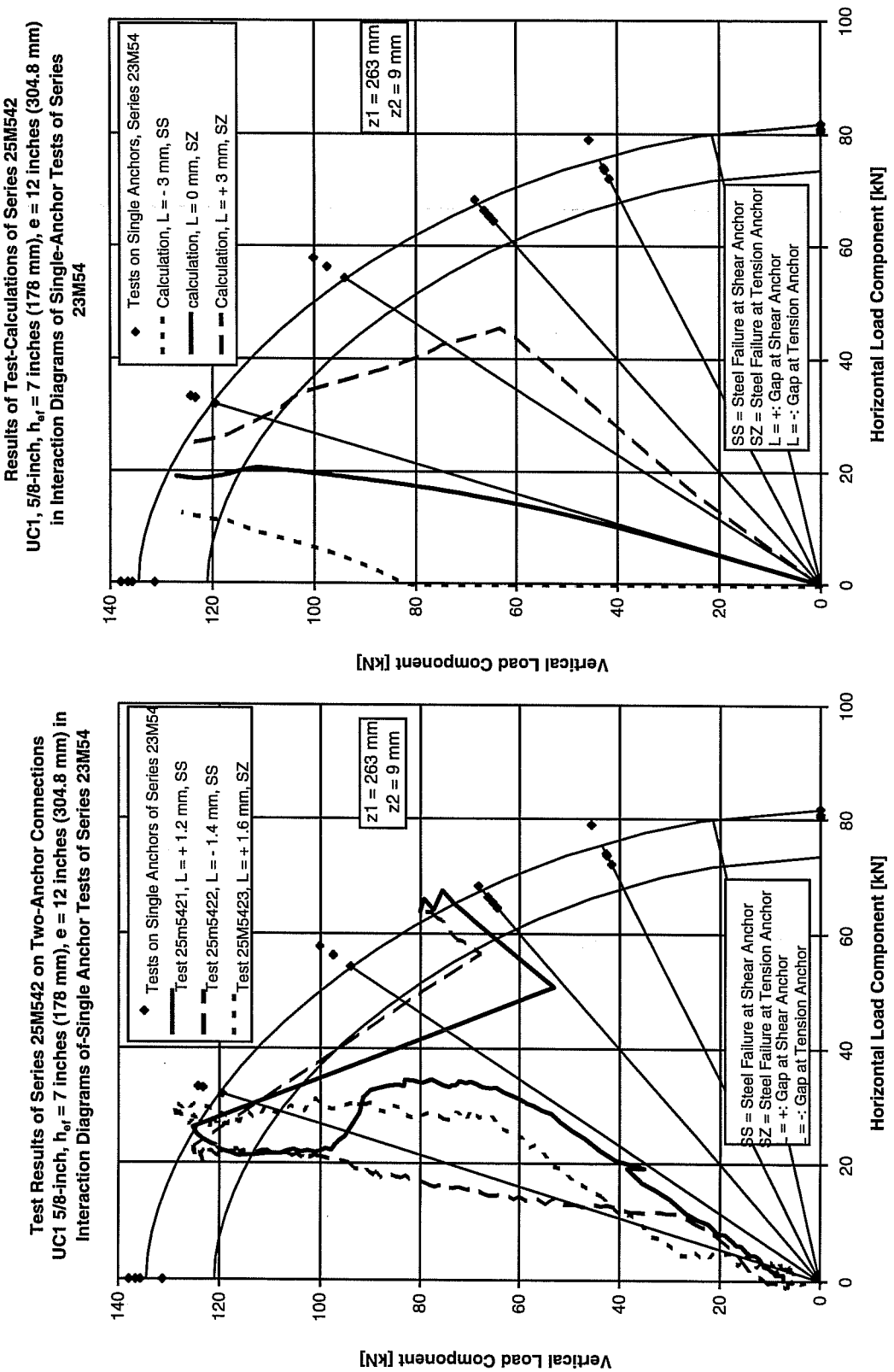
Results of Test-Calculations of Series 25M542
UC1, 5/8-inch, h_{ef} = 7 inches (178 mm), e = 12 inches (304.8 mm)
in Interaction Diagrams of Single-Anchor Tests of Series 23M54
Tests on Single Anchors, Series 23M54
Calculation, L = - 3 mm, SS
calculation, L = 0 mm, SZ
Calculation, L = + 3 mm, SZ
z1 = 263 mm
z2 = 9 mm
SS = Steel Failure at Shear Anchor
SZ = Steel Failure at Tension Anchor
L = +: Gap at Shear Anchor
L = -: Gap at Tension Anchor
Vertical Load Component [kN]
Horizontal Load Component [kN]
Test Results of Series 25M542 on Two-Anchor Connections
UC1 5/8-inch, h_{ef} = 7 inches (178 mm), e = 12 inches (304.8 mm) in
Interaction Diagrams of-Single Anchor Tests of Series 23M54
Tests on Single Anchors of Series 23M54
Test 25m5421, L = + 1.2 mm, SS
Test 25m5422, L = - 1.4 mm, SS
Test 25M5423, L = + 1.6 mm, SZ
z1 = 263 mm
z2 = 9 mm
SS = Steel Failure at Shear Anchor
SZ = Steel Failure at Tension Anchor
L = +: Gap at Shear Anchor
L = -: Gap at Tension Anchor
Vertical Load Component [kN]
Horizontal Load Component [kN]

Series 25M542, UC1 5/8", e = 12 inches (304.8 mm), f_c = 32.4 N/mm²

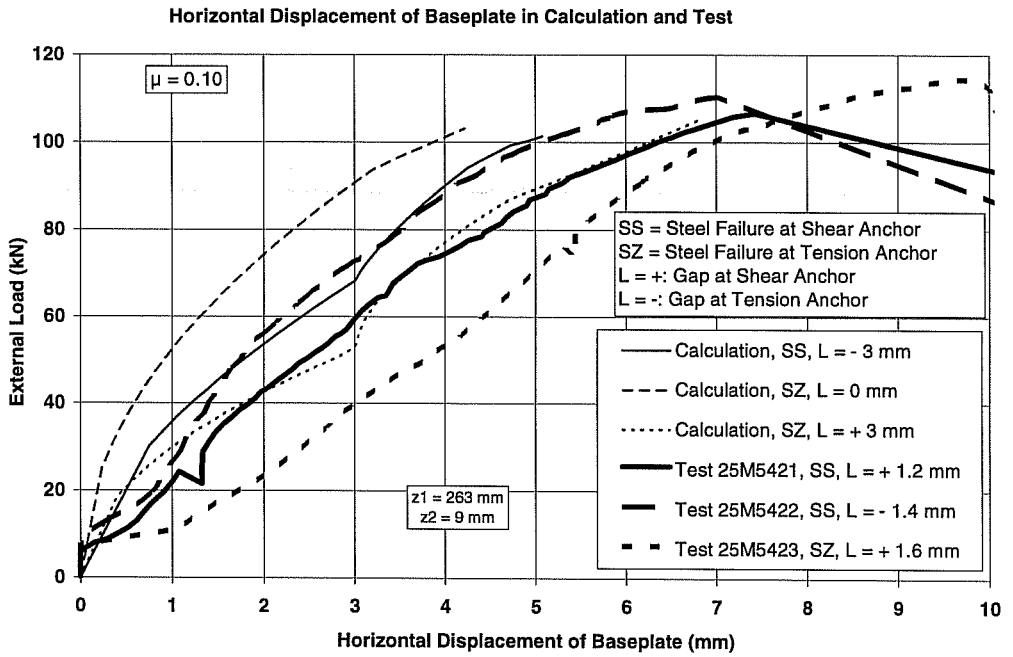

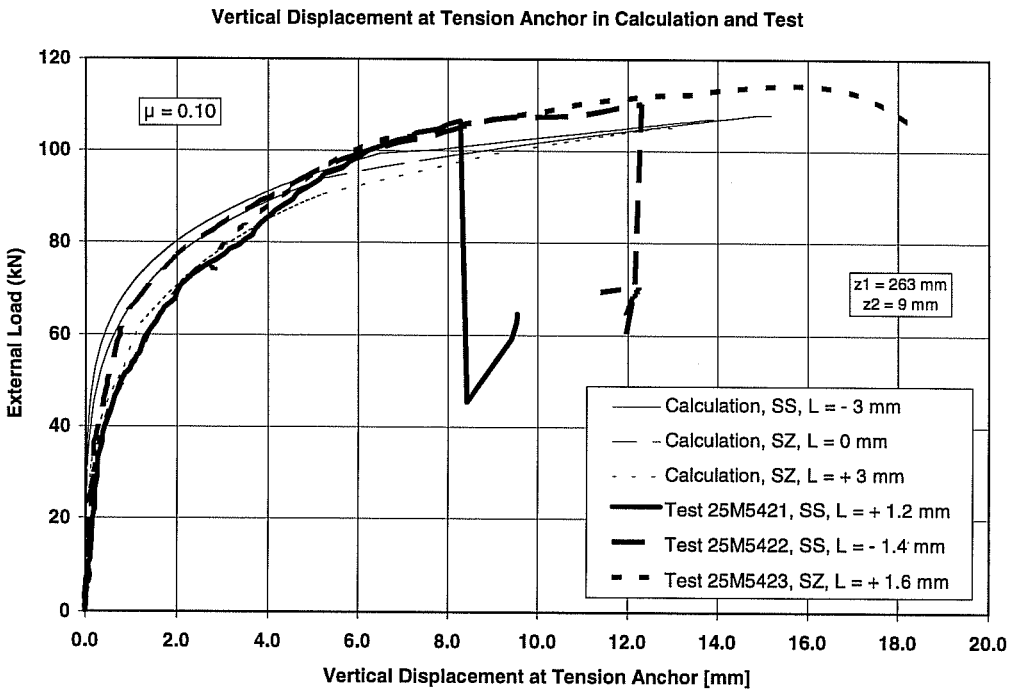

Series 25M542, UC1 5/8", e = 12 inches (304.8 mm), f_c = 32.4 N/mm²

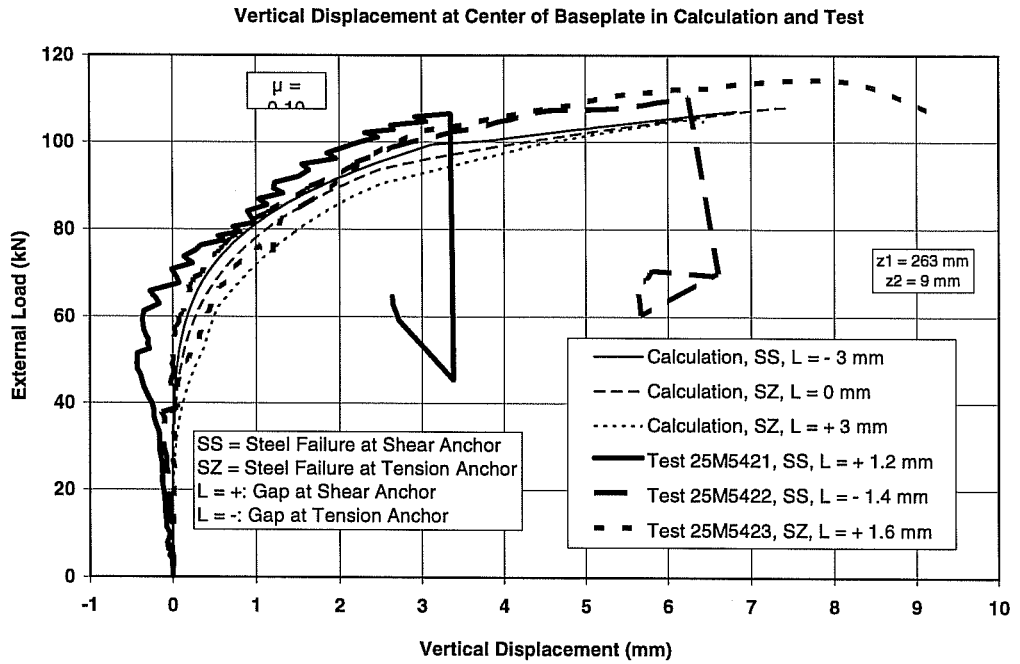

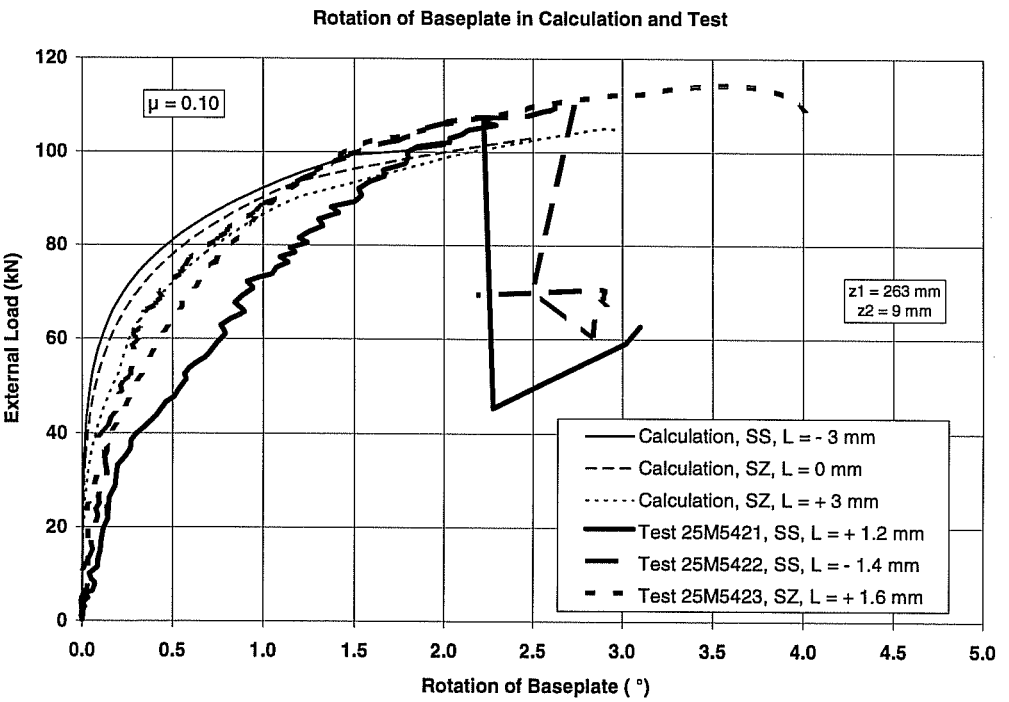

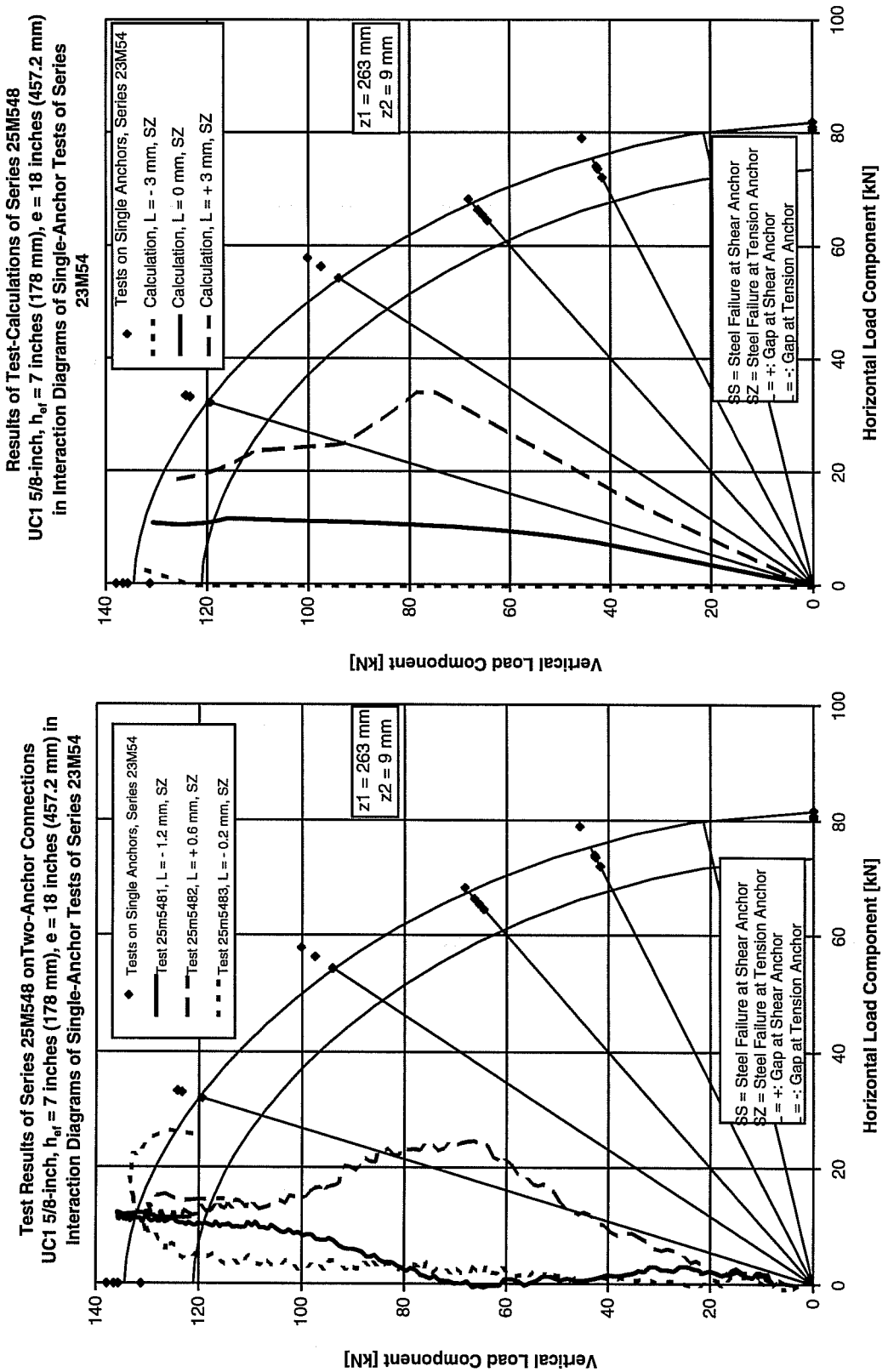
Test Results of Series 25M548 onTwo-Anchor Connections
UC1 5/8-inch, h_{ef} = 7 inches (178 mm), e = 18 inches (457.2 mm) in Interaction Diagrams of Single-Anchor Tests of Series 23M54
Tests on Single Anchors, Series 23M54
Test 25m5481, L = - 1.2 mm, SZ
Test 25m5482, L = + 0.6 mm, SZ
Test 25m5483, L = - 0.2 mm, SZ
z1 = 263 mm
z2 = 9 mm
SS = Steel Failure at Shear Anchor
SZ = Steel Failure at Tension Anchor
L = +: Gap at Shear Anchor
L = -: Gap at Tension Anchor
Vertical Load Component [kN]
Horizontal Load Component [kN]
0
20
40
60
80
100
120
140
Results of Test-Calculations of Series 25M548
UC1 5/8-inch, h_{ef} = 7 inches (178 mm), e = 18 inches (457.2 mm) in Interaction Diagrams of Single-Anchor Tests of Series 23M54
Tests on Single Anchors, Series 23M54
Calculation, L = - 3 mm, SZ
Calculation, L = 0 mm, SZ
Calculation, L = + 3 mm, SZ
z1 = 263 mm
z2 = 9 mm
SS = Steel Failure at Shear Anchor
SZ = Steel Failure at Tension Anchor
L = +: Gap at Shear Anchor
L = -: Gap at Tension Anchor
Vertical Load Component [kN]
Horizontal Load Component [kN]

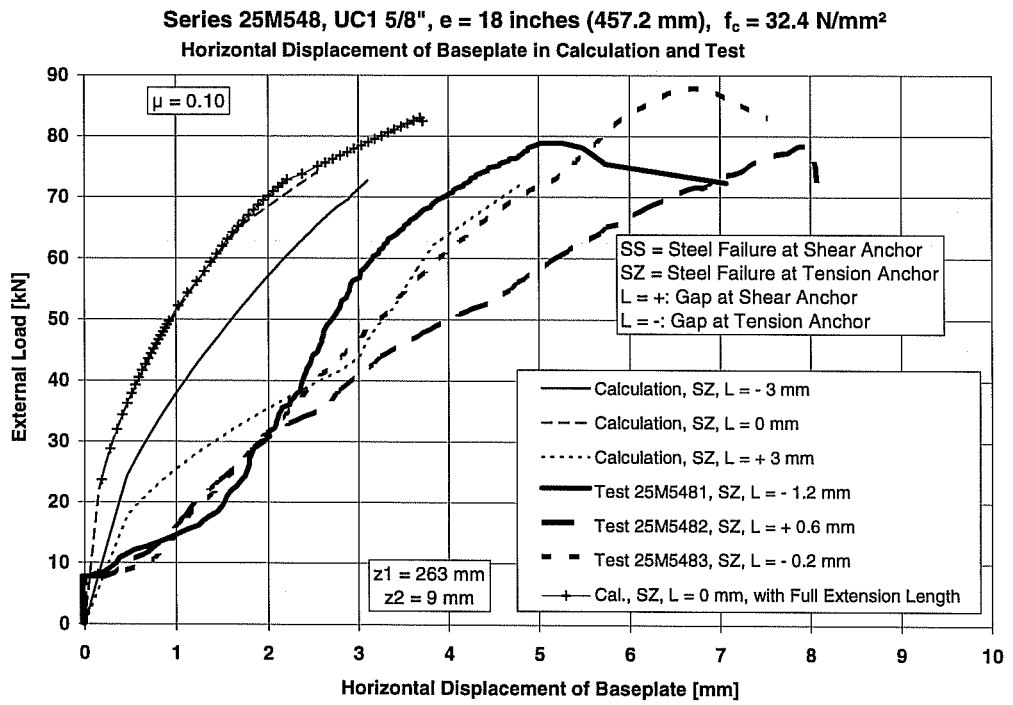
Series 25M548, UC1 5/8", e = 18 inches (457.2 mm), f_c = 32.4 N/mm²
Horizontal Displacement of Baseplate in Calculation and Test
μ = 0.10
SS = Steel Failure at Shear Anchor
SZ = Steel Failure at Tension Anchor
L = +: Gap at Shear Anchor
L = -: Gap at Tension Anchor
Calculation, SZ, L = - 3 mm
Calculation, SZ, L = 0 mm
Calculation, SZ, L = + 3 mm
Test 25M5481, SZ, L = - 1.2 mm
Test 25M5482, SZ, L = + 0.6 mm
Test 25M5483, SZ, L = - 0.2 mm
Cal., SZ, L = 0 mm, with Full Extension Length
z1 = 263 mm
z2 = 9 mm
External Load [kN]
Horizontal Displacement of Baseplate [mm]
0
10
20
30
40
50
60
70
80
90
0
1
2
3
4
5
6
7
8
9
10

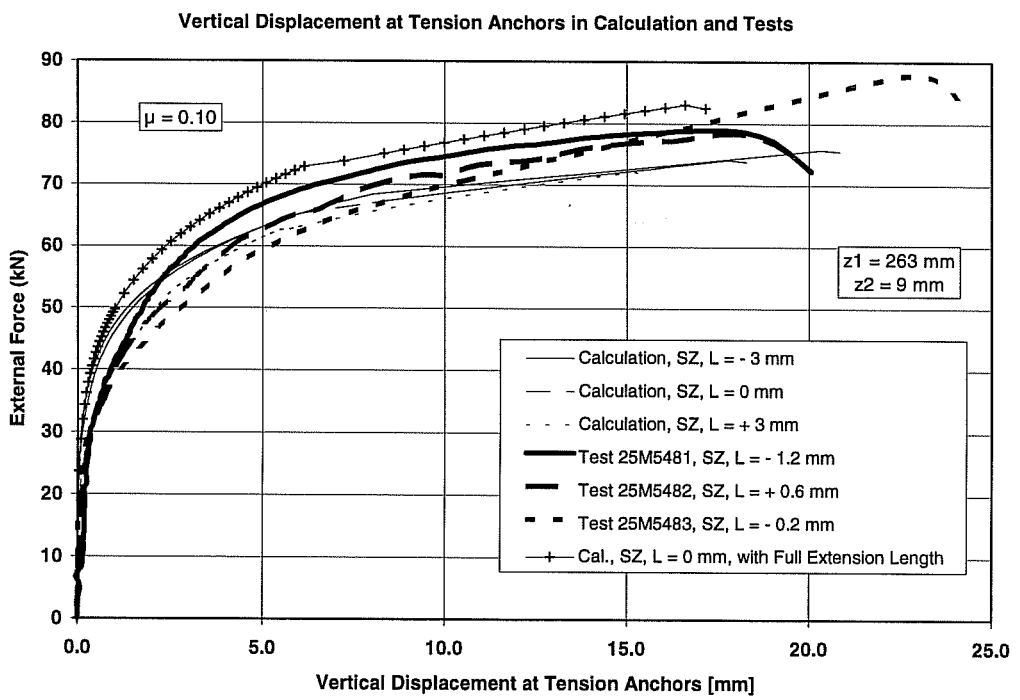
Vertical Displacement at Tension Anchors in Calculation and Tests
μ = 0.10
z1 = 263 mm
z2 = 9 mm
Calculation, SZ, L = - 3 mm
Calculation, SZ, L = 0 mm
Calculation, SZ, L = + 3 mm
Test 25M5481, SZ, L = - 1.2 mm
Test 25M5482, SZ, L = + 0.6 mm
Test 25M5483, SZ, L = - 0.2 mm
Cal., SZ, L = 0 mm, with Full Extension Length
External Force (kN)
Vertical Displacement at Tension Anchors [mm]
0
10
20
30
40
50
60
70
80
90
0.0
5.0
10.0
15.0
20.0
25.0

Series 25M548, UC1 5/8", e = 18 inches (457.2 mm), f_c = 32.4 N/mm²

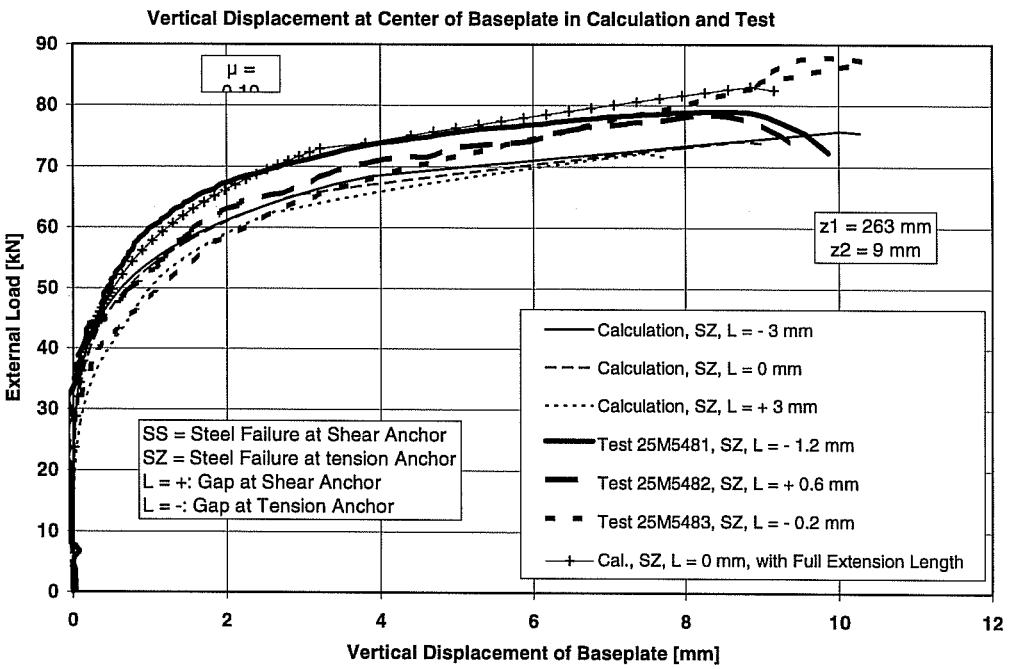

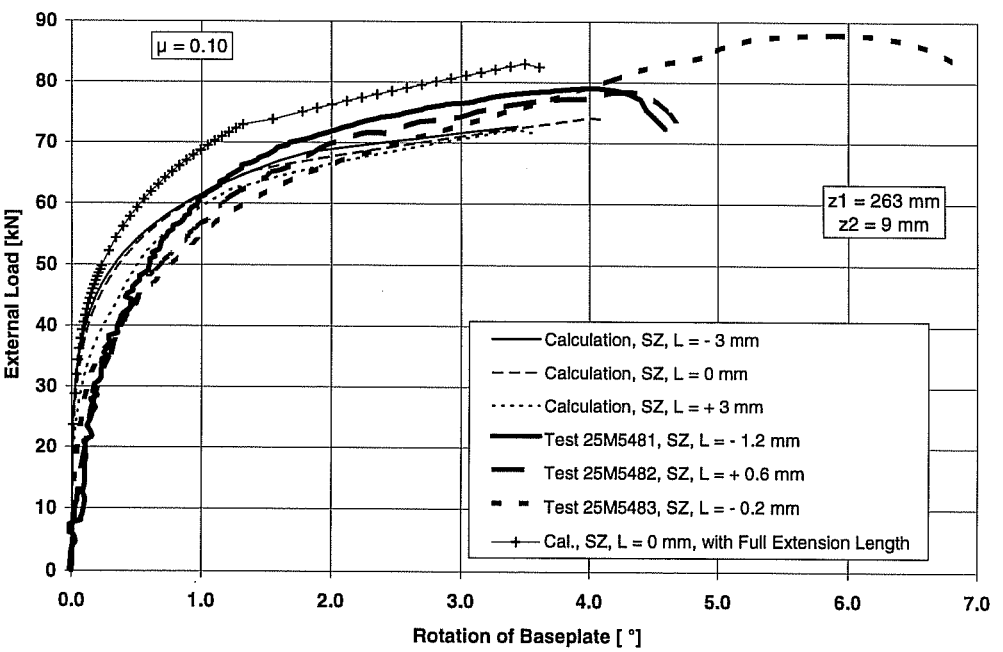

Comparison among Plastic Theory, Elastic Theory, Calculation with BDA5, and Test Results of Connections of Series 25M34

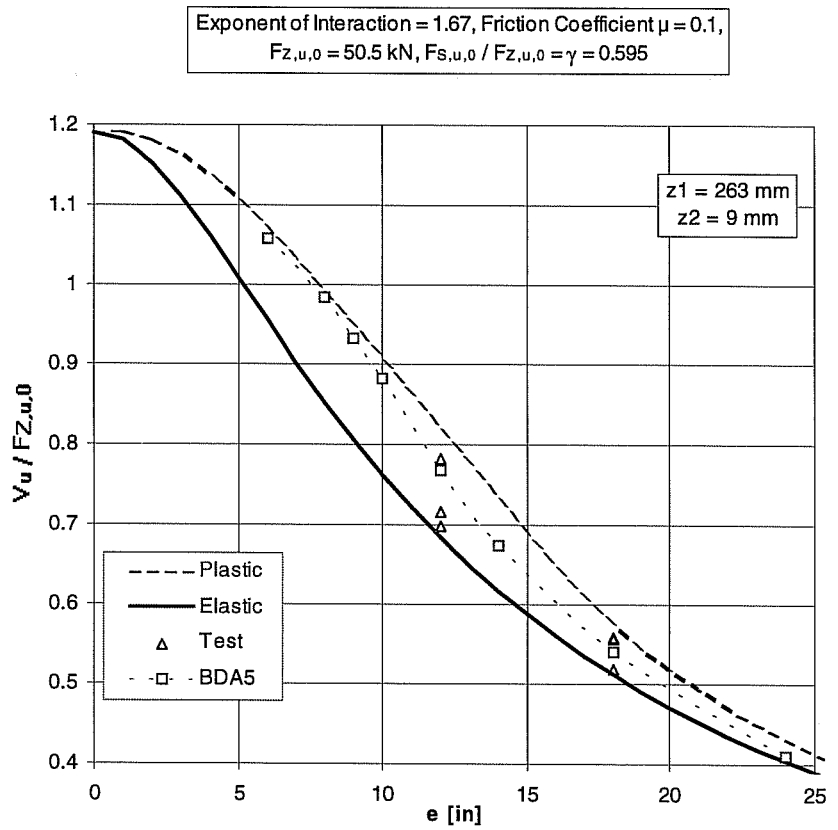

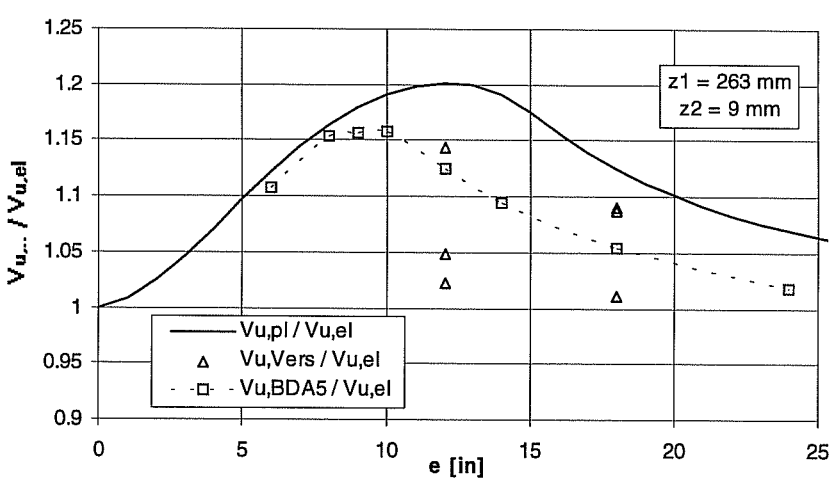

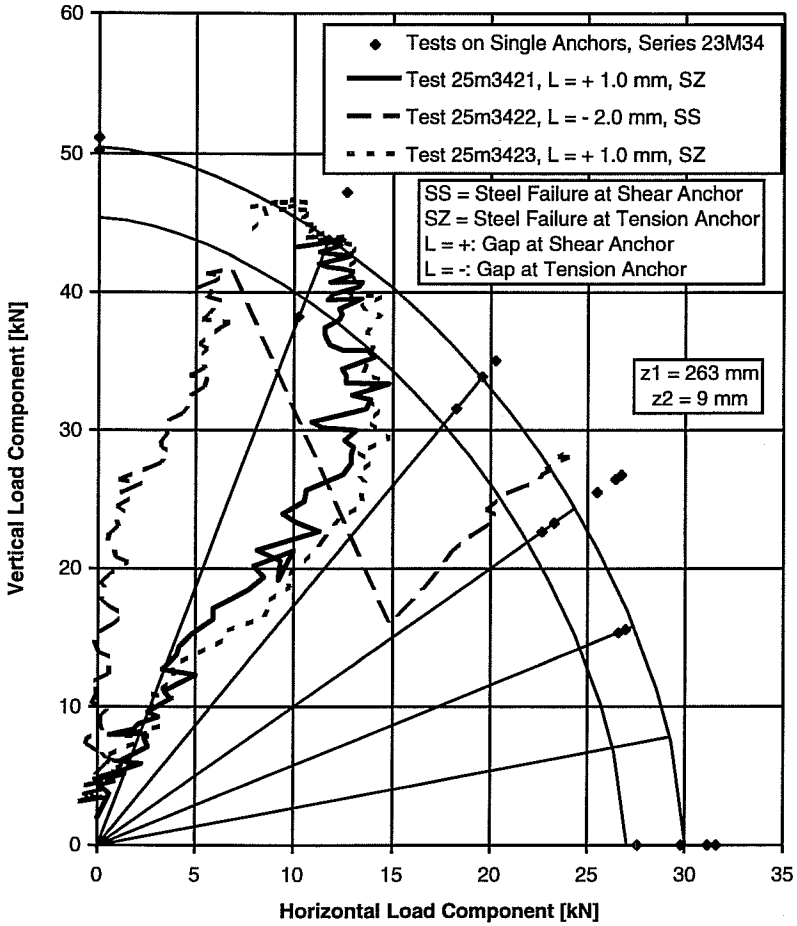
Test Results of Series 25M342 on Two-Anchor Connections
UC1 3/8-inch, h_{ef} = 7 inches (178 mm), e = 12 inches (304.8 mm) in Interaction Diagrams of Single-Anchor Tests of Series 23M34
Tests on Single Anchors, Series 23M34
Test 25m3421, L = + 1.0 mm, SZ
Test 25m3422, L = - 2.0 mm, SS
Test 25m3423, L = + 1.0 mm, SZ
SS = Steel Failure at Shear Anchor
SZ = Steel Failure at Tension Anchor
L = +: Gap at Shear Anchor
L = -: Gap at Tension Anchor
z1 = 263 mm
z2 = 9 mm
Vertical Load Component [kN]
Horizontal Load Component [kN]
0
10
20
30
40
50
60
0
5
10
15
20
25
30
35

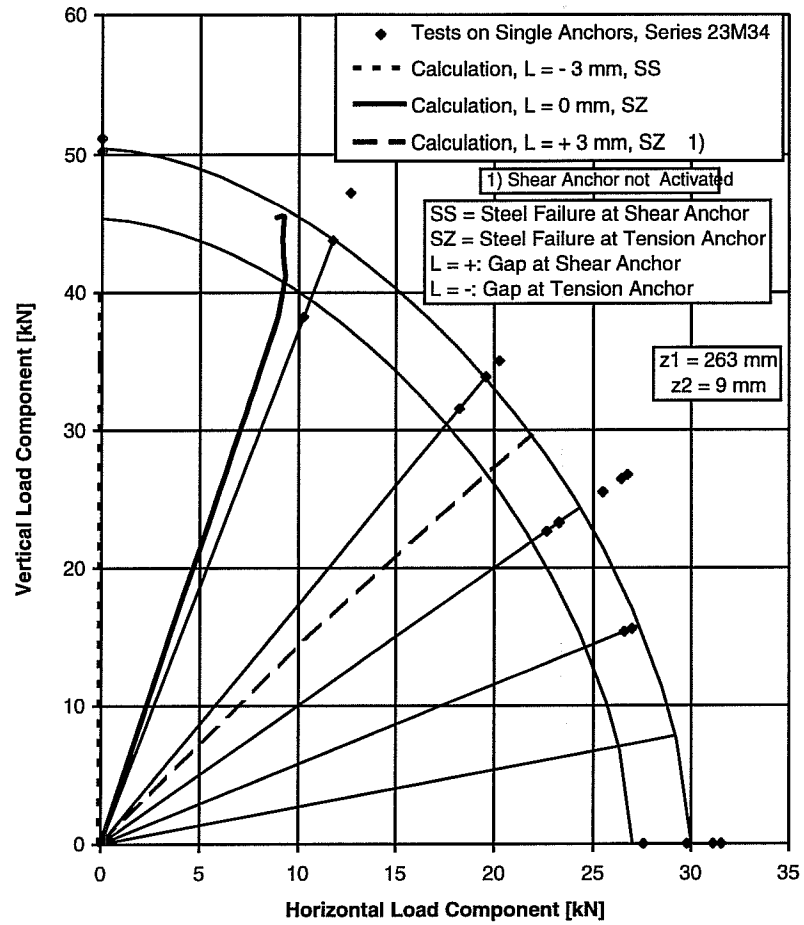
Results of Test-Calculations of Series 25M342
UC1 3/8-inch, h_{ef} = 7 inches (178 mm), e = 12 inches (304.8 mm) in Interaction Diagrams of Single-Anchor Tests of Series 23M34
Tests on Single Anchors, Series 23M34
Calculation, L = - 3 mm, SS
Calculation, L = 0 mm, SZ
Calculation, L = + 3 mm, SZ 1)
1) Shear Anchor not Activated
SS = Steel Failure at Shear Anchor
SZ = Steel Failure at Tension Anchor
L = +: Gap at Shear Anchor
L = -: Gap at Tension Anchor
z1 = 263 mm
z2 = 9 mm
Vertical Load Component [kN]
Horizontal Load Component [kN]
0
10
20
30
40
50
60
0
5
10
15
20
25
30
35

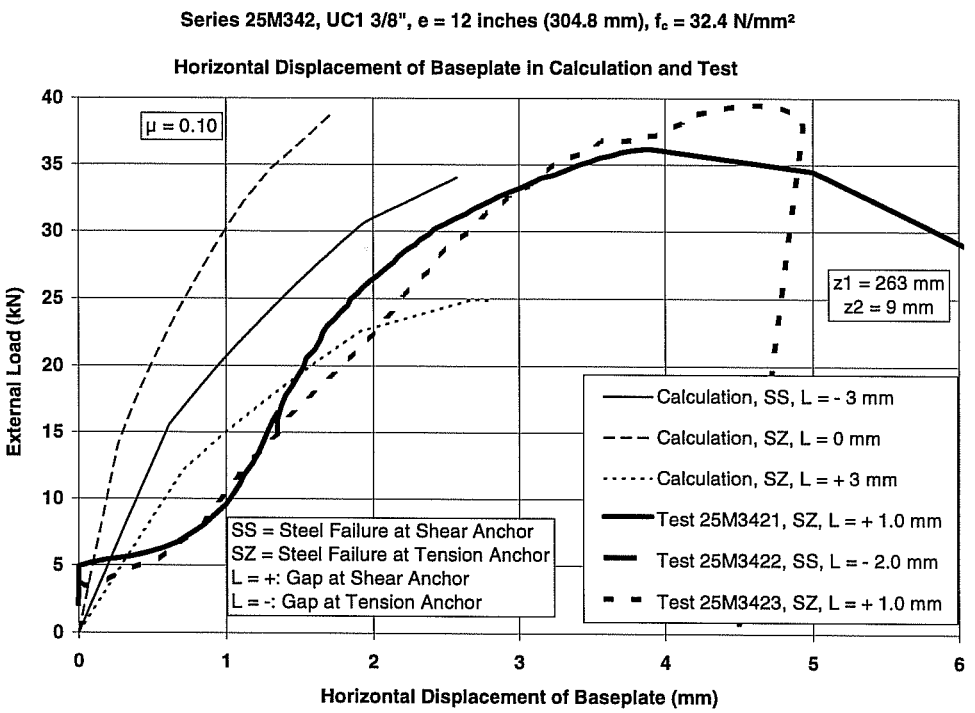
Series 25M342, UC1 3/8", e = 12 inches (304.8 mm), f_c = 32.4 N/mm²
Horizontal Displacement of Baseplate in Calculation and Test
μ = 0.10
z1 = 263 mm
z2 = 9 mm
SS = Steel Failure at Shear Anchor
SZ = Steel Failure at Tension Anchor
L = +: Gap at Shear Anchor
L = -: Gap at Tension Anchor
Calculation, SS, L = - 3 mm
Calculation, SZ, L = 0 mm
Calculation, SZ, L = + 3 mm
Test 25M3421, SZ, L = + 1.0 mm
Test 25M3422, SS, L = - 2.0 mm
Test 25M3423, SZ, L = + 1.0 mm
External Load (kN)
Horizontal Displacement of Baseplate (mm)
0
5
10
15
20
25
30
35
40
0
1
2
3
4
5
6

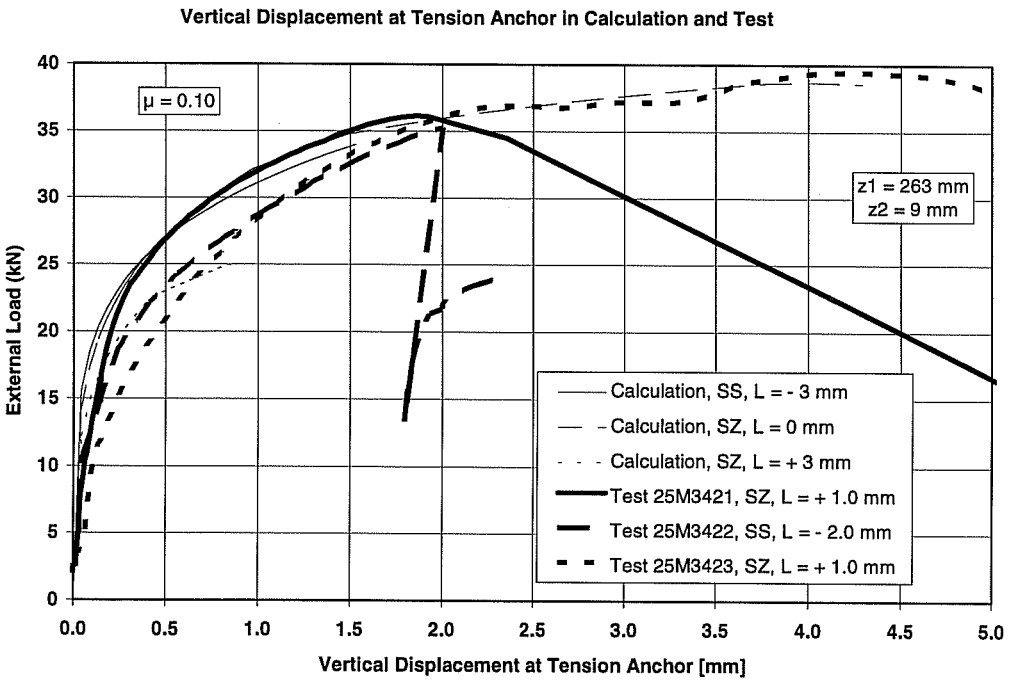
Vertical Displacement at Tension Anchor in Calculation and Test
μ = 0.10
z1 = 263 mm
z2 = 9 mm
Calculation, SS, L = - 3 mm
Calculation, SZ, L = 0 mm
Calculation, SZ, L = + 3 mm
Test 25M3421, SZ, L = + 1.0 mm
Test 25M3422, SS, L = - 2.0 mm
Test 25M3423, SZ, L = + 1.0 mm
External Load (kN)
Vertical Displacement at Tension Anchor [mm]
0
5
10
15
20
25
30
35
40
0.0
0.5
1.0
1.5
2.0
2.5
3.0
3.5
4.0
4.5
5.0

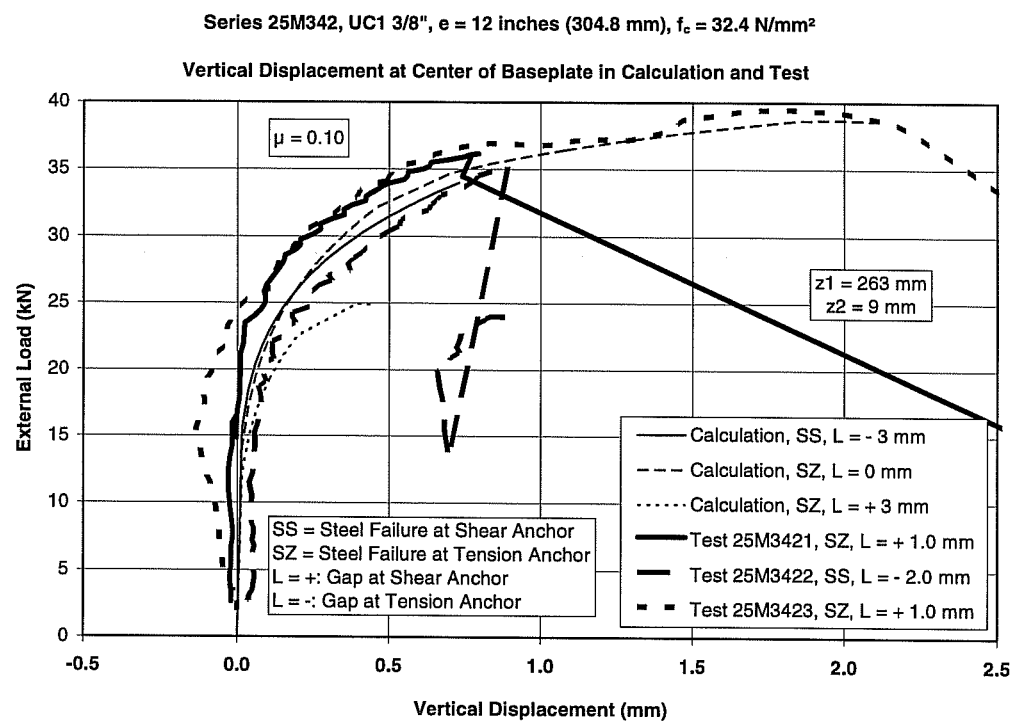
Series 25M342, UC1 3/8", e = 12 inches (304.8 mm), f_c = 32.4 N/mm²
Vertical Displacement at Center of Baseplate in Calculation and Test
μ = 0.10
z1 = 263 mm
z2 = 9 mm
SS = Steel Failure at Shear Anchor
SZ = Steel Failure at Tension Anchor
L = +: Gap at Shear Anchor
L = -: Gap at Tension Anchor
Calculation, SS, L = - 3 mm
Calculation, SZ, L = 0 mm
Calculation, SZ, L = + 3 mm
Test 25M3421, SZ, L = + 1.0 mm
Test 25M3422, SS, L = - 2.0 mm
Test 25M3423, SZ, L = + 1.0 mm
External Load (kN)
Vertical Displacement (mm)
40
35
30
25
20
15
10
5
0
-0.5
0.0
0.5
1.0
1.5
2.0
2.5

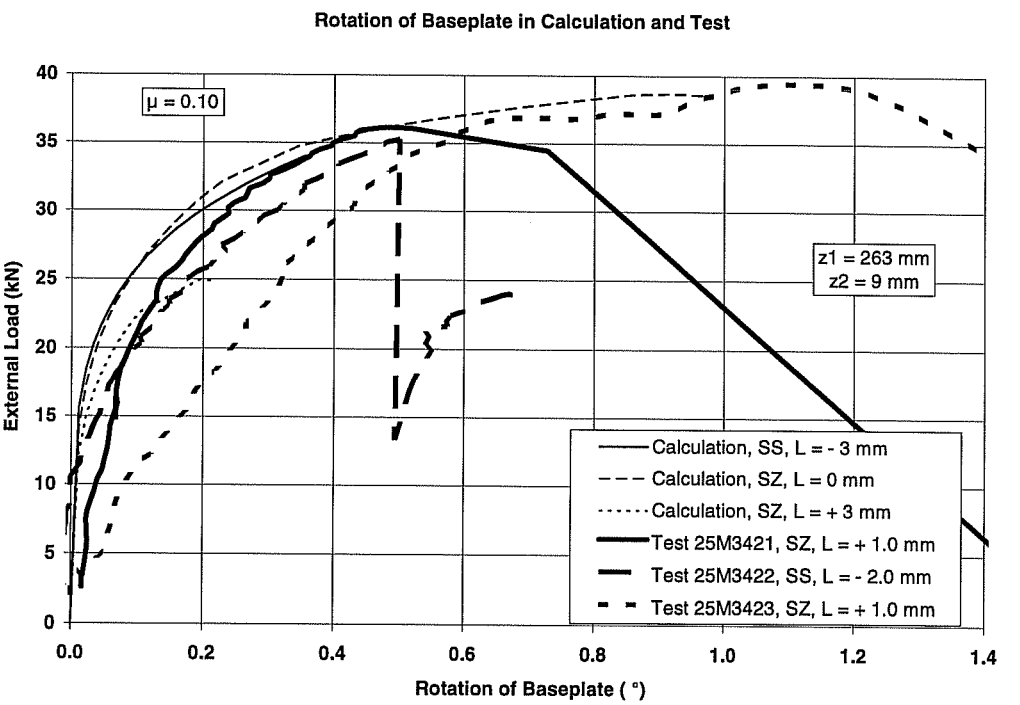
Rotation of Baseplate in Calculation and Test
μ = 0.10
z1 = 263 mm
z2 = 9 mm
Calculation, SS, L = - 3 mm
Calculation, SZ, L = 0 mm
Calculation, SZ, L = + 3 mm
Test 25M3421, SZ, L = + 1.0 mm
Test 25M3422, SS, L = - 2.0 mm
Test 25M3423, SZ, L = + 1.0 mm
External Load (kN)
Rotation of Baseplate (°)
40
35
30
25
20
15
10
5
0
0.0
0.2
0.4
0.6
0.8
1.0
1.2
1.4

Tests Results of Series 25M348 on Two-Anchor Connections UC1 3/8-inch, h_{ef} = 7 inches (178 mm), e = 18 inches (457.2 mm) in Interaction Diagrams of Single-Anchor Tests of Series 23M34

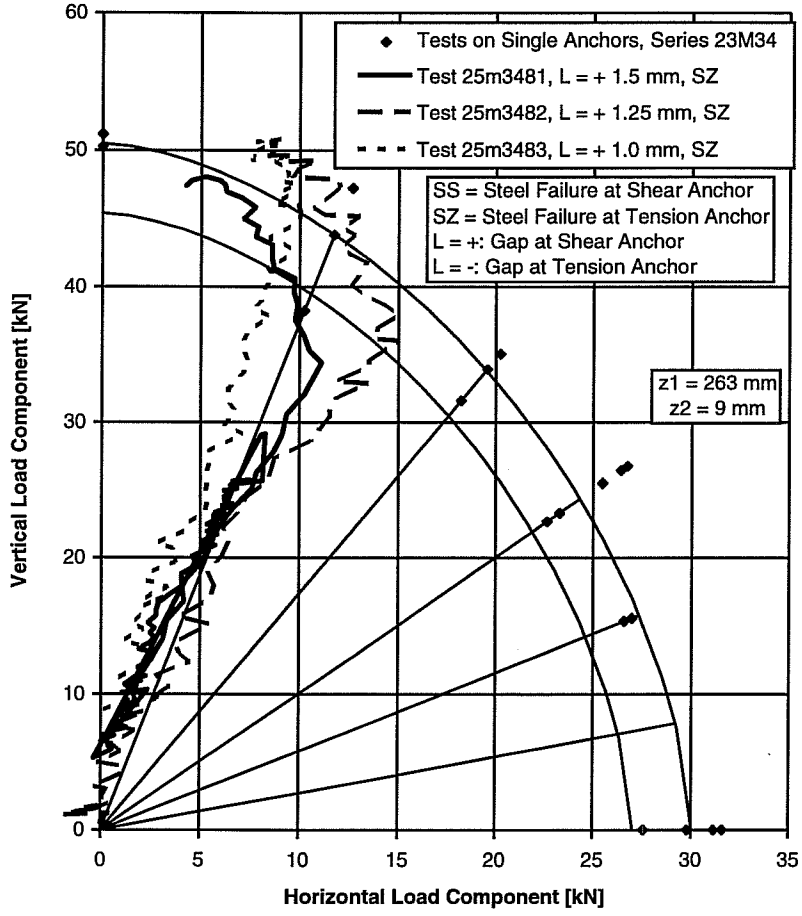

Results of Test-Calculations of Series 25M348 UC1 3/8-inch, h_{ef} = 7 inches (178 mm), e = 18 inches (457.2 mm) in Interaction Diagrams of Single-Anchor Tests of Series 23M34

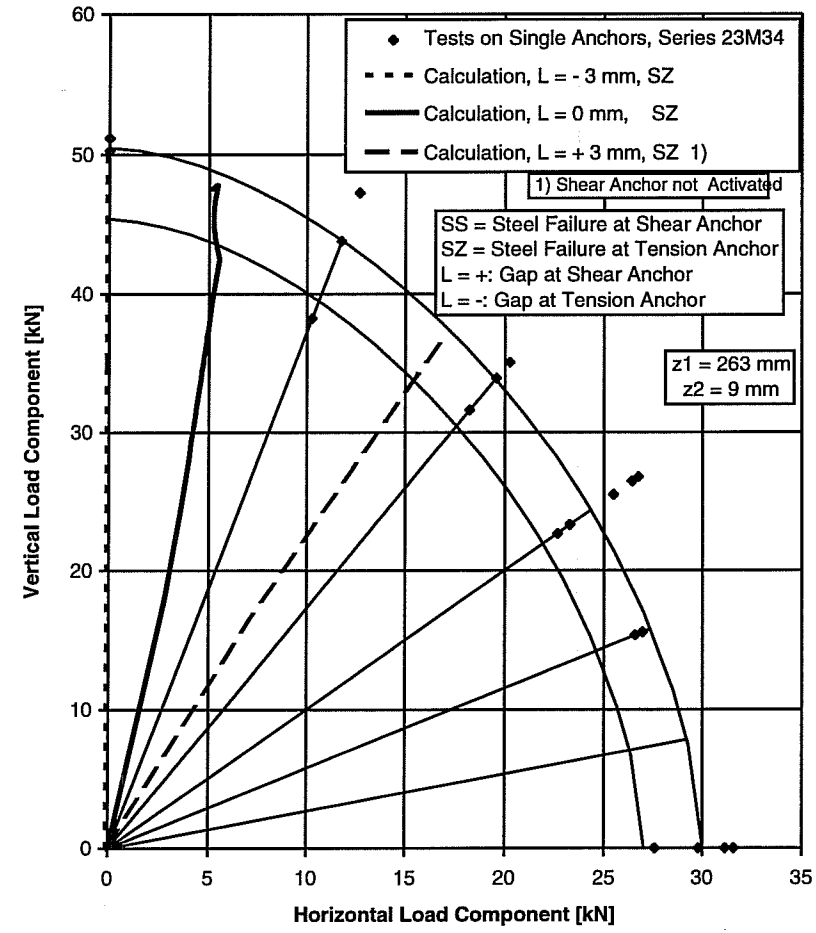

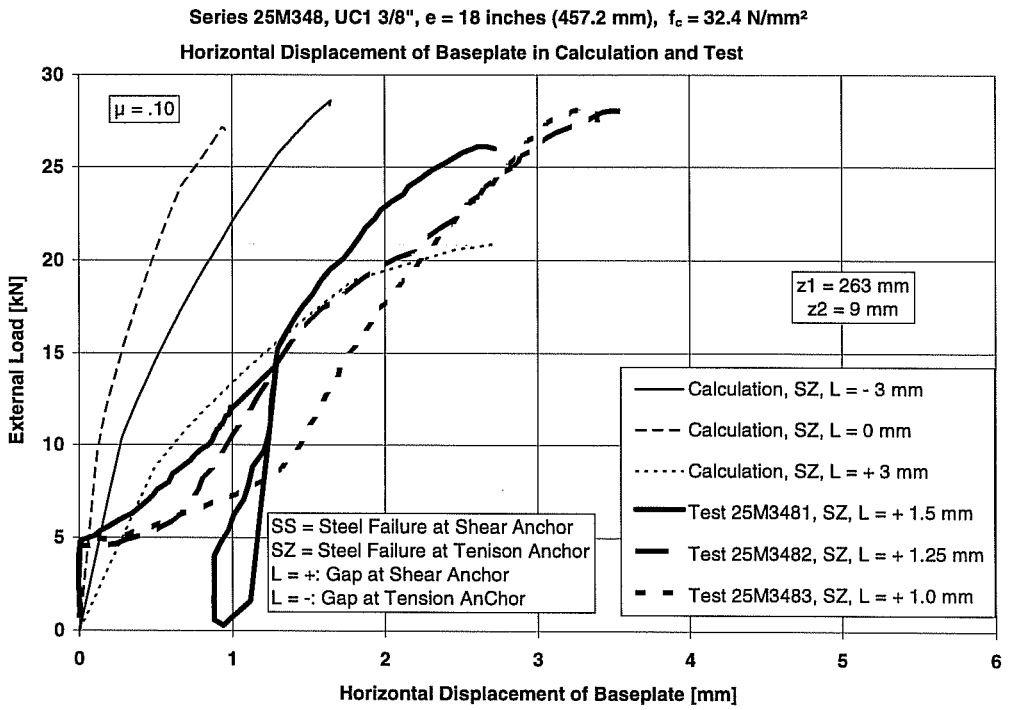
Series 25M348, UC1 3/8", e = 18 inches (457.2 mm), f_c = 32.4 N/mm²
Horizontal Displacement of Baseplate in Calculation and Test
μ = .10
z1 = 263 mm
z2 = 9 mm
SS = Steel Failure at Shear Anchor
SZ = Steel Failure at Tenison Anchor
L = +: Gap at Shear Anchor
L = -: Gap at Tension AnChor
Calculation, SZ, L = - 3 mm
Calculation, SZ, L = 0 mm
Calculation, SZ, L = + 3 mm
Test 25M3481, SZ, L = + 1.5 mm
Test 25M3482, SZ, L = + 1.25 mm
Test 25M3483, SZ, L = + 1.0 mm
External Load [kN]
Horizontal Displacement of Baseplate [mm]
0
5
10
15
20
25
30
0
1
2
3
4
5
6

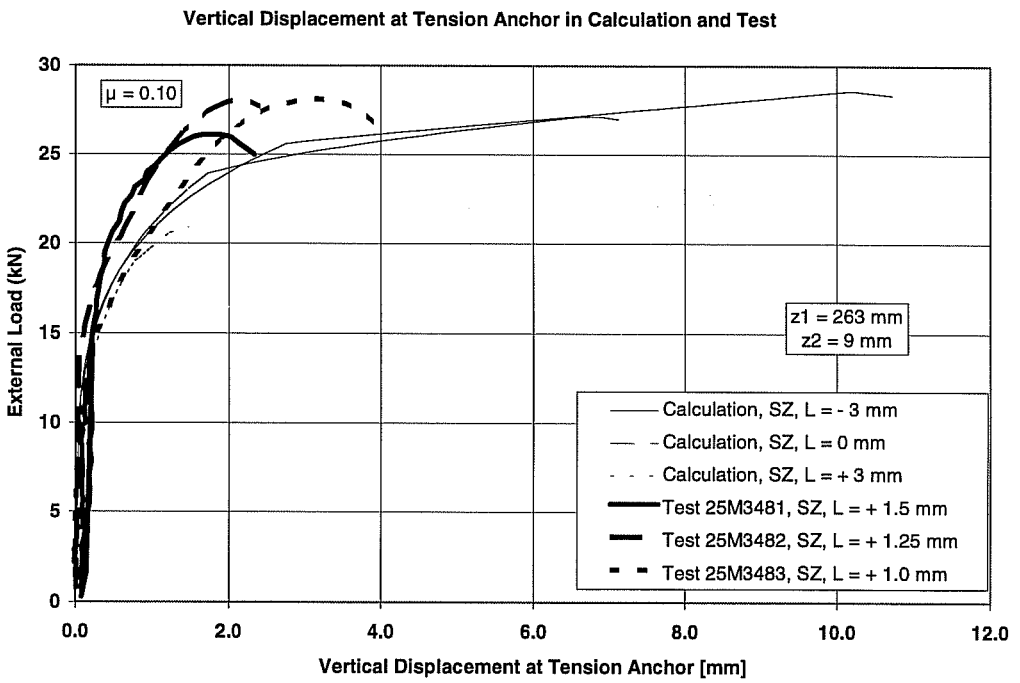
Vertical Displacement at Tension Anchor in Calculation and Test
μ = 0.10
z1 = 263 mm
z2 = 9 mm
Calculation, SZ, L = - 3 mm
Calculation, SZ, L = 0 mm
Calculation, SZ, L = + 3 mm
Test 25M3481, SZ, L = + 1.5 mm
Test 25M3482, SZ, L = + 1.25 mm
Test 25M3483, SZ, L = + 1.0 mm
External Load (kN)
Vertical Displacement at Tension Anchor [mm]
0
5
10
15
20
25
30
0.0
2.0
4.0
6.0
8.0
10.0
12.0

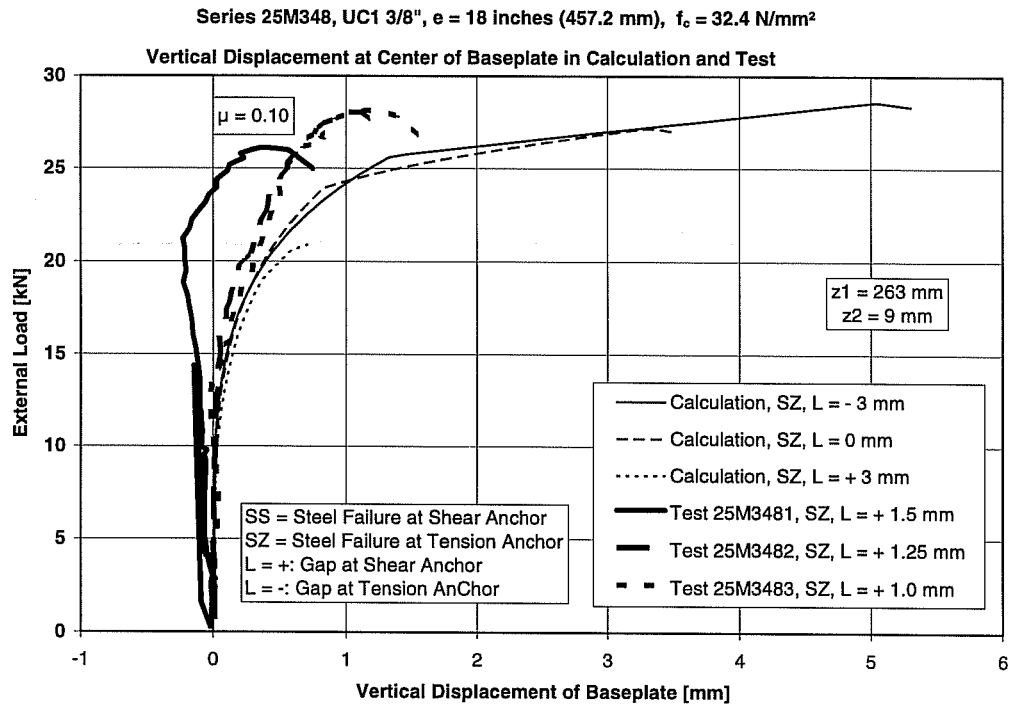
Series 25M348, UC1 3/8", e = 18 inches (457.2 mm), f_c = 32.4 N/mm²
Vertical Displacement at Center of Baseplate in Calculation and Test
μ = 0.10
z1 = 263 mm
z2 = 9 mm
SS = Steel Failure at Shear Anchor
SZ = Steel Failure at Tension Anchor
L = +: Gap at Shear Anchor
L = -: Gap at Tension AnChor
Calculation, SZ, L = - 3 mm
Calculation, SZ, L = 0 mm
Calculation, SZ, L = + 3 mm
Test 25M3481, SZ, L = + 1.5 mm
Test 25M3482, SZ, L = + 1.25 mm
Test 25M3483, SZ, L = + 1.0 mm
External Load [kN]
Vertical Displacement of Baseplate [mm]
0
5
10
15
20
25
30
-1
0
1
2
3
4
5
6

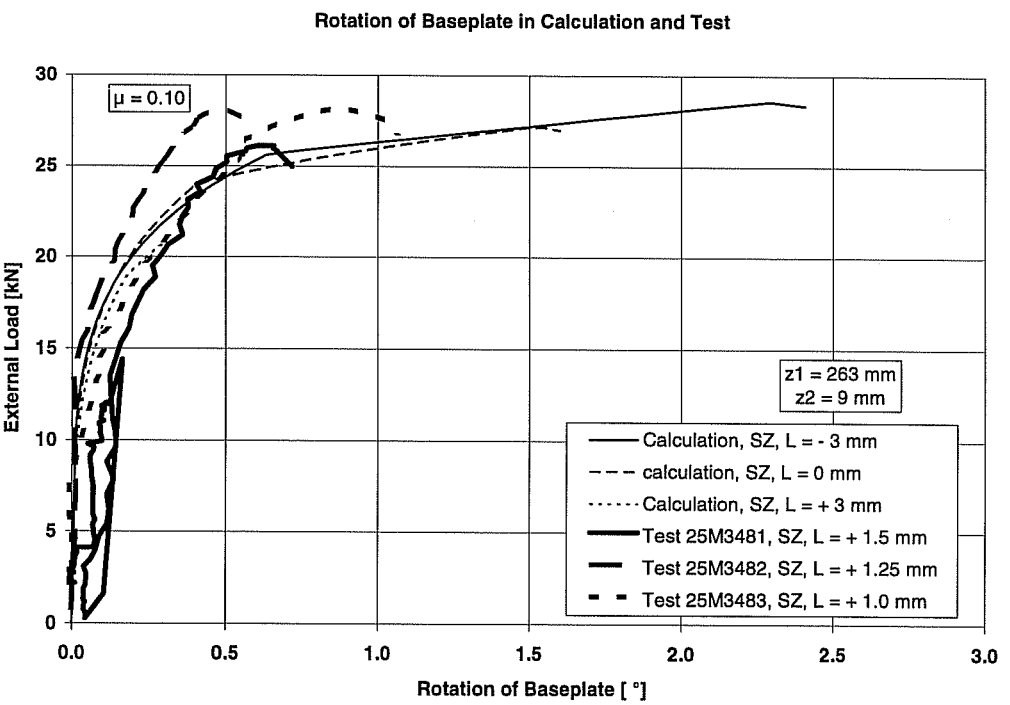
Rotation of Baseplate in Calculation and Test
μ = 0.10
z1 = 263 mm
z2 = 9 mm
Calculation, SZ, L = - 3 mm
calculation, SZ, L = 0 mm
Calculation, SZ, L = + 3 mm
Test 25M3481, SZ, L = + 1.5 mm
Test 25M3482, SZ, L = + 1.25 mm
Test 25M3483, SZ, L = + 1.0 mm
External Load [kN]
Rotation of Baseplate [°]
0
5
10
15
20
25
30
0.0
0.5
1.0
1.5
2.0
2.5
3.0

Comparison Among Plastic Theory, Elastic Theory, Calculation with bDA5, and Test Results of Connections of Series 26M54

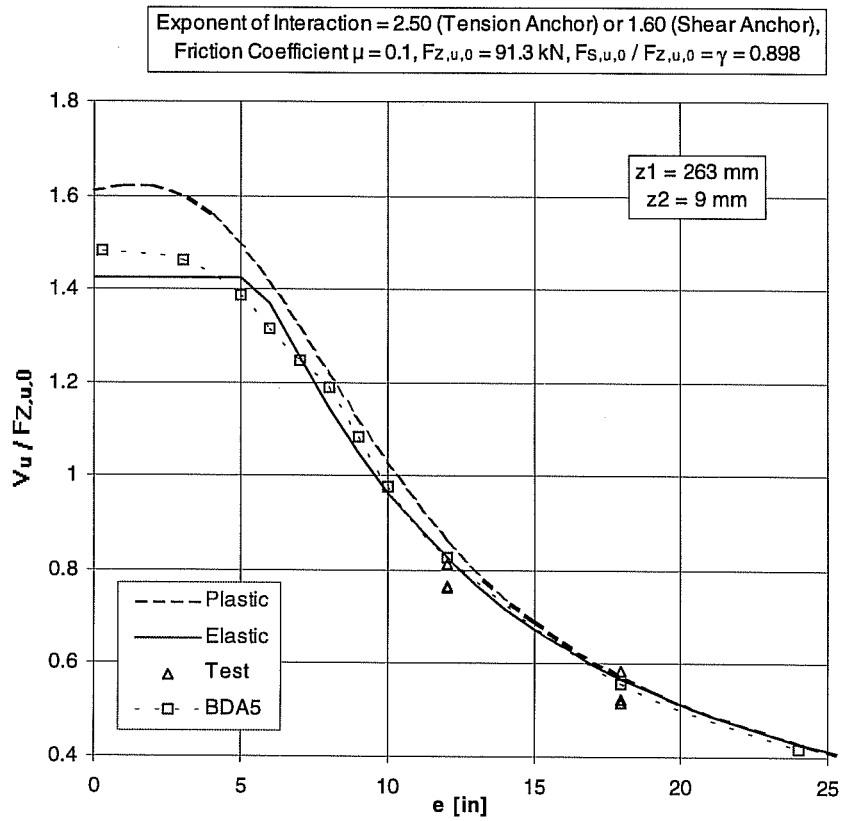

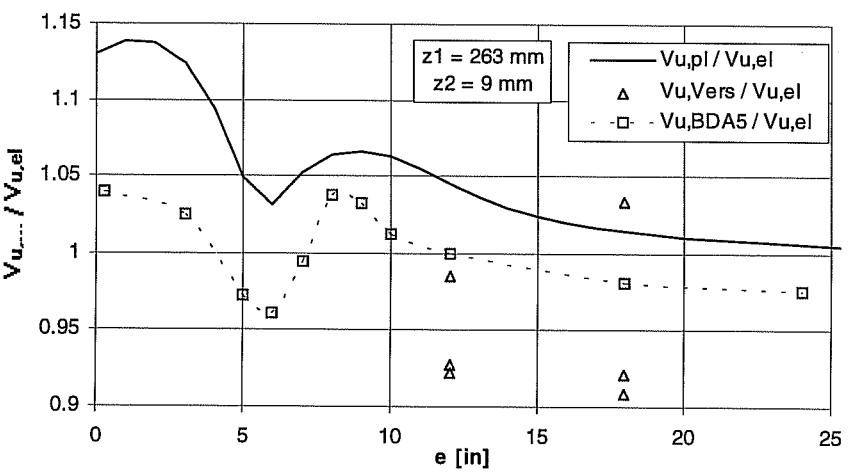

Results of Test-Calculations of Series 26M542
UC1 5/8-inch, h_{ef} = 3.5 inches (89 mm), e = 12 inches (304.8 mm) in Interaction Diagrams of Single-Anchor Tests of Series 23A54

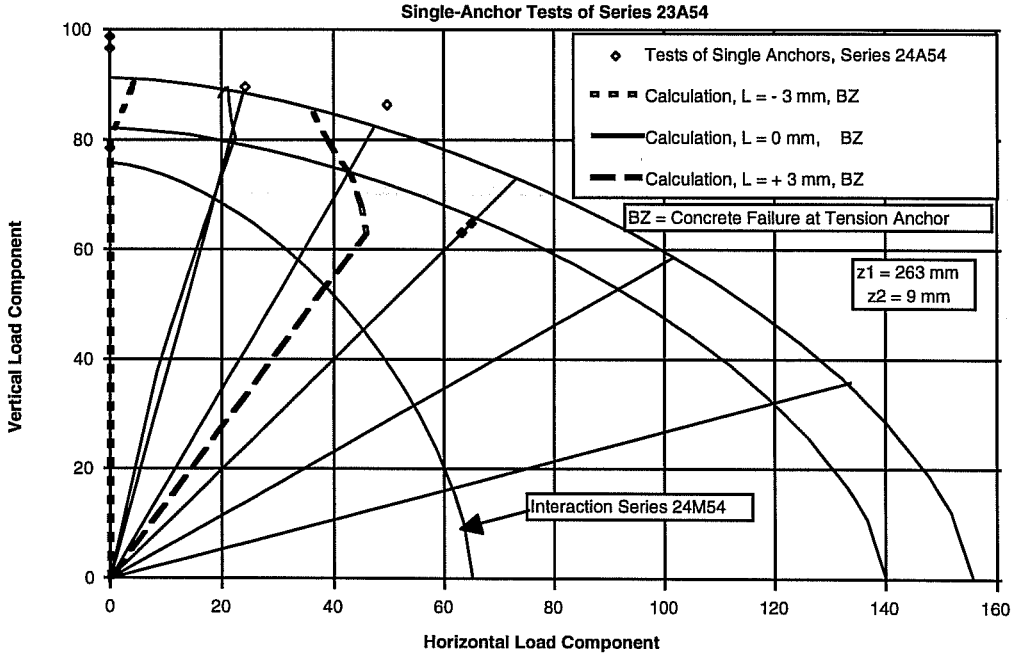

Test Results of Series 26M542 on Two-Anchor Connections
UC1 5/8-inch, h_{ef} = 3.5 inches (89 mm), e = 12 inches (304.8 mm) in Interaction Diagrams of Single-Anchor Tests of Series 23A54

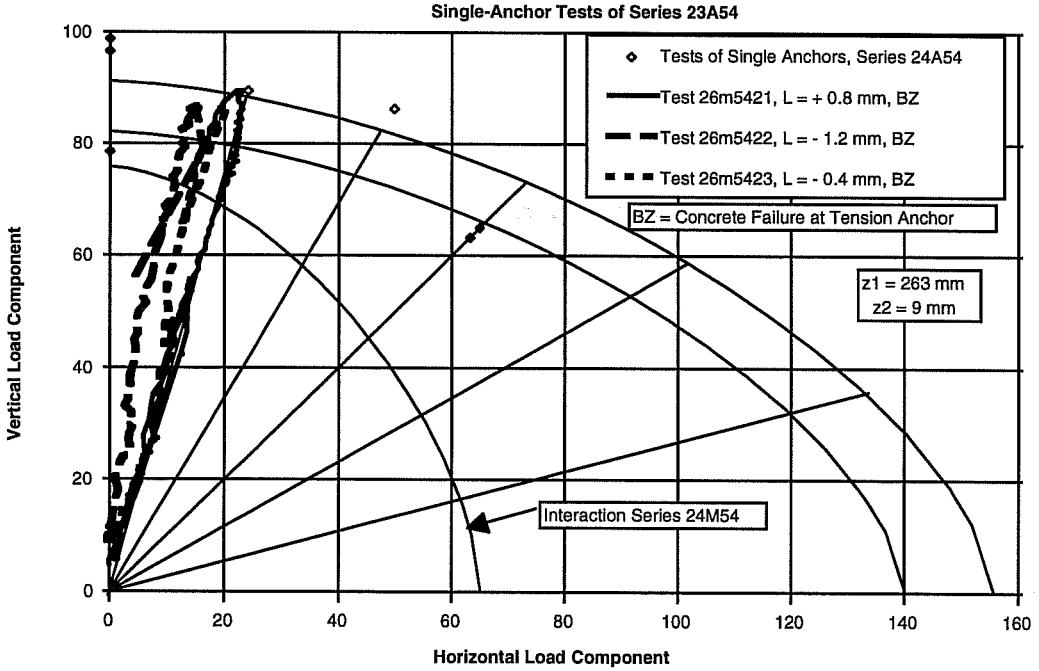

Series 26M542, UC1 5/8", e = 12 inches (304.8 mm), f_c = 32.4 N/mm²

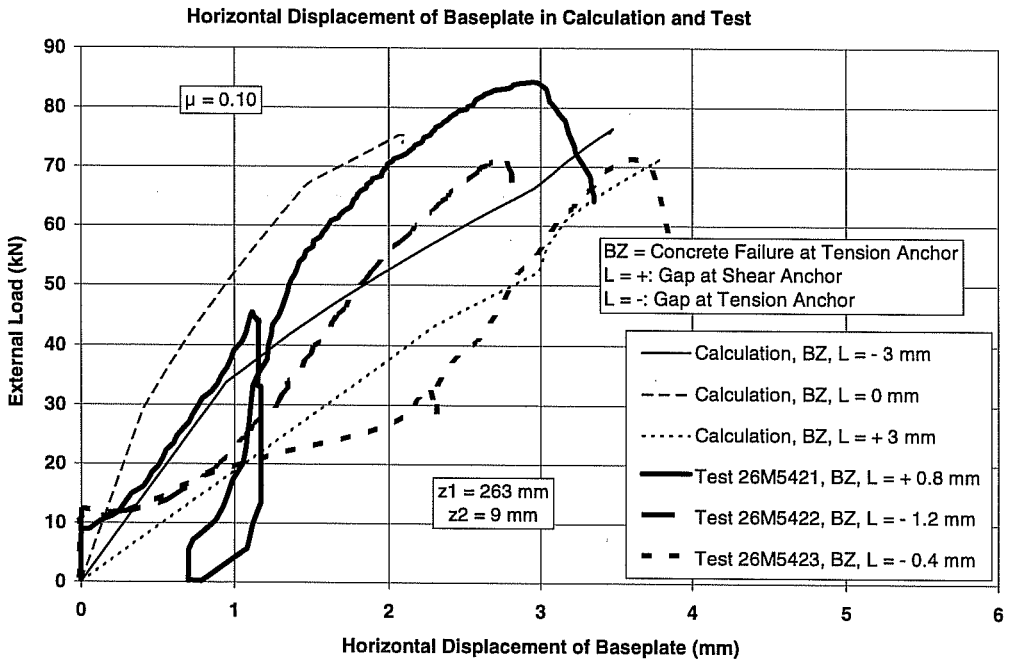

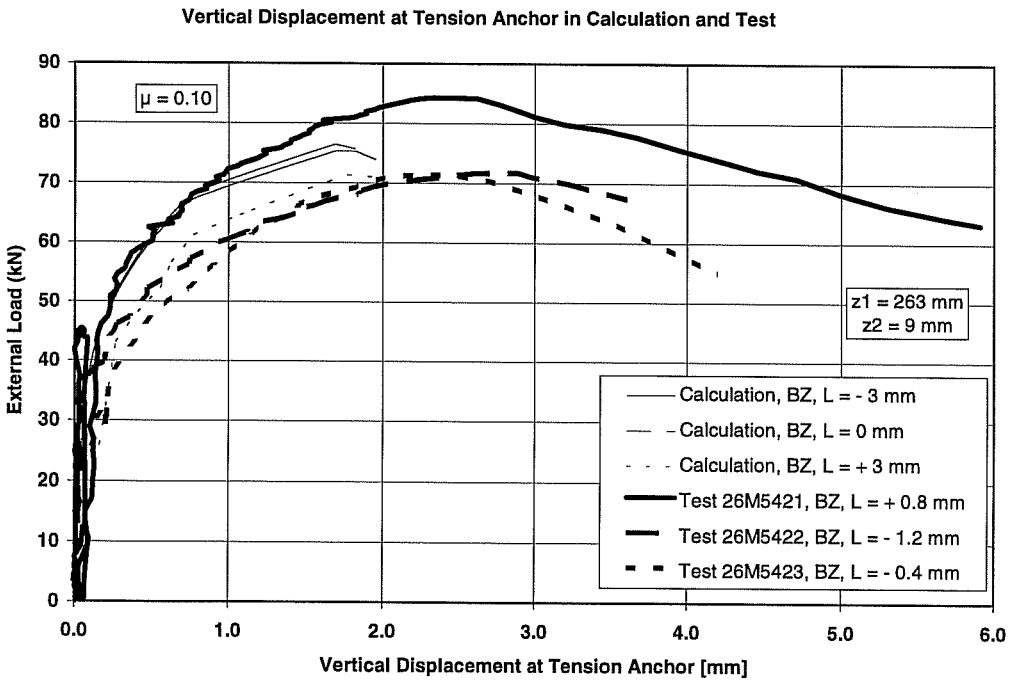

Series 26M542, UC1 5/8", e = 12 inches (304.8 mm), fc = 32.4 N/mm²

Vertical Displacement at Center of Baseplate in Calculation and Test

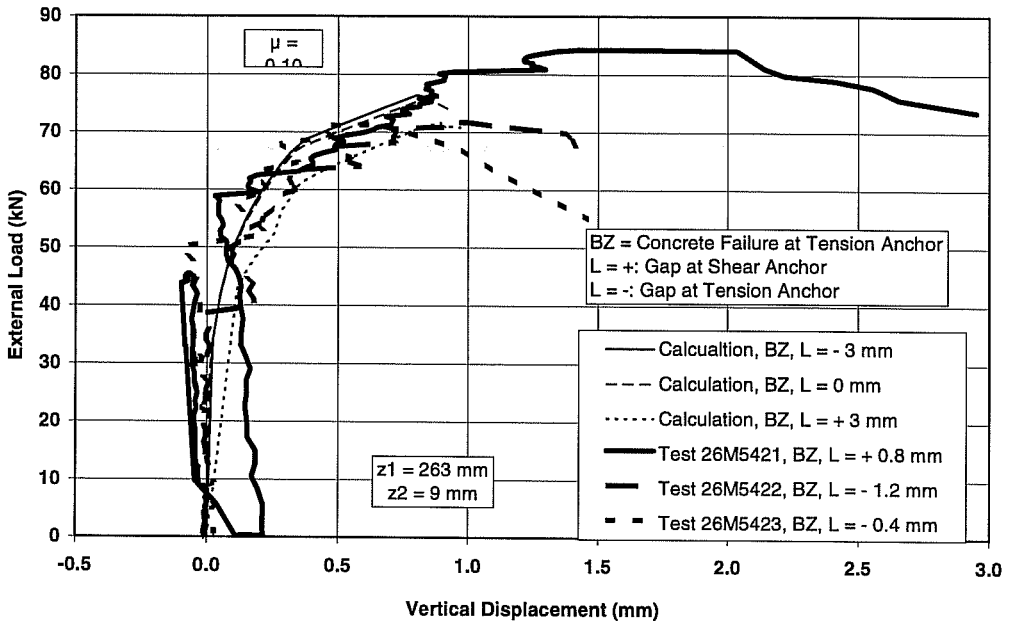

Rotation of Baseplate in Calculation and Test

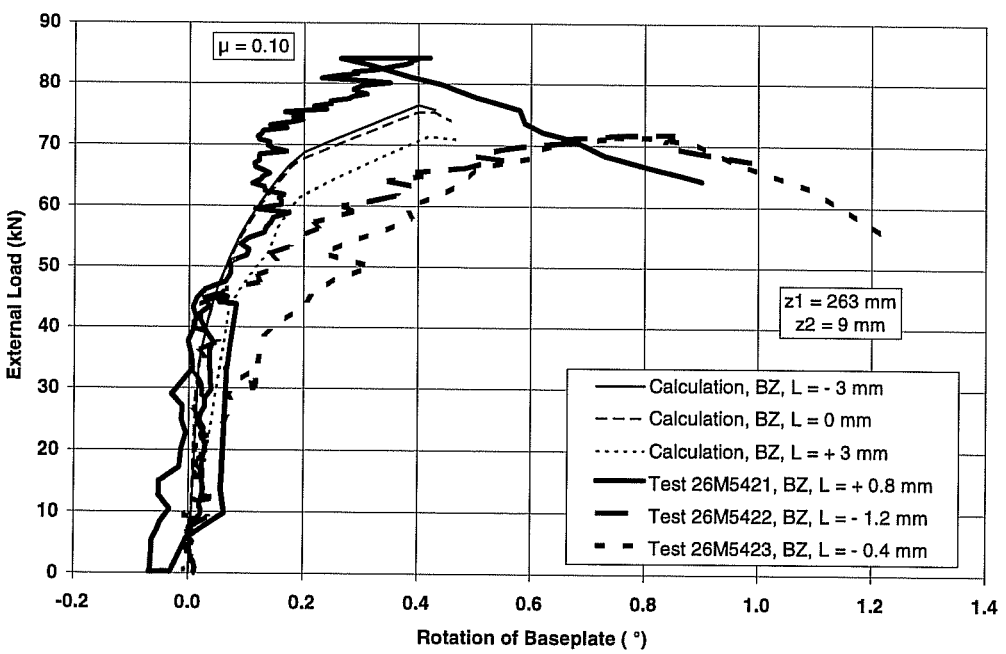

Tests Results of Series 26M548 on Two-Anchor Connections
UC1 5/8-inch, h_{ef} = 3.5 inches (89 mm), e = 18 inches (457.2 mm) in Interaction Diagrams of Single-Anchor Tests of Series 23A54

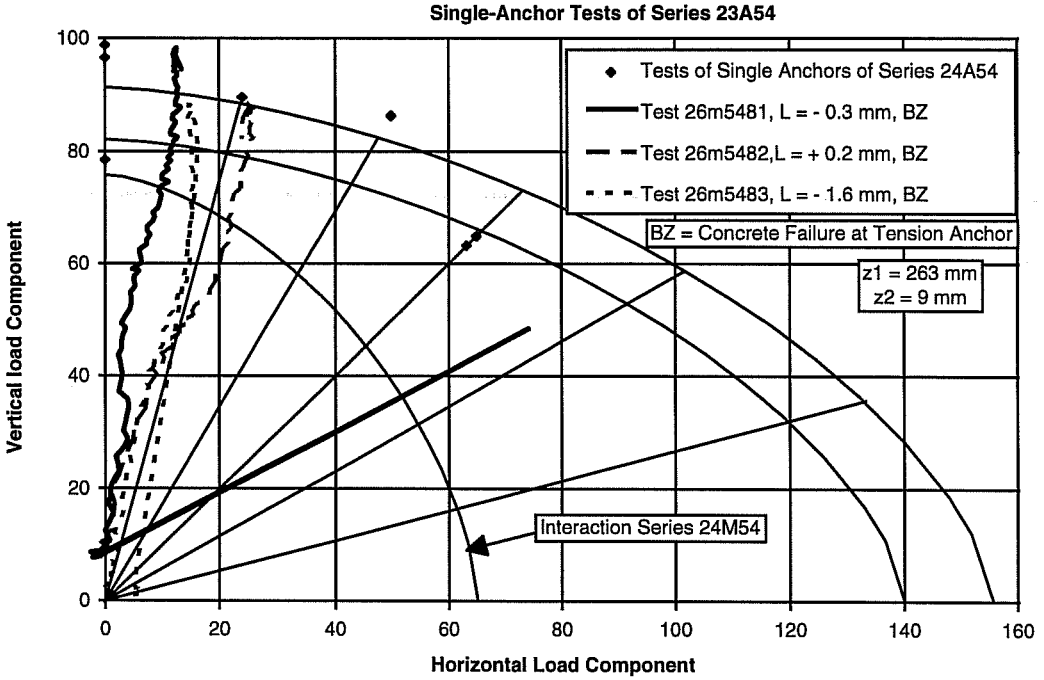

Results of Test-Calculations of Series 26M548
UC1 5/8-inch, h_{ef} = 3.5 inches (89 mm), e = 18 inches (457.2 mm) in Interaction Diagrams of Single-Anchor Tests of Series 23A54

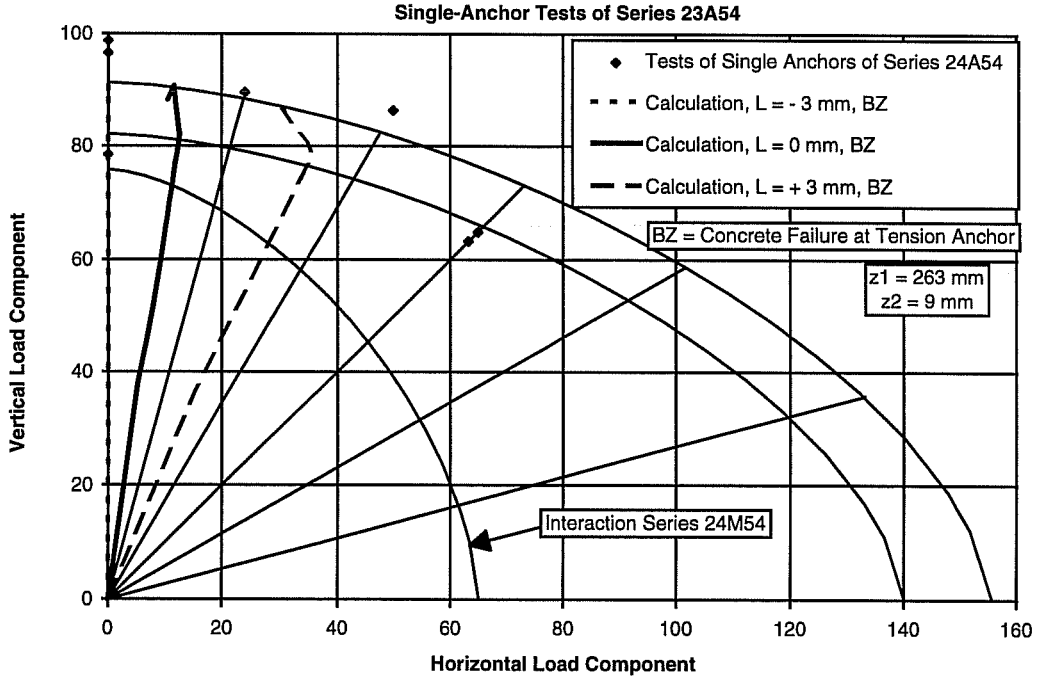

Series 26M548, UC1 5/8", e = 18 inches (457.2 mm), f_c = 32.4 N/mm²

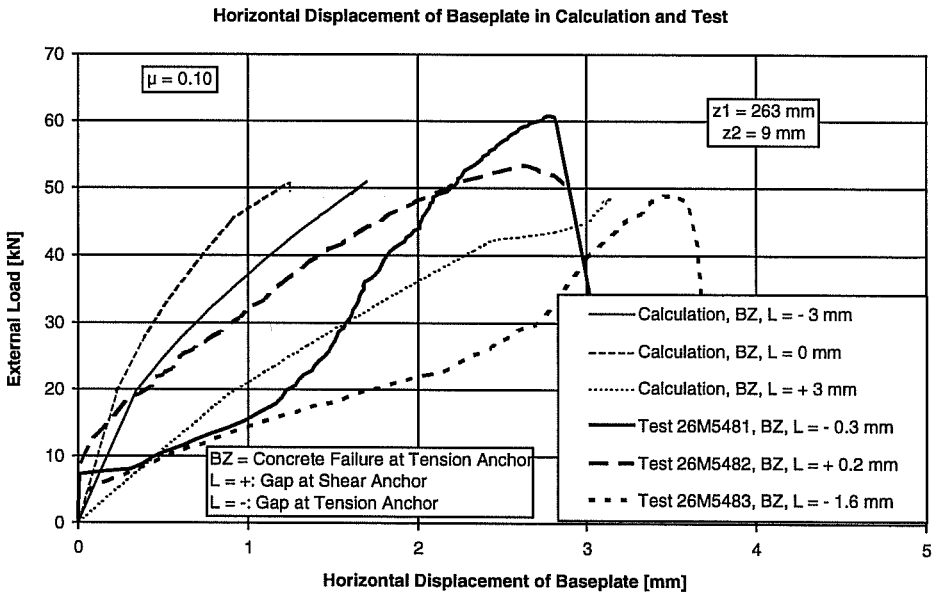

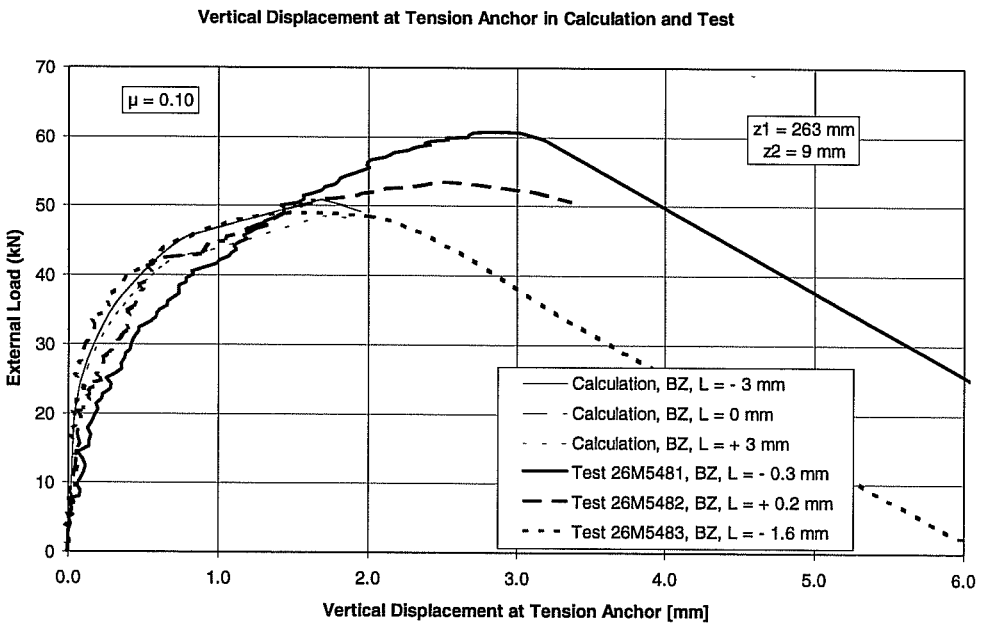

Series 26M548, UC1 5/8", e = 18 inches (457.2 mm), f_c = 32.4 N/mm²

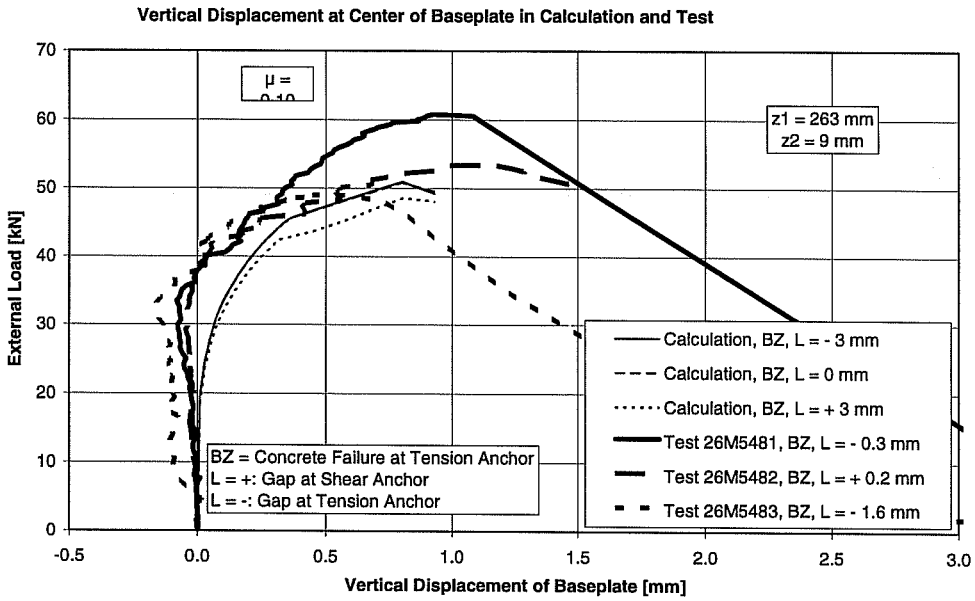

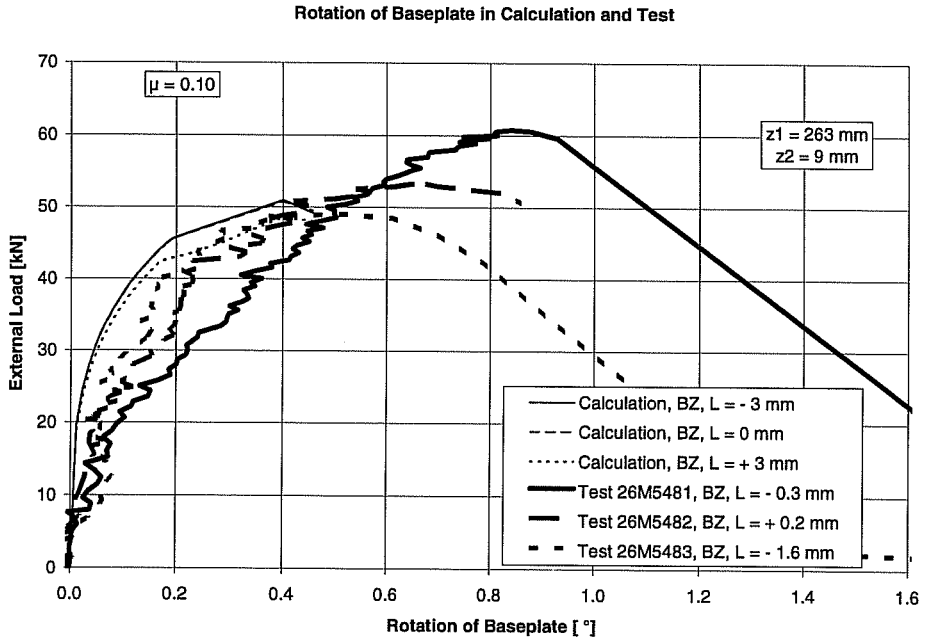

Comparison Among Plastic Theory, Elastic Theory, Calculation with BDA5, and Test Results of Cook (1989) on Connections with Two Anchor Rows and Stiff Baseplate

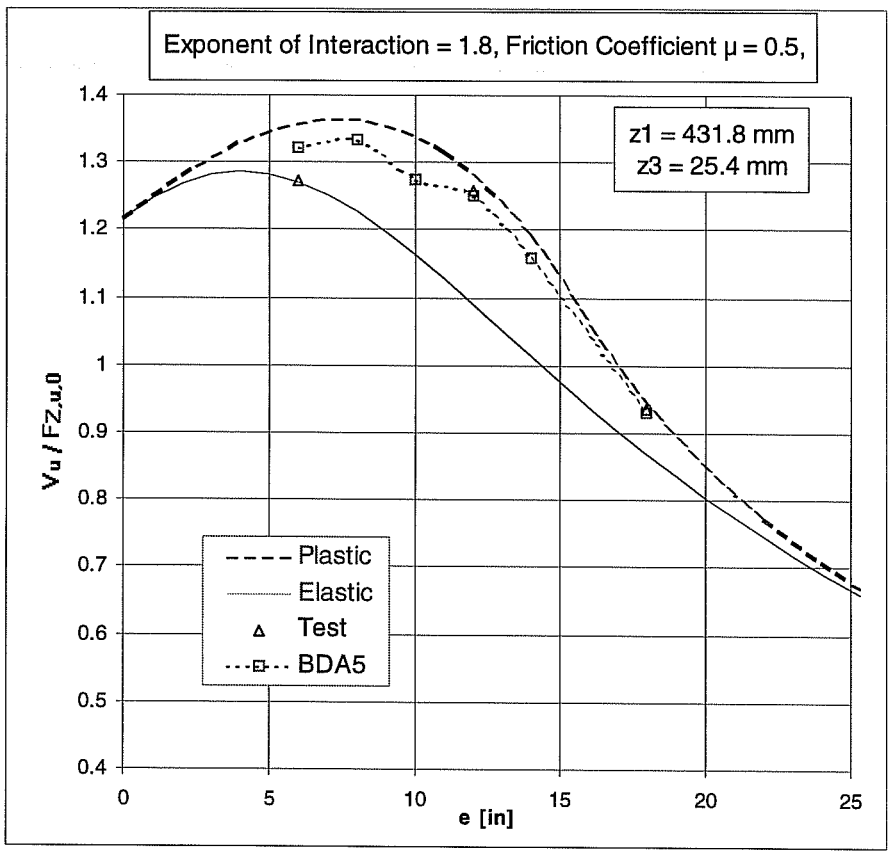

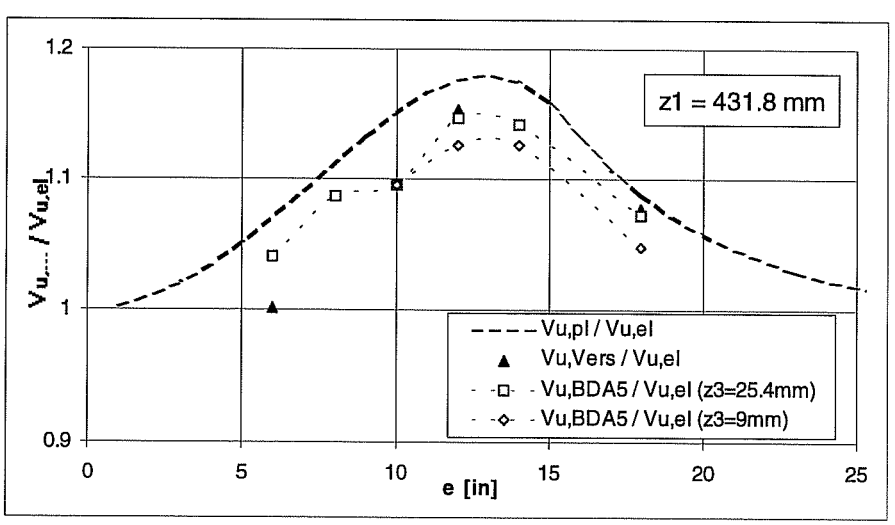

Comparison Among Plastic Theory, Elastic Theory, Calculation with BDA5, and Test Results of Cook (1989) on Connections with Three Anchor Rows and Stiff Baseplate

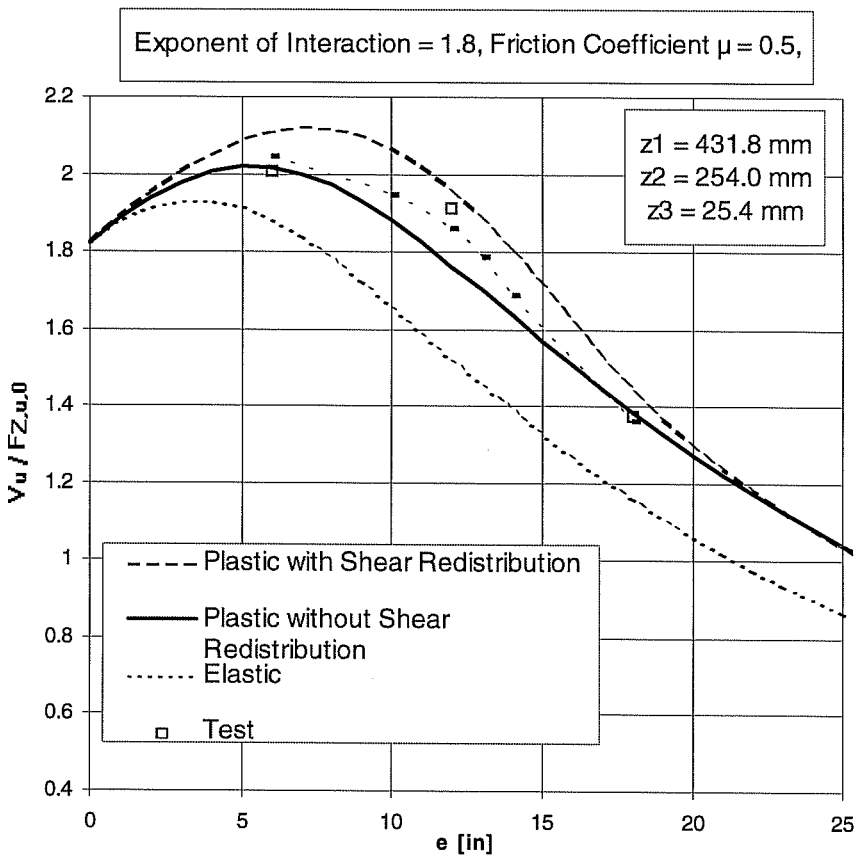

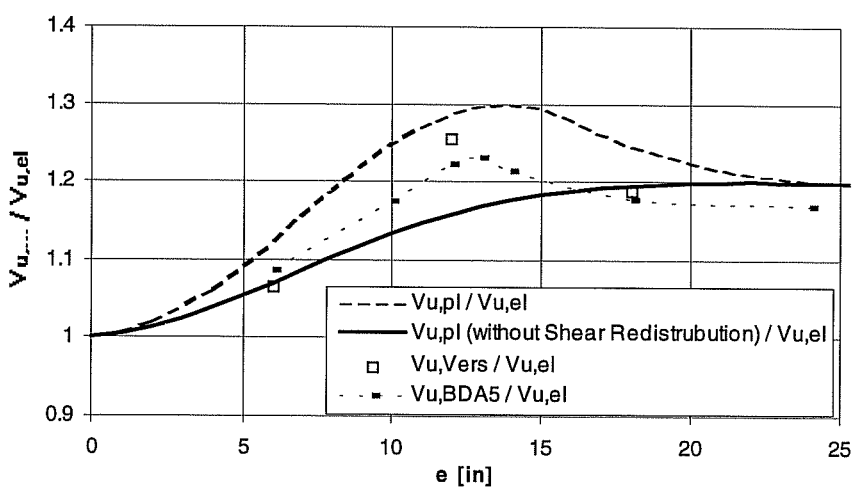

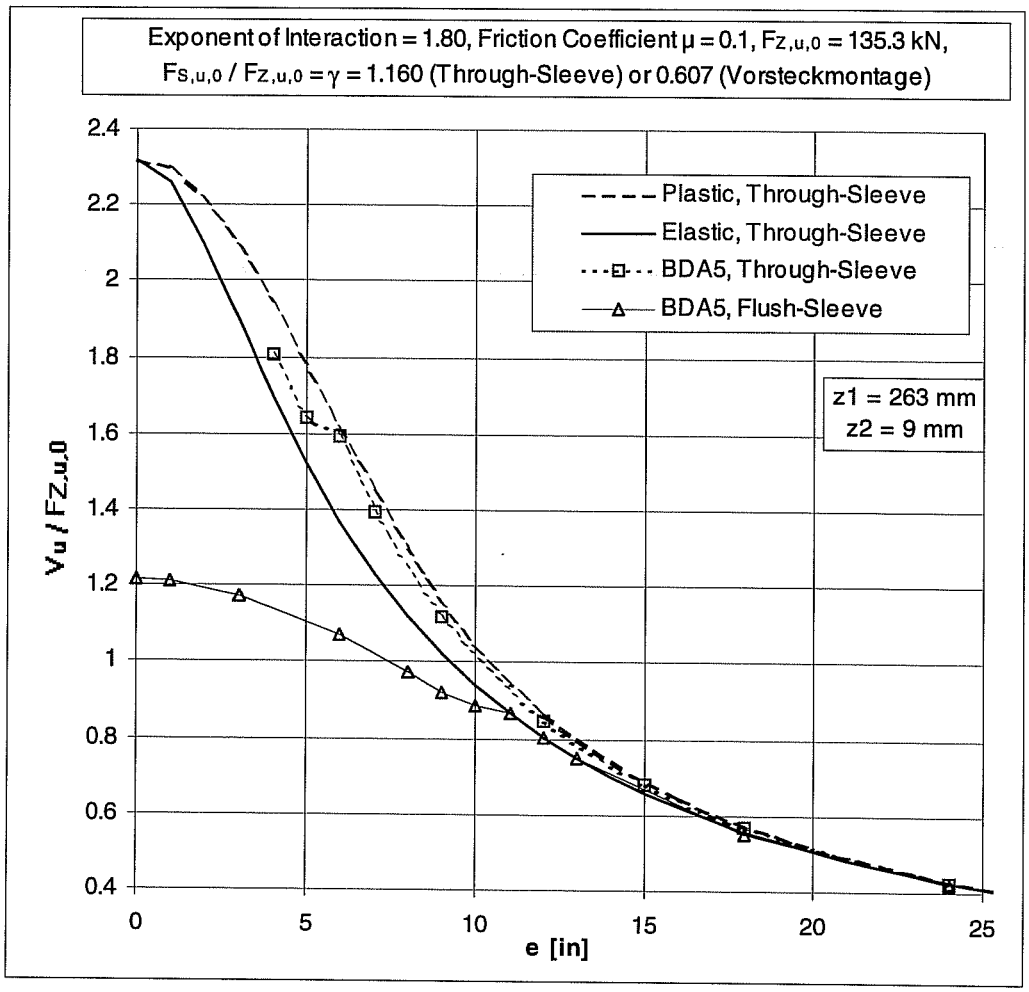
Exponent of Interaction = 1.80, Friction Coefficient μ = 0.1, Fz,u,0 = 135.3 kN,
Fs,u,0 / Fz,u,0 = γ = 1.160 (Through-Sleeve) or 0.607 (Vorsteckmontage)
Plastic, Through-Sleeve
Elastic, Through-Sleeve
BDA5, Through-Sleeve
BDA5, Flush-Sleeve
z1 = 263 mm
z2 = 9 mm
Vu / FZ,u,0
e [in]
2.4
2.2
2
1.8
1.6
1.4
1.2
1
0.8
0.6
0.4
0
5
10
15
20
25

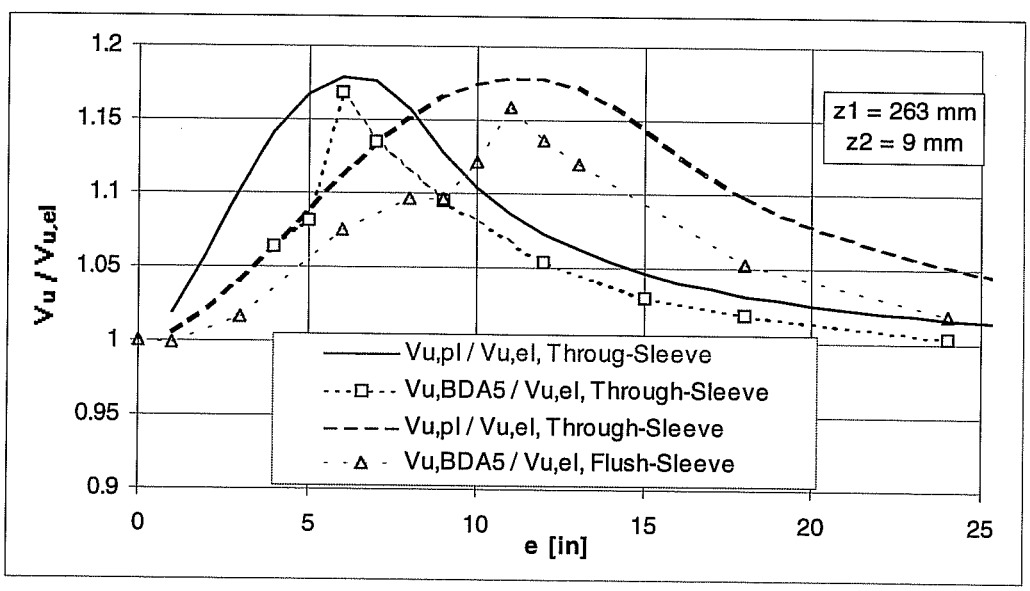
z1 = 263 mm
z2 = 9 mm
Vu,pl / Vu,el, Throug-Sleeve
Vu,BDA5 / Vu,el, Through-Sleeve
Vu,pl / Vu,el, Through-Sleeve
Vu,BDA5 / Vu,el, Flush-Sleeve
Vu / Vu,el
e [in]
1.2
1.15
1.1
1.05
1
0.95
0.9
0
5
10
15
20
25

Comparison Among Plastic Theory, Elastic Theory and Calculation with BDA5, Sleeve, Connections of Series 25H64 by Curves for Through-Sleeve Installation (Series 23H74)

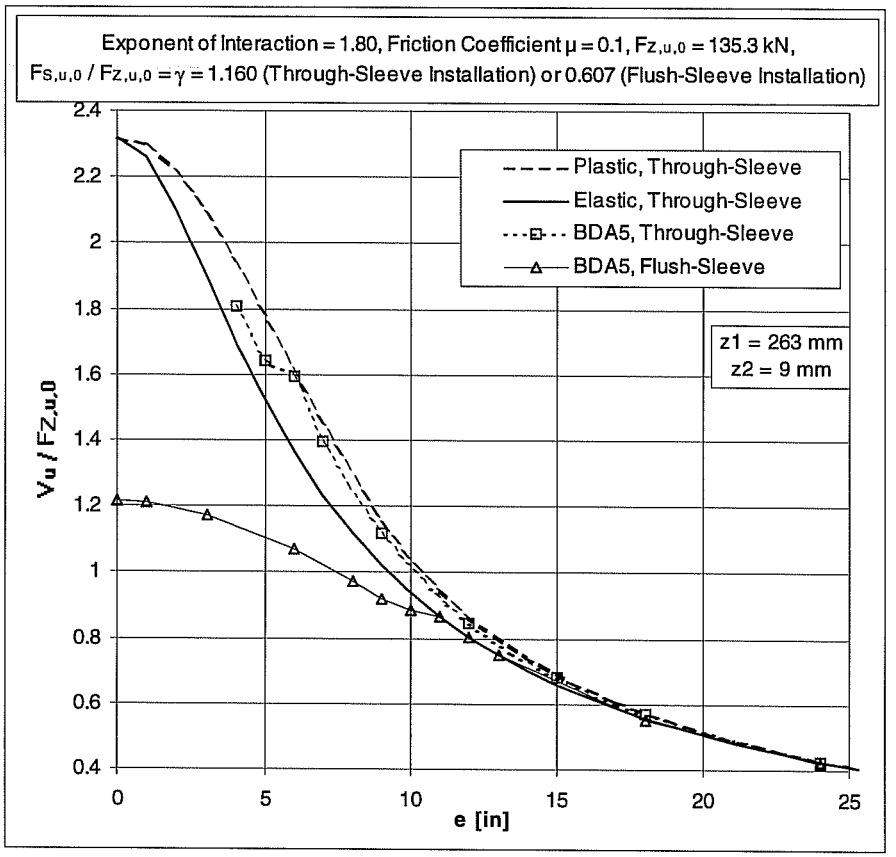

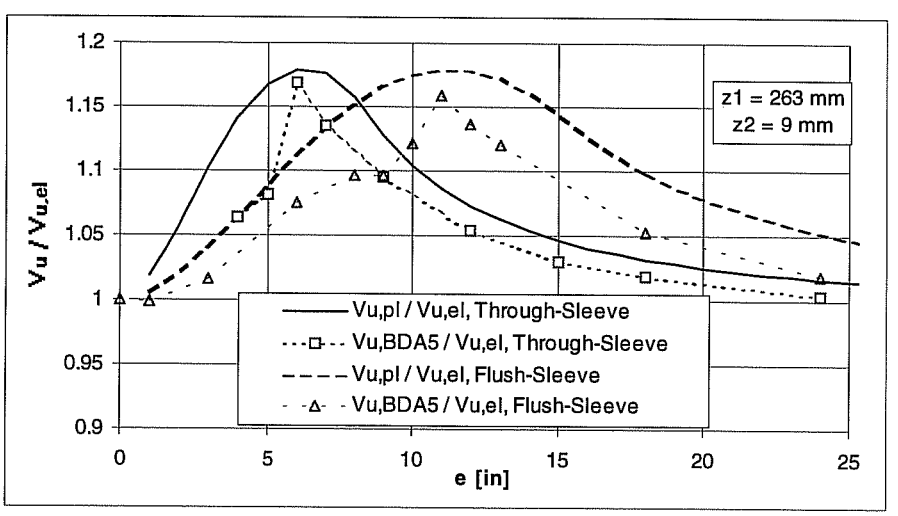

Comparison Among Plastic Theory, Elastic Theory and Calculation with BDA5, UC1, Influence of Concrete Strength, L-D Curves of Series 23M54 and 23M53

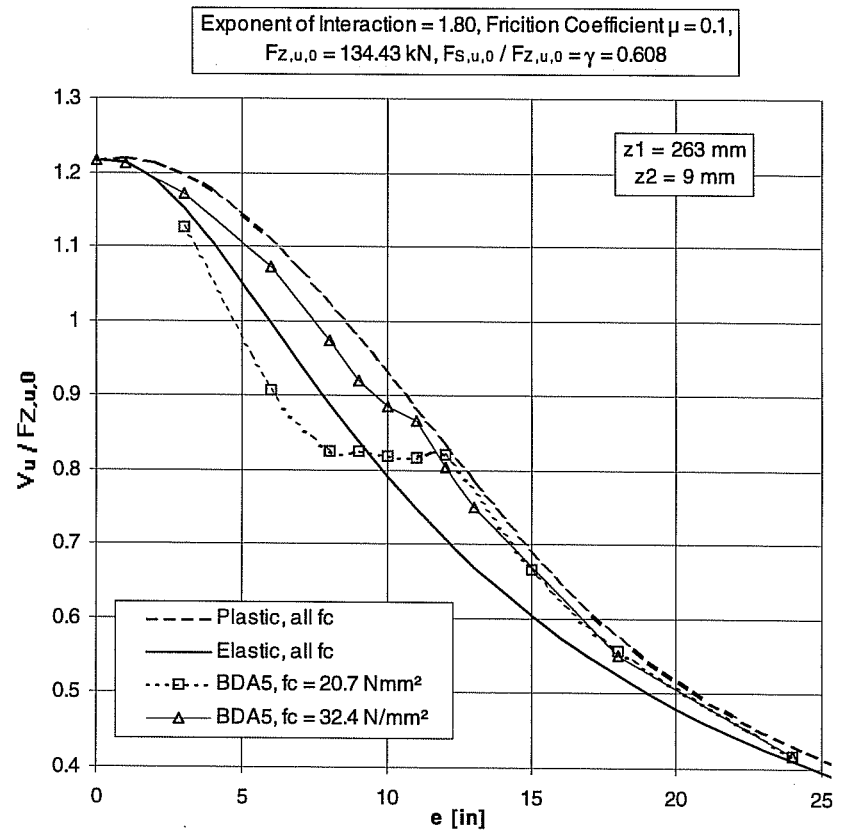

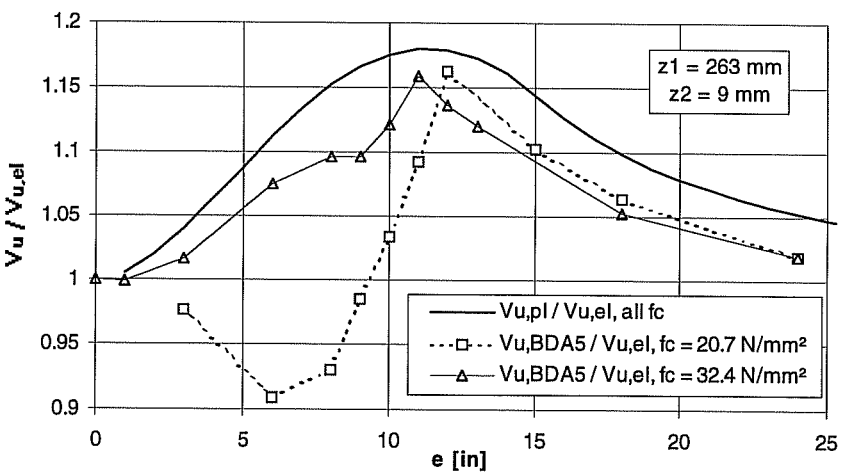

Comparison Among Plastic Theory, Elastic Theory and Calculation with BDA5, UC1, Influence of Friction, L-D Curves of Series 23M53 (f_c = 20.7 N/mm^2)

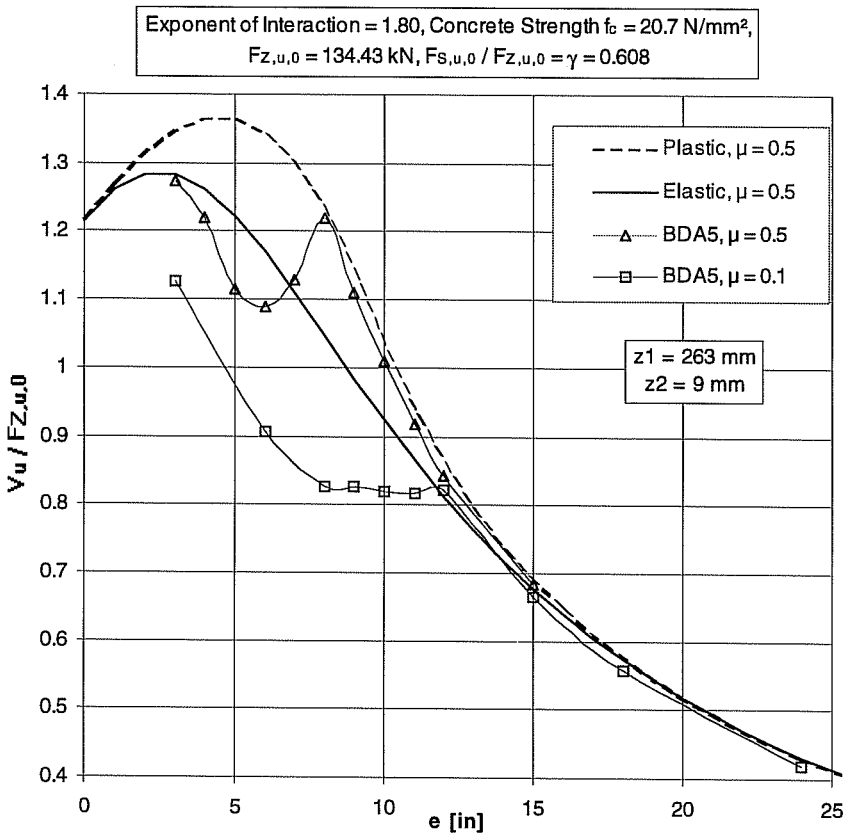

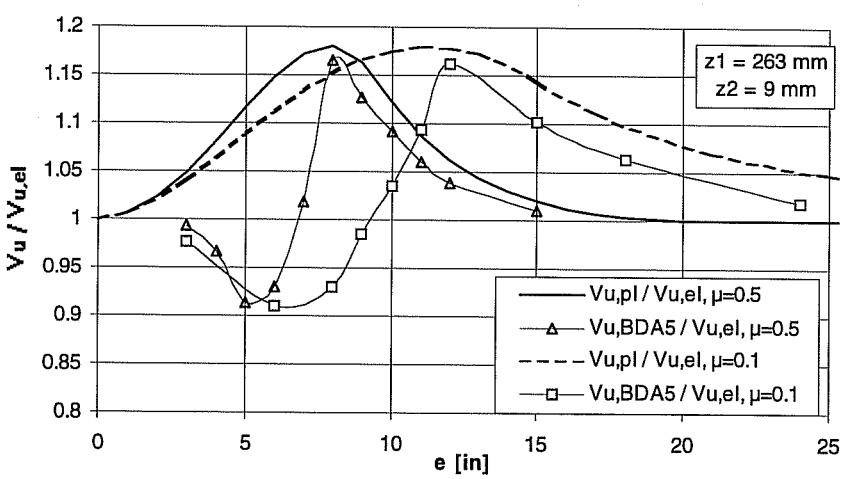

Comparison Among Plastic Theory, Elastic Theory and Calculation with BDA5, UC1, Influence of Friction, L-D Curves of Series 23M54 (f_c = 32.4 N/mm^2)